JOURNAL OF BIOLOGICAL REGULATORS & HOMEOSTATIC AGENTS

Volume 33, No. 2, March - April, 2019

CONTENTS

EDITORIAL

GUT MICROBIOTA AND IMMUNITY IN COMMON VARIABLE IMMUNODEFICIENCY: CROSSTALK WITH PRO-INFLAMMATORY CYTOKINES

L. FRANZA[1,2*], V. CARUSI[1*], S. ALTAMURA[1], A. GASBARRINI[3], A. CARAFFA[4], S.K. KRITAS[5], G. RONCONI[6], C.E. GALLENGA[7], F. DI VIRGILIO[8] and F. PANDOLFI[1]

[1]Clinical Immunology Laboratory, Department of Internal Medicine, Fondazione Policlinico Universitario A. Gemelli IRCCS - Università Cattolica del Sacro Cuore, Rome, Italy; [2]Department of Infective Diseases, Fondazione Policlinico Universitario A. Gemelli IRCCS - Università Cattolica del Sacro Cuore, Rome, Italy; [3]Gastroenterology Deparment, Fondazione Policlinico Universitario A. Gemelli IRCCS - Università Cattolica del Sacro Cuore, Roma, Italy; [4]School of Pharmacy, University of Camerino, Camerino, Italy; [5]Department of Microbiology and Infectious Diseases, School of Veterinary Medicine, Aristotle University of Thessaloniki, Macedonia, Greece; [6]Clinica dei Pazienti del Territorio, Fondazione Policlinico Gemelli, Rome, Italy; [7]Department of Biomedical Sciences and Specialist Surgery, Section of Ophthalmology, University of Ferrara, Ferrara, Italy; [8]Department of Morphology, Surgery and Experimental Medicine, University of Ferrara, Ferrara, Italy

Received January 11, 2019 – Accepted February 12, 2019

[*] These authors contributed equally to this article

In recent years, gut microbiota (GM) has emerged as a key factor in shaping the pathogenesis of a vast array of immune-mediated diseases, as well as in the response to immune-based treatments such as anti PD-1 and anti-CTLA4 therapy or influenza vaccination (1). In addition, GM has a significant role in the immune system development and is fundamental in developing mucosal immunity (2).

Recent data suggest that GM plays an important role in the immune system of immune deficient patients. In this review, we focus on primary immune deficiencies, discussing the possibilities and benefits of modulating GM in primary immune deficient patients.

Lastly, we discuss the effects of therapies used in immune deficiencies and their effects on patients, particularly concentrating on antibiotic use in this population.

As Robert Good said "primary immune deficiencies are experiments of nature which allow us to understand key factors of the immune system" (F.P. personal communication, Orvieto, 1994).

Gut microbiota and immunity: a complex cross-talk involving key cytokines

Over $10x10^{13}$ bacteria live in our gut, which is about 10 times the number of human cells. (3). Such bacteria can vary, based on many factors and particularly diet, which seems to be the primary driver of GM composition (4), age, sex, and stress (5). Even surgical procedures can completely change GM composition, not only temporary but for long periods of time (6). In a healthy condition, the GM varies considerably also based on the area of the gastrointestinal (GI) tract: in the esophagus the species mostly represented is the *Streptococcus*

Key words: gut; microbiota; immunodeficiency; inflammation; cytokine

Corresponding Author:
Prof. Franco Pandolfi,
Clinical Immunology Laboratory,
Department of Internal Medicine,
Fondazione Policlinico Universitario A. Gemelli IRCCS
Università Cattolica del Sacro Cuore, Rome, Italy
e-mail: franco.pandolfi@unicatt.it

0393-974X (2019)

group, in the stomach and in the small intestine there is an overall poorer microbial population, due to the acidic environment (3). Composition of the colorectal GM is, instead, extremely varied in species and localization. There appear to be three main genera, *Bacteroides*, *Prevotella* and *Ruminococcus*. Prevalence of one of these species determines in which main enterotype a person fits, even though many suggest that GM is better defined by a continuum, rather than specific categories (7).

GM directly contributes to the body's homeostasis: it is vital in the synthesis of vitamins B and K, determines how certain foods are digested, works as a mechanical barrier against pathogens and contributes to the gut homeostasis (8, 9). When the equilibrium of GM is altered, a condition known as dysbiosis, there is an increased inflammatory status in the gut (10), and there appear to be consequences in the whole body. Bacterial translocation and leaky gut are partly responsible for the long-term effects of dysbiosis, but many immunologic mechanisms are involved.

GM directly affects the innate and the adaptive immune system, through different pathways. Firstly, GM stimulates the gut-associated lymphatic tissue (GALT) through NOD-like receptor and toll-like receptor (TLR) signaling. The TLR-2 pathway works through MyD88 signaling, meaning that it affects both the IRAK-3 and the NF-kB pathways and it attracts hematopoietic stem cells to the spleen. Through TLR signaling, particularly TLR-2, GM also appears to play a role in differentiating cytokine production of lymphoid inducer tissue cells: TLR-2 enhances the interleukin-2 production, which stimulates the activation of innate lymphoid cells (ILC), but it also appears that the GM-activated TLR pathway may directly stimulate ILCs, particularly natural killers (NKs). Metabolites synthesized by the GM have some direct immune-modulating effects, which can be pro-inflammatory or anti-inflammatory: Lactobacillaceae and Bifidobacteriaceae produce short chain fatty acids (SCFAs), such as butyrate and propionate, that stimulate extra-thymic regulatory T-lymphocyte (Treg) differentiation, dependent on conserved non-coding sequence 1 and histone deacetylase inhibition, respectively. The Treg population significantly reduces the inflammatory status of the intestine and could benefit patients suffering from inflammatory bowel diseases (IBDs). Polysaccharide A (PSA), which is synthesized by Bacteroides fragilis, has also been linked to an increase in the number of Tregs. PSA induces CD4+ T-lymphocytes to differentiate into Foxp3+ Tregs, which produce IL-10. Such differentiation can take place also in an inflamed gut.

Cytokines are altered in common variable immune deficiency (CVID), and CVID is associated with elevated serum levels of CXCL-10/IP-10, IL-1R antagonist, TNF-α, IL-10, IL-12 (p40), CCL-2/MCP-1, G-CSF, and CCL-11/eotaxin. The cytokine profile observed in patients with CVID may be attributed to the activation of monocyte-macrophage and granulocyte lineages, possibly driven by the translocation of bacterial components across the gastrointestinal or respiratory tract mucosal barrier. In contrast, the levels of cytokines typically produced by CD4+ T helper cells of Th1 (IFN-γ, IL-2), Th2 (IL-9, IL-13), and Th17 (IL-17) subtypes are reduced in CVID. CVID is also associated with reduction of regulatory IL-10. Cytokines are also crucial for B-cell differentiation. In fact, it has been shown that responsiveness to interleukin-21(IL-21), a key cytokine for B cell differentiation, correlates with distinct clinical phenotypes in CVID. However, the poor immune response of patients lacking Ig production (particularly secretory IgA) may, in certain phases of the disease, result in gut inflammation with gut increase of inflammatory cytokines. In fact, Lipopolysaccharide (LPS) activates the immune system through TLR4 receptors on macrophages/monocytes. These cells cause local and systemic inflammation through the release of inflammatory cytokines such as TNF, IL-1β, and IL-12. Such inflammation is associated to specific microbiota patterns.

GM can also enhance inflammation, as adhesion of segmented filamentous bacteria (SFBs) to epithelial cell surface enhances T-helper 17 lymphocyte (Th17) induction, increasing the overall inflammatory status. Adhesion of SFBs activates a cascade of events that begins with epithelial cells releasing serum amylase A, which increases the production of IL-1β and IL-23 in CX3CR1+ phagocytes. ILC-3 synthesize more

IL-22, reinforcing the IL-1β production, lastly up-regulating the production of IL-17, which directs the differentiation of Th17 lymphocytes. A complex cross-talk takes place with gut eosinophils, as they are the main producers of IL-1Ra, a cytokine inhibiting IL-1β, thus modulating Th17 production.

Antibodies and GM cross-talk, too: antibodies appear to select the GM, which on the other hand is key in the production of different immunoglobulins (Ig). The interactions already start in the womb, where maternal IgG determine microbiota composition of the offspring, with lifelong consequences. IgA are responsible for mucosal immunity. Many studies report that GM is selected by IgA: *B. fragilis*, for example, needs the presence of IgA to colonize the intestine of the host. Dangerous pathogens (e.g. *Escherichia coli*) are instead inhibited by the presence of IgA. It is worth noting that production of IgA is impacted by MyD88, which is, as previously mentioned, regulated by GM.

A healthy GM stimulates correctly B-lymphocytes, avoiding IgG4 switch to IgE. It has been demonstrated that, in the presence of IL-4, a dysbiotic GM can substitute the co-signaling of $CD4^+$ T-lymphocytes and induce the switching of classes, which has consequences for the same GM: IgG control the GM's response to pathogens, maintaining homeostasis. At the same time, the GM influences the production of the IgG that controls it. Overall, B-lymphocytes have deep and complex interactions with the GM, shaping it and being shaped by it.

Primary immune deficiencies and gut microbiota: effects of disease and therapies

In 2015 there were updates in the classification of primary immune-deficiencies (PIDs). Nine main categories were identified, ranging from combined immune-deficiencies to more specific diseases to auto-inflammatory conditions.

PIDs are difficult to diagnose and require a complex, multidisciplinary management. Often immunologic therapies are not enough and long-term antibiotic prophylaxis have to be administered. Recent data suggest that PIDs are not as rare a condition as we used to think, but there still is a shortage of data on this group of conditions, in particular on the GM, in several PID.

As the GM has a key role in immune-regulation, it is likely that it also influences progression and response to therapies of patients with PIDs. Even though some specific features of PIDs have been studied, in literature, CVID and IgA deficit are the most studied diseases among PIDs in relation to GM.

CVID is a heterogeneous group of disorders characterized by hypogammaglobulinemia associated with defects of B, T and dendritic cells. The disease can be the result of at least 24 different mutations, affecting both B cells and T cells (more frequently CD26, LRBA, Taci, April, Icos and BAFF). Before the discovery of these mutations, an increased activity of $CD8^+$ mediated "immune-suppression" or a defect of T-helper cells have been suggested as possible causes of CVID.

Patients with CVID present a vast array of symptoms. Some patients present an inflammatory phenotype which could be linked to dysbiosis. There are different causes: an impaired immune surveillance in the gut, which leads to an increased bacterial translocation, which in this population can easily determine a symptomatic infection. Furthermore, dysbiosis also affects the host's response to infection, acting both as a risk and prognostic factor. LPS is a good marker of endotoxemia, caused by microbial translocation of Gram negative bacteria. CVID patients with an inflammatory phenotype present higher levels of circulating LPS than patients with other dominating symptoms. Overall, it appears that bacterial translocation creates an inflamed environment in the tissue, which can determine a more severe clinical presentation.

The hallmark of CVID is hypogammaglobulinemia, which means that also IgA production is impaired: the reduction of this population of antibodies is probably the reason why the GM in this group of patients is pro-inflammatory, as IgA are necessary for anti-inflammatory bacteria, such as *B. fragilis*, to colonize the gut. Function of T lymphocytes and dendritic cells is also impaired in these patients. In the T-lymphocyte population exhaustion is the main cause of this lack of functionality. Furthermore, recent studies

have shown that LPS levels directly correlate to PD-1 activation in lymphocytes of patients with CVID, suggesting that bacterial translocation plays a key role in CD4 T-cell exhaustion. Intravenous immunoglobulin (IVIg) treatment restores $CD4^+$ T-cell functions.

On the other hand, in dendritic cells, the reduced or absent cross-talk with IgA is partly the cause of hypo-reactivity. Dendritic cell hypo-reactivity causes a reduced stimulation of T-helper lymphocytes, overall worsening immune function in these patients.

Another key feature of CVID is the reduced number of Treg lymphocytes. While other features of this disease can improve after Ig replacement therapy, Tregs are not regained after therapy, indicating that there are other factors that interplay. Dysbiosis in the gut can lead to an absence of SCFA producing bacteria (e.g. *Clostridium strain IV*, *Lactobacillaceae*), increasing the inflammatory tone in the gut and reducing the stimuli for T lymphocytes to differentiate into Tregs.

CVID has been linked to a variety of enteropathies, which can even be the first symptom of CVID. A study published in 2010 described a small cohort of patients with CVID and autoimmune enteropathy, who presented similar symptoms to celiac disease but only a few benefitted from a gluten-free diet. It appears that a key factor in the development of enteropathies is the chronic presence of *Norovirus*: once the virus was eliminated, the enteropathy quickly disappeared. Overall, dysbiosis appears to be linked both to development and progression of intestinal disease in immune deficient patients. Alterations in the Th17 pathway and in the production of IgA are two of the mechanisms that create a vicious circle, through which dysbiosis reinforces itself, while also sustaining IBDs. For example, patients with immune deficiency are more likely to house non-typhoidal *Salmonella* in their GM, enhancing the IL-23 axis and potentiating the inflammatory stimuli in the intestine. IgA deficiency, on the other hand, reduces the presence of bacteria producing SCFAs, which have a potent anti-inflammatory effect. The importance of IgA in regulating GM has indeed been proven by the presence of enteropathies similar to the ones of CVID patients with a selective deficit of IgA. Exceedingly low levels of IgA and the presence of *Acinetobacter baumannii* have been reported in this population by Schulzhenko.

Different therapeutic strategies are used in treating CVID, but the cornerstone of therapy is Ig replacement therapy, which is highly effective in reducing hospitalizations due to infections. Equilibrium between the inflammatory and anti-inflammatory components of the immune system, however, is not fully restored, as it appears, indeed, that Ig replacement therapy cannot stimulate Treg production, even though it does partly reduce inflammatory activation. Also, it does not alleviate the gastrointestinal disorders caused by CVID. In CVID enteropathy steroids have been proven effective, and to avoid the systemic effects of steroids, budesonide has been proposed in these patients.

Antibiotic prophylaxis is also extremely important in these patients and is discussed below.

Patients who do not respond to conventional therapy or with malignancies can undergo allogeneic stem cell transplant (ASCT), even though there is a very high mortality (up to 52% of patients). Patients who did not face fatal consequences benefitted from the therapy in up to 92% of the cases. One of the indications for ASCT is severe IBD, which does not respond to therapy. GM is dramatically modified by ASC, following a similar transformation to the one that takes place in newborn, which confirms both that cross-talk between GM and the immune system is extremely complicated and that GM is a key element in modulating gastrointestinal symptoms in CVID.

Antibiotics and gut microbiota

Antibiotic prophylaxis is a therapeutical cornerstone in PIDs. The need for antibiotic therapy and prophylaxis in immune deficient patients is real but physicians need to evaluate how and when to administer it. Lankelma et al. have studied the effects of antibiotic therapy on GM and response to sepsis-like syndrome and found that broad spectrum antibiotics do change the GM, but there appear to be no consequences on the immune response, which could mean that the alterations of the GM are only temporary and do not interfere with immunity.

CONCLUSIONS

GM status has a remarkable impact on the immune system and in immune deficient patients this can lead to important consequences. The immune deficient status can determine dysbiosis, which can lead to a worsening of the clinical status of the patient, perpetrating a vicious circle.

Patients suffering from CVID share some of the alterations, particularly in terms of reduction of "good bacteria" and increase of pathogens, but the picture offered by those who suffer from CVID is far more complex from an immunologic point of view. However, as HIV-disease is a far more prevalent condition than CVID, the former population can give us important information on the latter. Another interesting aspect is that both HIV patients undergoing antiretroviral therapy and CVID patients undergoing Ig replacement therapy can regain acceptable immune system functionality, but GM dysbiosis does not improve significantly. The altered equilibrium of gastrointestinal flora can even impair the efficacy of therapies in these patients and it needs to be specifically targeted. Prebiotics are indeed a promising candidate in restoring GM homeostasis and improving immunity. Antibiotics are also capable of altering the microbial equilibrium, but they carry far more risks. As antimicrobial therapies and prophylaxis are often necessary in immune deficient patients, their use needs to be carefully evaluated, especially as antibiotic resistance is rising to a real global crisis.

REFERENCES

1. Oh JZ, Ravindran, R, Chassaing, B, et al. TLR5-mediated sensing of gut microbiota is necessary for antibody responses to seasonal influenza vaccination. Immunity 2014; 41(3): 478-92.
2. Cebra JJ. Influences of microbiota on intestinal immune system development. Am J Clin Nutr 1999; 69(5):1046-51S.
3. Thursby E, Juge N. Introduction to the human gut microbiota. Biochem J 2017; 474(11):1823-36.
4. Bibbo S, Ianiro G, Giorgio V, Scaldaferri F, Masucci L, Gasbarrini A, Cammarota G. The role of diet on gut microbiota composition. Eur Rev Med Pharmacol Sci 2016; 20(22):4742-49.
5. Gerard P. Gut microbiota and obesity. Cell Mol Life Sci 2016; 73(1):147-62.
6. Guyton K, Alverdy JC. The gut microbiota and gastrointestinal surgery 2017. Nat Rev Gastroenterol Hepatol; 14(1):43-54.
7. Knights D, Ward TL, McKinlay CE, Miller H, Gonzalez A, McDonald D, Knight R. Rethinking "enterotypes". Cell Host Microbe; 201416(4):433-37.
8. Harmsen HJ, de Goffau MC. The human gut microbiota. Adv Exp Med Biol 2016; 902:95-108.
9. Lin L, Zhang J. Role of intestinal microbiota and metabolites on gut homeostasis and human diseases. BMC Immunol 2017; 18(1):2.
10. Lucas C, Barnich N, Nguyen HTT. Microbiota, inflammation and colorectal cancer. Int J Mol Sci 2017; 18(6).

miR-1178-3p PROMOTES THE PROLIFERATION, MIGRATION AND INVASION OF NASOPHARYNGEAL CARCINOMA SUNE-1 CELLS BY TARGETING STK4

L.Q. WANG, A.C. DENG, L. ZHAO, Q. LI, M. WANG and Y. ZHANG

Department of Otolaryngology, Second Affiliated Hospital of Army Medical University, Chongqing, China

Received May 17, 2018 – Accepted September 7, 2018

Nasopharyngeal carcinoma (NPC) is a malignant tumor with high invasive and metastatic properties. Dysregulation of miRNAs may contribute to disease progression by targeting disease-related genes. In this study we aimed to elucidate the role and function of aberrantly expressed miRNA in NPC tumorigenesis. We found that miR-1178-3p was highly expressed in NPC tissues. Overexpression of miR-1178-3p promoted the proliferation, migration and invasion of NPC cells *in vitro*. In contrast, knocking down endogenous miR-1178-3p by miRNA-specific inhibitor significantly suppressed the above phenotypes. Moreover, miR-1178-3p was shown to negatively regulate serine/threonine-protein kinase 4 (STK4), an NPC-related tumor suppressor gene, in the post-transcriptional level. Furthermore, STK4 overexpression abolished miR-1178-3p-induced cell proliferation, migration and invasion through STK4-mediated dephosphorylation of AKT. Our results indicate that miR-1178-3p acts as an oncomiRNA in NPC by suppressing STK4 expression, and inhibition of miR-1178-3p may become a therapeutic potential for NPC.

Nasopharyngeal carcinoma (NPC) is a malignant tumor with highly invasive and metastatic properties. It is common in certain regions of southern China and southeast Asia (1, 2). Although traditional treatments such as chemotherapy and radiotherapy have achieved good therapeutic effects in NPC, little progress has been made to improve the five-year survival rate (3-5). About one-third of NPC patients develop distant metastasis, with reduced overall survival rate (6, 7). Previous studies have suggested that viral, environmental influences and genetic factors may be implicated in the disease pathogenesis (8), but the molecular mechanisms of NPC tumorigenesis remain unclear.

MicroRNAs (miRNAs) are small, non-coding RNAs of 20–24 nucleotides (nt), which play vital roles in the post-transcriptional regulation of gene expression (9). MiRNAs degrade target mRNAs, or inhibit their translation by sequence complementarity to the 3' untranslated region (3'UTR) of mRNAs (10). Aberrant miRNA expression has been linked to several cancer types, including NPC (11, 12). Dysregulation of specific miRNAs may contribute to NPC tumorigenesis, invasion and metastasis. Thus, elucidating the roles of disease-specific miRNAs holds great promise for the early detection and treatment of NPC.

Serine/threonine-protein kinase 4 (STK4) is a highly conserved protein across different species. STK4 is believed to be a pro-apoptotic protein that

Key words: miR-1178-3p, nasopharyngeal carcinoma, STK4, AKT signaling

Corresponding Author:
Dr Anchun Deng,
Department of Otolaryngology,
17th Floor, Main Ward Building,
Xinqiao Hospital, Shapingba District,
Chongqing City, P.R.China 400037
Tel.: +86 023 687755611 - Fax: +86 023 687755611
e-mail: denganchtt01@163.com

0393-974X (2019)

plays an important role in the apoptosis cascade (13, 14). As a tumor suppressor gene, STK4 also functions in cell cycle transition and inhibition of tumorigenesis (15). Previous studies have demonstrated the reduction of STK4 level in different types of cancers (15, 16), but the underlying mechanism remains obscure.

In the current study, we discovered that miR-1178-3p was highly expressed in NPC tissues. Overexpression of miR-1178-3p promoted the proliferation, migration and invasion of NPC cells *in vitro*. Moreover, STK4 was revealed to be the direct target gene of miR-1178-3p, and the tumorigenic effects induced by miR-1178-3p were reversed by STK4 re-introduction. Our findings suggest that miR-1178-3p promotes NPC cells proliferation, migration and invasion by regulating STK4 expression.

MATERIALS AND METHODS

Patients and clinical samples

In the present study, 60 NPC patients were recruited between January 2016 and September 2017 at The Second Affiliated Hospital of Army Medical University. The age distribution of the patients involved in the study was between of 25 and 65 years, and the male/female ratio was 27/33. Tumor tissues and adjacent normal nasopharyngeal epithelial tissues were collected from NPC patients at the time of surgery or biopsy. Tissue samples were immediately transferred into RNase-free centrifuge tubes and stored at -80°C until RNA isolation. This study was approved by the Ethics Committee of The Second Affiliated Hospital of Army Medical University, and written informed consent was obtained from each patient.

Cell culture and miRNA transfection

The human NPC cell line SUNE-1 was obtained from the Shanghai Institute of Cell Biology (Shanghai, China). Cells were cultured in Dulbecco's modified Eagle's medium (DMEM; Gibco, USA) supplemented with 10% fetal bovine serum (FBS; Gibco, USA) and 1% antibiotics (penicillin and streptomycin) with 5% CO_2 at 37°C.

The miRNA mimics, inhibitors and negative controls for miRNAs were purchased from GenePharma Company (Shanghai, China). The transfection concentrations for miRNA mimics, inhibitors and negative controls were 50 nM, 100 nM and 50 nM, respectively. Transfections were conducted in 6-well plates with Lipofectamine 3000 (Invitrogen, USA) according to the manufacturer's instructions. Cells were harvested for further analyses at 48h after transfection.

RNA isolation and quantitative real-time PCR (RT-PCR)

Trizol reagent (Invitrogen, USA) was used to harvest total RNA from clinical samples and SUNE-1 cells. For miRNA analysis, cDNAs of miR-1178-3p were reverse-transcribed with miR-1178-3p-specific primers. cDNAs of mRNAs were synthesized with random primers. RT-PCR was performed using the SYBR Green PCR Kit (Takara, Japan) according to the manufacturer's instructions. $2^{-\Delta\Delta CT}$ method was used to calculate fold changes. The expression levels of miRNA and mRNA were normalized to internal controls U6 or GAPDH, respectively.

Dual-luciferase assay

A fragment of wild-type STK4 3′UTR was amplified by PCR and cloned into Dual-luciferase reporter vector psiCHECK-2 (Promega, USA). The miR-1178-3p binding sites were mutated to generate the mutant 3′UTR plasmid. Cells were transfected with luciferase reporter plasmids along with miRNA mimics. Luciferase activity was analyzed by a microplate reader (Synergy Mx, Bio-Tek, USA) 24 hours after transfection.

Protein extraction and Western blotting

Cells were harvested and lysed in ice-cold RIPA buffer (Applygen, Beijing, China) containing 10% protease inhibitor cocktail and 1% phenylmethylsulfonyl fluoride (PMSF) for 30 min at 4°C. Cell lysates were centrifuged at 12000 rpm for 30 min to remove precipitate. Then, loading buffer was added and proteins were denatured at 100°C for 5 min. Samples were separated by SDS-PAGE and transferred to a PVDF membrane (Millipore, MA, USA) followed by 5% fat-free milk blocking, and incubated with primary antibodies (anti-STK4 1:500, anti-AKT 1:500, anti-phospho-AKT 1:500 and β-actin 1:1000, Cell Signaling Technology, USA) and horseradish peroxidase-conjugated secondary antibodies (1:2000 Sigma, USA). The signals were detected by Immobilon Western Chemiluminescent HRP Substrate (Millipore, USA) and visualized using Image Lab software (Bio-Rad, USA).

Cell proliferation assay

Cell count kit (CCK-8) (Obio Technology, China) was used to analyze cell proliferation. SUNE-1 cells were seeded in a 96-well plate at a density of 2000 cells/well. At time points 24 h, 48 h or 72 h, 10 μL of CCK-8 reagent was added into each well. Viability of cells was measured 4 h later at 450 nm absorbance with a microplate reader (Synergy Mx, Bio-Tek, USA).

Wound healing assay

Following miRNA mimics or inhibitor treatment, SUNE-1 cells were seeded into 6-well plates with 1 ml culture medium. When cells reached approximately 90% confluence, the cell monolayer was scratched linearly with a sterile pipette tip to generate an artificial wound. We measured wound distances at t= 0 h and 24 h under a microscope and the migration areas were determined by an image-analysis program.

Colony formation assay

SUNE-1 cells were transfected with miRNA mimics, inhibitors or negative controls with Lipofectamine 3000 (Invitrogen, USA) according to the manufacturer's instructions. Cells were seeded into 6-well plates containing Base Agar with the density of 1000 cells/well to perform colony formation assay. After 14 days, the colonies were fixed with 4% paraformaldehyde for 30 min, and stained with 0.1% crystal violet (Sigma, USA) for 20 min. Colonies were imaged with a digital camera.

Cell invasive assay

Cell invasion was evaluated by Transwell chambers (8 μm pore size; Corning, USA) coated with Matrigel (BD Biosciences, USA). Following treatment with miRNA mimics, inhibitors, negative controls or STK4 overexpression, SUNE-1 cells were harvested and re-seeded for 10^5 cell/well in the upper chamber in serum-free medium. Culture medium containing 10% FBS was added into the lower chambers. After 24 h, cells were then stained with 0.1% crystal violet for 15 min, and photographed using an upright microscope (Olympus, Japan).

Statistical analysis

Data are presented as the mean ± standard deviation (SD). Statistical analysis and graphical presentations were performed by GraphPad Prism 5.0 software. Student's *t*-test and one-way analysis of variance (ANOVA) were used to analyze two groups and multiple groups, respectively. $p<0.05$ was considered to be statistically significant.

RESULTS

MiR-1178-3p is highly expressed in nasopharyngeal carcinoma tissues

Our previous miRNA microarray analysis revealed that miR-1178-3p was significantly up-regulated in NPC patients (unpublished data). To further confirm our result, the expression levels of miR-1178-3p were measured in tumor and normal tissues of 60 NPC patients using RT-PCR. The expression levels of miR-1178-3p were significantly up-regulated in NPC tissues compared with that in normal nasopharyngeal epithelial tissues ($p<0.0001$, Fig. 1). Nonetheless, the functional role and underlying mechanism of aberrantly expressed miR-1178-3p in NPC remain to be elucidated.

MiR-1178-3p promotes SUNE-1 cell proliferation

In order to discover the potential function of miR-1178-3p in NPC, miR-1178-3p was overexpressed or inhibited in human NPC cell line SUNE-1. Relative expression level of miR-1178-3p was significantly increased upon miR-1178-3p mimics transfection, whereas cell transfected with miR-1178-3p-specific inhibitor showed opposite effect (Fig. 2A, $p<0.001$).

Cell proliferation was analyzed using the CCK-8 assay. Our results showed that the proliferation rate of SUNE-1 cells was elevated 48 h and 72 h after miR-1178-3p overexpression (Fig. 2B, left panel, $p<0.001$). In contrast, miR-1178-3p inhibition significantly reduced SUNE-1 cell proliferation compared to negative controls (Fig. 2B, right panel, $p<0.001$).

In the colony-formation assay, overexpression of miR-1178-3p in SUNE-1 cells resulted in increased colony formation compared to control miRNA-transfected cells (Fig. 2C, left panels). Conversely, cells transfected with miR1178-3p-specific inhibitor exhibited decreased colony number compared to those transfected with negative controls (Fig. 2C, right panels). These results indicate that miR-1178-3p promotes cancer cell proliferation in NPC.

MiR-1178-3p enhances SUNE-1 cell migration and invasion

In order to investigate the effect of miR-1178-3p on NPC cell migration and invasion, SUNE-1 cells were transiently transfected with miR-1178-3p mimics, inhibitor or negative controls, and wound healing assay was performed. Wound healing assay revealed that miR-1178-3p-overexpressed SUNE-1 cells migrated much faster than cells transfected with miRNA controls, resulting in narrower relative wound width after 24 h (Fig. 3A, left panel, $p<0.001$). However, the migration rate of SUNE-1 cells was reduced when endogenous miR-1178-3p was inhibited (Fig. 3A, right panel, $p<0.001$).

In Transwell invasion assay, overexpression of miR-1178-3p in SUNE-1 cells by mimics significantly increased the invasive ability of cells (Fig. 3B, left panel, $p<0.001$). Inhibition of endogenous miR-1178-3p by specific miRNA inhibitor decreased the number of cells that penetrated the membrane (Fig. 3B, right panel, $p<0.001$). These results demonstrate that miR-1178-3p is able to enhance migration and invasion of NPC cells *in vitro*.

STK4 is a direct target of miR-1178-3p via 3'UTR binding

To investigate the role of dysregulated miR-1178-3p and its potential mechanism in NPC tumorigenesis, computational prediction algorithms were used to predict the biological targets of miR-1178-3p. miR-1178-3p was predicted to regulate STK4, a cancer-related gene. The sequences of miR-1178-3p are complementary to nucleotides 168-174 and 4009-4015 of STK4 3'UTR (Fig. 4A, left panel). Next, we generated a dual-luciferase reporter construct by cloning STK4 3'UTR sequence downstream of luciferase reporter gene. Accordingly, miR-1178-3p markedly repressed luciferase activity when miR-1178-3p mimics were co-transfected with the wild-type reporter construct (Fig. 4A, right panel, lanes 1 and 2, $p<0.001$). We then mutated several binding sites in STK4 3'UTR to generate the mutant reporter construct, which was found to relieve miR-1178-3p-mediated transcriptional repression (Fig. 4A, right panel, lanes 3 and 4), indicating that these sequences are the genuine binding sites for miR-1178-3p.

Furthermore, we measured STK4 mRNA and

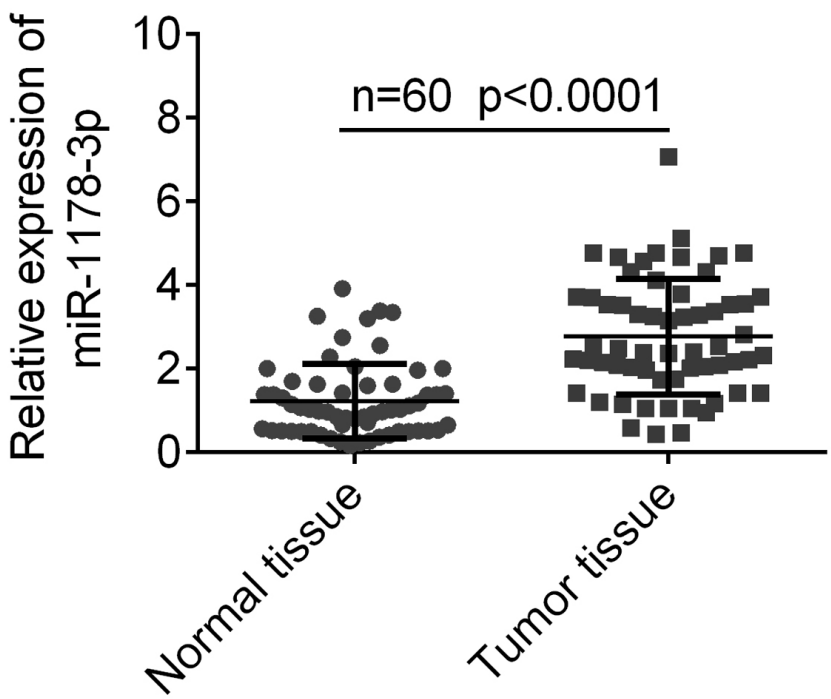

Fig. 1. *miR-1178-3p is highly expressed in NPC tissues. Expression levels of miR-1178-3p were measured in 60 NPC and 60 normal tissue samples by quantitative real-time PCR. The level of miR-1178-3p was significantly higher in tumor tissues ($p<0.0001$).*

protein levels following manipulation of miR-1178-3p expression. RT-PCR and Western blotting results showed marked reduction in the mRNA and protein levels of STK4 upon miR-1178-3p overexpression (Fig. 4B, upper panel and Fig. 4C, left panel, $p<0.001$), whereas transfection with miR-1178-3p inhibitor led to increased STK4 mRNA and protein levels (Fig. 4B, lower panel and Fig. 4C, right panel, $p<0.001$). Taken together, these results suggest that miR-1178-3p could negatively regulate the expression of STK4 by direct 3′ UTR binding.

Overexpression of STK4 abolishes mir-1178-3p-induced proliferation, migration and invasion in nasopharyngeal carcinoma cells

To investigate whether up-regulated miR-1178-3p could induce proliferation, migration and invasion through its direct regulation of STK4 expression, STK4 was re-introduced into miR-1178-3p-overexpressed cells. As shown in Fig. 5A, STK4 protein level was restored following STK4 overexpression in miR-1178-3p-transfected cells.

Furthermore, miR-1178-3p-treated SUNE-1 cells showed significantly decreased cell proliferation, invasion, and migration upon STK4 overexpression, which were confirmed by the CCK-8 assay (Fig. 5B), colony-formation assay (Fig. 5C), transwell invasion assay (Fig. 5D) and wound healing assay (Fig. 5D), respectively. These results demonstrate that miR-1178-3p promotes cell proliferation, migration and invasion by inhibiting STK4.

MiR-1178-3p promotes tumor cell survival by inhibiting STK4-mediated dephosphorylation of AKT signaling

Previous studies have demonstrated that

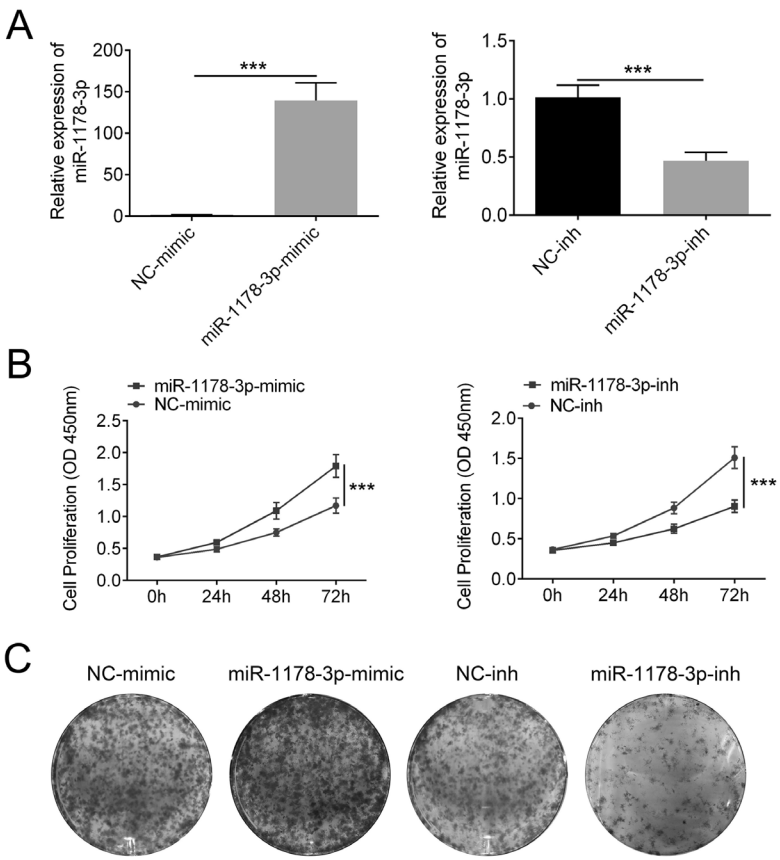

Fig. 2. *miR-1178-3p promotes the proliferation of SUNE-1 cells. **A**) Relative expression levels of miR-1178-3p were examined by quantitative real-time PCR following miR-1178-3p overexpression or inhibition. **B**) SUNE-1 cell proliferation was measured by CCK-8 assay upon miR-1178-3p overexpression or inhibition. **C**) Representative photographs of the colony-formation assay with SUNE-1 cells transfected with miR-1178-3p mimics, miR-1178-3p inhibitor or miRNA controls. (***p<0.001)*

activation of the AKT signaling plays a key role in cell proliferation, migration and invasion in different types of cancers (17-19), and STK4 may interact with AKT to regulate its kinase activity (15). Thus, we further explored whether miR-1178-3p may influence tumor cell survival by regulating STK-AKT signaling cascade. We found that overexpression of miR-1178-3p in SUNE-1 cells suppressed STK4 protein level and elevated downstream phospho-AKT level compared to negative controls. Re-introduction of STK4 into miR-1178-3p-overexpressed cells showed the opposite effects (Fig. 6A and B, left panel, $p<0.001$). In contrast, SUNE-1 cells transfected with miR-1178-3p inhibitor displayed elevated STK4 level and decreased phospho-AKT level, whereas STK4 knockdown in miR-1178-3p inhibitor-transfected cells had the opposite effects (Fig. 6A and B, right panel, $p<0.001$). Taken together, our results suggest that miR-1178-3p acts as an oncogenic miRNA in the NPC pathogenesis by suppressing STK4-mediated dephosphorylation of the AKT signaling.

DISCUSSION

MiRNAs play a vital role in the post-transcriptional regulation of genes and may be differentially expressed in normal and tumor tissues. In this study, we discovered that miR-1178-3p was highly expressed in NPC tissues compared with normal tissues. MiR-1178-3p inhibited STK4 expression through its binding sites in highly conserved regions of the 3'UTR of STK4 mRNA. MiR-1178-3p facilitated the proliferation, migration and invasion of NPC cells through inhibition of STK4-mediated dephosphorylation of AKT. We conclude that miR-1178-3p plays an oncomiR role and promotes a malignant phenotype in NPC.

MiR-1178 was first identified by microarray

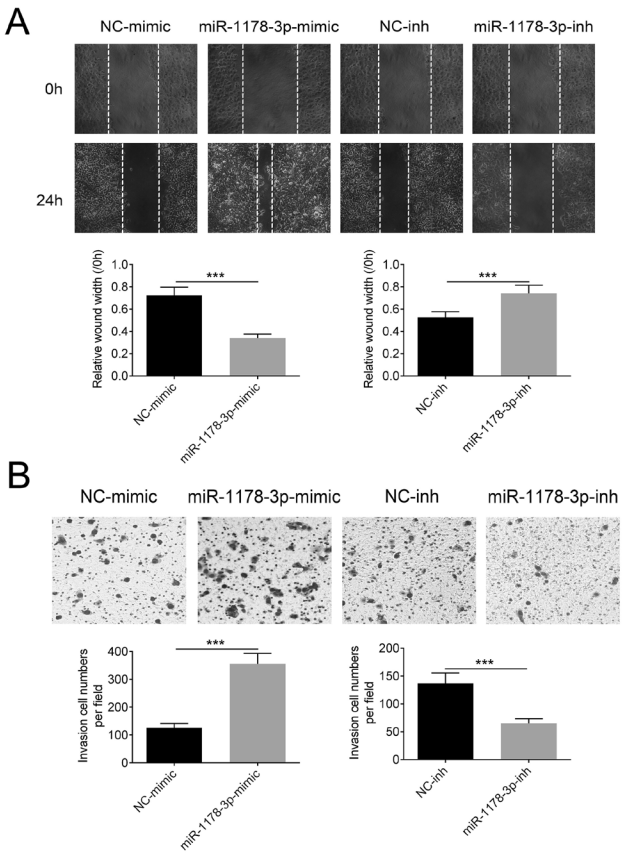

Fig. 3. *miR-1178-3p enhances SUNE-1 cell migration and invasion. **A)** Wound healing assay. Upper panels: representative photographs; lower panels: quantification. **B)** Transwell invasion assay. Upper panels: representative photographs; lower panels: quantification. (***p<0.001)*

technology and small RNA cloning approaches in human sarcoma samples in 2008 (20). To date, two separate studies have demonstrated the biological functions of miR-1178 and the association between miR-1178 and human cancers. Cao et al. reported that miR-1178 promotes the proliferation, G1/S transition, migration and invasion of pancreatic cancer cells by inhibiting CHIP expression (21). Moreover, miR-1178 is overexpressed in pancreatic cancer, and is an independent adverse prognostic indicator for pancreatic cancer patients. MiR-1178 promotes the invasion of cancer cells by regulating Stub1/FAK/MMP-9 signaling pathway (22). However, the potential role of miR-1178 in NPC has not been investigated. In our present study, miR-1178-3p was found to be significantly up-regulated in NPC tissues by quantitative RT-PCR, which is in accordance with the aforementioned diseases. CCK-8, colony-formation, transwell invasion, and wound healing assays demonstrated that miR-1178-3p could enhance the proliferation, migration and invasion of NPC cells *in vitro*. Thus, miR-1178-3p may have common roles and act as an oncomiR in different cancer types.

In order to investigate the underlying mechanism of miR-1178-3p up-regulation and tumorigenesis, bioinformatics algorithms were used to predict potential target genes of miR-1178-3p. We show that miR-1178-3p suppressed the expression of the tumor-suppressor gene STK4 through conserved binding to its 3'UTR, which was confirmed by dual-luciferase assay and Western blotting analysis. Aberrant up-regulation of miR-1178-3p in NPC resulted in down-regulated STK4 level, leading to impaired pro-apoptotic function. STK4 overexpression abolished miR-1178-3p-induced cell proliferation, migration and invasion.

We also investigated the associated regulatory

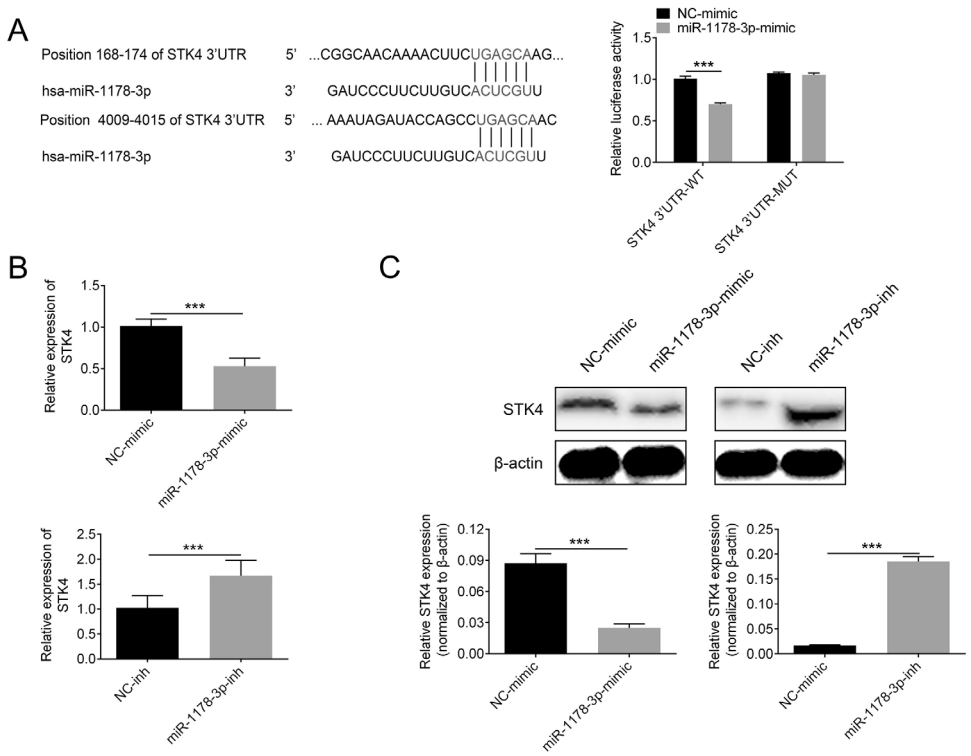

Fig. 4. *STK4 is a direct target of miR-1178-3p via 3'UTR binding.* ***A****) Bioinformatics analysis demonstrates the miR-1178-3p binding sites in STK4 3'UTR sequence. miR-1178-3p represses the relative activity of WT-STK4 3-UTR reporter, but has no effect on the mutant reporter.* ***B****) Relative STK4 mRNA expression levels were assessed by real-time PCR following cell transfection with miR-1178-3p mimics, inhibitors or negative controls.* ***C****) Relative expression levels of STK4 protein were detected by Western blotting following miR-1178-3p mimics, inhibitors or negative controls transfection. (***p<0.001)*

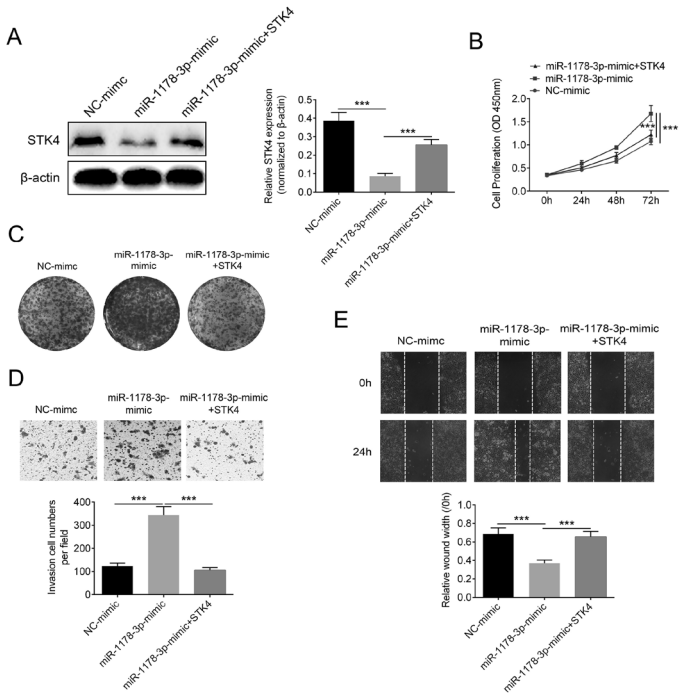

Fig. 5. *Overexpression of STK4 abolishes miR-1178-3p-induced proliferation, migration and invasion in NPC cells. SUNE-1 cells were transfected with negative control mimics, miR-1178-3pmimics, or miR-1178-3pmimics together with STK4 plasmid.* ***A)*** *Relative expression levels of STK4 protein were detected by Western blotting. Cell proliferation was measured by (****B****) CCK-8 assay and (****C****) colony-formation assay.* ***D)*** *Cell invasion was measured by transwell invasion assay.* ***E)*** *Cell migration was measured by wound healing assay. (***p<0.001).*

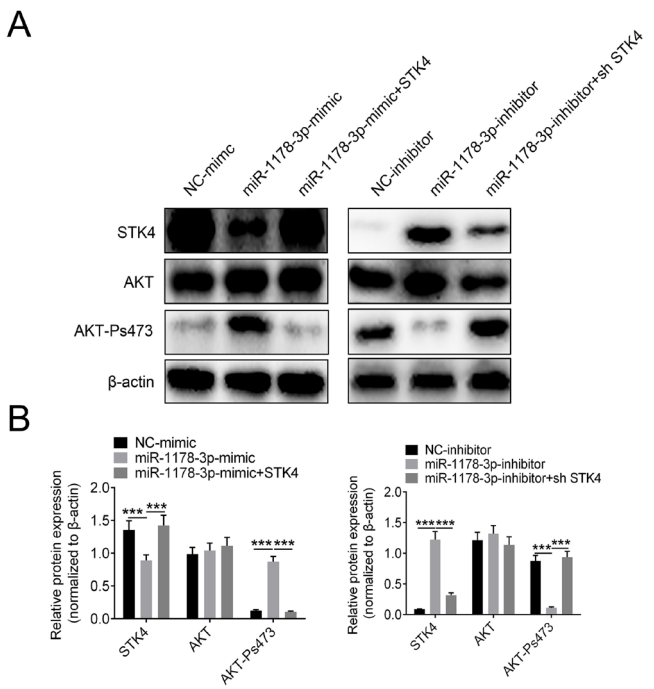

Fig. 6. *miR-1178-3p promotes tumor cell survival by suppressing STK4-mediated dephosphorylation of AKT signaling. A) Expression levels of STK4, AKT and p-AKT were examined by Western blotting following control miRNA, miR-1178-3p mimics, inhibitor, STK4 plasmid or shRNA for STK4 transfection in SUNE-1 cells. Relative expression levels are shown (****B****).*

mechanisms of miR-1178-3p-induced repression of STK4 on tumorigenesis. Previous studies have shown that STK4 interacts with AKT to regulate its kinase activity (15). As an inhibitory signal of apoptosis, the activation of AKT signaling has been linked to the cell cycle control, proliferation, migration and invasion of cancer cells (19, 21), including NPC (17). AKT overexpression leads to decreased apoptosis and cell differentiation, displaying a more aggressive cancer phenotype (23). Also, the activation of AKT signaling could affect the outcome of disease treatment (24). In this study, overexpression of miR-1178-3p in SUNE-1 cells decreased STK4 protein level and increased the downstream phospho-AKT level, suggesting that miR-1178-3p promotes tumor cell survival by suppressing STK4-mediated dephosphorylation of AKT signaling.

In conclusion, the present study demonstrates that miR-1178-3p promotes the proliferation, migration and invasion of NPC cells by targeting STK4 and downstream AKT signaling. Aberrant expression of certain miRNAs and the alteration of key signaling pathways may be the common mechanisms of tumorigenesis and disease progression. Meanwhile, modulating endogenous miR-1178-3p expression or rescuing STK4 expression may become therapeutic strategies for NPC treatment.

REFERENCES

1. Fang W, Li X, Jiang Q, et al. Transcriptional patterns, biomarkers and pathways characterizing nasopharyngeal carcinoma of Southern China. J Transl Med 2008; 6:32-42.
2. Chang ET, Adami HO. The enigmatic epidemiology of nasopharyngeal carcinoma. Cancer Epidemiol Biomarkers Prev 2006; 15(10):1765-77.
3. Zhuang K, Wu Q, Jin CS, Yuan HJ, Cheng JZ. Long non-coding RNA HNF1A-AS is upregulated and promotes cell proliferation and metastasis in nasopharyngeal carcinoma. Cancer Biomark 2016; 16(2):291-300.
4. Chua DT, Ma J, Sham JS, et al. Long-term survival after cisplatin-based induction chemotherapy and radiotherapy for nasopharyngeal carcinoma: a pooled data analysis of two phase III trials. J Clin Oncol 2005; 23(6):1118-24.
5. Ma BB, Hui EP, Chan AT. Systemic approach to improving treatment outcome in nasopharyngeal carcinoma: current and future directions. Cancer Sci 2008; 99(7):1311-18.
6. Yang L, Hong S, Wang Y, et al. Development and external validation of nomograms for predicting survival in nasopharyngeal carcinoma patients after definitive radiotherapy. Sci Rep 2015; 5:15638.
7. Jin Y, Shi YX, Cai XY, et al. Comparison of five cisplatin-based regimens frequently used as the first-line protocols in metastatic nasopharyngeal carcinoma. J Cancer Res Clin Oncol 2012; 138(10):1717-25.
8. Zhang F, Zhang J. Clinical hereditary characteristics in nasopharyngeal carcinoma through Ye-Liang's family cluster. Chin Med J (Engl) 1999; 112(2):185-87.
9. Bartel DP. MicroRNAs: target recognition and regulatory functions. Cell 2009; 136(2):215-33.
10. Ghildiyal M, Zamore PD. Small silencing RNAs: an expanding universe. Nat Rev Genet 2009; 10(2):94-108.
11. Li YQ, He QM, Ren XY, et al. MiR-145 inhibits metastasis by targeting fascin actin-bundling protein 1 in nasopharyngeal carcinoma. PLoS One 2015; 10(3):e0122228.
12. Liu N, Tang LL, Sun Y, et al. MiR-29c suppresses invasion and metastasis by targeting TIAM1 in nasopharyngeal carcinoma. Cancer Lett 2013; 329(2):181-188.
13. Lee KK, Ohyama T, Yajima N, Tsubuki S, Yonehara S. MST, a physiological caspase substrate, highly sensitizes apoptosis both upstream and downstream of caspase activation. J Biol Chem 2001; 276(22):19276-85.
14. Zhou D, Conrad C, Xia F, et al. Mst1 and Mst2 maintain hepatocyte quiescence and suppress hepatocellular carcinoma development through inactivation of the Yap1 oncogene. Cancer Cell 2009; 16(5):425-38.
15. Hsu TI, Hsu CH, Lee KH, et al. MicroRNA-18a is elevated in prostate cancer and promotes tumorigenesis through suppressing STK4 in vitro and in vivo. Oncogenesis 2014; 3:e99.
16. Li W, Xiao J, Zhou X et al. STK4 regulates TLR pathways and protects against chronic inflammation-

related hepatocellular carcinoma. J Clin Invest 2015; 125(11):4239-54.
17. Liu Y, Chen LH, Yuan YW, Li QS, Sun AM, Guan J. Activation of AKT is associated with metastasis of nasopharyngeal carcinoma. Tumour Biol 2012; 33(1):241-45.
18. Yao Z, Okabayashi Y, Yutsudo Y, Kitamura T, Ogawa W, Kasuga M. Role of Akt in growth and survival of PANC-1 pancreatic cancer cells. Pancreas 2002; 24(1):42-46.
19. Wolin EM. PI3K/Akt/mTOR pathway inhibitors in the therapy of pancreatic neuroendocrine tumors. Cancer Lett 2013; 335(1):1-8.
20. Subramanian S, Lui WO, Lee CH, et al. MicroRNA expression signature of human sarcomas. Oncogene 2008; 27(14):2015-26.
21. Cao Z, Xu J, Huang H, et al. MiR-1178 promotes the proliferation, G1/S transition, migration and invasion of pancreatic cancer cells by targeting CHIP. PLoS One 2015; 10(1):e0116934.
22. Cao Z, Zheng SL, Yang G, et al. Correlation between miR-1178 expression and clinicopathological significance in human pancreatic cancer. Zhonghua Wai Ke Za Zhi 2017; 55(6):468-73.
23. Kfir-Erenfeld S, Sionov RV, Spokoini R, Cohen O, Yefenof E. Protein kinase networks regulating glucocorticoid-induced apoptosis of hematopoietic cancer cells: fundamental aspects and practical considerations. Leuk Lymphoma 2010; 51(11):1968-2005.
24. Castaneda CA, Cortes-Funes H, Gomez HL, Ciruelos EM. The phosphatidyl inositol 3-kinase/AKT signaling pathway in breast cancer. Cancer Metastasis Rev 2010; 29(4):751-59.

LncRNA MALAT1 PROMOTES COLORECTAL CANCER DEVELOPMENT BY SPONGING miR-363-3p TO REGULATE EZH2 EXPRESSION

JJ. XIE[1*], WH. LI[2*], X. LI[1], W. YE[1] and CF. SHAO[1]

[1]Department of Anorectal Surgery, The First People's Hospital of Wenling, Zhejiang Province, China; [2]Department of General Surgery, The First People's Hospital of Wenling, Zhejiang Province, China

Received October 11, 2018 – Accepted January 15, 2019

[*]These authors contributed equally to this work and should be considered co-first authors

LncRNA MALAT1 is reported to play a potential role in human cancers. Hence, we investigated the effects of MALAT1 on colorectal cancer *in vitro* and *in vivo*, and further validated whether MALAT1 affected colorectal cancer development and EZH2 expression via regulating miR-363-3p. The fresh colorectal cancer tissues, adjacent non-tumor tissues, FHC, LOVO, SW620, CL40 and HCT116 cells were analyzed in this study. MALAT1, miR-363-3p and EZH2 expression levels were assessed using qRT-PCR and Western blot. Cell proliferation, migration and invasion were also measured. Binding effects between MALAT1 and miR-363-3p, or miR-363-3p and EZH2 3'UTR were detected by dual luciferase assay. We observed that MALAT1 was highly expressed in colorectal cancer tissues and cells, and MALAT1 knockdown inhibited cell proliferation as well as expression levels of EZH2 by upregulated miR-363-3p in cell models and *in vivo*. Moreover, miR-363-3p functions as a downstream target of MALAT1, meanwhile EZH2 was a target of miR-363-3p, suggesting MALAT1 might regulate miR-363-3p and/or EZH2 expression. Collectively, we concluded that MALAT1 functioned as a ceRNA to promote colorectal cancer development and EZH2 expression through sponging miR-363-3p *in vitro* and *in vivo*.

Considered as one of the most common malignancies, colorectal cancer (CC) shows an increasing disease incidence rate worldwide in recent years (1). Early symptoms of CC are insidious and advance rapidly. The disease could be diagnosed when patients showed several typical middle-stage symptoms, including bloody stool, diarrhea and local abdominal pain (2). In the late stages, systemic symptoms such as anemia and weight loss would occur (2-4). Therefore, the key to the current treatment and prognosis of CC is early detection, timely diagnosis and radical operation (5). However, the etiology of CC is not yet clear, but studies reveal that its onset factors are associated with environment, diet, lifestyle and genetic factors (6-9). It is becoming increasingly more important and urgent for academia and clinicians to clarify the pathogenic molecular mechanisms and regulation pathways of CC in consideration of its substantial morbidity and mortality rates.

Long non-coding RNAs (lncRNAs) are a type of non-coding RNAs with a length over 200 nucleotides (nt), which are involved in a number of important regulatory processes of cancer cells

Key words: MALAT1; Colorectal cancer; miR-363-3p; EZH2; Cancer development

Corresponding Author:
Dr. X. Li,
Department of Anorectal Surgery,
The First People's Hospital of Wenling,
Zhejiang province, China
Tel.: +86-0576-89668155
e-mail: lilydsa@163.com

0393-974X (2019)

(10). Metastasis-associated lung adenocarcinoma transcript 1 (MALAT1) is a highly conserved evolution gene located on chromosome 11q13 (11). MALAT1 has been reported to play a potential role in human cancer, including non-small cell lung cancer, gastric cancer and castration resistant prostate cancer (11-13). Several studies reported that MALAT1 functioned as a specific marker of early tumor metastasis and prognosis in patients who suffered from lung cancer. Interestingly, MALAT1 was highly expressed in lung, pancreas and other healthy organs (11, 14). Furthermore, lung cancer cell migration was significantly inhibited when it interfered with M gene expression.

In addition, microRNAs (miRNAs) are non-coding small RNA molecules encoded by the genome of higher eukaryotes with a length of ~22nt, which have been reported to play an important role in almost all types of cancers, including initiation, progression, and transmission of cancer microenvironments (15). A large number of studies suggest that miRNA could affect cancer cell apoptosis, proliferation, migration and invasion. For example, miR-181a and miR-630 were reported to diminish cell cycle arrest (16), miR-146a inhibited androgen-dependent prostate cancer cell growth (17), and miR-363-3p decreased gastric cancer cell growth and migration (18).

This study was carried out with the aim to investigate the effects of MALAT1 on CC tissues and in cell models, and to reveal whether MALAT1 affects CC development by sponging miR-363-3p that regulates enhancer of zeste homolog 2 (EZH2) expression.

MATERIALS AND METHODS

Tissue collection

Fresh CC tissues and adjacent non-tumor tissues were obtained from 30 patients (20 male and 10 female), who had undergone surgery between September 2012 and November 2013 in the First People's Hospital of Wenling, China. The clinicopathological parameters of CC tissues, such as the locations, sizes and differentiation of tumors, American Joint Committee on Cancer (AJCC) stage and vascular invasion, are summarized in Table I. Overall survival of the patients was tested by Kaplan–Meier curve analysis. Tissues were cut into patches of 5 mm for the preparation of total RNA extraction, and stored at -80°C. The participants were informed and agreed before the operation. All experiment protocols were approved by the Ethics Committee of the First People's Hospital of Wenling.

Cell culture

Human normal colonic mucosa cell line FHC, human CCcell lines LOVO, SW620, CL40 and HCT116 were obtained from the American Type Culture Collection (ATCC, Manassas, USA). FHC and CL40 cells were cultured in Dulbecco's Modified Eagle Medium/ Nutrient Mixture F-12 (DMEM: F12; Thermo Fisher Scientific, Waltham, USA) Medium with 10% fetal bovine serum (FBS, Thermo Fisher Scientific) and 10% dimethylsulfoxide (DMSO; Thermo Fisher Scientific). LOVO cells were cultured in Kaighn's Modification of Ham's F-12 Medium (Thermo Fisher Scientific) containing 10% FBS and 10% DMSO. SW620 cells were cultured in Leibovitz's L-15 Medium (Thermo Fisher Scientific) with 10% FBS and 10% DMSO. HCT116 cells were cultured in McCoy's 5A Medium (Thermo Fisher Scientific) with 10% FBS, 10% DMSO and 1× Trypsin-Ethylene Diamine Tetraacetic Acid (EDTA) Solution (Thermo Fisher Scientific).

Cell transfection

Lipofectamine 2000 Reagent (Life Technologies Corporation, Carlsbad, USA) was used to transfect siMALAT1 and shRNA-MALAT1 into cells following the manufacturer's instruction. Small interfering RNA (siRNA) MALAT1 (siMALAT1) was transfected into SW620 and HCT116 cells to knock down MALAT1. miR-363-3p mimics, inhibitors and their miR-NCs were transfected into LOVO and CL40 cells. Short-hairpin RNA (shRNA)-MALAT1 was transfected into SW620 cells.

Cell proliferation assay

*C*ell proliferation rate was determined using 3-(4, 5)-dimethylthiahiazol-(-z-y1)-3, 5-diphenytetrazolium bromide (MTT) Cell proliferation Kit (Sigma-Aldrich, St. Louis, USA). 48 h post-transfection, cells were suspended by trypsin, added into 10 μl MTT solutions, and incubated at 37°C for 4 h. Cells were washed by 1×phosphate buffer saline (1×PBS) twice, added into 150 μl DMSO, and

samples were measured at the wavelength of 490 nm (OD 490) by Microplate Reader (Sigma-Aldrich) at 12, 24, 48 and 72 h time points. Subsequently, transfected cells were seeded on 65 mm dishes. After 10 days, cells were fixed by 4% polyoxymethylene (PFA; Sigma-Aldrich), stained with 0.5% crystal violet (Solarbio, Beijing, China) for 30 min, and colony numbers were counted under the microscope (Leica Microsystems, Weitzlar, Germany).

Cell migration assay

Cell migration rate was detected by cell wound healing assay. Briefly, LOVO, CL40, SW620 and HCT116 cells were seeded in 6-well plates with 5 mm horizontal line for 24 h at 37°C. Then, the plates were marked perpendicular to the horizontal line using a pipette tip. Cells were washed by 1×PBS twice, incubated at 37°C for 12 h, and recorded using a Nikon Microscope (Nikon, Tokyo, Japan).

Cell invasion assay

Cell invasion was determined by Transwell assay. LOVO, CL40, SW620 and HCT116 cells were incubated on the upper compartment of 24-well plates at 37°C for 24 h post-transfection. The lower compartment was added with 500 µl of DMEM with 10% FBS. Subsequently, cells were fixed by 95% methanol for 30 min and stained with 0.1% crystal violet for 30 min. The non-traversed cells were wiped off the upper surface, and then the traversed cells randomly selected 9 fields of vision to count under the microscope (Leica Microsystems).

Dual luciferase activity assay

The cells were co-transfected with empty pmir-GLO-NC, pmir-GLO-MALAT1-Wt, pmir-GLO-MALAT1-Mut, EZH2 3'-UTR-Wt or EZH2 3'-UTR-Mut (GenePharma) and miR-363-3p or scramble using Lipofectamine 2000. The relative luciferase activities were measured according to Dual-Luciferase® Reporter Assay System Protocol (Promega, Madison, USA).

RNA binding protein immunoprecipitation (RIP) assay

RIP assays were performed using RIP™ RNA-Binding Protein Immunoprecipitation Kit (Millipore, Billerica, USA) according to the manufacturer's instructions. Cells were lysed in RIP lysis buffer. 100 µl of cell lysates were incubated with RIP wash buffer containing magnetic beads that conjugated to human anti-Ago2 antibody at 4°C overnight. IgG functions was a negative control. The coprecipitated RNAs were isolated by TRIzol (Life Technologies Corporation, Carlsbad, USA) and detected by qRT-PCR. At the same time, the total RNAs (input

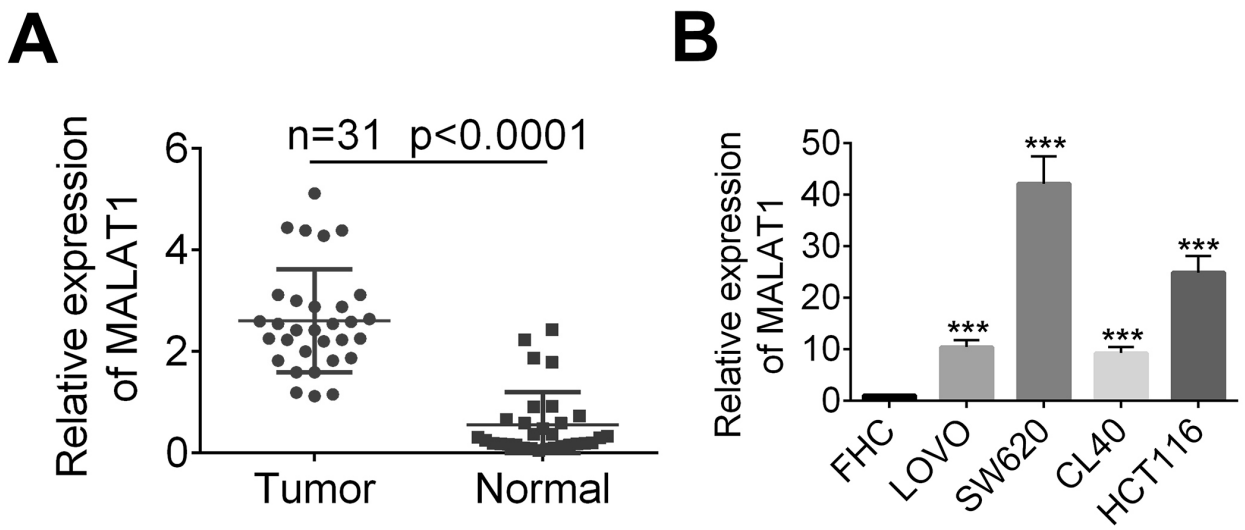

Fig. 1. *MALAT1 was overexpressed in colorectal cancer tissues and cells. MALAT1 mRNA expression level was assessed in (**A**) colorectal cancer tissues and adjacent non-tumor tissues and in (**B**) human normal colonic mucosa cell line FHC, human colorectal cancer cell lines LOVO, SW620, CL40 and HCT116. **C**) Overall survival was tested by Kaplan-Meier curve analysis. (n=30; ***p <0.001).*

controls) and IgG were also detected with the aim to prove that the signal was the result of RNAs specifically binding to Ago2.

Quantitative real-time polymerase chain reaction (qRT-PCR

The total RNA was extracted from cells using Trizol (Life Technologies Corporation) and reversed to cDNA by using an mRNA Selective PCR kit (TaKaRa, Dalian, China). The One Step SYBR® PrimeScript™RT-PCR Kit (TaKaRa) was used to detect MALAT1 and EZH2 expression levels. In addition, the Taqman MicroRNA Reverse Transcription Kit (Applied Biosystems, Foster City, USA) was used to detect the expression level of miR-363-3p. The GAPDH and U6 were used to normalize MALAT1, EZH2 and miR-363-3p levels, respectively. Fold changes were calculated as $2^{-\Delta\Delta Ct}$ (19).

Western blotting

The total proteins were extracted by using Lysis Buffer (Thermo Fisher Scientific) with 100 mM PMSF on ice for 30 min. The proteins were separated by 10% SDS-PAGE, and transferred to the Polyvinylidene Difluoride (PVDF) membrane. EZH2 and GADPH antibodies (1:1,000; Abcam, Shanghai, China) were diluted in 1×TBST. The membrane proteins were incubated at room temperature

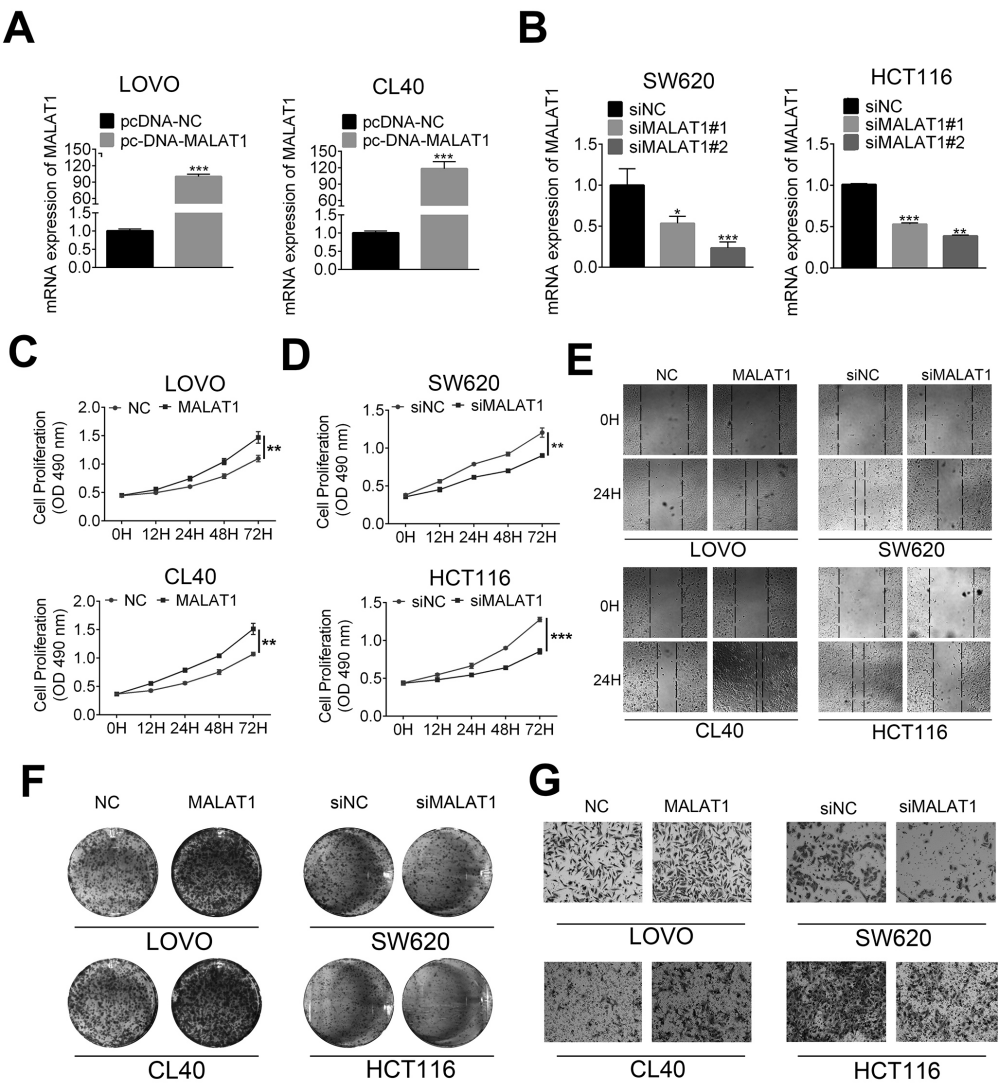

Fig. 2. *MALAT1 regulated colorectal cell proliferation, invasion and migration. Cells were respectively transfected with MALAT1 or NC, siMALAT1 or siNC.* ***A-C****) cell proliferation was measured by MTT and crystal violet assay.* ***D****) Cell migration was assessed by using cell wound healing assay.* ***E****) Cell invasion was measured by Transwell assay. (**p <0.01).*

for 1 h and washed twice by 1×TBST. Secondary antibody (1:2,000) marked by horseradish peroxidase (HRP) contacted with the PVDF membrane and incubated at room temperature for 1 h. The PVDF membranes were displayed and fixed in an X-light clip. The band intensity and molecular weight was quantified using Image Lab™ Software (Bio-Rad, Shanghai, China).

Establishment of xenograft mouse model

Nude mice weighing 60-80 g were purchased from Beijing Vital River Laboratory Animal Technology Co., Ltd (Beijing, China), and raised in specific-pathogen-free (SPF) room with a humidity of 40-60 at 26-28°C. SW620 cells were transfected with shRNA-MALAT1 or shRNA, and subsequently incubated at 37°C for 48 h. Transfected cells (2×10^6/ml) were injected into the subcutaneous of nude mice for 4 weeks. The tumor weights and volumes were measured and calculated weekly according to the formula (20):

Tumor volume=(the longest diameter of the tumor ×the shortest diameter of the tumor)^2/2.

The tumor tissues were excised from sacrificed nude mice and fixed in 4% paraformaldehyde solution. All experimental procedures and protocols followed the Guide for the Care and Use of Laboratory Animals published by the US National Institutes of Health and approved by the Ethics Committee of the First People's Hospital of Wenling.

Statistical analysis

The three parallel experimental data were expressed by the mean ± standard deviation (SD). The p-values of comparisons were calculated using Student's *t*-test or *chi*-square test. In this study, $p<0.05$ was considered as

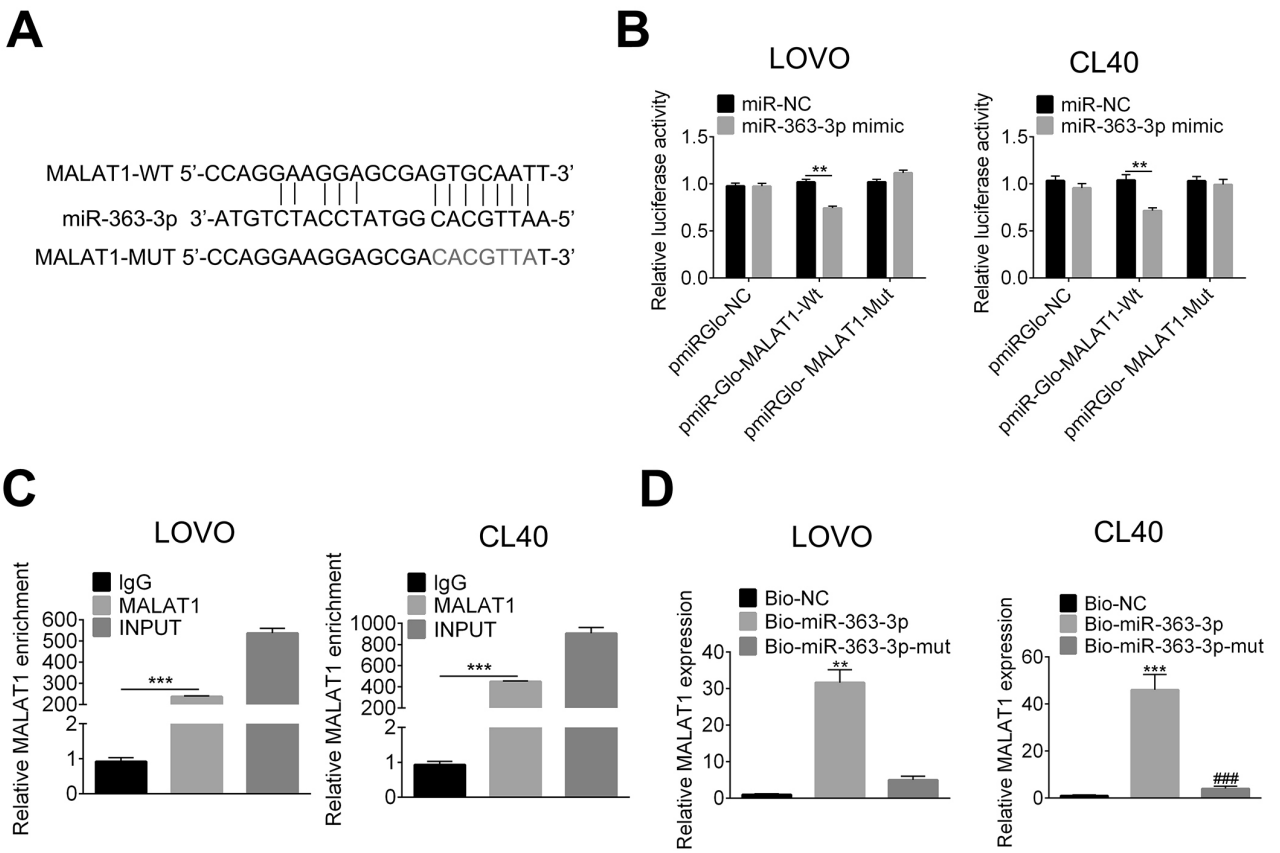

Fig. 3. *miR-363-3p was a target of MALAT1 in colorectal cells. LOVO and CL40 cells were severally transfected with miR-NC or miR-363-3p mimic.* ***A****) The potential binding sequences between MALAT1 and miR-363-3p was analyzed via bioinformatics analysis.* ***B****) The relative luciferase activities of MALAT1 were measured.* ***C****) The MALAT1 enrichment was measured by using RIP assay. (**p <0.01; ***p <0.001).*

statistically significant (*p<0.05, **p<0.01, ***p<0.001).

RESULTS

MALAT1 was overexpressed and had associations with several clinicopathological parameters in colorectal cancer. To explore the effect of MALAT1 on colorectal cancer, MALAT1 expression level was detected in CC tissues and cell models.

In Fig. 1A, the relative expression level of MALAT1 in CC tissues was more than that in adjacent non-tumor tissues (***p<0.0001). Similarly, MALAT1 expression level was increased in LOVO, SW620, CL40 and HCT116 cells compared to human normal colonic mucosa FHC cells (Fig. 1B, ***p<0.001). Among them, the expression of MALAT1 was the highest in SW620 cells. Then, we analyzed the relationship between the MALAT1 expression and clinicopathological parameters of patients. In Table I, the results show MALAT1 expression was significantly correlated with AJCC stage, vascular invasion, lymph node metastasis and distant metastasis (*p<0.05). In order to analyze the prognostic value of MALAT1 expression for colorectal cancer, overall survival of patients was tested by Kaplan–Meier curve analysis. Data in Fig. 1C suggested that overall survival in the low MALAT1 expression group was higher than that in the high MALAT1 expression group. Collectively, MALAT1 expression level was fortified in CC tissues and cell models, and had effects on prognosis of colorectal cancer.

MALAT1 overexpression increased colorectal cell proliferation, migration and invasion

Cell proliferation, invasion and migration rate were then assessed with the aim to investigate the effect of MALAT1 on colorectal cells.

MALAT1 and NC were transfected into LOVO and CL40 cells, while siMALAT1 and siNC were transfected into SW620 and HCT116 cells. Data in Fig. 2, A and B show that cell proliferation was significantly increased when MALAT1 overexpression in LOVO and CL40 cells (**p<0.01). Conversely, cell proliferation was decreased when MALAT1 silencing in SW620 and HCT116 cells

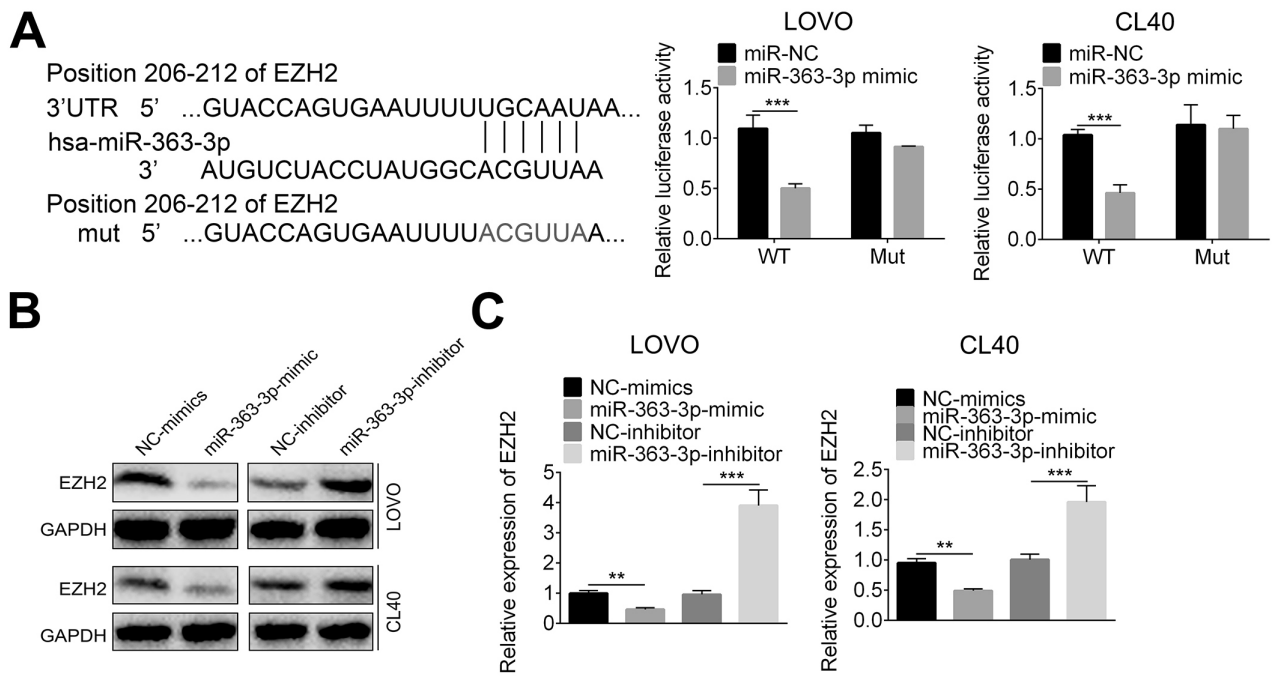

Fig. 4. *EZH2 was a target of miR-363-3p in colorectal cells. LOVO and CL40 cells were severally transfected with miR-NC, miR-363-3p mimic, NC-inhibitor or miR-363-3p inhibitor.* ***A)*** *The relative luciferase activities of EZH2 were detected. The expression of EZH2 was assessed by using* ***(B)*** *Western blot and* ***(C)*** *qRT-PCR. (***p <0.001).*

(**p<0.01 or ***p<0.001). Furthermore, crystal violet staining results showed that cell colony numbers in the MALAT1 or siNC group were higher than that in the NC or siMALAT1 group (Fig. 2C). In Fig. 2,D and E, cell wound healing and Transwell assay indicated that cell migration and invasion rate were increased in the MALAT1 group then NC group, and were clearly decreased when MALAT1 knockdown. In short, MALAT1 overexpression could increase colorectal cell development; similarly, MALAT1 silencing could reduce cell proliferation, migration and invasion.

miR-363-3p was a target of MALAT1 in colorectal cells.

Wang et al. reported that MALAT1 could adsorb miR-363-3p through sponging to regulate the expression of MCL-1 as competing endogenous RNA (ceRNA) in gallbladder carcinoma. Hence, in this study, we used the online program TargetScan database (http://www.targetscan.org/) to predict the potential binding sequences between lncRNA MALAT1 and miR-363-3p (Fig. 3A).

Experimental results suggested the relative luciferase activities were significantly lessened in LOVO and CL40 cells that transfected with pmiR-Glo-MALAT1-Wt compared to those transfected with pmiRGlo-NC (**p<0.01), while transfection using pmiE-Glo-MALAT1-Mut showed no obvious effect on relative luciferase activities (Fig. 3B). In Fig. 3C, RIP assay results suggested that miR-363-3p was enriched by MALAT1 in LOVO and CL40 cells (***p<0.001). Therefore, the above results suggested miR-363-3p was a target of MALAT1.

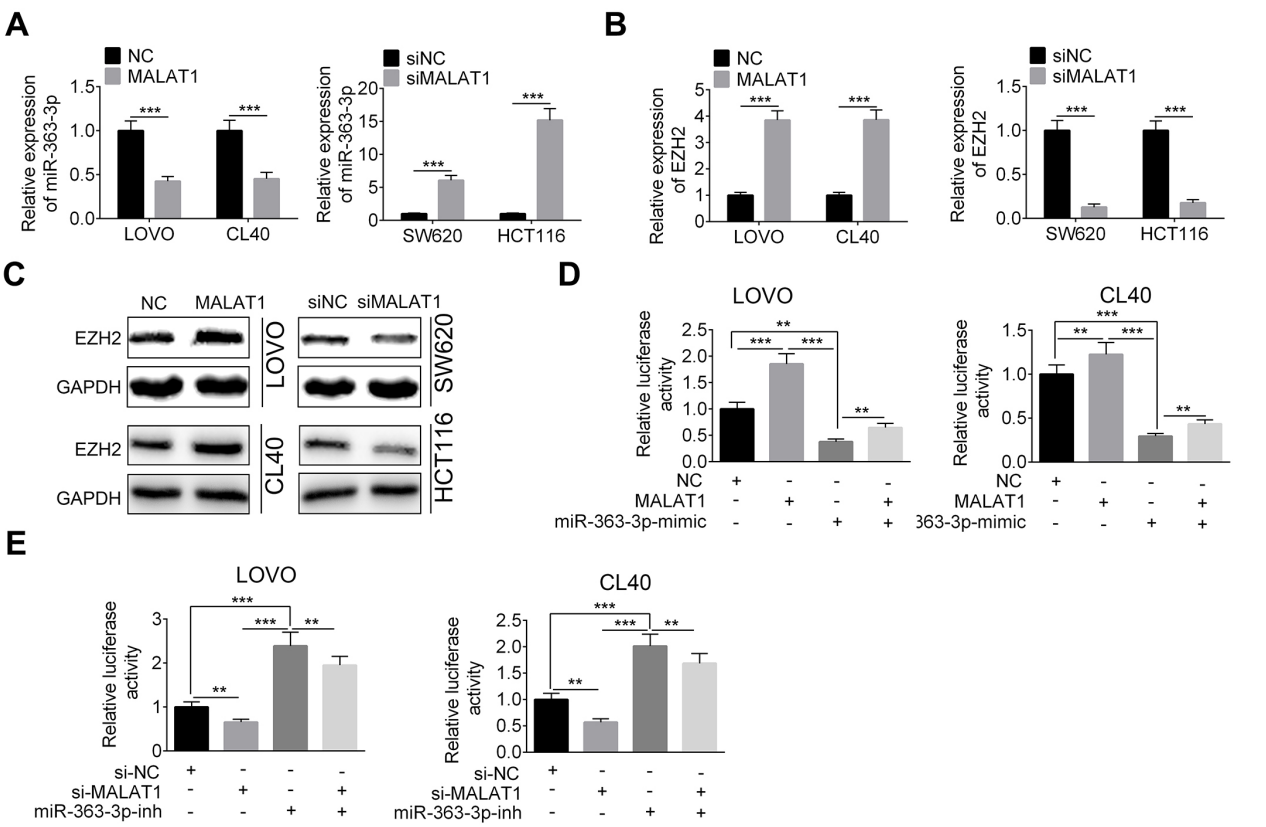

Fig. 5. *MALAT1 promoted EZH2 expression by regulating miR-363-3p in colorectal cells. Cells were respectively transfected with MALAT1, NC, miR-363-3p mimic, siMALAT1, siNC or miR-363-3p inhibitor. The mRNA levels of (**A**) MALAT1 and (**B**) EZH2 were detected by using qRT-PCR. (**C**) The protein expression level of EZH2 was assessed by using western blotting. (**D**) The potential binding sequences between EZH2 and miR-363-3p was predicted by using bioinformatics analysis. (**E-F**) The relative luciferase activities of EZH2 were detected in cell models. (**p <0.01; ***p <0.001).*

EZH2 was a target of miR-363-3p in colorectal cells.

Using microRNA database (http://www.microrna.org/), we discovered that EZH2 might be a potential target gene in the downstream of miR-363-3p. Subsequently, dual luciferase activity assay was applied to verify whether EZH2 was a target of miR-363-3p.

Fig. 4A suggested the relative luciferase activities were remarkably decreased when miR-363-3p overexpression in EZH2 3'-UTR-Wt transfected LOVO and CL40 cells (***p< 0.001). Meanwhile, the relative luciferase activities of cells transfected with EZH2 3'-UTR-Mut did not change significantly. Subsequently, we detected the expression levels of EZH2. As shown in Fig. 4B and 4C, EZH2 expressions were decreased when miR-363-3p overexpressed in LOVO and CL40 cells (**p<0.01). On the contrary, the expression levels of EZH2 were distinctly up-regulated in the miR-363-3p-inhibitor group than in the NC-inhibitor group (***p<0.001). Collectively, it is suggested that miR-363-3p was a negative upstream regulator of EZH2.

MALAT1 promoted EZH2 expression by regulating miR-363-3p in colorectal cells

LOVO and CL40 cells were transfected with MALAT1 and NC respectively, while SW620 and HCT116 cells were transfected with siMALAT1 and

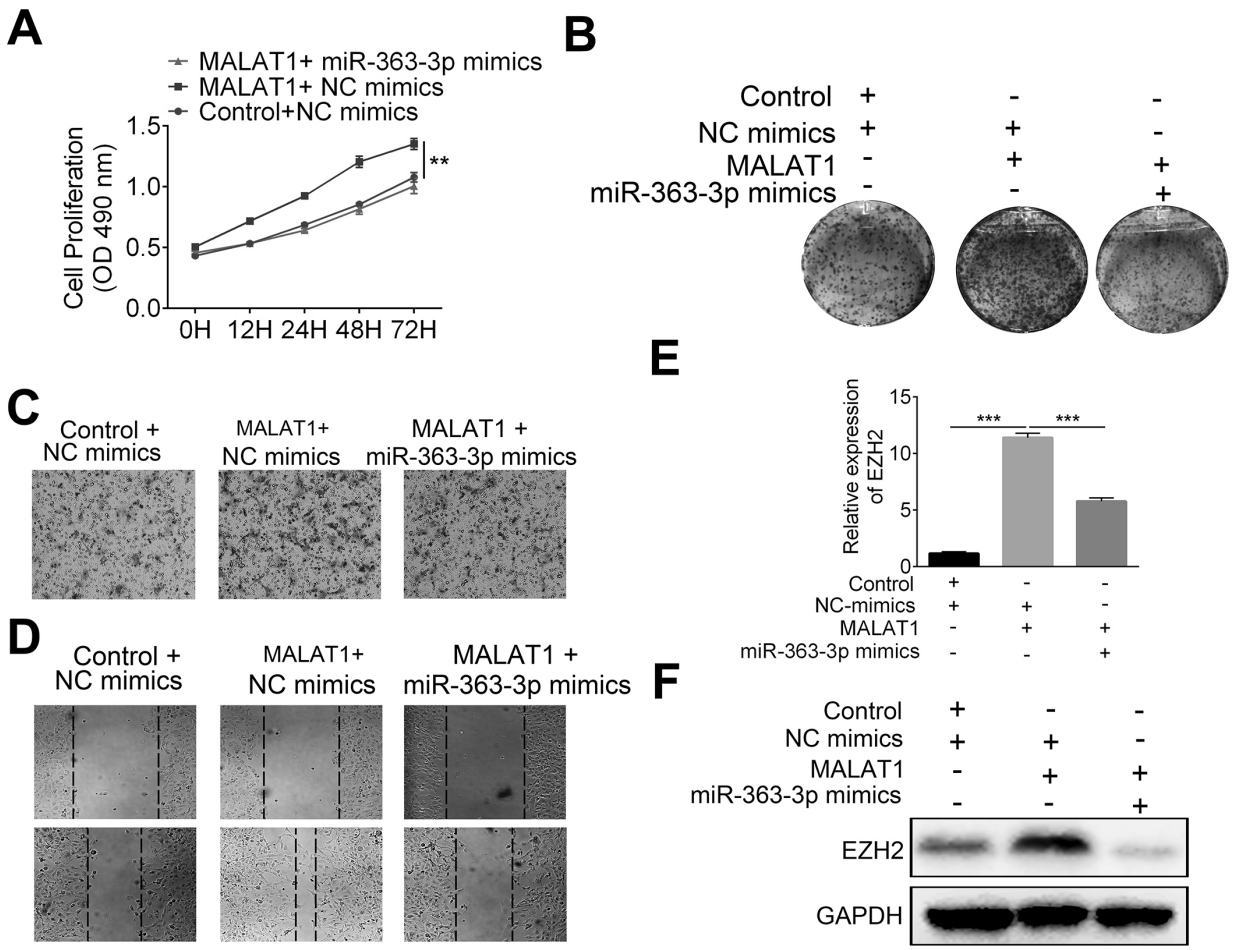

Fig. 6. *MALAT1 knockdown inhibited the growth of cancer and EZH2 expression by miR-363-3p overexpression. CL40 cells were transfected with MALAT1, NC or miR-363-3p mimics. Cell proliferation was measured by using (**A**) MTT and (**B**) crystal violet assay. Cell migration and invasion were assessed by using (**C**) Transwell assay and (**D**) cell wound healing assay. The expression levels of EZH2 (**E**) mRNA and (**F**) EZH2 protein were assessed. (**p <0.01; ***p <0.001).*

siNC. The effects of MALAT1 on the expression levels of EZH2 and miR-363-3p were assessed by qRT-PCR and Western blotting.

As seen in Fig. 5A, overexpression of MALAT1 inhibited miR-363-3p mRNA levels, and MALAT1 knockdown significantly increased miR-363-3p levels in colorectal cells (***p<0.001). As shown in Fig. 5 B-C, mRNA and protein levels of EZH2 were both increased in the MALAT1 group compared to the NC group (***p<0.001). Conversely, EZH2 were significantly down-regulated in the siMALAT1 group than in the siNC group (***p<0.001).

Furthermore, the potential binding sequences between miR-363-3p and EZH2 were analyzed, as shown in Fig. 5D. Based on these results, dual luciferase activity assay was applied to evaluate the binding status and abilities between MALAT1, miR-363-3p and EZH2.

As shown in Fig. 5E, it is suggested that the relative luciferase activities of EZH2 were increased when MALAT1 was overexpressed (***p<0.001), which was clearly decreased in content of miR-363-3p overexpression (**p<0.01; ***p<0.001). Meanwhile, cells that co-transfected with MALAT1 and miR-363-3p mimic ameliorated the effects of such decrease (**p<0.01). Contrarily, MALAT1 silencing reduced, while miR-363-3p knockdown significantly increased the relative luciferase activity in HCT116 and SW620 cells (**p<0.01; ***p<0.001). The increased activity was alleviated when MALAT1 and miR-363-3p were both knocked down (**p<0.01, Fig. 5F). In summary, these results indicated MALAT1 could affect EZH2 transcriptional levels by regulating miR-363-3p expression.

MALAT1 knockdown inhibited the growth of cancer and EZH2 expression by miR-363-3p overexpression

To investigate the effects of MALAT1 and miR-363-3p on the regulation of cell growth, we detected cell proliferation, migration and invasion rates in CL40 cells.

MTT and crystal violet assays revealed that MALAT1 overexpression promoted cell proliferation, while miR-363-3p overexpression partially inhibited these additions (**p< 0.01, Fig. 6 A-B). Similarly, Transwell and cell wound healing assay suggested that increase of cell migration and invasion caused by MALAT1 overexpression were inhibited when miR-363-3p mimics transfected into cells (Fig. 6C and 6D). Furthermore, Fig. 6E and 6F demonstrated that the expression levels of EZH2 were alleviated in the MALAT1+miR-363-3p mimics group than that in the MALAT1+NC mimics group (***p<0.001). In addition, to accurately investigate the regulatory relationship between MALAT1 and miR-363-3p or miR-363-3p and EZH2, qRT-PCR was utilized

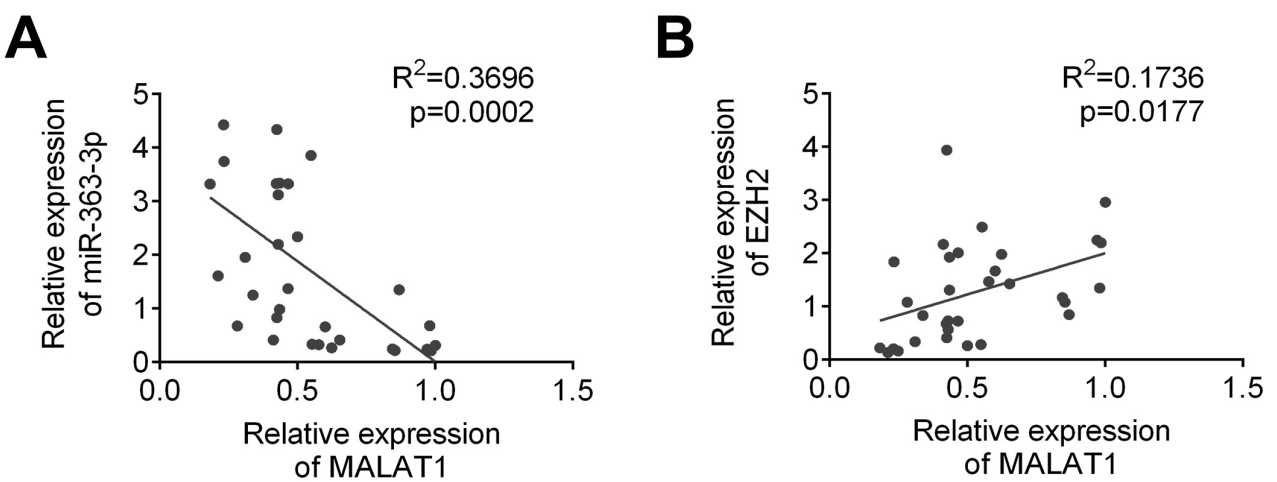

Fig. 7. *MALAT1 negatively regulated miR-363-3p, and positively regulated EZH2 expression. The expressions of (**A**) miR-363-3p and (**B**) EZH2 were detected in colorectal cancer tissues and adjacent non-tumor tissues.*

to assess their expression levels in CCtissues and adjacent non-tumor tissues. In Fig. 7A-B, MALAT1 negatively regulated miR-363-3p, and positively regulated EZH2 expression levels. To sum up, MALAT1 knockdown inhibited cell development and EZH2 expression by upregulating miR-363-3p.

MALAT1 knockdown decreased tumor growth and EZH2 expression, and increased miR-363-3p expression in vivo

A xenograft mouse model was established to verify the effects of MALAT1 on tumor growth *in vivo*.

Fig. 8A-C suggested that tumor sizes, weights and volumes were significantly decreased when MALAT1 was knocked down (***$p< 0.001$). As shown in Fig. 8D, cell proliferation ability *in vivo* was also reduced in the shRNA-MALAT1 group comopared to the sh-Ctrl group. Furthermore, qRT-PCR and Western blotting results confirmed that MALAT1 knockdown increased miR-363-3p expression (***$p<0.001$), which also remarkably reduced the protein levels of EZH2 *in vivo*.

DISCUSSION

The age of onset of CC patients gradually tends to aging, and the studies regarding its molecular pathogenesis have also received increasing attention (2-4, 6). In this study, we observed that MALAT1 was highly expressed in CC tissues and cell models and had a correlation with clinicopathological parameters. We also observed MALAT1 knockdown inhibited cell proliferation, migration and invasion by miR-363-3p up-regulation. miR-363-3p was a downstream target of MALAT1, and EZH2 was a target of miR-363-3p. Moreover, MALAT1 silencing decreased CCgrowth and EZH2 expression, and increased miR-363-3p expression *in vivo*.

LncRNAs can regulate or maintain gene expression to promote or inhibit tumor growth, and their abnormal expressions often lead to the occurrence, development and metastasis of tumors (21). Some studies revealed that MALAT1 promotes cell proliferation, motility and invasion, while MALAT1 expression was increased in various types of cancers, such as gallbladder cancer, triple-negative breast cancer and CC (22-24). Moreover, Jin et al. found that knockdown of MALAT1 could inhibit the growth of tumor *in vivo* (24). Our experimental results were consistent with the above results, indicating that MALAT1 was highly expressed and promoted CC cell development *in vitro* and *in*

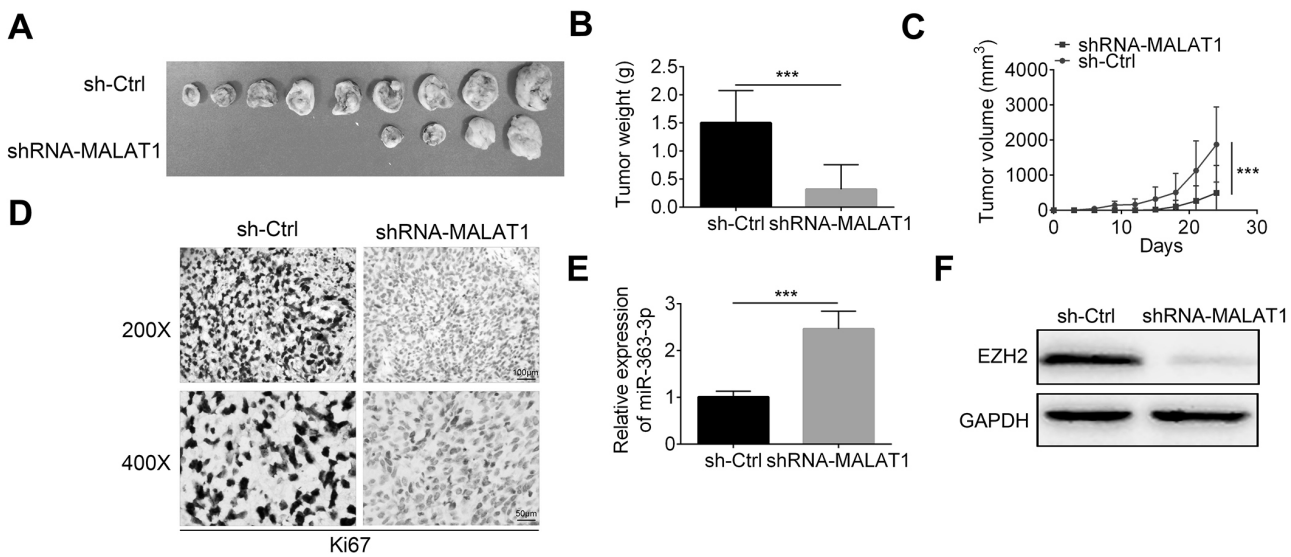

Fig. 8. *MALAT1 knockdown decreased tumor growth and EZH2 expression, and increased miR-363-3p expression in vivo. SW620 cells were transfected with shRNA-MALAT1, which were transplanted subcutaneously into nude mice. Tumor (**A**) sizes, (**B**) weights and (**C**) volumes were measured and calculated. **D**) Cell proliferation, the expression levels of (**E**) miR-363-3p and (**F**) EZH2 were assessed. (***p <0.001).*

Table I. *Correlation between MALAT1 expression and clinicopathological parameters of colorectal cancer patients (n=30).*

	Number of cases	Low MALAT1 expression(%)	High MALAT1 expression(%)	p value
Gender				0.784
Male	10	7	3	
Female	20	13	7	
Age(years)				0.796
≤65	16	11	5	
>65	14	9	5	
Location				0.584
Left	20	14	6	
Right	10	6	4	
Tumor size(cm)				0.439
≤3	15	9	6	
>3	15	11	4	
AJCC stage				
I	4	4	0	0.035*
II	8	7	1	
III	13	8	5	
IV	5	1	4	
Differentiation				0.845
Well	11	8	3	
Moderate	13	8	5	
Poor	6	4	2	
Vascular invasion				0.018*
Yes	12	5	7	
No	18	15	3	
Depth of invasion				0.754
T1	2	1	1	
T2	7	5	2	
T3	9	7	2	
T4	12	7	5	
Lymph node metastasis				0.034*
N0	12	11	1	
N1	12	7	5	
N2	6	2	4	
Distant metastasis				0.015*
M0	25	19	6	
M1	5	1	4	

**p<0.05. AJCC: American Joint Committee on Cancer.*

vivo. In addition, MALAT1 expression also affected overall survival of patients. We hypothesized that there might be a certain relationship between the expression levels of MALAT1 and the occurrence of colorectal cancer.

Current studies have found the effects of lncRNAs on cancer development is through regulation of miRNAs expression (16, 18, 24, 25). However,

there are still lots of unknowns in the regulatory mechanisms between MALAT1 and microRNAs in colorectal cancer. Only Jie and Zhao reported that MALAT1 accelerated cell development via miR-129-5p in colon cancer (25). Moreover, Wang et al. reported MALAT1 functioned as a ceRNA through sponging miR-363-3p to modulate the expression of MCL-1in gallbladder cancer (23). Therefore, we hypothesized that MALAT1 could affect the development of CC through regulating miR-363-3p expression. In our study, results demonstrated that MALAT1 knockdown decreased cell development by miR-363-3p up-regulation, while overexpression of MALAT1 decreased miR-363-3p levels. Interestingly, luciferase reporter assay testified that miR-363-3p was a target of MALAT1. These experimental results are consistent with our previous assumptions.

EZH2 is a member of the epigenetic inhibitory factor polycomb group (PcG) family (26). It inhibits target genes transcription and participates in the regulation of cell cycle, cell senescence, cell determination and other physiological or pathological processes through trimethylation of H3K27me3 by histone methyltransferase activity (26, 27). Overexpression of EZH2 in tumor tissues is reported to be closely related to malignancy, poor prognosis and low survival rate of tumors (28). A large number of reports have demonstrated that miRNAs regulate EZH2 expression by combining with EZH2 3 'UTR, such as miR-144, miR-26a and miR-205, which can inhibit EZH2 expression via targeting EZH2 in bladder cancer, breast cancer and renal cell carcinoma (29-31). However, in our study, we forecast that EZH2 might be a potential target gene in the downstream of miR-363-3p and confirmed that EZH2 was a target of miR-363-3p in colorectal cells through dual luciferase reporter assay. In addition, down-regulation of EZH2 by siRNAs and/or shRNAs can also inhibit cell proliferation and the growth of tumor tissues (32). Furthermore, our results suggested that MALAT1 could positively regulate EZH2 expression and functioned as a ceRNA, as well as promote CC cell development by sponging miR-363-3p to regulate EZH2 expression. *In vivo*, MALAT1 knockdown could decrease tumor size, weight and volume, and EZH2 expression levels. LncRNA MALAT1 could function as a miRNA sponge to promote CC development and EZH2 expression, while negatively regulating miR-363-3p expression. The regulatory network of MALAT1/miR-363-3p/EHZ2 might provide a novel molecular basis for future research and treatments of colorectal cancer. In future experiments, we will study the regulatory role of MALAT1 on more miRNAs with the aim to identify more regulatory networks in CC to develop novel therapeutic strategies from bench to clinic.

REFERENCES

1. Siegel R, Ward E, Brawley O, Jemal A. Cancer statistics, 2011: the impact of eliminating socioeconomic and racial disparities on premature cancer deaths. CA Cancer J Clin 2011; 61:212-36.
2. Giardiello FM, Gurbuz AK, Bayless TM, Goodman SN, Yardley JH. Colorectal cancer in ulcerative colitis: survival in patients with and without colorectal cancer symptoms. Inflamm Bowel Dis 1996; 2:6-10.
3. Astin M, Griffin T, Neal RD, Rose P, Hamilton W. The diagnostic value of symptoms for colorectal cancer in primary care: a systematic review. Br J Gen Pract 2011; 61:e231-43.
4. Majumdar SR, Fletcher RH, Evans AT. How does colorectal cancer present? Symptoms, duration, and clues to location. Am J Gastroenterol 1999; 94:3039-45.
5. Marshall JL, Haller DG, de Gramont A, Hochster HS, Lenz HJ, Ajani JA, Goldberg RM.. Adjuvant Therapy for Stage II and III Colon Cancer: Consensus Report of the International Society of Gastrointestinal Oncology. Gastrointest Cancer Res 2007; 1:146-54.
6. Potter JD, Slattery ML, Bostick RM, Gapstur SM. Colon cancer: a review of the epidemiology. Epidemiol Rev 1993; 15:499-545.
7. Shephard RJ. Exercise in the prevention and treatment of cancer. An update. Sports Med 1993; 15:258-80.
8. Thune I, Lund E. Physical activity and risk of colorectal cancer in men and women. Br J Cancer 1996; 73:1134-40.
9. Faivre J, Bouvier AM, Bonithon-Kopp C. Epidemiology and screening of colorectal cancer. Best Pract Res Clin

Gastroenterol 2002; 16:187-99.
10. Yarmishyn AA, Kurochkin IV. Long noncoding RNAs: a potential novel class of cancer biomarkers. Front Gene 2015; 6:145.
11. Ji P, Diederichs S, Wang W, et al. MALAT-1, a novel noncoding RNA, and thymosin beta4 predict metastasis and survival in early-stage non-small cell lung cancer. Oncogene 2003; 22:8031-41.
12. Xia H, Chen Q, Chen Y, et al. The lncRNA MALAT1 is a novel biomarker for gastric cancer metastasis. Oncotarget 2016; 7:56209-18.
13. Ren S, Liu Y, Xu W, et al. Long noncoding RNA MALAT-1 is a new potential therapeutic target for castration resistant prostate cancer. J Urol 2013; 190:2278-87.
14. Gutschner T, Hammerle M, Eissmann M, et al. The noncoding RNA MALAT1 is a critical regulator of the metastasis phenotype of lung cancer cells. Cancer Res 2013; 73:1180-89.
15. Catana CS, Pichler M, Giannelli G, Mader RM, Berindan-Neagoe I. Non-coding RNAs, the Trojan horse in two-way communication between tumor and stroma in colorectal and hepatocellular carcinoma. Oncotarget 2017; 8:29519-34.
16. Galluzzi L, Morselli E, Vitale I, et al. miR-181a and miR-630 regulate cisplatin-induced cancer cell death. Cancer Res 2010; 70:1793-803.
17. Lin SL, Chiang A, Chang D, Ying SY. Loss of mir-146a function in hormone-refractory prostate cancer. Rna 2008; 14:417-24.
18. Bo S, Jin Y, Chao L, Zhou H, Zheng Y. Tumor suppressor role of miR-363-3p in gastric cancer. J Exp ClinRes 2015; 21:4074-80.
19. Livak KJ, Schmittgen TD. Analysis of relative gene expression data using real-time quantitative PCR and the 2(-Delta Delta C(T)) method. Methods 2001; 25:402-8.
20. Herchenhorn D, Souza AL, Souza AM, et al. Prognostic impact of radiology response and tumor volume among patients with locally advanced squamous cell carcinoma of the head and neck (LASCHNC) treated with concomitant chemoradiation. J Clin Oncol 2009; 27:15S, e17035-e17035.
21. Li X, Wang Z. The role of noncoding RNA in thyroid cancer. Gland Surg 2012; 1:146-50.
22. Yang MH, Hu ZY, Xu C, Xie LY, Wang XY, Chen SY, Li ZG. MALAT1 promotes colorectal cancer cell proliferation/migration/invasion via PRKA kinase anchor protein 9. Biochim Biophys Acta 2015; 1852:166-74.
23. Wang SH, Zhang WJ, Wu XC, et al. The lncRNA MALAT1 functions as a competing endogenous RNA to regulate MCL-1 expression by sponging miR-363-3p in gallbladder cancer. J Cell Mol Med 2016; 20:2299-308.
24. Jin C, Yan B, Lu Q, Lin Y, Ma L. Reciprocal regulation of Hsa-miR-1 and long noncoding RNA MALAT1 promotes triple-negative breast cancer development. Tumour Biol 2016; 37:7383-94.
25. Wu Q, Meng WY, Jie Y, Zhao H. LncRNA MALAT1 induces colon cancer development by regulating miR-129-5p/HMGB1 axis. J Cell Physiol 2017; 233(9):6750-57.
26. Bracken AP, Pasini D, Capra M, Prosperini E, Colli E, Helin K. EZH2 is downstream of the pRB-E2F pathway, essential for proliferation and amplified in cancer. Embo j 2003; 22:5323-35.
27. Sauvageau M, Sauvageau G. Polycomb group proteins: multi-faceted regulators of somatic stem cells and cancer. Cell Stem Cell 2010; 7:299-313.
28. Zhang J, Chen L, Han L, Shi Z, Zhang J, Pu P, Kang C. EZH2 is a negative prognostic factor and exhibits pro-oncogenic activity in glioblastoma. Cancer Lett 2015; 356:929-36.
29. Hirata H, Hinoda Y, Shahryari V, et al. Long noncoding RNA MALAT1 promotes aggressive renal cell carcinoma through Ezh2 and interacts with miR-205. Cancer Res 2015; 75:1322-31.
30. Guo Y, Ying L, Tian Y, et al. miR-144 downregulation increases bladder cancer cell proliferation by targeting EZH2 and regulating Wnt signaling. FEBS J 2013; 280:4531-38.
31. Zhang B, Liu XX, He JR, et al. Pathologically decreased miR-26a antagonizes apoptosis and facilitates carcinogenesis by targeting MTDH and EZH2 in breast cancer. Carcinogenesis 2011; 32:2-9.
32. Chang CJ, Hung MC. The role of EZH2 in tumour progression. Br J Cancer 2012; 106:243-47.

CYTOSINE 5-HYDROXYMETHYLATION REGULATED KIT GENE EXPRESSION IN ACUTE MYELOID LEUKEMIA

YM. XUE[1], HC. CHENG[2], JH. WANG[1], W. WANG[1] and L. MIAO[3]

[1]Department of Hematology, The Second Affiliated Hospital of Harbin Medical University, Harbin, China; [2]Institute of Harbin Hematology & Oncology, The First Hospital of Harbin, Harbin, China; [3]Department of Respiratory Medicine, The First Hospital of Harbin, Harbin, China

Received October 17, 2018 – Accepted January 22, 2019

5-methyl cytosine (5mC) can be oxidized to 5-hydroxymethyl cytosine (5hmC) under the action of TET protein family, and 5hmC plays important roles in the pathogenesis of various tumors including acute myeloid leukemia (AML). In this study, we evaluated the role of 5mC and 5hmC levels in HL60 AML cells and bone marrow samples from AML patients for KIT gene expression to analyze 5hmC level in AML pathogenesis. Results showed that the expression and 5hmC level increased significantly of the KIT gene but the change of its 5mC level was not obvious after being treated by decitabine (DAC) in HL60 cells. IDH1 and IDH2 expression increased followed by increased KIT 5hmC level. In AML patients with IDH1 or IDH2 mutation, KIT expression and 5hmC were much lower than in those without mutation. The study indicated that the expression of KIT gene was regulated by 5hmC level in HL60 cells, and the 5hmC level was regulated by IDH1 and IDH2.

5-methyl cytosine (5mC) as an important epigenetic modification plays important roles in gene expression, embryonic development and disease progression. In tumors, including acute leukemia, the genome-wide hypomethylation and hypermethylation of promoter regions lead to transcriptional silencing of some genes of DNA damage repair, apoptosis and cell cycle regulation, which promotes the pathogenesis of various tumors (1). For example, hypermethylation of SFRP1/2 silenced its expression and was an adverse risk factor for overall survival in AML patients (2).

Recently, two papers reported that 5mC could be oxidized to 5-hydroxymethyl cytosine (5hmC) by TET protein family (3, 4). Stroud et al. (5) indicated that 5hmC is mainly involved in gene promoters and enhancer, and plays an important role in regulation of gene expression. Orr et al. (6) found that the degree of malignancy was associated with a decrease of 5hmC levels in gliomas. In breast cancer, the level of 5hmC is closely related to the hypoxia, malignancy and poor prognosis (7). In addition, Thomson et al. (8) showed that changes in 5hmC levels occur earlier than changes in 5mC, and that the changes are very stable. In short, the 5hmC level is a potential marker for early tumor diagnosis and may be predictive of prognosis. However, studies are limited on 5hmC of single gene, especially in AML.

Acute myeloid leukemia (AML) is a group of hematological malignancies and is characterized by abnormal proliferative, clone and differentiation of stem cells (9). The development of AML is

Key words: DNA methylation; hydroxymethylation; KIT; AML

Corresponding Author:
Dr Jing-Hua Wang,
The Department of Hematology,
The Second Affiliated Hospital
Harbin Medical University,
No. 148 of Baojian Road, Harbin, 150081, China
e-mail: hayida_jinghua@163.com

0393-974X (2019)

associated with the accumulation of acquired genetic alterations and epigenetic changes in hematopoietic progenitor cells, such as abnormal expression of tumor suppressor genes and oncogenes (10). The oncogene KIT encodes the cellular homolog of the feline sarcoma viral oncogene KIT and is involved in cell signal transduction pathways, such as MAPK, PI3K and JAK (11). KIT could lead to tumor growth through impairment of cellular growth regulation (12). KIT over-expression leads to a significant inhibition of cellular proliferation, and over-expressing cells showed a regression of typical morphological features of malignancy (13). Some papers reported that KIT expression was highly expressed or mutated in various tumors including leukemia cells (14-16), however there is no report on 5mC or 5hmC of KIT gene.

MATERIALS AND METHODS

Cell culture and treatment

HL60 AML cells were kindly provided by Professor

Table I. *Names and sequences of all primers.*

Name	Primer sequences (5'→3')
ASXL1F	CTGTGGGTCTAATGAAGCC
ASXL1R	TCGCCTGTGAGGAAGC
KITF	TACAACGATGTGGGCAAGA
KITR	TACGAAACCAATCAGCAAAG
NRASF	CTCAGGGTTGTATGGG
NRASR	CCTCCAGGGAAGTCAG
KRASF	GAGGGAGATCCGACAA
KRASR	CAACACCCAGATTACATT
RUNX1F	GTTTGTCGGTCGAAGTG
RUNX1R	TTTGATGGCTCTGTGGTA
KITMF	TCAGCCTGGCCGTCCACATC
KITMR	GCCCCTGCTCTTTCGACGTG
TET1F	GCACATAAGATAAGGGCAGTGG
TET1R	ACTTCAGGTTGCACGGTCTCAG
TET2F	AGAAAGGAGACCCGACTG
TET2R	GCAAAGGCAAGTAAACAAT
IDH1F	CTCTGTCTAAGGGTTGG
IDH1R	ACTGGGACTTGTACTGC
IDH2F	GGGCGTTTCAAGGACA
IDH2R	CAAAGCCACCCGAAGA

Note: F and R indicate the upstream and downstream primers. KITMF and KITMR indicate the primers used for 5mC and 5hmC detection.

Amin from MD Anderson Cancer Center (Houston, TX, USA). Cells were cultured in DMEM-1640 medium with 10% FBS and 5% CO2. When the cells reached 80% confluence, they were reseeded at a dilution of 1:3. HL60 cells (10^5 per well) were treated with various concentrations of demethylation drug decitabine, referred to as DAC (Sigma, MO, USA), for 48 h. Then the cells were used for cell viability analysis, and DNA, RNA and protein extraction.

Patient samples

Bone marrow (BM) samples from AML patients (n=56) were collected at the Second Affiliated Hospital of Harbin Medical University between August 2016 and July 2017 after informed consent. The median age was 48 (18 to 65 years). All subjects were newly diagnosed AML patients (except for M3) and were detected by two generation sequencing with AML panel. Among the 56 AML patients, 10 and 12 patients had IDH1 and IDH2 mutations, respectively. No mutation was found in the other patients.

Cell viability assay

Cell viability analysis was determined with the MTT method. HL60 cells (2×10^4cells/well) were seeded in triplicate into 96 well plates in normal growth media for 24 h. Then the cells were supplemented with various concentrations of DAC or DMSO as controls for 48 h. After treatment for 48 h, cells were added with 20 μL MTT (5mg/mL) in each well and then incubated for 4 h. Subsequently, supernatant was removed and 180 μL DMSO was added after centrifugation. The optical density was measured at 490 nm using a microplate spectrophotometer. Percentage of cell growth inhibition was calculated as (ODcontrol-ODdrug)/ODcontrol× 100%.

RNA isolation and real-time RT-PCR

Total RNA from HL60 cells of each group was isolated with TRIzol reagent (Invitrogen, Carlsbad, CA, USA) according to the manufacturer's instructions. The RNA samples were treated with Amplification Grade DNase I (TaKaRa, Tokyo, Japan) at room temperature for 60 min to prevent of DNA pollution. First strand cDNA was synthesized with RevertAid™ First Strand cDNA Synthesis Kit (MBI) and the real-time PCR was performed by an ABI 7500 system using SYBR®Premix Ex Taq™ (Takara, Dalian, China). The house-keeping gene β-actin was used as internal controls to evaluate the relative expression. All the primer sequences for expression, 5mC and 5hmC analysis are all listed in Table I.

Western blot analysis

After the exposure to DAC for 48 h, the cells were collected and the total protein was isolated with lysis

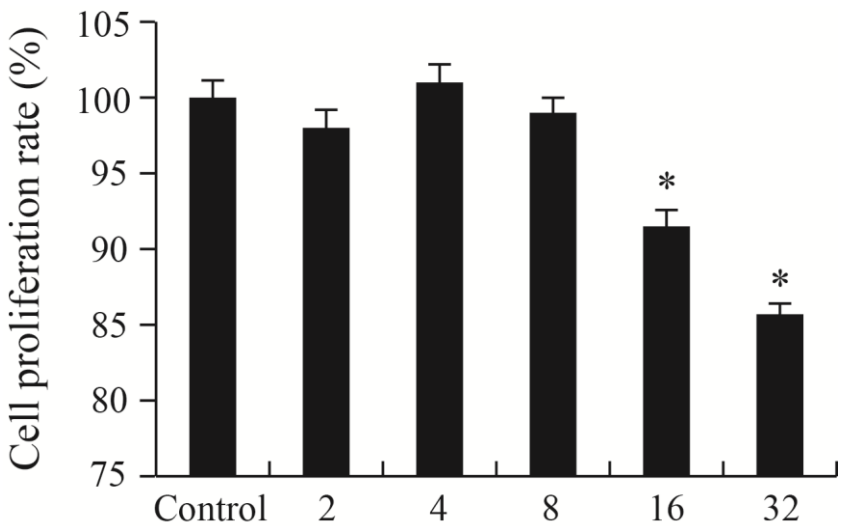

Fig. 1. *Effect of DAC on HL60 cell proliferation. Control, 2, 4, 8, 16 and 32 indicate HL60 cells treated with DMSO and various concentrations (uM) of DAC. *P<0.05 vs control.*

buffer and PMSF. Proteins were separated on 10% SDS-PAGE, transferred to a PVDF membrane and detected with anti-KIT and anti-β-actin antibodies (Cell signaling technology, Boston, MA, USA).

DNA isolation and 5mC analysis

HL60 cells of each group were extracted for genomic DNA using a DNA Extraction Kit (Tiangen, Beijing, China) according to the manufacturer's instructions. Before analyzing 5mC levels, genomic DNA was treated with a BisulFlash DNA Modification Kit (Zymo Research, Irvine, CA, USA) to convert unmethylated cytosine to thymine, but the methylated cytosine remained unchanged. In order to make the detection more accurate, we used real time PCR and PCR products cloning sequencing methods to detect the 5mC level. The specific procedures of the two methods were previously described in Ma et al. (17).

Detection of 5hmC

The Quest 5hmC Detection Kit™ (Zymo Research, Irvine, CA, USA) was used for 5hmC analysis. Firstly, DNA was glycosylated according to the manufacturer's instructions, after which glucose-5hmC-sensitive restriction endonucleases were able to cut the C and 5mC sites, but not the 5hmC sites. As a result, KIT 5hmC could be detected with real-time PCR using the treated DNA as template. We used ΔΔCt values (glucosylated-unglucosylated) to assess the 5hmC levels in all detected samples.

Statistical analysis

All data are presented as the average of three independent experiments. The $2^{-\Delta\Delta Ct}$ method was used to

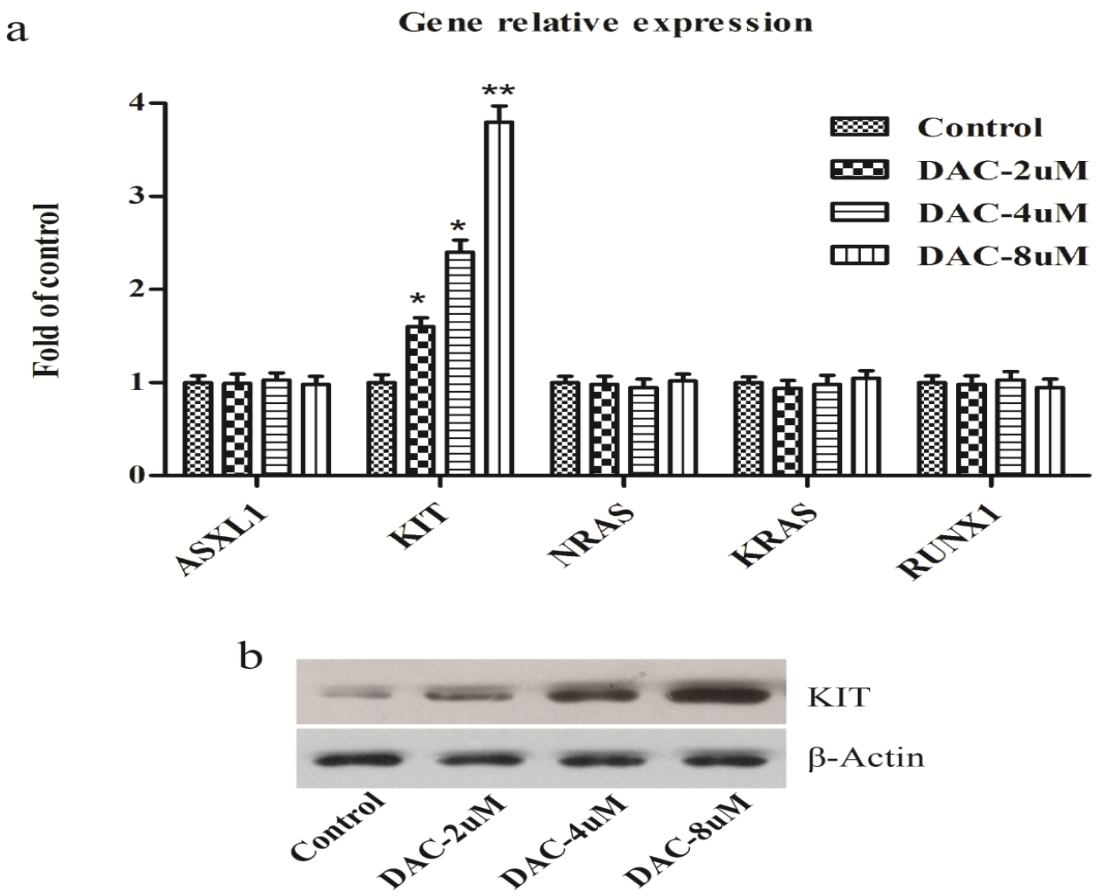

Fig. 2. *Gene relative expression with real time PCR (**a**) and Western blot (**b**). Controls indicates HL60 cells treated with DMSO. *P<0.05, **P<0.01 vs control.*

calculate the relative expression, 5mC and 5hmC levels in each gene. Statistical analysis was carried out using unpaired Student's *t*-test. Values of $p<0.05$ and $p<0.01$ are criteria for evaluating significant and much more significant differences.

RESULTS

Effect of DAC on cell viability

HL60 cells were treated with DAC at concentrations of 2 μM, 4 μM, 8 μM, 16 μM and 32 μM for 48 h and the cell viability was determined by MTT assay. Because the half-life of DAC is short, we replaced the medium with a proper concentration of DAC after being treated for 24 h. The MTT results indicated that DAC had almost no inhibition on HL60 cell growth at concentrations of 2 μM, 4 μM and 8 μM. The inhibition rates of DAC were only 8.5% and 14.3% at concentrations of 16 μM and 32 μM (Fig.1). To avoid the effect on gene expression by inhibition of cell proliferation, we chose the concentrations of 2 μM, 4 μM and 8 μM to study the demethylation of DAC on HL60 cells.

DAC increased KIT expression in HL60 cells

We detected the expression of ASXL1, KIT, NRAS, KRAS and RUNX1 genes in HL60 cells treated by DMSO, 2 μM, 4 μM and 8 μM DAC. Real time PCR results showed that DAC increased KIT expression significantly, but it had no significant effect on ASXL1, NRAS, KRAS and RUNX1 expression (Fig. 2a). The increased expression of KIT treated by DAC was in a dose-dependent manner; the increased times were 1.6, 2.4 and 3.8 at 2 μM, 4 μM and 8 μM, respectively. To verify the uniformity between mRNA and protein levels, we carried out Western blotting analysis of KIT gene. Western blotting results showed that KIT protein levels were also increased significantly in HL60 cells after treatment by DAC (Fig. 2b).

Detection of 5mC and 5hmC of KIT

Because DAC is a demethylation drug and KIT expression increased after treatment by DAC, we detected the 5mC and 5hmC levels of KIT in HL60 cells to study the role of methylation in the regulation of gene expression. Three *Msp*I sites in promoter and 5' untranslated regions of KIT were used to analyze 5mC and 5hmC levels in HL60 cells before and after treatment by various concentrations of DAC. Real time PCR results showed the difference of 5mC was not significant (Fig. 3a). Subsequently, we detected the 5mC of this fragment with direct sequencing of clones to verify the accuracy of the

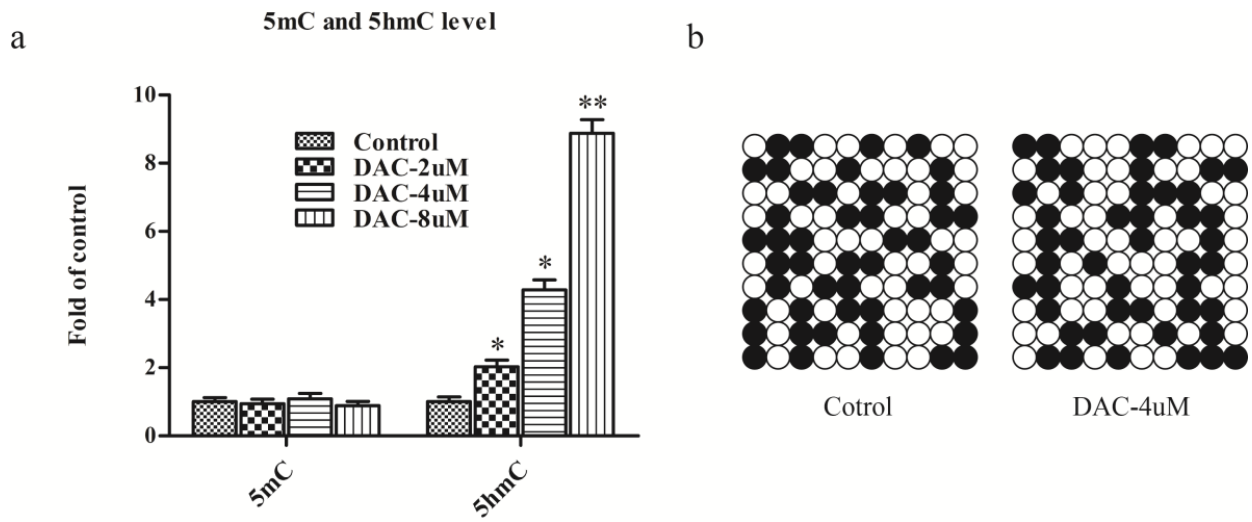

Fig. 3. *5mC and 5hmC analysis with real time PCR (**a**) and 5mC analysis with PCR products sequencing (**b**) of KIT gene. Controls indicates HL60 cells treated with DMSO. *P<0.05, **P<0.01 vs control. Filled and open circles represent methylated and unmethylated CG dinucleotide.*

above method. Sequencing results indicated that the average 5mC percentages were 48% and 46% in HL60 cells and those treated by 4 μM DAC, and the statistical analysis was not significant (Fig. 3b). For 5hmC analysis, the ΔΔCt values (glucosylated-unglucosylated) were used to assess the 5hmC levels in different samples. Statistical analysis showed that the difference of KIT 5hmC was significant, and the difference was in a dose-dependent manner. The ΔΔCt values were -0.24, -1.26, -2.34 and -3.39 in control, respectively. In other words, the increased times of 5hmC levels were 2.03, 4.29 and 8.88 in HL60 cells treated by 2 μM, 4 μM and 8 μM DAC compared to control, respectively (Fig. 3a).

DAC increased IDH1 and IDH2 expression

In order to further study the regulatory factors of 5hmC, we detected the expression of TET1, TET2, IDH1 and IDH2 which play important roles in the generation and transformation of 5hmC. Real-time quantitative PCR results showed that the difference of TET1 and TET2 expression was not significant in cells treated by DAC compared to controls (Fig. 4). However, the expression of IDH1 and IDH2 increased significantly after DAC treatment, and the trend of expression was also in a dose-dependent manner similar to KIT expression (Fig. 4).

KIT expression decreased in patients with IDH1 or IDH2 mutation

Fifty-six AML patients were chosen for the study on the effect of IDH1 and IDH2 on 5hmC of KIT gene *in vivo*. All patients were divided into control (n=34), IDH1 (n=10) and IDH2 (n=12) mutated groups. All specimens in each group were evenly mixed for expression, 5mC and 5hmC detection. Real time results indicated that KIT expression decreased significantly in patients with IDH1 or IDH2 mutation compared to controls. The change trend of 5hmC of KIT was consistent with its expression. It was also much lower in patients with IDH1 or IDH2 mutation than controls. However, the difference of 5mC was not significant between the control, IDH1 and IDH2 mutation groups (Fig. 5).

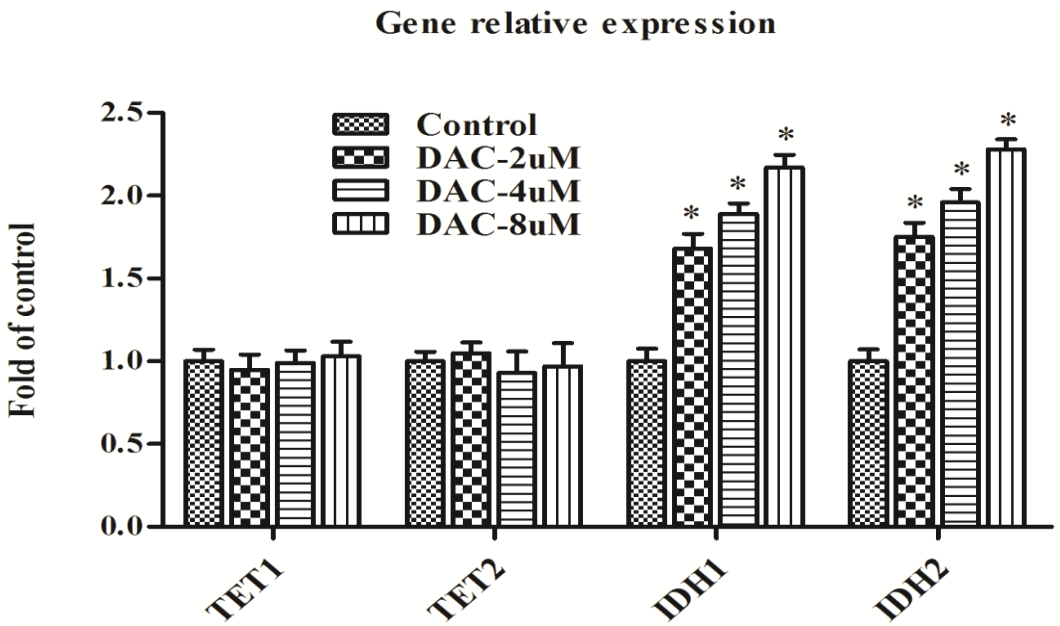

Fig. 4. *TET1, TET2, IDH1 and IDH2 genes expression with real time PCR. Controls indicates HL60 cells treated with DMSO. *P<0.05 vs control.*

DISCUSSION

The evolution of leukemia is a sequential and multistep process of genetic variation, such as abnormal gene expression or gene mutation. The main gene types of genetic variation include tumor suppressor gene, and DNA methylation-related genes (18). Alterations in DNA methylation of many genes occur in hematological malignancies. Generally, hypermethylation of tumor suppressor genes and hypomethylation of oncogenes are involved in the development of leukemia (19). DAC had been applied to AML because it could reactivate expression of silenced genes due to its demethylation effect (20, 21). In this study, KIT expression increased significantly but the difference in DNA methylation was not significant in HL60 cells treated by DAC, which indicated that KIT expression could be regulated by other mechanisms rather than DNA methylation.

Unlike 5mC, 5hmC is a stable marker of the genome. Ficz et al. (22) showed that the content of 5hmC and 5mC would maintain a relative balance. The balance is frequently deregulated in cancer, leading to aberrant methylation and hydroxymethylation patterns (23). The damage of 5hmC in promoter region may affect the binding of methylated binding proteins to these sequences, thereby affecting the expression of these genes. In the study, the 5mC level of KIT gene was not changed although its expression increased significantly after being treated by DAC. Considering the extensive demethylation of DAC and the relationship of 5mC and 5hmC, we detected 5hmC of KIT. Real time PCR results showed that 5hmC level increased followed by its expression, although 5mC level had no change at the same 5' UTR region, which indicated that DAC did not affect only demethylation, but also hydroxymethylation on some genes. Meanwhile, the results also indicated that 5hmC but not 5mC regulated KIT expression after treatment with DAC.

TET1 and TET2 are key enzymes in the process of DNA hydroxylation and both could catalyze 5mC into 5hmC (24). IDH1 and IDH2 could catalyze decarboxylation of citric acid to produce alpha glutaric acid (α-KG). Alpha-KG could regulate DNA hydroxylation process by interfering with the activity of a variety of enzymes that depend on its

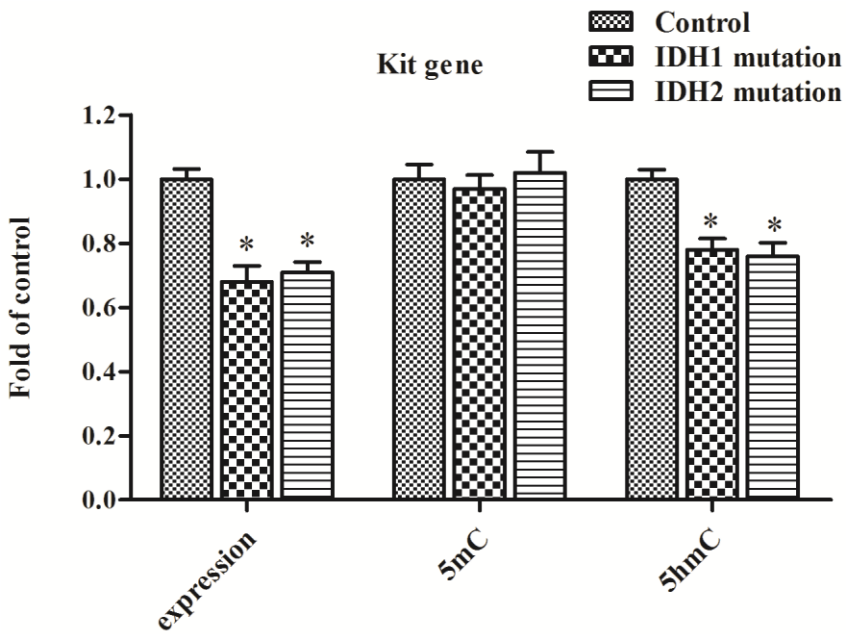

Fig. 5. *Expression, 5mC and 5hmC analysis of KIT gene. Control indicates HL60 cells treated with DMSO. *P<0.05 vs control.*

factor (25). Therefore, we detected TET1, TET2, IDH1 and IDH2 expression in HL60 cells before and after treatment with DAC. The fluorescent quantitative PCR results showed that IDH1 and IDH2 expression increased but TET1 and TET2 expression had no obvious change in HL60 cells after being treated with DAC, which indicated that IDH1 and IDH2 may participate in the regulation of DNA hydroxylation. The results were similar with those that Chen (26) and Chou (27) reported - that the decreased expression of IDH1 and IDH2 led to 5hmC level decrease in renal cell carcinoma and gastric cancer.

Magotra et al. (28) reported that IDH1 and IDH2 mutation could cause defective conversion of 5mC into 5hmC and impair demethylation of DNA, leading to decreased 5hmC. In order to further verify the effect of IDH1 and IDH2 on KIT hydroxylation *in vivo*, we detected KIT expression and 5hmC in AML patients with IDH1 or IDH2 mutation or without as control. Quantitative PCR results showed that KIT expression and 5hmC level both decreased in IDH1 or IDH2 mutated patients, which is similar with the results of Liu et al. (29) in gliocytoma. The paper reported that IDH1 mutation could increase histone methylation level and inhibit the activity of a variety of α-KG-dependent double oxygenase in glioma, and reduce the level of 5hmC. In summary, DAC could increase KIT expression in HL60 cells, and 5hmC regulates its expression. IDH1 and IHD2 play important roles in regulating KIT 5hmC level. The relationship between KIT 5hmC level and clinical features and whether it could be used as a molecular biological marker still needs further clinical trials in AML patients.

In conclusion, KIT gene expression and 5hmC level increased significantly after treatment by decitabine (DAC) in AML HL60 cells. The expression of KIT gene was regulated by 5hmC level in HL60 cells and patients. IDH1 and IDH2 could regulate 5hmC level of KIT gene.

ACKNOWLEDGEMENTS

This study was supported by Harbin Technology and Innovation Foundation for Youth (Grant number 2016RAQXJ188).

REFERENCES

1. Irizarry RA, Ladd-Acosta C, Wen B, et al. The human colon cancer methylome shows similar hypo- and hypermethylation at conserved tissue-specific CpG island shores. Nat Genet 2009; 41(2):178-86.
2. Guo H, Zhang TJ, Wen XM, et al. Hypermethylation of secreted frizzled-related proteins predicts poor prognosis in non-M3 acute myeloid leukemia. Onco Targets Ther 2017; 10:3635-44.
3. Kriaucionis S, Heintz N. The nuclear DNA base 5-hydroxymethylcytosine is present in Purkinje neurons and the brain. Science 2009; 324(5929):929-30.
4. Tahiliani M, Koh KP, Shen Y, et al. Conversion of 5-methylcytosine to 5-hydroxymethylcytosine in mammalian DNA by MLL partner TET1. Science 2009; 3249(5929):930-35.
5. Stroud H, Feng S, Morey Kinney S, Pradhan S, Jacobsen SE. 5-Hydroxymethylcytosine is associated with enhancers and gene bodies in human embryonic stem cells. Genome Biol 2011; 12(6):R54.
6. Orr BA, Haffner MC, Nelson WG, Yegnasubramanian S, Eberhart CG. Decreased 5-hydroxymethylcytosine is associated with neural progenitor phenotype in normal brain and shorter survival in malignant glioma. PLoS One 2012; 7(7):e41036.
7. Wu MZ, Chen SF, Nieh S, et al. Hypoxia drives breast tumor malignancy through a TET-TNFα-p38-MAPK signaling axis. Cancer Res 2015; 75(18):3912-24.
8. Thomson JP, Hunter JM, Lempiäinen H, Müller A, Terranova R, Moggs JG, Meehan RR. Dynamic changes in 5-hydroxymethylation signatures underpin early and late events in drug exposed liver. Nucleic Acids Res 2013; 41(11):5639-54.
9. Döhner H, Weisdorf DJ, Bloomfield CD. Acute myeloid leukemia. New England J Med 2015; 373(12):1136-52.
10. Rostami S, Nadali F, Alibakhshi R, et al. Aberrant methylation of APAF-1 gene in acute myeloid leukemia patients. Int J Hematol Oncol Stem Cell Res 2017; 11(3):225-30.
11. Sanlorenzo M, Vujic I, Posch C, et al. Oncogenic KIT mutations in different exons lead to specific changes in melanocyte phospho-proteome. J Proteomics 2016; 144:140-47.
12. Sehitoglu I, Bedir R, Cure E, Cure MC, Yuce S,

Dilek N. Evaluation of the relationship between c-Kit expression and mean platelet volume in classic Kaposi's sarcoma. An Bras Dermatol 2016; 91:430-35.
13. Franceschi S, Lessi F, Panebianco F, et al. Loss of c-KIT expression in thyroid cancer cells. PLoS One 2017; 12(3):e0173913.
14. Matsumura Y, Umemura S, Ishii G, et al. Expression profiling of receptor tyrosine kinases in high-grade neuroendocrine carcinoma of the lung: a comparative analysis with adenocarcinoma and squamous cell carcinoma. J Cancer Res Clin Oncol 2015; 141(12):2159-70.
15. Yu G, Yin C, Jiang L, et al. Amyloid precursor protein cooperates with c-KIT mutation/overexpression to regulate cell apoptosis in AML1-ETO-positive leukemia via the PI3K/AKT signaling pathway. Oncol Rep 2016; 36(3):1626-32.
16. Chen EC, Karl TA, Kalisky T, et al. KIT Signaling promotes growth of colon xenograft tumors in mice and is up-regulated in a subset of human colon cancers. Gastroenterology 2015; 149(3):705-17.
17. Ma EG, Bai YF, Cao W, Cao Y, Huang YG, Cheng HC, An RH. Cytosine 5-hydroxymethylation regulates VHL gene expression in renal clear cell carcinoma. Oncotarget 2017; 8(38):63780-87.
18. Ley TJ, Miller C, Ding L, et al. Genomic and epigenomic landscapes of adult de novo acute myeloid leukemia. N Engl J Med 2013; 368(22):2059-74.
19. Yao H, Duan M, Lin L, et al. TET2 and MEG3 promoter methylation is associated with acute myeloid leukemia in a Hainan population. Oncotarget 2017; 8(11):18337-47.
20. Claus R, Pfeifer D, Almstedt M, Zucknick M, Hackanson B, Plass C, Lübbert M. Decitabine induces very early in vivo DNA methylation changes in blasts from patients with acute myeloid leukemia. Leuk Res 2013; 37(2):190-96.
21. Xiang L, Zhou J, Gu W, et al. Changes in expression of WT1 during induced differentiation of the acute myeloid leukemia cell lines by treatment with 5-aza-2'-deoxycytidine and all-trans retinoic acid. Oncol Lett 2016; 11(2):1521-26.
22. Ficz G, Gribben JG. Loss of 5-hydroxymethylcytosine in cancer: cause or consequence. Genomics 2014; 104(5):352-57.
23. Kroeze LI, van der Reijden BA, Jansen JH. 5-Hydroxymethylcytosine: An epigenetic mark frequently deregulated in cancer. Biochimica et Biophysica Acta 2015; 1855(2):144-54.
24. Mohr F, Döhner K, Buske C, Rawat VP. TET genes□new players in DNA demethylation and important determinants for stenmess. Exp Hematol 2011; 39(3):272-81.
25. Xu W, Yang H, Liu Y, et al. Oneometabolite 2-hydroxyglutarate is a competitive inhibitor of a-ketoglutarate-dependent dioxygenases. Cancer Cell 2011; 19(1):17-30.
26. Chen K, Zhang J, Guo Z, et al. Loss of 5-hydroxymethylcytosine is linked to gene body hypermethylation in kidney cancer. Cell Res 2016; 26(1):103-18.
27. Chou NH, Tsai CY, Tu YT, et al. Isocitrate Dehydrogenase 2 Dysfunction Contributes to 5-hydroxymethylcytosine Depletion in Gastric Cancer Cells. Anticancer Res 2016; 36(8):3983-90.
28. Magotra M, Sakhdari A, Lee PJ, et al. Immunohistochemical loss of 5-hydroxymethylcytosine expression in acute myeloid leukaemia: relationship to somatic gene mutations affecting epigenetic pathways. Histopathology 2016; 69(6):1055-65.
29. Liu Y, Jiang W, Liu J, Zhao S, Xiong J, Mao Y, Wang Y. IDH1 mutations inhibit multiple α-ketoglutarate-dependent dioxygenase activities in astroglioma. J Neurooncol 2012; 109(2):253-60.

EFFECTS OF CD133 ON THE BIOLOGICAL FEATURES AND *IN-VIVO* ONCOGENICITY OF GLIOMA CELLS

R. GAO[1] and TT. SUN[2]

[1]Department of Neurosurgery, General Hospital of Ningxia Medical University, Yinchuan, Ningxia Hui Autonomous Region, China; [2]Department of General Medicine, Daqing Longnan Hospital, Daqing, Heilongjiang Province, China

Received November 9, 2018 – Accepted January 10, 2019

This study aimed to investigate the effect of CD133 on the proliferation and migration of glioma cells and expressions of genes related to cancer stem cells/tumor stem cells (CSC/TSC) as well as their *in-vivo* oncogenicity. CD133-overexpressing U251-CD133 and U251-mock glioma cells were constructed. The effect of CD133 on *in-vitro* proliferation and the neurosphere-forming ability of glioma cells was determined by cell count and neurosphere formation assay. Real-Time PCR was performed to detect the expressions of CSC/TSC-related genes in the CD133-transfected cells. Nude mouse subcutaneous tumor formation assay was used to determine the effect of CD133 on the *in-vivo* oncogenicity of glioma cells. In serum-containing medium, human CD133 had no impact on the proliferation of U251 glioma cells, but the neural stem cells placed in serum-free medium promoted neurosphere formation. In the presence of CD133, the expressions of CSC/TSC-related genes were upregulated to varying degrees in glioma cells; CD133 greatly enhanced the *in-vivo* oncogenicity. In conclusion, CD133 promoted the upregulation of CSC/TSC-related genes in glioma cells, while enhancing the neurosphere-forming ability and *in-vivo* oncogenicity.

Glioma is a common intracranial cancer, featured by high malignancy, high recurrence and poor prognosis (1, 2). In 2003, Singh et al. first reported cancer stem cells/tumor stem cells (CSC/TSC), for which CD133 is a specific marker (3). Many studies have shown that $CD133^+$ CSC/TSC in glioma is closely related to tumor grading and prognosis. The higher the expression of CD133, the higher the tumor malignancy and the worse the prognosis (4-6). It is indicated that CD133 plays a role in angiogenesis, high drug resistance, and radiochemotherapy tolerance in glioma (3, 7), though more studies are required to investigate the biological functions and working mechanism of CD133 (8, 9). In order to determine the role of CD133 in the development of glioma, the full-length CD133 was inserted into retrovirus vector pEGZ-term, and the gene-transfected cell line stably expressing human CD133 was constructed. By using the retrovirus vector pEGZ-term, the CD133 gene was introduced to the genome of U251 glioma cells, so that the transfected cell line could stably express CD133 in the long term. After repeated freeze/thaw cycles, the cell line could maintain the ability of stably overexpressing CD133. The research findings lay the basis for understanding the effect of CD133 on the growth, proliferation, *in-*

Key words: glioma; CD133; oncogenicity; biological features

Corresponding Author:
Dr Rong Gao,
Department of Neurosurgery,
General Hospital of Ningxia Medical University,
Yinchuan, 750001,
Ningxia Hui Autonomous Region, China
e-mail: gaorongbiosci01@163.com

0393-974X (2019)

vitro and *in-vivo* oncogenicity, cytokine secretion and signal transduction of glioma cells.

MATERIALS AND METHODS

Animals

Thirty-six nude mice aged 6 weeks were purchased from Shanghai Jiandun Biological Technology Co., Ltd., and maintained in a specific pathogen-free (SPF) environment at the room temperature of 25±2°C, noise of less than 60 dB, humidity of 50-60%, and illumination of 12 h/d. They were fed with aseptic diet and sterile water. After one week, the nude mice were randomly divided into three groups (12 mice in each group). The experiment was approved by the ethics committee of General Hospital of Ningxia Medical University.

pEGZ-Term-CD133 construction

Primers were designed based on CD133 gene sequence (Gene Bank AF0272081) (General Hospital of Ningxia Medical University, China). Restriction sites for BamH I and Smi I were introduced to the two flanks of CD133 cDNA by PCR. The primer sequences were as follows:

upstream
'-TGGATTTAAATATGGCCCTCGTACTCGGCTC-3';
downstream
5'-GTGTGGATCCCTATCAATGTTGTGATGGGCTTG-3'.

PCR products were retrieved. Restriction endonucleases BamH I and Smi I (Thermo Fisher Scientific, USA) cut the PCR products and vector pEGZ-Term (Thermo Fisher Scientific, USA). The purified products were joined together by the T4 ligase. The competent *E. coli* Top10 cells (Shanghai Xinyu Biotechnology Co., Ltd., China) were transformed and the negative colonies were picked. After colony PCR, double digestion verification and sequencing, it was indicated that the recombinant plasmid was successfully constructed and named pEGZ-Term-CD133.

Construction of CD133-transfected glioma cell lines

For preparation of recombinant retroviruses, 293T cells at logarithmic growth stage were taken and inoculated to 6-well plates (1×10^5 /well). When the cell confluency reached 80 ~ 90%, the recombinant plasmid pEGZ-Term-CD133 and its helper vector pHIT456 and pHIT60 (Shanghai Huashun Biotechnology Co., Ltd., China) were introduced into 293T cells by liposomes. The intact retroviruses were packaged and the virus-containing cell culture supernatant was collected 48 h later and stored at -20°C until use.

In order to construct the gene transfected cell lines, U251 cells (Shanghai Tianda Bioengineering Co., Ltd., China) at logarithmic growth stage were inoculated to 24-well plates (1×10^5 /well). After the cells adhered to the wall, 0.5 ml of virus supernatant was added to each well, and Polybrene was added at 8μg/ml for culture for 48 h. Cells were digested and diluted, and then they were inoculated in 24-well plates for zeocin pressure screening (500μg/ml). When the resistant clones were large enough, they were inoculated into the culture flask and were named U251-CD133. Meanwhile, 293T cells were transfected with pCMV-Neo-Bam pEGZ-Term, and negative control U251 mock cell lines were prepared with the same method.

The expression of CD133 mRNA in gene transfected cell lines was detected by RT-PCR and Real Time PCR: the total RNAs of gene transfected cell lines were transfected and reversely transcribed into cDNA. The CD133 cDNA fragment was amplified by RT-PCR and Real Time PCR with the U251, U251-mock and U251-CD133 as templates, respectively.

Flow cytometry was used to detect the expression of CD133 on the surface of gene transfected cell lines: 5×10^5/test U251-CD133, U251-mock and U251 cells at the logarithmic growth stage were taken, and they were washed twice with PBS buffer containing 0.3%FCS; 1 μl of CD133 mAb-PE antibody was added for staining, and the cells were incubated at 4°C for 30 min, and were washed once in PBS buffer. The expressions of GFP and CD133 molecules on the cell surface were detected with flow cytometry. Meanwhile, mouse IgG-PE isotype control antibody stained cells were used as the control.

Detection of in vitro proliferative ability

U251, U251-mock and U251-CD133 cells in good growth status were digested with trypsin and re-suspended in 10% FCS 1640 medium. The cell concentration was adjusted to 5×10^4/ml, and the cells were inoculated into the 96-well plate at 100 μl per well, i.e., 5000 cells per well. The cells in each well were calculated daily, until the end of the experiment. The growth curves were plotted and the proliferative status was compared.

Determination of migration ability of gene-transfected cells by scratch assay

After reaching the log phase of growth, U251, U251-mock and U251-CD133 cells were inoculated into the 24-well plate at 5×10^5 per well. The cells were incubated overnight to form a cell monolayer. The next day, the cells were scratched using the tip of 200 µl pipette, and then washed with PBS once to remove the cells floating to the middle of the scratch. Images were taken under the microscope. The migration of the cells towards the scratch was observed every two days and images were taken.

Detection of colony-forming ability of the gene-transfected cells

DMEM-F12 medium containing B27, bFGF 1ng/ml and EGF 0.5ng/ml was prepared. The U251, U251-mock and U251-CD133 cells in good growth status were digested with trypsin and washed with PBS three times to remove the residual serum in the medium. The cells were counted and the cell concentration was adjusted to 5×10^4/ml. The cells were further re-suspended in the above-mentioned medium containing the corresponding cytokines, and inoculated into the 96-well plate at 100 µl per well. Cell morphology was observed every two days, and neurosphere formation was captured by taking images. The number of neurospheres formed in five random visual fields was counted under the microscope.

Real-Time PCR detection of CSC/TSC-related genes

Total RNA was extracted from the cells using Trizol method. RNA integrity was verified by electrophoresis and the absorbance values of RNA at 260 nm and 280 n were measured by using a spectrophotometer. The extracted products with OD260nm/OD280nm>1.8 were reversely transcribed into cDNA, and the expressions of CSC/TSC-related genes were measured using SYBR Green dye.

Subcutaneous inoculation of tumor cells to mice

The two constructed cell lines U251-mock and U251-CD133 were inoculated to the RPMI 1640 medium containing 10% FBS (Thermo Fisher Scientific, USA) and placed at 37°C in a 5% CO_2 incubator. The cell growth status was observed every two days and the passage was performed for the two cells simultaneously so that their *in-vitro* growth speed was basically the same. U251-mock and U251-CD133 cells of the log phase were harvested and digested with trypsin. After centrifugation at 1200 rpm for 5 min, the supernatant was discarded. The cells were washed with sterile PBS twice to remove the residual FBS. The cell concentration was adjusted to 2×10^7/ml, 6×10^6/ml and 2×10^6/ml, respectively, using sterile PBS. The two cell lines were inoculated subcutaneously to flanks of the nude mice (three groups) at the dose of 1×10^6/site, 3×10^5/site and 1×10^5/site, respectively, with 50 µl at each site. The general conditions of nude mice and tumor formation were observed regularly, and the time of tumor formation was recorded. The major diameter (a) and short diameter (b) of the tumor were measured with a vernier caliper. After the tumor grew to a diameter of about 15 mm, the nude mice were sacrificed. The tumor size was calculated using the formula $V=a\times b^2/2$, and the tumor-forming curve and growth curve were plotted.

Statistical analysis

All data were analyzed statistically using SPSS 19.0 software. Measurements were reported as $\bar{x} \pm s$, and $P<0.05$ indicated significant difference.

RESULTS

pEGZ-Term-CD133 construction

Restriction enzyme cutting sites of BamH I and Smi I were introduced into both wings of CD133 cDNA by PCR, and CD133 gene was transfected into pEGZ-Term expression vector plasmids by double enzyme digestion. The competence *Escherichia coli* were transformed, and after the bacteria were amplified, plasmids were extracted and verified with double enzyme digestion (Fig. 1). The results showed that the recombinant pEGZ-Term-CD133 was able to release fragments similar to the full-length CD133 gene in size after double enzyme digestion of BamH I and Smi I. DNA sequencing showed that the correct CD133 full-length gene had been successfully cloned into pEGZ-Term retrovirus surface vectors.

As shown in Fig. 1, double digestion of recombinant plasmid pEGZ-Term-CD133 with BamH I and Smi I produced fragments of similar size as the full-length CD133 gene. As verified by DNA sequencing, the full-length CD133 gene was successfully cloned to the retrovirus vector pEGZ-Term.

Construction of CD133-transfected glioma cells

Total RNA was extracted from U251, U251-mock and U251-CD133 cells, and the products were reversely transcribed to cDNA. Using the three cDNAs as templates, the target gene fragments of CD133 and β-actin were amplified, and β-actin was obtained by amplification using all the three cDNA as templates. Using cDNA from U251-CD133 cell line as the template, the fragment of expected size was obtained. But when using DNA from U251 and U251-mock cells as templates, only a very light band was obtained by amplification. This is probably attributed to the extremely low expression of CD133 in the two cell lines. Based on Real-Time PCR, the CD133-transfected cell line had an overexpression of CD133 mRNA. It was also indicated by flow cytometry that the U251-CD133 cell line overexpressed GFP and CD133.

The U251, U251-mock and U251-CD133 cells were inoculated on the glass slide. After fixation and blocking, the cells were stained with anti-human CD133 mAb-PE, and incubated in the dark. The nuclei were stained with DAPI. Then, the cells were sealed and observed under a fluorescence microscope. As shown in Fig. 2, the U251-CD133 cells expressing report gene green fluorescent protein and CD133 molecules were observed by fluorescence microscopy.

As shown in Fig. 2 (A, B, C), compared with the higher expression of CD133 mRNA on U251-mock, U251 cells and U251-CD133 cells [(7400.2±5003.4) *vs* (2.0±1.1), (1.0±2.2), P=0.0007), infected pEGZ-

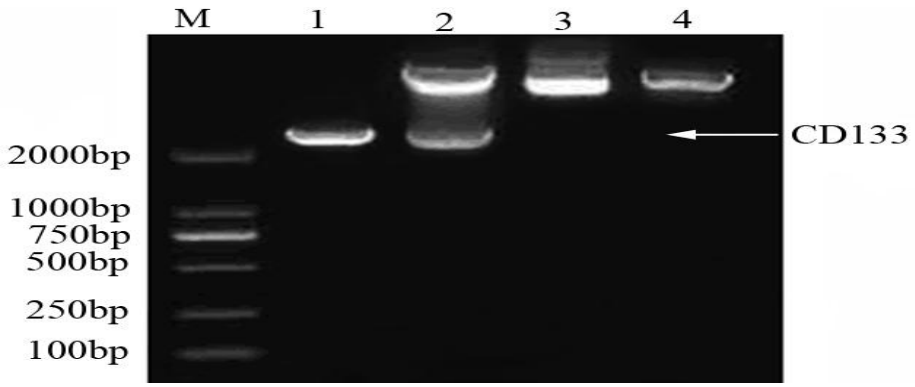

Fig. 1. *Double digestion verification of recombinant plasmid pEGZ-Term-CD133 (M: DL2000 DNA marker; 1: Full-length CD133; 2: Products of double digestion of recombinant plasmid pEGZ-Term-CD133 by BamH I and Smi I; 3: pEGZ-Term-CD133 plasmid before digestion; 4: Products of double digestion of pEGZ-Term plasmid by BamH I and Smi I).*

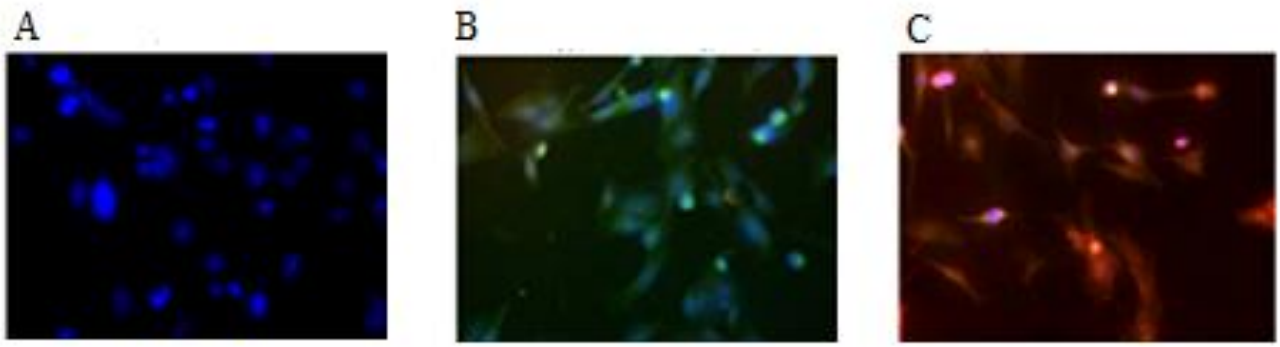

Fig. 2. *Determination of CD133 expressions on the surface of gene-transfected cells by immunohistochemistry (×100). **A**) U251 cell line was the template; **B**) U251-mock cell line was the template; **C**) U251-CD133 cell line was the template.*

Term-CD133 had no effect on the proliferation of U251 cells *in vitro* (P>0.05). However, under serum-free neural stem cell culture, the number of nerve spheres formed by U251-CD133 cells was significantly higher than that of U251-mock and U251 cells [(34.0±7.5) *vs* (14.6±2.3), (11.5±1.3), P < 0.01]. When the inoculation volume was 1×105 cells, the tumorigenesis time (32 days) of U251-CD133 cells in nude mice was less than that of U251-mock cells (38 days) and the tumorigenesis rate was higher (100% *vs* 30%). At day 41, tumor volume increased significantly [(180.3±146.8) *vs* (4.0±0.0) mm^3, P=0.003].

In order to further explore the role of CD133 molecules in the occurrence and development of brain glioma, CD133 full-length gene was transfected into pEGZ-Term reverse transcription expression virus vectors, and 293T cells were co-transfected with the

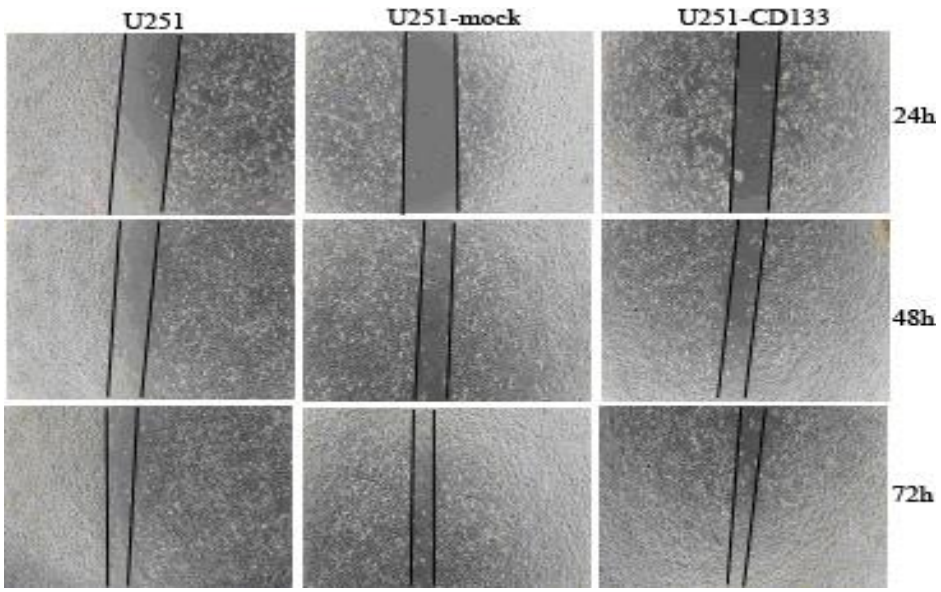

Fig. 3. *Effects of CD133 on the migration ability of glioma cells (×40).*

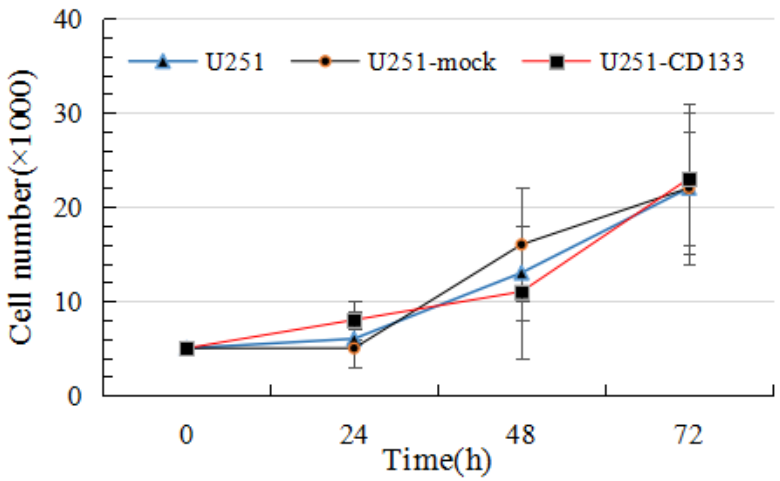

Fig. 4. *Effects of CD133 transfection on the growth of glioma in the presence of serum (×100).*

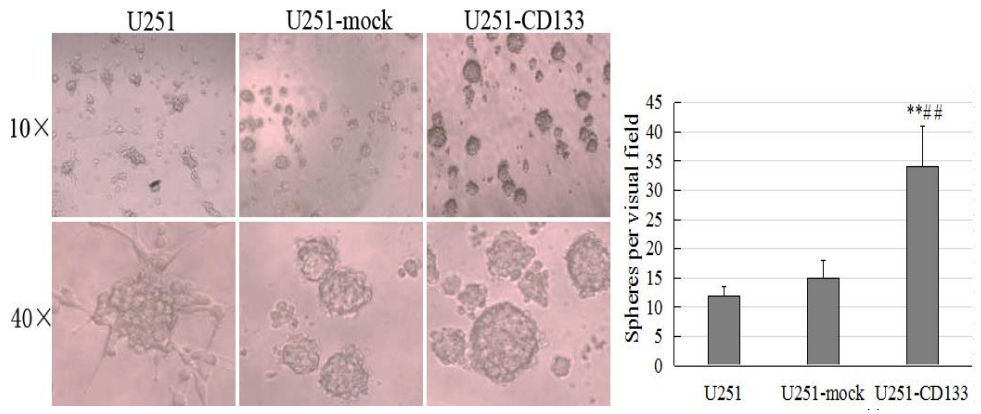

Fig. 5. *Effects of CD133 on the neurosphere-forming ability of glioma cells.* $^{**}P<0.01$*, compared with U251 cells;* $^{\#\#}P<0.01$*, compared with U251-mock cells.*

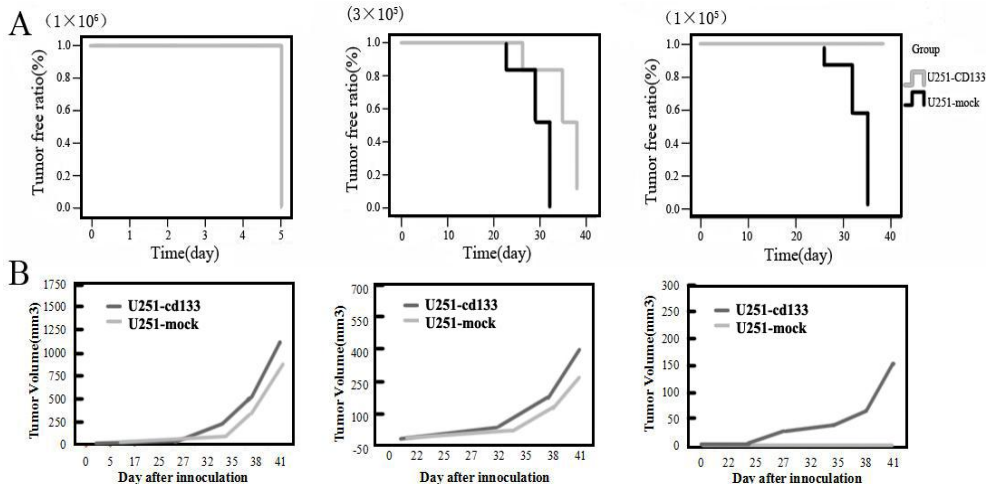

Fig. 6. *Effects of CD133 on the oncogenicity of glioma cells.* ***A)*** *Tumor formation curve;* ***B)*** *Tumor growth curve.*

helper virus vector into the virus with intact package, which were then infected with glioma U251 cell line. After Zeocine pressurized screening, flow cytometry, Real Time PCR and cellular immunochemical detection, the gene transfected cell lines with stable expressions of human CD133 molecules were successfully constructed. Since CD133 gene was introduced into U251 cell line genome with reverse transcription virus expression vectors, CD133 molecules could be expressed stably in the gene transfected cell line for a long time. After repeated cryopreservation and resuscitation, the molecule was stably expressed. Therefore, the disadvantages of unstable expressions of CD133 molecules after the selection of $CD133^+$ cells from traditional tumor cell lines were overcome, laying a foundation for further study on the role of CD133 molecules in the growth characteristics, migration ability, tumorigenicity *in vitro* and *in vivo*, cytokine secretion and signal transduction of glioma cells.

Effects of CD133 on the migration ability of glioma cells

Scratch assay is a simple and feasible test to detect the migration and invasion ability of tumor cells. In this study, the migration ability of U251, U251-mock and U251-CD133 cells was analyzed

by scratch assay. As shown in Fig. 3, all three cells migrated towards the scratch without significant difference. This indicated that CD133 had no impact on the migration ability of glioma cells.

Effects of CD133 on the proliferation of glioma cells in the presence of serum

U251, U251-mock and U251-CD133 cells of good growth were resuspended in 10% FCS1640 medium and inoculated into 96-well plates (5×10^4 / well). At 24 h, 48 h and 72 h, the number of all three types of cells was counted and the growth curve was drawn. All three cell lines adhered to the wall and the number of cells was similar at 24 h, 48 h and 72 h (Fig. 4), which indicated that the proliferative ability of the CD133-transfected cells was not changed significantly. In other words, CD133 had no impact on the proliferative ability of glioma cells in the presence of serum.

Effects of CD133 on neurosphere formation of glioma cells in the presence of serum

CSC/TSC showed a neurosphere-like growth in

Table I. *Real-Time PCR detection of CSC/TSC-related genes in the gene-transfected cell lines.*

	Cell line	Mean CT value of the target gene	Mean CT value of internal reference	ΔCT	ΔΔCT	2-ΔΔCT
Nanog	U251	28.28±0.17	11.61±0.18	16.67±0.13	0.00±0.11	1.00±0.12
	U251-mock	27.81±0.22	10.93±0.23	16.88±0.22	0.12±0.22	0.95±0.24
	U251-CD133	30.27±0.11	16.52±0.21	13.75±0.08	-2.81±0.08	7.32±0.33
KLF4	U251	30.57±0.15	14.56±0.34	16.01±0.12	0.00±0.13	1.00±0.16
	U251-mock	29.59±0.26	15.11±0.11	14.48±0.24	-1.47±0.23	2.93±0.24
	U251-CD133	32.81±0.14	20.58±0.12	12.23±0.18	-3.82±0.17	14.15±1.25
OCT4	U251	31.25±0.13	14.54±0.35	16.71±0.21	0.00±0.22	1.00±0.14
	U251-mock	29.15±0.16	15.11±0.16	14.04±0.13	-2.65±0.17	6.45±0.73
	U251-CD133	32.34±0.18	20.45±0.21	11.89±0.15	-5.08±0.22	35.12±3.07
STAT3	U251	22.72±0.07	14.58±0.31	8.14±0.13	0.00±0.06	1.00±0.21
	U251-mock	21.58±0.08	15.11±0.11	6.47±0.05	-1.51±0.09	2.86±0.44
	U251-CD133	26.66±0.03	20.57±0.14	6.09±0.08	-2.11±0.08	4.32±0.32
SOX2	U251	24.26±0.13	15.61±0.16	8.65±0.13	0.00±0.15	1.00±0.32
	U251-mock	22.65±0.17	15.91±0.18	6.74±0.16	-1.88±0.17	3.81±0.46
	U251-CD133	27.16±0.16	20.99±0.13	6.17±0.13	-2.41±0.15	5.26±0.44
IL-6	U251	26.69±0.23	15.61±0.31	11.08±0.15	0.00±0.23	1.00±0.09
	U251-mock	26.61±0.15	15.95±0.35	10.66±0.11	-0.46±0.21	1.43±0.21
	U251-CD133	28.88±0.22	20.97±0.15	7.91±0.16	-3.07±0.12	8.66±0.15
FoxD3	U251	29.72±0.17	11.81±0.31	17.91±0.11	0.00±0.04	1.00±0.12
	U251-mock	31.15±0.36	10.88±0.14	20.27±0.31	2.42±0.05	0.20±0.11
	U251-CD133	31.88±0.41	16.78±0.36	15.10±0.24	-2.65±0.41	6.81±1.65
LIN28	U251	31.33±0.36	11.83±0.16	19.50±0.41	0.00±0.34	1.00±0.34
	U251-mock	30.46±0.21	10.95±0.18	19.51±0.17	0.15±0.12	0.97±0.33
	U251-CD133	30.82±0.15	16.77±0.32	14.05±0.11	-5.42±0.11	45.82±1.43

the stem cell culture medium. Therefore, the gene-transfected cells were incubated in the neural stem cell culture medium. U251-CD133 cells always had a semi-adherent growth or suspension growth, forming larger and denser neurosphere-like clusters. The cells around the neurospheres were transparent with clear structures. The cells in the middle had a higher density, poor transparency and obscure contour. In the control group, some U251 and U251-mock cells always adhered to the wall, forming fewer neurospheres with loose structures (Fig. 5). This indicated that CD133 could promote neurosphere formation of glioma cells as well as the growth of tumor cells in stem cell culture medium.

Effects of CD133 on the upregulation of CSC/TSC-related genes in glioma cells

Tumor stem cells are very similar to normal stem cells, and some specific genes of stem cells are expressed in tumor stem cells to varying degree. To study the changes of the expression of stem cell-related genes in glioma cell lines transfected with CD133 gene, Real Time PCR was used to detect the expression of stem cell-related genes Nanog, SOX2, KLF4, LIN28, IL-6, STAT3, FoxD3 and OCT4 in the three cell lines. As shown in Table I, compared with the other two cell lines, there was an upregulation of "stem cell"-related genes in U251-CD133 cells to varying degree. For example, Nanog was up-regulated about 7 times, KLF4 was up-regulated 14 times, and OCT4 was up-regulated about 35 times ($p<0.01$); STAT3 was upregulated about 4 times and SOX2 was upregulated about 5 times, with significant difference ($p<0.05$). The results indicated that CD133 might be involved in the maintenance of undifferentiated status of glioma cells by upregulating the stem cell-related genes.

Growth of the transplanted tumor

At day 5 after inoculation, visible tumors were formed in both U251-CD133 and U251-mock 1×10^6 groups. The growth status was observed every 3 days after that, and the results were as follows:

(a) Time of tumor formation: The time of tumor formation in U251-CD133 1×10^6, 3×10^5 and 1×10^5 groups was 4 days, 22 days and 27 days, respectively; that of U251-mock at the three doses was 5 day s, 25 days and 39 days, respectively. The tumor was formed earlier in the U251-CD133 3×10^5 and 1×10^5 groups than in the U251-mock cells (Fig. 6A); (b) Tumor formation rates: The tumor formation rate was all 100% in the U251-CD133 1×10^6, 3×10^5 and 1×10^5 groups; and that of U251-mock cells at the corresponding dose was 100%, 100% and 30%, respectively; the tumor formation rate in the U251-mock 1×10^5 group was only 30%, which was much lower than that in the U251-CD133 1×10^5 group (Fig. 6A); (c) Tumor size: The U251-CD133 3×10^5 group had a larger tumor size than the U251-mock group ($P<0.05$); and that of the U251-CD133 1×10^5 group was significantly larger than that of the U251-mock group ($P<0.05$) (Fig. 6B).

Compared with the U251-mock ($CD133^-$) cells, the U251-CD133 ($CD133^+$) cells formed tumors earlier, with a higher tumor formation rate and larger tumor size. This trend was even more pronounced when fewer cells were inoculated. It was inferred that CD133 transfection significantly enhanced the *in-vivo* oncogenicity of glioma cells.

DISCUSSION

Infiltrative growth is a salient feature of glioma cells (10). Our study showed that the migration ability of glioma cells was not affected by CD133, probably because the glioma is not prone to migrate to other tissues. Nor was the proliferation of glioma cells influenced by CD133, which is in agreement with the reports by Dong et al. (11) and Elsaba et al. (12). Beier et al. (13) separated the $CD133^+$ and $CD133^-$ cells from the fresh glioma tissues. The $CD133^-$ cells adhered to the wall during growth in the neural stem cell culture medium without neurosphere formation; in contrast, the $CD133^+$ cells had a neurosphere-like growth and could be passaged in the long term. $CD133^+$ cells may be the origin for infinite proliferation of tumors. In the present study, U251-CD133 cells were inoculated into the serum-free neural stem cell culture medium. Compared with the U251-mock cells, the U251-CD133 cells were able to form more typical and larger neurospheres with higher density and proliferative capacity. It was

suggested that CD133 promoted the proliferation of glioma in the neural stem cell culture medium, which was completely different from the serum-containing culture medium. CD133 may be related to the stemness features of CSC/TSC.

Nanog, SOX2, KLF4, LIN28, FoxD3 and OCT4 are very important embryonic stem cell-related genes and are expressed in early embryos; they play an important role in maintaining pluripotency of embryonic stem cells (14-16). Our study found that Nanog, SOX2, KLF4, STAT3, IL-6, LIN28, FoxD3 and OCT4, the stem cell-related genes, were all upregulated in glioma to varying degrees, which means that CD133 promoted the upregulation of stem cell-related genes in glioma cells. It was probable that CD133 is involved in the maintenance of undifferentiated status of CSC/TSC in glioma by upregulating the CSC/TSC-related genes. However, the relevant signaling pathways and molecular mechanism remain to be further clarified.

Tumor tissues are highly heterogenous (17-19), and the growth and differentiation degrees of each component vary. Not all tumor cells can overcome the effect of growth inhibitory factors in the outer environment and proliferate continuously, finally forming a new tumor (20, 21). Beier et al. (22) divided glioma cells into $CD133^+$ and $CD133^-$ cells, which were respectively inoculated to the brain, abdominal cavity and subcutaneous region of nude mice. The results showed that the $CD133^-$ cells were not oncogenic, but that the oncogenic rate of $CD133^+$ cells was 50-100%. To further investigate the effect of CD133 on glioma cells *in vivo*, we inoculated subcutaneously the U251-CD133 and U251-mock cells in the nude mice, respectively, and observed tumor growth. U251-CD133 cells formed subcutaneous tumors earlier, with a higher tumor formation rate and larger tumor size. The U251-CD133 cells at the dose of 3×10^5 and 1×10^5 formed a tumor much larger than that of the U251-mock cells ($P<0.05$). The difference was significant at the dose of 1×10^5 ($P<0.01$). These results indicated that CD133 promoted self-renewal and proliferation of tumor cells *in vivo*.

To conclude, CD133 promoted the growth and proliferation of glioma cells in the neural stem cell culture medium, by upregulating the CSC/TSC-related genes and enhancing the *in-vivo* oncogenicity of glioma cells in nude mice.

REFERENCES

1. Böttger K, Hatzikirou H, Chauviere A, Deutsch A. Investigation of the migration/proliferation dichotomy and its impact on avascular glioma invasion. Math Model Nat Phenom 2012; 7(01):105-35.
2. Bai J, Mei PJ, Liu H, et al. BRG1 expression is increased in human glioma and controls glioma cell proliferation, migration and invasion in vitro. J Cancer Res Clin Oncol 2012; 138(6):991-98.
3. Venugopal C, Hallett R, Vora P, et al. Pyrvinium targets CD133 in human glioblastoma brain tumor-Initiating cells. Clin Cancer Res 2015; 21(23):5324-37.
4. Zhao WP, Chen QX. Effects of HMGB1 on proliferation and apoptosis of human brain glioma CD133 cells. Bratisl Lek Listy 2015; 116(8):480-85.
5. Griguer CE, Oliva CR, Gobin E, Marcorelles P, Benos DJ, Lancaster JR Jr, Gillespie GY. CD133 is a marker of bioenergetic stress in human glioma. PLoS One 2008; 3(11):e3655.
6. Choi SA, Wang KC, Phi JH, Lee JY, Park CK, Park SH, Kim SK. A distinct subpopulation within CD133 positive brain tumor cells shares characteristics with endothelial progenitor cells. Cancer Lett 2012; 324(2):221-30.
7. Bi CL, Fang JS, Chen FH, Wang YJ, Wu J. Chemoresistance of CD133 (+) tumor stem cells from human brain glioma. Zhong Nan Da Xue Xue Bao Yi Xue Ban 2007; 32(4):568-73 (Chinese).
8. Sun B, Wan Z, Shen J, et al. DNA hypomethylation of CD133 promoter is associated with recurrent glioma. Oncol Rep 2016; 36(2):1062-68.
9. Barrantes-Freer A, Renovanz M, Eich M, et al. CD133 Expression is not synonymous to immunoreactivity for AC133 and fluctuates throughout the cell cycle in glioma stem-like cells. PLoS One 2015; 10(6):e0130519.
10. Qin K, Tian G, Li P, et al. Anti-glioma response of autologous T cells stimulated by autologous dendritic cells electrofused with $CD133^+$ or $CD133^-$ glioma cells. J Neuroimmunol 2012; 242(1-2):9-15.
11. Cao CL, Lan F, Shen L. Overexpression of CD133

promotes the phosphorylation of Erk in U87MG human glioblastoma cells. Neurosci Lett 2010; 484(3):210-14.
12. Elsaba TMA, Luisa M P, Robins AR, et al. The stem cell marker CD133 associates with enhanced colony formation and cell motility in colorectal cancer. PLoS One 2010; 5(5):e10714.
13. Beier D, Hau P, Proescholdt M, et al. $CD133^{+}$ and $CD133^{-}$ Glioblastoma-derived cancer stem cells show differential growth characteristics and molecular profiles. Cancer Res 2007; 67(9):4010-5.
14. Milhavet O, Lemaitre JM. Senescent-derived pluripotent stem cells are able to redifferentiate into fully rejuvenated cells. Genes Dev 2011; 25(21):2248-53.
15. Shi Y, Desponts C, Do JT, Hahm HS, Schöler HR, Ding S. Induction of pluripotent stem cells from mouse embryonic fibroblasts by Oct4 and Klf4 with small-molecule compounds. Cell Stem Cell 2008; 3(5):568-74.
16. Riggi N1, Suvà ML, De Vito C, et al. EWS-FLI-1 modulates miRNA145 and SOX2 expression to initiate mesenchymal stem cell reprogramming toward Ewing sarcoma cancer stem cells. Genes Dev 2010; 24(9):916-32.
17. Zhang J, Hao G, Yao C, Hu S, Hu C, Zhang B. Paramagnetic albumin decorated CuInS2/ZnS QDs for CD133+ glioma bimodal MR/fluorescence targeted imaging. J Mater Chem B 2016; 4(23):4110-18.
18. Altaner C. Glioblastoma and stem cells. Neoplasma 2008; 55(5):369-74.
19. Spencer DA, Auffinger BM, Murphy JP, Muroski ME, Qiao J, Gorind Y, Lesniak MS. Hitting a moving target: glioma stem cells demand new approaches in glioblastoma therapy. Curr Cancer Drug Targets 2017; 17(3):236-54.
20. Song WC, Fei XF, Dong J. Preliminary interpretation on the relationship between the phenotype of CD133+ cells and niche in transplanted human glioma in mice. Zhonghua Zhong Liu Za Zhi 2010; 32(8):564-69.
21. Cho JH, Kim AR, Kim SH, Lee SJ, Chung H, Yoon MY. Development of novel imaging agent using peptide-coated gold nanoparticles toward brain glioma stem cell marker CD133. Acta Biomater 2017; 47:182-92.
22. Beier D, Hau P, Proescholdt M, et al. $CD133(^{+})$ and $CD133(^{-})$ glioblastoma-derived cancer stem cells show differential growth characteristics and molecular profiles. Cancer Res 2007; 67(9):4010-5.

EFFECTS OF ACARBOSE AND SIGLITINE ON BLOOD GLUCOSE FLUCTUATION AND ISLET β-CELL FUNCTION IN PATIENTS WITH TYPE 2 DIABETES MELLITUS

RR. WANG[1*], ZM. LV[2*], YP. DAN[2], KY. CHEN[2] and C. ZHANG[2]

[1]Department of Endocrinology, Jiamusi Central Hospital of Heilongjiang Province, Jiamusi, Heilongjiang, China; [2]Department of Endocrinology, The First Affiliated Hospital of Jiamusi University, Jiamusi, Heilongjiang, China

Received September 3, 2018 – Accepted January 8, 2019

[*]These authors contributed equally to this work

The effects of acarbose and sitagliptin on blood glucose fluctuation and islet β-cell function in patients with type 2 diabetes mellitus (T2DM) were studied. One hundred and three patients with poorly controlled T2DM with insulin aspart 30 were selected and randomly divided into three groups: group A [continuous subcutaneous insulin infusion (CSII) treatment group], group B (CSII combined with acarbose treatment), group C (CSII combined with sitagliptin treatment). The treatment lasted for two weeks and the clinical indicators in the three groups were measured. The insulin dosage was adjusted according to the blood glucose statuses of the three groups of patients. In the final three days, 72 h of continuous glucose monitoring (CGM) were carried out, and the OGTT test was performed again. The results showed that the MODD (absolute means of daily difference), intra-day blood glucose fluctuation indices [(24 h MBG (mean blood glucose), LAGE (largest amplitude of glycemic excursions) and MAGE (average blood glucose fluctuation)] and postprandial blood glucose fluctuation indices [PGS (postprandial glucose spike), Δt, PPGE (postprandial glucose excursion) and T (time) total] in group C and group B were significantly lower than those in group A. Compared with group B, the difference in blood glucose fluctuation indices in group C was not statistically significant (P>0.05). The HOMA-islet (homeostasis model assessment of islet) (CP-DM) index and FC-P (Fasting c-peptide) levels in group C and group B were significantly higher than those in group A (P<0.01). The HOMA-IR (CP) index of groups B and C was significantly lower than that of group A (P<0.01), and there was no statistically significant difference between groups B and C (P>0.05). Sitagliptin combined with intensive insulin pump therapy can reduce blood glucose fluctuation throughout the day, reduce insulin dosage, improve islet B cell function and reduce hypoglycemia better than intensive insulin pump therapy alone.

The incidence of type 2 diabetes mellitus (T2DM) is increasing yearly around the world, and its chronic complications gradually increase with the prolongation of disease course (1-3). Strict glycemic control can prevent or delay the occurrence of chronic complications of diabetes (4). Measures of glycated hemoglobin (HbAlc) remain the gold standard for the long-term control of blood glucose in diabetic patients (5, 6). However, an increasing number of studies have shown that blood glucose fluctuations are also a non-negligible indicator of complications and prognosis for diabetic patients

Key words: acarbose; sitagliptin; type 2 diabetes; blood glucose fluctuation; islet β cell function

Corresponding Author:
Dr Chao Zhang,
Department of Endocrinology,
First Affiliated Hospital, Jiamusi University,
No.348 Dexiang Street, Jiamusi,
154002, Heilongjiang, China
e-mail: zhchao754160@163.com

0393-974X (2019)

(7-9). Therefore, even if the overall blood glucose control in T2DM patients is ideal, effective measures should be taken to reduce blood glucose fluctuations (10). This requires considering a reduction of the risk of postprandial blood glucose drift and hypoglycemia in the choice of therapeutic drugs (11, 12). Traditional anti-diabetic drugs have varied limitations, such as weight gain, hypoglycemia and even gastrointestinal reactions. They also differ in reducing blood sugar fluctuations (13-15). Sitagliptin acts as a glucose-dependent insulin to control blood sugar and represents a new class of drugs for the treatment of T2DM. Sitagliptin has been shown to play a role in the regulation of α and β cytokines. It has the advantage of rarely causing adverse reactions, such as hypoglycemia and weight gain (16, 17). As a traditional oral hypoglycemic agent, acarbose has characteristics which include an exact curative effect, fewer side effects and decreased hypoglycemia (18). Therefore, this study seeks to explore the effects, efficacy and safety of acarbose and sitagliptin on blood glucose variability in insulin-treated T2DM patients, and to thus provide a new basis for clinical treatment decisions.

MATERIALS AND METHODS

Patients

One hundred and three patients who were treated at Jiamusi Central Hospital of Heilongjiang Province from October 2016 to May 2018 were selected. All patients were previously diagnosed with T2DM and exhibited poor insulin control. All procedures were approved by the Ethics Committee of Jiamusi Central Hospital of Heilongjiang Province. Participants provided written informed consent prior to the study.

Inclusion criteria: conformance with the 1999 WHO diagnostic criteria for T2DM (19): Symptoms of diabetes + plasma glucose ≥ 11.1 mmol/L (200 mg/dl), or fasting blood glucose ≥ 7.0 mmol/L (126 mg/dl), or (oral glucose tolerance test, OGTT) 2 h blood glucose ≥ 11.1 mmol/L (200 mg/dl). The above steps need to be repeated once for the diagnosis to be established. $19kg/m^2 \leq BMI \leq 35kg/m^2$; age 20-70 years. No oral hypoglycemic agents, antidepressants, salicylic acid preparations or other drugs were used in the month prior to subject selection. Blood glucose control must have been undertaken through diet, exercise therapy and subcutaneous insulin injection (insulin aspart 30, injection 2 or more times) with a stable dosage for more than 6 months, and a fasting plasma glucose (FPG) value between 7.5~16.0mmol/L or HbAlc 7.0%~10%. Selected patients did not participate in any drug trials within the first three months of the trial.

Exclusion criteria: type 1 diabetes; gestational diabetes and diabetes with pregnancy; disease stress state; patients with other endocrine diseases and mental illness such as depression; serious complications; poor compliance.

Screening period

All patients underwent a two-week screening period and discontinued medications that affect blood glucose fluctuations. All subjects were given a daily calorie supply as appropriate. Body weight was measured weekly to keep the weight unchanged. The patients were hospitalized at the end of screening period.

Groups

A total of 103 subjects were randomly divided into three groups: a simple continuous subcutaneous insulin injection group (group A); an acarbose combined with CSII group (group B); and a sitagliptin combined with CSII group (group C).

Group A (34 subjects): T2DM patients only underwent continuous subcutaneous insulin aspart injection (Insulin Aspart 30 Injection [NovoMix 30], Denmark Novo Nordisk A/S), adjusting the basic amount and pre-three-meal insulin dosage; Group B (32 subjects): T2DM patients underwent continuous subcutaneous insulin aspart injection in addition to taking acarbose [Acarbose Tablets [Glucobay], Bayer Vital GmbH, Germany], 50 mg orally three times per day with meals; Group C (37 subjects): T2DM patients underwent continuous subcutaneous insulin injection in addition to taking sitagliptin phosphate tablets [JANUVIA], Merck Sharp & Dohme Pty Ltd, Italy, 100 μg orally three times per day.

At the time of enrollment, the ages, duration, and severities of the three patient groups were similar.

Collection and detection of specimens

All patients discontinued subcutaneous injection of insulin aspart 30 on the day of admission, and each patient then fasted for 8-12 h. On an empty stomach, at 6:00-8:00 in the morning of the second day, blood was taken from the elbow vein to measure FPG, CP, INS (Insulin), HbAlc, liver and kidney function, blood lipid composition, inflammatory markers (hs-CRP). Then, the OGTT test was carried out (82.59 g glucose powder was dissolved in 250-300 ml water, and the patients drank it off in 5 min), and blood sugar was measured after 120 min (2-h postprandial plasma glucose, i.e. 2h PG). INS and C-P specimens were detected by radioimmunoassay in the isotope chamber, and the remaining blood specimens were independently completed by the hospital biochemical laboratory.

Treatment methods

The three groups of patients were then treated with CSII for two weeks. The amount of insulin was adjusted according to the blood sugar condition, so that the blood sugar could reach the standard as much as possible: fasting 3.9~7.0 mmol/L, postprandial blood glucose (2-h postprandial plasma glucose, i.e. 2h PG) 3.9~10.0 mmol/L. In addition, group B was given acarbose 50 mg/time for chewing three times a day. Group C received 100 mg of Sigliptin orally once a day after meals. Seventy-two hours of CGM was performed in the final 3 days. Insulin adjustment program: the patient's body weight (kg) multiplied by 0.4~0.8U body weight (kg) × 0.4~0.8U is the total amount for the whole day; 50% of the total amount was put into the base amount, and 50% was put as the load before the three meals. The insulin base was divided into six periods (0:00~3:00, 3:00~7:00, 7:00~12:00, 12:00~17:00, 17:00~22:00, 22:00~0:00) by the insulin pump (TOP, Japan) for continuous administration to the patient. The dosage of the meal was adjusted according to the insulin sensitivity coefficient 1800 rule, i.e., the insulin sensitivity coefficient (mmol/L) = 1800/(total insulin total × 18). All patients were monitored for blood glucose at eight time points: before breakfast, after breakfast, before lunch, after lunch, before dinner, after dinner, before bedtime and at night at 3:00. Before each evening meal, the basal rate of the insulin pump was adjusted once to bring the blood glucose in line with the standard as quickly as possible (fasting: 3.9~7.0 mmol/L; blood glucose after eating (2h PG): 3.9~10.0 mmol/L).

Dynamic blood glucose monitoring system: On the 11th day of the experiment, the patients wore a dynamic blood glucose monitor (East Instrument Technology Co., Ltd., China) for 72 h CGMS (Continuous Glucose Monitoring System). During this period, fingertip blood glucose before and after the three meals and before bedtime was corrected, while significant events, such as diet, exercise, treatment, and hypoglycemia, were also documented. On the 14th day, the probe was removed in the morning, and the data was extracted for processing.

After 2 weeks, CGMS was used to observe blood glucose control, daily insulin dose, hypoglycemia rates, blood glucose compliance rates, 8 average daily blood glucose profiles and blood glucose fluctuations. At the same time, the biochemical indicators of the three groups of patients were reviewed, the OGTT test was repeated, and measures of the above indicators were repeated.

Blood glucose assessment

Daytime blood glucose variation: MODD (Mean of Daily Differences) represents the mean value of the absolute difference of blood sugar between 2 consecutive days of blood profile at the same time point. The study selected the data from the last 2 days of CGMS treatment, evaluated the MODD after treatment, and calculated the MODD value.

Blood glucose fluctuations during the day: 24 hMBG represents the average of 288 measurements made during the CGMS 24-h monitoring period. LAGE is the difference between the maximum and minimum blood glucose values during the CGMS 24-h monitoring period. MAGE is currently the "gold standard" for assessing intraday blood glucose fluctuations. According to the blood glucose fluctuations of all amplitudes ≤1SD, the patients' 24-h drift amplitudes (AGE) were calculated; drift amplitude was calculated from the drift peak to the valley value. MAGE is the average value of all blood glucose drift amplitudes. In this study, the

blood glucose level monitored for the last 24 hours was selected as the observation index.

Blood sugar fluctuations after meals: PGS represents the highest value of postprandial blood glucose during CGMS monitoring. Δt is the time after the postprandial blood glucose drifts to a peak. PPGE is the difference between the peak postprandial blood glucose and the blood glucose immediately before the meal. Total T represents the total time of blood glucose drift after meals in the day. (upper limit: 11.1 mmol/L low limit: 3.9 mmol/1)

Risk of hypoglycemia: hypoglycemia (final blood glucose below 3.9 mmol/L) during treatment is considered a hypoglycemic event.

Indicator calculations

The incidence of hypoglycemia (%) = (the number of occurrences of MBG ≤ 3.9 mmol/L)/the total number of experimental subjects; Blood glucose compliance rate (%) = number of patients with blood glucose compliance/total number of experimental groups; BMI = weight/height (kg/m^2); Mean change in each metabolic parameter (Δ) = post-treatment level - baseline level; Insulin resistance and islet β cell function: HOMA-IR (CP) = 1.5 + FPG (mmol/L) × fasting C-P (pmol/L)/2800; HOMA-islet (CP-DM) = 0.27 x fasting C-P/(FPG-3.5).

Statistical analysis

The data measured in this study were analyzed using SPSS 22.0 statistical software. Data conforming to normal distribution were represented by mean value ± standard deviation (x ± s) and in cases where data did not conform to a normal distribution, the natural logarithm was converted into a normal distribution and analyzed, including HOMA-IR (CP), HOMA-islet (CP-DM), LAGE, MAGE. The paired *t*-test was used before and after treatment of measurement data. The difference between groups was analyzed by the independent sample *t*-test. The comparison of multiple groups was analyzed by one-way ANOVA. The comparison of the rank data of the counts was performed by the rank sum test and the χ^2 test. $P < 0.05$ was considered statistically significant.

RESULTS

General clinical characteristics statistics

As shown in the data in Table I, there were no significant differences in age, gender, duration of disease, BMI, HbAlc, SBP, or DBP among the three groups (P>0.05). There were no significant differences in biochemical parameters: TG, LDL-C, FPG, 2hPG, hs-CRP, FC-P, HOMA-IR (CP) and HOMA-islet (CP-DM) (P>0.05).

Statistics of biochemical indicators

Table II shows that FPG, 2hPG, TG, and hs-CRP after treatment in group A were significantly lower than those before treatment (P<0.05). FC-P and HOMA-islet (CP-DM) were significantly higher than before treatment (P<0.05). HOMA-IR (C-P) and LdL-C decreased after treatment (P>0.05). There was no significant change before and after HDL-C treatment (P>0.05). FPG, 2hPG, TG, LDL-C, hs-CRP and Homa-IR (C-P) in group B were significantly lower than those before treatment (P<0.05). FC-P and Homa-islet (CP-DM) were significantly higher than before treatment (P<0.05). There was no significant difference before and after HDL-C treatment (P>0.05). The FPG, 2hPG, TG, LDL-C, hs-CRP and Homa-IR (C-P) in group C were significantly lower than those before treatment (P<0.05). FC-P and Homa-islet (CP-DM) were significantly higher than before treatment (P<0.05). There was no significant difference before and after HDL-C treatment (P>0.05).

Comparison of blood lipids and hs-CRP before and after treatment

The TG of groups A, B and C decreased, and the decrease of TG in group C and group B was significantly higher than that in group A (P<0.05). The LdL-C of group A, group B and group C decreased, and the decrease of LdL-C in group C was significantly higher than that in group A (P<0.05). There were no significant differences in the efficacy of the three groups in regulating HdL-C and hs-CRP (P>0.05). Comparison of differences between groups before and after treatment is shown in Table III.

Table I. *Comparison of the general situation and main biochemical indicators of the three groups before intervention.*

Category	Group A	Group B	Group C	P value
Gender (M/F)	14/20	15/17	17/20	0.72
Age	52.33±10.11	55.12±9.53	55.43±10.93	0.34
HbAlc (%)	8.45±2.03	8.68±2.13	8.03±1.84	0.28
Course of disease (year)	6.58±5.83	6.69±4.96	6.14±5.77	0.21
BMI (kg/m^2)	23.67±7.12	24.12±4.56	24.76±6.77	0.38
SBP (mmHg)	118.35±28.13	119.76±28.54	117.58±20.16	0.22
DBP (mmHg)	69.58±16.22	70.15±24.35	69.64±15.65	0.66
FPG (mmol/L)	11.44±7.34	10.76±7.71	11.81±9.14	0.61
2hPG (mmol/L)	16.54±7.76	16.58±9.22	16.89±6.56	0.76
TG (mmol/L)	3.86±0.89	3.91±0.74	3.87±0.79	0.85
LDL-C (mmol/L)	3.32±0.96	3.36±0.87	3.28±0.56	0.91
HDL-C (mmol/L)	1.31±0.35	1.32±0.23	1.29±0.25	0.82
FC-P (pmol/L)	323.46±160.73	326.32±153.62	323.48±119.14	0.66
HOMA-IR(CP)	2.97±0.64	2.95±0.56	3.08±0.65	0.54
HOMA-islet (CP-DM)	16.69±2.75	16.58±2.73	17.04±2.62	0.56
Hs-CRP (mg/dL)	1.84±0.33	1.82±0.19	1.88±0.39	0.91

M: male; F: female; TG: triglyceride; LDL-C: low density lipoprotein cholesterol; HDL-C: high-level data link control; SBP: systolic blood pressure; DBP: diastolic blood pressure

Table II. *Comparison of biochemical indicators before and after treatment in each group.*

Group	Category	Before treatment	After treatment	P value
A	FPG(mmol/L)	11.44±7.34	6.45±1.15*	<0.001
	2hPG(mmol/L)	16.54±7.76	9.122±2.31*	<0.001
	TG(mmol/L)	3.86±0.89	3.51±0.64*	0.03
	LDL-C(mmol/L)	3.32±0.96	2.88±0.62	0.05
	HDL-C(mmol/L)	1.31±0.35	1.27±0.16	0.33
	FC-P(pmol/L)	323.46±160.73	381.21±214.65*	<0.001
	Homa-IR(CP)	2.97±0.64	2.68±0.48	0.12
	Homa-islet(CP-DM)	16.69±2.75	26.28±11.45*	<0.001
	Hs-CRP(mg/dL)	1.84±0.33	1.60±0.41*	0.04
B	FPG(mmol/L)	10.76±7.71	5.65±1.12*	<0.001
	2hPG(mmol/L)	16.58±9.22	7.82±2.04*	<0.001
	TG(mmol/L)	3.91±0.74	3.35±0.53*	0.003
	LDL-C(mmol/L)	3.36±0.87	2.77±0.68*	0.04
	HDL-C(mmol/L)	1.32±0.23	1.39±0.36	0.43
	FC-P(pmol/L)	326.32±153.62	387.37±172.86*	<0.001
	Homa-IR(CP)	2.95±0.56	2.46±0.43*	0.003
	Homa-islet(CP-DM)	16.58±2.73	28.13±15.16*	<0.001
	Hs-CRP(mg/dL)	1.82±0.19	1.56±0.27*	0.01
C	FPG(mmol/L)	11.81±9.14	5.81±0.93*	<0.001
	2hPG(mmol/L)	16.89±6.56	7.72±2.05*	<0.001
	TG(mmol/L)	3.87±0.79	3.31±0.63*	0.008
	LDL-C(mmol/L)	3.28±0.56	2.96±0.75*	0.04
	HDL-C(mmol/L)	1.29±0.25	1.47±0.23	0.08
	FC-P(pmol/L)	323.48±119.14	391.34±201.63*	<0.001
	Homa-IR(CP)	3.08±0.65	2.549±0.52*	<0.001
	Homa-islet(CP-DM)	17.04±2.62	28.62±10.63*	<0.001
	Hs-CRP(mg/dL)	1.88±0.39	1.43±0.27*	0.005

**P<0.05 in comparison of before- and after-treatment values.*

Table III. *Comparison of biochemical indicators before and after treatment in group B.*

Category	Before treatment	After treatment	P value
FPG (mmol/L)	10.76±7.71	5.65±1.12*	<0.001
2hPG (mmol/L)	16.58±9.22	7.82±2.04*	<0.001
TG (mmol/L)	3.91±0.74	3.35±0.53*	0.003
LDL-C (mmol/L)	3.36±0.87	2.77±0.68*	0.04
HDL-C (mmol/L)	1.32±0.23	1.39±0.36	0.43
FC-P (pmol/L)	326.32±153.62	387.37±172.86*	<0.001
HOMA-IR (CP)	2.95±0.56	2.46±0.43*	0.003
HOMA-islet (CP-DM)	16.58±2.73	28.13±15.16*	<0.001
Hs-CRP (mg/dL)	1.82±0.19	1.56±0.27*	0.01

**P<0.05 compared with before and after treatment.*

Table IV. *Comparison of hypoglycemia rate and blood glucose compliance rate in the three groups after treatment.*

Category	Group A	Group B	Group C	P value
Hypoglycemia rate	15.2%	3.9%	0%*	0.07
Blood glucose compliance rate	69.8%	84.9%	92.3%*	0.08

*Groups B and C are compared with group A, *P < 0.05.*

Comparison of islet β-cell function related indexes before and after treatment

In terms of insulin resistance, the HOMA-IR (CP) index of the three groups decreased. Group B and C were significantly higher than group A (P<0.01), but there was no significant difference between group C and group B (P>0.05). In terms of islet β cell secretory function, the HOMA-islet (CP-DM) index and FC-P level of the three groups were elevated. The HOMA-islet (CP-DM) index and FC-P level in group B and group C were significantly higher than those in group A (P<0.01). There was no statistical difference between the elevated levels of HOMA-islet (CP-DM) and FC-P in group C (P>0.05). Comparison of islet function in the three groups after treatment is shown in Table IV.

Comparison of blood glucose control and insulin dosage after treatment

The FPG and blood glucose levels 2 h after meals were significantly lower in group B and group C after 2 weeks of treatment (P<0.05). Group C was not inferior to group B in terms of blood glucose control (P>0.05). In addition, the three groups of initial insulin levels were approximately the same. After 2 weeks of treatment in the three groups, it was found that the total amount of insulin used in group B and group C was significantly lower than that in group A (P<0.05). The difference between group B and group C was not significant (P>0.05). Comparison of blood glucose control and insulin dosage in three groups after treatment is shown in Fig. 1.

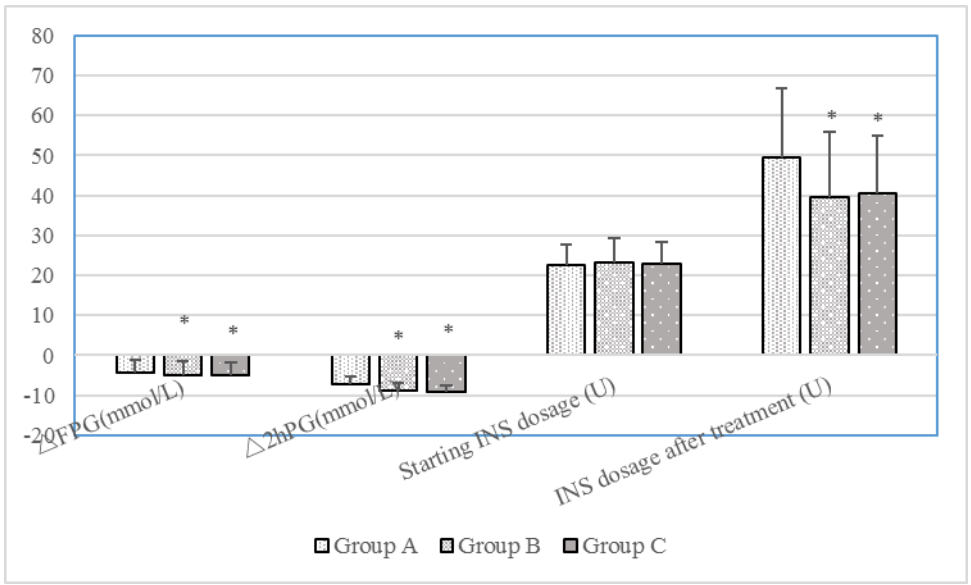

Fig. 1. *Comparison of blood glucose control and insulin dosage in the three groups after treatment (Groups B and C compared with group A, *P<0.05)*

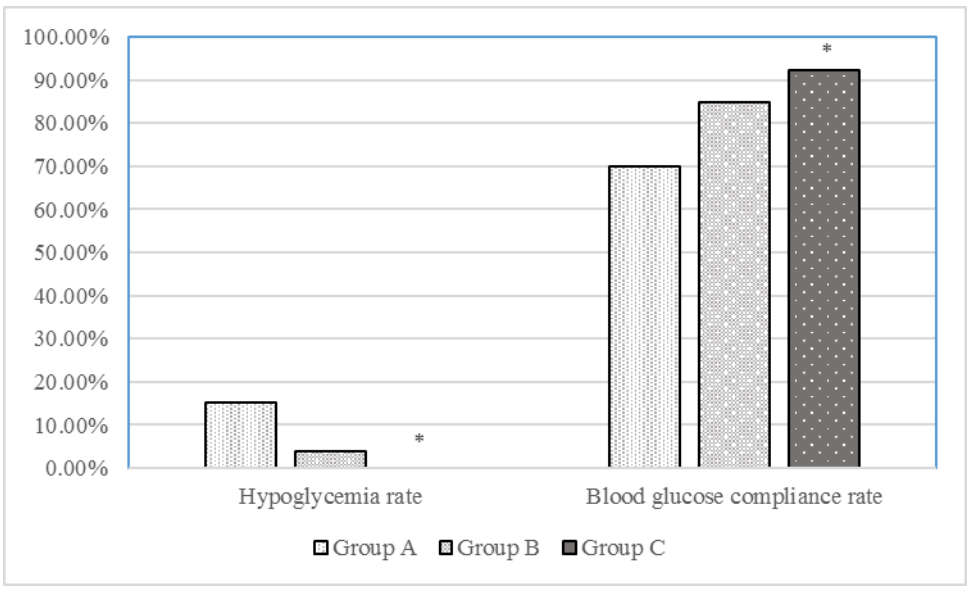

Fig. 2. *Comparison of hypoglycemia rate and blood glucose compliance rate between the three groups after treatment (Groups B and C are compared with group A, *P<0.05)*

Comparison of hypoglycemia rate and blood glucose compliance rate after treatment

The blood glucose compliance rate of group C was significantly better than that of group A (P<0.05), and the incidence of hypoglycemia was lower than that of group A (P<0.05). There was no significant difference in the rate of blood glucose compliance and hypoglycemia between group B and group C (P>0.05). Comparison of hypoglycemia rate and blood glucose compliance rate between the two groups after treatment is shown in Fig. 2.

Comparison of CGMS indicators

Blood glucose fluctuations in daytime and intraday:

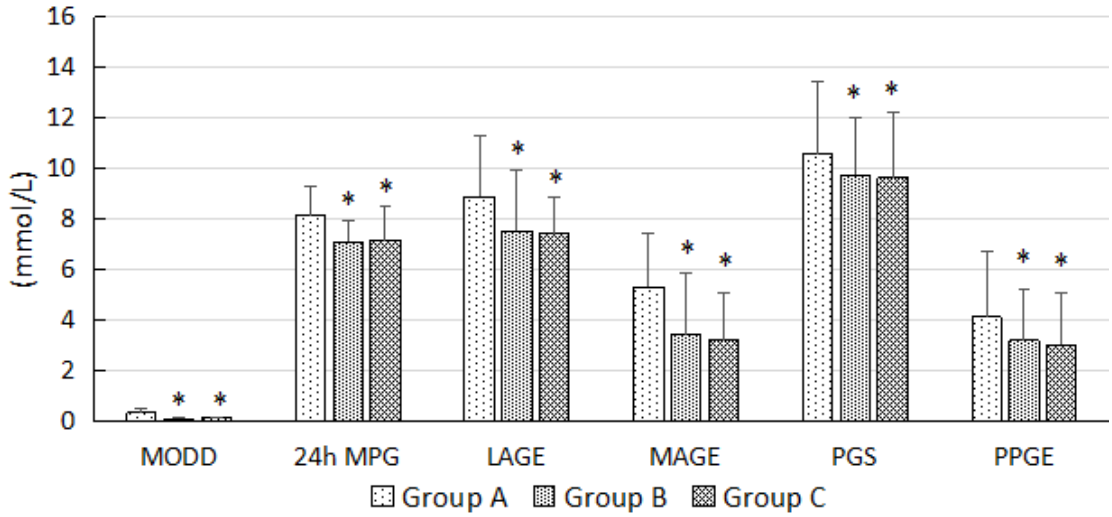

Fig. 3. *Indicators of blood glucose fluctuations during daytime, intraday, and after meal by CGMS in the three groups after treatment (Groups B and C are compared with group A, *P<0.05).*

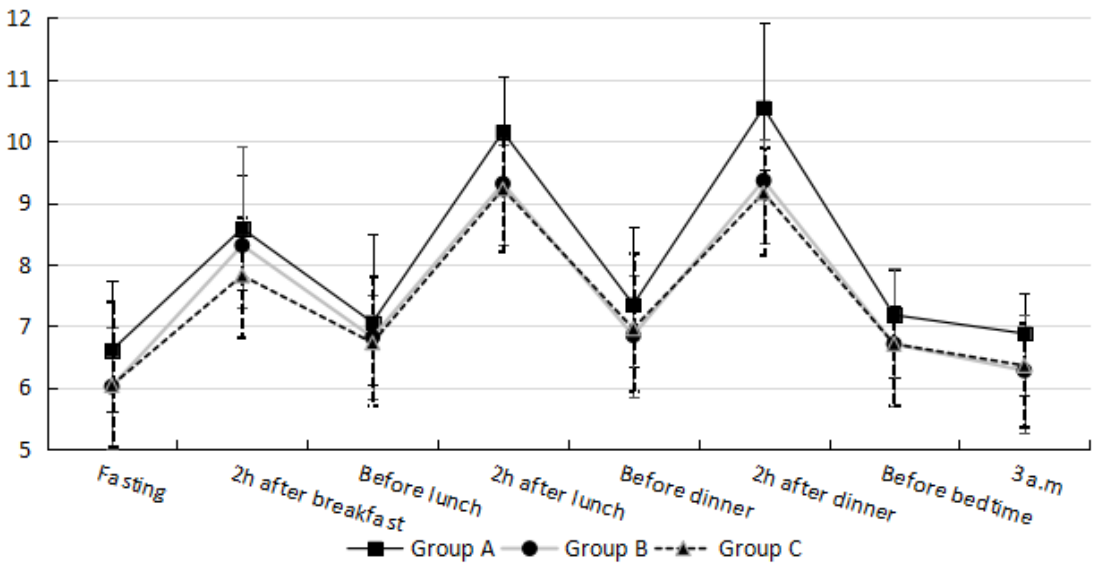

Fig. 4. *Comparison of blood glucose profiles in the three groups after treatment*

After 2 weeks of treatment, the 24-h MBG, LAGE and MAGE of groups B and C were significantly lower than group A (P<0.01). There was no significant difference between group B and group C (P>0.05).

Blood glucose fluctuations after meals: After 2 weeks of treatment, the total PGS, PPGE, Δt (Group A: 68.44±25.35; Group B: 58.53±20.43; Group C: 57.37±21.37) and T (Group A: 189.34±21.28; Group B: 169.17±19.96; Group C: 170.02±20.38) in group B and group C were significantly lower than those in group A (P<0.001). There was no significant difference between group B and group C (P>0.05). Indicators of blood glucose fluctuations during daytime, intraday, and after meal by CGMS in the three groups after treatment is shown in Fig. 3.

Comparison of blood glucose profiles after treatment

After treatment, the blood glucose levels of

groups B and C were lower than those of group A while fasting, before going to bed, and at 3:00 am ($P<0.05$). There was a significant decrease in blood glucose at 2 h after lunch and 2 h after dinner ($P<0.01$). The blood glucose at 2 h after the morning meal in group C was significantly lower than that in group B and in group A ($P<0.05$). The specific data is shown in Fig.4.

DISCUSSION

The blood sugar of normal people shows fluctuations; 10 minutes after the start of a meal, the blood glucose concentration begins to rise, and the blood glucose concentration reaches a peak within 1 hour after the meal. T2DM patients exhibit excessive shifts in blood glucose for a longer period, with a delay in blood glucose spikes (20, 21). MODD is the absolute value of the difference between the corresponding measured values within two consecutive days; the average value was then calculated (22, 23).

GLP-1 has a potential protective effect on the morphology and function of islet β cells and prevents β cell apoptosis (24-26). This may be related to the effect of sitagliptin on controlling the blood glucose concentration by increasing the concentration of GLP-1 and preventing the apoptosis of β cells, thereby ensuring the secretion of insulin (27, 28).

In summary, this study demonstrates that insulin combined with sitagliptin is not inferior to the combined application of acarbose, but it can more smoothly lower blood glucose and reduce its fluctuation throughout the day. At the same time, the risk of gastrointestinal side effects and hypoglycemia is lower, and sitagliptin has potential cardiovascular protective effects. Therefore, the combination of sitagliptin in patients with poorly controlled insulin aspart 30 is an optimal treatment for diabetes and is worthy of clinical application.

ACKNOWLEDGEMENTS

This work was supported by Jiamusi University Science and Technology School Level Project (13Z1201550).

REFERENCES

1. Elmore LK, Baggett S, Kyle JA, Skelley JW. A review of the efficacy and safety of canagliflozin in elderly patients with type 2 diabetes. Consult Pharm 2014; 29(5):335-46.
2. Copeland KC, Silverstein J, Moore KR, et al. Management of newly diagnosed type 2 Diabetes Mellitus (T2DM) in children and adolescents. Pediatrics 2013; 131(2):364-82.
3. Schober E, Rami B, Grabert M, et al. Phenotypical aspects of maturity-onset diabetes of the young (MODY diabetes) in comparison with Type 2 diabetes mellitus (T2DM) in children and adolescents: experience from a large multicentre database. Diabet Med 2009; 26(5):466-73.
4. Ridderstråle M, Jensen MM, Gjesing RP, Niskanen L. Cost-effectiveness of insulin detemir compared with NPH insulin in people with type 2 diabetes in Denmark, Finland, Norway, and Sweden. J Med Econ 2013; 16(4):468-78.
5. Ryskjaer J, Deacon CF, Carr RD, Krarup T, Madsbad S, Holst J, Vilsbøll T. Plasma dipeptidyl peptidase-IV activity in patients with type-2 diabetes mellitus correlates positively with HbAlc levels, but is not acutely affected by food intake. Eur J Endocrinol 2006; 155(3):485-93.
6. Pareek A, Chandurkar N, Thomas N, et al. Efficacy and safety of hydroxychloroquine in the treatment of type 2 diabetes mellitus: a double blind, randomized comparison with pioglitazone. Curr Med Res Opin 2014; 30(7):1257-66.
7. Nowicki M, Rychlik I, Haller H, Warren ML, Suchower L, Gause-Nilsson I; D1680C00007 Investigators. Saxagliptin improves glycaemic control and is well tolerated in patients with type 2 diabetes mellitus and renal impairment. Diabetes Obes Metab 2011; 13(6):523-32.
8. Urrutia-Rojas X, Menchaca J, Wadley W, et al. Cardiovascular risk factors in Mexican-American children at risk for type 2 diabetes mellitus (T2DM). J Adolesc Health 2004; 34(4):290-99.
9. Souto SB, Souto EB, Braga DC, Medina JL. Prevention and current onset delay approaches of type 2 diabetes mellitus (T2DM). Eur J Clin Pharmacol 2011; 67(7):653-61.

10. Kosmalski M, Drozdowska A, Sliwinska A, Drzewoski J. Inappropriate metformin prescribing in elderly type 2 diabetes mellitus (T2DM) patients. Adv Med Sci 2012; 57(1):65-70.
11. Klimontov VV, Tyan NV, Fazullina ON, Myakina NE, Orlov NB, Konenkov VI. [Acute-phase serum proteins and adipocytokines in women with type 2 diabetes mellitus: Relationships with body composition and blood glucose fluctuations]. Ter Arkh 2016; 88(10):35-41.
12. Maggi D, Bordone C, Briatore L, et al. Glucose-targeted therapy for subjects with type 2 diabetes mellitus: primum non nocere. Eur J Clin Invest 2017; 47(10):691-93.
13. Adeniyi OV, Yogeswaran P, Longo-Mbenza B, Ter Goon D. Uncontrolled hypertension and its determinants in patients with concomitant type 2 diabetes mellitus (T2DM) in rural South Africa. PLoS One 2016; 11(3):e0150033.
14. Azzi M, Constantino M, Pont L, Mcgill M, Twigg S, Krass I. Medication Safety: an audit of medication discrepancies in transferring type 2 diabetes mellitus (T2DM) patients from Australian primary care to tertiary ambulatory care. Int J Qual Health Care 2014; 26(4):397-403.
15. Cho M, Park JS, Nam J, et al. Association of Abdominal Obesity with Atherosclerosis in Type 2 Diabetes Mellitus (T2DM) in Korea. J Korean Med Sci 2008; 23(5):781-88.
16. Iwamoto Y, Taniguchi T, Nonaka K, Okamoto T, Okuyama K, Arjona Ferreira JC, Amatruda J. Dose-ranging efficacy of sitagliptin, a dipeptidyl peptidase-4 inhibitor, in Japanese patients with type 2 diabetes mellitus. Endocr J 2010; 57(5):383-94.
17. McGuire DK, Van de Werf F, Armstrong PW, et al. Association between sitagliptin use and heart failure hospitalization and related outcomes in type 2 diabetes mellitus: secondary analysis of a randomized clinical Trial. JAMA Cardiol 2016; 1(2):126-35.
18. Willms B, Ruge D. Comparison of acarbose and metformin in patients with Type 2 diabetes mellitus insufficiently controlled with diet and sulphonylureas: a randomized, placebo-controlled study. Diabet Med 1999; 16(9):755-61.
19. Davidson MB, Schriger DL, Peters AL, Lorber B. Relationship between fasting plasma glucose and glycosylated hemoglobin: potential for false-positive diagnoses of type 2 diabetes using new diagnostic criteria. JAMA 1999; 281(13):1203-10.
20. Whittaker A, Dinu M, Cesari F, et al. A khorasan wheat-based replacement diet improves risk profile of patients with type 2 diabetes mellitus (T2DM): a randomized crossover trial. Eur J Nutr 2017; 56(3):1191-200.
21. Del Prato S, Tiengo A. The importance of first-phase insulin secretion: implications for the therapy of type 2 diabetes mellitus. Diabetes Metab Res Rev 2001; 17(3):164-74.
22. Schipf S, Werner A, Holle R, et al. P2-269 Regional differences in the prevalence of type 2 diabetes mellitus: results from five population-based cohort studies in Germany (DIAB-CORE consortium). 2011, 65(Suppl 1):A296-A296.
23. Kelly J, Edney K, Moran C, et al. Gender differences in physical activity levels of older people with type 2 diabetes mellitus. Diabet Med 2012; 29(7):e88-95.
24. Salehi M, Gastaldelli A, D'Alessio DA. Altered islet function and insulin clearance cause hyperinsulinemia in gastric bypass patients with symptoms of postprandial hypoglycemia. J Clin Endocrinol Metab 2014; 99(6):2008-17.
25. Young A. Inhibition of glucagon secretion.Adv Pharmacol 2005; 52:151-71.
26. Ahlkvist L, Omar B, Valeur A, Fosgerau K, Ahrén B. Defective insulin secretion by chronic glucagon receptor activation in glucose intolerant mice. J Endocrinol 2016; 228(3):171-78.
27. Røge RM, Klim S, Ingwersen SH, et al. The Effects of a GLP-1 analog on glucose homeostasis in type 2 diabetes mellitus quantified by an integrated glucose insulin model. CPT Pharmacometrics Syst Pharmacol 2015; 4(1):e00011.
28. Østergaard L, Frandsen CS, Madsbad S. Treatment potential of the GLP-1 receptor agonists in type 2 diabetes mellitus: a review. Expert Rev Clin Pharmacol 2016; 9(2):241-65.

INHIBITION OF THE NF-κB SIGNALING PATHWAY ON ENDOTHELIAL CELL FUNCTION AND ANGIOGENESIS IN MICE WITH ACUTE CEREBRAL INFARCTION

X. SUI

The Second Internal Medicine-Neurology, The Third Affiliated Hospital of Qiqihar Medical University, Tiefeng District, Qiqihar City, Heilongjiang Province, China

Received January 13, 2019 – Accepted January 30, 2019

This study was aimed to investigate whether interferon (IFN)-induced protein 35 (IFI35) affects the signaling pathway of nuclear factor-kappa B (NF-κB) and to observe the effect of different expressions of IFI35 on the proliferation of endothelial cells and angiogenesis in rats with acute cerebral infarction. A suture method was adopted to prepare a mouse model of permanent middle cerebral artery occlusion (PMCAO). After the treatment of cerebral artery occlusion in 200 healthy male mice (weighting 20g-40g), 47 mice were selected and the double luciferase assay was used to identify different structural domains of IFI35; for the remaining 153 mice, RT-PCR and immunohistochemical assays were used to detect the mRNA expression of glioma-associated oncogene homolog 1 (Gli1), vascular endothelial growth factor (VEGF), basic fibroblast growth factor (bFGF), and CD105 (endoglin). The results showed that IFI35 could reduce the level of p65 protein (REL-A) in the nucleus while affecting the production of p-p65 in the cytoplasm. At the same time, IFI35 could be used in combination with a NID1 protein domain + Nmi protein to inhibit the signaling pathway of NF-κB. Expressions of Gli1, VEGF, bFGF, and CD105 in the IFI35 treatment group were all significantly reduced (P<0.05). In conclusion, IFI35 could suppress the activation of the NF-κB signaling pathway, reduce the proliferating potential of vascular endothelial cells, and lower the expression of vascular growth factors, thereby inhibiting angiogenesis in mice with acute cerebral infarction.

Cerebrovascular diseases (1) are caused by the abnormal growth of cerebral blood vessels, which directly lead to the dysfunction of brain function. Recently, the incidence of cerebrovascular diseases is on the rise, due to the acceleration in population aging, and the average age of these patients is becoming younger. As a major type of cerebrovascular diseases, ischemic cerebrovascular disease (2) is caused by a short pause in brain activity resulting in serious damage to the blood supply of the brain tissue. Among all brain components, the cerebral cortex has a larger blood flow and therefore is more sensitive to ischemia and hypoxia.

Cerebrovascular endothelial cells (3) play an important role in maintaining the homeostasis of the vascular system. Fang et al. (4) confirmed that endothelial cells can promote the excessive hyperplasia of vascular intima and lead to arterial endothelial cell injury, which in turn can lead to platelet aggregation (5), blood vessel thrombosis, inflammatory reactions, infiltration of smooth muscle cells into the intima, and excessive proliferation of vascular endothelial cells. The studies of Heiss et al. have confirmed (6) that damage to endothelial

Key words: IFI35; NF-κB signaling pathway; endothelial cells; angiogenesis; inhibition

Corresponding Author:
Dr Xin Sui,
The Second Internal Medicine-Neurology,
The Third Affiliated Hospital, Qiqihar Medical University,
Tiefeng District, Taishun Street No 27,
Qiqihar City 161000, Heilongjiang Province, China
e-mail: suixin_neuro@163.com

0393-974X (2019)

cells induced the release of a large number of active transcription factor nuclear factor-kappa B (NF-κB) from microglia and I-kappa B protein from neurons. The binding of active NF-κB and the target gene locus on DNA can induce the activation of tumor necrosis factor (TNF-α) and the proliferation of immune inflammatory cells, microglia and astrocytes, and promote recruitment of white blood cells to the nervous system, which can initiate inflammatory cascade reaction, further enhancing brain damage. Therefore, inhibiting the signal pathway of NF-κB can reduce the brain damage caused by endothelial cell injury.

According to Kiefel et al.'s report (7), the expression of molecules involved in the NF-κB signaling pathway is increased after cerebral ischemia, suggesting that NF-κB signal is activated in ischemic brain tissues after cerebral infarction. Using ischemic models, including myocardial ischemia models and arterial ischemia models, Li et al. confirmed (8) that the NF-κB signaling pathway can promote the formation of blood vessels, while the use of exogenous solvents can promote the conduction of NF-κB signal, thus promoting the proliferation of vascular endothelial cells and accelerating the regeneration of blood vessels (9). In fact, many growth factors and cytokines, including Gli1 (10), VEGF (vascular endothelial growth factor) (11), bFGF (b fibroblast growth factor) (12) and CD105 (13), are involved in the process of blood vessel regeneration. As an interference protein (14) which can reduce the incidence of inflammatory reactions upon viral infection (15), IFI35 can alleviate rheumatoid arthritis (16, 17), Sezary syndrome (18) and appendicitis (19) by reducing inflammatory reactions and enhancing the immunity of patients. It is confirmed that IFI35 plays an important role in antivirus-related immune inflammation. Meanwhile, immune inflammation plays an important role in endothelial cell proliferation and angiogenesis after vascular endothelial cell injury. Therefore, it is hypothesized that IFI35 may participate in cell proliferation and angiogenesis after endothelial cell injury. In order to verify the hypothesis, the effect of IFI35 expression on the proliferation of endothelial cells and angiogenesis was studied in mice with acute cerebral infarction in this study.

MATERIALS AND METHODS

Animals

Two hundred healthy male BALB/c mice (weight, 20-40g; age, 15 weeks) were selected and housed in a ventilated environment with sufficient food and water. All mice were fasted for 10-12 h before surgery. The feeding conditions of mice were as follows: room temperature 19-24°C, noise less than 60 dB, humidity 50%-60%, illumination 12 h/d, autoclave sterilization of feed and cushion, and strictly-pasteurized drinking water. All mice were provided by the laboratory animal center of our college and all mice experiments were approved by the medical ethics committee of The Third Affiliated Hospital of Qiqihar Medical University.

The external carotid artery (ECA) and its branches were blocked without exposing the pterygopalatine artery (PPA). The extracranial blood supply was cut off, and the internal carotid artery (ICA) was obstructed by suspending braided thread and clamping the artery. Finally, ECA was inserted by the embolism line, which leads to cerebral artery occlusion in mice. After weighing, mice were anesthetized by intraperitoneal injection of 12% chloral hydrate at a dose of 0.4ml/85g. Forty-seven mice were randomly selected, and the head skin was cut open to quickly extract endothelial cells from cerebral artery vessels. The effect of IFI35 on the proliferation of vascular endothelial cells was investigated by inhibiting the NF-κB signaling pathway with different protein domains of IFI35. The other 153 mice were randomly divided into sham operation group, cerebral infarction model group and IFI35 treatment group, with 51 mice in each group. The mice in various groups were subjected to different periods of ischemia, namely 8 h, 24 h and 48 h, respectively. Among these mice, the mice in the IFI35 treatment group received an injection of 0.16mg/kg IFI35 into the cerebral artery at the time of ischemia, while the same dose of solvent was injected into the mice of the sham operation and model groups. The mRNA expression of Gli1, VEGF, bFGF and CD105 in cerebral ischemic cortex was then detected by RT-PCR and immunohistochemical assays.

Model setting of experimental mice

The mice were then fixed on the operating table and a 2 cm incision was opened in the middle of the neck under conventional conditions to isolate various glands, muscles,

aponeurosis, vagus nerves and left common carotid arteries (CCAs). In the bifurcation of the left carotid artery, the interior carotid artery (ICA) and the exterior carotid artery (ECA), the main artery of the left external carotid artery was isolated. Subsequently, both ends of each artery were clamped with arteriole clamps, while the separated left main artery was clamped with an arteriole clamp and bandaged. A small incision was then made using a small scalpel at the bifurcation of the common carotid artery and about 2 mm away from the heart, and a bolted fishing line was inserted into the incision to connect the common carotid artery with the internal carotid artery. The distal end of the fishing line was about 16 mm away from the total bifurcation of the neck. After reaching an obstacle, the fishing line was inserted into the left cerebral aorta of the mice before the incision was sutured. In the experiment to analyze the effect of IFI35 on neovascularization, the mice in the model and IFI35 groups were subjected to the same procedure described above. For mice in the sham operation group, the same procedure was also used except that their blood vessels were separated without inserting the bolted fishing line.

Fluorescence staining of immune cells

Endothelial cells were collected and infected with an adenovirus vector carrying siRNA. After 48 h of culture, a single cell suspension was obtained by trypsinization, centrifugation and resuspension. Subsequently, the single cell suspension was washed by phosphate buffered saline (PBS), fixed in 5 ml of 5% paraformaldehyde for 1 h, blocked for 1 h with a mixture of 500 µl of Triton-X100 solution (Sigma, Germany) and 500 µl of bovine serum albumin (BSA) solution (Shanghai Biotech Co., Ltd.), and then stained with 200 µl of 1% p65 antibody solution (CST, USA) at 4°C for 24 h. After PBS washing, the samples were stained with a 0.5% goat anti-rabbit fluorescence antibody solution in a 37□ and 5% CO_2 cell culture incubator (Thermo Scientific, USA). Finally, the samples were washed by a Tris Buffered Saline Tween (TBST) solution (Shanghai Biotech Co., Ltd., China), stained with 200 µl of DAPI (4',6-diamidino-2-phenylindole) staining solution (Gibco, USA) in the dark for 15 min, and evaluated with fluorescence quantitative PCR (ABI, USA).

Extraction of nucleoprotein and cytoplasmic protein of endothelial cells

Endothelial cells were infected by an adenovirus vector carrying si-RNA for 48 h, digested by trypsin, centrifuged and resuspended in a complete culture medium (DMEM, Gibco, USA) to obtain a single-cell suspension. Then, CER I and CER II solutions were added into the single-cell suspension, incubated on a high-speed shaker for 10 s and placed on ice for 2 min before the mixture was centrifuged at 16000 g to obtain cytoplasmic protein. Another part of the single-cell suspension was incubated with a NER solution on a high-speed shaker at 4°C for 30 min and then centrifuged to obtain nuclear protein.

Construction of an IFI35 plasmid and a corresponding mutant with deletions

Using the pCMV-C-His plasmid as a template, an IFI35 plasmid (Santa Cruz, USA) was constructed with homologous recombination and a ClonExpress II One Step Cloning Kit Enzymes Hind III and Xho I were used for restriction digestion and a pCMV-C-His vector (Abcam, USA) was linearized in the next step of recombination reaction. Then, the purified IFI35 plasmid was cloned into the pCMV-C-His plasmid using homologous recombination to create a pCMV-C-IFI35 plasmid, which was used as the template for structural deletion of IFI35. Homologous recombinant primers were designed for the region of deletion, while plasmid sequences were amplified with PCR, followed by homologous recombination to obtain the complete plasmid.

Cell growth analysis and double luciferase assay

A "blood/tissue/cell genome extraction kit" produced by Tiangen Biotech Co., Ltd. was used for DNA extraction from cells. A dual Luciferase reporter plasmid was constructed using a pGL3-Basic plasmid as the blank vector and a pGL-Control plasmid as the control vector. A Dual-Luciferase Reporter Assay kit was used for the detection of luciferase activity following the instruction of the kit.

Determination of Gli1 mRNA expressions in the occlusion cerebral cortex of mice using RT-PCR

PCR (Transgene, USA) amplification was carried out for Gli-1 and GLYPD mRNA (glyceraldehyde-3-phosphate dehydrogenase, Proteintech, USA). In brief, 10 µl of RNA samples were mixed in 2 ml of Diethylpyrocarbonate (DEPC) water before the absorbance value of the solution was used to calculate the concentration of isolated RNA. Subsequently, 10 µl of RNA samples were mixed with 2 µl of Anchored

Oligo, an ES Reaction Mix, an EasyScript RT/RI Enzyme Mix, and 20 μl of DEPC water for reverse transcription to amplify mRNA of Gli-1 and GLYPD. Finally, the RT-PCR product was loaded onto an agarose gel for electrophoresis and image analysis (Shanghai Bio-Tech Co., Ltd, China) to determine the mRNA expression of Gli-1.

Determination of protein expressions of VEGF, bFGE and CD105 in the occlusion cerebral cortex of mice by immunohistochemistry

Mice in the sham operation group, model group and IFI35 group were given secondary anesthesia before their limbs were disinfected with normal saline. When the limbs of the mice became white, their brain was taken out to cut off and place the left side with cerebral infarction in a 5% paraformaldehyde solution for fixation. Subsequently, paraffin sections were obtained by paraffin embedding, stained with xylene, and then treated with ethanol, a citric acid antigen repair solution, hydrogen peroxide and other solutions. During the staining process, VEGF antibody with a dilution ratio of 1: 250 (Santa Cruz, Usa), bFGF antibody with a dilution ratio of 1: 200 (Santa Cruz, USA) and CD105 antibody with a dilution ratio of 1:200 (Santa Cruz, USA) were added. Finally, the stained sections were placed under a microscope (Olympus, Japan) for analysis of integrated option density (IOD).

Statistical analysis

SPSS17.0 statistical software was used for data analysis. The experimental data were expressed as x±s. One-Way ANOVA was used for data comparison among different groups. $P<0.05$ indicated that the difference was statistically significant.

RESULTS

Inhibition of the NF-kB signaling pathway by IFI35

An Ov-IFI35 adenovirus vector overexpressing IFI, an Ovad control adenovirus vector, an adenovirus vector carrying IFI35 si-RNA (si-IFI35), and an adenovirus vector carrying control si-RNA (si-Co) were used in this study. P65 is an important transcription factor of the NF-κB signaling pathway. In Fig. 1(A), p65 was expressed in both the nucleus and cytoplasm. Overexpression of IFI35 in vascular endothelial cells inhibited the translocation of p65 into the nucleus, and the inhibition of IFI35 promoted the translocation. Therefore, to clarify

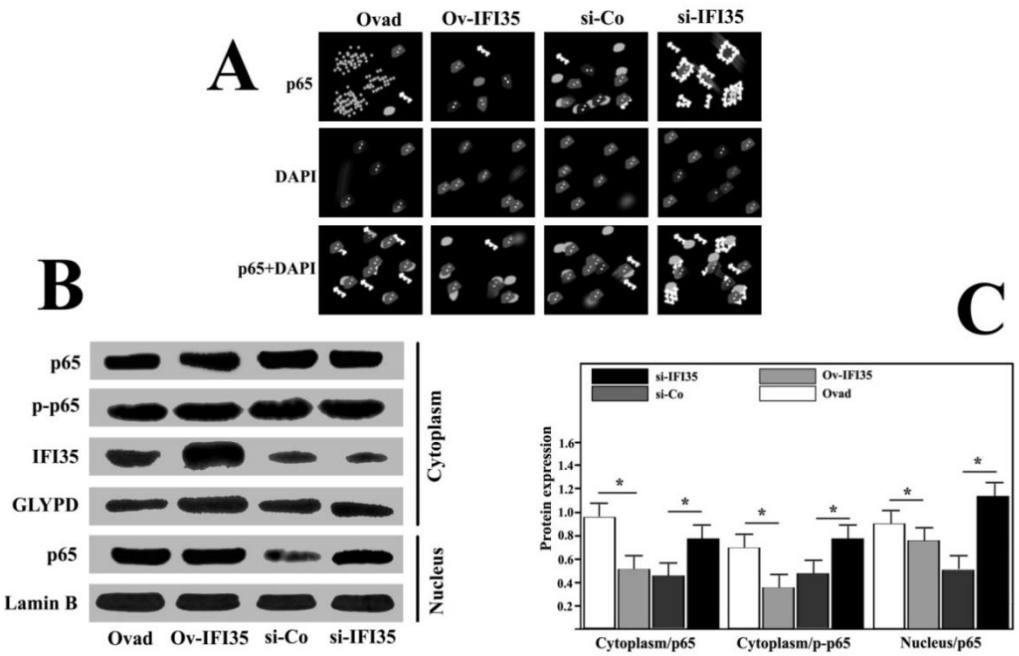

Fig. 1. *The NF-κB signaling pathway was inhibited by IFI35.* ***A****) Expression of IFI35 was regulated in endothelial cells.* ***B****) Effect of IFI35 on the nucleation of p65.* ***C****) Expressions of p65/p-p65 in the cytoplasm and nucleus, *P<0.05*

whether IFI35 suppresses the activation of the NF-kappa B signaling pathway, the cytoplasmic and nuclear distribution of p65 protein was analyzed and is shown in Fig. 1, B and C. When IFI35 was overexpressed, the expression of p65 was decreased in the nucleus and cytoplasm. When the expression of IFI35 was lowered, the expression of p65 in the nucleus and cytoplasm was increased along with an increased cytoplasmic expression of p-p65 (CST, USA), suggesting that IFI35 inhibited the activation of the NF-κB signaling pathway.

Effect of NF-κB signaling pathway inhibition on IFI35-mediated endothelial cell proliferation

When IFI35 was lowered, the number of endothelial cells was significantly increased after the introduction of a PDTC inhibitor (Sigma, Germany) to inhibit IFI35 expressions (Fig. 2A). The number of bright spots was increased while the proliferation ability of endothelial cells was decreased when a PDTC inhibitor was added (Fig. 2A). Fig. 2B shows that this trend became more obvious. After the inhibition of IFI35 by PDTC, the proportion of active endothelial cells was significantly higher than that of the si-RNA control and si-IFI35 groups ($P<0.05$).

Inhibition of the NF-κB signaling pathway by IFI35 via interaction between its NIDI and Nmi protein domains

In Fig. 3, the 1-290 amino acid segment represents the complete sequence of IFI35; the 5-26 amino acid segment represents the leucine-zipper domain of leucine; the amino acid segment of 9-80 represents the structural domain of N-terminus; the amino acid segment of 81-172 represents the structural domain of NID1, and the amino acid segment of 183-268 represents the structural domain of NID2.

The effect of IFI35 on suppressing the NF-κB signaling pathway was analyzed by deleting different structural domains of IFI35 (Fig. 4). When Leucine-zipper, N-terminus, and NID2 domains were deleted, the inhibitory effect of IFI35 on p65 and p-p65 was not affected. When NID1 domain was deleted, the inhibitory effect of IFI35 on p65 and p-p65 was significantly reduced (Fig. 4, A and B).

The effect of deleting the structural domains of IFI35 on NF-κB transcription was analyzed (Fig 4C). It was found that the deletion of N-terminus, NID2 domains, and Leucine-zipper domains did not attenuate the transcription ability of NF-κB. However, when the NID1 domain was deleted, the inhibitory effect of IFI35 on the transcription of NF-

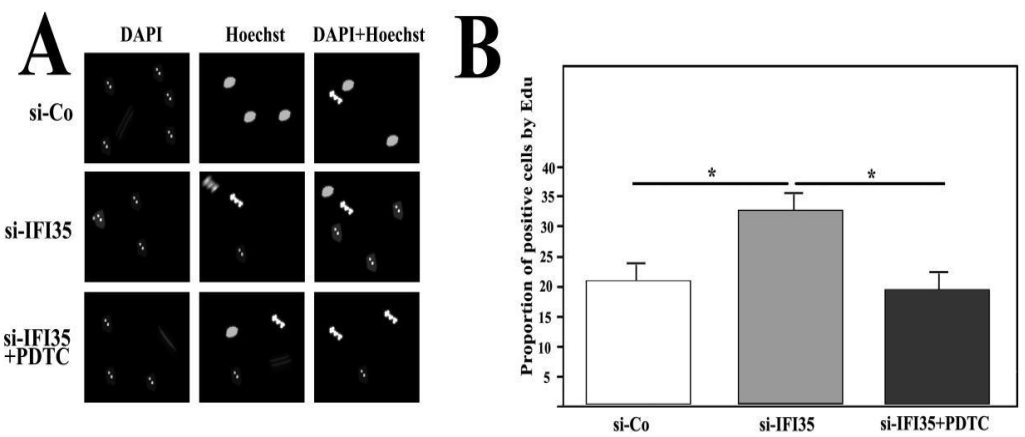

Fig. 2. *The effect of the NF-κB signaling pathway inhibition on IFI35-mediated endothelial cell proliferation.* ***A)*** *Effect of IFI35 expressions and a PDTC inhibitor on the activation of the NF-kB signaling pathway.* ***B)*** *Effect of IFI35 expressions and a PDTC inhibitor on the cells of cerebral infarction, *P<0.05*

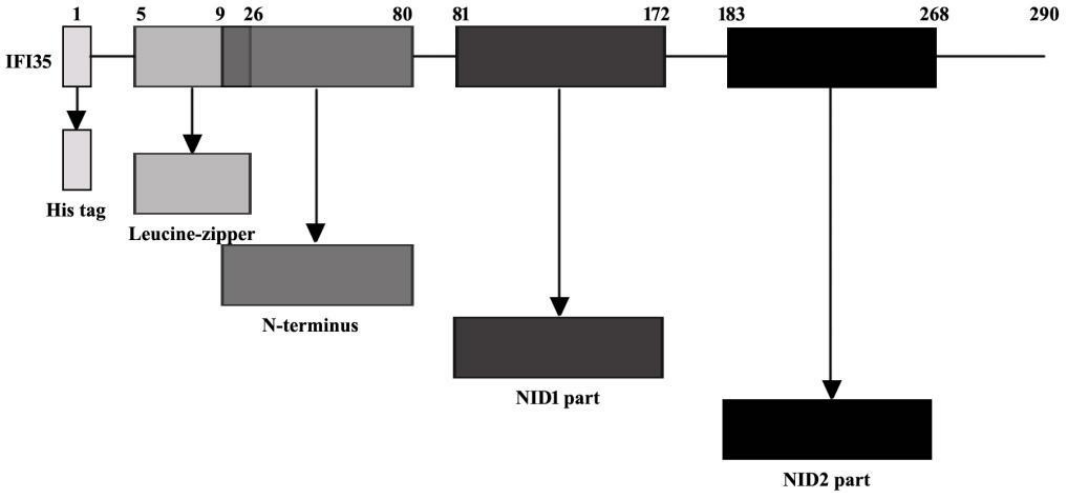

Fig. 3. *Structure diagram of IFI35 with domain deletions*

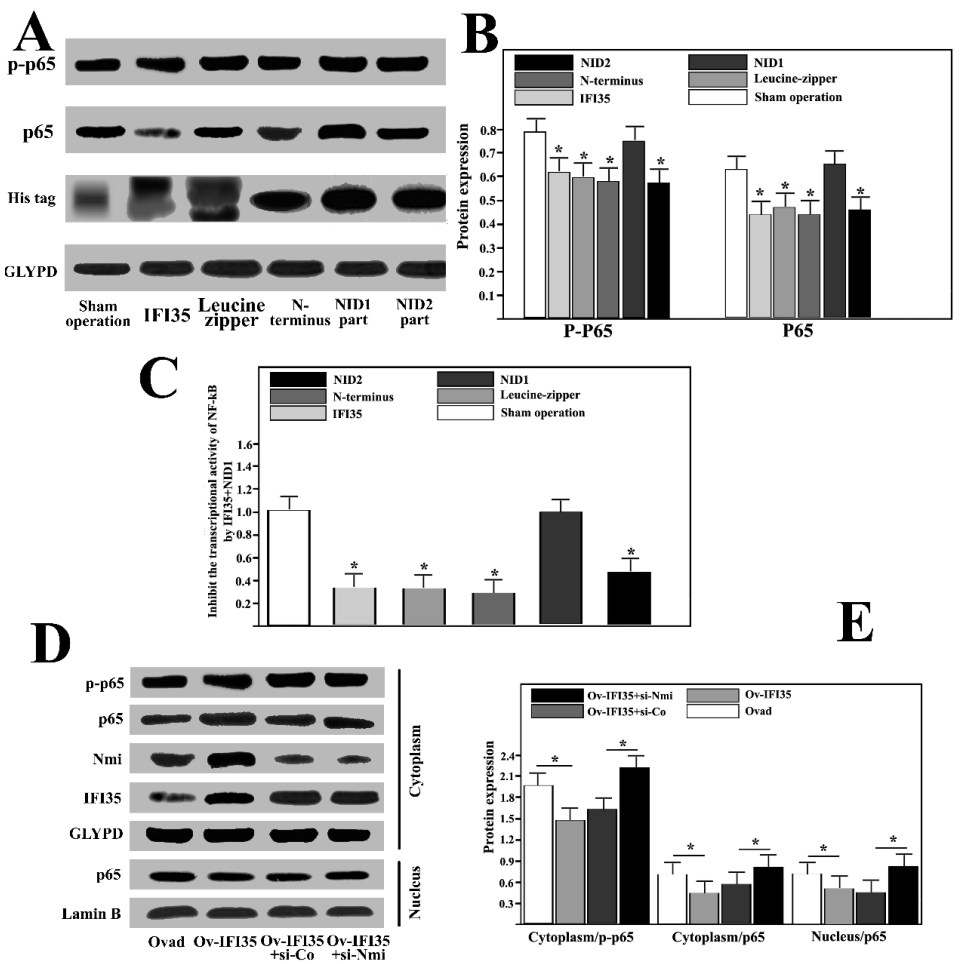

Fig. 4. *Inhibition of NF-κB signaling pathway activation by IFI35 was achieved via the interaction between the Nmi and NID1 structural domains of IFI35.* ***A, B****) Inhibition of NF-κB signaling pathway activation by the NID structural domain of IFI35.* ***C****) Inhibition of transcriptional activity of NF-κB by the NID1 structural domain of IFI35.* ***D, E****) The effect of reduced Nmi expressions on the inhibitory effect of IFI on NF-κB signaling, *P<0.05.*

κB promoter was significantly reduced, indicating that the NID1 structural domain of IFI35 could significantly inhibit the transcriptional ability of NF-κB ($P<0.05$).

To verify that the inhibitory effect of IFI35 on the NF-κB signaling pathway was exerted via the Nmi domain, the expression of IFI35 was increased. It was found that the expression of p65 in the cytoplasm and the expression of p-p65 in the nucleus were decreased by increased expressions of IFI35. However, when the expression of Nmi domain was reduced, the inhibitory effect of IFI35 on p65 and p-p65 expressions in the cytoplasm and nucleus was significantly reduced ($p <0.05$) (Fig. 4, D and E).

Effect of Nmi domain on the inhibitory effect of IFI35 on endothelial cell proliferation

Whether Nmi domain (Abcam, American) played a role in the inhibitory effect of IFI35 on NF-κB signaling was investigated (Fig. 5), and it was found that the increased expression of IFI35 inhibited the proliferation of endothelial cells. However, a decreased level of Nmi could reduce the inhibitory effect of IFI35 on the proliferation of endothelial cells.

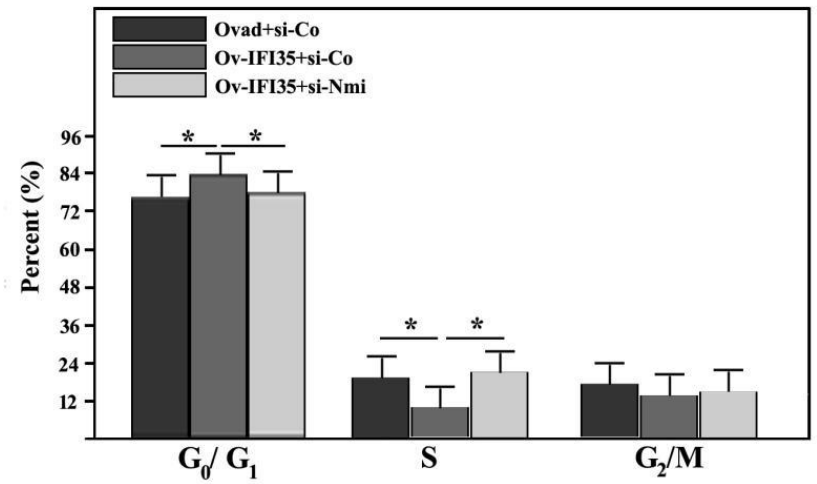

Fig. 5. *Effect of Nmi domain on the inhibitory effect of IFI35 on endothelial cell proliferation*

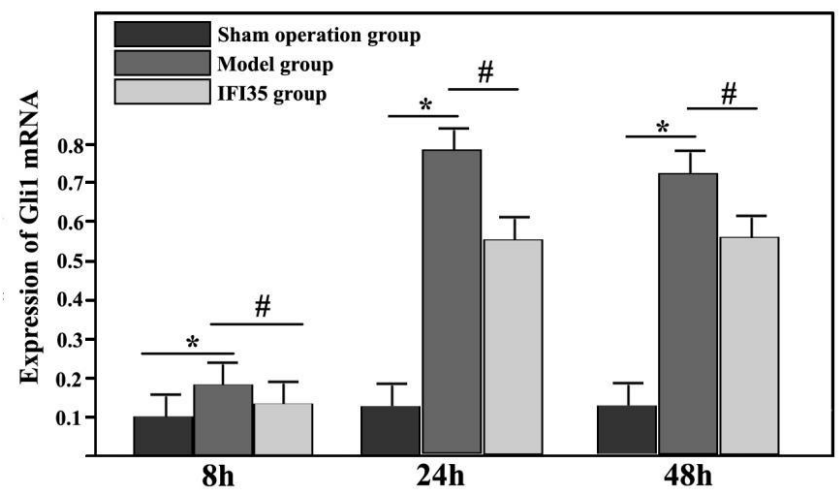

Fig. 6. *Effect of NF-κB signaling inhibition on the mRNA expression of Gli1 in occluded lateral cerebral cortex*

Therefore, Nmi plays an increasingly significant role in the transformation of endothelial cells from the growth stage of G_0/G_1 to the S stage, indicating that Nmi is involved in the inhibitory effect of IFI35 on endothelial cell proliferation.

Effect of NF-κB signaling inhibition on the mRNA expression of Gli1 in occluded lateral cerebral cortex of mice

In Fig. 6, the Gli1 expression in the sham operation and IFI35 treatment groups was significantly lower than that in the model group (P<0.05).

Effect of NF-kB signaling inhibition on the expression of VEGF, bFGE, and CD105 in occluded lateral cerebral cortex of mice

The expression of VEGF, bFGF, and CD105 in the sham operation and IFI35 treatment groups was significantly lower than that in the model group (P<0.05) (Fig. 7).

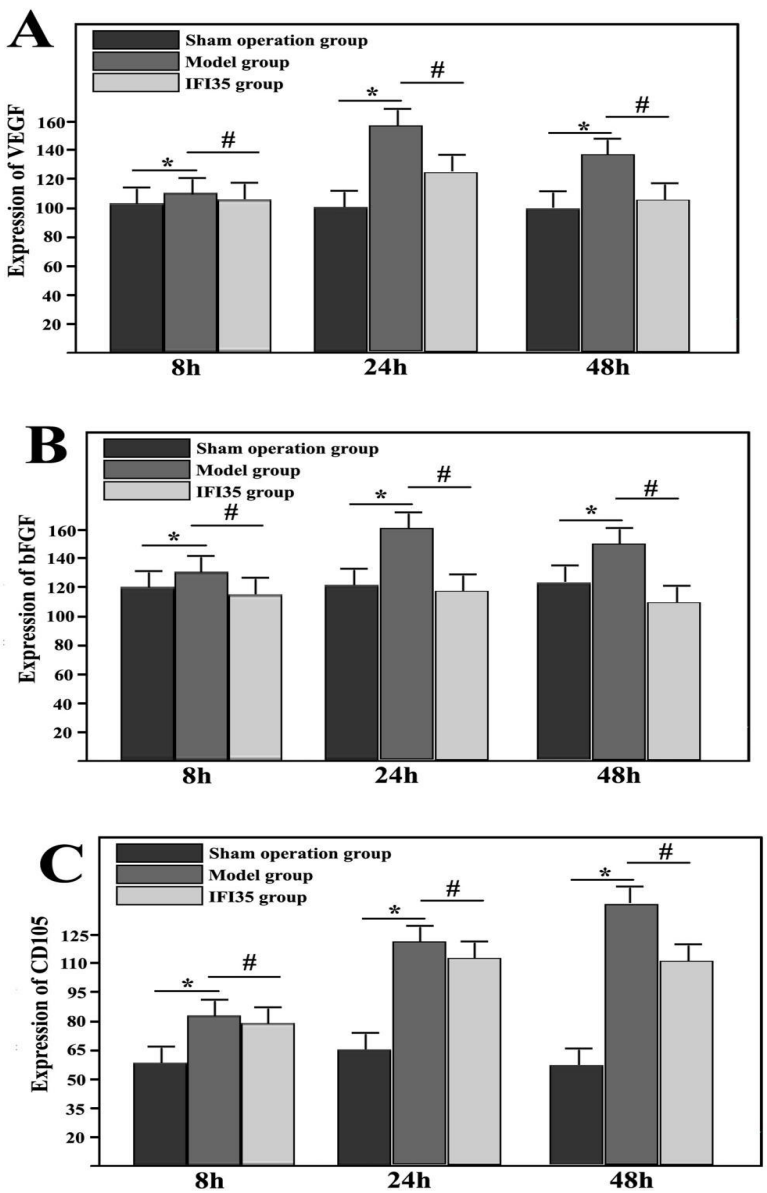

Fig. 7. *Effect of NF-κB signaling inhibition on the level of angiogenic factors in cerebral cortex.* ***A****) Effect of NF-κB signaling inhibition on the level of VEGF in cerebral cortex.* ***B****) Effect of NF-κB signaling inhibition on the level of bFGF in cerebral cortex.* ***C****) Effect of NF-κB signaling inhibition on the level of CD105 in cerebral cortex, *P<0.05*

DISCUSSION

NF-κB is distributed in neurons, astrocytes, microglia and oligodendrocytes of the nervous system (20, 21). The activation and inhibition of NF-κB are affected by inhibitory subunit of NF-κB and IκB-kinase (22). NF-κB signaling pathway plays an important role in regulating cell proliferation and cell migration. After activation of the NF-κB signaling pathway, the p50-p65 complex in the nuclei activates transcription of the gene in the region of vascular endothelial growth factor Receptor 2 (VEGFR2) (23). Therefore, the proliferation of endothelial cells and the generation of angiogenesis are promoted. Meanwhile, activation of the signaling pathway promotes the transcription of CCND1 (Cyclin D1)(24).

In this study, the binding of IFI35 and Nmi inhibited the growth of endothelial cells by suppressing the NF-κB signaling pathway. Nmi protein is combined with other different functional proteins, including signal transducers and activators of transcription (STAT), breast cancer gene 1 (BRCA1), proto-oncogenes (c-Myc and N-Myc), and plays an important role in cell proliferation, cell cycle regulation and inflammatory response (25).

IFI35 plays an important role in antivirus-related immune inflammation. Meanwhile, immune inflammation plays an important role in endothelial cell proliferation and angiogenesis after vascular endothelial cell injury. The results of study showed that: i) after IFI35 was inhibited by PDTC, the proportion of active endothelial cells was significantly higher than that of the si-RNA control and si-IFI35 groups; ii) the inhibitory effect of IFI35 on the transcription of NF-κB promoter was significantly reduced, indicating that the NID1 structural domain of IFI35 could significantly inhibit the transcriptional ability of NF-κB; iii) Nmi was involved in the transformation of cell cycle from stage G_0/G_1 to stage S; iv) endothelial cells were treated with IFI35, an the expression of vascular growth factor related (VEGF, bFGF, and CD105) in endothelial cells showed a decline trend.

In conclusion, it was confirmed that IFI35 inhibited the proliferation of endothelial cells and the expression of angiogenic factors by suppressing the NF-kappa B signaling pathway, but it was not related to endothelial cell proliferation and angiogenesis. Further studies are required to verify the findings above.

REFERENCES

1. Olmez I, Ozyurt H. Reactive oxygen species and ischemic cerebrovascular disease. Neurochem Int 2012; 60(2):208-12.
2. Celikbilek A, Ismailogullari S, Zararsiz G. Neutrophil to lymphocyte ratio predicts poor prognosis in ischemic cerebrovascular disease. J Clin Lab Anal 2014; 28(1):27-31.
3. Doll DN, Hu H, Sun J, Lewis SE, Simpkins JW, Ren X. Mitochondrial crisis in cerebrovascular endothelial cells opens the blood-brain barrier. Stroke 2015; 46(6):1681-89.
4. Fang T, An LC, Liu MM, Hua J, Xu KL, Zeng LY. Effects of liver sinusoid endothelial cell injury in mouse hepatic veno-occlusive disease. Zhongguo Shi Yan Xue Ye Xue Za Zhi 2012; 20(6):1457-62.
5. Li T, Li D, Xu H, Zhang H, Tang D, Cao H. Wen-Xin decoction ameliorates vascular endothelium dysfunction via the PI3K/AKT/eNOS pathway in experimental atherosclerosis in rats. BMC Complement Altern Med 2016; 16:27.
6. Heiss C, Rodriguez-Mateos A, Kelm M. Central role of eNOS in the maintenance of endothelial homeostasis. Antioxid Redox Signal 2015; 22(14):1230-42.
7. Kiefel H, Bondong S, Pfeifer M, et al. EMT-associated up-regulation of L1CAM provides insights into L1CAM-mediated integrin signalling and NF-κB activation. Carcinogenesis 2012; 33(10):1919-29.
8. Li L, Krymskaya L, Wang J, et al. Genomic editing of the HIV-1 coreceptor CCR5 in adult hematopoietic stem and progenitor cells using zinc finger nucleases. Mol Ther 2013; 21(6):1259-69.
9. Dong X, Tong F, Qian C, Zhang R, Dong J, Wu G, Hu Y. Nemo modulates radiation-induced endothelial senescence of human umbilical veins through NF-DU signaling pathway. Radiat Res 2015; 183(1):82-93.
10. Zhao L, Yu Y, Deng C. Protein and mRNA expression of Shh, Smo and Gli1 and inhibition by cyclopamine in hepatocytes of rats with chronic fluorosis. Toxicol Lett 2014; 225(2):318-24.

11. Thomas JL, Eichmann A. The power of VEGF (vascular endothelial growth factor) family molecules. Cell Mol Life Sci 2013; 70(10):1673-74.
12. Pepper MS, Mandriota SJ, Jeltsch M, Kumar V, Alitalo K. Vascular endothelial growth factor (VEGF)-C synergizes with basic fibroblast growth factor and VEGF in the induction of angiogenesis in vitro and alters endothelial cell extracellular proteolytic activity. J Cell Physiol 1998; 177(3):439-52.
13. Karzai FH, Apolo AB, Cao L, et al. A phase i study of TRC105 anti-CD105 (endoglin) antibody in metastatic castration-resistant prostate cancer. BJU Int 2015; 116(4):546-55.
14. Imaizumi T, Yano C, Numata A,et al. Interferon (IFN)-induced protein 35 (IFI35), a type I interferon-dependent transcript, upregulates inflammatory signaling pathways by activating toll-like receptor 3 in human mesangial cells. Kidney Blood Press Res 2016; 41(5):635-42.
15. Diamond MS, Farzan M. The broad-spectrum antiviral functions of IFIT and IFITM proteins. Nat Rev Immunol 2013; 13(1):46-57.
16. Bahari G, Hashemi M, Taheri M, Naderi M, Eskandari-Nasab E, Atabaki M. Association of IRGM polymorphisms and susceptibility to pulmonary tuberculosis in Zahedan, Southeast Iran. ScientificWorldJournal 2012; 2012:950801.
17. Felson DT, Anderson JJ, Boers M, et al. American College Of Rheumatology. preliminary definition of improvement in rheumatoid arthritis. Arthritis Rheum 1995; 38(6):727-35.
18. McKenzie RC, Jones CL, Tosi I, Caesar JA, Whittaker SJ, Mitchell TJ. Constitutive activation of STAT3 in Sézary syndrome is independent of SHP-1. Leukemia 2012; 26(2):323-31.
19. Bhangu A, Søreide K, Di Saverio S, Assarsson JH, Drake FT. Acute appendicitis: modern understanding of pathogenesis, diagnosis, and management. Lancet 2015; 386(10000):1278-87.
20. Zhang Q, Lenardo MJ, Baltimore D. 30 Years of NF-κB: A blossoming of relevance to human pathobiology. Cell 2017; 168(1-2):37-57.
21. Tang X, Sun L, Wang G, Chen B, Luo F. RUNX1: A regulator of NF-kB signaling in pulmonary Diseases. Curr Protein Pept Sci 2018; 19(2):172-178.
22. Gao X, Wu L, Wang K, et al. Ubiquitin carboxyl terminal hydrolase L1 Attenuates TNF-α-mediated vascular smooth muscle cell migration through suppression of NF-κB activation. Int Heart J 2018; 59(6):1409-15.
23. Dong F, Zhou X, Li C, et al. Dihydroartemisinin targets VEGFR2 via the NF-κB pathway in endothelial cells to inhibit angiogenesis. Cancer Biol Ther 2014; 15(11):1479-88.
24. Guan F, Shan Y, Wang Q. Induction of apoptosis by Bigelovii A through inhibition of NF-κB activity. Mol Med Rep 2018; 18(2):1600-608.
25. Hou J, Wang T, Xie Q, Deng W, Yang JY, Zhang SQ, Cai JC. N-Myc-interacting protein (NMI) negatively regulates epithelial-mesenchymal transition by inhibiting the acetylation of NF-κB/p65. Cancer Lett 2016; 376(1):22-33.

LETTER TO THE EDITOR

CHANGES IN POSTPRANDIAL SERUM FIBROBLAST GROWTH FACTOR 19 IN NEWLY DIAGNOSED TYPE-2 DIABETIC PATIENTS AND THE CLINICAL SIGNIFICANCE

L. ZHAO[1], Y. CAO[2] and Y. LIU[1]

[1]Department of Endocrinology, The 309th Hospital of Chinese People's Liberation Army, Beijing, China; [2]Department of Endocrinology, Chinese PLA General Hospital, Beijing, China

Received August 9, 2018 – Accepted December 5, 2018

The present study aims to investigate changes in serum fibroblast growth factor 19 (FGF19) levels two hours after oral use of 75 g of glucose in newly diagnosed type-2 diabetic patients, and explore its influence factors. Fifty newly diagnosed type-2 diabetic patients, admitted to our hospital from January 2015 to December 2015, were randomly enrolled in the present study (T group), while 50 age- and gender-matched subjects, who presented with normal physical examination results were enrolled in the control group. All subjects underwent oral glucose tolerance test (OGTT). Serum FGF19 levels at two hours after sugar use were compared, and the related influence factors of serum FGF19 were determined. The difference between the two groups was not statistically significant (*P*>0.05). The comparison of related indexes after OGTT revealed that serum FGF19 levels were lower in the T group (198.06 pg/ml, range: 120.03-346.46 pg/ml) than in the control group (222.27 pg/ml, range: 126.92-382.62 pg/ml), but the difference was not statistically significant (*P*>0.05). Among these influence factors, postprandial serum FGF19 level was positively correlated with LDL-C and postprandial blood glucose in the T group, while postprandial serum FGF19 level was positively correlated with HbA1c in the control group. There was no significant difference in postprandial serum FGF19 level between patients with type-2 diabetes mellitus and healthy subjects. LDL-C and postprandial blood glucose may be independent factors for serum FGF19 levels in type-2 diabetic patients, and there is a positive correlation among these.

To the Editor,

The prevalence of type-2 diabetes mellitus (T2DM) continues to increase in China (1). In recent years, a study revealed that some human fibroblast growth factors (FGFs) can regulate the function and metabolism of endocrine-related tissues and organs, in which FGF19 is involved in the regulation of glycolipid metabolism (2), and acts against obesity and diabetes. Serum FGF19 level will remain stable as the age of the human body increases. FGF19 is involved in regulating the process of energy metabolism, particularly during eating or under a hungry state. FGF19 is secreted in the intestines after eating, and assumes the role of the negative regulation of the synthesis and secretion of bile acids. As an anaphase hormone, FGF19 improves glucose tolerance, insulin sensitivity, and fat and energy metabolism. In particular, serum FGF19 level is reduced in patients with diabetes, obesity and metabolic syndrome (3). It was reported that

Key words: FGF19; T2DM; postprandial blood glucose; OGTT

Corresponding Author:
Dr Lin Zhao,
Department of Endocrinology,
The 309th Hospital of Chinese People's Liberation Army,
No. A17 of Heishanhu Street, Haidian District,
Beijing 100091, China
Tel.: +86 15330066199 - Fax: +86 010 66775029
e-mail: linzhao_dr@163.com

0393-974X (2019)

an injection of FGF19 can reduce lipodieresis to improve blood glucose levels in hyperglycemic rats (4). Another study also revealed that under the fasting state, serum FGF19 level was lower in patients with T2DM and impaired fasting glucose tolerance (IFT), compared to healthy subjects, while serum FGF19 level in patients with impaired glucose tolerance (IGT) was not significantly different from that of normal subjects (5). After the oral glucose tolerance test (OGTT), the 2-hour postprandial serum FGF19 level increased, compared with that under the fasting state (6).

Both clinical and laboratory studies have revealed that this hormone plays an important role in glycolipid metabolism in the gastrointestinal tract. In order to enrich the clinical evidence for FGF19 level, in the present study, postprandial serum FGF19 level and its influence factors were analyzed in newly diagnosed T2DM patients.

MATERIALS AND METHODS

The research subjects in the present study are a general population in Beijing, China. Fifty newly diagnosed T2DM patients, who were treated at the Department of Endocrinology of our hospital from January 2015 to December 2015, were randomly enrolled (T group). In addition, 50 age- and gender-matched subjects, who presented with normal physical examination results during the past two years, were enrolled from the Health Checkup Center of our hospital, and were assigned as the control group. In the T group, 30 patients were male and 20 patients were female, and the average age was 55.5±9.5 years. In the control group, 27 patients were male and 23 patients were female, and the average age was 51.7±8.7 years. The differences in age and gender between these two groups were not statistically significant (P>0.05), hence, the two groups were comparable. Patients in the T group met the 1999 World Health Organization (WHO) diagnostic criteria. The course of diabetes was less than six months. The two groups of subjects had no medication history for the regulation of blood lipid and bile acid in the pprevious three years, had no other diseases, such as cardiovascular and cerebrovascular diseases, diseases of the liver, kidney or other organs, and did not have a history of cancer or major surgery. This study was conducted in accordance with the Declaration of Helsinki and approved by the Ethics Committee of our hospital. Written informed consent was obtained from all participants.

Methods

The height, weight, waist circumference, hip

Table I. *Comparison of general information between the two groups.*

Indexes	T group	Control group	P value
BMI (kg/m^2)	25.7±2.5	22.6±1.9	P < 0.001
WC	102±11.5	92±11.5	P < 0.05
WHR	0.97±1.72	0.82±1.5	P < 0.05
HbA1C	8.5±1.3	6.1±0.7	P < 0.001
TG	3.51±0.6	0.9±0.4	P < 0.001
LDL-C	3.4±0.97	2.12±0.42	P < 0.001
HDL-C	1.12±0.15	1.21±0.2	0.23
FBG	8.7±2.5	4.5±0.5	P< 0.001
FINS (pmol/L)	7.9±1.8	4.7±0.8	P< 0.05
FGF19 (pg/ml)	244.77 (139.69-399.79)	276.21 (152.72-459.27)	0.08

Note: WC: waist circumference; WHR: waist-to-hip ratio; FBG: Fasting blood glucose; FGF19: fibroblast growth factor 19.

circumference and body mass index (kg/m^2) of subjects in the two groups were measured in the early morning under a fasting state, and the body fat of these subjects were calculated. Subjects in both groups underwent 75-g OGTT. Fasting blood samples were taken immediately and two hours after glucose use, and the serum was separated. The collected serum was used for biochemical testing, and the remaining samples were preserved for further FGF19 detection. Glycated hemoglobin (HbA1c) was detected using ion-exchange high-performance liquid chromatography, and the instrument used was a hemoglobin photometer. Fasting blood glucose (FBG) and 2-hour postprandial glucose (2hPG) were determined using the glucose oxidase method (Beckman, USA). Serum triglyceride (TG), total cholesterol (TC) and high density lipoprotein cholesterol (HDL-C) were determined using the enzymic method. Low density lipoprotein cholesterol (LDL-C) was detected by homogenous assay, using an automatic biochemical analyzer (Beckman, USA). Fasting insulin (FIns), fasting C-peptide, 2-hour postprandial insulin and 2-hour postprandial C-peptide were determined using a fully automated chemiluminescence analyzer (Beckman, USA). Serum FGF19 was detected using an enzyme-linked immunosorbent kit according to the manufacturer's instructions as follows: control dilution, sample processing, sample loading, plate washing, the addition of detection antibodies, the addition of streptavidin-conjugated horseradish peroxidase (STP-HRP), coloration, termination, colorimetry and the calculation of concentration.

Statistical analysis

SPSS software 20.0 (SPSS, Chicago, IL, USA) was used for statistical analysis. The quantitative variables were analyzed using *t*-test, and the classification variables were analyzed using χ^2-test or the 2×2 four-fold table exact probability test (Fisher's exact test). The influence factors were evaluated using Pearson's Correlation, and independent influence factors were analyzed using multiple linear regression (stepwise method). Some data were transformed to normal distribution by natural logarithm prior to the statistical analysis. $P<0.05$ was considered statistically significant.

RESULTS

Comparison of test results

The characteristics of the clinical and metabolic indicators are presented in Table I. The differences in age, gender and HDL-C between the T group and control group were not statistically significant ($P>0.05$). However, the differences in other

Table II. *Comparison of related indexes after OGTT between the two groups.*

Indexes	T group	Control group	P value
2hPG	16.2±2.7	7.1±0.5	P < 0.001
INS (pmol/L)	14.9±1.2	8.7±1.8	P < 0.05
FGF19 (pg/ml)	188.06 (120.03-346.46)	222.27 (146.92-392.62)	0.24

Note: 2hPG: 2-hour postprandial glucose; FGF19: fibroblast growth factor 19.

Table III. *Comparison of indexes influencing postprandial serum FGF19 levels.*

Indexes	T group		Control group	
	r	P value	r	P value
2hPG	0.253	0.047	-0.134	0.335
HbA1c	-0.146	0.197	0.288	0.036
LDL-C	0.241	0.030	-0.006	0.961

Note: FGF19: fibroblast growth factor 19; 2hPG: 2-hour postprandial glucose.

indicators between the two groups were statistically significant ($P<0.05$). In addition, the difference in serum FGF19 level in the fasting state between the two groups was not statistically significant ($P>0.05$).

In the present study, the comparison of related indexes after OGTT between the T group and control group revealed that serum FGF19 levels were lower in the T group (198.06 pg/ml, range: 120.03-346.46 pg/ml), compared with the control group (222.27 pg/ml, range: 126.92-382.62 pg/ml), but the difference was not statistically significant ($P>0.05$, Table II).

Analysis of factors influencing postprandial serum FGF19 levels

Postprandial serum FGF19 level was positively correlated with LDL-C and postprandial blood glucose level in the T group, while postprandial serum FGF19 level was positively correlated with HbA1c in the control group. These results are presented in Table III.

DISCUSSION

FGF19 can reduce TG and blood glucose, and promote the synthesis of glycogen and liver protein. In addition, FGF19 transgenic mice had lower TC and TG levels in serum and the liver, when compared to wild-type mice. Furthermore, the intraperitoneal injection of recombinant FGF19 in these transgenic mice could decrease plasma apo1ipoprotein A (APOA) level by 32%, and decrease liver APOA mRNA by 47%.

The serum FGF19 level in T2DM patients with obesity (BMI $\geq$30 kg/m^2) was lower than the normal level, but the difference was not statistically significant. Wang et al. (7) revealed that after OGTT, the increase in FGF19 level was positively correlated to the increase in age, and was negatively correlated to abnormal glycemic regulation and statin therapy. Weight reduction could increase the expression of FGF19 in the distal small intestine (8). Furthermore, a recent study revealed that FGF19 levels were not correlated to abnormal glucose tolerance induced by the increase in visceral fat (9).

The present study revealed that there was no significant difference in serum FGF19 level between T2DM patients and healthy subjects in Beijing, China in the fasting and postprandial states. Furthermore, postprandial serum FGF19 level was positively correlated with LDL-C and postprandial blood glucose in T2DM patients, while postprandial serum FGF19 was positively correlated with HbA1c in normal subjects. This factor is the influence factor for serum FGF19 in the normal population. Most of the conclusions in the present study are in contrast with those reported by other studies, and the reason may be the regional influence. Hence, there is a need to further expand the sample size and increase the variety of serological indicators in future studies, in order to further clarify these differences in clinical data.

REFERENCES

1. Bragg F, Holmes MV, Iona A, et al. Association between diabetes and cause-specific mortality in rural and urban areas of China. JAMA 2017; 317:280-89.
2. Wu X, Ge H, Baribault H, et al. Dual actions of fibroblast growth factor 19 on 1ipid metabolism. J Lipid Res 2013; 54:325-32.
3. Zhang F, Yu L, Lin X, et al. Minireview: Roles of fibroblast growth factors 19 and 21 in metabolic regulation and chronic diseases. Mol Endocrinol 2015; 29:1400-13.
4. Perry RJ, Lee S, Ma L, Zhang D, Schlessinger J, Shulman GI. FGF1 and FGF19 reverse diabetes by suppression of the hypothalamic-pituitary-adrenal axis. Nat Commun 2015; 6:6980.
5. Fang Q, Li H, Song Q, et al. Serum fibroblast growth factor 19 levels are decreased in Chinese subjects with impaired fasting glucose and inversely associated with fasting plasma glucose levels. Diabetes Care 2013; 36:2810-14.
6. Zhang J, Li H, Zhou H, et al. Lowered fasting chenodeoxycholic acid correlated with the decrease of fibroblast growth factor 19 in Chinese subjects with impaired fasting glucose. Sci Rep 2017; 7:6042.
7. Wang JS, Lee CL, Lee WJ, et al. Factors associated with fibroblast growth factor 19 increment after oral glucose loading in patients who were previously admitted for coronary angiography. Clin Chim Acta 2015; 450:237-42.
8. Patton A, Khan FH, Kohli R. Impact of fibroblast

growth factors 19 and 21 in bariatric metabolism. Dig Dis 2017; 35:191-96.
9. Hu X, Xiong Q, Xu Y, et al. Association of serum fibroblast growth factor 19 levels with visceral fat accumulation is independent of glucose tolerance status. Nutr Metab Cardiovasc Dis 2018; 28:119-25.

LETTER TO THE EDITOR

BILATERAL OVARIO-HYSTERECTOMY INDUCED OSTEOPOROTIC RABBIT MODEL

ES. JIN[1,2], JY. KIM[2], JK. MIN[2], SR. JEON[2,3], KH. CHOI[2,4], MS. LEE[5] and JH. JEONG[2,6]

[1]Department of Internal Medicine, College of Medicine, Kyung Hee University; Seoul, Republic of Korea; [2]Laboratory of Stem Cell Therapy, College of Medicine, Asan Medical Center, University of Ulsan, Ulsan, Republic of Korea; [3]Department of Neurological surgery, Asan Medical Center, College of Medicine, University of Ulsan, Ulsan, Republic of Korea; [4]Department of Rehabilitation Medicine, Asan Medical Center, College of Medicine, University of Ulsan, Ulsan, Republic of Korea; [5]OSTEONIC, Co., Ltd., Seoul, Republic of Korea; [6]Department of Neurosurgery, Soonchunhyang University Bucheon Hospital, Gyunggi-do, Republic of Korea

Received September 13, 2018 – Accepted January 11, 2019

Rabbit models have been proposed for the study of postmenopausal osteoporosis by bilateral ovariectomy with reduced dietary calcium intake or glucocorticoid administration. However, restricting dietary calcium intake or administering a glucocorticoid can cause secondary osteoporosis and is not representative of a pure postmenopausal osteoporosis model. The aim of this study was to establish an experimental rabbit model of osteoporosis induced by ovario-hysterectomy alone. Fourteen female New Zealand rabbits were separated into two groups of a sham (control) group and an ovario-hysterectomy-induced osteoporosis group. Tibiae were extracted 24 weeks after ovario-hysterectomy and were scanned by micro-computed tomography. The evaluation parameters were bone mineral density (BMD), trabecular bone volume (BV/TV), trabecular number (Tb.N), trabecular thickness, and trabecular separation (Tb. Sp). The tibial samples were evaluated after hematoxylin and eosin and Masson's trichrome staining. The sham group had significantly higher BMD, BV/TV, and Tb.N values and the lowest Tb.Sp value compared to the ovario-hysterectomy group. The histological analyses revealed a loss of the bony trabeculae and an increase in osteoporotic changes in the bone of the ovario-hysterectomy-induced osteoporosis group compared to the control group. Our results indicate that an ovario-hysterectomy-induced rabbit model would be a safe, reproducible model for postmenopausal osteoporosis studies.

To the Editor,

Several animal models have been developed to study postmenopausal osteoporosis. Because of the low cost and ease of management, the ovariectomized rat model represents the standard for postmenopausal osteoporosis studies and demonstrates cancellous bone defects, such as postmenopausal bone loss. However, the rat model has several weaknesses, including incomplete skeletal maturity, deficient Haversian canals with a lack of intra-cortical bone remodeling, and a small-sized anatomy for fixation of orthopedic implants (1).

Rabbit models have been used to study the bone–implant interface (1). Unfortunately, ovariectomy (OVX) alone is insufficient to produce osteoporosis in rabbits, so other osteoporosis models with

Key words: animal model; micro-computed tomography; osteoporosis; ovariectomy; rabbit

Corresponding Author:
Je Hoon Jeong, M.D., Ph.D.,
Department of Neurosurgery,
Soonchunhyang University Bucheon Hospital,
1174 Jung-1-dong, Wonmi-gu, Bucheon-si,
Gyunggi-do, 424-767, Republic of Korea
Tel.: +82 32 621 6709 - Fax: +82 32-621 5016,
e-mail: neuri71@gmail.com

0393-974X (2019)

combined therapy have been proposed, such as reducing dietary calcium or administering a glucocorticoid (1-6). However, reducing dietary calcium or administering a glucocorticoid are causes of secondary osteoporosis and do not represent a pure postmenopausal osteoporosis model. Moreover, there are relatively few publications on rabbit models with only OVX to evaluate trabecular bone mineral density (BMD) (7-10).

The purpose of the present study was to establish and illustrate a rabbit model of osteoporosis by ovario-hysterectomy (OHX) without administering a glucocorticoid or other specific adjuvant therapies.

MATERIALS AND METHODS

Grouping and bilateral ovario-hysterectomy

Fourteen 24-week-old female New Zealand rabbits (weight, 3–3.5 kg) were divided into two groups of a sham (control) group and a bilateral OHX-induced osteoporosis group. Rabbits were anesthetized with Alfaxan (1.6 ml mg/kg i.m.) and Rompun (0.4 ml mg/kg, i.m.). The abdomen, flank, and groin areas were shaved and surgically prepared using povidone-iodine and alcohol. A 3–5 cm midline incision was made through the skin between the umbilicus and the pelvis. After finger dissection and externalization of the ovaries and uterus, the ovarian blood vessels and the uterine arteries were identified and ligated. Finally, the uterus and ovaries were removed. The animals received an i.m. antibiotic (cefazole 10 mg/kg and ketoprofen 5 mg/kg) injection over the first 3 postoperative days. This study was approved by the Institutional Animal Care and Use Committee of Asan Institute for Life Sciences Seoul, Republic of Korea

Ex-vivo micro-computed tomography (micro-CT) evaluation

Both tibiae were extracted and scanned by high-resolution micro-CT (Skyscan N.V., Kontich, Belgium) 25 weeks after OHX. A region of interest was selected as the maximal trabeculae area in the upper portion of the proximal growth plate of the tibia (Fig. 1) The volume of interest was chosen as a column diameter of 3 mm and height of 4.507 mm (126 slices). The acquisition settings were 70 kV and 357 μA. A 1 mm-thick aluminum filter was used to reduce beam hardening artifacts. Pixel size was 35.78 mm. Exposure time was 350 ms using a stepwise mode and rotation was 0.7° with a complete rotation. We reconstructed and analyzed the images using Skyscan software (Skyscan N.V.). We evaluated the following parameters: bone mineral density (BMD; g/cm^2), trabecular bone volume (BV/TV; %), trabecular number (Tb.N;/mm), trabecular thickness (Tb.Th; mm), and trabecular separation (Tb.Sp; mm).

Hematoxylin and eosin (H&E) staining

After the extracted tibia were decalcified and fixed in paraffin, they were cut longitudinally at a thickness of 3 μm using a microtome (Leica Microsystems, Wetzlar, Germany). Each section was mounted on a slide and kept at 55°C. The sections were de-paraffinized in four 5-min changes of xylene and dehydrated in 2 min by changes in sequentially decreasing alcohol solutions (100%, 95%, 80%, and 70%). The slides were washed in flowing purified

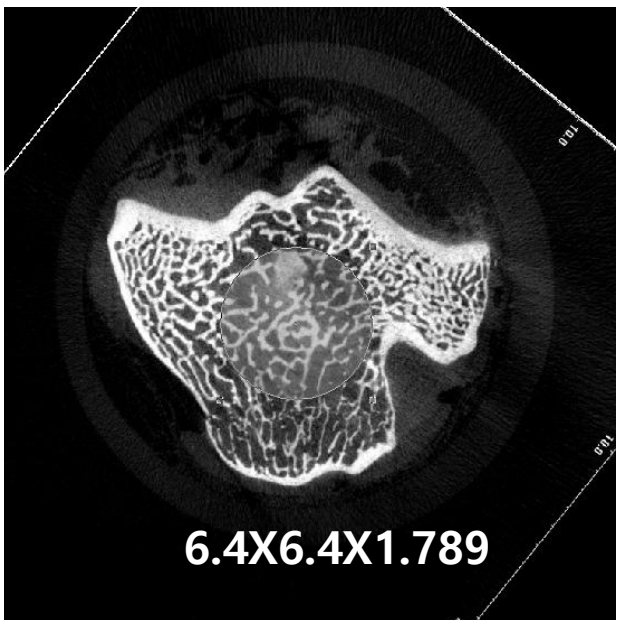

Fig. 1. *Volume of interest for evaluation of the osteoporotic changes in micro-computed tomography. The volume of interest (VOI) was selected as a column with a diameter 3.0 mm and a height of 4.507 mm (126 slices) which was defined as the maximal trabeculae bone region upper portion of the proximal growth plate of the tibia.*

water for 1 min and dipped in Harris hematoxylin-I, (YD-Diagnostics, Yong In, South Korea) for 5 min, followed by a 1 min wash in running purified water. The sections were blued in ammonia water for 30 sec and then washed under running tap water for 3 min. The sections were then stained with Eosin Y (Sigma-Aldrich, St. Louis, MO, USA) for 2 min 30 s and dehydrated in 95–100% ethanol. The remaining stain was washed away using flowing purified water. Each section was mounted (Shandon Synthetic Mountant; Thermo Fisher Scientific, Waltham, MA, USA).

Masson's trichrome stain

After deparaffinization and hydration, the sections were mounted in a 5% iron aluminum solution and dried in a 56°C drying oven for 30 min. The sections were washed in flowing purified water for 5–6 min to remove the picric acid. The sections were stained with Weigert's iron hematoxylin for 10 min and rinsed in distilled water. They were then stained with Biebrich Scarlet Acid Fuchsin (Sigma-Aldrich) for 5 min and rinsed in flowing purified water. The sections were placed in phosphomolybdic-phosphotungstic acid solution for 5 min, rinsed in distilled water, and clarified in 1% glacial acetic acid solution for 3 min. The remaining stain was washed off in flowing purified water.

Statistical analysis

Data are shown as mean ± standard deviation. The Mann–Whitney *U*-test was applied to identify the parameter (body weight and micro-CT measurements) differences between the two groups. A p-value ≤ 0.05 was considered significant. All analyses were performed using R (version 3.3.2, the R Foundation for Statistical Computing, Vienna, Austria).

RESULTS

None of the rabbits developed an infection or wound dehiscence, and all animals tolerated the procedure. Representative 3D-micro-CT images (Fig. 2) illustrate the bone osteoporotic changes in the OHX group. The sham group had higher BMD, BV/TV, and Tb.N values and the lowest Tb.Sp values compared to the OHX group (Fig. 3).

The histological findings of H&E and Masson's trichrome staining in the 24-week samples following OHX revealed loss of the trabeculae and increased

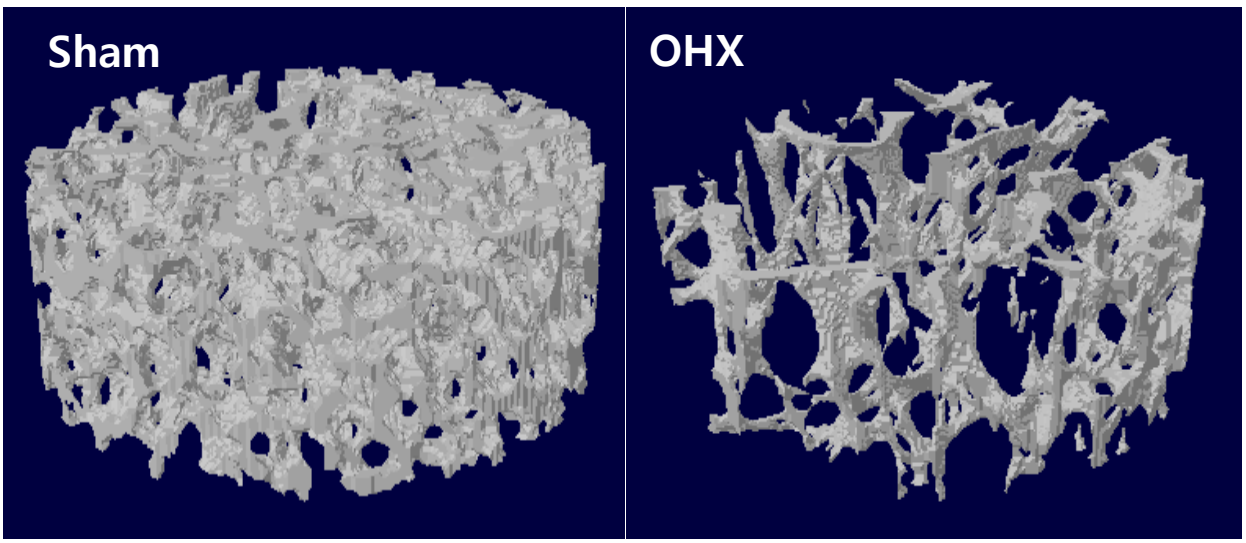

Fig. 2. *Representative 3-dimensional micro-computed tomography images of the volume of interest This photography shows osteoporotic changes of bone in OHX group after ovariectomy.*

adipose tissue in the bone marrow in the OHX group compared to the control group (Fig. 4).

DISCUSSION

Postmenopausal osteoporosis in rabbits by bilateral OVX alone has been described as a primary osteoporosis model (8-10). Yildiz et al. (9) reported an OVX model involving 12 rabbits that achieved a reduction in tibial BMD over 16 weeks. Furthermore, other studies have shown significant reductions in OVX-only model BMD over longer periods, but a prolonged period limits the usefulness of these models (11). In our study, we checked the change in BMD 24 weeks after OHX. The sham group had significantly higher BMD, BV/TV, and Tb.N values and the lowest Tb.Sp value compared to the OHX group.

The cause for the delay and insignificant reductions in BMD in the OVX-induced rabbit model can be explained by reflex ovulation or ectopic production of sex hormones. To overcome this limitation, other researchers have used glucocorticoids to accelerate and increase the degree of BMD loss following OVX (11). It is well known that glucocorticoids cause loss of cortical and trabecular bone (1), upregulate osteoclastic resorption, downregulate new bone formation, and arrest osteoblastic differentiation. However, these methods are similar to secondary osteoporosis. For preventing the reflex ovulation or ectopic production of sex hormones and accelerating the process of osteoporosis, we only performed bilateral OHX to remove the ectopic source in this study.

The rabbit has an active Haversian remodeling

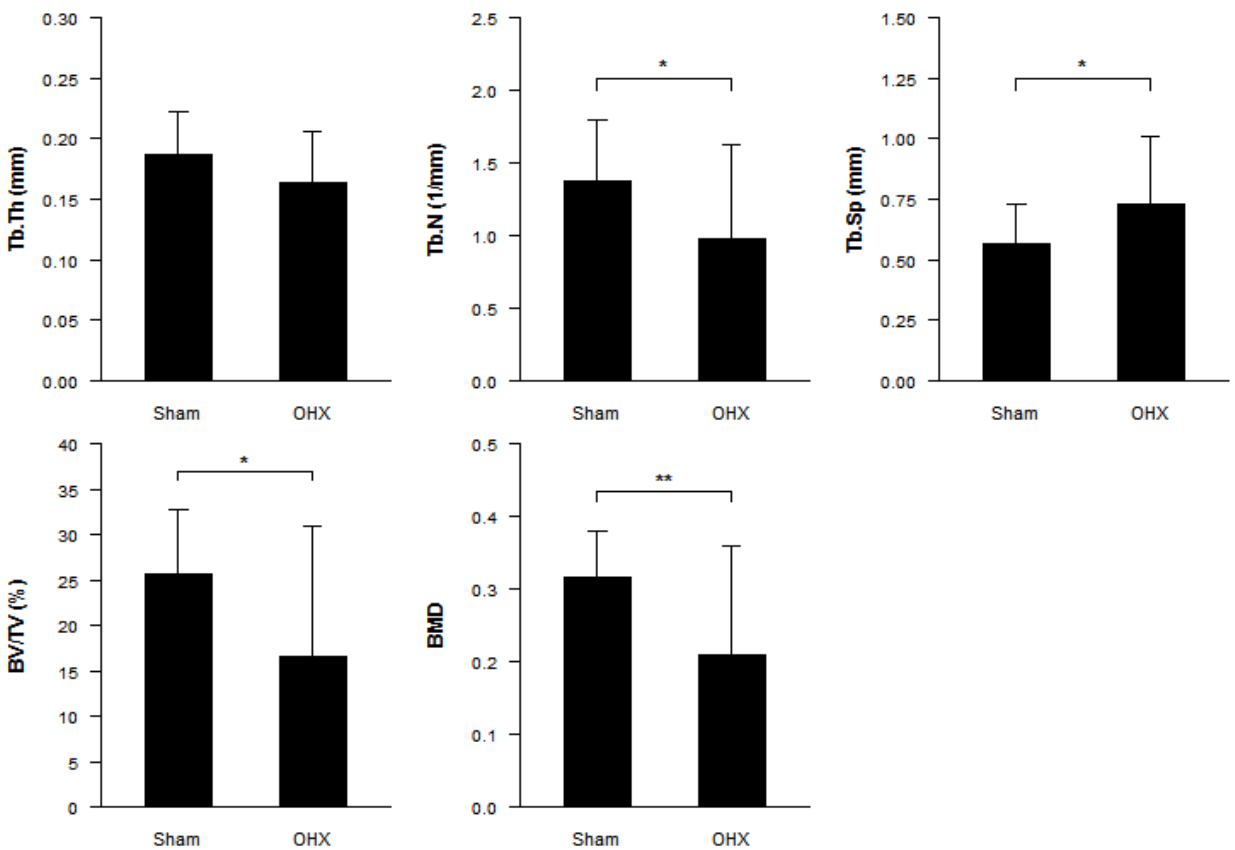

Fig. 3. *Comparing the tibia feasures measured at 16 weeks between sham and bilateral ovario-hysterectomy group * $p<0.05$; ** $p<0.01$. (Sham; control group, OHX; bilateral ovario-hysterectomy group)*

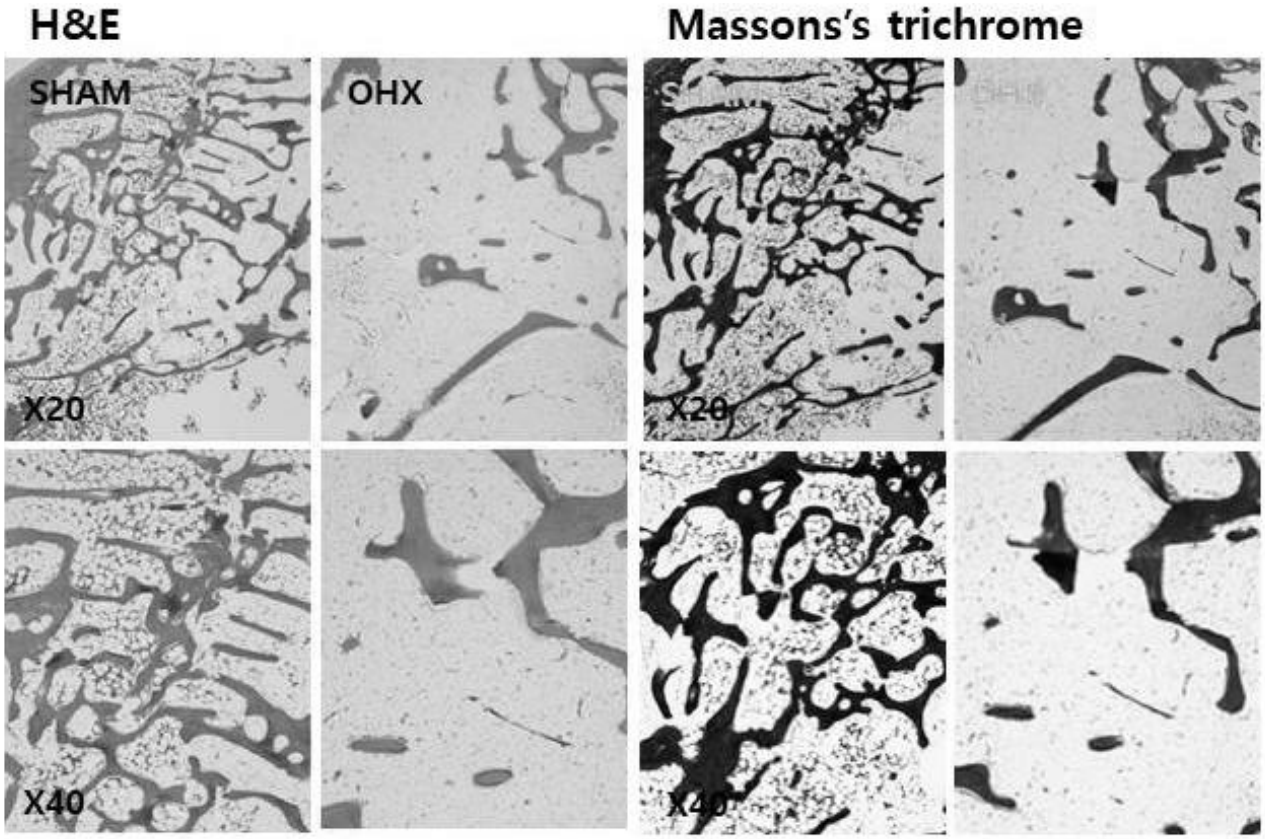

Fig. 4. *Representative photographs of the H&E staining of Volume of interest in the tibia. Photographs show a loss of the bony trabeculae and increased adipose tissue in the bone marrow in the OHX groups as compared to the shaml group (Magnification, 20x, 40x). (Sham; control group, OHX; bilateral ovario-hysterectomy group).*

system in cortical bone, which is of benefit when studying bone remodeling-associated drugs with strong anabolic effects (1). However, there is a lack of cancellous bone in rabbits and only a small portion in the knee joint and spine. Therefore, it is difficult to verify cancellous bone BMD. We cannot confirm that the BMD measurements taken with dual energy X-ray absorptiometry are insufficient to identify minimal bone loss. However, OVX rabbits showed a tendency to lose BMD. Thus, we performed a histomorphometric analysis by applying micro-CT to the knee area. Representative 3D-micro-CT images (Fig. 3) illustrate the osteoporotic changes of bone in the OHX group after OHX.

In conclusion, our results indicate that an ovario-hysterectomy-induced rabbit model would a safe, reproducible model for postmenopausal osteoporosis studies.

ACKNOWLEDGEMENTS

This research was supported by the Ministry of Trade, Industry & Energy (MOTIE), Korea Institute for Advancement of Technology (KIAT) through the Encouragement Program for The Industries of Economic Cooperation Region (Grant Number: R0005237), and was also supported by the Soonchunhyang University Research Fund.

REFERENCES

1. Castañeda S, Calvo E, Largo R, González-González R, de la Piedra C, Díaz-Curiel M, Herrero-Beaumont G. Characterization of a new experimental model of osteoporosis in rabbits. J Bone Miner Metab 2008; 26:53-59.
2. Wen B, Zhu F, Li Z, Zhang P, Lin X, Dard M. The

osseointegration behavior of titanium-zirconium implants in ovariectomized rabbits. Clin Oral Implants Res 2014; 25:819-25.
3. Baofeng L, Zhi Y, Bei C, Guolin M, Qingshui Y, Jian L. Characterization of a rabbit osteoporosis model induced by ovariectomy and glucocorticoid. Acta Orthop 2010; 81:396-401.
4. Li GW, Tang GY, Liu Y, Tang RB, Peng YF, Li W. MR spectroscopy and micro-CT in evaluation of osteoporosis model in rabbits: comparison with histopathology. Eur Radiol 2012; 22:923-29.
5. Martin-Monge E, Tresguerres IF, Blanco L, Khraisat A, Rodríguez-Torres R, Tresguerres JA. Validation of an osteoporotic animal model for dental implant analyses: an in vivo densitometric study in rabbits. Int J Oral Maxillofac Implants 2011; 26:725-30.
6. Oue H, Doi K, Oki Y, et al. Influence of implant surface topography on primary stability in a standardized osteoporosis rabbit model study. J Funct Biomater 2015; 6:143-52.
7. Liu X, Lei W, Wu Z, Cui Y, Han B, Fu S, Jiang C. Effects of glucocorticoid on BMD, micro-architecture and biomechanics of cancellous and cortical bone mass in OVX rabbits. Med Eng Phys 2012; 34:2-8.
8. Sevil F, Kara ME. The effects of ovariectomy on bone mineral density, geometrical, and biomechanical characteristics in the rabbit femur. Vet Comp Orthop Traumatol 2010; 23:31-36.
9. Yildiz A, Esen E, Kürkçü M, Damlar I, Dağlioğlu K, Akova T. Effect of zoledronic acid on osseointegration of titanium implants: an experimental study in an ovariectomized rabbit model. J Oral Maxillofac Surg 2010; 68:515-23.
10. Ye X, Zhang P, Xue S, Xu Y, Tan J, Liu G. Adipose-derived stem cells alleviate osteoporosis by enhancing osteogenesis and inhibiting adipogenesis in a rabbit model. Cytotherapy 2014; 16:1643-55.
11. Wanderman NR, Mallet C, Giambini H, et al. An ovariectomy-induced rabbit osteoporotic model: A new perspective. Asian Spine J 2018; 12:12-17.

JOURNAL OF BIOLOGICAL REGULATORS & HOMEOSTATIC AGENTS Vol. 33, no. 2, 397-401 (2019)

LETTER TO THE EDITOR

OVERVIEW OF THE DIFFERENT METHODS USED IN THE PRIMARY CULTURE OF ORAL MUCOSA CELLS

A. BRYJA[1], M. POPIS[1], B. BOROWIEC[1], M. DYSZKIEWICZ-KONWIŃSKA[1,2], I. KOCHEROVA[1], A. ANGELOVA-VOLPONI[3], K. MEHR[4], M. BRUSKA[1], M. NOWICKI[5] and B. KEMPISTY[1,5,6]

[1]Department of Anatomy, Poznan University of Medical Science, Poznań, Poland; [2]Department of Biomaterials and Experimental Dentistry, Poznan University of Medical Sciences, Poznań, Poland; [3]Centre for Craniofacial and Regenerative Biology, Faculty for Dentistry, Oral & Craniofacial Sciences, King's College University of London, London, United Kingdom; [4]Department of Dental Prosthetics, Pomeranian Medical University in Szczecin, Szczecin, Poland; [5]Department of Histology and Embryology, Poznan University of Medical Science, Poznań, Poland; [6]Department of Obstetrics and Gynecology, University Hospital and Masaryk University, Brno, Czech Republic

Received September 25, 2018 – Accepted January 11, 2019

The culture of primary cells *in vitro* has enabled to gain knowledge in the field of cell biology, disease mechanisms and to offer great potential in drug testing. To date, two main techniques of isolating and culturing oral mucosal cells, the direct explant method and the enzymatic method, dominate the literature and practice. In the present study, both techniques are discussed in detail, comparing the advantages and disadvantages of the two approaches in setting up a primary culture of oral mucosal cell. The direct explant technique is well-established and has been commonly used for the past 20-30 years. Although the method of setting up the cultures did not show much variations in the methodology described by authors, the culturing conditions varied according to the aims of the projects. The enzymatic methods showed many prominent variations as different enzymes, concentrations and other conditions were introduced. Both methods of setting up the primary cell cultures of oral mucosal cells proceed to culturing conditions adapted to the purpose of the study. The variations of the methods aimed at maintaining the purity (free from microbial contamination), identity and stability through maintenance of the genotype and phenotype during growth and passage.

To the Editor,

The main function of epithelial tissues is to cover the outside of the body and line organs, vessels (blood and lymph), and cavities. The epithelial tissues are composed of epithelial cells that are very closely packed together acting as a barrier with protective function.

These tissues are classified into three broad categories: keratinizing stratified squamous epithelia, non-keratinizing stratified epithelia, and non-stratified epithelia.

The mucous membrane of the oral cavity consists of two layers: stratified squamous epithelium, and an underlying layer of connective tissue (lamina

Key words: direct explant method; enzymatic method; oral mucosa; primary culture

Corresponding author:
Bartosz Kempisty PhD,
Department of Histology and Embryology,
Department of Anatomy, Poznan University of Medical Sciences,
6 Święcickiego St., 60-781 Poznań, Poland
Tel./Fax: +48 61 8546418/+48 61 8546440
e-mail: bkempisty@ump.edu.pl

0393-974X (2019)

propria). The oral epithelia consist of tissues classified into both the stratified epithelial categories. Keratinizing epithelium and non-keratinizing epithelium can be distinguished in this tissue. The oral mucosa exhibits both epithelial and connective tissue structural modifications in different areas of the oral cavity (1). The epithelial tissue is composed mostly by keratinocytes, and the connective tissue is commonly composed of fibroblasts.

While *in vitro* expansion of the fibroblast population is relatively easy. They are characterised with easy attachment to the culturing surface and do not require feeder cells or coating. The culturing of the epithelial cells (keratinocytes) has been proven to be more complex. For a long period, the culturing approach to keratinocytes was by using feeder cell population (fibroblasts produce keratinocyte growth factor, that promote oral epithelial growth and proliferation), most commonly: i) the mitotically inhibited murine 3T3 cells, or a choice of substances to "coat" the culturing surface for increased cell attachment; ii) substances like collagens, fibronectin, laminin; iii) regulation of Ca^{2+} concentration; iv) conditioned medium; or v) dedicated medium used for keratinocyte *in vitro* culture.

Oral mucosa cell isolation methods

Two main methods are commonly used in laboratories to establish primary culture of the oral mucosa cells *in vitro*. The first one is direct explant technique; the protocols for this method are less complicated and less variations in the steps are observed in the literature. The main differences in the protocols refer to the methods of disinfection of the tissue sample and the choice of culturing media used for establishing culture and subsequent expansion. The second isolation method involves more variable protocols, with the variation mainly concerning the concentrations of digestion enzymes used. Both of the approaches are outlined below.

Direct explant method

Direct explant technique consists in placing small pieces of the extracted tissue on a culture dish, obtaining attachment and supplying carefully controlled conditions: culturing media; temperature and gases (CO_2 and O_2). The basic principle used in this method is cell migration from the edges of the attached to culturing surface piece of tissue (2). This technique has been used successfully for 20-30 years in experiments including cultures of human gingival and buccal tissues (3).

In the direct explant method, the important step is the disinfection of the tissue. Wanichpakorn et al. suggested disinfection of gingival specimens in 10% povidone-iodine solution for 2-3 min. and then washing in culture media, before setting up the culture (3).

Other authors suggested different approaches as Guzman-Uribe et al., who, in order to disinfect the samples, preserved the tissue fragments in the phosphate buffered saline (PBS), supplemented with 100 µg/ml streptomycin, 100 IU/mg penicillin and 10 µg/ml amphotericin B, at 4°C for 12 h (4) before setting up cultures. Heller et al. sterilized gingiva samples using sterillium, for 15 s, and 70% ethanol for the next 15 s. Then they washed the samples twice in sterile PBS (5).

In order to separate the epithelial tissue from the underlying connective tissue, some authors, such as Bayer et al., offered a simple method using a surgical pen to mark the epithelial surface (2).

Klingbeil et al. compared efficiency of two methods of keratinocyte isolation. In the direct explant method, a tissue sample, after washing and disinfection, was cut into small pieces and placed, with epithelial surface directly adjacent, on the culture dish area (6). To separate keratinocytes from the total cell volume, they used selective medium composed of DMEM and Ham's F12 (2:1), and cultured cells on the 3T3 feeder layer (6). Islam et al., using direct explant technique, analysed four culture media and measured: cell attachment, outgrowth, proliferation and phenotype for samples that were taken from rat hard palates, buccal mucosa, lower lip and transition zone of the lower lip. (7). The tested media were: i) EpiLife- is serum-free, has low Ca^{2+} content and promotes an undifferentiated phenotype; ii) Oral Keratinocyte Medium (OKM) that has a positive effect on cells viability; iii) Dulbecco's modified Eagle's medium/Ham's F12 (DMEM/F12); iv) Roswell Park Memorial Institute 1640

medium (RPMI) (7). DMEM was supplemented with commonly used cholera toxin and epidermal growth factors (EGF) to increase the proliferation capacity of oral epithelial cells (6- 8). These four analyzed media had similar attachment ability, while DMEM generated a higher fold outgrowth than OKM and EpiLife (7).

Enzymatic method

For the enzymatic technique, three enzymes are usually used: collagenases, dispase and trypsin. It was speculated that dispase works from the stromal side, because the epithelial structure contains a tight and adherents junction. With dispase II we can separate connective tissue and epithelial tissue (8). Trypsin is used to separate cells of the epithelial tissue (9). Collagenases, including matrix metalloproteinase 1 (MMP-1), digest type I, II, III, V and IX collagen (10).

There are many protocols of isolation of oral mucosal cells using an enzymatic method. The differences between the isolation protocols are mainly dependent on the type of isolated cells. When keratinocytes are isolated, the digestion is usually trypsin based (6).

Klingbeil et al., while employing the enzymatic method, used 0.05% trypsin solution for keratinocyte isolation. The fragments of tissue were cut into small pieces and were digested in trypsin solution at 37°C. Then the supernatant that contained cell suspension was collected every 30 min., with trypsin activity neutralized with culture medium. After that, cells were seeded on a feeder-layer (6).

Nakamura et al. isolated oral epithelial cells by explant incubation at 37°C, for 1 h, in 1.2 IU dispase and then treated them with 0.25% trypsin-EDTA solution for 30 min at room temperature (9).

For fibroblast isolation, collagenase is used (8). Chinnathambi et al. separated epithelium and connective tissue mechanically and then treated connective tissue with 0.2% collagenase for 1 h at 37°C (8).

Conclusions from direct explant technique and enzymatic technique

Klingbeil et al. compared two methods of human oral mucosa keratinocyte isolation: direct explant and enzymatic methods. In their study, they measured colony formation efficiency, life-span of the cultured cells and the time before the first cell harvest. In the conclusions they wrote that the enzymatic method provided the best results for human oral keratinocyte primary culture, compared to the direct explant method. The authors suggested that the enzymatic method allowed to obtain the best cell yield within the shortest time (6).

Oral mucosa culturing methods

It is well known that connective tissue has both instructive and permissive effects on the development and differentiation of the epithelial tissues (8). The influence of the connective tissue on the epithelia was presented by Chinnathambi et al. They showed that oral fibroblasts induced the expression of the oral keratins K4, K13 and K19 in the skin keratinocytes (8).

Keratinocytes grow better in a low concentration of Ca^{2+} and serum-free medium. The higher concentration Ca^{2+} can induce differentiation (11, 12). On the other hand, fibroblasts require a higher level of Ca^{2+} (physiological concentration) to proliferate (12). This problem is significant when we have co-culture of keratinocytes and fibroblasts. In the study by Costea, the author described that FAD medium (1:3 mixture of DMEM and Hams' F12 media) was superior compared to other media (KSFM, MEM) for optimal growth and differentiation of human oral mucosa (12). In the case of keratinocyte cultures, it should be taken into account that the serum promotes progress towards terminal differentiation. Spontaneous immortalization of keratinocytes also seems to be an interesting issue. Parikh et al. cultured keratinocytes using low Ca^{2+} medium. After 2-3 passages, the keratinocytes entered a crisis phase in which the majority of cells underwent apoptosis. The few surviving keratinocytes became spontaneously immortalized (11).

It is also important to add growth promoting supplements to the culture media as they play a significant role in cell proliferation (7, 13). Formanek et al., in their study, described that adding 5µg/ml hydrocortisone, 5µg/ml insulin and 10 ng/ml EGF to DMEM with 10% FCS promoted keratinocyte growth (13). Contrary to this result, Islam et al.,

in their study, had higher outgrowth from mucosal pieces placed in supplemented DMEM and RPMI that not been supplemented with EGF, insulin and hydrocortisone (7).

Oral mucosa can be used in tissue engineering and regenerative medicine. Studies conducted by Guzman-Uribe et al. found its application as a skin substitute particularly promising. (4). Izumi et al. described production of an oral mucosa equivalent composed of keratinocytes and AlloDerm (14). In regenerative medicine, it is essential that cells are grown on media that do not contain animal components. Izumi et al. used MCDM153 medium without FBS in their cultures. This elimination did not affect planting of primary cultures of oral keratinocytes. For trypsin deactivation a 0.03% solution of soybean tissue inhibitor was used (14).

A different direction in the experiments concerning oral mucosa cell culture is the discovery and characterization of the mesenchymal stem cells (MSCs) that can be used in tissue engineering. Du et al. described a technique of MSC isolation from gingiva using the limiting dilution method (15). They incubated minced gingival tissue in collagenase type I and dispase for 2 h at 37°C. The cells were cultured in supplemented A-MEM. They isolated single cell-derived colonies using colony rings, then each colony was transferred primarily to a 96-well plate and later to a 6-well plate (15).

Izumi et al. isolated and characterized small-sized, cultured oral keratinocyte population containing progenitor/stem-cell-enriched population that could be used to fabricate a human *ex-vivo*-produced oral mucosa equivalent (EVPOME) (16). They digestated samples of oral mucosa overnight, using 0.04% trypsin solution, at room temperature. Dissociated keratinocytes were resuspended in a chemically defined culture system. After second passage, keratinocytes were sorted by fluorescence-activated cell sorting (FACS). Sorted keratinocytes from the 8th passage were used to generate day 11 EVPOME (D11E) (16).

Madhira et al. cultured oral mucosal epithelial cells on human amniotic membrane (HAM), for ocular surface reconstruction (17). Epithelium was removed from HAM using 0.25% trypsin for 30 min, followed by mechanical separation. Oral tissue samples were placed on the deepithelialized HAM. Cells were cultured in human corneal epithelium (HCE) medium, with contained Minimal Essential Medium (MEM) and Ham's F12 (1:2), 10% FCS, epidermal growth factor and insulin. Human oral mucosal epithelial cells for ocular surface reconstruction were also cultured by Nakamura et al. in a serum-free, feeder-free culture system, where the keratinocytes were grown as cell sheets. (18). They also used a denuded amniotic membrane, and for the feeder-free culture, they used a medium mixture composed of DMEM/F12 and defined keratinocyte-SFM (1:2) supplemented with EGF, hydrocortisone, epigallocatechin gallate and Dextran 40 (18).

In another study, Roh et al. described a method for generating 3D cell sheets of oral mucosa tissue without animal products. They used the medium containing autologous serum collected from blood samples. Tissues obtained from the patient were treated with dispase and collagenase. The resulting keratinocytes and fibroblasts were seeded onto separate dishes. In the next steps, the serum collected from blood and fibroblasts were used to make fibrin glue as a source of scaffolds. This mixture was allowed to solidify in cell culture inserts and, after 60 min, inserts were placed in plates with medium, and keratinocytes were seeded onto prepared inserts. Later, cell sheets were detached with forceps and prepared for grafting (19).

CONCLUSION

In both culture methods, it is possible to obtain and propagate oral keratinocytes in *in vitro* culture (6). The direct explant technique requires less involvement at the beginning than the enzymatic method. However, using the enzymatic method, in a short time, many more cells can be yielded from the culture (6). The *in vitro* cultured epithelial cells offer potential clinical applications. However, the problem of culture contamination with oral microbiological flora from tissue samples is a major obstacle in the process of their development.

Although the direct explant technique is older than the enzymatic technique, both techniques have

been widely used in laboratories with success. In the United Kingdom a survey was carried out which that 21 out of 34 laboratories in England which returned the questionnaire reported that they used the enzymatic method, with variation in the type and of the enzymes (20). Both protocols have their pros and cons, with the choice and evaluation of the method largely dependent on the author's preference (3).

REFERENCES

1. Jankowski M, Dyszkiewicz-Konwińska M, Budna J, et al. Does migrative and proliferative capability of epithelial cells reflect cellular developmental competence? Med J Cell Biol 2018; 6:1-7.
2. Bayar GR, Gulses A. Ex-vivo production of oral mucosa keratinocytes by the direct explant method. Int J Oral Maxillofac Surg 2013; 42:417-18.
3. Wanichpakorn S, Kedjarune-Laggat U. Primary cell culture from human oral tissue: gingival keratinocytes, gingival fibroblasts and periodontal ligament fibroblasts. Songklanakarin J Sci Technol 2010; 32:327-31.
4. Guzmán-Uribe D, Alvarado-Estrada KN, Pierdant-Pérez M, Torres-Álvarez B, Sánchez-Aguilar JM, Rosales-Ibáñez R. Oral mucosa. J Appl Oral Sci 2017; 25:186-95.
5. Heller M, Frerick-Ochs EV, Bauer H-K, et al. Tissue engineered pre-vascularized buccal mucosa equivalents utilizing a primary triculture of epithelial cells, endothelial cells and fibroblasts. Biomaterials 2016; 77:207-15.
6. Klingbeil MFG, Herson MR, Cristo EB, dos Santos Pinto D, Yoshito D, Mathor MB. Comparison of two cellular harvesting methods for primary human oral culture of keratinocytes. Cell Tissue Bank 2009; 10:197-204.
7. Islam R, Eidet JR, Badian RA, et al. Tissue harvesting site and culture medium affect attachment, growth, and phenotype of ex vivo expanded oral mucosal epithelial cells. Sci Rep 2017; 7:674.
8. Chinnathambi S, Tomanek-Chalkley A, Ludwig N, et al. Recapitulation of oral mucosal tissues in long-term organotypic culture. Anat Rec A Discov Mol Cell Evol Biol 2003; 270:162-74.
9. Nakamura T, Endo K-I, Cooper LJ, et al. The successful culture and autologous transplantation of rabbit oral mucosal epithelial cells on amniotic membrane. Invest Ophthalmol Vis Sci 2003; 44:106.
10. Lipka D, Boratyński J. Metaloproteinazy MMP. Struktura i funkcja. Postepy Hig Med Dosw 2008; 62.
11. Parikh N, Nagarajan P, Sei-ichi M, Sinha S, Garrett-Sinha LA. Isolation and characterization of an immortalized oral keratinocyte cell line of mouse origin. Arch Oral Biol 2008; 53:1091-100.
12. Costea DE. Epithelial - mesenchymal interactions in normal and neoplastic human oral mucosa. A study on *in vitro* organotypic models, University of Bergen, Bergen, Norway, 2005.
13. Formanek M, Millesi W, Willheim M, Scheiner O, Kornfehl J. Optimized growth medium for primary culture of human oral keratinocytes. Int J Oral Maxillofac Surg 1996; 25:157-60.
14. Izumi K, Terashi H, Marcelo CL, Feinberg SE. Development and characterization of a tissue-engineered human oral mucosa equivalent produced in a serum-free culture system. J Dent Res 2000; 79:798-805.
15. Du L, Yang P, Ge S. Isolation and characterization of human gingiva-derived mesenchymal stem cells using limiting dilution method. J Dent Sci 2016; 11:304-14.
16. Izumi K, Tobita T, Feinberg SE. Isolation of human oral keratinocyte progenitor/stem cells. J Dent Res 2007; 86:341-46.
17. Madhira SL, Vemuganti G, Bhaduri A, Gaddipati S, Sangwan VS, Ghanekar Y. Culture and characterization of oral mucosal epithelial cells on human amniotic membrane for ocular surface reconstruction. Mol Vis 2008; 14:189-96.
18. Nakamura T, Yokoo S, Bentley AJ, et al. Development of functional human oral mucosal epithelial stem/progenitor cell sheets using a feeder-free and serum-free culture system for ocular surface reconstruction. Sci Rep 2016; 6:37173.
19. Roh J□L, Lee J, Jang H, Kim EH, Shin D. Use of oral mucosal cell sheets for accelerated oral surgical wound healing. Head & Neck 2018; 40:394-401.
20. Daniels JT, Kearney JN, Ingham E. Human keratinocyte isolation and cell culture: a survey of current practices in the UK. Burns 1996; 22:35-39.

LETTER TO THE EDITOR

I-LEVEL POSITIVE AIRWAY PRESSURE VENTILATION FOR PATIENTS WITH HYPOXEMIA AFTER CORONARY ARTERY BYPASS GRAFTING

WW. CAI, J. HU, H. WANG, GJ. ZHU, S. CHEN and XP. CHEN

Luoyang Central Hospital Affiliated to Zhengzhou University, Luoyang, China

Received July 21, 2018 – Accepted December 6, 2018

Coronary artery bypass grafting (CABG) is an effective scheme for treatment of myocardial ischemia. Hypoxemia is a common complication of CABG, which can affect surgical effect and prognosis and even induce multiple organ failure. To explore the clinical efficacy of bi-level positive airway pressure ventilation in the treatment of CABG-associated hypoxemia, 216 patients who were admitted to our hospital between August 2015 and April 2017 and developed CABG-associated hypoxemia were selected and randomly divided into 2 groups, an observation group (n=108) and a control group (n=108). Patients in the control group were given conventional treatment including continuous oxygen inhalation through nasal tube, anti-infection, bronchodilation, phlegm resolving, nutrition support, analgesia, cardiac function maintenance, coronary dilatation, anticoagulation and maintenance of stable internal environment, while patients in the observation group were given positive airway pressure ventilation via a breathing machine or nasal mask besides the conventional treatment. The arterial blood gas indexes and blood circulation indexes of patients in the two groups were detected before and after treatment, the number of cases of reintubation was recorded, and the curative effects were analyzed. The results demonstrated that the arterial gas indexes and blood circulation indexes of patients in the observation group improved after treatment, and the improvement of the observation group was significantly superior to that of the control group (P<0.05). The intensity of hypoxia of the observation group was higher, and the number of cases of reintubation of the observation group was lower than that of the control group (P<0.05). Thus bi-level positive airway pressure ventilation is an effective non-invasive ventilation mode for treating CABG-associated hypoxemia because it can improve p(O_2), reduce p(CO_2) in a short time, relieve blood circulation, and reduce the rate of reintubation. Patients who develop hypoxemia after removal of tracheal intubation are advised to undergo bi-level positive airway pressure in the early stage.

To the Editor,

Coronary heart disease patients of an advanced age who have critical illness and organ dysfunction usually need surgical treatment. Coronary artery bypass grafting (CABG), which can effectively relieve myocardial ischemia and anoxia, is a safe treatment (1). Though CABG is being improved and incidence of complications has been reduced, CABG-associated hypoxemia still cannot be ignored. Hypoxemia has an incidence of 23-27%, which usually happens 1 or 2 hours after surgery (2). The occurrence of hypoxemia is associated to heart dysfunction, pulmonary atelectasis, obesity, smoking, deep hypothermic circulatory arrest and systemic

Key words: coronary artery bypass grafting; hypoxemia; bi-level positive airway pressure

Corresponding Author:
Dr Xingpeng Chen,
No. 288 Zhongzhou Road,
Luoyang Central Hospital
Affiliated to Zhengzhou University,
Luoyang, 471000, China
e-mail: chenxingpengdd@163.com

0393-974X (2019)

inflammatory response (3). The basic treatment (4) of hypoxemia includes increasing oxygen supply, reducing oxygen consumption and improving blood circulation. Postoperative occurrence of hypoxemia will delay the removal of tracheal intubation or lead to reintubation and a longer hospital stay. Severe hypoxemia can be life-threatening. When conventional drug treatment is ineffective in the treatment, mechanical ventilation as the last treatment means can save the lives of patients (5). However, one study (6) suggested that mechanical ventilation could not only increase pain in patients, but also induce complications such as ventilator-associated pneumonia. With the development of minimally invasive technology in recent years, non-invasive breathing machine assisted ventilation as a brand-new minimally invasive technology has gradually been applied in the treatment of respiratory system diseases (7). Meneses et al. (8) found that non-invasive breathing machine assisted ventilation treatment could significantly reduce the incidences of adverse reactions and complications and rapidly relieve dyspnea and hypoxemia in the treatment of respiratory distress syndrome. The present study was carried out to explore the clinical effect of bi-level positive airway pressure ventilation in the treatment of CABG-associated hypoxemia.

MATERIALS AND METHODS

Two hundred and sixteen patients who developed hypoxemia within 24 h after CABG and were admitted to our hospital between August 2015 and April 2017 were selected. There were 117 males and 99 females aged 46~68 years who had body mass index (BMI) between 24 kg/m^2 and 31 kg/m^2. There were 122 cases of hypertension, 52 cases of diabetes and 108 cases of smoking history. The subjects were randomly divided into a control group and an observation group, 108 in each group. The differences of basic data such as gender,

Table I. *General data of the two groups.*

Baseline data		Observation group (n=108)	Control group (n=108)
Gender	Male	56	61
	Female	52	47
Average age (years)		56.37±5.26	55.91±6.37
BMI (kg/m^2)		27.83±1.55	27.71±1.63
BSA (m^2)		1.91±0.24	1.90±0.22
Euro Score		6.12±1.28	6.15±1.25
LVEF (%)		55.67±6.81	55.81±7.02
With history of smoking		52	56
Accompanying diseases	Hypertension	56	66
	Diabetes	28	24

age, BMI, BSA, Euro Score, left ventricular ejection fraction (LVEF), accompanying diseases and history of smoking between the two groups had no statistical significance (P>0.05; Table I). This study has gained the approval from the ethical committee of our hospital, and all the patients signed informed consent.

Inclusion and exclusion criteria

The included patients were those who underwent CABG, developed hypoxemia within 24 h after tracheal extubation, had conscious mind and 60% FiO_2 and PaO_2 < 120 mm Hg when admitted to the intensive care unit (ICU).

Patients who had severe primary diseases in the liver or kidney, blood or immune function disorders, history of atrial fibrillation and hyperthyroidism, unstable hemodynamics, preoperative pulmonary diseases, such as chronic obstructive pulmonary disease (COPD), asthma and pneumothorax, severe postoperative complications, weak or stopped autonomous respiration, or disturbance of consciousness, attended trails previously or were attending other trials were excluded.

Treatments

Patients in the control group were given comprehensive treatment including continuous oxygen inhalation through a nasal tube, anti-infection, bronchodilation, phlegm resolving, nutrition support, analgesia, diuresis, cardiac function maintenance, coronary dilatation, anticoagulation and maintenance of stable internal environment. Patients in the observation group were given positive pressure ventilation via face or nasal mask using bi-level positive airway pressure breathing machine besides the comprehensive treatment. The breathing machine was set at spontaneous/timed mode. The respiratory frequency was set as 12~18 times/min; the inhale pressure was set as 8~10 cm H_2O initially and then increased to 16~18 cm H_2O; the respiratory pressure was set 0~4 cm H_2O. The parameters were adjusted according to blood gas analysis. The ventilation treatment lasted for 24 h, and an interval

Table II. *Arterial blood gas analysis of the two groups before and after treatment.*

Group		$p(O_2)$/mmHg	$P(CO_2)$/mmHg	SpO_2/%	PO_2/FiO_2
Observation group	Before treatment	70.24±9.26	39.36±2.27	91.21±2.23	141.23±21.55
	After treatment	140.1±21.54*#	34.48±2.05*#	99.42±0.48*#	284.72±34.17*#
Control group	Before treatment	70.02±9.43	39.45±2.33	90.94±2.18	140.57±20. 88
	After treatment	119.3±20.01*	36.16±2.07*	96.63±1.27*	235.52±29.64*

(*mean±SD). *P<0.05 compared to before treatment; # P<0.05 compared to the control group.*

of 15~30 min was allowed during ventilation. To prevent rebreathing of CO_2, a non-return valve was used in the mouth-nose mask. The breathing machine was removed if the patient had conscious mind and had stable pressure.

Observation of indexes

Indexes such as arterial blood gas, including arterial partial pressure of oxygen ($p(O_2)$), arterial carbon dioxide partial pressure ($p(CO_2)$), oxygen saturation (SpO_2), oxygenation index (PO_2/FiO_2), and blood circulation indexes including heart rate (HR), mean arterial pressure (MAP), LVEF, were detected before and after treatment, respectively. The disease conditions of the patients were closely observed were followed up during the treatment, and the number of cases of reintubation was recorded.

Statistical analysis

All the data were statistically analyzed using SPSS ver. 20.0. Measurement data were expressed as mean±standard deviation (SD). Comparison between groups was performed using *t*-test. Enumeration data were processed using *Chi*-squared test. Difference was considered statistically significant if $P<0.05$.

RESULTS

Arterial blood gas analysis

The difference of the arterial blood gas indexes between the two groups had no statistical significance before treatment ($P>0.05$). $p(O_2)$, SpO_2 and $p(O_2)/FiO_2$ of both groups increased, $p(CO_2)$ decreased after treatment, and the differences before and after treatment had statistical significance ($P<0.05$). The improvement of the indexes of the observation group was significantly superior to that of the control group (Table II).

Analysis of blood circulation indexes

The differences of the blood circulation indexes between the two groups were not statistically significant before treatment ($P>0.05$). After treatment, the HR and MAP of the two groups decreased, and LVEF increased; the differences had statistical significance ($P<0.05$). Moreover the improvement of the indexes of the observation group was significantly superior to that of the control group (Table III).

Table III. *Blood circulation indexes before and after treatment.*

Group		HR/(time/min)	MAP/mmHg	LVEF/%
Observation group	Before treatment	94.13±5.41	92.36±7.81	50.11±4.09
	After treatment	81.04±4.79*#	77.68±5.46*#	56.38±4.29*#
Control group	Before treatment	94.90±5.26	92.51±7.80	50.09±3.93
	After treatment	83.47±4.46*	81.02±5.56*	53.25±4.11*

*(mean±SD). * $P<0.05$ compared to before treatment; # $P<0.05$ compared to the control group.*

Comparison of postoperative symptoms and signs between the two groups

In the observation group, 73 patients (67.6%) had controlled disease conditions, i.e. HR between 80 and 100 times/min, respiratory frequency between 18 and 20 times/min, disappeared dyspnea and conscious mind; 34 patients (31.5%) had relieved symptoms, and 2 patients (1.9%) underwent reintubation; none of the patients had breathing machine-associated complications such as barotrauma or pneumothorax. In the control group, 55 patients (50.9%) had controlled disease conditions, 42 patients (38.9%) had relieved symptoms, and 11 patients (10.2%) underwent reintubation. The percentage of cases of reintubation of the observation group was significantly lower than that of the control group (χ^2=3.168, P<0.05).

DISCUSSION

Hypoxemia is an important complication of CABG which can lead to delayed postoperative recovery, extended hospitalization and increased medical expense and affect the survival and prognosis of patients. It is one of key factors affecting postoperative recovery (9), therefore it is of great importance to treat CABG-associated hypoxemia with effective therapies.

Previously, CABG-associated hypoxemia was usually treated by invasive mechanical ventilation or oxygen inhalation, but the effects of these two therapies were found limited in practice. With the development of medical technology, non-invasive bi-level positive airway pressure ventilation has emerged. Differing from the conventional tracheal intubation-assisted ventilation, non-invasive positive airway pressure ventilation can increase alveolar ventilation volume, relieve the state of hypoventilation, inhibit atrophy of pulmonary alveoli, regulate ventilation/perfusion ratio, strengthen the binding of tissues and oxygen, relieve left ventricle load, transform negative pressure in the pleural cavity to positive pressure, reduce ventricular wall pressure, and increase cardiac output (10, 11). The research results demonstrated that the arterial blood gas indexes and blood circulation indexes of the observation group were significantly superior to those of the control group, which conformed to the aforementioned mechanism. It indicated that bi-level positive airway pressure was reliable in relieving the clinical symptoms of patients with CABG-associated hypoxemia in a short time.

Moreover, bi-level positive airway pressure ventilation has obvious advantages, including little trauma, lower incidence of breathing machine-associated pneumonia, retention of cough, speaking and swallowing of patients and less pain. Moreover, it extends the application range of a breathing machine. In this study, the rate of reintubation of the observation group was significantly lower than that of the control group, which is similar to the research results of Joshi et al. (12). In conclusion, patients with hypoxemia are advised to undergo bi-level positive airway pressure ventilation in the early stage. But those who have no relief of symptoms and no improvement or even aggravation of blood gas indexes and hemodynamic indexes after non-invasive ventilation should establish smooth and closed artificial airway and be given invasive breathing machine-assisted ventilation.

REFERENCES

1. Shi S, Gao Y, Wang L, Liu J, Yuan Z, Yu M. Elevated free fatty acid level is a risk factor for early postoperative hypoxemia after on-pump coronary artery bypass grafting: association with endothelial activation. J Cardiothorac Surg 2015; 10(1):122.
2. Herlitz J, Wognsen G B, Haglid M, et al. Risk indicators for cerebrovascular complications after coronary artery bypass grafting. Thorac Cardiovasc Surg 2015; 46 (1):20-24.
3. Ji Q, Mei Y, Wang X, et al. Study on the risk factors of postoperative hypoxemia in patients undergoing coronary artery bypass grafting. Circ J 2008; 72(12):1975-80.
4. Mckiernan C, Chua LC, Visintainer PF, Allen H. High flow nasal cannula therapy in infants with bronchiolitis. J Pediatr 2010; 156(4):634-38.
5. Neves FH, Carmona MJ, Auler JO, Rodrigues RR, Rouby JJ, Malbouisson LM. Cardiac compression of lung lower lobes after coronary artery bypass

graft with cardiopulmonary bypass. PLoS One 2013; 8(11):e78643.
6. Bhandari V. Nasal intermittent positive pressure ventilation in the newborn: review of literature and evidence-based guidelines. J Perinatol 2010; 30(8):505-12.
7. Li JQ, Li N, Han GL, et al. Clinical research about airway pressure release ventilation for moderate to severe acute respiratory distress syndrome. Eur Rev Med Pharmacol Sci 2016; 20(12):2634-41.
8. Meneses J, Bhandari V, Alves JG, Herrmann D. Noninvasive ventilation for respiratory distress syndrome: a randomized controlled trial. Pediatrics 2011; 127(02):300-307.
9. Huffmyer JL, Groves DS. Pulmonary complications of cardiopulmonary bypass. Best Pract Res Clin Anaesthesiol 2015; 29(2):163-75.
10. Di Blasi RM. Neonatal noninvasive ventilation techniques: do we really need to intubate? Respir Care 2011; 56(9):1273-94.
11. Emr B, Gatto LA, Roy S, et al. Airway pressure release ventilation prevents ventilator-induced lung injury in normal lungs. JA-MA Surg 2013; 148(11):1005-12.
12. Joshi G, Tobias JD. A five year experience with the use of BiPAP in a pediatric intensive care unit population. Intensive Care Med 2007; 22:38-43.

LETTER TO THE EDITOR

EFFECT OF γ-SECRETASE INHIBITOR ON TREG IN PBMC OF RESPIRATORY SYNCYTIAL VIRUS BRONCHIOLITIS CHILDREN

LX. LIU[1*], XJ. ZHANG[2*], FL. WU[2] and X. HE[2]

[1]Child Healthcare Department, Zibo Maternal and Child Health Hospital, Zibo, China;
[2]Department of Pediatrics, the Affiliated Hospital of Binzhou Medical University, Binzhou, China

Received July 25, 2018 – Accepted January 9, 2019

[*]These Authors contributed equally to this work

Bronchiolitis is a widespread lower respiratory tract infection in infants and young children, and is closely related to the incidence of asthma, and T regulatory cells (Tregs) play a role in its pathogenesis. Notch signaling pathways are closely related to T cells and play a role in respiratory syncytial virus (RSV) bronchiolitis. In this study, we observed the changes in Treg and the level of FoxP3 mRNA in PBMCs in children with RSV bronchiolitis after blocking Notch signaling pathway by γ-secretase inhibitor MW167, which provides a new idea for RSV bronchiolitis immunotherapy. The study enrolled 30 patients with RSV bronchiolitis and 25 normal controls. PBMC was separated and divided into a normal control group, an RSV group, and an MW167 group. The percentage of Tregs was detected by flow cytometry, and the level of FoxP3 mRNA was detected by real-time fluorescent quantitative PCR. Compared with the normal group, the percentage of Tregs in the RSV group was decreased, and the levels of FoxP3 mRNA were significantly decreased. Compared with the RSV group, the percentage of Tregs in the MW167 group was increased, and the levels of FoxP3 mRNA were increased. There are changes in the percentage of Tregs and the level of transcription factor FoxP3 in PBMCs of children with RSV bronchiolitis, and γ-secretase inhibitor MW167 can reverse this change to a certain extent.

To the Editor,

Bronchiolitis caused by respiratory syncytial virus (RSV) infection is a lower respiratory tract infectious disease that occurs in winter and spring and is mostly seen in infants under the age of one year, and is closely related to asthma (1). Severe RSV bronchiolitis in early infancy can lead to lifelong changes in airway remodeling (2, 3). The peripheral blood of children with RSV has immune dysfunction, which is manifested as Th1/Th2 imbalance. In recent years, it has been found that $CD4^+CD25^+$ regulatory T cells (Treg) are a subgroup of T cells with immunomodulatory effects. Treg plays an immunomodulatory role *in vivo* (4, 5), inhibiting the overexpression of Th2 cytokines and playing an important role in reducing the occurrence of allergic diseases. Notch signaling pathway is a ubiquitous signal sequence that is highly conserved and can regulate the differentiation and development of T cells (6, 7). γ-secretase inhibitor (GSI) MW167 is its inhibitor. However, to date, there are few studies on the effects of γ-secretase inhibitor on Tregs. The purpose of this study was to study the effect of γ-secretase inhibitor (GSI) on peripheral

Key words: Treg; RSV; bronchiolitis; Notch signaling pathway; γ-secretase inhibitor

Mailing address:
Dr Fuling Wu,
No.661 Huanhe 2nd Road,
Department of Pediatrics,
the Affiliated Hospital
Binzhou Medical University, Binzhou, 256603, China
e-mail: wufulinggc@163.com

0393-974X (2019)

blood mononuclear cell (PBMC) Tregs in children with RSV bronchiolitis, and to seek new ideas for the immunotherapy of RSV bronchiolitis.

MATERIALS AND METHODS

All human studies are legal and were approved by Binzhou Medical University Ethics committee, and informed consent was obtained from the families of the children. The bronchitis group included infants who were diagnosed as RSV bronchiolitics and hospitalized in Binzhou Medical University Affiliated Hospital from August 2016 to February 2017; there were 19 male children and 11 female children. The average age was (5.6±3.6) months. All patients were under 2 years of age. The course of disease was within 2 days. Serum specific RSV antibody IgM was detected by solid-phase enzyme-linked immune adsorption assay. In the early stage of upper respiratory tract infection, the patients presented with persistent dry cough and paroxysmal dyspnea. Auscultation showed different degrees of wheezing in the lungs. Chest radiographs showed obstructive emphysema, peribronchitis and enlarged lung texture of different severity. The diagnosis was consistent with bronchiolitics diagnostic criteria of Practical Pediatrics of Zhu Futang. Uninfected infant samples were obtained from children with normal physical examination without cause of RSV infection. There were 13 males and 12 females. The average age was (5.3±3.4) months. All of the controls had no history of allergic or chronic diseases, and family history of allergies and asthma were not found. There was no history of infection or medication within the previous 2 weeks. The sex and age of the three groups were not statistically significant.

Sample collection and PBMC separation

After admission, 3 mL of peripheral venous blood was collected from each patient and processed by heparin for anticoagulation. 3 mL of lymphocytes separation medium was added in a new centrifuge tube. The blood of the patient was slowly added to the surface of the medium, and shaking was avoided. Then it was centrifuged at 500 g and room temperature for 30 min. There were 4 layers of liquid in the centrifuge tube: layer of red blood cells (red), layer of separating medium (transparent), PBMC layer (layer of white membrane) and layer of plasma (faint yellow). The layer of white membrane was moved to a new centrifuge tube and mixed with 10 mL of cell cleaning solution. Then it was centrifuged at 250 g for 10 min. After removal of the supernatant, the above operations were repeated. The sediment at the bottom of the centrifuge tube was PBMC.

Cell processing and culture

PBMC was obtained by resuspension using RPMI1640 medium which contained 10% fetal bovine serum. The concentration of the cells was adjusted to 1×10^6/ mL. It was inoculated into a 24-well plate, 1 mL each well. The cells were divided into a normal group, an RSV group and an MW167 group. The normal group included PBMC obtained by separation of peripheral blood of children in the control group; each well was added with 2 μL of dimethylsulfoxide (DMSO). The RSV group included PBMC obtained by separation of peripheral blood of children in the observation group; each well was added with 2 μL of DMSO. The MW167 group included PBMC obtained by the separation of peripheral blood of children in the observation group; each well was added with 2 μL of MW167 (1 mg of MW167 was dissolved in 141.7 μL of DMSO). Each well in the groups mentioned above was added with 10 μg/mL phytohemagglutinin. Then they were cultured in an incubator (37°C, 5% CO2). After 48 h, the cells were collected, and the supernate was cultured.

Flow cytometry

The percentage of Treg cells of the subjects in each group was detected using flow cytometry. Three flow cytometry tubes were taken and marked with blank control tube, isotype control tube and experimental tube respectively. 10 μl of anti-human CD4-FITC m Ab and 10 μl of Ig G1-FITC/Ig G1-PE-Cy5/Ig G1-PE were added to the isotype control tube. 10 μl of anti-human CD4-FITC m Ab, 5 μl of anti-human CD25PE-Cy5 m Ab and 10 μl of anti-human CD127-PE m Ab were added to the experimental tube. Then the three tubes were added with 50 μl of anticoagulant and then incubated at room temperature in the dark for 15 min. Then hemolysis and fixation were performed. It was detected by flow cytometry within 24 h after incubation. CD4+ cells were distinguished by CD4 histogram gating, after which the percentage of CD25+CD127- cells in CD4+ cells was detected.

Real-Time PCR

Total RNA was extracted from PBMC using TRIzol and reversely transcribed into first stranded complementary DNA (cDNA). In a 20 μl reaction system, the cDNA was 2 μl, and then Real-time PCR was performed using cDNA-specific primers. The SYBR Green Master Mix kit (Roche) was used for real-time PCR using the Bio-Rad iCycler iQ system (Bio-Rad). Real-time PCR was carried out under the following conditions: 95°C for 1 min, followed by 95°C for 5 s and 60°C for 30 s for 40 cycles. As a control, each cDNA sample was subjected to GAPDH amplification at the same time. The real-time PCR primers used are shown in Table I. The product length of GAPDH was 138 bp, and the product length of FoxP3 was 122bp. The threshold cycle (Ct) of each sample was determined, and the final statistical results were expressed as $2^{-\Delta\Delta Ct}$. All results were normalized to GAPDH expression.

Statistical analysis

Data are reported as mean ± SD. All data were analysed with SPSS17.0 statistical software. The normality and variance homogeneity test were performed on different groups. One-way ANOVA was used for analysis of metrological data. $P<0.05$ meant difference had statistical significance.

RESULTS

MW167 treatment affected the expression of Tregs

The percentages of Tregs in PBMCs were measured after 48 hours of *in vitro* culture. The proportion of Tregs in the three groups is shown in Table II. The ratio of Tregs in the RSV group was lower than that in the normal group ($^{*}P<0.01$), while the proportion of Tregs in the MW167 group increased ($^{*}P<0.01$).

Table I. *Primers of RT-PCR.*

	GAPDH	FoxP3
Forward primers	5'-GGTGTGAACCATGAGAAGTATGACA-3'	5'-TCCCAGAGTTCCTCCACAAC-3'
Reverse primers	5'-GTCCTTCCACGATACCAAAGTTGT-3'	5'-ATTGAGTGTCCGCTGCTTCT-3'

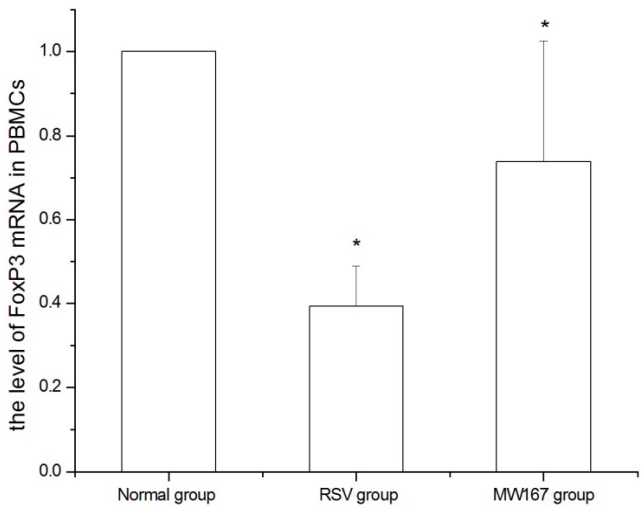

Fig 1. *Level of FoxP3 mRNA in PBMCs.*

Table II. *Proportion of Treg in the PBMC of children with RSV bronchiolitics.*

Group	n	Tregs(%)
Normal group	25	3.26±0.98825*
RSV group	30	1.18±0.44373
MW167 group	30	2.82±0.53918*

MW167 Effects on expression of Foxp3

The mRNA levels of Foxp3 were detected by real-time PCR in the normal group, RSV group and MW167 group at 48 h after separating PBMCs. The levels of FoxP3 mRNA in PBMCs are shown in Fig 1. Compared with the normal group, the level of FoxP3 mRNA in the RSV group was lower (*P<0.01); compared with the RSV group, the level of FoxP3 mRNA in the MW167 group was higher.

DISCUSSION

Bronchiolitis is mainly caused by RSV infection accompanied with strong inflammatory response. Overexpression of Th2 and/or immune deficiency reaction of Th1 plays an important role in the pathogenesis of RSV bronchiolitis (9).

$CD4^+CD25^+$Treg has an important role in $CD4^+$T cell lineage, which participates in the maintenance of immunoregulation and immune balance. Treg cells are involved in inhibition of the synthesis and secretion of Th2 and can indirectly participate in immunosuppression of the human body through regulating inflammatory cytokines (10, 11). Fox P3 is a member of the transcription regulator family. It is specifically expressed on $CD4^+CD25^+$Treg and plays an important role in the development, expression and maintenance of its function (12). It can reflect the activity level of $CD4^+CD25^+$Treg. In this study, the flow cytometry and real-time fluorescence quantitative RT-PCR detection showed that the ratio of $CD4^+CD25^+$Treg in peripheral blood and the expression of FOXP3 m RNA in the RSV group were lower than those in the normal control group at the same age. It indicated that a large amount of effector $CD4^+$T cells, especially Th2 cells, were activated because of insufficiency of $CD4^+CD25^+$Treg and decline of immunosuppressive function and a large number of pro-inflammatory cytokines generated. In addition, the number of $CD4^+CD25^+$Treg and the expression of FOXP3 mRNA in the MW 167 group increased, approaching the normal level, suggesting that GSI may inhibit Notch pathway and regulate Treg level to participate in inflammatory response. In conclusion, Notch signal pathway provides a new way for the treatment of bronchiolitis.

ACKNOWLEDGEMENTS

This study was supported by a grant from the Shandong Province Natural Science Foundation (ZR2014HL001) and grants from Soft Science Research Project of Binzhou (2016BRK19).

REFERENCES

1. de Steenhuijsen Piters WA, Heinonen S, Hasrat R, et al. Nasopharyngeal microbiota, host transcriptome, and disease severity in children with respiratory syncytial virus infection. Am J Resp Crit Care Med 2016; 194(9):1104-15.
2. Colak D, Saglik I, Mutlu D, Sarinoglu RC, Inan D, Gunay N. Detection and molecular characterization of respiratory syncytial virus (RSV) in children with lower respiratory tract infections. J Clin Virol

2015; 70:S72-S72.
3. Wyffels V, Smulders M, Gavart S, Fleischhackl R, Mazumder D, Gupta N, Nguyen-Van-Tam J. Evaluation of resource utilization among infants, young children and elderly patients diagnosed with Rsv infection in the United States. Value Health 2017; 20(9):A790-A791.
4. Chauhan A, Singh M, Agarwal A, Paul N. Correlation of TSLP, IL-33, and CD4+CD25+FOXP3+T regulatory (Treg) in pediatric asthma. J Asthma 2015; 52(9):868-72.
5. Dal Ben ER, do Prado CH, Baptista TS, Bauer ME, Staub HL. Patients with systemic lupus erythematosus and secondary antiphospholipid syndrome have decreased numbers of circulating CD4+CD25+Foxp3+Treg and CD3–CD19+B cells. Rev Bras Reumatol (English Edition) 2014; 54(3):241-46.
6. Amsen D, Helbig C, Backer RA. Notch in T Cell differentiation: all things considered. Trends Immunol 2015; 36(12):802-14.
7. Kobayashi M, Nabinger SC, Bai Y, et al. Protein tyrosine phosphatase PRL2 mediates Notch and Kit Signals in early T cell progenitors. Stem Cells 2017; 35(4):1053-64.
8. Jiang SS, Han SW, Chen JY, Li XJ, Che HL. Inhibition effect of blunting Notch signaling on food allergy through improving TH1/TH2 balance in mice. Ann Allerg Asthma Im 2017; 118(1):94-102
9. Scheltema NM, Gentile A, Lucion F, et al. Global respiratory syncytial virus-associated mortality in young children (RSV GOLD): a retrospective case series. Lancet Glob Health 2017; 5(10):e984-991
10. Li J, Dong XJ, Zhao L, et al. Natural killer cells regulate Th1/Treg and Th17/Treg balance in chlamydial lung infection. J Cell Mol Med 2016; 20(7):1339-51
11. Smith KA, Maizels RM. IL-6 controls susceptibility to helminth infection by impeding Th2 responsiveness and altering the Treg phenotype in vivo. Eur J Immunol 2014; 44(1):150-61.
12. Picca CC, Caton AJ. The role of self- peptides in the development of CD4+CD25+regulatory T cells. Curr Opin Immunol 2005; 17(4):131-36.

JOURNAL OF BIOLOGICAL REGULATORS & HOMEOSTATIC AGENTS Vol. 33, no. 2, 415-420 (2019)

LETTER TO THE EDITOR

MEGALIN – A FACULTATIVE MARKER OF OBESITY-RELATED GLOMERULOPATHY IN CHILDREN

D. OSTALSKA-NOWICKA[1*], K. MACKOWIAK-LEWANDOWICZ[1*], B. PEREK[2], K. ZAORSKA[3], J. ZACHWIEJA[1] and M. NOWICKI[3]

[1]Department of Pediatric Cardiology, Nephrology and Hypertension, Poznan University of Medical Sciences, Poznan, Poland; [2]Department of Cardiac Surgery, Poznan University of Medical Sciences, Poznan, Poland; [3]Department of Histology and Embryology, Poznan University of Medical Sciences, Poznan, Poland

Received July 30, 2018 – Accepted December 4, 2018

*These Authors contributed equally to this work

Obesity-related glomerulopathy (ORG) is an increasingly detected syndrome present in children with obesity. Megalin, a constitutive proximal tubule cell protein, when present in urine, can be considered as a biomarker indicating renal injury in these children. The aim of the study was to analyze 24-hour urine megalin excretion in children with obesity and compare its clinical usefulness to both urine (u) and serum (s) concentrations of neutrophil gelatinase-associated lipocalin (NGAL) and angiotensinogen (AGT). The study group consisted of 112 patients with obesity; the control group was composed of 90 age-matched healthy children. Daily urine megalin excretion, NGAL and AGT concentrations in serum and urine were estimated using ELISA assays. Obesity was defined by Body Mass Index (BMI) z score ≥ 2. GFR was calculated using Filler formula. An increased daily urine megalin excretion was detected in normo- and hypo-filtrating children with obesity (2.1±2.1 mg/kg b.w./24h and 12.4±3.6 mg/kg b.w./24h, respectively). In hyperfiltering children with obesity this excretion was found within control values (1.5±2.1 mg/kg b.w./24 h). sNGAL, uNGAL and uAGT concentrations were significantly increased in hyper- and hypo-filtering children with obesity. Normofiltering children with obesity (corresponding to individuals with asymptomatic ORG), presented significantly increased uAGT concentration. Elevated sNGAL and uNGAL concentrations are useful for characterization of both hyper- and hypo-filtration states in ORG. An increased daily urine megalin excretion in normofiltrating children with obesity, accompanied by elevated uAGT concentration, may indicate asymptomatic ORG in these children.

To the Editor,

Over the last decade, overweight and obesity have become a significant problem affecting the European pediatric population (1). Excess visceral fat, likewise, the accumulation of cervical adipose tissue, has been shown to be associated (even in children and adolescents) with hypertension, insulin resistance, type 2 diabetes, dyslipidemia, metabolic syndrome, nonalcoholic fatty liver disease and, what is particularly interesting, glomerulosclerosis (2).

Key words: obesity; obesity-related glomerulopathy; megalin; NGAL; BMI; a Body Shape Index; children

Corresponding Author:
Dr Michal Nowicki,
Department of Histology and Embryology,
Poznan University of Medical Sciences,
Swiecickiego st. 6, 60-781 Poznan, Poland
Tel.: +48618546453 - Fax: +48618546440
e-mail: mnowicki@ump.edu.pl

0393-974X (2019)

Obesity-related glomerulopathy (ORG) is an increasingly detected syndrome present in patients with class I (moderate) or class II (severe) obesity. The clinical manifestations of ORG, at the very beginning, are mainly proteinuria, a higher rate of renal plasma flow and, to some extent, increased glomerular filtration (3).

The etiopathogenesis of ORG is not fully understood, but some authors indicate the important initial role of renin-angiotensin-aldosterone system (RAAS) activation. Angiotensin II (Ang II), the main effector RAAS protein, has been shown to induce both glomerular and proximal tubule cell (PTC) injury, contributing to the progression of various incipient glomerulopathies (4). In this regard, megalin - the multiligand receptor and an endocytotic protein expressed exclusively in the brush border of the proximal tubule - can be considered as a protein whose normal function and/or presence in PTCs will be impaired following RAAS activation.

In line with above, the aim of the present study was to analyze daily megalin urine excretion in children with obesity and compare its clinical usefulness to both urine and serum concentrations of highly specific factors indicating the duration and extent of kidney damage - neutrophil gelatinase-associated lipocalin (NGAL) (5) and angiotensinogen (AGT) (6).

MATERIALS AND METHODS

Study population

A total number of 202 children (including 118 boys and 84 girls) was analyzed in the present report. The study group was composed of 112 patients diagnosed with moderate obesity (70 boys and 42 girls, mean age 10.1±1.4 years), admitted to the Department of Pediatric Cardiology, Nephrology, and Hypertension, Poznan University of Medical Sciences between October 1st 2014 and October 31st, 2017. Inclusion criteria were age from 7 to 14 years and diagnosis of moderate obesity (BMI z score ≥ 2). Children and adolescents affected by genetic obesity or familial hyperlipidemia were excluded from the study protocol. No study participant was taking antihypertensive, antidiabetic or lipid-lowering medicines, nor corticosteroids.

Ninety age-matched healthy children served as the control group (48 boys and 42 girls, mean age 10.4±1.6 years).

Based on the additional laboratory tests performed in both analyzed groups, no endocrine, cardiovascular, liver, nephrological disorders nor arterial hypertension were found. The clinical and biochemical data in studied children are summarized in Table I.

The study was conducted by the ethical principles of the Declaration of Helsinki. Poznan University of Medical Sciences Local Ethics Committee approved the research protocol (No. 0152/14), and an informed written consent was obtained from all the parents of studied children.

Anthropometric measurements

Weight and height were measured using a certified columnar scale (SECA 799, Hamburg, Deutschland) with BMI function. Obtained BMI values were transformed into BMI z scores using WHO reference values for pediatric BMI (7).

Waist circumferences was measured in centimeters using inextensible tape parallel to the ground. The measurement area corresponded to half the length between the lowest rib and the iliac crest, at the end of normal expiration. aBSI was calculated by employing the following formula $aBSI = WC(m)/(BMI^{2/3} \times H\,(m)^{1/2})$ (8). It was then converted to age and sex specific z scores calculated based on USA population normals (9).

Blood pressure

Systolic (SBP) and diastolic blood pressure (DBP) was measured using an aneroid sphygmomanometer 3 times after the patient sat still for at least 5 min. Hypertension was defined as blood pressure ≥ 95th percentile for age, sex and height.

Biomarkers for the diagnosis of obesity-related glomerulopathy

Five ml of peripheral blood and the 24-hour urine collection were obtained from all the studied children on the first day of hospitalization. The 24-hour urine amount was measured after thorough mixing. Ten mL of each urine sample was then centrifuged within 2 h after collection at 1000 rpm for 10 min to remove cellular debris. The cleaned urine samples were stored at −72°C until measurement. The laboratory tests included standard biochemical settings as well as megalin, NGAL and AGT evaluations.

All the children in the study and control groups were assessed for plasma concentration of creatinine, uric acid, cysC, glucose, and cholesterol. Additionally, daily urine collection for detection of microalbuminuria and/or proteinuria was carried out.

The presence of protein in the urine, assessed quantitatively as a trace, was defined as proteinuria <10mg/kg body weight in a portion of urine. Glomerular filtration rate (GFR) was assessed by Schwartz (10) and Filler (11) formulas in both groups. Hyperfiltration was defined as GFR > 130 ml/min/1.73m^2. In contrast, a reduced GFR (hypofiltration) was defined as GFR < 90 ml/min/1.73m^2.

Daily megalin excretion was estimated using Human LRP2/Megalin ELISA assay (LS-F11978-1, BD BioSciences, Warsaw, Poland). The concentrations of NGAL and ANG were estimated both in urine and serum samples using Human Lipocalin-2/NGAL Quantikine ELISA Kit (R&D Systems, Minneapolis, MN) and Human Angiotensinogen ELISA Kit (code 0797h, Wuhan EIAab Science Co., Warsaw, Poland) respectively.

The samples from patients and controls were run in duplicates. The assays were performed according to the manufacturer's instructions. The optical density (OD) value was determined twice using a microplate reader set to 450 nm and 540 nm as a wavelength correction. The readings at 540 nm were subtracted from the readings at 450 nm to correct for optical imperfections in the plate. The concentrations of NGAL, and ANG were calculated based on the standard curve. These standards were also assayed in duplicates.

Statistical analysis

All continuous variables are expressed as the mean±SD. Initially, they were assessed for normality with the Shapiro-Wilk *W* test. When they showed a normal

Table I. *Daily urine megalin excretion and mean concentrations of NGAL and AGT evaluated in the serum and urine of examined children.*

Parameter	Study group (n=112)			Control group (n=90)
	GFR > 130 ml/min/1.73m^2 (n=11)	90 ≤ GFR ≤ 130 ml/min/1.73m^2 (n=21)	GFR < 90 ml/ min/1.73m^2 (n=80)	
urine megalin excretion (mg/ kg/24h)	3.9±4.9*			1.0±0.6
	1.5±2.1	2.1±2.1*	12.4±3.6*	
(s)NGAL (ng/ml)	53.5±18.3*			45.5±8.1
	60.4±21.7*	44.9±8.6	77.6±21.8*	
(u)NGAL (ng/ml)	6.4±2.6*			5.3±1.8
	6.8±3.1*	5.6±1.2	9.2±2.8*	
(s)AGT (ng/ ml)	159.6±13.6			168.8±12.8
	155.2±12.8	161.4±14.3	158.7±13.9	
(u)AGT (ng/ ml)	14.4±1.8*			0.9±0.3
	13.1±1.4*	14.3±2.3*	15.8±1.8*	

*s: serum; u: urine; GFR: glomerular filtration rate (by Filler formula); NGAL: neutrophil gelatinase-associated lipocalin; AG: angiotensinogen; * p < 0.001 as compared with control group*

distribution, a subsequent analysis of variance (ANOVA) was employed, which was then followed by *post-hoc* comparisons of means (Tukey honest significant difference test for an unequal samples sizes in a group – Spjotvoll/ Stoline test). Non-parametric continuous variables were compared using the Kruskal-Wallis test. Pearson χ^2 test was employed to analyze nominal data.

The statistical analyses were performed using the Statistica 13.1 PL software package (Dell, Poland). A value of $p<0.05$ was considered to be statistically significant.

RESULTS

Clinical and biochemical analysis

Children composing study and control groups did not differ in serum concentrations of creatinine, glucose, and cholesterol. Significantly higher concentrations of serum cystatin C and uric acid were observed in the study group ($p<0.0001$). According to Schwartz formula, GFR values did not differ significantly between the study and control groups (109.7±6.4 ml/min/1.73m^2 and 113.4±3.8 ml/min/1.73m^2, respectively). As far as Filler formula was employed, mean GFR in the study group was 106.8±8.5 ml/min/1.73m^2 and 112.9±3.4 ml/min/1.73m^2 in the control group ($p=0.0017$).

The percentage of children with hyperfiltration (in the study group) was 14.3% using Schwartz formula and 19.6% by Filler formula (not significant). On the other hand, hypofiltration was found in only 10.7% of children with obesity by Schwartz formula and in as many as 37.5% of children composing the study group by Filler formula ($p=0.0023$).

A trace of protein in urine was found in 24 patients with obesity (13 boys and 11 girls), while in the control group proteinuria was not detected. Patients with obesity and control children had similar mean systolic and diastolic blood pressure.

Mean BMI z score in the study group was 2.57±0.67; mean aBSI in this group was 0.089±0.02 SD).

Mean serum and urine concentrations of NGAL and ANG, as well as mean 24-hour urine megalin excretion differed between children with obesity and control subjects. Mean daily urine megalin excretion was 3.9±4.9 mg/kg b.w./24 h in these children. In control subjects mean daily urine megalin excretion was 1.0±0.6 ($p<0.0001$). Similarly, the increased concentrations of serum NGAL, urine NGAL and urine AGT were noticed in patients with obesity ($p<0.001$). There was no significant difference in serum concentration of AGT between the two analyzed groups of patients (detailed information is shown in Table I).

According to the Filler formula, children with obesity were divided into "hyperfiltering" subjects (GFR>130 ml/min/1.73m^2; n=11), "normofiltering" children (90≤GFR≤130 ml/min/1.73m^2; n=21) and "hypofiltering" individuals (GFR<90 ml/min/1.73m^2; n=80).

Daily urine megalin excretion was found within control values (1.5±2.1 mg/kg b.w./24h) in hyperfiltering children. However, serum NGAL, urine NGAL and urine AGT concentrations were significantly increased as compared to controls (60.4±21.7 ng/ml, 6.8±3.1 ng/ml and 13.1±1.4 ng/ml, respectively).

Hypofiltering subjects were found to have significantly increased concentrations of serum NGAL (77.6±21.8 ng/ml), urine NGAL (9.2±2.8 ng/ml) and urine AGT (15.8±1.8 ng/ml) as well as 24-hour urine megalin excretion (12.4±3.6 mg/kg b.w./24h) compared to healthy children.

Interestingly, normofiltering patients with obesity showed only significantly increased expression of urine AGT (14.3±2.3 ng/ml) and elevated daily urine megalin excretion (2.1±2.1 mg/kg b.w./24h). This information is summarized Table I.

Clinical and biochemical factors associated with early kidney damage

Pearson correlation showed a high negative correlation between GFR (calculated by Filler formula) and serum NGAL (-0.5484), urine AGT (-0.5260) concentrations and daily urine megalin excretion (-0.8018).

Serum NGAL concentration was strongly positively correlated with BMI z score (0.57348), aBSI (0.56471), urine NGAL (0.54404) and 24-hour urine megalin excretion (0.64012). Finally, a high correlation was found between daily urine megalin excretion and urine NGAL concentration (0.53946) as well as BMI z score and aBSI (0.90819).

Detailed information is presented as matrix of correlations in Table II.

DISCUSSION

At present, several early kidney disease biomarkers can be listed. The most important include NGAL (5) and AGT (6). In reference to the literature, NGAL and AGT strongly negatively correlate with GFR values in ORG (12). Similar observations have been made in the current study. A significantly increased concentrations of serum NGAL, urine NGAL and urine AGT were observed in hyperfiltrating patients. In normofiltrating individuals with obesity, serum NGAL and urine NGAL were found within control values. Serum concentration of AGT did not differ between study and control children. However, urine concentration of AGT was found to increase linearly. Its concentration was significantly higher than in the control group, but it was not different between hyperfiltrating, normofiltrating and hypofiltrating children.

Can it therefore be concluded that only the elevated concentration of uAGT in normofiltering children is sufficient to diagnose ORG? Certainly not. Such a comprehensive analysis must be completed by determining at least one more factor. In our opinion, this might be megalin. The data presented in the correlation matrix shows that daily urine excretion of megalin negatively correlates with GFR, but positively with serum NGAL and urine NGAL. It does not correlate with urine AGT. For this reason 24-hour urine megalin excretion can be regarded as an independent (from urine AGT) ORG biomarker.

ACKNOWLEDGEMENTS

Financial support: grant number NR 13 0033 10/2010 State Committee for Scientific Research, NCBR. We thank Professor Geoffrey Shaw for his assistance with the English text.

Table II. *Correlation matrix of selected factors in the study group.*

	BMI Z score	aBSI	GFR	sNGAL	uNGAL	Megalin	uAGT
BMI Z score		**0.90819**	-0.3542	**0.57348**	0.28463	0.49267	0.17791
	aBSI		-0.3821	**0.56471**	0.36541	0.54548	0.20732
		GFR		**-0.5484**	-0.4223	**-0.8018**	**-0.5260**
			sNGAL		**0.54404**	**0.64012**	0.26629
				uNGAL		**0.53946**	0.31818
					Megalin		0.46650

BMI: body mass index; aBSI: a Body Shape Index; GFR: glomerular filtration rate (by Filler formula); sNGAL: serum neutrophil gelatinase-associated lipocalin; uNGAL: urine neutrophil gelatinase-associated lipocalin; AGT: angiotensinogen; ***bold:*** *high and very high correlation in J. Gilville's classification*

REFERENCES

1. NCD Risk Factor Collaboration (NCD-RisC). Worldwide trends in body-mass index, underweight, overweight, and obesity from 1975 to 2016: a pooled analysis of 2416 population-based measurement studies in 128.9 million children, adolescents, and adults. Lancet 2017; 16:2627-42.
2. Franchini S, Savino A, Marcovecchio ML, Tumini S, Chiarelli F, Mohn A. The effect of obesity and type 1 diabetes on renal function in children and adolescents. Pediatr Diabetes 2015; 16:427-33.
3. Adelman RD. Obesity and renal disease. Curr Poin Nehrol Hypertens 2002; 11:331-35.
4. Rutkowski P, Klassen A, Sebekova K, Bahner U, Heidland A. Renal disease in obesity: the need for greater attention. J Ren Nutr 2006; 16:216-23.
5. Devarajan P. NGAL in acute kidney injury: from serendipity to utility. Am J Kidney Dis 2008; 52:395-99.
6. Aroor A, Zuberek M, Duta C, Meuth A, Sowers JR, Whaley-Connell A, Nistala R. Angiotensin II stimulation of DPP4 activity regulates megalin in the proximal tubules. Int J Mol Sci 2016; 60:108-16.
7. Kêkê LM, Samouda H, Jacobs J, et al. Body mass index and childhood obesity classification systems: A comparison of the French, International Obesity Task Force (IOTF) and World Health Organization (WHO) references. Rev Epidemiol Sante Publique 2015; 63:173-82.
8. Krakauer NY, Krakauer JC. A new body shape index predicts mortality hazard independently of body mass index. PLoS One 2012; doi: 10.1371/journal.pone.0039504.
9. Krakauer NY, Krakauer JC. An Anthropometric Risk Index based on combining height, weight, waist, and hip measurements. J Obes 2016; doi: 10.1155/2016/8094275.
10. Mian AN, Schwartz GJ. Measurement and estimation of glomerular filtration rate in children. Adv Chronic Kidney Dis 2017; 24:348-56.
11. Bacchetta J, Cochat P, Rognant N, Ranchin B, Hadj-Aissa A, Dubourg L. Which creatinine and cystatin C equations can be reliably used in children? Clin J Am Soc Nephrol 2011; 6:552-60.
12. Kashani K, Cheungpasitporn W, Ronco C. Biomarkers of acute kidney injury: the pathway from discovery to clinical adoption. Clin Chem Lab Med 2017; 55:1074-89.

LETTER TO THE EDITOR

GPROTEIN-COUPLED ESTROGEN RECEPTOR 30 AND EXTRACELLULAR SIGNAL-REGULATED KINASE 1/2 IN ENDOMETRIAL ADENOCARCINOMA

YM. LI[1], YB. ZHANG[2] and HL. YANG[3]

[1]Department of Gynecology, Binzhou people's Hospital, Binzhou, Shandong, China; [2]Department of Radiology, Binzhou people's Hospital, Binzhou, Shandong, China; [3]Department of Oncology, Binzhou people's Hospital, Binzhou, Shandong, China

Received August 12, 2018 – Accepted December 11, 2018

Endometrial cancer which originates from the malignant proliferation and differentiation of endometrial epithelium cells, along with cervical cancer and ovarian cancer, are the three most malignant cancers in thereproductive system of females. The incidence of endometrial cancer ranked the second among the malignant cancers of reproductive system of females. Endometrial adenocarcinoma is the main pathological category, with an incidence of 20-30%. The current target treatment of endometrial adenocarcinoma is still being explored. Therefore it is of great significance to study the expression of signal pathway and gene proteins in the cancerous development of endometrial epithelium cells and their invasion and metastasis process. To investigate the expression of gprotein-coupled estrogen receptor 30 (GPR30) and phosphorylated extracellular signal-regulated kinase 1/2 (p-ERK1/2) in endometrial adenocarcinoma and its significance, the expressions of GPR30 and p-ERK1/2 in the tissues from 24 cases of endometrial adenocarcinoma, 24 cases of endometrial atypical hyperplasia (EAH) and 24 cases of normal endometrium were detected using streptavidin-perosidase method. The results demonstrated that the positive expression rate of GPR30 in the EAH and endometrial adenocarcinoma group significantly increased, and the differences with the normal endometrium group had statistical significance (P<0.05). The positive expression rate of p-ERK1/2 was the highest in the EAH group, and the difference with the normal endometrium group was statistically significant (P<0.05). The expression of GPR30 in endometrial cancer with different depth of myometrial invasion was significantly different; the deeper the myometrial invasion, the higher the positive expression rate (P<0.05). The expressions of GPR30 and p-ERK1/2 was in no correlation with the other clinicopathological parameters. There was no correlation between the expressions of GPR30 and p-ERK1/2 in the normal endometrium tissues (r_s=0.032, P>0.05), but there was a positive correlation between the expressions of GPR30 and p-ERK1/2 in the EAH and endometrial adenocarcinoma group (r_s=0.601, 0.557, P<0.05). Thus, it can be concluded that GPR30 may play its regulatory role in endometrial adenocarcinoma via p-ERK1/2 signal pathway.

To the Editor,

Endometrial adenocarcinoma, an endometrial epithelium derived malignant cancer, has an incidence of 20-30% among malignant cancers of the female reproductive system (1). There are 142,000 new cases, and about 42,000 females die of endometrial

Key words: endometrial adenocarcinoma; gprotein-coupled estrogen receptor 30; phosphorylated extracellular signal-regulated kinase 1/2

Corresponding Author:
Dr Yongmei Li,
No.515 Huanghe 7th Road,
Department of Gynaecology,
Binzhou people's Hospital,
Binzhou, Shandong, 256610, China
e-mail: liyongmeiag@163.com

0393-974X (2019)

DISCLOSURE: ALL AUTHORS REPORT NO CONFLICTS OF INTEREST RELEVANT TO THIS ARTICLE.

adenocarcinoma worldwide every year (2). Recent studies (3, 4) found a novel 7-transmembrane gprotein-coupled estrogen receptor 30 (GPR30) on human breast cancer cytomembrane which can rapidly combine with microestrogen to activate intracellular second messengers and mitogen-activated protein kinases (MAPK) and play the nongenomic effect of estrogen. Extracellular signal-regulated kinase (ERK) is a subtribe of the MAPk family, and the overactivation of signal transduction pathway is in a close correlation with the occurrence of tumor (5). ERK1 and ERK2 are two important members proved to be involved in the regulation of proliferation, differentiation and multiple metabolic functions of cells (6). Filardo et al. (7) found that estrogen could activate ERK in Michigan Cancer Foundation-7 cells (MCF-7) with positive expression of GPR30, but could not activate ERK in MDA-MB-231 cells which lack GPR30 unless being transfected with GPR30. Thus GPR30 plays an important role in ERK/MAPK signal pathway. Based on the aforementioned studies, the role of GPR30 in the pathogenesis of endometrial adenocarcinoma and the signal pathway mechanism of GPR30 in the participation of regulation of non-nuclear effect of estrogen were investigated in this study to provide a theoretical basis to search for new targets for treatment of endometrial adenocarcinoma.

MATERIALS AND METHODS

General data

Seventy-two patients who were admitted to hospital between April 2016 and April 2017 and had complete preoperative fractional curettage, hysteroscopy and postoperative pathological diagnosis data were selected. Patients who underwent surgical-pathological staging, had complete pathological and clinical data and signed the informed consent were included. Patients who had incomplete pathological and clinical data or developed other malignant cancers were excluded. There were 24 cases of endometrial adenocarcinoma, 24 cases of EAH and 24 normal cases. Tissues were collected from 24 patients (aged 46~68 years: median 55 years) with endometrial adenocarcinoma and prepared in paraffin-embedded samples. The revised International Federation of Gynecology and Obstetrics (FIGO) staging method was used; there were 6 cases of high differentiation (G1), 13 cases of moderate differentiation (G2) and 5 cases of low differentiation (G3). The EAH patients were aged 40~56 years (median 47.5 years). The normal patients were aged 40~61 years (median 48.5 years). All the cases were definitely diagnosed by more than two professional pathologists. The age of patients in the three groups was comparable.

Detection methods for the expressions of GPR30 and p-ERK1/2

The streptavidin-perosidase method was used according to the manufacturer's instructions. Antigen was repaired using a microwave. Positive controls and negative controls were set for each experiment. The positive sections were taken as the positive controls. Phosphate buffer solution (PBS) was taken as negative controls. Rabbit anti-human GPR30 polyclonal antibody ab98075 (Abcam company, USA) at a working concentration of 1:50, rabbit anti-human p-ERK1/2 polyclonal antibody BS4621 (Bioworld Company, USA) at a working concentration of 1:50, horse radish peroxidase labelled goat anti-rabbit second antibody 111-035-003 (Jackson Company, USA), immunohistochemical kit (SP9001) and DAB (3,3′-diaminobenzidine (Beijing Beijing Zhongshan Golden Bridge Biotechnology Co., Ltd., China) were used.

Determination criteria for results

The expression of GPR30 was found located in the cytoplasm and cell membrane under a light microscope, and the expression of p-ERK1/2 located in the cytoplasm and cell nucleus, manifested as brownish yellow or brown particles. The cells were counted using the double-blind method. Six fields were randomly chosen for each section under a high power lens (×400), and the percentage of positive cells was calculated. The score was given based on the staining degree and number of positive cells, and the standards referred to literature (8). The staining degree was scored as 0 points if all the stained cells were negative (-), as 1 point if the stained cells were weakly positive (+), as 2 points if the stained cells were moderately positive (++), and as 3 points if

the stained cells were strongly positive (+++). Cells were determined as positive if the staining intensity was stronger than the non-specifically stained cells in the background. Six high power fields in which the cancer cells concentrated intensively were randomly selected, and then at least 100 cancer cells were counted to observe their positive expression. It was scored as 1 point if the positive expression rate was smaller than 1%, as 2 points if the positive expression rate was between 1% and 10%, as 3 points if the positive expression rate was between 11% and 33%, as 4 points if the positive expression rate was between 34% and 66%, and as 4 points if the positive expression rate was between 67% and 100%. The antigen expression was determined as positive if the sum of the two scores was between 5 and 8 points; otherwise it was determined as negative. Each section was scored by two pathologists; the scoring was performed again if the scoring results of the two pathologists were inconsistent.

Statistical analysis

Data were statistically processed by SPSS. ver. 21.0. Enumeration data were expressed as rate. Comparison was performed using *Chi*-squared test and calibration *Chi*-squared test. Spearman's rank correlation was performed, and r=0.05 was regarded as the criteria for determining the correlation. Difference was considered significant if $P \leq 0.05$.

RESULTS

Expression of GPR30 and p-ERK1/2 in different tissues

In the endometrial adenocarcinoma tissues, GPR30 strongly expressed in the cytoplasm and cell membrane, manifested as brown yellow particles. The expression of p-ERK1/2 located in the cell nucleus and cytoplasm, mainly in the cell nucleus, manifested as brownish yellow particles which distributed as focally or dispersed. In the EAH tissues, GPR30 moderately expressed in the cytoplasm and cell membrane; the positive signals of p-ERK1/2 significantly enhanced, mostly in brownish yellow and sepia, and the cytoplasm and cell nucleus manifested as positive. In the normal endometrial tissues, the majority of GPR30 weakly expressed in cytoplasm, manifested as light yellow; the majority of p-ERK1/2 weakly expressed in the cytoplasm, manifested as light yellow.

The positive expression rates of GPR30 were 16.67% (4/24), 41.67% (10/24) and 70.83% (17/24) in the normal endometrial tissues, EAH tissues and endometrial adenocarcinoma tissues, respectively.

Table I. *The expression of GPR30 and p-ERK1/2 in different endometrial tissues [n(%)].*

Group	GPR30		p-ERK1/2	
	Positive	Negative	Positive	Negative
Endometrial adenocarcinoma	17 (70.83)[ab]	7(29.17)	11(45.83)	13(54.17)
EAH	10(41.67)[a]	14(58.33)	16(66.67)[a]	8(33.37)
Normal	4(16.67)	20(83.33)	7(29.17)	17(70.83)

[a] P<0.05 comparing with the normal group; [b] P<0.05 comparing with the EAH group.

The positive expression rate of the endometrial adenocarcinoma group was significantly higher than that of the other two groups (P<0.05). The positive expression rate of GPR30 in the EAH group was also obviously higher than that in the normal group (P<0.05). The positive expressions of p-ERK1/2 were 29.17% (7/24), 66.67% (16/24) and 45.83% (11/24) respectively in the normal endometrial tissues, EAH tissues and endometrial adenocarcinoma tissues. The positive expression rate of p-ERK1/2 in the EAH group was significantly higher than that in the normal group (P< 0.05; Table I).

Correlation between the expressions of GPR30 and p-ERK1/2

The expression of GPR30 was in no correlation with the expression of p-ERK1/2 in the normal endometrial tissues, but the EAH group and endometrial adenocarcinoma group suggested a positive correlation (P<0.05; Table II).

Correlations between the expressions of GPR30 and p-ERK1/2 and the clinicopathological parameters of endometrial adenocarcinoma

The analysis of the expression of GPR30 and clinical data of the endometrial adenocarcinoma group suggested that the expression of GPR30 was only correlated to the depth of myometrial invasion; the deeper the myometrial invasion, the higher the positive expression rate (P=0.003). No correlation was observed between the expression of p-ERK1/2 and different clinicopathological parameters (Table III).

DISCUSSION

GPR30-mediated estrogen non-genomic signals extensively participate in the physiological and pathological processes of the human body, including the occurrence and development of cancer (9). The results of this study showed that GPR30 had a low, moderate, or even no expression in the normal endometrium and EAH tissues, however high expression of GPR30 also existed, but the expression of GPR30 was moderate or high in the endometrial adenocarcinoma, which was similar to the results of a previous study (9). Moreover, there was a significant correlation between the expression of GPR30 and the depth of myometrial invasion. The further analysis found that the expression of GPR30 was in no obvious correlation with FIGO stage, degree of differentiation and metastasis of lymph nodes, revealing that GPR30 might not be directly involved in the process of biological behaviors such as tumor metastasis, but the involvement of GPR30

Table II. *Correlation between the expressions of GPR30 and p-ERK1/2 in different endometrial tissues [n(%)].*

P-ERK1 /2	GPR30					
	Normal		EAH		ECC	
	Positive	Negative	Positive	Negative	Positive	Negative
Positive	3(12.50)	4(16.67)	10(41.67)	6(25.00)	11(45.83)	0
Negative	1(4.17)	16(66.66)	0	8(33.33)	6(25.00)	7(29.17)
rs	0.032		0.601		0.557	
P	0.901		0.005		0.008	

Table III. *Correlation between the expressions of GPR30 and p-ERK1/2 and the clinicopathological parameters of endometrial adenocarcinoma.*

Pathological characteristics		GPR30			P-ERK1/2		
		Positive	Negative	P	Positive	Negative	p
Age	>55	7(70.00)	3(30.00)	0.433	6(60.00)	4(40.00)	0.122
	≤55	10(71.43)	4(28.57)		5(35.71)	9(64.29)	
Menstruation	Pre-menopause	6(60.00)	4(40.00)	0.217	7(70.00)	3(30.00)	0.143
	Post-menopause	11(78.57)	3(21.43)		7(50.00)	7(50.00)	
Histological stage	G1	4(66.67)	2(33.33)	0.069	3(50.00)	3(50.00)	0.147
	G2	9(69.23)	4(30.77)		6(46.15)	7(53.85)	
	G3	4(80.00)	1(20.00)		2(40.00)	3(60.00)	
FIGO stage	Stage I	7(58.33)	5(41.67)	0.485	4(33.33)	8(66.67)	0.492
	Stage II	5(71.43)	2(28.57)		3(42.86)	4(57.14)	
	Stage III	5(100.00)	0		4(80.00)	1(20.00)	
Lymphatic metastasis	Metastasis	5(83.33)	1(16.67)	0.352	3(50.00)	3(50.00)	0.227
	No metastasis	12(66.67)	6(33.33)		8(44.44)	10(55.56)	
Myometrial invasion	>1/2	10(100.00)	0	0.002	6(60.00)	4(40.00)	0.118
	≤1/2	7(50.00)	7(50.00)		5(35.71)	9(64.29)	

in a series of signal transduction pathways which were activated by estrogen might be one of the key ways in tumor proliferation and progress.

Whether ERK1/2 signal pathway is involved in the malignant process of endometrium is still controversial (10, 11). The results of this study demonstrated that p-ERK1/2 only had a high expression in the EAH tissues. Differing from the high expression of p-ERK1/2 in breast cancer and colon cancer (12), the expression of p-ERK1/2 in the endometrial adenocarcinoma tissues was low or moderate, which was mildly lower than that in the EAH group. It was assumed that ERK1/2 might have two different signal conditioning mechanisms in EAH and endometrial adenocarcinoma. In the experiment, the expression of p-ERK1/2 in the endometrial adenocarcinoma was in no obvious correlation with different clinical characteristics; therefore it was assumed that ERK1/2 signal pathway might not directly participate in the development of endometrial adenocarcinoma.

In conclusion, the specific mechanisms of p-ERK1/2 and GPR30 remain to be further studied. The results of this study may provide a new target for the treatment of endometrial adenocarcinoma.

REFERENCES

1. Stewart CJR, Doherty DA, Havlat M, et al. Transtubal spread of endometrial carcinoma: Correlation of intraluminal tumour cells with tumour grade, peritoneal fluid cytology, end extra-uterine metastasis. Pathol 2013; 454(16):4786-91.
2. Ren SJ. Pathological characteristics of endometrial

carcinoma in different ages. Southwest National Defense Med 2016; 23(06):621-24.
3. Albanito L, Madeo A, Lappano R, et al. Gprotein-coupled receptor 30 (GPR30) mediates gene expression changes and growth response to 17b-estradiol and selective GPR30 ligand G-1 in ovarian cancer cells. Cancer Res 2007; 67:1859-66.
4. Thomas P, Pang Y, Filardo E. J, et al. Identity of an estrogen membrane receptor coupled to a G-protein in human breast cancer cells. Endocrinol 2005; 146:624-32.
5. Liu T, Liu Y, Bao X, et al. Overexpression of TROP2 predicts poor prognosis of patients with cervical cancer and promotes the proliferation and invasion of cervical cancer cells by regulating ERK signaling pathway. PLoS One 2013; 8(9):e75864.
6. Wygrecka M, Dahal BK, Kosanovic D, et al. Mast cells and fibroblasts work in concert to aggravate pulmonary fibrosis: role of transmenbrance SCF and the PAR-2/PKC-a/Raf-1/p44/42 signaling pathway. Am J Pathol 2013; 182(6):2094-108.
7. Filardo EJ, Graeber CT, Quinn JA, et al. Distribution of GPR30, a seven membrane-spanning estrogen receptor, in primary breast cancer and its association with clinicopathologic determinants of tumor progression. Clin Cancer Res 2006;12 (21):6359-66.
8. Leake R, Barnes D, Pinder S, et al. Immunohistochemical detection of steroid receptors in breast cancer: a working protocol. UK Receptor Group, UK NEQAS, The Scottish Breast Cancer Pathology Group, and The Receptor and Biomarker Study Group of the EORTC. J Clin Pathol 2000; 53:634-35.
9. Maggiolini M, Picard D. The unfolding stories of GPR30, a new membrane-bound estrogen receptor. J Endoerinol 2010; 204(2):105-14.
10. Peng Y, Yang H, Zhu T, et al. The antihepatic fibrotic effects of fluorofenidone ria MAPK signalling pathways. Eur J Clin Invest 2013; 43(4):358-68.
11. He YY, Cai B, Yang YX, et al. Blackwell Publishing Asia Estrogenic G protein-coupled receptor 30 signaling is involved in regulation of endometrial carcinoma by promoting proliferation, invasion potential, and interleukin-6 secretion via the MEK/ERK mitogen-activated protein kinase pathway. Cancer Sci 2009; 100(6):1051-61.
12. Sebolt-Leopold JS, Herrera R. Targeting the mitogen-activated protein kinase cascade to treat cancer. Nat Rev Cancer 2004; 4(12):937-947.

LETTER TO THE EDITOR

EVALUATION OF GLUCOCORTICOID TREATMENT ON DIFFERENT PATHOLOGICAL TYPES OF PRIMARY NEPHROTIC SYNDROME

Y. ZHANG, YY. WANG, R. FU and X. YAN

Nephrology Department, The Second Affiliated Hospital of Qiqihar Medical University, Qiqihar City, China

Received October 25, 2018 – Accepted January 11, 2019

This study aimed to assess the distribution of pathotypes in primary nephrotic syndrome (PNS) and their relationship with glucocorticoid treatment efficacy. The study included 120 patients who were treated in the nephrology, internal medicine and pediatrics wards of The Second Affiliated Hospital of Qiqihar Medical University between March 2014 and October 2017 and who underwent renal biopsy to confirm PNS. The patients with PNS were divided into a child group (40 cases, aged 0~17 years) and an adult group (80 cases, aged over 18 years). We evaluated the correlation of the curative effect of glucocorticoid with age, pathological type, renal tubulointerstitial damage retinol binding protein and total urine protein. The main pathological types of PNS were glomerular minor lesion (GML) and mesangial proliferative nephritis (MPGN). The glucocorticoid treatment had an improved effect on children compared to adults, and also the effect decreased with age. The pathotypes of PNS were correlated with hormone resistance: tubulointerstitial lesions were associated with glucocorticoid resistance which was also associated with the degree of tubular damage. In both adults and children the retinol binding protein (RBP) urinary levels were positively associated with the degree of renal tubular injury. In conclusion, age, pathological type, renal tubulointerstitial damage, and RBP urinary level were related to the therapeutic effect of glucocorticoid treatment in adults and children with PNS.

To the Editor,

Primary nephrotic syndrome (PNS) is a glomerulopathy caused by a variety of renal pathologies. If it is not treated in time, it may eventually develop into end stage renal failure (ESRF) (1). Two major types of complications can appear in PNS, one related to the treatment and known as drug-induced complications (e.g. cyclophosphamide, cyclosporin A, corticosteroids) and the other related to the disease and known as disease-related complications. The most severe disease-related complications are the infections such as sepsis or peritonitis with germs resistant to the usual antibacterial therapy (eg Gram-negative bacteria, pneumococci) (2). Because of the hyperlipidemia that exists in PNS, the risk of cardiovascular disease is high in these patients. Some liver diseases, such as viral hepatitis C, non-alcoholic fatty liver disease, persistent proteinuria and severe hypoalbuminaemia, may greatly influence hypercholesterolemia (3).

Nowadays, the treatment of PNS is mainly based on glucocorticoids (GLU) (4). In this clinical condition, the management includes preventing infection, anti-coagulation treatment and lipid regulation, to slow down or reverse the evolution of the disease. Primary nephrotic syndrome can be divided into hormone

Key words: primary nephrotic syndrome; pathotype; glucocorticoids; hormone sensitivity/resistance

Corresponding Author:
Dr Xu Yan,
Nephrology Department,
The Second Affiliated Hospital
Qiqihar Medical University,
Qiqihar City 161000, China
e-mail: dryanxuyx@163.com

0393-974X (2019)

sensitive PNS and hormone resistant PNS. Hormone resistant PNS can easily progress towards end stage renal failure (ESRF), which is difficult to treat (5). Therefore, early diagnosis and early treatment with hormonal therapies for delaying the progression of PNS into ESRF are critical in renal disease. There are many factors that influence the response to hormonal therapy. Therefore, in order to understand the influence of various factors of the therapeutic effect in PNS, this study proposed to analyze the impact of age, renal injury and other factors relative to the response to hormonal therapy in PNS.

MATERIALS AND METHODS

Patients

The study included 120 patients from the nephrology, internal medicine and pediatrics wards of The Second Affiliated Hospital of Qiqihar Medical University between March 2014 and October 2017, with clinical primary nephrotic syndrome (PNS) who underwent renal biopsy. The clinical diagnosis of primary nephrotic syndrome was based upon Diagnostic Criteria of Nephrotic Syndrome. The patients were divided according to age into a child group (40 cases, aged 0~17 years) and an adult group (80 cases, aged over 18 years). The study was approved by the Ethics Committee of The Second Affiliated Hospital of Qiqihar Medical University and all subjects included in the study signed an inform consent to participate in the study or informed written consent was given by the family or guardian.

Inclusion criteria: (i) meeting the diagnostic criteria of PNS; (ii) age 0-65 years; (iii) signing the consent to use glucocorticoids and received regular hormone therapy; (iv) the control group included subjects with normal renal function (normal serum creatinine, urea nitrogen, etc., creatinine clearance rate greater than 60 ml/min or no obvious abnormal renal B-mode ultrasound. Exclusion criteria: (i) those who do not meet the inclusion criteria; (ii) patients with systemic diseases such as lupus nephritis, obesity-related glomerulopathy and paraproteinemia who do not have obvious clinical symptoms at the initial stage or for which the staging of renal disease was not easily established by laboratory examination after consent to renal biopsy; (iii) pregnant or lactating women; (iv) patients with serious primary diseases, such as cardiac insufficiency, respiratory failure or hematological diseases; (v) patients with severe complications, such as severe infections, uncontrollable hypertension or deep venous thrombosis; (vi) patients with poor compliance or mental disorders.

Hormone therapy

After routine examination to exclude contraindications of hormone use, the subjects received prednisone 2 mg/kg ▪ day, orally, divided into 3 doses per day. The glucocorticoid therapy was associated with calcium carbonate D3 one tablet per day (morning), diet management and heparin as anticoagulant.

Observation indexes

The effect of glucocorticoid treatment was evaluated by the following outcomes: total urine protein, biochemical parameters, blood cytology, blood coagulation and histopathological findings. Total urine protein was measured by IQ200 series automatic urine analyzer (Beckman Coulter, USA) 24 h before and 8 weeks after hormone treatment. Biochemical parameters determined by Architect c8000 biochemical analyzer (Abbott Diagnostics, USA) included: blood urea nitrogen (BUN), Creatinine (Cr), Triglycerides (TG), cholesterol (CH), Total protein (TP), Albumin (ALB), complement 3 (C3), and complement 4 (C4).

Retinol binding protein (RBP) levels in the urine were determined using RBP Urinary Competitive ELISA Kit (Thermo Scientific, USA).

Before renal biopsy routine tests were performed for blood cytology (DxH800 hematology analyzer, Beckman Coulter, USA), blood coagulation (PUN-2048 series semi-automatic coagulation analyzer, Beijing Perlong New Technology, China) and cardiopulmonary function (Cardiopulmonary function instrument, Shanghai Slpoo Medical Equipment, China). After the renal tissue sampling, the samples were prepared for light microscopy, electron microscopy and immunofluorescence. The renal disease was divided based on immunofluorescence into glomerular minor lesion (GML), mesangial proliferative nephritis (MPGN), membranous nephropathy (MN), focal segmental sclerosing glomerular inflammation (FSGS), IgA nephropathy (IgAN), sclerosing glomerulonephritis (SGN).

The evaluation of the degree of renal tubulointerstitial

injury was based on the semi-quantitative method described by Abe et al. (6). The renal injury was staged into four grades: no damage, slight damage (damage area<20), moderate damage (damage area in 20%~50%) and severe damage (damage area >50%).

Statistical analysis

The data obtained in this study was processed using SPSS19.0 software. The continuous variables were expressed in the form of mean ± standard deviation. Differences between groups of patients were analyzed used *Chi*-squared test for count data, and analysis of variance (ANOVA) or independent samples Student's *t*-test for continuous data. Correlation analysis was performed by Spearman Rank correlation method. A statistically significant difference between groups was considered when P<0.05.

RESULTS

Distribution of pathotypes

The relationship between the degree of renal tubulointerstitial injury and the sensitivity to hormone treatment is shown in Fig.1. In the glomerulonephritis form and mesangial proliferative nephritis, the correlation was strong both in adults and children.

Relationship between the degree of renal tubulointerstitial damage and the sensitivity to glucocorticoids

We observed a significant difference of the glucocorticoid sensitivity between the four degrees of renal tubulointerstitial damage (P<0.05). The level of urinary RBP and the degree of renal tubulointerstitial damage were positively correlated with sensitivity to glucocorticoid treatment (P<0.05). For all degrees of renal injury, the RBP urinary levels were higher in hormone resistant PNS compared with hormone sensitive PNS (P<0.05) (Table I).

Relationship between the protein content of urine and the sensitivity to glucocorticoids

There was a significant difference in the total amount of 24-h urine protein before and after the treatment in the hormone-sensitive group (P<0.05). There was no significant difference in the total amount of 24-h urine protein before and after

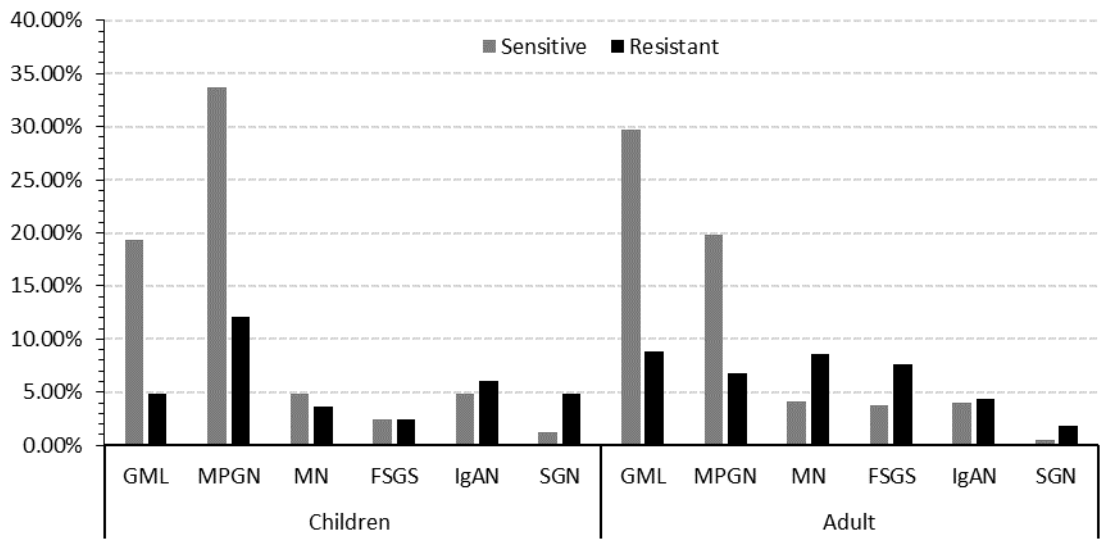

Fig. 1. *Distribution chart of sensitivity to hormone treatment in various pathological types of PNS. GML: glomerular minor lesion, MPGN: mesangial proliferative glomerulonephritis, MN: membranous nephropathy, FSGS: focal segmental sclerosing glomerular inflammation, IgAN: IgA nephropathy, SGN: sclerosing glomerulonephritis*

Table I. *Comparison of the relationship between urine RBP and 24-h total urine protein before and after the treatment and hormone sensitivity in PNS patients.*

		Adults			Children		
		Hormone sensitive (n=27)	Hormone resistant (n=13)	P value	Hormone sensitive (n=50)	Hormone resistant (n=30)	P value
No damage	Cases	21	2		10	1	
	RBP(mg/L)	0.36±0.19	0.97±0.67	0.031*	0.31±0.23	1.18±0.85	
	#P value	-	-		-	-	
	@P value	-	-		-	-	
Slight damage	Cases	21	18		13	7	
	RBP(mg/L)	1.19±0.87	3.03±1.02	0.026*	1.09±1.32	3.21±1.23	
	#P value	>0.05	0.001*		0.043*	0.014*	
	@P value	0.033*	0.041*		0.032*	0.028*	
Moderate damage	Cases	7	9		3	3	
	RBP(mg/L)	2.96±2.02	4.85±2.12	0.023*	2.03±1.53	3.62±1.34	
	#P value	0.008*	0.003*		0.003*	0.022*	
	@P value	0.025*	0.028*		0.027*	0.015*	
Severe damage	Cases	1	1		1	2	
	RBP(mg/L)	0.36±0.19	5.84±3.04	0.031*	3.38±2.13	4.98±1.67	
	#P value	0.001*	0.036*		0.001*	0.034*	
	@P value	0.007*	0.011*		0.012*	0.009*	
All cases	24 h TUP BT (mg/L)	4782±3581	5334±3465		3812±2024	3487±2132	
	24 h TUP AT (mg/L)	1302±1536	4753±3246		1065±632	3261±1016	
	₮P value	0.024*	0.082		0.034*	0.263	

*Note: # indicates that the group is compared with the group with normal renal tubular structure; @difference between levels before and after hormonal treatment; ₮difference between levels before and after hormonal treatment; *significant difference, P<0.05.PNS: Primay nephrotic syndrome, RBP: Retinol binding protein (RBP), 24-h TUP BT: levels of 24-h total urine protein before hormonal treatment, 24-h TUP AT: levels of 24-h total urine protein after hormonal treatment.*

Table II. *Biochemical and immunological parameters in adults and children before treatment. Blood urea nitrogen (BUN), Cr (Creatinine), TG (Triglycerides), cholesterol (CH), TP (Total protein), ALB (Albumin), complement 3 (C3), and complement 4 (C4).*

Categories	Children			Adult		
	Hormone sensitive (n=27)	Hormone resistant (n=13)	P	Hormone sensitive (n=50)	Hormone resistant (n=30)	P
ALB(g/L)	19.24±8.23	21.88±8.02	0.335	19.64±6.67	20.67±7.22	0.519
BUN(mmoL/L)	5.41±4.35	5.24±4.17	0.907	39.35±31.32	8.87±5.32	<0.001
C3(g/L)	1.18±0.32	1.10±0.16	0.402	1.04±0.06	1.01±0.31	0.507
C4(g/L)	0.23±0.08	0.24±0.09	0.724	0.26±0.07	0.28±0.11	0.323
Cr(μmoL/L)	54.65±35.12	61.43±43.52	0.600	101.36±70.23	115.02±71.41	0.405
CH(mmoL/L)	9.11±3.54	8.92±3.13	0.870	10.61±5.52	15.03±11.20	0.021
TG(mmoL/L)	2.49±1.21	2.28±1.13	0.6028	2.76±2.01	2.82±2.10	0.899
TP(g/L)	41.31±8.35	24.76±8.78	<0.001	42.09±9.24	42.13±8.73	0.985

*Note: *levels before treatment significantly differed compared with levels after treatment, P<0.05. BUN: blood urea nitrogen; Cr: creatinine; TG: Triglycerides; CH: cholesterol; TP: total protein; ALB: albumin; C3: complement 3; C4: complement 4*

treatment in the hormone-resistant group (P>0.05) (Table I).

Comparison of biochemical parameters, C3, and C4 before treatment with the sensitivity to glucocorticoids

In adult hormone treatment-sensitive patients there was a significant increase of BUN and a mild decrease of cholesterol (P<0.05), and in children a significant increase of total protein in hormone-sensitive patients. There was no significant difference in the rest of the biochemical parameters and C3 and C4 levels in adults and children before treatment between the hormone-sensitive group and hormone-resistant group, respectively (P>0.05) (Table II).

DISCUSSION

In our study, the main pathotypes in adults and children are GML and MPGN. Our data was different from the results of other studies, that could be related to racial differences (7). The hormone sensitivity of these two pathotypes was relatively higher, which could be related to the mild pathological changes and relatively good curative effect. The proportion of GML in hormone-sensitive children was lower than that in hormone-sensitive adults. This may be due to the transformation of this pathotype into focal segmental glomerulonephritis, thus affecting the efficacy of hormone (8), but the prognosis is quite good in this case. In the hormone-resistant group, the adult main pathotypes were FSGS, MN and GML, as in other reports (9). The main pathotypes in children were MPGN and IgAN.

The current study found that the sensitivity to glucocorticoid hormonal treatment was directly proportional with the degree of tubule-interstitial injury (P<0.05). This could be related to the induction of cytokine production (9, 10). RBP is a small molecule protein, with a normal low urinary level that increases when the tubular reabsorption is blocked (11), making it a good biomarker for the

evaluation of renal tubulointerstitial damage. Our study confirmed this hypothesis. In addition, the current study showed that in adults and children, the total proteins in 24-h urine decreased significantly after treatment in hormone-sensitive PNS patients, while in resistant PNS patients no changes were observed.

This study only assessed the physiological changes of patients with nephrotic syndrome before and after glucocorticoid treatment, but the underlying mechanism needs further research.

REFERENCES

1. Mok CC, Tse SM, Ho LY. AB0558 Association of the Metabolic Syndrome (Mets) with Vascular Complications, End Stage Renal Failure (ESRF) and Mortality in Patients with Systemic Lupus Erythematosus (SLE): A Cohort Analysis. Ann Rheum Dis 2015; 74(Suppl 2):1086:3-87.
2. Teodoru I, Rusu E, Radulian G. A 4 years study in diabetic chronic kidney disease patients on ketoaminoacids treatment in Bucharest. Results after 1-year follow-up. Farmacia 2018; 66(2): 296-301.
3. Agrawal S, Zaritsky JJ, Fornoni A, Smoyer WE. Dyslipidaemia in nephrotic syndrome: mechanisms and treatment. Nat Rev Nephrol 2017; 14(1):57-70.
4. Liang Y, Chen Y, Chen Y, Gong Y. Role of the glucocorticoid receptor in the recurrence of primary nephrotic syndrome. Exp Ther Med 2015; 10(4):1556-62.
5. Banaga AS, Mohammed EB, Siddig RM et al. Causes of end stage renal failure among haemodialysis patients in Khartoum State/Sudan. Bmc Res Notes 2015; 8:502.
6. Abe S, Amagasaki Y, Iyori S, Konishi K, Kato E, Sakaguchi H. Significance of tubulointerstitial lesions in biopsy specimens of glomerulonephritic patients. Am J Nephrol 1989; 9(1):30-37.
7. Arias LF, Henao J, Giraldo RD, Carvajal N, Rodelo J, Arbeláez M. Glomerular diseases in a Hispanic population: review of a regional renal biopsy database. São Paulo Med J 2009; 127(3):140-44.
8. Zhao Y, Su BG, Xiao HJ, et al. Clinical characteristics of glucocorticoid-induced eye adverse reactions in children with primary nephrotic syndrome. Beijing Da Xue Xue Bao Yi Xue Ban 2017; 49(5):794-97.
9. Zhang Y, Yang X, Jia LY, et al. Tripterygium glycosides for treatment of nephrotic syndrome: A systematic review and meta-analysis of randomised controlled trials. Eur J Integr Med 2018; 20:131-45.
10. Wagrowskadanilewicz M, Danilewicz M. Current position of electron microscopy in the diagnosis of glomerular diseases. Pol J Pathol 2007; 58(2):87-92.
11. Domingos MA, Moreira SR, Gomez L, et al. Urinary retinol-binding protein: relationship to renal function and cardiovascular risk factors in chronic kidney disease. Plos One 2016; 11(9):e0162782.

LETTER TO THE EDITOR

ANALYSIS OF IMAGING CHARACTERISTICS OF PATENT FORAMEN OVALE-RELATED CRYPTOGENIC STROKE

H. WANG, W. CHU, YH. KOU and SY. ZHANG

Ultrasonic Department, Luoyang Central Hospital Affiliated to Zhengzhou University, Henan, China

Received August 27, 2018 – Accepted January 9, 2019

Cryptogenic ischemic stroke (CS) is an important risk factor for the death and disability of young and middle-aged individuals. With the constant development of clinical medicine, it was found that patients with patent foramen ovale (PFO) have apparently higher risks of stroke than healthy people. Many scholars and some clinical scientists consider PFO as the main cause of stroke of unknown origin occurring in young and middle-aged. This study aimed to investigate the correlation between PFO and cryptogenic ischemic stroke and analyze the characteristics of cerebral Diffusion-weighted magnetic resonance imaging (DW-MRI) of CS patients with PFO. One hundred and sixty-two young and middle-aged patients with CS who were admitted to our hospital between June 2014 and December 2016 were selected. They were divided into a CS-PFO positive group (n = 106) and a CS-PFO negative group (n = 56) according to the results of contrast echocardiography of the right heart and transesophageal echocardiography. The results demonstrated that the percentage of CS patients with PFO was significantly higher than that without PFO, but the baseline data of the two groups had no significant difference (P>0.05). The results of DWI suggested that infarct lesions of the CS-PFO negative group were mainly located in the cortex and sites which were more than 15 mm below the cortex compared to the CS-PFO positive group, and the difference was statistically significant (P<0.05). Regarding vascular distribution, infarct lesions of the two groups mainly located at the middle cerebral arteries (MCA), but the difference had no statistical significance (P>0.05). Thus, it is concluded that PFO may be an important pathogenic factor for CS patients, infarct lesions of patients with CS and PFO mainly locate at the sites which were more than 15 mm below the cortex, and paradoxical embolism may be the most probable pathogenesis of PFO-induced cerebral infarction.

To the Editor,

Ischemic stroke has become one of the major diseases threatening the health of human because of its constantly escalating incidence, high disability rate, fatality rate and increasingly higher incidence among young people (1,2). Stroke which is not induced by common pathogenic factors is attributed to unknown causes and is called cryptogenic ischemic stroke (CS) (3, 4), and accounts for 30-40% of all strokes. Etiotropic and effective prevention and treatment can be carried out if the pathogenesis is definite (5).

It was found that patients with patent foramen ovale (PFO) had significantly higher risk of diseases

Key words: cryptogenic ischemic stroke; patent foramen ovale; diffusion weighted imaging

Corresponding Author:
Dr Wen Chu,
No.288 Zhongzhou Road,
Luoyang Central Hospital
Affiliated to Zhengzhou University,
Henan, 47009, China
e-mail: chuwencwly@163.com

0393-974X (2019)

such as cerebral infarction and migraine compared to healthy people (6~8). One study regarding whether PFO can induce CS (9) suggested that the incidence of CS among young people aged 15-45 years increased from 8.3% to 64.2%. Therefore some scholars assumed that PFO might be correlated to CS. Diffusion-weighted imaging (DWI) is recognized as having high specificity and sensitivity in the diagnosis of acute ischemic stroke. However, the imaging characteristics of PFO-related cryptogenic cerebral infarction are controversial. It is not clear whether the category and characteristics of infarction of CS patients with PFO are different from those of infarction induced by large artery atherosclerosis or small artery occlusion. Therefore this study investigated the correlation between PFO and CS and analyzed whether the imaging characteristics of infarct lesions of patients with or without PFO had statistical differences. This study aimed to provide an assistance for the clinical diagnosis and treatment of young people with CS.

MATERIALS AND METHODS

Research subjects

One hundred and sixty-two young and middle-aged patients who were diagnosed with cryptogenic stroke and admitted to hospital between June 2014 and December 2016 were selected as research subjects. The included patients satisfied the Guidance for the Diagnosis and Treatment of Acute Ischemic Stroke of China (2010), were definitely diagnosed by head computed tomography (CT) or Magnetic Resonance Imaging (MRI), and were classified as cryptogenic stroke according to Trial of Origin Acute Stroke Treatment (TOAST) subtyping after admission. Those who had atherosclerotic cerebral infarction, small vascular cerebral infarction and cardiogenic embolism which was not induced by PFO according to TOAST subtyping, cerebral hemorrhage, cerebral arteritis, severe impairment of the heart, liver and kidney, hematological diseases, malignant tumors or lacunar infarction which was highly suspected being induced by microangiopathy were excluded. This study was reviewed and approved by the ethics committee of Luoyang Center Hospital Affiliated to Zhengzhou University, Henan, China, and all the research subjects signed informed consent.

Detection methods

All the subjects underwent right heart contrast echocardiography and transesophageal echocardiography.

Echocardiography and vascular ultrasound: Philips I E33 diasonograph was used for transthoracic echocardiography (M3S phased array probe, 1.5~4 MHz) and TEE (X7-2 matrix array probe, 2~7 MHz). Cervical vascular ultrasonic examination was performed using Philips IU22 diasonograph (linear array probe, 3~9 MHz). TEE finished within one week after attack. Before examination, the existence of foramen ovale and its size were observed in double atriums and four-chamber view after oral mucosal anesthetic was used. The examination results were divided into negative and positive. The main examination content included the existence of PFO, atrial septal aneurysm (ASA) and left atrial and auricle thrombus and relevant measurement. PFO was classified into three types, i.e. large PFO with a diameter no smaller than 4 mm, medium PFO with a diameter between 2 mm and 3.9 mm and small PFO with a diameter smaller than 2 mm, according to the diameter of foramen (2). The diagnostic criterion for ASA was lengthy and thin interatrial septum protruding to the right and right atriums or the sum of swing height of the two atriums larger than 11 cm.

Right heart contrast echocardiography: Saline microbubble contrast agent was prepared. Two 10-ml injectors were taken: one extracted 8 mL of normal saline, and the other extracted 1 mL of air. They were connected with two ports of a three-way valve respectively, and another port was connected with a 7 gauge scalp needle. After elbow venous puncture, 1 mL of venous blood was extracted from each subject and transferred to the injector which contained 8 mL of normal saline. After the three-way rotary knob was adjusted, the mixture was pulled into the injector which contained 1 ml of air. Then it was pushed back and forth rapidly for 15 times to make the blood, normal saline and air fully mixed. Right heart contrast echocardiography started after the mixture was rapidly injected via the elbow vein. During Valsalva manoeuvre, saline microbubble contrast agent was injected via the elbow vein. The existence of PFO was confirmed if there was more than three microbubbles in four cardiac cycles after the imaging of the right atrium (9).

Diffusion-weighted magnetic resonance imaging (DW-MRI)

All the patients underwent cerebral MRI and DWI

analysis within one week after admission. Signa 1.5 Tesla superconducting scanner (GE company, USA) was used. Gradient field was 200 mT/m; DWI adopted single-shot echo planner imaging (EPI) sequence, and diffusion sensitivity coefficient was 1000 s/mm^2; pulse repetition time/time of echo = 10000/20 ms, the size of matrix was 128 × 128; the thickness of layer was 5 mm; the spacing was 0, and the number of excitation was 1. Two experienced radiologists made double-blind analysis on all the imaging data, and the results were unified after discussion. The distribution and area of infarct lesions of different patients were mainly analyzed. Infarct lesions were divided into single infarct lesions including cortical infarct lesions and cortical-subcortical infarct lesions (less than 15 mm under the cortex) or cortical-subcortical infarct lesion (more than 15 mm under the cortex) and multiple infarct lesions including small diffused infarct lesions and large fused infarct lesions, i.e., multiple infarct lesions in the vascular dominance area (unilateral anterior cerebral circulation artery, unilateral cerebral posterior circulation artery, anterior cerebral artery, middle cerebral artery, posterior cerebral artery, anterior choroid artery, superior cerebellar artery, anterior inferior cerebellar artery and posterior inferior cerebellar artery involved simultaneously) according to DW-MRI results.

Statistical analysis

Data were statistically analyzed using SPSS ver. 20.0. Enumeration data were expressed by number and percentage; comparison between groups was performed using *chi*-squared test. Measurement data were expressed as mean ± standard deviation (SD); comparison between groups was performed using *t*-test. $P<0.05$ indicated that the difference had statistical significance.

RESULTS

Comparison of clinical data between the two groups

A total of 163 patients with cryptogenic stroke were included, of whom 106 (65.43%) were found having PFO by right heart contrast echocardiography and transesophageal echocardiography, and 56 patients (34.57%) had no PFO. The difference of number of patients with and without PFO had statistical significance ($\chi^2=5.364$, $P<0.05$). A typical case is shown in Figs. 1 and 2. The statistical analysis suggested no significant difference between patients with and without PFO in age, gender, vascular risk factors and National Institutes of Health Stroke Scale (NIHSS) score which was used for evaluating the severity of stroke ($P>0.05$, Table I).

Table I. *Clinical data between the two groups.*

Baseline data	CS-PFO positive group	CS-PFO negative group	t/X^2	P
Age (years)	44.81±5.73	44.76±5.37	0.754	>0.05
Gender (male)	89(84.0%)	45(80.4%)	0.542	>0.05
Hypertension	42(39.6%)	25(44.6%)	0.731	>0.05
Hyperlipidaemia	19(17.9%)	9(16.1%)	0.106	>0.05
Diabetes	10(9.4%)	6(10.7%)	0.084	>0.05
Smoking	12(11.3%)	6(10.7%)	0.619	>0.05
ASA	3(2.8%)	0(0%)	0.141	>0.05
Arrhythmia	6(5.7%)	1(1.8%)	0.739	>0.05
Coronary heart disease	20(18.9%)	10(17.8%)	0.621	>0.05
NIHSS (point)	3.44±2.83	4.20±3.18	0.946	>0.05

Table II. *Distribution characteristics of infarct lesions on DWI, n(%).*

Group		CS-PFO positive group	CS-PFO negative group
Single infract lesions	Cortical	15(14.2)	7(12.5)
	Corticosubcorti-cal < 15 mm	14(13.2)	13(23.2)
	Corticosubcorti-cal ≥ 15 mm	45(42.4)*	9(16.1)
Multiple lesions	Unilateral AC	16(15.1)	9(16.1)
	Unilateral PC	1(1.0)	4(7.1)
	Bilateral AC	6(5.7)	5(8.9)
	Bilateral PC	3(2.8)	2(3.6)
	Anterior and posterior circulations	8(7.5)	7(12.5)

* *P<0.05 comparing to the CS-PFO negative group*

Table III. *Vascular distribution area of infarct lesions, n(%).*

Group	CS-PFO positive group	CS-PFO negative group
Middle cerebral artery	69(65.1)	30(53.4)
Anterior cerebral artery	8(7.5)	1(1.8)
Anterior choroidal artery	3(2.8)	4(7.1)
Posterior cerebral artery	10(9.4)	9(16.1)
Basilar artery	8(7.5)	5(8.9)
Inferior cerebellar artery	0	0
Superior cerebellar artery	7(6.6)	3(5.4)
Middle cerebellar artery	1(1.0)	4(7.1)

Distribution characteristics of infarct lesions on DWI

The percentage of single infarct lesions was higher than that of multiple infarct lesions in the CS-PFO positive group; fifteen patients had single infarct lesions in the cortex (14.2%), 14 had single infarct lesions in the cortex and the site which was less than 15 mm under the cortex (13.2%), and 45 patients had single infarct lesions in the cortex and the site which was no less than 15 mm under the cortex (42.4%). The percentage of single infarct lesions was close to that of multiple infarct lesions in the CS-PFO negative group; 7 patients had lesions in the cortex (12.5%), 13 patients had lesions in the cortex and the site which was less than 15 mm under the cortex (23.2%), and 9 patients had lesions in the cortex and the site which was no less than 15 mm under the cortex (16.1%). Lesions in the CS-PFO positive group were mainly single lesions which involved the cortex and the site which was no less than 15 mm under the cortex, and the difference between the two groups had statistical significance (χ^2=7.169, P<0.05). The two groups had no significant difference in distribution characteristics of multiple infarct lesions in cerebral anterior and posterior circulation (Table II).

Distribution area of infarct lesions in DWI

The infarct lesions of the CS-PFO negative and positive groups mainly located in the middle

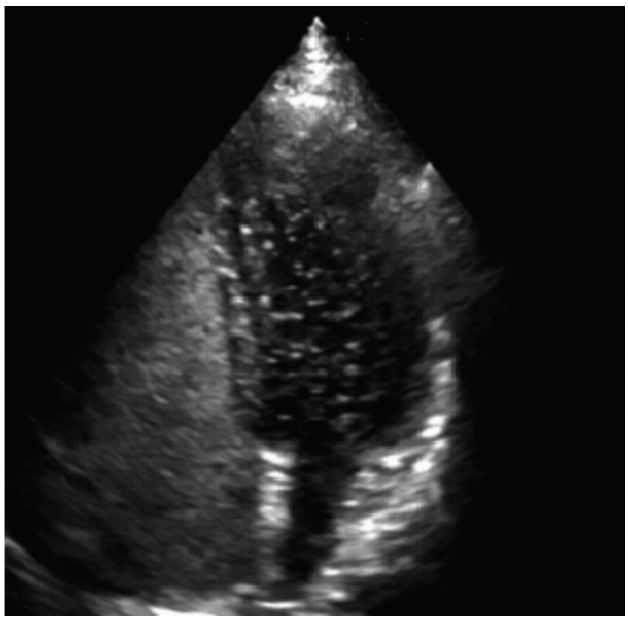

Fig. 1. *Right heart contrast echocardiography suggested a large number of microbubbles in the left atrium, indicating the presence of PFO,*

cerebral artery, but the vascular distribution of the infarct lesions in the two groups had no significant difference (Table III).

DISCUSSION

With the improvement of detection rate of PFO, PFO is considered as an important cause for patients with cryptogenic stroke, and it is assumed that its pathogenesis was that embolus of the venous system directly enters the left atrium-left ventricle-arterial circulation system via the abnormal channel, PFO, i.e., paradoxical embolism (10). The main purpose of this study was to analyze the correlation between CS and PFO and to explore the DW-MRI features of cryptogenic stroke-associated PFO by comparing the differences of infarct lesions between the CS-PFO positive group and CS-PFO negative group. To make results more reliable, right heart contrast echocardiography combined with transesophageal echocardiography was used in the diagnosis of PFO, which is more stringent than the previous study (11). Finally it was found that CS-PFO positive patients were significantly more than CS-PFO negative patients, suggesting that PFO might be an important pathogenic factor in patients with cryptogenic stroke. The results of this study also showed that the infarct lesions of the CS patients with PFO were mainly single lesions located in the subcortical layer (≥ 15 mm), which was consistent with previous research conclusions (12). These single infarct lesions were mainly located in the anterior circulation and most lesions of the two groups located in the middle cerebral artery region.

In conclusion, the risk of cerebral stroke in patients with PFO is significantly higher than that in normal subjects. Lesions of CS-PFO patients are mainly single lesions in the site which is no less than 15 mm under the anterior cerebral circulation cortex. Paradoxical embolism may be the most likely pathogenesis of PFO-induced cerebral stroke.

ACKNOWLEDGEMENTS

This study was supported by the Medical and Health Project of Science and Technology Plan of Luoyang (fund name: clinical application of detecting PFO using cTTE and cTCD and TEE in the diagnosis and treatment of young and middle-aged patients with cerebral infarction; fund number: 1721001A-1).

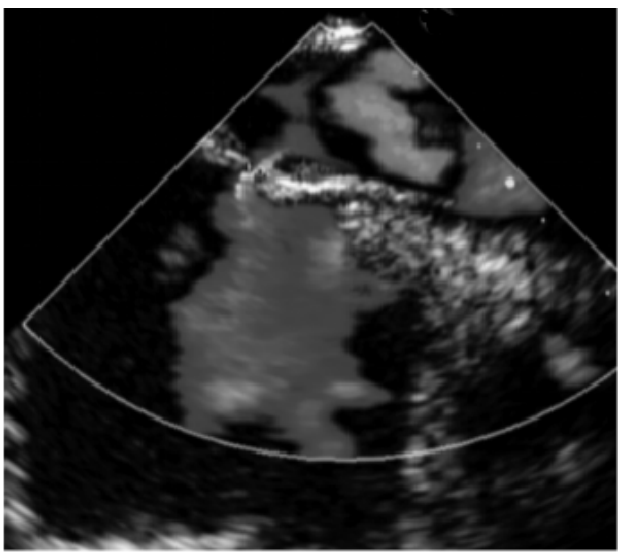

Fig. 2. *Transesophageal echocardiography suggested PFO (the diameter of foramen ovale: 1.9 mm).*

REFERENCES

1. Handke M. Harloff A. Olschewski M, et al. Patent foramenovale and dryptogenic stroke in older patients. N Engl J Med 2007; 357(22):2262-68.
2. Kent D M, Ruthazer R, Weimar C, et al. An index to identify strokerelated vs incidental patent foramen ovale in cryptogenic stroke. Neurol 2013; 81(7):619-25.
3. Furlan A J, Reisman M, Massaro J, et al. Closure or medical therapy for cryptogenic stroke with patent foramen ovale. N Engl J Med 2012; 366(11):991-99.
4. Piechowski-Jozwiak B, Bogousslavsky J. Stroke and patent foramen ovale in young individuals. Eur Neurol 2013; 69(2):108-17.
5. Carroll JD, Saver JL, Thaler DE, et al. Closure of patent foramen ovale versus medical therapy after cryptogenic stroke. N Engl J Med 2013; 368(12):1092- 100.
6. Tariq N, Tepper SJ, Kriegler JS. Patent foramen ovale and migraine: closing the debate-a review. Headache 2016; 56(3):462-78.
7. Fonseca AC, Ferro JM. Cryptogenic stroke. Eur J Neurol 2015; 22(4):618-23.
8. Akhondi A, Gevorgyan R, Tseng CH, et al. The association of patent foramen ovale morphology and stroke size in patients with paradoxical embolism. Circ Cardiovasc Interv 2010; 3(5):506-10.
9. Ferro JM, Massaro AR, Mas JL. Aetiological diagnosis of ischaemic stroke in young adults. Lancet Neurol 2010; 9(11):1085-96.
10. Sidia B, Saleh C, El Issa M, Mono M. Management of patent foramen ovale in patients with cryptogenic stroke: Is device closure superior to medical treatment? A brief review. Surg Neurol Int 2018; 9(1):132.
11. Stortecky S, da Costa BR, Mattle HP, et al. Percutaneous closure of patent foramen ovale in patients with cryptogenic embolism: a network meta-analysis. Eur Heart J 2015; 36(2):120-28.
12. Boutet C, Rouffiange-Leclair L, Garnier P, et al. Brain magnetic resonance imaging findings in cryptogenic stroke patients under 60 years with patent foramen ovale. Eur J Radio 2014; 83(5):824-28.

LETTER TO THE EDITOR

EFFECT OF TICAGRELOR AND CLOPIDOGREL ON PLATELET AGGREGATION FUNCTION AFTER PERCUTANEOUS CORONARY INTERVENTION IN PATIENTS WITH ACUTE CORONARY SYNDROME

Z. SUI and P. QU

Department of Cardiology, The Second Affiliated Hospital of Dalian Medical University, Dalian, China

Received October 1, 2018 – Accepted December 17, 2018

In this study, phosphorylation levels of vasodilator stimulated phosphoprotein (VASP) were detected by flow cytometry (FCM) to investigate the effects of ticagrelor and clopidogrel on platelet aggregation function (PAF) after percutaneous coronary intervention (PCI) in patients with acute coronary syndrome (ACS). Eighty patients with ACS treated by PCI were enrolled in this study. They were randomly divided into a ticagrelor group (group A, 40 cases) and clopidogrel group (group B, 40 cases). The levels of VASP phosphorylation in platelets were measured with FCM before drug treatment and at 24 hours, 7 days and 1 month after PCI treatment. In addition, the platelet reactivity index (PRI) was calculated and recorded, while the incidence of major adverse cardiovascular events (MACE) and bleeding events within 1 month after PCI intervention in the two groups was analyzed. The results showed that the PRI of group A was significantly lower than that of group B at 24 hours, 7 days and 1 month after PCI intervention (P<0.001). Significant difference was observed in the PRI of the two groups before drug treatment and at 24 hours, 7 days and 1 month after PCI intervention (P<0.001). The overall mean values of PRI between the two groups were also significantly different (P < 0.001). Furthermore, the percentage of PRI ≥ 50% in group A at different time points was significantly lower than that of group B (P<0.01). Nevertheless, there was no significant difference between the two groups in terms of the incidence of MACE and bleeding events within 1 month after PCI (P>0.05). In conclusion, compared to clopidogrel, ticagrelor reduces PAF more strongly and faster, which effectively reduced recurrence of post-PCI intervention ischemic cardiovascular events without increasing the risk of bleeding during a short period.

To the Editor,

Acute coronary syndrome (ACS) is a clinically serious type of coronary heart disease (CHD), which is usually caused by severe stenosis in the coronary artery (1). When the level of platelet activity increases, secondary platelet aggregation or thrombosis leads to a sharp increase in lumen stenosis (2). It has been shown that inflammatory factors, hyperlipidemia, hyperglycemia and other factors induce vascular endothelial damage and stimulate the activation, aggregation and thrombosis of platelets, the main pathophysiological mechanisms involved in ACS (3-5). ACS needs to be treated with an anti-platelet, anti-coagulation, or timely interventional therapy or a drug therapy (6). Although PCI has shown great clinical benefits in ACS patients, there is a risk of stent thrombosis after the treatment, therefore, an adequate anti-platelet therapy is required (7).

Currently, aspirin combined with $P2Y_{12}$ receptor inhibitor is more effective in reducing the probability

Key words: ticagrelor; clopidogrel; VASP; acute coronary syndrome; platelet aggregation function

Corresponding Author:
Dr Peng Qu,
Department of Cardiology,
The Second Affiliated Hospital
Dalian Medical University, No. 467 Zhongshan Road,
Shahekou District, Dalian, China
e-mail: qupengqp777@163.com

0393-974X (2019)

DISCLOSURE: ALL AUTHORS REPORT NO CONFLICTS OF INTEREST RELEVANT TO THIS ARTICLE.

of ischemic cardiovascular events after PCI intervention than aspirin alone (8). $P2Y_{12}$ receptor inhibitors include thienopyridines and cyclopentyl triazolopyrimidine. Ticagrelor reversibly binds to the $P2Y_{12}$ receptor, thereby blocking the adenosine diphosphate (ADP) pathway to inhibit platelet aggregation (9, 10). Therefore, FCM was employed in this study to measure levels of VASP phosphorylation to investigate the effect of ticagrelor on post-PCI platelet aggregation function (PAF) on ACS patients. In addition, the incidence of MACE and bleeding events was analyzed to optimize the application of post-PCI anti-platelet therapy in ACS patients.

MATERIALS AND METHODS

Patients

A total of 80 patients, initially diagnosed as ACS by coronary angiography and who underwent PCI between April 2017 and June 2018 in the Department of Cardiovascular Medicine at The Second Hospital of Dalian Medical University, were enrolled in this study. Patients and their families signed the informed consent and were able to insist on the review and follow-up with complete data. The study was approved by the Ethics Committee of The Second Affiliated Hospital of Dalian Medical University.

Inclusion criteria: ACS diagnosis was conformed to the ACS diagnostic criteria (11), including unstable angina pectoris (UAP), non-ST segmental elevation myocardial infarction (NSTEMI), and ST segment elevation myocardial infarction (STEMI); the patient had at least one stenosis in the coronary arteriography requiring PCI treatment; the patient first developed the disease and successfully completed PCI treatment within 12 hours; age, 35-75 years; the patients were treated for the first time and had not been taking any drugs within one month prior to admission that could affect platelet aggregation; the patients had at least one stenosis in the coronary artery requiring PCI treatment.

Exclusion criteria: patients taking glucocorticoids and non-steroidal anti-inflammatory drugs for nearly 2 weeks; those who had contraindications for ticagrelor or clopidogrel, such as abnormal coagulation, peptic ulcer, aortic dissection; those who had undergone surgery, or had severe trauma, shock or active bleeding in the previous 4 weeks; hypertension was not controlled (systolic pressure > 180 mmHg or diastolic pressure > 110 mmHg); those who had an arrhythmia, and the New York Heart Function Rating (NYHA) grade IV; those who suffered from severe liver insufficiency (glutamic-pyruvic transaminase reached more than 2 times the normal upper limit), severe renal insufficiency (requiring dialysis), and malignant tumors; pregnant and lactating women; patients taking drugs within one month prior to admission that may affect platelet function; those who took drugs affecting the activity of CYP enzyme within 3 months prior to admission; those who had serious multiple coronary artery stenosis or acute myocardial infarction requiring coronary artery transplantation; those who underwent surgery in February, 2017; those who underwent blood vessel surgery within 2 weeks; those who suffered from tumor and autoimmune diseases and hence had a higher risk of bleeding; those who suffered from organ failure, severe anemia, thrombocytopenia, or severe diseases of the blood system; those who had refractory hypertension with blood pressure higher than 180/110 mmHg after drug treatment; those who were allergic to drugs; those who had active peptic ulcer or ulcerative colitis; those who had history of moderate to severe cerebral hemorrhage or extensive cerebral infarction in the previous six months.

Definition of general characteristics

Diagnosis of hypertension: the blood pressure of subjects was measured twice or multiple times on different days during rest, which showed a systolic blood pressure (SBP) of ≥140 mmHg and/or diastolic blood pressure (DBP) of ≥90 mmHg. In addition, the subjects had history of hypertension.

Diagnosis of diabetes mellitus: a fasting plasma glucose (FPG) level of ≥ 7.0 mmol/L, a blood glucose level of ≥ 11.1 mmol/L at 2 h after food intake, and a random blood glucose level of ≥ 11.1 mmol/L along with clinical symptoms of hyperglycemia or hyperglycemia crisis.

Diagnosis of hyperlipidemia: triglyceride (TG) of ≥ 2.27 mmol/L; total cholesterol (TC) of ≥ 6.19 mmol/L; high-density lipoprotein (HDH-c) of ≤ 1.04 mmol/L; and low-density lipoprotein (LDL-c) of ≥ 4.14 mmol/L (11).

Smoking history: No less than 10 cigarettes per day on average that continued for more than half a year. If the

Body mass index (BMI) value of a subject was ≤ 18.5, the weight of the subject was considered to be too light. If the BMI value of a subject ranged from 18.5 to 24.99, the weight of the subject was considered normal. If the BMI value of a subject was 25-28, the subject was considered overweight. If the BMI value of a subject was 28-32, the subject was considered obese. If the BMI value of a subject was ≥ 32, the subject was considered extremely obese.

Coronary TIMI blood flow: the blood flow of infarct-related vessels during acute myocardial infarction, which was divided into 4 levels by coronary arteriography. TIMI level 0: no perfusion, that is, no forward flow (contrast agent) filling at the occlusion site and the distal end. TIMI level I: micro-perfusion, that is, the contrast agent passed through the occlusion site, but at any time there was no forward blood flow through the distal vessel of the occlusion segment. TIMI level II: partial perfusion, contrast agent passed through the occlusion segment and reached the distal vessel, but its filling rate was significantly slower than normal vessels. TIMI level III: complete perfusion, the forward blood flow filled the distal blood vessels quickly and completely.

Grouping and treatment

Eighty subjects were randomly divided into a ticagrelor group (group A, 40 cases) and a clopidogrel group (group B, 40 cases). All patients were given subcutaneous injection of low molecular weight heparin (70 UI/Kg) twice a day, 10 mg of rosuvastatin calcium tablets once a day, and 40 mg of isosorbide mononitrate once a day. Hypertension and diabetes were treated accordingly. The injection of tirofiban was given after the PCI operation: patients in group A were given 180 mg of ticagrelor and 300 mg of aspirin enteric-coated tablets initially, followed by 90 mg of ticagrelor twice a day and 100 mg of aspirin enteric-coated tablets once a day. Patients in group B were also given 300 mg of clopidogrel and 300 mg of aspirin enteric-coated tablets initially, followed by 75 mg of clopidogrel once a day and 100 mg of aspirin enteric-coated tablets once a day. Patients in both groups were given corresponding oral medications for at least 12 months.

Steps and methods of the test

Blood samples were taken from each patient and placed in a plastic tube containing 0.109 M sodium citrate (anticoagulation ratio, 9:1). The collected samples were stored at 18-25°C. Phosphorylation of platelet VASP in both groups was detected by Shanghai Bogoo Biological Technology Co., Ltd according to the manufacturer's instructions.

Three flow test tubes were selected and labeled as T1, T2 and T3. PGE1 (prostaglandin E1) was added to test tube T1, while PGE1 + ADP was added to test tubes T2 and T3; 10 mL of whole blood was then added to test tube T1, T2, and T3, which was then vortexed and warmed for 10 min. A stationary liquid was added to T1, T2, and T3, and the mixture was stirred and then warmed for 5 min. Mouse monoclonal antibody + permeabilization liquid were then added to T1 and T2, while a negative quality control antibody + permeabilization liquid were added to T3 before the mixture was stirred and warmed up. The staining reagent was then added to T1, T2, and T3, and the specimens were stored at 2-8°C after the treatment. The phosphorylation level of platelet VASP in each tube was analyzed by flow cytometry within 2 h, and the "updated" values of mean fluorescence intensity (MFI) in T1, T2, and T3 were recorded. PRI was calculated according to the following formula:

$$MFIc_{(PGE1)}=MFIc_{(T1)}=MFI_{(T1)}-MFI_{(T3)}$$

$$MFIc_{(PGE1+ADP)}=MFIc_{(T2)}=MFI_{(T2)}-MFI_{(T3)}$$

$$PRI=[(MFIc_{(PGE1)}-MFIc_{(PGE1+ADP)})/MFIc_{(PGE1)}]*100\%$$

The phosphorylation levels of VASP in both groups were measured at 24 h, 7 days and 1 month after PCI, respectively, and the PRI was calculated and recorded accordingly. PRI ≥ 50% indicates an increased risk of ischemia. Therefore, if PRI is < 50%, the aggregation of platelets can be effectively inhibited. In contrast, a PRI value of < 16% indicates a possible risk of bleeding (12).

Follow-up

The occurrence of MACE events (myocardial infarction, angina pectoris, stent thrombosis, stroke and death), major bleeding events (hemorrhage in the digestive tract, hemoglobin decreased by more than 3 g/dL, transfusion of 2-3 units of whole blood or red blood cells due to bleeding, or cerebral hemorrhage), and secondary bleeding events (hematoma at the puncture site, skin ecchymosis, oral gingival bleeding or nasal bleeding with a necessity of tamponade treatment) within 1 month after PCI were recorded, and compared between

the two groups. The patients were followed-up daily during hospitalization and once every week by telephone after discharge. Finally, the patients were reviewed at the outpatient clinic 1 month after discharge.

Statistical analysis

SPSS 22.0 software was used for statistical analysis. The measurement data in the study were represented by ($\bar{x} \pm s$). PRI at different time points was compared between the two groups using the independent sample *t*-test. In addition, categorical variables were expressed as percentage (%) and evaluated using χ^2 test or Fisher's exact test. PRI was compared between the two groups by repeated measures analysis of variance, while PRI at different time points was compared by using one-way ANOVA. P <0.05 was considered statistically significant.

RESULTS

General clinical data

There was no significant difference in the baseline data between the two groups (P>0.05), as shown in Table I. The imaging results showed no significant difference between the two groups in terms of the number of vascular lesions and the number of implanted stents (P>0.05), as shown in Table II.

Levels of VASP phosphorylation

The flow cytometry histogram of platelets was displayed on the flow cytometer by FSLOG×SS LOG and FL1 LOG×FL2 LOG, as shown in Fig. 1A. The phosphorylation region of VASP was marked by the resting state T1, the activated state

Table I. *Comparison of baseline data between the two groups*

Category	Group A	Group B	P value
Age (years)	59.14±8.22	58.79±7.38	0.98
Gender (male/female)	29/11	27/13	0.71
BMI (kg/m^2)	26.33±2.12	26.45±1.56	0.84
LVEF (%)	53.45±6.37	55.27±6.73	0.19
AST (U/L)	23.65±20.12	24.89±18.54	0.81
ALT (U/L)	22.67±16.08	23.12±13.43	0.90
Creatinine (μmol/L)	95.66±42.18	84.49±33.51	0.36
PLT (10^9/L)	241.27±50.18	236.92±57.82	0.62
Smoking history (cases)	18	17	0.63
Hyperlipidemia (cases)	27	33	0.15
Hypertension (cases)	22	23	0.61
Diabetes (cases)	22	19	0.66
CHD family history (cases)	8	11	0.43
NSTEMI (cases)	10	8	0.74
UA (cases)	30	32	0.71
β - blocker (cases)	33	32	0.70
Statin (cases)	40	40	1
ACEI/ARB (cases)	27	24	0.45
PPI (cases)	10	14	0.33

Note: CHD: coronary heart disease; NSTEMI: non-ST-segment elevation myocardial; UA: unstable angina; ACEI/ARB: angiotensin converting enzyme inhibitor; PPI: proton pump inhibitor; LVEF: left ventricular ejection fraction; PLT: platelet; β- blocker was metoprolol succinate sustained-release tablet.

T2 and the negative homogeneity quality control T3, respectively, as shown in Fig. 1B. The average fluorescence intensity was recorded to calculate the PRI of each patient according to the above formula.

The overall mean values of PRI at each time point were compared between group A and group B, and there was no significant difference before the drug treatment (P>0.05). When the overall mean values of PRI at 24 h, 7 days and 1 month after PCI were compared between group A and B, the values in group A were significantly lower than those in group B (P<0.001);

There was significant difference between the two groups in terms of overall mean values of PRI (P < 0.001). In addition, significant difference was found in the overall mean values of PRI between the two groups before the drug treatment and at 24 h, 7 days and 1 month after PCI (P<0.001). Furthermore, there was an intergroup effect of time on the overall mean values of PRI in the two groups (P<0.001).

After PCI intervention, the percentage of subjects with a PRI value of ≥ 50% was significantly higher in group B than that in group A at different time points (P < 0.001). See Table III.

Incidence of MACE and bleeding events within 1 month after PCI

Within 1 month after PCI, there was no ischemic event in group A, while 4 patients suffered a MACE event in group B. However, there was no significant difference between the two groups in terms of the incidence of MACE (P>0.05). In addition, the incidence of bleeding events was higher in group A than that in group B, although the difference was not statistically significant (P>0.05).

Table II. *Comparison of coronary angiography and intervention.*

Category		Group A	Group B	P value
Number of vascular lesions (cases)	Single-vessel	12	10	0.55
	Double-vessel	20	18	
	Triple-vessel	8	12	
Number of stents		1.76 ± 0.50	1.84 ± 0.80	0.59

Table III. *Comparison of PRI values at different time points between the two groups*

		Before drug treatment	24 hours after surgery	7 days after surgery	1 month after surgery
Group A	PRI (%)	73.02±13.23	25.11±13.57	23.87±12.69	22.62±13.46
	PRI ≥ 50% (cases)	38	3	2	2
Group B	PRI (%)	75.58±12.15	56.51±13.35*	54.47±12.48*	53.15±11.33*
	PRI ≥ 50% (cases)	39	30*	26*	12*

*Note: *P<0.005, compared with group A.*

DISCUSSION

The decrease in PAF was closely related to the blockage of P2Y12 receptor. In this study, PGE1 (Alprostadil) induced phosphorylation of VASP, and P2Y12 receptor also promoted phosphorylation of VASP by binding to the drugs.

The inhibitors of the $P2Y_{12}$ receptor effectively reduced inflammatory responses. However, ticagrelor exerted a lower inhibitory effect on interleukin 6 (IL-6) and C-reaction protein (CRP) than clopidogrel, which might be related to its dual inhibition on platelet $P2Y_{12}$ receptor and ENT-1. Our study showed that the incidence of adverse events, such as stent thrombosis and revascularization, was significantly lower in group A than in group B. In addition, there was no significant difference between the two groups in terms of the incidence of major adverse cardiovascular and cerebrovascular events. However, compared with group B, group A showed an increased level of mild bleeding events. Within 1 month after PCI, the overall mean value of PRI in group A was lower than that in group B, indicating the effectiveness and stability of ticagrelor against platelet aggregation.

In summary, the level of VASP phosphorylation in platelets was detected by FCM in this study, and the effect of ticagrelor on PAF was evaluated. The results showed that ticagrelor was highly effective and stable in inhibiting platelet aggregation without significantly increasing the risk of bleeding in patients with ACS.

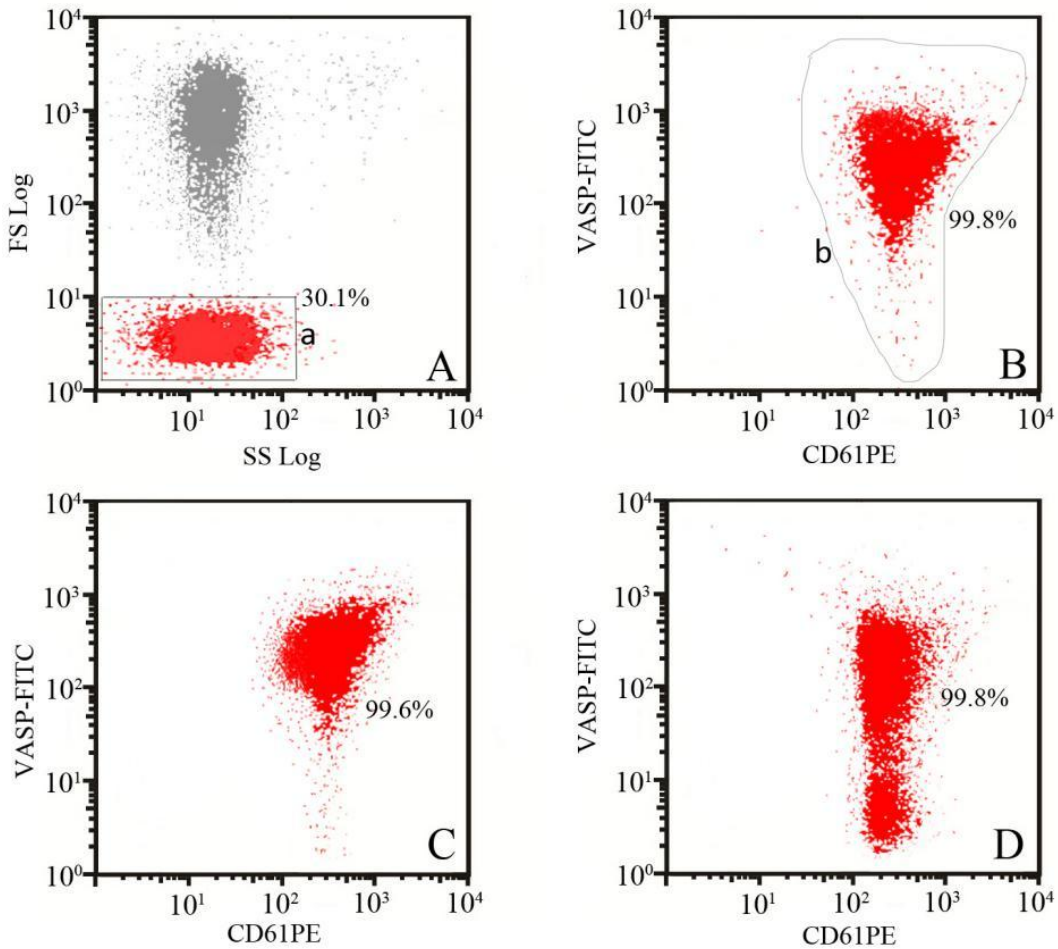

Fig. 1. *Levels of VASP phosphorylation measured by flow cytometry.* ***A****) Platelet population;* ***B****) expression of VASP-P under PGE1 conditions;* ***C****) expression of VASP-P under PEG1+ADP conditions;* ***D****) negative quality control under PEG1+ADP conditions.*

REFERENCES

1. Kastorini CM, Milionis HJ, Ioannidi A, et al. Adherence to the Mediterranean diet in relation to acute coronary syndrome or stroke nonfatal events: a comparative analysis of a case/case-control study. Am Heart J 2011; 162(4):717-24.
2. Schwartz GG, Olsson AG, Abt M. Effects of dalcetrapib in patients with a recent acute coronary syndrome. N Engl J Med 2012; 367(22):2089-99.
3. Alexander JH, Lopes RD, James S, et al. Apixaban with antiplatelet therapy after acute coronary syndrome. N Engl J Med 2011; 365(8):699-708.
4. Romagnoli E, Biondi-Zoccai G, Sciahbasi A, et al. Radial versus femoral randomized investigation in ST-segment elevation acute coronary syndrome: the RIFLE-STEACS (Radial Versus Femoral Randomized Investigation in ST-Elevation Acute Coronary Syndrome) study. J Am Coll Cardiol 2012; 60(24):2481-89.
5. Widera C, Gupta SK, Lorenzen JM, et al. Diagnostic and prognostic impact of six circulating microRNAs in acute coronary syndrome. J Mol Cell Cardiol 2011; 51(5):872-75.
6. Aungraheeta R, Conibear A, Butler M, Kelly E, Nylander S, Mumford A, Mundell SJ. Inverse agonism at the P2Y12 receptor and ENT1 transporter blockade contribute to platelet inhibition by ticagrelor. Blood 2016; 128(23):2717-28.
7. Senoo T, Motohiro M, Kamihata H, et al. Contrast-induced nephropathy in patients undergoing emergency percutaneous coronary intervention for acute coronary syndrome. Am J Cardiol 2010; 105(5):624-28.
8. Moseley AD, Collado FM, Volgman AS, Schaer GL, Snell RJ. duration of dual antiplatelet therapy in coronary artery disease: a review article. Curr Atheroscler Rep 2016; 18(7):45.
9. Gurbel PA, Bliden KP, Butler K, et al. Randomized double-blind assessment of the ONSET and OFFSET of the antiplatelet effects of ticagrelor versus clopidogrel in patients with stable coronary artery disease: the ONSET/OFFSET study. Circulation 2009; 120(25):2577-85.
10. Dayoub EJ, Seigerman M, Tuteja S, Kobayashi T, Kolansky DM, Giri J, Groeneveld PW. Trends in platelet adenosine diphosphate P2Y12 receptor inhibitor use and adherence among antiplatelet-naive patients after percutaneous coronary intervention, 2008-2016. JAMA Intern Med 2018; 178(7):943-50.
11. Anderson JL, Adams CD, Antman EM, et al. 2011 ACCF/AHA Focused update incorporated into the ACC/AHA 2007 guidelines for the management of patients with unstable angina/non-st-elevation myocardial infarction: a report of the American College of Cardiology Foundation/American Heart Association Task Force on Practice Guidelines. Circulation 2011; 123(18):e426-579.
12. Aleil B, Ravanat C, Cazenave JP, Rochoux G, Heitz A, Gachet C. Flow cytometric analysis of intraplatelet VASP phosphorylation for the detection of clopidogrel resistance in patients with ischemic cardiovascular diseases. J Thromb Haemost 2005; 3(1):85-92.

LETTER TO THE EDITOR

CHARACTERIZATION OF BACTERIAL MICROBIOTA DIVERSITY IN TIBETAN PIGS FED WITH GREEN FORAGE IN LINZHI OF THE TIBET AUTONOMOUS REGION

ZD. SHANG[1,2,*], ZK. TAN[1,2,*], SZ. LIU[1,2,], JK. LI[1,3], YZ. QIANG-BA[1,4], P. SHANG[1,4] and HH. WANG[1,2,*]

[1]College of Animal Science, Tibet Agricultural & Animal Husbandry University, Linzhi, People's Republic of China; [2]Tibetan Plateau Feed Processing Research Center, Linzhi, People's Republic of China; [3]Laboratory of Detection and Monitoring of Highland Animal Disease, Linzhi, Tibet, People's Republic of China; [4]Tibetan pig Collaborative Research Center (Open platform), Linzhi, Tibet, People's Republic of China

Received October 3, 2018 – Accepted January 25, 2019

The acute shortage of forage resources is a serious problem for Tibetan pigs in the Tibet region, and the composition of feed can change the structure of the intestinal flora. This study first reported the effect of *Alfalfa* and *Chenopodium glaucum* feeding on the microbial diversity in Tibetan pigs, contributing to the forage exploitation of Tibetan pigs in the Tibet region. Results showed that the replacement of concentrate by green forage did not affect the feed intake of THE pigs. The daily weight gain of pigs fed with 45% green forage was significantly lower ($p<0.05$), whereas it remained unchanged for the other groups. A total of 483,570 high-quality sequences were obtained from 12 fecal samples. The alpha diversity index revealed no variation in the evenness of community, but a significant difference was found in the richness of community among the feeding groups. Principal component analysis showed an obvious alteration among the principal components of the microbial community structure in the different feeding groups. At the phylum and genus levels, 6 phyla and 16 genera differed among the four groups ($p<0.05$) but did not include the harmful bacteria. The intestinal microbiota of Tibetan pigs mainly involved 12 metabolic functions, among which, the mean proportion of amino acid metabolism and biosynthesis of other secondary metabolites were higher in the experimental groups. Although the structure of intestinal microflora changed, harmful bacteria in the pigs did not increase when they were fed with *Alfalfa* and *C. glaucum*. These findings indicated that alfalfa and *C. glaucum* could be used as forage grass for Tibetan pigs.

To the Editor,

Tibetan pig is an ancient primitive breed and the only pig breed that lives at high and cool altitudes in China. Under long-term harsh natural environmental conditions, Tibetan pigs have developed cold resistance, high disease resistance and herbivorous and other typical characteristics which make them indispensable for pig production in the plateau. However, green forage resources are scarce in winter and spring because of the traditional feeding method (grazing) of the pigs, the short growing period of crops and the extremely low level of pasture production

Key words: microbial diversity, bacteria, Alfalfa, Chenopodium glaucum, Tibetan pig

Corresponding Author:
Dr Zhenda Shang,
College of Animal Science,
Tibet Agricultural & Animal Husbandry University,
Linzhi, 860000, Tibet,
People's Republic of China
e-mail: 446809464@qq.com

0393-974X (2019)

in Tibet. This shortage in resources has become a problem that severely restricts the development of the Tibetan pig and the economic development of the Tibet region.

The intestinal tract is the main site where a host digests and absorbs food, and these processes involve the gut microbiota (1-2). The diverse and large gut microbiota in the intestinal tract have a mutual relationship with its host (3). These microbiota provide nutrition, participate in host metabolism, maintain the microecological balance and ensure the health of the intestine. The dynamic distribution of the intestinal microflora in animals is related to dietary composition (4). Elucidating the correlation between different diet compositions and characteristics of gut microbiota diversity is beneficial to the development of forage for Tibetan pigs.

Alfalfa and *Chenopodium glaucum*, widely cultivated in Tibet, are used as forage grass. Therefore, in the present study, we analyzed the effect of replacing concentrate with green forage on growth performance and bacterial diversity in fattening Tibetan pigs in Linzhi of the Tibet Autonomous Region.

MATERIALS AND METHODS

Animal feeding and sample collection

Feeding of Tibetan pigs and collection of fecal samples were approved and instructed by the Tibetan Pig Collaborative Research Center of Tibet Agriculture and Animal Husbandry College, Tibet, China (Unified social credit code:12540000MB0P013721). Twelve healthy Tibetan pigs that had an average weight of 15.27±0.73 kg, came from the same breeding environment and were approximately 4 months old were randomly assigned to four groups (groups A, B, C and D, n=3). Group A (A1, A2 and A3) was fed with full concentrate, group B (B1, B2 and B3) received a diet consisting of 85% concentrate and 15% green forage, group C (C1, C2 and C3) were given a diet composed of 70% concentrate and 30% green forage, and group D (D1, D2 and D3) was administered with a diet containing 55% concentrate and 45% green forage (green forage consisted of a mixture of fresh alfalfa and *C. glaucum*). The feeding experiment lasted 6 weeks. During the experiment, the pigs were kept in a positioning column, where the space could allow free movement, and they were subjected to free feeding and drinking. After they were fed daily, the positioning columns and the pigs' houses were cleaned. After each week, the feed intake and daily gain of the pigs were calculated. After the experiment was conducted, fresh fecal samples of each pig were collected in 50 mL sterilised tubes and immediately frozen at −20°C for analysis of the bacterial diversity.

Total DNA extraction

Fresh fecal samples were pretreated using a similar method from a previous study. The total microbial genomic DNA was extracted from the samples by using QIAamp Fast DNA Stool Mini Kit (QIAGEN, Hilden, Germany) in accordance with the manufacturer's directions. The concentration and quality of DNA were detected with a nucleic acid detector and 0.8% agarose gel electrophoresis, respectively.

Gene amplification of V3-V4 hypervariable regions

The standard bacteria V3-V4 hypervariable regions gene PCR primers (ACTCCTACGGGAGGCAGCA and GGA-CTACHVGGGTWTCTAAT) were used. The PCR amplification system contained 5 μL of 5× reaction buffer, 5 μL of 5× GC buffer, 2 μL of dNTP (2.5 mM), 1 μL of forward primer (10 μM), 1 μL of reverse primer (10 uM), 2 μL of DNA template, 8.75 μL of ddH_2O and 0.25 μL of Q5 DNA polymerase in a total volume of 25 μL. PCR amplification was performed under the following conditions: initial denaturation at 98°C for 2 min; 28 cycles of denaturation at 98°C for 15 s, annealing at 55°C for 30 s and extension at 72°C for 30 s; and a final extension at 72°C for 5 min. The PCR amplification products were detected via 2% agarose gel electrophoresis, and target fragments were recovered using AXYGEN's gel recovery kit.

Sequencing library preparation

The sequencing library was constructed using a TruSeq Nano DNA LT Library Prep kit (Illumina). The prominent base was removed at the 5′-end of the DNA sequence by using End Repair Mix 2, and a phosphate group was added at the 3′ end to repair the amplified product. Library enrichment products were repurified using BECKMAN AMPure XP beads. The final fragment of the library was purified and selected throguh 2% agarose gel electrophoresis with Greengenes. Library

quality control and quantitative assay were separately conducted with an Agilent High-sensitivity DNA kit with an Agilent bioanalyzer and a Quant-iT PicoGreen dsDNA assay kit with Promega QuantiFluor. Then, the paired end sequencing of DNA fragments was performed with Illumina MiSeq equipment (MiSeq Reagent Kit V3) (Personalbio, Shanghai, China).

Sequence data processing and statistical analysis

The question sequences were identified and eliminated using Quantitative Insights Into Microbial Ecology (QIIME) software v1.8.0. The sequences were established as operational taxonomic units (OTUs) via Uclust with over 97% similarity (5). Then, OTUs were taxonomically classified and grouped by comparing with those in the Greengenes databases. Alpha diversity index (Chao1, ACE, Simpson and Shannon) was calculated using the Mothur software. Beta diversity was analysed by utilising the similarity of the microbial community structure among different feeding groups through principal component analysis (PCA). The data of the microbial community structure at different classification levels (phylum, class, order, family and genus) of the four groups were statistically analysed using the QIIME software. A Metastats statistical algorithm was used to examine the discrepancy of microbial community between groups at phylum and genus levels. A heat map was drawn using the R software. PICRUSt functional predictive analysis was achieved by comparing the Greengenes database with the KEGG PATHWAY database (6). The feed intake and daily gain of Tibetan pigs were evaluated through one-way ANOVA, and deviations were assessed with a significant level of $p<0.05$ by using SPSS Statistics 22.0 (IBM).

RESULTS

Feed intake and growth of Tibetan pigs in four groups

In the present study, group A was given the concentrate at an intake of 862.50 g. Groups B, C and D received the concentrate at intakes of 733.25, 604.00 and 474.75 g, respectively, and their forage intakes were 146.85, 265.00 and 405.42 g, respectively. The daily gains of the Tibetan pigs in groups A, B, C and D were 262.5, 229.5, 225.7 and 188.2, respectively (Fig. 1). No significant differences were observed between the other three groups except the significant decrease in group D ($p<0.05$).

Characterisation of the microbial community of Tibetan pigs in four groups

In this study, 483,570 high-quality sequences

Table I. *The microbial community diversity index of each sample in four groups.*

Group	Simpsom	Shannon	ACE	Chao1
GroupA	0.974±0.011^{a}	7.713±0.433^{a}	1377.94±111.82^{a}	1348.44±93.56^{a}
GroupB	0.972±0.022^{a}	8.283±0.741^{a}	1683.44±90.83^{ab}	1648.49±78.47^{ab}
GroupC	0.953±0.023^{a}	7.493±0.375^{a}	1818.11±226.61^{b}	1750.02±270.93^{b}
GroupD	0.939±0.021^{a}	7.300±0.294^{a}	1617.75±169.87^{ab}	1547.03±135.21^{ab}

Note: In the same row, values with different small letter superscripts mean significant difference ($p<0.05$), while with the same letter superscripts mean no significant difference ($p>0.05$). The same as below.

Table II. *The microbial community structure in different levels in four groups.*

Classification level	Bacteria	Group (%)			
		A	B	C	D
Phylum	*Firmicutes*	67.20±4.71^{a}	52.00±17.72^{ab}	42.03±9.13^{b}	43.70±9.33^{b}
	Bacteroidetes	24.10±2.16^{a}	24.00±6.05^{a}	28.73±6.28^{a}	29.53±1.87^{a}
	Spirochaetes	6.10±5.86^{a}	18.36±12.65^{a}	24.80±9.09^{a}	22.13±8.99^{a}
	Actinobacteria	0.56±0.15^{b}	1.10±0.36^{ab}	1.26±0.55^{a}	1.43±0.20^{a}
	Other	2.03±0.45^{b}	4.53±0.70^{a}	3.16±1.20^{ab}	3.20±0.88^{ab}
Class	*Clostridia*	30.13±0.56^{a}	41.63±11.38^{a}	35.46±9.96^{a}	41.90±8.94^{a}
	Bacteroidia	67.20±4.71^{a}	52.00±17.72^{ab}	42.03±9.13^{b}	43.70±9.33^{b}
	Spirochaetes	6.10±5.86^{a}	18.36±12.65^{a}	24.80±9.09^{a}	22.13±8.99^{a}
	Bacilli	36.60±4.06^{a}	9.50±6.55^{b}	4.63±6.75^{b}	1.16±1.19^{b}
	Other	3.06±0.41^{b}	6.50±1.25^{a}	6.40±2.52^{a}	5.40±0.85^{ab}
Order	*Clostridiales*	30.13±0.56^{a}	41.63±11.38^{a}	35.46±9.96^{a}	41.90±8.94^{a}
	Bacteroidales	24.10±2.16^{a}	24.00±6.05^{a}	28.70±6.27^{a}	29.40±1.70^{a}
	Spirochaetales	5.93±5.93^{a}	18.23±12.65^{a}	24.66±9.07^{a}	21.93±8.93^{a}
	Lactobacillales	36.56±4.11^{a}	9.43±6.60^{b}	4.60±6.79^{b}	1.13±1.23^{b}
	Other	3.26±0.49^{b}	6.70±1.15^{a}	6.56±2.53^{a}	5.63±1.00^{ab}
Family	*Spirochaetaceae*	5.93±5.93^{a}	18.23±12.65^{a}	24.66±9.07^{a}	21.93±8.93^{a}
	Lachnospiraceae	13.23±7.38^{a}	19.60±14.22^{a}	17.83±10.29^{a}	19.40±13.02^{a}
	Lactobacillaceae	36.53±4.10^{a}	9.33±6.60^{b}	4.56±6.73^{b}	0.16±0.28^{b}
	Ruminococcaceae	9.30±3.89^{a}	10.10±4.15^{a}	9.23±2.02^{a}	11.76±5.42^{a}
	Paraprevotellaceae	4.60±6.18^{a}	5.80±0.87^{a}	10.83±7.32^{a}	9.90±6.35^{a}
	Other	30.40±8.60^{a}	36.93±5.57^{a}	32.86±8.96^{a}	36.83±7.51^{a}
Genus	*Treponema*	5.93±5.93^{a}	18.23±12.65^{a}	24.66±9.07^{a}	21.93±8.93^{a}
	Lactobacillus	36.53±4.10^{a}	9.33±6.60^{b}	4.56±6.73^{b}	0.16±0.28^{b}
	YRC22	4.16±6.04^{a}	5.06±1.17^{a}	10.46±7.34^{a}	9.56±6.24^{a}
	Prevotella	2.46±1.31^{a}	5.96±5.75^{a}	2.33±1.45^{a}	3.06±2.00^{a}
	Ruminococcus	1.50±0.43^{a}	2.36±2.45^{a}	2.16±0.32^{a}	3.93±2.14^{a}
	Fibrobacter	0.46±0.20^{b}	1.96±1.10^{a}	0.83±0.23^{ab}	0.83±0.66^{ab}
	Paludibacter	0.36±0.28^{a}	1.26±0.47^{a}	0.93±1.09^{a}	1.16±0.58^{a}
	Oscillospira	1.16±0.77^{a}	0.93±0.55^{a}	0.80±0.34^{a}	0.60±0.43^{a}
	Other	47.40±8.88^{a}	54.86±11.16^{a}	53.23±18.94^{a}	58.73±16.28^{a}

Note: In the same row, values with different superscript letters mean significant difference ($p<0.05$), while with the same superscript letters mean no significant difference ($p>0.05$).

were obtained from 12 fecal samples, and the effective sequences in each sample exceeded 35,000. The average length of these sequences was 400-500 bp. The effective sequences were copolymerised into 6,350 OTUs. Of the total OTUs in the four experimental groups, 804 core sequences accounting for 12.66% were found. Interestingly, only 623 OTUs were found in group A, 945, 657 and 836 OTUs were identified in groups B, C and D only (Fig. 2). We utilised various alpha indices to measure the microbial community diversity (Table I). Chao1 and ACE indices revealed a visible difference in the flora richness between the four groups ($p<0.05$). The Shannon and Simpson indices demonstrated that no significant difference was observed in the flora evenness among the four groups ($p>0.05$). Likewise, PCA showed that all of the samples from the four groups could be distinguished clearly, and the microbial community structure changed after the pigs were fed with different diets (Fig. 2).

At the phylum level (Table II), *Firmicutes*, *Bacteroidetes* and *Spirochaetes* were the dominant microflora in all of the treatment groups. The abundance of *Firmicutes* in group A (67.20%) was significantly higher than that in groups B, C and D (52.00%, 42.03% and 43.70%, respectively) ($p<0.05$). The abundance of *Bacteroidetes* had no significant difference among all groups ($p>0.05$). The abundance of *Spirochaetes* in group A (6.10%) was lower than that in the other groups (18.36%, 24.80% and 22.13%, respectively), but the difference was not significant ($p>0.05$). At the class level, the abundance of Bacilli in group A was significantly higher than that in the other groups ($p<0.05$). At the order level, the abundance of *Spirochaetales* in group A was lower than that in the other groups ($p>0.05$), and the abundance of *Lactobacillales* in group A was significantly higher than that in the other groups ($p<0.05$). At the family level, the abundances of *Spirochaetaceae* and *Lachnospiraceae* in group A were lower than those in the other groups ($p>0.05$), and the abundance of *Lactobacillaceae* in group A was significantly higher than those in the other groups ($p<0.05$). At the genus level, the abundance of *Treponema* in group A was lower than that in the other groups ($p>0.05$). The abundance of *Lactobacillus* in group A was significantly higher than that in the other groups ($p<0.05$).

The absolute abundance of each taxon in the four groups was compared at the phylum and genus levels. At the phylum level, the abundance of one phylum (*Actinobacteria*) significantly differed

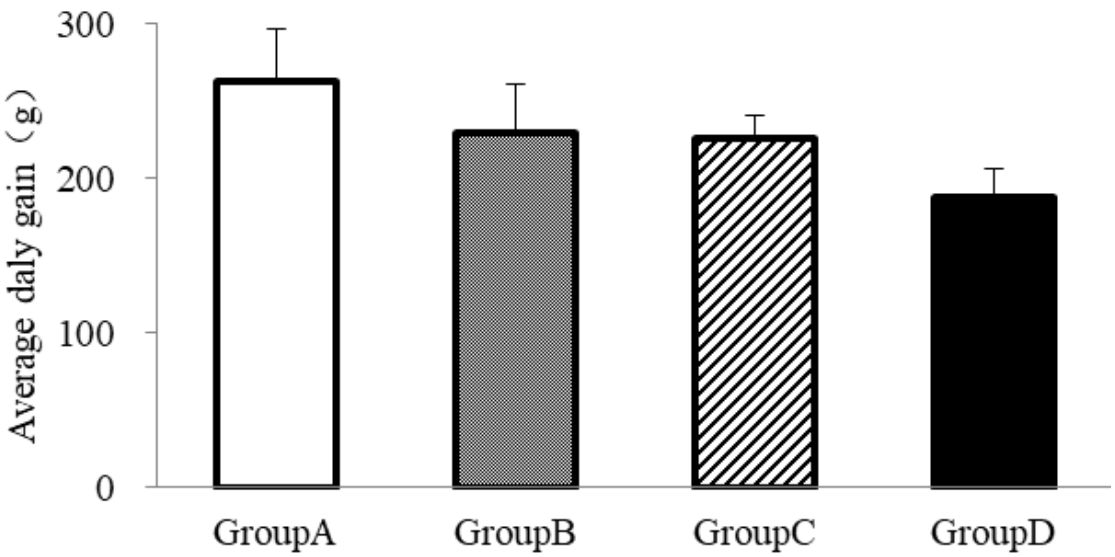

Fig. 1. *The average daily gain of Tibetan pigs in four groups (g).*

between groups A and B. Two phyla (Firmicutes and Spirochaetes) also significantly varied between groups A and C. Five phyla (*Actinobacteria, Firmicutes, Bacteroidetes, Spirochaetes* and *Cyanobacteria*) significantly differed between groups A and D. *Tenericutes* significantly varied between groups B and C. At the genus level, nine genera (*Lachnospira, Adlercreutzia, Anaeroplasma, Lactobacillus, Fibrobacter, Paludibacter, Parabacteroides, Phascolarctobacterium* and *Mogibacterium*) exhibited significant differences between groups A and B. Seven genera (*Treponema, Lactobacillus*, *CF231*, *Mogibacterium, Lachnospira, Ruminococcus* and *p-75-a5*) showed significant

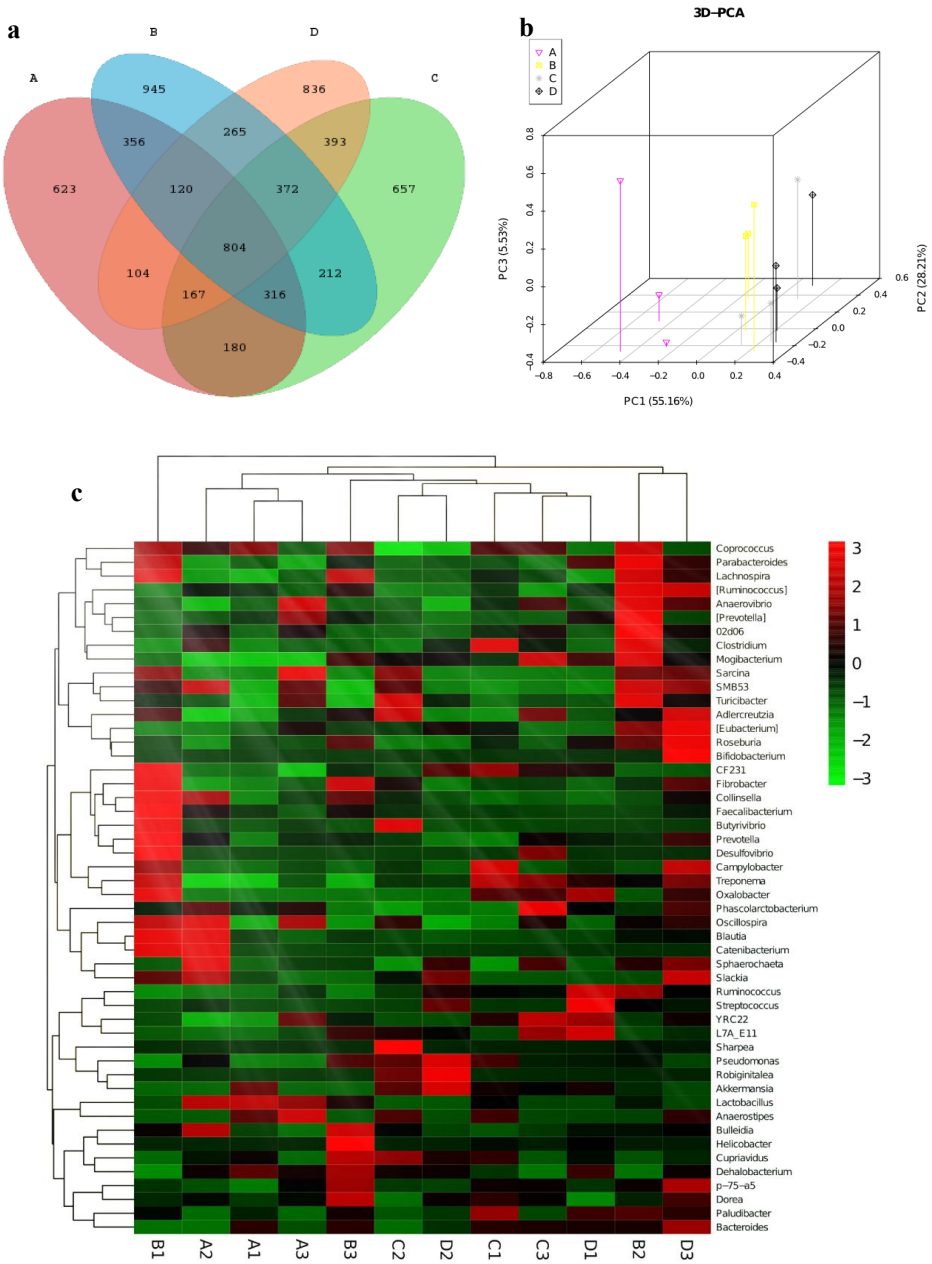

Fig. 2. *Gut microbiota compositions for Tibetan pigs in different groups.* ***a****) Venn diagram shows various comparisons of OUTs in four groups.* ***b****) The principal component analysis of the microbial community structure in four groups.* ***c****) Heat map of the microflora composition at Genus level of each group.*

variations between groups A and C. Seven genera (*Lactobacillus, Parabacteroides, Treponema, Mogibacterium, Paludibacter, Sharpea* and *Ruminococcus*) significantly varied between groups A and D. Four genera (*Lachnospira, Anaeroplasma, Coprococcus* and *Ruminococcus*) had significant difference between groups B and C. Two genera (*Lachnospira* and *Coprococcus*) had significant difference between groups B and D. *Genera Parabacteroides* also had significant difference between groups C and D. On the basis of the results of heat map analysis (Fig. 2), we concluded that the microflora composition of all of the samples in each group differed. The similarity of the microflora composition between groups A and B and between groups C and D was higher.

Analysis of the microbial metabolic function

In the KEGG second-level functional groups (Fig. 3), 12 functions were mainly involved in metabolic pathways. Among these functions, the metabolism of amino acids and the biosynthesis of other secondary metabolites in group A had significantly lower abundance than that in the other groups. Nucleotide metabolism, enzyme families, terpenoid and polyketide metabolism, xenobiotic biodegradation and metabolism in group A had a significantly higher proportion than that in the other groups ($p<0.05$). The metabolism of carbohydrate, cofactors and vitamins, lipid, enzyme, other amino acids, the biosynthesis and metabolism of glycan had no significant difference among the groups ($p>0.05$).

DISCUSSION

The serious shortage of green forage resources has become a problem that severely restricts the development of Tibetan pigs in the Tibet region. In this study, we first reported the effect of partly replacing concentrate with green forage on the

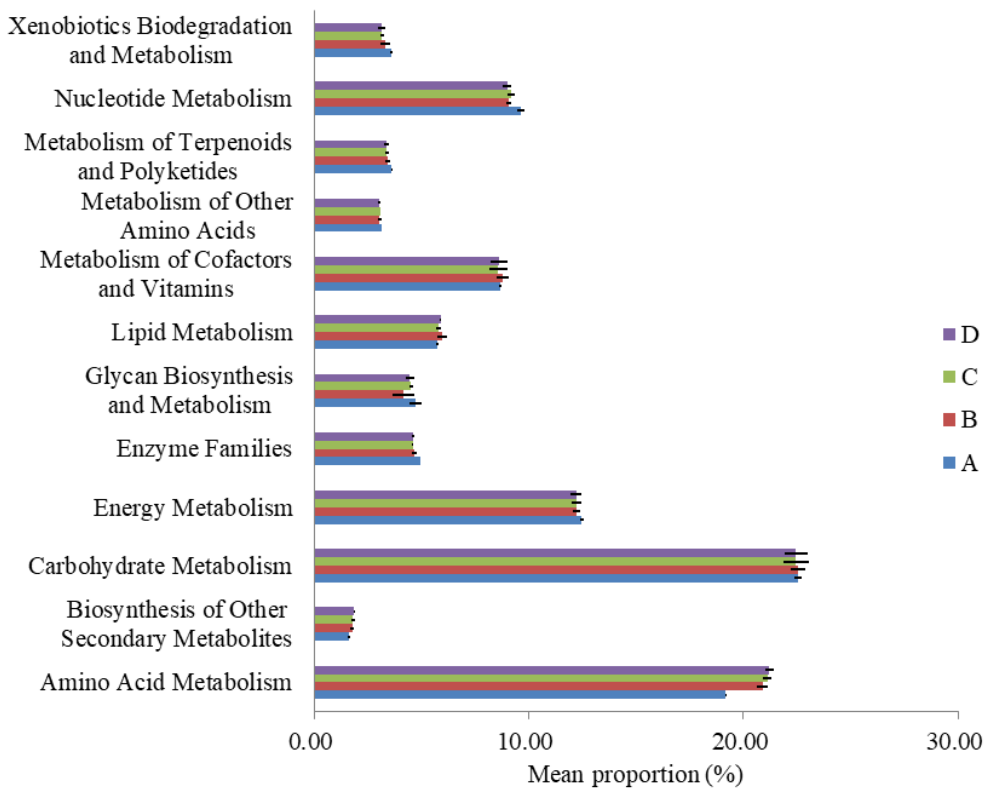

Fig. 3. *Mean proportion and the differences in microbial metabolism function between four groups.*

growth performance and intestinal microbial diversity of Tibetan pigs. The results showed that the pigs did not show any difference in feed intake after the concentrate was replaced by green forage. The daily weight gain of the pigs fed with 45% green forage significantly decreased, whereas no significant difference was observed in the other groups possibly because of the low intake of dry matter and digestive energy.

This study indicated that the change in dietary composition would affect the structure of intestinal microflora in Tibetan pigs, and this phenomenon was consistent with that described in previous studies (7). Overall, *Firmicutes, Bacteroidetes*, *Spirochaetes* and *Proteobacteria* were the dominant bacteria in the intestines of Tibetan pigs. As the proportion of green forage increased, the value of *Firmicutes*/*Bacteroides* significantly decreased, indicating that it could affect the decomposition of fodder fiber because the feed composition changed, thereby reducing the efficiency of forage utilisation in Tibetan pigs (8-9). This phenomenon might be related to the high crude fiber content in green feed. The abundance of *Proteobacteria* does not significantly change as forage composition changes, and no harmful bacteria belonging to *Proteobacteria* are found in the dominant flora at other classification levels (10). This finding showed that the abundance of harmful bacteria did not increase as the proportion of green feed increased, thereby maintaining the stability of the intestinal microbial diversity and ensuring the health of Tibetan pigs. Various bacteria, such as *Ruminococcus*, *Bacteroides*, *Prevotella*, *Fibrobacter* and *Lachnospira*, associated with herbivore characteristics have been detected in Tibetan pigs (11). The content of beneficial bacteria, such as *Treponema*, in these pigs can be increased by feeding green forage (12). The dietary composition could change the intestinal microflora which affected the metabolic functions of the animals.

In summary, alfalfa and *C. glaucum* were used to feed Tibetan pigs. Although the composition and structure of intestinal microflora changed, the population of harmful bacteria did not increase. This study first reported the effect of alfalfa and *C. glaucum* feeding on microbial diversity in Tibetan pigs and contributed to the forage exploitation of these pigs in the Tibet region.

ACKNOWLEDGEMENTS

This research was supported by the Tibetan plateau feed processing research center Project & Natural Science Foundation of China (31760673). The organizational unit was the Science and Technology Department of the Tibet Autonomous Region.

REFERENCES

1. Kim HB, Borewicz K, White BA, Singer RS, Sreevatsan S, Tu ZJ, Isaacson RE. Microbial shifts in the swine distal gut in response to the treatment with antimicrobial growth promoter, tylosin. Proc Natl Acad Sci 2012; 109:15485-90.
2. Yatsunenko T, Rey FE, Manary MJ, et al. Human gut microbiome viewed across age and geography. Nature 2012; 486:222-27.
3. Macfarlane GT, Macfarlane S. Models for intestinal fermentation: association between food components, delivery systems, bioavailability and functional interactions in the gut. Current Opinion in Biotechnology 2007; 18:156-62.
4. Looft T, Johnson TA, Allen HK, et al. In-feed antibiotic effects on the swine intestinal microbiome. Proceedings of the National Academy of Sciences of the United States of America 2012; 109:1691-96.
5. Bokulich NA, Subramanian S, Faith JJ, et al. Quality-filtering vastly improves diversity estimates from Illumina amplicon sequencing. Nat Methods 2013; 10:57-59.
6. Langille MG, Zaneveld J, Caporaso JG, et al. Predictive functional profiling of microbial communities using 16S rRNA marker gene sequences. Nature Biotechnol 2013; 31:814-21.
7. Chen YH, Penner GB, Li MJ, Oba M, Guan LL. Changes in bacterial diversity associated with epithelial tissue in the beef cow rumen during the transition to a high-grain diet. Appl Environ Microbiol 2011; 77:5770-81.
8. Brulc JM, Antonopoulos DA, Miller ME, et al. Gene-centric metagenomics of the fiber-adherent bovine rumen microbiome reveals forage specific

glycoside hydrolases. Proc Natl Acad Sci USA 2009; 106: 1948-53.

9. Turnbaugh PJ, Ley RE, Mahowald MA, Magrini V, Mardis ER, Gordon JI. An obesity-associated gut microbiome with increased capacity for energy harvest. Nature 2006; 444:1027-31.
10. Evans NJ, Brown JM, Murray RD, Getty B, Birtles RJ, Hart CA, Carter SD. Characterization of novel bovine gastrointestinal tract Treponema isolates and com parison with bovine digital dermatitis treponemes. Appl Environ Microbiol 2011; 77:138-47.
11. Zhu L, Wu Q, Dai J, Zhang S, Wei F. Evidence of cellulose metabolism by the giant panda gut microbiome. Proceedings of the National Academy of Sciences 2011; 108:17714-19.
12. Edrington TS, Dowd SE, Farrow RF, Hagevoort GR, Callaway TR, Anderson RC, Nisbet DJ. Development of colonic microflora as assessed by pyrosequencing in dairy calves fed waste milk. J Dairy Sci 2012; 95:4519-25.

LETTER TO THE EDITOR

CONTRIBUTIONS OF THE SUPEROXIDE DISMUTASE 1 AND ZINC FINGER PROTEIN 469 (ZNF469) GENES TO KERATOCONUS

E. LOUKOVITIS[1], E. TSOTRIDOU[2,3], T. VAKALIS[3], S. ASTERIADIS[3], T. SOUSOURAS[3], Z. ZACHARIADIS[3], P. TRANOS[3], N. KOZEIS[3], M. BALIDIS[3] and G. ANOGEIANAKIS[3,4]

Hellenic Army Medical Corps and Ophthalmica Eye Institute, Thessaloniki, Greece; [2]Faculty of Medicine, Aristotle University of Thessaloniki, Greece; [3]Ophthalmica Eye Institute, Thessaloniki, Greece; [4]Association for Training in Biomedical Technology, Thessaloniki, Greece

Received October 15, 2018 – Accepted December 18, 2018

Keratoconus (KC) is a multifactorial, progressive, degenerative corneal disorder with an incidence of approximately 1 in 2,000 subjects. Although, the most frequent type of KC is sporadic, there are many cases of familial KC, mainly inherited through an autosomal dominant pattern. KC is characterized by genetic heterogeneity as it has been associated with a plurality of genes. The present report focuses on superoxide dismutase 1 (SOD1) and zinc finger protein 469 (ZNF469) genes which are involved in many cases of KC and other corneal pathologies including the relation of the ZNF469 mutations with Brittle Cornea Syndrome (BCS).

To the Editor,

Keratoconus (KC) is a mainly bilateral, progressive, non-inflammatory corneal disease. It is associated with corneal steepening and thinning that results in irregular astigmatism (1) and blurred vision. KC has a prevalence varying from 8.8 to 2,300 per 100,000 people and an incidence of approximately 1 in 2,000 (2). Although, KC is mainly sporadic, there are cases of familial KC, which are mainly inherited through an autosomal dominant pattern, with first degree family members being at a higher risk (1). KC affects both men and women, but recent studies report that there is a preponderance of men over women (1). Beside the fact that KC is described as a non-inflammatory disease, recent studies prove that there is overexpression of inflammatory mediators such as interleukin 6 (IL-6) in tears of KC patients. There is also a degradation of the corneal extracellular matrix (ECM), characterized by increased levels of inflammatory molecules such as Matrix metalloproteinase-9 (MMP-9) and Tumor necrosis factor alpha (TNF-α), as well as by an increase in oxidative stress (1). KC, therefore, is a multifactorial disease that stems from the interaction of genetic, environmental and behavioral factors that include chronic eye rubbing, contact lens wear, ultraviolet irradiation and atopy (2). The genetic etiology is also evidenced by the association between KC and genetic disorders such as Down syndrome, Leber's congenital amaurosis and the ethnic differences in KC prevalence and incidence (2).

KC genetic heterogeneity is evidenced by Genome Wide Association Studies (GWAS). These studies have reported, to date, more than 150 polymorphisms in over 60 genes/loci. They also support the notion that KC pathophysiology is the result of interplay of several genes rather than a single one (2). One meta-analysis reported that

Corresponding Author:
Prof. George Anogeianakis,
Ophthalmica Eye Institute,
Vas Olgas 196 & Ploutonos 27,
54655 Thessaloniki, Greece
Tel.: +30 6976637334
e-mail: anogian@auth.gr

0393-974X (2019)

there are 8 SNPs in 6 genes/loci which are mostly associated with KC; *BANP-ZNF469* rs9938149, *FOXO1* rs2721051, *FNDC3B* rs4894535, *IMMP2L* rs757219 and rs214884, *COL4A4* rs2229813 and rs2228557 and *RXRA-COL5A1* rs1536482 (2). Two genes whose role in KC pathogenesis was recently investigated are superoxide dismutase 1 (SOD1) and zinc finger protein 469 (ZNF469).

SOD1 Gene

SOD1 has been implicated in the pathogenesis of KC (3, 4) albeit without definitive association. SOD1 encodes the superoxide dismutase enzymes (4) that contribute to the binding of zinc and copper ions and metabolise free superoxide radicals to produce molecular oxygen. They are thus protecting the cell from superoxide radical damage (3, 5). It is noteworthy that the distribution of superoxide dismutase isoenzymes differs between healthy and the KC corneas (4). In addition, mutations in SOD1 may result in ocular colobomas, brain malformations, ichthyosis, post-cholecystectomy syndrome, endocrine abnormalities and they have been implicated in amyotrophic lateral sclerosis (2).

SOD1 is located on chromosome 21q22.11. A SOD1 variant with a seven-base deletion in intron 2 (IVS2+50del7bp), is associated with KC (3, 4). mRNA analysis showed the presence of 2 additional transcript splice variants coding for proteins lacking the active site of the SOD1 enzyme (4). In addition, a deletion has been identified within intron 2 close to the 5' splice junction of SOD1 in 3 KC patients (4). Skipping of SOD1 exon 2 or SOD1 exon 2+3 results in weak protein expression or no expression at all, due to diminished enzyme levels and activities (4).

Four other sequence changes (g.12035 C>A; g.13978 T>A; g.12037 G>A and g.11931 A>C) are present with the same frequency in both KC patients and normal controls; this indicates that the SOD1 gene may not play a vital role in KC pathogenesis at least at the sequence level (6). The presence of c.169 þ 50delTAAACAG change is implicated in sporadic KC, but further study is needed (6). It is probable that mutations on chromosome 21 may be related to the effects of oxidative stress on the cornea given that trisomy 21 is associated with increased risk of KC (6), an association which implies that increased oxidative damage may also be involved in Down syndrome (4).

SOD isoenzymes and reactive oxygen species

Oxygen tension, light exposure and high metabolic activity contribute to the production of reactive oxygen species (ROS) (5). The human eye is particularly vulnerable to oxidative stress (5). There are three superoxide dismutase (SOD) isoenzymes (SOD1, SOD2 and SOD3) which are compartmentalized in the cytosol, the mitochondrial matrix and the extracellular space and they trigger the generation of hydrogen peroxide and molecular oxygen by catalyzing the dismutation of the superoxide radicals (5). Oxidative stress is mainly caused by environmental stimuli like ultraviolet exposure and epithelial trauma and it leads to the destruction of the mitochondria, the nucleus and, eventually, of the whole cell (7). In KC these antioxidant enzymes are altered (4) and result in an increase of the byproducts of the nitric oxide and lipid peroxidation pathways (7). Furthermore, the increase in reactive oxygen species (ROS), results in a decrease in mitochondrial membrane potential, in mitochondrial DNA damage, in apoptosis of corneal fibroblasts and in oxidative damage. Oxidative damage, in particular, results in the upregulation of altered proteins, degradation of enzymes, high levels of oxidative stress, cellular dysfunction and damage to the DNA (8).

ZNF 469 gene

ZNF469 is a two-exon gene, which codes a 413kDa protein consisting of 3,925 amino acid residues (9). It is detected, among many other tissues, and in the human cornea (10). ZNF469 shows a 30% sequence similarity to the helical parts of COL1A1 (which encodes the pro-alpha1 chains of type I collagen which is abundant in the cornea), COL1A2 (which encodes the pro-alpha2 chains of type I collagen which is also abundant in the cornea), and COL4A1 (which encodes a type IV collagen alpha protein that belongs to the integral components of basement membranes). The COL1A1, COL1A2 and COL4A1 genes are highly expressed in the cornea

(10), while, as there is a 30% protein homology between ZNF469 and the helical parts of the three different collagen types, ZNF469 may function as a transcription factor or extra-nuclear regulator that contributes to the synthesis and organization of collagen fibers and ECM proteins of the human cornea (9, 11). Thus, ZNF469 functional mutations may affect the homogeneity and regular properties of collagen corneal fibrils (9).

There are five classical C2H2 zinc finger domains (ZNFs) in the C-terminus, which are the most important parts of the ZNF469 protein. ZNFs work as sequence-specific DNA-binding motifs that regulate specific transcription processes (10). Although the role of ZNF469 is not well established, evidence shows that it regulates the development and maintenance of the ECM (11). Recent studies show a downregulation of ECM component genes like GPC6 (glypican-6), THBS1 (thrombospondin), CLU (clusterin) and PCOLCE2 (procollagen C-endopeptidase enhancer 2, in ZNF mutant fibroblasts) (10). This organization of the collagen fibers occurs in conjunction with the gene PRDM5 (which encodes a transcription factor that belongs to the PR-domain protein family). Heterozygous mutations of PRDM5 have been linked with a mildly reduced) Central Corneal Thickness (CCT) (480 – 505 μm), KC and blue sclera (11). CCT can affect eye disorders such as primary open glaucoma and KC (9).

Apart from ZNF469 being considered as a significant genetic contributor to KC, mutations in ZNF469 cause brittle cornea syndrome (BCS). Potentially pathogenic heterozygous ZNF469 alleles are present in 12.5% of European KC patients (9), making ZNF469 probably the most important genetic factor responsible for KC (12).

CCT meta-analysis of a sample of more than 20,000 individuals revealed 27 CCT-associated loci (2). There is a nominal association with KC for 11 SNPs, while after correction for multiple testing 6 showed a significant association (2). Of 27 CCT-associated loci, 11 were identified in healthy European and Asian populations, with common SNPs 100kb upstream of ZNF469 (MIM 612078), the gene most strongly associated with CCT (2). Five loci with 6 independent SNPs associated with KC have been reported. Two of them increase KC risk in an independent cohort of patients of European origin (2). These are rs1324183, upstream of MPDZ (Multiple PDZ Domain Crumbs Cell Polarity Complex Component), and rs9938149, upstream of ZNF469. It is not known if there is any relevance between other SNPs found in European patients and those found in Asians (2).

Upstream of the ZNF469 gene, there are two SNPs that have been identified, rs12447690 and rs9938149 (2), in Australian, UK, Malay, Indian, Croatian, Caucasian, Scottish and Latino populations (2, 12), suggesting the involvement of these SNPs in CCT variation. More specifically, ZNF469 is the closest to the SNP rs9938149 and thus genetic variation within this gene may account for the association at rs9938149 as well as for its contribution to the susceptibility to CCT and KC (10). However, other rare potentially pathogenic variants do not contribute to KC pathogenesis (10). Studies from Australia and the UK revealed two genome-wide significant signals at 16q24.2 and 13q14.1, in intragenic regions, which influence the genes ZNF469 and FOX01, respectively (10). However, sequencing analysis of ZNF469 in patients with KC and high myopia did not identify any significant variants (9).

There are conflicting results concerning the variants that contribute to the progress of KC. It is reported that ZNF469 variants may not be important genetic factors for KC in Polish patients, while mutations in ZNF469 in a New Zealand population (at a frequency of 23%) and in the Han population seem to be important contributing genetic factors (9). Thus, variants that may be pathogenic in one population, may not be pathogenic in other populations, or among different regions, reflecting the pleiotropic function of ZNF469 in KC, and keeping ZNF469 involvement contentious (9).

Brittle cornea syndrome

BCS is a tissue disorder characterized by extremely thin and prone to spontaneous rupture corneas even after minor trauma. It is associated with homozygous mutations in ZNF469, suggesting the role of ZNF469 in the structural integrity of the cornea (12). It is

inherited with autosomal recessive form and is a connective tissue disorder characterized by extreme corneal thinning between 220–450 μm, which poses a high risk of corneal rupture that can lead to blindness (12). BCS comorbidities include joint hypermobility, scoliosis and deafness, that lead to combined sensory deprivation (10).

There are two types of BCS. BCS type 1 (OMIM #229200) results from homozygous mutations in the ZNF469 gene and features all the signs mentioned above (10). As previously mentioned, the gene was originally mapped to chromosome 16q24 (10) and five homozygous mutations of the ZNF469 have been reported. These include a homozygous frameshift mutation, (c.9527delG) which results in a premature termination codon (p.Gln3178ArgfsX23 and p.Gly1983AlafsX16), p.Phe717SerfsX14, p.Gln1392X and p.Gln1757X, as well as one homozygous missense mutation (p.Cys3339Tyr) (12).

BCS type 2 results from homozygous mutations in the PRMD5 (PR/SET Domain 5) of the ZNF469 gene. BCS type 2, like BCS1, is an autosomal recessive condition (12). These mutations in ZNF469 apparently increase the risk of isolated KC and BCS type 1 in patients of different ethnicities (12.5% of the European KC patients from three different cohorts, 23% of patients with KC in New Zealand and 50% of Maori or Polynesian KC patients). A rare missense mutation in ZNF469 was also reported to be in 23% of the KC patients in Polynesian populations (12).

In conclusion, the role of a plurality of genes has been studied in relation to the pathogenesis of KC, often with conflicting results. In order to have safer results, larger studies with larger samples will be needed in the future.

REFERENCES

1. Moussa S, Grabner G, Ruckhofer J, Dietrich M, Reitsamer H. Genetics in keratoconus–what is new? Open Ophthalmol J 2017; 11:201-10.
2. Rong SS, Ma STU, Yu XT, et al. Genetic associations for keratoconus: a systematic review and meta-analysis. Sci Rep 2017; 7(1):4620.
3. Udar N, Atilano SR, Small K, Nesburn AB, Kenney MC. SOD1 haplotypes in familial keratoconus. Cornea 2009; 28(8):902-7.
4. Udar N, Atilano SR, Brown DJ, Holguin B, Small K, Nesburn AB, Kenney MC. SOD1: a candidate gene for keratoconus. Invest Opthalmol Vis Sci 2006; 47(8):3345-51.
5. Zelko IN, Mariani TJ, Folz RJ. Superoxide dismutase multigene family: a comparison of the CuZn-SOD (SOD1), Mn-SOD (SOD2), and EC-SOD (SOD3) gene structures, evolution, and expression. Free Radic Biol Med 2002; 33(3):337-49.
6. Al-Muammar AM, Kalantan H, Azad TA, Sultan T, Abu-Amero KK. Analysis of the SOD1 gene in keratoconus patients from Saudi Arabia. Ophthalmic Genet 2015; 36(4):373-75.
7. Saee-Rad S, Raoofian R, Mahbod M, et al. Analysis of superoxide dismutase 1, dual-specificity phosphatase 1, and transforming growth factor, beta 1 genes expression in keratoconic and non-keratoconic corneas. Mol Vis 2013; 19:2501-7.
8. Wang X, Simpkins JW, Dykens JA, Cammarata PR. Oxidative damage to human lens epithelial cells in culture: estrogen protection of mitochondrial potential, ATP, and cell viability. Invest Opthalmol Vis Sci 2003; 44(5):2067-75.
9. Karolak JA, Gambin T, Rydzanicz M, et al. Evidence against ZNF 469 being causative for keratoconus in Polish patients. Acta Ophthalmol 2016; 94(3):289-94.
10. Abu A, Frydman M, Marek D, Pras E, Nir U, Reznik-Wolf H, Pras E. Deleterious mutations in the zinc-finger 469 gene cause brittle cornea syndrome. Am J Hum Genet 2008; 82(5):1217-22.
11. Burkitt Wright EM, Spencer HL, Daly SB, et al. Mutations in PRDM5 in brittle cornea syndrome identify a pathway regulating extracellular matrix development and maintenance. Am J Hum Genet 2011; 88:767-77.
12. Lechner J, Porter LF, Rice A, et al. Enrichment of pathogenic alleles in the brittle cornea gene, ZNF469, in keratoconus. Hum Mol Genet 2014; 23(20):5527-35.

LETTER TO THE EDITOR

GENES INVOLVED IN HORMONE METABOLISM AND CELLULAR RESPONSE IN HUMAN OVARIAN GRANULOSA CELLS

M. BRĄZERT[1], D. IŻYCKI[2], W. KRANC[3], B. BOROWIEC[3], M. POPIS[3], K. OŻEGOWSKA[1], A. BRĘBOROWICZ[4], D. RACHOŃ[5], M. NOWICKI[6] and B. KEMPISTY[3,6,7]

[1]Division of Infertility and Reproductive Endocrinology, Department of Gynecology, Obstetrics and Gynecological Oncology, Poznan University of Medical Sciences, Poznan, Poland; [2]Department of Cancer Immunology, Poznan University of Medical Sciences, Poznan, Poland; [3]Department of Anatomy, Poznan University of Medical Sciences, Poznan, Poland; [4]Department of Pathophysiology, Poznan University of Medical Sciences, Poznan, Poland; [5]Department of Clinical and Experimental Endocrinology of the Medical University of Gdansk, Poland; [6]Department of Histology and Embryology, Poznan University of Medical Sciences, Poznan, Poland; [7]Department of Obstetrics and Gynecology, University Hospital and Masaryk University, Brno, Czech Republic

Received August 15, 2018 – Accepted December 21, 2018

Endocrinal interactions are one of the most crucial regulatory mechanisms that maintain the state of homeostasis in humans. Processes such as oogenesis, folliculogenesis, menstruation and pregnancy remain under hormonal control. A key role in folliculogenesis is played by granulosa cells. Moreover, granulosa cells take part in corpus luteum formation after ovulation. Because of that, it is important to understand the ways in which the granulosa cells, associated with those processes, respond to hormonal stimulus. In the present study, a transcriptomic analysis of human granulosa cells (GCs) was carried out with the use of expression microarrays. The results were validated by RT-qPCR. The total RNA was isolated after 1st, 7th, 15th and 30th days of long-term primary cultures. The main focus of this work was placed on the genes belonging to "Response to estradiol", "Response to follicle-stimulating-hormone", "Cellular response to hormone stimulus", "Cellular hormone metabolic process" and "Hormone biosynthetic process" gene ontology groups. These groups of genes have been associated with GC hormone metabolism and cellular response to hormones. Eighty genes belonging to these groups were identified. Those that were members of more than one of the analyzed gene ontology groups, or exhibited unique expression patterns, were selected for further analysis. All of the selected genes were described, with their expression patterns detailed. In this manuscript, two gene expression patterns have been described. The first one showed large downregulation of genes in the later stages of culture, with the second one presenting upregulation of expression after day 1 of IVC. The present research was focused on six genes found to be the most important for steroidogenesis: STAR, POR, *CYP11A1, ADM, GCLC, IL1B,* as well as three genes of higher expression at the later stages of long-term *in vitro* culture: *NR2F2*, *BMP4, COL1A1*. The main goal of the presented study was to select genes involved in response to hormonal stimulus and hormone metabolism in GC long-term *in vitro* culture.

Key words: human granulosa cells; hormone metabolism; cellular response

Corresponding Author:
Bartosz Kempisty PhD,
Department of Anatomy,
Department of Histology and Embryology,
Poznan University of Medical Sciences,Poznan, Poland
Tel.: +48 61 8546418 - Fax: +48 61 8546440
e-mail: bkempisty@ump.edu.pl

0393-974X (2019)

To the Editor,

Hormonal regulation is one of the aspects having the most influence over the proceedings of reproduction. Under physiological conditions, due to the influence of FSH, granulosa cells (GCs) secrete the most active form of estrogen, 17-beta estradiol, into the follicular fluid and blood. The high concentration of estrogens in the blood suppresses the secretion of FSH by the pituitary gland on the principle of negative feedback. The LH causes ovulation and subsequent development of the corpus luteum. This begins the luteal phase of the ovarian cycle. The corpus luteum is responsible for the production of progesterone (5).

The above processes are closely related to cells of the granulosa layer located inside the ovarian follicle. Even after the follicular rupture and ovulation, GCs that remain in the follicle transform into granulosa lutein cells and continue their role in the maintenance of the menstrual cycle or potential pregnancy. The basis of the role of GCs in effective reproduction is also well known - oocyte-cumulus interactions, estradiol production, etc. (1). However, advanced clinical approaches involving tissue and cell engineering, gene therapy, as well as understanding the exact causes of multiple diseases of the reproductive system, require understanding the molecular basis of GC function (3). The aim of this study is to analyze the genes belonging to: "Response to estradiol", "Response to follicle-stimulating-hormone", "Cellular response to hormone stimulus", "Cellular hormone metabolic process" and "Hormone biosynthetic process" gene ontology groups, to gain a deeper understanding of the genetic basis of GC *in-vitro* function in the context of hormone metabolism and cellular response. That knowledge could translate into future advancement in understanding the mechanism of GC action, hence, in the wider perspective, various processes associated both with the menstrual cycle and others that involve GCs and the hormones that they express.

MATERIALS AND METHODS

Patients and collection of granulosa cells

The GCs were derived from patients undergoing *in vitro* fertilization (IVF) procedures, who had given their informed consent to be included in this protocol. The group of 20 patients, aged 18-40 years, with diagnosed infertility, referred to the Division of Infertility and Reproductive Endocrinology, Poznan University of Medical Sciences, Poland, were examined. The patients underwent IVF procedure, based on controlled ovarian hyperstimulation protocol, adjusted to the patient's initial infertility workup and ovarian response. Stimulation was performed with human recombinant FSH (Gonal-F, Merck Serono) and highly purified human menopausal gonadotropin - hMG - HP (Menopur, Ferring). The injections with cetrorelix acetate (Cetrotide, Merck Serono) were administered in an adequate dose, to suppress pituitary function. Triggering of ovulation was based on subcutaneous injection of 6,500 U of human Chorionic Gonadotropin (Ovitrelle, Merck-Serono). GC containing follicular fluid was collected during transvaginal, ultrasound guided oocyte pick-up, 36 h after hCG administration. The fluid was collected from oocytes of over 16 mm in diameter. It was immediately passed to an embryologist who isolated the oocyte and pooled the follicular fluid from each ovary. Fresh follicular fluid was centrifuged for 10 min at 200 x g, to separate and collect GCs. Patients with polycystic ovary syndrome (PCOS), endometriosis, and diminished ovarian reserve [serum antimüllerian hormone (AMH) less than 0.7 ng/mL and/or day 2-3 FSH serum level higher than 15 mU/mL and/or antral follicle count less than 9] were excluded from the study. This study was approved with resolution 558/17 by the Bioethical Committee at the Poznan University of Medical Sciences. All participants gave written informed consent to the research.

Primary granulosa cell culture

Collected GCs were centrifuged at 200 x g for 10 min at room temperature (RT). Afterwards, they were washed with culture medium. The medium consisted of Dulbecco's Modified Eagle's Medium (DMEM/F12, Sigma-Aldrich, USA), 2% fetal bovine serum FBS (FBS; Sigma-Aldrich Co., St. Louis, MO, USA), 4 mM L-glutamine (stock 200 mM, Invitrogen, Carlsbad, CA, USA), 10 mg/ml gentamicin (Invitrogen, USA), 10,000 units/ml penicillin, and 10,000 μg/ml streptomycin (Invitrogen, Carlsbad, CA, USA). GCs were cultured at 37°C under aerobic conditions (5% CO_2). When the cells achieved 90% confluence, the culture were detached with 0.05% trypsin-EDTA (Invitrogen, USA) for 1-2 min. Granulosa cells were counted using a "neubauer

improved" counting chamber (ISO LAB Laborgerate GmbH, DIN EN ISO CERTIFIED 9001) and trypan blue (Sigma-Aldrich, Co., St. Louis, MO, USA). Three mln cells were seeded onto one flask (Nunclon 25cm^3 Cell Culture Flask; Sigma-Aldrich Co., St. Louis, MO, USA). GCs from all patients were cultured in long-term *in vitro* culture (30 days). Medium was changed twice a week. Finally, total RNA was isolated from the GCs after 24 h, 7 days, 15 days and 30 days of IVC.

Total RNA isolation

Total RNA was isolated from the GCs at 4 time periods, after 24 h, 7 days, 15 days, and 30 days culture. Improved Chomczyński-Sacchi method was used for total RNA isolation. The GCs were suspended in 1 ml of guanidine thiocyanate and phenol monophasic solution (TRI Reagent®, Sigma-Aldrich, USA, St. Louis, USA). Chloroform was then added and the sample centrifuged to separate 3 phases. The RNA was located in upper phase – an aqueous phase. The resulting RNA was intact with little or no contaminating DNA and protein. The last step was to strip the RNA with 2-propanol (Sigma-Aldrich, St. Louis, USA, catalog number I9516), in an amount adequate per 1 mL of TRI-reagent, and the sample was washed with 75% ethanol. RNA prepared in that way was used for further analysis. The total mRNA was determined from the optical density at 260 nm. The purity of total RNA was determined by the 260/280 nm absorbance ratio (NanoDrop spectrophotometer, Thermo Scientific, ALAB, Poland). Samples with 260/280 absorbance ratio greater than 1.8 were used in the study. The RNA samples were re-suspended in 20 µl of RNase-free water and stored at -80°C until further analysis.

Microarray expression analysis and statistics

Total RNA (100 ng) from each sample was subjected to two rounds of sense cDNA amplification (Ambion® WT Expression Kit). In this reverse transcription procedure, total RNA is primed with engineered primers containing a T7 promoter sequence. The reaction synthesizes single-

Table I. *Oligonucleotide sequences of primers used for RT-qPCR analysis.*

Gene	Gene accession number	Primer sequence (5'-3')	Product size (bp)
CYP11A1	NM_000781.2	AGCCAGCATCAAGGAGACAC AATTTTCCGGGTCGAAGAAG	170
ADM	NM_001124.2	CGTCGGAGTTTCGAAAGAAG CCCTGGAAGTTGTTCATGCT	232
GCLC	NM_001197115.1	ACCATCATCAATGGGAAGGA GCGATAAACTCCCTCATCCA	182
STAR	NM_000349.2	GGCATCCTTAGCAACCAAGA TCTCCTTGACATTGGGGTTC	199
Il1B	NM_000576.2	GGGCCTCAAGGAAAAGAATC TTCTGCTTGAGAGGTGCTGA	205
POR	NM_000941.2	CACAAGGTCTACGTCCAGCA GCCACGATGTCGTAGAAGGT	143
GAPDH	NM_002046	TCAGCCGCATCTTCTTTTGC ACGACCAAATCCGTTGACTC	90
ACTB	NM_001101	AAAGACCTGTACGCCAACAC CTCAGGAGGAGCAATGATCTTG	132
HPRT	NM_000194	TGGCGTCGTGATTAGTGATG ACATCTCGAGCAAGACGTTC	141

stranded cDNA containing a T7 promoter sequence. In the second step, single-stranded cDNA is converted to double-stranded cDNA, which acts as a template for transcription. The reaction uses DNA polymerase and RNase H to simultaneously degrade the RNA and synthesize second-strand cDNA. The obtained cDNA was used for biotin labeling and fragmentation with the use of Affymetrix GeneChip® WT Terminal Labeling and Hybridization (Affymetrix, Santa Clara, CA, USA). Biotin-labeled fragments of cDNA (5.5 µg) were hybridized to the Affymetrix® Human Genome U219 Array (48°C/20 h). Microarrays were then washed and stained according to the technical protocol using the Affymetrix GeneAtlas Fluidics Station. The array strips were scanned using the Imaging Station of the GeneAtlas System. Preliminary analysis of the scanned chips was performed using Affymetrix GeneAtlas™ Operating Software. The quality of gene expression data was confirmed according to the quality control criteria provided by the software. The obtained CEL files were imported into downstream data analysis software. The CEL file stores the results of the intensity calculations on the pixel values of the scanned microarray (DAT) file. This includes an intensity value, standard deviation of the intensity, the number of pixels used to calculate the intensity value, a flag to indicate an outlier as calculated by the algorithm and a user defined flag indicating the feature should be excluded from future analysis. The file stores the previously stated data for each feature on the probe array.

All of the presented analyses and graphs were performed using Bioconductor and R programming languages. Each CEL file was merged with a description file. In order to correct background, normalize, and summarize results, the Robust Multiarray Averaging (RMA) algorithm was used. To determine the statistical significance of the analyzed genes, moderated t-statistics from the empirical Bayes method were performed. The obtained p-value was corrected for multiple comparisons using Benjamini and Hochberg's false discovery rate. The selection of significantly altered genes was based on a p-value beneath 0.05 and expression higher than two-fold. The differentially expressed gene list (separated for up- and down-regulated genes) was uploaded to DAVID software (Database for Annotation, Visualization and Integrated Discovery).

Subsequently, sets of differentially expressed genes from selected GO BP terms, were submitted to Search Tool for the Retrieval of Interacting Genes/Proteins (STRING) software for interaction prediction. STRING is a database containing information on protein/gene interactions, including experimental data, computational prediction methods and public text collections.

In order to further investigate the chosen gene sets, we investigated their mutual relations with the use GOplot package. Moreover, GOplot package allowed us to calculate the z-score (the number of up- regulated genes minus the number of down- regulated genes divided by the square root of the count). Z-score analysis allowed us to compare the enrichment of selected Gene Ontology Biological Process (GO BP) terms.

Reverse transcription and RT-qPCR

The results obtained during microarray analysis were validated using the quantitative RT-qPCR method. For the reverse transcription, 1 ug of RNA isolated from GCs in particular time intervals (after 24 h, 7 days, 15 days, 30 days

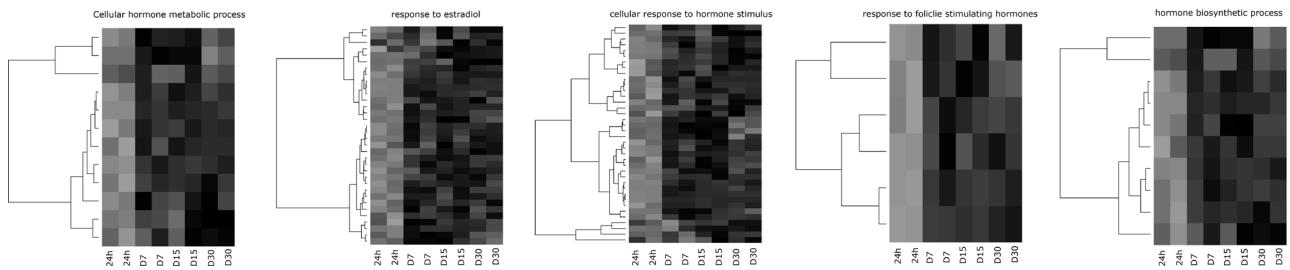

Fig. 1. *Heat map representation of differentially expressed genes belonging to the "response to estradiol", "response to follicle-stimulating-hormone", "cellular response to hormone stimulus", "cellular hormone metabolic process" and "hormone biosynthetic process" GO BP terms. Log2 signal intensity values for any single gene were resized to Row Z-Score scale (from -2, the lowest expression to +2, the highest expression for single gene).*

of culture) was used. Reverse transcription was conducted based on the protocols and reagents from SABiosciences (RT^2 First Stand Kit - 330401), using a Veritimer 96 well Thermal Cycler.

Real-time PCR was performed using the Light Cycler® 96 (Roche Diagnostic GmbH, Germany), RT^2 SYBR® Green ROX™ qPCR Master Mix (Qiagen Sciences, Maryland, USA) and sequence-specific primers (Table I). To quantify the granulosa cell specific genes, expression levels of specific mRNAs were calculated in relation to *Glyceraldehyde-3-phosphate dehydrogenase (GADPH),* and *β-actin (ACTB)* and *Hypoxanthine phosphoribosyltransferase 1 (HRPT1)* were used as reference genes. Gene expression was analyzed using the relative quantification (RQ) method. The q-PCR starters were designed using Primer3Plus software (http://primer3plus.com/cgi-bin/dev/primer3plus.cgi).

One RNA sample of each preparation was processed without the RT-reaction to provide a negative control for subsequent PCR.

To ensure the integrity of these results, the additional housekeeping gene was used as an internal standard to demonstrate that *GAPDH, HPRT* and *ACTB* mRNAs were not differentially regulated in the granulosa cell sample.

RESULTS

Changes of the GC morphology were presented using photos from an inverted microscope that employed relief contrast. The GC system achieved the spindle-shaped morphology in the primary stages of long-term primary culture. After 30 days long-term IVC, the GCs exhibited fibroblast-like cell morphology. In some of the GC primary long-term cultures, several epithelial-origin cells (e.g. ovarian follicle cells, inadvertently collected during puncture) were visible. These cultures were immediately discarded from further RNA isolation, microarray assays and/or cell freezing.

Whole transcriptome profiling using Affymetrix® Human HgU 219 Array microarray allowed to analyze the genes involved in GCs' hormone metabolism and cellular response during long-term primary *in-vitro* culture**.** In that way, the expression of 22480

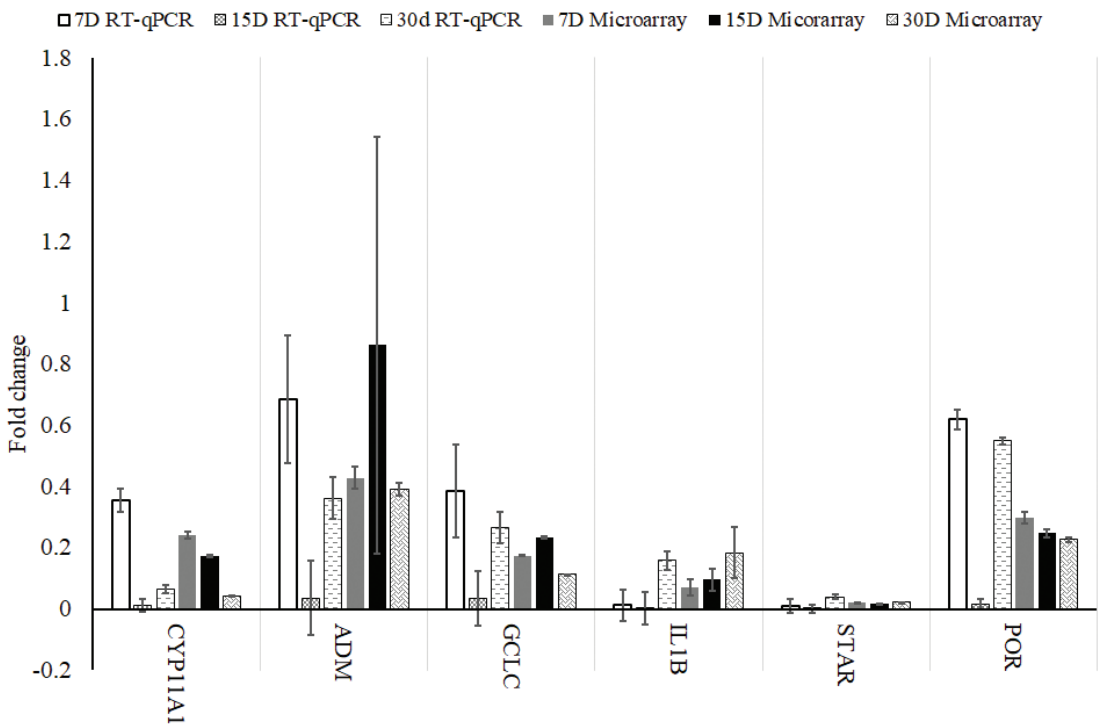

Fig. 2. *Results of RT-qPCR validation of microarray results presented as a bar graph.*

transcripts was identified. Genes with fold change higher than |2| and with corrected p value lower than 0.05 were considered differentially expressed. This set of genes consisted of 2278 different transcripts.

DAVID was used for extraction of the genes belonging to the analyzed GO BPs. Up and down regulated gene sets were subjected to the DAVID search separately, and only the gene sets which displayed adjusted p value lower than 0.05 were selected. The DAVID software analysis yielded differently expressed genes belonging to 582 Gene ontology groups and 45 KEGG pathways. In this paper we focused on "response to estradiol" (GO:0032355), "response to follicle-stimulating-hormone" (GO:0032354), "cellular response to hormone stimulus" (GO:0032870), "cellular hormone metabolic process" (GO:0034754) and "hormone biosynthetic process" (GO:0042446) GO BP terms. These sets of genes were subjected to hierarchical clusterization procedure and presented as heatmaps (Fig. 1).

RT-qPCR was also employed, with its results

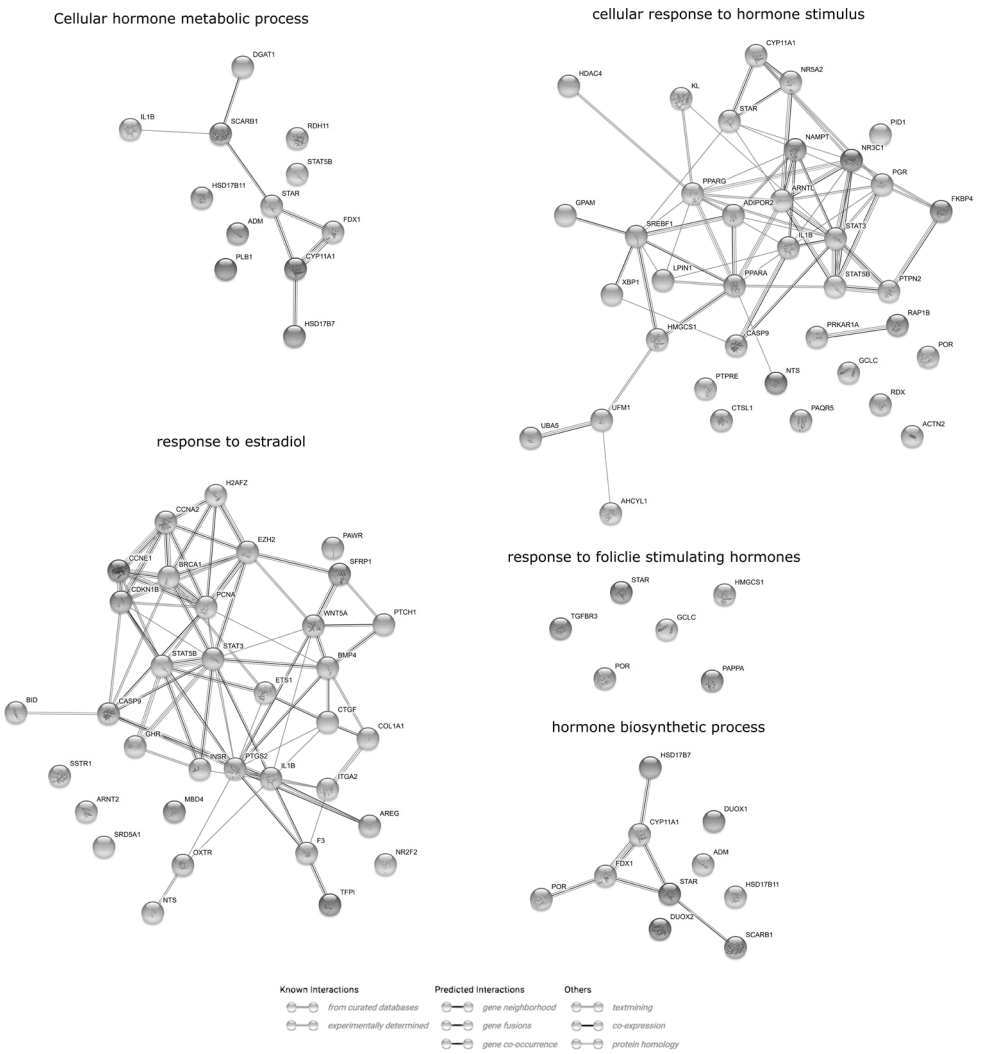

Fig. 3. *STRING-generated interaction network among differentially expressed genes belonging to the "response to estradiol", "response to follicle-stimulating-hormone", "cellular response to hormone stimulus", "cellular hormone metabolic process" and "hormone biosynthetic process" GO BP terms. The intensity of the edges reflects the strength of interaction score.*

confirming the presence of analyzed gene transcripts in the samples. Comparison between the results from microarrays and RT-qPCR (Fig. 2) confirmed the direction of changes in expression. However, as RT-qPCR is a quantitative method, as compared to qualitative microarrays, the fold changes of expression often varied between those two methods. As can be seen, all of the analyzed genes expressed downregulation of expression when tested by both the microarrays and RT-qPCR. Some of them present high scale of changes (*STAR*), while most of them change in moderate to low manner (*ADM*).

All of the genes analyzed by RT-qPCR (*CYP11A1, ADM, GCLC, IL1B, STAR* and *POR*) exhibited the lowest fold change of gene expression on day 15 of GCs primary *in vitro* culture, in reference to the starting point. Moreover, in most of the genes, except *STAR* and *IL1B*, the highest fold change was observed on day 7. The highest fold change was observed on day 30 of *in vitro* primary culture for *STAR* and *IL1B* genes. The most downregulated among these terms was the "cellular hormone metabolic process" GO, and the least regulated term was "response to follicle-stimulating-hormone".

STRING was used to generate interaction network among differentially expressed genes belonging to each of selected GO BP terms. The main goal of the STRING database is to analyze protein-protein interactions, including direct (physical) links and indirect (functional) links. Functional interrelations depict the relationship between particular proteins contributing to a common biological goal. Fig. 3 illustrates the molecular interaction network formed between protein products of studied genes.

DISCUSSION

hGCs are the primary cell type forming the follicle, being present in the folliculogenesis and oogenesis. The presented research was focused on three genes with higher expression after 30 days of long-term *in vitro* culture: *NR2F2*, *BMP4, COL1A1*.

Nuclear Receptor Subfamily 2 Group F Member 2 (*NR2F2*)- this ligand, an activated nuclear receptor/ transcription factor, plays a key role in angiogenesis, neural development, organogenesis, homeostasis and cell fate determination (10). In addition, this gene has been identified in mouse embryonic ovaries and plays a key role in maintaining a balance between estrogen and progesterone, thus enabling normal embryo imagination in the uterus, which is also confirmed by the research presented by our team (8).

The second gene belonging to the "Response to estradiol" ontological group is bone morphogenic protein 4 (*BMP4)*. It is a secreted ligand of the transforming growth factor beta (TGF-beta) protein superfamily. Ligands of TGF-betas bind their respective receptors on the cell surface, causing their phosphorylation. This activates a signaling cascade involving recruitment and activation of SMAD transcription factors, which then translocate to the nucleus to regulate gene expression. *BMP4* plays a major role in embryonic development, especially in induction of dorsal-venal axis and neurogenesis (9, 11). It also performs numerous functions during organogenesis, including lung morphogenesis, limb patterning and tooth development (1). Under physiological conditions, BMP4 inhibits the GC luteinization process. In addition, BMP4 reduces the expression of the gap junction intercellular communication (GJIC) genes (3). In the context of our research, we can conclude that the increase in BMP4 gene expression suggests changes in GC properties during long-term *in vitro* culture. BMP4 is responsible for processes related to cell differentiation. The next gene, *COL1A1*, provides information for production of a component of type I collagen, called the pro-alpha 1 chain. These molecules arrange and cross-link to produce mature type I collagen. This type of collagen is abundant in most connective tissue (bones, tendon, dermis and cornea) (12). The presented studies indicate a decrease in gene expression closely related to steroidogenesis and GC response to steroid hormones.

ACKNOWLEDGEMENTS

This work was supported by the Poznan University of Medical Sciences under Grant numbers 502-14-02227367-10694, UMO-2012/07/N/NZ5/00069 and 502-01-02227367-08414, as well as grant number 2014/15/B/NZ7/00999 from the Polish National

Centre of Science. All of the experiments were conducted in Poznan University of Medical Sciences.

REFERENCES

1. Bei M, Maas R. FGFs and BMP4 induce both Msx1-independent and Msx1-dependent signaling pathways in early tooth development. Development 1998; 125(21):4325-33.
2. Chachuła A, Kranc W, Budna J, et al. The differentiation of mammalian ovarian granulosa cells living in the shadow of cellular developmental capacity. J Biol Regul Homeost Agents 2016; 30(3):627-34.
3. Chang H-M, Cheng J-C, Leung PCK. Theca-derived BMP4 and BMP7 down-regulate connexin43 expression and decrease gap junction intercellular communication activity in immortalized human granulosa cells. J Clin Endocrinol Metab 2013; 98(3):437-45.
4. Ciesiółka S, Budna J, Jopek K, et al. Time- and dose-dependent effects of 17 beta-estradiol on short-term, real-time proliferation and gene expression in porcine granulosa cells. Biomed Res Int 2017; 2017:1-9.
5. Gregoraszczuk EL. Effect of FSH on progesterone secretion by porcine large and small luteal cells isolated from early-developing corpora lutea. Exp Clin Endocrinol Diabetes 2009; 103(4):272-74.
6. Kempisty B, Ziółkowska A, Ciesiółka S, et al. Association between the expression of LHR, FSHR and CYP19 genes, cellular distribution of encoded proteins and proliferation of porcine granulosa cells in real-time. J Biol Regul Homeost Agents 2014; 28(3): 419-31.
7. Kossowska-Tomaszczuk K, De Geyter C, De Geyter M, Martin I, Holzgreve W, Scherberich A, Zhang H. The multipotency of luteinizing granulosa cells collected from mature ovarian follicles. Stem Cells 2009; 27(1):210-19.
8. Kurihara I, Lee D-K, Petit FG, et al. COUP-TFII mediates progesterone regulation of uterine implantation by controlling ER activity. PLoS Genet 2007; 3(6):e102.
9. Mira H, Andreu Z, Suh H, et al. Signaling through BMPR-IA regulates quiescence and long-term activity of neural stem cells in the adult hippocampus. Cell Stem Cell 2010; 7(1):78-89.
10. Pereira LO, Rubini MR, Silva JR, Oliveira DM, Silva ICR, Poças-Fonseca MJ, Azevedo RB. Comparison of stem cell properties of cells isolated from normal and inflamed dental pulps. Int Endod J 2012; 45(12):1080-90.
11. De Robertis EM, Kuroda H. Dorsal-ventral patterning and neural induction in Xenopus embryos. Annu Rev Cell Dev Biol 2004; 20:285-308.
12. Sengupta P, Xu Y, Wang L, Widom R, Smith BD. Collagen alpha1(I) gene (COL1A1) is repressed by RFX family. J Biol Chem 2005; 280(22):21004-14.

LETTER TO THE EDITOR

EFFECTS OF EUPHORBIA KANSUI ON THE SERUM LEVELS OF IL-6, TNF-α, NF-κB, sTNFR AND IL-8 IN PATIENTS WITH SEVERE ACUTE PANCREATITIS

XJ. MO[1], XZ. YE[2] and YP. LI[1]

[1]Department of Emergency Intensive Care Unit (EICU), The Third Affiliated Hospital of Wenzhou Medical University, Wenzhou, Zhejiang, P.R. China; [2]Ultrasonic Department, Physical Examination Center, The Third Affiliated Hospital of Wenzhou Medical University, Wenzhou, Zhejiang, P.R. China

Received October 8, 2018 – Accepted January 11, 2019

In this study, effects of euphorbia kansui on serum levels of inflammatory factors in patients with severe acute pancreatitis were investigated, and the mechanisms underlying the role of Euphorbia kansui in the treatment of severe acute pancreatitis were discussed. 36 patients hospitalized in the Third Affiliated Hospital of Wenzhou Medical University from March 2017 to May 2018 due to severe acute pancreatitis were selected and divided into two groups using a randomized grouping method. ELISA (enzyme-linked immunosorbent assay) was used to detect expressions of various inflammatory cytokines, such as tumor necrosis factor α (TNF-α), soluble TNF receptors (sTNFR), nuclear factor-κB (NF-κB), interleukin-6 (IL-6), and interleukin-8 (IL-8), in the serum of patients at different time points. The results showed no significant difference between the two groups in terms of age, gender, predisposing factors, Balthaza CT scores, and APACHEII (Acute Physiology and Chronic Health Evaluation) scores. According to the experimental results, euphorbia kansui effectively reduced the expression of inflammation related cytokines, such as NF-κB, TNF-α, sTNFR, IL-6, and IL-8, in the serum of patients with severe acute pancreatitis. It was also proposed that euphorbia kansui hindered the release of inflammatory factors and treated SAP by inhibiting the activation of the NF-κB signaling pathway.

To the Editor,

In recent years, with the continuous innovation and research progress in the field of traditional Chinese medicine (TCM), many kinds of TCM have been used in the treatment of critically ill patients (1). In particular, the combination of euphorbia kansui and Western therapies was used to treat severe acute pancreatitis (SAP) (2). After a long-term study, it was shown that the above method was effective in the treatment of SAP (3). There is also evidence indicating that cytokines play an important role in the pathogenesis of SAP (4, 5). In particular, the nuclear transcription factor NF-κB is activated in the nuclei of inflammatory cells to promote gene transcription of pro-inflammatory cytokines such as TNF-α, sTNFR, IL-6, and IL-8. When secreted by

Key words: Euphorbia kansui; severe acute pancreatitis; inflammatory factors

Corresponding Author:
Dr Youpeng Li,
Department of Emergency Intensive Care Unit (EICU),
The Third Affiliated Hospital
Wenzhou Medical University,
No. 108 Wansong Road, Ruian, Wenzhou,
Zhejiang 325200, P.R. China
e-mail: lyp_liyoupeng108@163.com

0393-974X (2019)

inflammatory cells, proinflammatory cytokines can further promote the activation of NF-Kb (6, 7). Kansui also effectively prevents the progression of SAP in early bacterial translocation and hence reduces the incidence of subsequent pancreatic and peripancreatic infections (8). Meanwhile, kansui also improves microcirculation of the gastrointestinal tract and the outcomes of SAP, therefore may be significant in the treatment of severe acute pancreatitis (9). This study proposed a possible signaling pathway underlying the pharmacological effect of kansui by identifying its potential targets. Finally, it was demonstrated that there was a dose-response relationship in the treatment of SAP by Gansui.

MATERIALS AND METHODS

Patients

A total of 36 SAP patients who were admitted to the Third Affiliated Hospital of Wenzhou Medical University from March 2017 to May 2018 were enrolled in this study. The subjects were randomly divided into two groups: the control group and the Euphorbia injection group, with 18 cases in each group. Informed consent was signed by all patients and/or their family members, and the protocol was approved by the Ethics committee of the Third Affiliated Hospital of Wenzhou Medical University.

Inclusion criteria: patients with SAP admitted to the Department of Hepatobiliary, Pancreatic and Splenic Surgery, the Third Affiliated Hospital of Wenzhou Medical University; acute pancreatitis patients with organ dysfunction, necrosis, pseudocyst, abscess and other local complications; in line with three and more of Ranson criteria; acute physiology and chronic health status scores (APACHEII) of ≥8; Balthaza CT grade of II or above (10); patients who gave written informed consent.

Exclusion criteria: patients who did not meet the above diagnostic criteria; Patients with advanced tumors; patients with primary dysfunction in the heart, brain, blood vessels, lungs, liver, kidneys and other important organs; patients who also suffered from uncontrolled immune system diseases and endocrine diseases; patients who also suffered from acute peptic ulcer, gastrointestinal bleeding, gastrointestinal perforation, and gastrointestinal tract infarction; patients who were deemed unsuitable for the clinical research.

Grouping

The treatment (conventional treatment) of patients in the control group included: fasting, indwelling gastrointestinal tube (gastrointestinal decompression) or endoscopic indwelling nasointestinal tube, indwelling catheter within 12 h of admission; proton pump inhibitors + Shanning to inhibit the secretion of gastric acid and trypsin; preventive use of antibiotics: third-generation Cephalosporin (quinolones for allergies) and ornidazole for anaerobic bacteria; drugs to maintain water, electrolytes and acid-base balance; drugs to prevent septic shock; ECG monitoring and oxygen inhalation were used when necessary; nutritional support treatment; analgesia and spasmolysis treatment were given if necessary; after the recovery of gastrointestinal functions, the diet of patients was gradually changed to a fluid diet. 20 mL of saline was injected as a placebo via the nasointestinal or gastric tube, once a day for 7 days.

Euphorbia kansui treatment group: as well as the conventional treatment, patients were also treated with powdered kansui (The Third Affiliated Hospital of Wenzhou Medical University, Wenzhou, China) consecutively for 7 days. In this treatment, 20 mL of saline was added to 50 mg of powdered kansui to create a suspension, which was administered daily via a gastric tube. The gastric tube was clamped once a day for 30-60 min. All drugs were provided within 2 h of admission (the dose was calculated as 80 mg/m^2 according to each patient's surface area).

Detection of serum levels of inflammatory factors in the patients

Peripheral venous blood samples were collected from the patients in the control and experimental groups on days 1, 3, 5 and 7. The samples were then centrifuged for 10 min at 40°C and 3000 r/min. 1 ml of upper serum was taken and stored at -80°C. The ELISA test was performed on the collected serum according to the instructions of the ELISA Kit (Boster Biology, California, USA). The kit was removed from the refrigerator and equilibrated at room temperature for 20 min, and all reagents were carefully mixed while the concentrated detergent was diluted with double distilled water at a ratio of 1:19; 0.5mL of standard diluent was added into the standard tube and gently mixed for 15 min until the material was thoroughly dissolved and the final concentration of the standard was 6000pg/mL, which was then diluted to 3000pg/mL, 1500pg/mL, 750pg/mL, 375pg/mL, and 187.5pg/mL, respectively. The

pipette tip was carefully rinsed, and the enzyme labeling solution was used to set up sample wells (by adding 50 uL of diluted standard or test samples into each well, respectively), along with blank wells (blank control wells without samples or enzyme labeling reagent), followed immediately by the addition of 50uL/well antibody labeled with biotin. The plate was incubated for 30 min at room temperature before adding the biotinylated antibody working fluid (100uL/well). Enzyme conjugate solution (100uL/well) was added, and sealed with a piece of sealing tape before it was incubated at room temperature for 20 min. l00uL of color TMB was added into each well, gently mixed and incubated at room temperature for 20 min in the dark. 50 uL of TMB terminator was added to each well to terminate the reaction (at this point, the blue color in the standard well should turn yellow immediately). The plate was then assayed on an enzyme labeling instrument for 1 min under shaking.

Statistical analysis

SPSS 17 statistical software was used for data analysis. T was used to detect the normal distribution with continuous variables, and data were expressed in mean ± standard deviation ($\underline{x}$±s). Analysis of variance was used for comparison of continuous variables in more than two groups. For the same variables involving multiple groups, analysis of variance was adopted. The multivariate analysis of variance was used to compare multiple groups.

Table I. *Effects of euphorbia kansui on serum levels of NF-κB in SAP patients (x±S, n=18).*

	serum levels of NF-κB				serum levels of TNF			
Day	Euphorbia kansui group	Control group	F	P	Euphorbia kansui group	Control group	F	P
1	70.175±4.561	70.308±3.174	3.5354	0.001	42.107±4.476	41.564±6.368	-0.817	0.4195
3	51.253±5.174	70.283±3.725	-13.521	<0.001	36.316±4.813	38.432±4.247	-3.899	0.0004
5	40.536±2.122	54.526±2.467	-16.513	<0.001	29.212±4.452	33.721±4.253	-3.874	0.0004
7	31.254±2.243	46.543±3.125	-18.003	<0.001	20.573±1.752	28.256±4.263	-9.429	<0.001

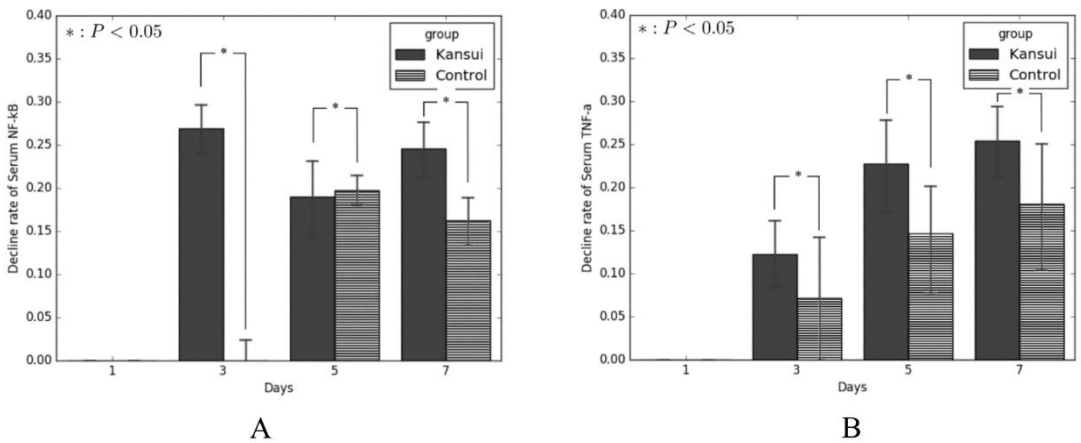

Fig. 1. *Effect of Euphorbia kansui* on serum NF-*κB and TNF-α. **A)** Euphorbia kansui reduced the serum levels of NF-κB more rapidly in SAP patients. **B)** Euphorbia kansui reduced the serum levels of TNF more rapidly in SAP patients.*
** P<0.05, compared with the control group.*

RESULTS

Comparison of clinical data between two groups

The effects of age, gender and predisposing factors on the treatment efficacy of the patients were studied. There was no significant difference in terms of age, sex, inducement, Balthaza CT classification and APACHEII scores on day 1 between the two groups (P>0.05).

Effects of euphorbia kansui on serum levels of NF-κB in SAP patients at each time point

The serum levels of NF-κB in the patients of the kansui group showed significant difference on days 1, 3, 5 and 7 (P = 0.000).The serum levels of NF-κB in the patients of the control group were significantly different on days 1, 3, 5 and 7 (P = 0.000).

The serum levels of NF-κB in the patients taking kansui and the controls were significantly different on each day (P=0.000). The results showed that the serum levels of NF-κB in patients of the two groups were decreased significantly on days 3, 5, and 7. In addition, the level of NF-κB in the euphorbia kansui group was significantly lower than that in the control group (Table I), and the rate of NF-κB reduction in

Table II. *Effects of euphorbia kansui on serum levels of sTNFR in SAP patients (x±S, n=18).*

Day	Euphorbia kansui group	Control group	F	P
1	52.812±3.457	53.145±2.763	0.206	0.8379
3	37.524±1.115	41.738±2.164	-6.468	<0.001
5	31.211±1.325	36.263±1.427	-14.105	<0.001
7	23.865±2.327	33.362±2.453	-12.698	<0.001

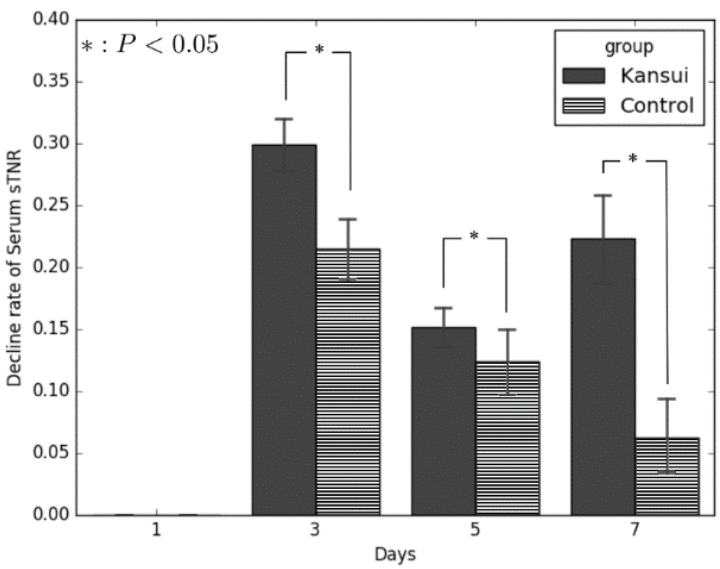

Fig. 2. *Euphorbia kansui reduced the serum levels of sTNR more rapidly in SAP patients * P<0.05, compared with the control group.*

the euphorbia kansui group was significantly higher than that in the control group (Fig. 1). The rates of NF-κB reduction were 27.56%, 42.57% and 55.33%, respectively, in the euphorbia kansui group on days 3, 5, and 7, while the corresponding values in the control group were 21.78%, 29.67% and 34.85%, respectively.

Effects of euphorbia kansui on serum levels of TNF-α in SAP patients

The serum levels of TNF-α in the kansui group at days 1, 3, 5 and 7 were measured and analyzed, which showed significant difference (P=0.000).The serum levels of TNF-α in the control group at days 1, 3, 5 and 7 were measured and analyzed, which showed significant difference (P=0.000).The serum levels of TNF-α at different time points in the kansui group were compared with those in the control group via analysis of variance. There was significant difference in the serum levels of TNF-α between the two groups (P=0.000).

The experimental results showed that the serum levels of TNF-α in the patients of the euphorbia kansui group were significantly lower than those in the control group (Table I). In addition, the level of serum TNF-α declined more rapidly in the euphorbia kansui group than that in the control group (Fig. 1). On day 3, 5 and 7, the rates of TNF-α reduction in the euphorbia kansui group were 11.21%, 29.02% and 49.59%, respectively, while the corresponding values in the control group were 7.09%, 18.12% and 32.06%, respectively.

Effects of euphorbia Kansui on serum levels of sTNFR in SAP patients

The serum levels of sTNFR at days 1, 3, 5 and 7 in the kansui group were measured and analyzed, and showed significant difference (P = 0.000). The serum levels of sTNFR at day 1, 3, 5 and 7 in the control group were measured and analyzed, and showed significant difference (P = 0.000).The serum levels of sTNFR at different time points in the kansui group were compared with those in the control group via analysis of variance. There was significant difference in the serum levels of sTNFR between the two groups (P=0.000).

The experimental results showed that the serum levels of sTNFR in the patients of the euphorbia kansui group were significantly lower than those in the control group (Table II). In addition, the level of serum sTNFR declined more rapidly in the euphorbia kansui group than that in the control group (Fig. 2). On days 3, 5 and 7, the rates of sTNFR reduction in the euphorbia kansui group were 30.17%, 42.26% and 55.51%, respectively, while the corresponding values in the control group were 21.13%, 31.45% and 37.29%, respectively.

Effects of euphorbia kansui on serum levels of IL-8 in SAP patients

The serum levels of IL-8 at days 1, 3, 5 and 7 were measured and analyzed, and showed significant difference (P = 0.000). The serum levels of IL-8 at days 1, 3, 5 and 7 in the control group were measured and analyzed, which showed significant difference (P=0.000).The serum levels of IL-8 at different time points in the kansui group were compared with those in the control group via analysis of variance. There was significant difference in the serum levels of IL-8 between the two groups (P=0.000).

The experimental results showed that the serum levels of IL-8 in the patients of the euphorbia kansui group were significantly lower than those in the control group (Table III). In addition, the level of serum IL-8 declined more rapidly in the euphorbia kansui group than that in the control group (Fig. 3). On days 3, 5 and 7, the rates of IL-8 reduction in the euphorbia kansui group were 29.11%, 52.08% and 69.65%, respectively, while the corresponding values in the control group were 21.66%, 35.08% and 51.25%, respectively.

Effects of euphorbia Kansui on serum levels of IL-6 in SAP patients

The serum levels of IL-6 at days 1, 3, 5 and 7 were measured and analyzed, and showed significant difference (P = 0.000).The serum levels of L-6 at days 1, 3, 5 and 7 in the control group were measured and analyzed, and showed significant difference (P=0.000).The serum levels of IL-6 at different time points in the kansui group were compared with those in the control group. There was no significant difference in the serum levels of IL-6 between the two groups on day 1 (P=0.823>0.05), while there was significant difference between the two groups on days 3, 5 and 7 (P < 0.05).

Table III. *Effects of euphorbia kansui on serum levels of IL-8 in SAP patients (x±S, n=18).*

	serum levels of IL-8				serum levels of IL-6			
Day	Euphorbia kansui group	Control group	F	P	Euphorbia kansui group	Control group	F	P
1	65.412±4.738	65.526±5.637	-0.575	0.5683	85.158±4.124	83.683±3.691	2.992	0.0049
3	46.343±3.875	51.328±3.215	-4.9597	<0.001	54.134±5.863	58.235±4.469	-2.175	0.0360
5	31.284±3.592	42.518±2.726	-10.577	<0.001	37.328±4.147	47.481±4.425	-7.142	<0.001
7	19.827±2.287	32.879±2.842	-17.144	<0.001	29.587±4.316	38.217±3.513	-7.194	<0.001

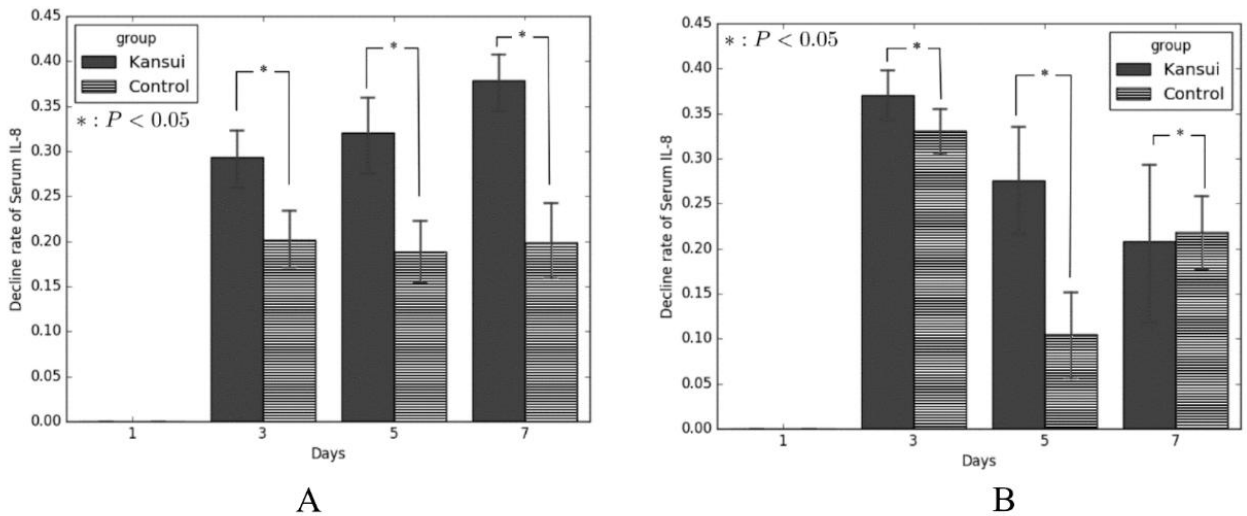

Fig. 3. *Effect of Euphorbia kansui on serum IL-8 and IL-6.* ***A)*** *Euphorbia kansui reduced the serum levels of IL-8 more rapidly in SAP patients.* ***B)*** *Euphorbia kansui reduced the serum levels of TNF more rapidly in SAP patients. * P<0.05, compared with the control group.*

The experimental results showed that the serum levels of IL-6 in the patients of the euphorbia kansui group were significantly lower than those in the control group (Table III). In addition, the level of serum IL-6 declined more rapidly in the euphorbia kansui group than that in the control group (Fig.3). On days 3, 5 and 7, the rates of IL-6 reduction in the euphorbia kansui group were 36.47%, 55.05% and 65.14%, respectively, while the corresponding values in the control group were 31.44%, 44.02% and 55.04%, respectively.

DISCUSSION

The results of this study suggested that NF-κB was the initiator and core factor in triggering inflammatory responses during SAP. It was also suggested that kansui may improve SAP by inhibiting the transcriptional activity of NF-κB, reducing the release of TNF-α, sTNFR, NF-κB, IL-6 and IL-8, and controlling the severity of inflammatory reactions.

Relevant clinical studies have shown that kansui not only promotes the gastrointestinal tract

accumulation of dirt and excretion of toxin in SAP patients, but also absorbs intra-peritoneal fluid and enables toxin excretion from the intestinal tract, thus alleviating the systemic toxic symptoms of SAP (10). It is also suggested that kansui can promote the remission of SAP, shorten the disease cycle, and significantly reduce the incidence of complications and mortality, although the specific mechanisms underlying the role of kansui remain unclear (11). Numerous studies have shown that among the various inflammatory mediators and cytokines released during SAP, NF-κB interacts with TNF-α, IL-6, IL-8, and sTNFR to stimulate inflammatory responses, thus resulting in systemic inflammatory damages and organ failure (8).

This study showed that the combined treatment of SAP using Western medicine and euphorbia kansui produced a significantly higher efficacy than the treatment using Western medicine only. With the prolonged treatment time, the inhibitory effect of euphorbia kansui on the expression of inflammatory factors became more significant. Therefore, it can be conferred that euphorbia kansui inhibits the release of NF-κB, TNF-α, NF-κB, sTNFR, IL-6, and IL-8 by decreasing the transcriptional activity of TNF-α. In addition, euphorbia kansui may be used to alleviate SAP and to control inflammatory responses.

REFERENCES

1. Bazerbachi F, Haffar S, Hussain MT, et al. Systematic review of acute pancreatitis associated with interferon-α or pegylated interferon-α: Possible or definitive causation? Pancreatology 2018; 18(7):691-99.
2. Song J, Zhong Y, Lu X, et al. Enteral nutrition provided within 48 hours after admission in severe acute pancreatitis: A systematic review and meta-analysis. Medicine (Baltimore) 2018; 97(34):e11871.
3. Mandalia A, Wamsteker EJ, Dimagno M. Recent advances in understanding and managing acute pancreatitis. F1000Res 2018; 7.
4. Shah AP, Mourad MM, Bramhall SR. Acute pancreatitis: current perspectives on diagnosis and management. J Inflamm Res. 2018; 11:77-85.
5. Roberts KM, Nahikian-nelms M, Ukleja A, Lara LF. Nutritional aspects of acute pancreatitis. Gastroenterol Clin North Am. 2018; 47(1):77-94.
6. Shen J, Kai J, Tang Y, Zhang L, Su S, Duan JA. The chemical and biological properties of euphorbia kansui. Am J Chin Med. 2016; 44(2):253-73.
7. Jiang D, Kang A, Yao W, et al. Euphorbia kansui fry-baked with vinegar modulates gut microbiota and reduces intestinal toxicity in rats. J Ethnopharmacol 2018; 226:26-35.
8. Zhang JS, Weng HZ, Huang JL, Tang GH, Yin S. Anti-inflammatory ingenane diterpenoids from the roots of euphorbia kansui. Planta Med 2018; 84(18):1334-39.
9. Kim YM, Ahn J, Chae HS, Choi YH, Kim J, Chin YW. Two new lathyrane-type diterpenoid glycosides with IL-6 production inhibitory activity from the roots of Euphorbia kansui. Bioorg Med Chem Lett 2018; 28(7):1207-10.
10. Fonteh P, Smith M, Brand M. Adaptive immune cell dysregulation and role in acute pancreatitis disease progression and treatment. Arch Immunol Ther Exp (Warsz) 2018; 66(3):199-209.
11. Lin Y, Zhang Y, Shang E, et al. Effect of glycyrrhiza on the diuretic function of euphorbia kansui: an ascites mouse model. Evid Based Complement Alternat Med 2016; 2016:7620817.

JOURNAL OF BIOLOGICAL REGULATORS & HOMEOSTATIC AGENTS Vol. 33, no. 2, 477-483 (2019)

LETTER TO THE EDITOR

VITAMINS B12 and D DEFICIENCIES AND MACRO- AND MICROELEMENT DISTURBANCES AMONG DIABETIC ELDERLY PATIENTS

S. DZIEGIELEWSKA-GESIAK[1], E. FATYGA[1], G. KASIARZ[2], T. WILCZYNSKI[2], M. MUC-WIERZGON[1] and T. KOKOT[1]

[1]Department of Internal Medicine, School of Public Health in Bytom, Medical University of Silesia, Katowice, Poland; [2]Students' Scientific Association by the Department of Internal Medicine, School of Public Health in Bytom, Medical University of Silesia, Katowice, Poland

Received October 17, 2018 – Accepted December 21, 2018

Vitamin and mineral disturbances may interfere with glucose metabolism. Elderly persons with diabetes type 2 (T2DM) are more prone to mineral disturbances and vitamin deficiencies. The aim of this study was to analyze concentrations of vitamins B12 and D and macro- and microelements among diabetic elderly patients. The study enrolled 347 patients with T2DM of whom 247 were elderly (median 76 years of age) (SenDM group) and 100 younger T2DM (median 59 years of age) (Y-DM group), and 320 patients aged 65 years and above without T2DM (mean 77 years of age) – Sen-nonDM - as a control group. Patient clinical and biochemical characteristics were recorded (drugs taken and glucose concentration, glycated hemoglobin level, complete blood count, concentration of Na, K, Ca, Fe and serum vitamins D and B_{12} levels). All elderly patients had insufficient/deficient vitamin D concentration. Vitamin B_{12} levels were below the reference limit for 15.6% of the SenDM group. No significant differences in Na, K, were observed among the investigated groups. 30.7% of the SenDM were Fe-deficient. In the SenDM group, vitamin B_{12}-deficient patients did not develop macrocytic anaemia while Fe-deficient patients with T2DM tended to develop microcytic anaemia. The prevalence of vitamin deficiencies in elderly patients with T2DM is clinically relevant. Elderly patients with T2DM are clinically predisposed to Fe deficiencies. We suggest to monitor vitamin B12 and Fe concentration toward developing a full clinical picture as it may accelerate the treatment options and improve elderly patients' outcome.

To the Editor,

Glucose homeostasis requires a complex interaction between the liver, muscle, adipocytes, pancreas and neuroendocrine system (1). Thus diabetes hyperglycemia frequently is linked to macro- and microelement disturbances and vitamin deficiencies. On the other hand vitamin deficiencies and macro- and microelement disturbances may contribute to inappropriate glucose metabolism. The glycemic target range for patients with T2DM should be individualized according to age, stage of disease, complications, cognitive status, overall prognosis and life expectancy (2).

Clinical practice, especially in geriatrics, should be based on evidence-based medicine (3). Among elderly persons, vitamin B_{12} deficiency may result in macrocytic anemia, neuropathy, cognitive dysfunction and mental changes. Metformin is the oral drug of choice for the treatment of T2DM and may increase the risk of vitamin B_{12} deficiency

Key words: elderly; diabetes type 2; macroelements; microelements; vitamin B_{12}; vitamin D

Corresponding Author:
Prof. Małgorzata Muc-Wierzgoń,
Department of Internal Medicine,
Medical University of Silesia in Katowice,
Żeromskiego 7 Str.,44-902 Bytom, Poland
Tel./Fax: +48 32 2812122
e-mail: mwierzgon@sum.edu.pl

0393-974X (2019)

DISCLOSURE: ALL AUTHORS REPORT NO CONFLICTS OF INTEREST RELEVANT TO THIS ARTICLE.

through several mechanisms (4).

Uptake of B_{12} vitamin in distal ileal enterocytes are calcium-dependent and calcium concentration is affected by vitamin D, the agent that, when present in optimal concentrations, influences mineral balance (5). Moreover, evidence exists that serum 25(OH)D concentration, the major circulating form of vitamin D, may exert positive effects on β cells, insulin

Table I. *The investigated patients characteristic and comparison between the groups: young type 2 diabetes patients vs elderly type 2 diabetes patients groups (p*) and elderly type 2 diabetes patients vs elderly patients without type 2 diabetes groups (p**).*

	Y-DM median (interquartile range)	SenDM median (interquartile range)	Sen-nonDM median (interquartile range)	p*	p**
Age [years]	59.0 (52.0-61.0)	76.0 (71.0-83.0)	77.0 (71.0-83.0)	def	NS
Glu [mmol/l]	9.1 (6.8-19.3)	8.6 (6.7-12.9)	6.6 (5.6-8.0)	NS	def
$HbA1_c$ [%]	7.6 (5.9-10.7)	6.6 (5.8-7.6)	-	<0.02	-
Mean glu [mg/dl]	171.4 (122.6-260.4)	142.7 (119.8-171.4)	-	<0.02	-
$HbA1_c$ (IFCC) [mmol/mol]	59.2 (40.7-92.9)	48.4 (39.6-59.2)	-	<0.02	-
Vitamin B_{12} [pg/ml]	524.4 (365.2-910.0)	350.8 (225.7-541.3)	433.2 (304.7-477.3)	<0.003	<0.003
25(OH) Vitamin D [ng/ml]	14.1 (7.0-21.8)	8.0 (6.8-14.1)	9.6 (7.6-25.0)	NS	NS
Fe [µg/dl]	64.3 (40.4-123.4)	55.2 (27.0-75.7)	102.8 (40.0-106.3)	<0.02	NS
Na [mmol/l]	135.6 (132.8-139.2)	136.6 (132.1-139.5)	137.8 (133.8-140.4)	NS	<0.02
K [mmol/l]	4.4 (4.0-5.0)	4.3 (4.0-4.9)	4.2 (4.3-4.8)	NS	NS
Ca [mmol/l]	-	2.3 (2.0-2.5)	2.3 (2.2-2.5)	-	NS
Creatinine [µmol/l]	78.0 (59.2-107.5)	92.4 (72.6-123.6)	76.9 (61.4-105.4)	NS	<0.002
eGFR [ml/min/1,73 m^2]	60.0 (58.4-60.0)	56.6 (40.9-60.0)	60.0 (45.4-60.0)	NS	<0.003
WBC [tys/µl]	8.6 (7.0-13.3)	9.6 (7.0-13.3)	9.2 (6.2-13.5)	NS	NS
RBC [mln/µl]	4.4 (4.0-5.0)	4.2 (3.6-4.6)	4.1 (3.5-4.6)	NS	NS
HCT [%]	40.0 (35.6-43.7)	37.1 (31.8-40.7)	36.6 (329.9-41.0)	NS	NS
HGB [g/dl]	13.8 (12.1-15.5)	12.6 (10.7-14.0)	12.5 (10.8-14.1)	NS	NS
MCV [fl]	89.0 (86.5-93.3)	89.2 (84.8-92.6)	90.5 (85.9-94.6)	NS	NS
MCH [pg]	31.1 (29.4-32.4)	30.3 (29.0-31.9)	30.5 (28.9-32.2)	NS	NS
MCHC [g/dl]	34.5 (33.4-35.5)	34.1 (33.0-35.0)	33.6 (32.5-34.5)	NS	NS
PLT [tys/µl]	221.5 (180.0-280.0)	232.0 (177.0-310.0)	232.0 (173.0-315.0)	NS	NS

Y-DM: young type 2 diabetes patients group; SenDM: elderly type 2 diabetes patients group; Sen-nonDM: elderly patients without type 2 diabetes; p: p value compared group Y-DM and SenDM; p**: p value compared SenDM and Sen-nonDM; NS: not significant; def: different by definition; Glu: glucose on admission; $HbA1_c$: glycated haemoglobin; Mean glu: mean glucose derived from glycted haemoglobin; $HbA1_c$ (IFCC): glycated haemoglobin according to International Federation of Clinical Chemistry; Fe: iron; Na: sodium; K: potassium; Ca: calcium; eGFR: estimated glomerluar filtration rate; WBC: white blood cells; RBC: red blood cells; HCT: hematocrite; HGB: haemoglobin; MCV: mean corpuscular volume; MCH mean corpuscular haemoglobin; MCHC: mean corpuscular haemoglobin concentration; PLT: platelets*

secretion and insulin sensitivity, either indirectly through a modulation of calcium metabolism or directly through vitamin D receptor (VDR) and/or vitamin D binding protein (DBP) (6). Thus, vitamin D deficiency may predispose a patient to glucose intolerance, altered insulin secretion, insulin resistance and T2DM.

Thus, the aim of the study was to evaluate vitamins B12 and D deficiencies and macro- and microelement disturbances among elderly diabetic patients.

MATERIALS AND METHODS

The study was performed in accordance with the Declaration of Helsinki of 1975 for Human Research revised in 2008 and the study protocol was approved by the Bioethics Committee of the Medical University of Silesia in Katowice (statements number: KNW/0022/KB1/38/IV/16/17/18). All subjects gave informed, signed consent to participate in the study.

Among the 1,010 patients hospitalized in 2016 in the Department of Internal Medicine of the Medical University of Silesia, Poland, we included those with T2DM (newly diagnosed to 10 years of disease). The study included elderly patients with diabetes (according to the World Health Organization - 65 years old and over, the group termed: SenDM) and younger patients with diabetes (less than 65 years old, the group termed: Y-DM). Moreover, for the SenDM group, we also matched elderly hospitalized patients without diabetes (Sen-nonDM) to serve as controls.

Additional inclusion criteria included: hypertension, angina pectoris CCS (Canadian Cardiovascular Society) I-II stage, heart failure NYHA (New York Heart Association) I-II stage. We also included patients with chronic kidney diseases with eGFR (estimated Glomerular Filtration Rate) >30 ml/min/1.73m2. No subjects adhered to a special diet or used vitamin or mineral supplements.

Exclusion criteria included: end stage of heart failure,

Table II. *Anti-diabetic drugs used by investigated type 2 diabetes patients: all diabetic patients in young type 2 diabetes patients group, and elderly type 2 diabetes patients group.*

	Y-DM, n=100	SenDM, n=247	p
Diet	10.0%	9.4%	NS
Metformin	28.0%	32.4%	NS
Sulfonylurea	11.0%	25.0%	p<0.01
Insulin:			
Rapid acting	4.0%	2.4%	p<0.0001
Short acting	19.2%	18.8%	NS
Intermediate	5.0%	7.8%	NS
Long acting	11.0%	4.9%	p<0.05
Mixed	21.0%	18.4%	NS
Other (acarbose, SGLT2)	1.0%	0.4%	NS

T2DM: all diabetics; Y-DM: young diabetics group; SenDM: elderly diabetics group; NS: not significant; SGLT2: sodium-glucose co-transporter 2 inhibitor.

positive history of stroke, neoplastic disease, liver cirrhosis and kidney failure.

In total, this observational study enrolled: 347 T2DM patients of whom 247 were 65 years old and over (SenDM group) and 100 patients with T2DM aged under 65 years (Y-DM group), and 320 patients aged 65 years and over without T2DM (Sen-nonDM group).

Blood sampling and biochemical analysis

Upon hospital admission, fasting blood was collected

Table III. *The correlation coefficients between vitamins, minerals and biochemical parameters in the studied type 2 diabetes patients (all at p<0.05).*

	DM	**Y-DM**	**SenDM**	**SenDM & B_{12} deficiency**	**SenDM & Fe deficiency**
HbA_{1c}	& age -0.2014 & Vit D +0.2814 & Na -0.2656 & K +0.1910 & Glu +0.7392	& age -0.2475 - & Na -0.4305 - & Glu +0.7713	- - **& Na -0.1743** **& K +0.2391** **& Glu +0.6837**	-	- - & Na -0.3828 - & Glu +0.6910
Vit B_{12}	& Na -0.2083 & crea +0.1805 & eGFR -0.2096 & Glu +0.1698	& Na -0.5312 - - -	- **& crea +0.2801** **& eGFR -0.2916** **& Glu +0.1698**	- - - - & WBC +0.5953	- - - - & WBC +0.4449 & RBC -0.3935
Vit D	& age -0.3379 & K +0.3219 - - & HbA_{1c} +0.2814	- - - - -	**& age -0.3034** - **& crea +0.3237** **& eGFR -0.3940**	-	-
Fe	& eGFR +0.2217 & WBC -0.4134 & HCT +0.1998 & HGB +0.2818 & MCV +0.2382 & MCH +0.3792 &MCHC +0.4457 & PLT -0.4385 -	- & WBC -0.6533 & HCT +0.3064 & HGB +0.3769 & MCV +0.5418 & MCH +0.6091 &MCHC+0.3781 & PLT -0.3830 & K -0.3212	- **& WBC -0.3330** - **& HGB +0.2025** **& MCV +0.2418** **& MCH +0.2954** **&MCHC +0.4188** **& PLT -0.4405** -		- - - & HGB +0.3175 & MCV +0.3418 & MCH +0.3799 &MCHC+0.4720 & PLT -0.3446 -
Na	& crea -0.2111 & eGFR +0.2057 & Glu -0.3503 & HbA_{1c} -0.2656	- - & Glu -0.4898 &HbA_{1c} -0.4305	**& crea -0.2869** **& eGFR +0.2057** **& Glu -0.3036** **& HbA_{1c} -0.1743**	- - - - & WBC -0.4628	- - & Glu -0.4961 & HbA_{1c}-0.3828
K	& crea +0.1849 & eGFR -0.1494	& krea +0.3777 & eGFR -0.3468 & WBC +0.2780	- - - **&HbA_{1c} +0.2391**	-	-

DM: all type 2 diabetes patients; SenDM: elderly type 2 diabetes patients; Y-DM: young type 2 diabetes patients; Vit B_{12}: vitamin B_{12}; Vit D: vitamin D; Glu: glucose; HbA_{1c}: glycated haemoglobin; Fe: iron; Na: sodium; K: potassium; crea: creatinine; eGFR: estimated glomerluar filtratio rate; WBC: white blood cells; RBC: red blood cells; HCT: hematocrite; HGB: haemoglobin; MCV: mean corpuscular volume; MCH: mean corpuscular haemoglobin; MCHC: mean corpuscular haemoglobin concentration; PLT: platelets

by ulnar vein puncture. For each patient, a complete blood count (CBC) was obtained by hematological analyzer Sysmex 4500 (Siemens, Los Angeles, the USA). Serum glucose was measured using the COBAS Integra 400 (Roche Diagnostics, Basel, Switzerland) with sensitivity of 0.6 mg/dL (0.04 mmol/L) and precision 1.4%. Glycated hemoglobin (HbA_{1c}) was measured using a turbidimetric inhibition immunoassay (TINA) using the COBAS Integra 400 (Roche Diagnostics, Basel, Switzerland). The final results were expressed as HbA_{1c} percent and were calculated from the HbA_{1c}/Hb ratio, including a conversion equation to match a high performance liquid chromatography reference method. HbA_{1c} (%) = HbA_{1c}/Hb × 91.5 + 2.15.

Plasma concentrations of sodium - Na (reference range 135.0 – 145.0 mmol/l), potassium – K (reference range 3.5 - 5.1 mmol/l), calcium – Ca (reference range 2.15 - 2.55 mmol/l) and iron – Fe (reference range 33-193 µg/dl) as well as creatinine – crea (reference range 44 - 88 µmol/l) were assessed automatically on the COBAS Integra System (Roche Diagnostics, Basel, Switzerland). Moreover, the estimated glomerular filtration rate (eGFR) was calculated using the modified diet in real disease formula (MDRD): eGFR (mL/min/1.73 m^2) = {186 x [creatinine]$^{-1.154}$ × [age]$^{-0,203}$ × 0.742 [for women] × 1.210 [for Afro-American]}.

Serum levels of vitamin B_{12} and 25-OH-vitamin D were measured by electrochemiluminescence binding assay (ECLIA) (Elecsys 2010 Analyzer, Roche Diagnostics, Basel, Switzerland). Vitamin D insufficiency was defined as 25(OH)D levels between 21-30ng/ml and deficiency 20ng/ml or less. Vitamin B_{12} deficiency was defined as 197pg/ml and less.

Statistical analysis

Statistica for Windows (version 12.5, StatSoft, Cracow, Poland) was used for statistical analyses. The normality of the distribution was assessed using the Shapiro-Wilk test. To assess the significance of the differences between groups, Mann–Whitney U tests were used. *Chi*-squared analysis was used to test categorical variables. As the value distribution was non-Gaussian, the results were presented as medians and interquartile range for continuous variables and number of cases and percent from total for categorical variables. Bivariate correlations are expressed as Pearson's correlation coefficient. A p-value < 0.05 was considered statistically significant.

RESULTS

The patients characteristics and comparisons between T2DM patients (SenDM and Y-DM groups) as well as comparisons between hospitalized elderly patients with and without T2DM (SenDM and Sen-nonDM groups) are shown in Table I.

No significant differences in CBC, electrolytes (Na, K), kidney function and vitamin D levels were observed among investigated patients with diabetes type 2 (SenDM *vs* Y-DM), however, the SenDM group tended to have lower glucose levels upon hospital admission. HbA_{1c} was lower in the SenDM group compared to the Y-DM group ($p < 0.02$). Lower concentrations of vitamin B_{12} and Fe were found in the SenDM *vs* Y-DM ($p < 0.003$ and $p < 0.02$, respectively). Significantly lower vitamin B_{12} concentrations (SenDM vs. Y-DM) were still observed ($p < 0.02$) even after excluding patients who used to take metformin.

No significant differences in CBC, electrolytes (K, Ca, Fe), or vitamin D levels were observed among elderly patient groups (SenDM *vs* Sen-nonDM). Seniors with T2DM compared to seniors without T2DM had lower concentrations of vitamin B_{12} and Na, and higher creatinine concentrations, and lower eGFR levels ($p < 0.003$; $p < 0.02$; $p < 0.002$ and $p < 0.003$, respectively).

Table II lists the anti-diabetic drugs used by both T2DM groups: Y-DM *vs* SenDM (as mono- or combination therapy). Concerning these anti-diabetic drugs, we noted higher intake of sulfonylureas in the SenDM group compared to the Y-DM ($p < 0.02$) while the Y-DM group used to take more frequent, rapid, and long-acting insulin compared to the SenDM group ($p < 0.0001$ and $p < 0.05$, respectively). Both groups had comparable diets and metformin intake.

Furthermore, mineral disturbances and vitamin levels were analyzed among the patients with T2DM. Concentrations of Na and K below and above reference limits were comparable in both groups (Na below 38.3% SenDM *vs* 39.0% Y-DM; Na above 1.7% SenDM *vs* 1.0% Y-DM and K below 10.8% SenDM *vs* 8.6% Y-DM; K above 21.3% SenDM *vs* 22.6% Y-DM). Ca was measured only in the SenDM group, 27.8% of whom were below the

reference limit and 13.9% were above. The SenDM group had concentration of Fe below the reference limit more often compared to the Y-DM group (30.7% *vs* 11.4% respectively; $p < 0.02$). Those with Fe concentrations above the reference were comparable between the SenDM and Y-DM groups (4.1% *vs* 6.8%, respectively). Concerning vitamins status, all T2DM patients had vitamin D levels below the reference limit. Insufficient levels were seen in 11.3% of the SenDM group *vs* 31.8% of the Y-DM group ($p < 0.02$) and deficiencies were seen in 88.7% of the SenDM group *vs* 68.2% of the Y-DM group ($p < 0.03$). Vitamin B_{12} levels were below the reference limit for 15.6% of the SenDM group *vs* 3.3% of the Y-DM group ($p < 0.004$).

Correlation tests between two variables are shown in Table III. Among patients with T2DM, HbA_{1c} correlated negatively with age in the whole diabetic group and in the Y-DM group. Vitamin D correlated negatively with age in the whole diabetic group and in the SenDM. In the SenDM group, vitamin D and vitamin B_{12} were dependent on kidney function. In the SenDM group, vitamin B_{12}-deficient patients did not develop macrocytic anemia while Fe-deficient patients with T2DM tended to develop microcytic anemia. Na disturbances correlated with the kidney function, glucose concentration, and HbA_{1c} level in the SenDM group. Also in this group, K disturbances were positively correlated with HbA_{1c} levels. Concerning Ca, there were no significant correlations with any parameters in the investigated groups.

DISCUSSION

In the present study the prevalence of low serum vitamin B12 was comparable with the NHANES III data (7) for the Y-DM group, while the SenDM group had a higher prevelance of B12 deficiency. However, we investigated both metformin and non-metformin users in this study. Moreover, vitamin B12 correlated positively with creatinine and negatively with eGFR in the SenDM group and their kidney function was poorer in comparison to the Sen-nonDM group. Recent studies have shown that kidneys, besides their role in water-electrolytes balance, vitamin D production and erythropoesis, play a central role in glucose homeostasis (8). In the present study, in the SenDM subjects investigated, HbA_{1c} correlated inversely with Na and positively with K. Moreover, Na correlated with kidney function, indicating that chronic kidney diseases may represent a relevant clinical complication in the SenDM group. Additionally, the SenDM group had poorer kidney function compared to the Sen-nonDM group. The former developed microcytic anemia whereas we did not notice macrocytic anemia in those with vitamin B_{12} deficiency.

Low plasma concentrations of vitamin D have been reported in patients with diabetes (9). Our study confirmed 25-OH vitamin D deficiency in patients with T2DM, regardless of age. However, those who were older more often had a deficiency rather than an insufficiency. This may be due to a greater, but not significant, decrease in kidney function compared to the Y-DM patients. This is in agreement with Al-Shoumer et al. who demonstrated prevalent vitamin D deficiency in patients with insulin-resistant T2DM (10).

In conclusion, the prevalence of vitamins B12 and D deficiencies in elderly patients with T2DM is clinically relevant. Elderly patients with T2DM are clinically predisposed to Fe deficiencies. We suggest to monitor vitamin B12 and Fe concentration toward developing a full clinical picture. It may accelerate the treatment options and improve elderly patients' outcome.

REFERENCES

1. DeFronzo RA. Banting Lecture. From the triumvirate to the ominous octet: a new paradigm for the treatment of type 2 diabetes mellitus. Diabetes 2009; 58:773-95.
2. Ismail-Beigi F, Moghissi E, Tiktin M, Hirsch IB, Inzucchi SE, Genuth S. Individualizing glycemic targets in type 2 diabetes mellitus: implications of recent clinical trials. Ann Intern Med 2011; 154:554-59.
3. Płóciniczak A, Dzięgielewska-Gęsiak S, Brożek A, Blacha A, Nowicki M, Formanowicz D. High sensitivity C-reactive protein as a cardiovascular risk marker in indeendent community-living persons. J Biol Regul Agents 2018; 32(5):887-890.
4. Fogelman Y, Kitai E, Blumberg G, Golan-Cohen A, Rapoport M, Carmeli E, Vitamin B12 screening in

metformin-treated diabetics in primary care: were elderly patients less likely to be tested? Aging Clin Exp Res 2016; 29(2):135-39.

5. Heaney RP. Vitamin D and calcium interactions: functional outcomes. Am J Clin Nutr 2008; 88:541S-544S.
6. Cimbek A, Gursoy G, Kirnap NG, Acar Y, Kilic Z, Gungor F, Ozasik I. Relation of obesity with serum 25 hydroxyvitamin D3 levels in type 2 diabetic patients. J Res Med Sci 2012; 17:1119-23.
7. Evatt M, Terry PD, Ziegler TR, Oakley GP. Association between vitamin B12-containing supplement consumption and prevalence of biochemically defined B12 deficiency in adults in NHANES III (third national health and nutrition examination survey) Public Health Nutr 2010; 13:25-31.
8. Stone M, Martyn L, Weaver CM. Potassium intake, bioavailability, hypertension, and glucose control. Nutrients 2016; 8(7). doi: 10.3390/nu8070444.
9. Esteghamati A, Aryan A, Esteghamati A, Nakhjavani M. Vitamin D deficiency is associated with insulin resistance in nondiabetics and reduced insulin production in type 2 diabetics. Horm Metab Res 2015; 47(4):273-79.
10. Al-Shoumer KA, Al-Asoosi AA, Ali AH, Nair VS. Does insulin resistance in type 2 diabetes alter vitamin D status? Prim Care Diabetes 2013; 7(4):283-87.

LETTER TO THE EDITOR

TICAGRELOR FOR PATIENTS WITH ST-SEGMENT ELEVATION MYOCARDIAL INFARCTION AFTER EMERGENCY PERCUTANEOUS CORONARY INTERVENTION

L. HAN[1], JJ. ZHANG[1], HF. JING[2] and L. QIN[1]

[1]Ward II of Cardiovascular Department, Zhengzhou Central Hospital Affiliated to Zhengzhou University, ZhengZhou, China; [2]Radiology Department, Zhengzhou Central Hospital Affiliated to Zhengzhou University, ZhengZhou, China

Received August 27, 2018 – Accepted December 10, 2018

Acute ST-segment elevation myocardial infarction (STEMI) is one of the most common cardiovascular emergencies. With the improvement of living standards, the incidence and mortality rate of STEMI has shown a significant growth trend. Percutaneous coronary intervention (PCI) is the preferred choice for the treatment of STEMI, and the rational use of antiplatelet drugs is an important factor for its success. Therefore, the correct use of antiplatelet agglutination drugs has become a widespread concern. In order to evaluate the clinical efficacy of emergency PCI for patients with acute STEMI, 120 patients who underwent emergency PCT in our hospital between January 2016 and December 2017 were randomly selected and grouped into a clopidogrel group (clopidogrel + aspirin) and a ticagrelor group (ticagrelor + aspirin) 60 per group. The thrombolysis in myocardial infarction (TIMI) flow grade of infarct related arteries, platelet aggregation rate and P2Y12 response unit before and after PCI and the major adverse cardiovascular events (MACE), bleeding events and cardiac function after 30 days were compared between the two groups. The results suggested that the proportion of the TIMI flow grade 3 of the ticagrelor group was significantly higher than the clopidogrel group after PCI, but the platelet aggregation rate and P2Y12 response unit were significantly lower, and the differences had statistical significance (P<0.05). After 30 days of follow up, it was found that the incidence of re-infarction and cardiac death, left ventricular end diastolic diameter (LVEED) and left ventricular end systolic diameter (LVESD) of the ticagrelor group were significantly lower than those of the clopidogrel group, but the left ventricular ejection fraction (LVEF) of the ticagrelor was obviously higher; the differences had statistical significance (P<0.05). None of the patients had severe bleeding events, and the difference of the incidence of mild bleeding between the two groups had no statistical significance. Therefore, in conclusion, ticagrelor has better performance in inhibiting platelet than clopidogrel and better blood perfusion effect for STEMI patients who undergo PCI and it will not increase bleeding risks while improving the short-term prognosis.

To the Editor,

Coronary artery disease, especially acute myocardial infarction, is the most common cause of death worldwide. More than 7 million people die of coronary artery disease every year, accounting for 12.8% of all-cause mortality. In Europe, one in 6 men and one in 7 women will die of myocardial infarction (1). Reperfusion therapy in a time window

Key words: ST-segment elevation myocardial infarction; percutaneous coronary intervention; ticagrelor

Corresponding Author:
Dr Jingjing Zhang,
No.195 Tongbai Road,
Ward II of Cardiovascular Department,
Zhengzhou Central Hospital
Affiliated to Zhengzhou University,
ZhengZhou, Henan, 450000, China
e-mail: zhangjingjingai11@163.com

0393-974X (2019)

is the main treatment for acute ST-segment elevation myocardial infarction (STEMI) (2, 3). As a drug treatment, antiplatelet drugs play an important role in inhibiting platelet aggregation and preventing stent thrombosis (4). Aspirin and clopidogrel were previously often used before surgery, but the clinical application of clopidogrel has limitations because of its slow acting speed and the existence of drug resistance in some patients (5, 6).

Ticagrelor is a new oral anti-platelet drug, characterized by faster and stronger anti-platelet aggregation. It is the first drug which has been proved of being capable of significantly reducing risks of cardiovascular events (7). Therefore, many international guidelines have recommended ticagrelor as an important anti-platelet drug for PCI. However, some Chinese researchers have reported the clinical efficacy and short-term prognosis of ticagrelor combined with aspirin for STEMI patients who undergo emergency PCI. The purpose of this study was to evaluate the clinical efficacy and short-term prognosis of ticagrelor combined with aspirin in the treatment of STEMI patients who underwent emergency PCI.

MATERIALS AND METHODS

General data

One hundred and twenty STEMI patients who underwent emergency PCI in our hospital between January 2016 and December 2017 were selected, including 74 males and 46 females. They were randomly divided into a ticagrelor group (N=60) and a clopidogrel group (N=60). The patients or their family members signed informed consent before treatment, and the study protocol has been approved by the medical ethics committee of our hospital. In the ticagrelor group, there were 31 males and 29 females; they aged 53~75 years old (average (66.92±8.33) years old); the interval between the onset and surgery was 2~9 h (average (4.1±1.4) years old). In the clopidogrel group, there were 33 males and 27 females; they aged 55~79 years old (average (67.21±8.04) years); the interval between the onset and surgery was 3~10 h (average (4.2±1.3) h). The differences of baseline data between the two groups had no statistical significance (P>0.05); hence the results were comparable.

Inclusion and exclusion criteria

Patients who satisfied the diagnostic criteria of STEMI released by WTO (8), hospitalized within 12 h after onset, aged below 80 years, and had two or more continuous ST-segment elevation in electrocardiography (chest lead > 0.2 mV and limb lead > 0.1 mV) were included.

Patients who had hepatic and renal insufficiency, immune disease, infectious disease, severe coagulation function, hematological system disease or malignant tumor, could not tolerate surgery, or were allergic to treatment drugs were excluded.

Treatment

All the patients took 300 mg of aspirin (approval number of State Food and Drug Administration: J20130078; Bayer Health Care Co., Ltd., Germany) by chewing after definite diagnosis. Patients in the clopidogrel group were given 600 mg of clopidogrel (approval number State Food and Drug Administration: H20123115; Henan Xinshuaike Pharmaceutical Inc., China), and patients in the ticagrelor group orally took 180 mg of ticagrelor (approval number State Food and Drug Administration: J20130020; AstraZeneca AB). Then PCI was performed. Femoral artery was firstly punctured using percutaneous puncture; then an artery sheath catheter was inserted for angiography; a guide wire was inserted into the target vessel along the guide catheter; dilation started once the sacculus arrived the stricture site. After PCI, patients in both groups were given anti-platelet maintenance treatment, i.e., orally took 100 mg of aspirin, once a day. Moreover, patients in the clopidogrel group were given 75 mg of clopidogrel once a day for at least one year, while patients in the ticagrelor group were given 90 mg of ticagrelor, twice a day for at least one year.

Observation indexes

The TIMI grade of infarction related forward arterial blood flow of the two groups was observed before and after PCI. No forward blood flow in the distant end of vascular occlusion was determined as TIMI grade 0; if partial contrast agent passed through the occlusion site, but failed to fill the distant end of blood vessels, it was determined as TIMI grade 1; if contrast agent could completely fill the distant

end of coronary artery, but the filling and removal speed of contrast agent was slower than normal coronary artery, it was determined as TIMI grade 2; if contrast agent completely and rapidly filled the distant end of blood vessels and were rapidly removed, then it was determined as TIMI grade 3. The function of platelet was detected before treatment and 24 h after treatment. Two samples of fasting venous blood was collected from each patient, one for detection of adenosine diphosphate (ADP) induced platelet aggregation rate using turbidimetry and the other for detection of P2Y12 reaction unit. The incidence of major adverse cardiovascular events (MACE) including re-infarction, cardiac death, malignant arrhythmia and intractable angina at the postoperative 30th day of the two groups was recorded. Moreover, the incidence of bleeding events of the two groups was also recorded. The bleeding severity of the patients was divided into mild bleeding and severe bleeding according to TIMI criteria. They were followed up for 30 days. LVEF, LVEDD and LVESD were detected using ultrasonic cardiogram.

Statistical analysis

Data were statistically analyzed using SPSS ver. 21.0. Measurement data were expressed as mean ± standard deviation (SD) and processed by t test. Categorical data was expressed as rate (%) and processed by *Chi*-squared test. $P<0.05$ meant the difference had statistical significance.

Table I. *Comparison of TIMI flow grade.*

Group	TIMI flow grade before PCI				TIMI flow grade after PCI			
	Grade 0	Grade 1	Grade 2	Grade 3	Grade 0	Grade 1	Grade 2	Grade 3
Ticagrelor group	10(15.15)	28(42.42)	23(34.85)	5(7.58)	0	1(1.51)	5(7.58)	60(90.91)
Clopidogrel group	11(16.67)	29(43.94)	22(33.33)	4(6.06)	1(1.51)	2(3.03)	11(16.67)	52(78.79)
χ^2	0.976	0.901	0.879	0.852	1.357	0.632	7.639	8.833
P	>0.05	>0.05	>0.05	>0.05	>0.05	>0.05	<0.05	<0.05

Table II. *Comparison of platelet function between the two groups before and after PCI.*

Group	Time	Platelet aggregation rate	P2Y12 reaction unit
Ticagrelor group	Before surgery	66.6±4.7	231.3±18.2
	24 h after surgery	50.7±4.4*#	180.7±17.9*#
Clopidogrel group	Before surgery	67.1±4.3	229.2±17.1
	24 h after surgery	55.3±4.2*	196.3±15.1*

(*mean±SD); *P<0.05 compared to before surgery; #P<0.05 compared to the clopidogrel group.*

RESULTS

The comparison of TIMI flow grade between the two groups before and after PCI

Before emergency PCI, the TIMI grade of infarction related arterial blood flow of the two groups had no significant difference (P>0.05). After PCI, the proportion of infarction related arterial blood flow TIMI grade 3 of the ticagrelor group was significantly higher than the one of the clopidogrel group (P<0.05, Table I).

Comparison of platelet function between the two groups before and after PCI

There was no significant difference in platelet aggregation rate and P2Y12 reaction unit between the two groups before operation (P>0.05). The platelet aggregation rate and P2Y12 reaction unit of the patients in the ticagrelor group were significantly lower than those in the clopidogrel group 24 h after PCI, and the difference was statistically significant (P<0.05, Table II).

Comparison of the short-term MACE between the two groups after treatment

Patients in the two groups were followed up for 30 days after treatment. In the ticagrelor group, there were 2 cases of re-infarction, 1 case of cardiac death, 3 cases of malignant arrhythmia and 5 cases of intractable angina; the incidence of MACE was 16.67%. In the clopidogrel group, there were 4 cases of re-infarction, 2 cases of cardiac death, 4 cases of malignant arrhythmia and 6 cases of intractable angina; the incidence of MACE was 24.24%. The difference of incidence of MACE between the two groups had statistical significance (χ^2=6.334, P<0.05).

Comparison of incidence of bleeding events between the two groups after treatment

None of the patient in the two groups had severe bleeding events in the 30-day follow up. The incidence of mild bleeding of the ticagrelor group was slightly higher than the clopidogrel group (6.06% *vs* 4.55%). The main bleeding events in the two groups were gingival bleeding, mucocutaneous hemorrhage, melena and gross hematuria. The difference of the incidence of bleeding events between the two groups was not statistically significant (χ^2=0.976, P>0.05).

Comparison of cardiac function between the two groups after treatment

At the postoperative 30th day, the LVEF in the ticagrelor group was significantly higher than the one of the clopidogrel group, while the LVEDD and LVESD of the former were significantly lower than those of the latter (P<0.05, Table III).

Table III. *Comparison of cardiac function between the two groups after treatment.*

Group	LVEED(mm)	LVESD(mm)	LVEF(%)
Ticagrelor group	49.1±2.0	37.3±1.7	55.3±2.6
Clopidogrel group	53.2±2.9	40.3±2.1	51.7±2.8
t	7.027	7.812	7.258
P	<0.05	<0.05	<0.05

DISCUSSION

Aspirin in combination with clopidogrel as a previously used antiplatelet aggregation treatment scheme has been found having limitations of long onset time and low response or no response in some patients (9). Compared to oral administration of clopidogrel, the antiplatelet aggregation rate of oral administration of ticagrelor (180 mg) was equivalent to the one of clopidogrel (600 mg) within 30 min. Moreover, the binding of ticagrelor and its receptor is reversible, and platelet functions can be restored after drug withdrawal to effectively reduce risk of bleeding (10, 11).

The results of this study suggested that ticagrelor could significantly improve the TIMI grade of infarction related arterial blood flow after PCI, which might be correlated to that the effectiveness of ticagrelor in reducing platelet aggregation rate and P2Y12 reaction unit. It is similar to the research results of Gurbel et al. (12). It indicated that ticagrelor had stronger platelet aggregation inhibition effect than clopidogrel, without the presence of resistance to ADP receptor antagonist. Moreover, relevant studies have demonstrated that ticagrelor can significantly reduce the incidence of MACE of patients with acute coronary acute coronary syndrome compared to clopidogrel. The results of this study suggested that ticagrelor could significantly reduce the incidences of re-infarction and cardiac death of STEMI patients who underwent PCI in 30 days of follow up, but the differences of the incidence of malignant arrhythmia and intractable angina between the two groups had no statistical significance, which might be related to the small sample size and short follow-up time. The further study suggested that ticagrelor in combination with aspirin could significantly enhance the cardiac function of the STEMI patients who underwent PCI.

In conclusion, ticagrelor combined with aspirin can effectively reduce the platelet aggregation rate in STEMI patients who undergo emergency PCI, which is beneficial to the improvement of the clinical efficacy and prognosis.

REFERENCES

1. Steg PG, James SK, Atar D, et al. ESC guidelines for the management of acute myocardial infarction in patients presenting with ST-segment elevation. Eur Heart J 2012; 33(20):2569-19.
2. Zeymer U, Hochadel M, Lauer B, et al. Use, efficacy and safety of prasugrel in patients with ST segment elevation myocardial infarction scheduled for primary percutaneous coronary intervention in clinical practice. Results of the prospective ATACS-registry. Int J Cardiol 2015; 184:122-27.
3. Wang JW, Zhou ZQ, Chen YD, Wang CH, Zhu XL. A risk score for no reflow in patients with st-segment elevation myocardial infarction after primary percutaneous coronary intervention. Clin Cardiol 2015; 38(4):208-215.
4. Koltowski L, Koltowskahaggstrom M, Filipiak KJ, et al. Quality of life in patients with ST-segment elevation myocardial infarction undergoing percutaneous coronary intervention-radial versus femoral access (from the OCEAN RACE Trial). Am J Cardiol 2014; 114(4):516-21.
5. Gurbel PA, Bliden KP, Butler K, et al. Response to ticagrelor in clopidogrel nonresponders and responders and effect of switching therapies: the RESPOND study. Circulation 2010; 121(10):1188-99.
6. Youn YN, Yi U, Lee S, Joo HC, Yoo KJ. Posttreatment platelet reactivity on clopidogrel is associated with the risk of adverse events after off-pump coronary artery bypass. Am Heart J 2014; 167(6):818-25.
7. Myat A, Tantry US, Kubica J, Gurbel PA. Current controversies in the use of aspirin and ticagrelor for the treatment of thrombotic events. Expert Rev Cardiovasc Ther 2016; 14(12):1361-70.
8. Antman EM, Anbe DT, Armstrong PW, et al. ACC/AHA guidelines for the management of patients with ST-elevation myocardial infarction-executive summary:a report of the American College of Cardiology/American Heart Association Task Force on Practice Guidelines(Writing Committee to Revise the 1999 Guidelines for the Management of Patients With Acute Myocardial Infarction).Circulation 2004; 110(5):588-636.
9. Abergel E, Nikolsky E. Ticagrelor: an investigational oral antiplatelet treatment for reduction of major adverse cardiac events in patients with acute coronary syndrome. Vasc Health Risk Manag 2010; 6:963-77.
10. Steblovnik K, Blinc A, Mijovski MB, Fister M, Mikuz U, Noc M. Ticagrelor versus clopidogrel in comatose

survivors of out-of-hospital cardiac arrest undergoing percutaneous coronary intervention and hypothermia: a randomized study. Circulation 2016; 134(25):2128-30.

11. Wang Y, Zhao X, Lin J, et al. Association between CYP2C19 loss-of-function allele status and efficacy of clopidogrel for risk reduction among patients with minor stroke or transient ischemic attack. JAMA 2016; 316(1):70-78.
12. Gurbel PA, Bliden KP, Butler K, et al. Response to ticagrelor in elopidogrel nonresponders and responders and effect of switching therapies: the RESPOND study. Circulation 2010; 121(10):1188-99.

LETTER TO THE EDITOR

DIVERSITY OF PHENYLALANINE TOLERANCE IN PREGNANT PHENYLKETONURIA PATIENTS HOMOZYGOUS FOR THE p.R408W MUTATION: THE NEED FOR IMPROVED UNDERSTANDING OF PHENYLALANINE HOMEOSTASIS

K.K. HOZYASZ[1] and J. ŻÓŁKOWSKA[2]

[1]Institute of Health Sciences, State School of Higher Education, Biała Podlaska, Poland
[2]PKU Polyclinic, Institute of Mother and Child, Warsaw, Poland

Received September 5, 2018 – Accepted January 10, 2019

Dietetic treatment of phenylketonuria (PKU) includes a low-phenylalanine (phe) diet that provides sufficient phe for maintenance and growth plus special phe-free formulas with amino acids to meet requirements for protein, energy and micronutrients. Rules for predicting phenylalanine tolerance changes during the course of pregnancy are not clear. The purpose of this report is to describe phe tolerance in pregnant PKU patients with the *PAH* genotype p.R408W/p.R408W. Low-phe diet was started before the pregnancies. The reviewed cases included three PKU women with two pregnancies and four PKU women with one pregnancy. Phe restriction in a patient's diet was determined upon the amount of this amino acid intake, which allows for stable blood phe concentrations within the target range of 120–360µmol/L. Daily phe tolerance increased from 344±85mg in the pre-conceptional period up to 1348±466mg at the end of the third trimester. Before delivery, the lowest and highest phe tolerance expressed per kg of the pregnant women's body weight were 6.8 mg and 26.9 mg respectively. Phe tolerance varies greatly even between pregnancies of patients with the same PKU genotype. Further research on pregnant PKU patients is essential to identify biological regulators of phe tolerance during pregnancy and provide evidence-based guidelines to optimise the dietetic care.

To the Editor,

Classical phenylketonuria (PKU, OMIM 261600) is an inborn error of amino acids metabolism caused by a deficiency of the cytosolic enzyme phenylalanine hydroxylase (PAH, EC 1.14.16.1), encoded by the *PAH* gene (1, 2). There is a large scale of severity of the PAH deficiency. The majority of *PAH* variants are missense, usually resulting in protein misfolding and impairment of tetrahydrobiopterin-dependent catalytic functions. The R408W (c.1222C>T) mutation is the commonest phenylketonuria-causing mutation in Northern Europe, arising from at least two independent founder events, and which was later diffused outside Europe (3). Neonates are screened for PKU by measuring phe concentrations in blood after birth (1, 2). Early dietary intervention restricting phenylalanine (phe) intake has converted PKU to a disease with essentially normal neurodevelopment and social integration (1, 2). Phe tolerance (mg/day) is the amount of phe in the diet that maintains blood phe levels within the acceptable range. Clinical determination of phe tolerance relies on frequent

Key words: PKU; phenylalanine tolerance; pregnancy

Corresponding Author:
Kamil K.Hozyasz, M.D., Ph.D.
Institute of Health Sciences,
State School of Higher Education
95/97 Sidorska Str., 21-500 Biała Podlaska, Poland
Tel.: +48 602336954
e-mail: khozyasz@verco.com.pl

0393-974X (2019)

DISCLOSURE: ALL AUTHORS REPORT NO CONFLICTS OF INTEREST RELEVANT TO THIS ARTICLE.

assessment of blood phe levels in relation to phe intake from detailed daily food count forms. For optimal pre-conception care, stable blood phe control within the therapeutic range of 120–360µmol/L should be maintained before females with PKU conceive (1,2). Phe intake should provide the minimum requirement for this essential amino acid needed to maintain physiological protein turnover for current body mass of mother and foetus/es. It should be noted, however, that there is limited evidence for the practical management of pregnant PKU patients (1,2,4). For example, rules for the prediction of phenylalanine tolerance changes during the course of pregnancy are not clear.

The purpose of this report is to describe phe tolerance in pregnant PKU patients with the *PAH* genotype pR408W/pR408W from a mono-ethnic population.

MATERIALS AND METHODS

Patient population and study design

A retrospective review of the singleton pregnancies cared for in the PKU Polyclinic of the Institute of Mother and Child in Warsaw from 2005 to 2018 was performed by examining dietetic and medical notes. Inclusion criteria for the study were: a medical diagnosis of PAH deficiency due to the *PAH* genotype p.R408W/p.R408W, not having co-morbidities (e.g. hypertension, diabetes), full medical history of at least one single pregnancy on low-phe diet initiated before conceiving and more than 50% blood phe assessments <360µmol/L. Continuing contraception was advised until phe levels in the recommended range were achieved for at least one month. There is no evidence that maintaining blood phe concentrations within the target range for a period of several months *vs* two weeks prior to conception is associated with a better outcome (2). Gestational age was expressed as the number of weeks after the last menstrual period.

For this project, the IRB issued a waiver since the study is retrospective and only anonymized data was used.

Measurement of phenylalanine, dietary records and anthropometric data

Fasting blood phe was measured from blood spots on filter paper cards by using tandem mass spectrometry (Ms/Ms). The blood target range for this amino acid was set at 120–360µmol/L, according to national recommendations (Polish PKU Consensus) (5). Phe concentrations, as well as daily dietary records, were assessed at least two times weekly during pregnancy with at least quartely clinic visits and one time weekly prior to conception (5). Food records were analysed to calculate the intake of phe (mg/day). PKU-patients' weight was measured weekly in light clothing without shoes. Standing height was measured to the nearest cm with no hair accessories or shoes.

Offspring data

The offspring outcome variables were birth body weight, body length, occipitofrontal circumference, results of newborn PKU screening and examinations for congenital anomalies.

RESULTS

Baseline characteristics

Four PKU women with one pregnancy and three PKU women with two pregnancies fulfilling the inclusion criteria were identified. All patients were Caucasians of Polish origin diagnosed by newborn screening and categorised as classical PKU. Global IQ assessed with the Wechsler Adult Intelligence Scale ranged from 85 to 128. Table I includes descriptive characteristics of pregnancies and infant birth measurements. Half of the participants were under the age of 30 years at conception. The course of the pregnancies was normal in all ten cases and they lasted at least 38 weeks. Infants with normal birth weight and occipitofrontal circumference were born.

In the month preceding conception mean phe concentration was 196±193µmol/L. During pregnancy, the mean proportion of time when the phe concentrations were >360 µmol/L was lower in comparison to the mean proportion of time when phe concentrations were in the desirable range, as well as <120 µmol/L (Table I).

Dietetic treatment and phe tolerance

The pre-pregnancy low-phe diet was begun at least three months before conception (Table I). General vitamin, including folic acid, and mineral

Table I. *Characteristics of maternal PKU pregnancies.*

Demographic features of seven PKU patients (genotype p.R408W/p.R408W) during the course of ten singleton pregnancies and their offsprings' birth measurements	
Age at conception, mean±SD (yrs)	29.5±3.6
Low-phe diet initiated before pregnancy (%)	100
Duration of pre-conception dietary treatment, mean±SD (months)	9.6±6.1
Unrestricted diet before pre-conception dietary treatment (%)	50
Pre-pregnancy weight, mean±SD (kg)[1]	53.2±6.3
Pre-pregnancy BMI, mean±SD (kg/m^2)	20.4±3.0
Weight gain during pregnancy, mean ±SD (kg)	19.5±4.0
Pre-delivery BMI, mean±SD (kg/m^2)	27.0±4.1
Phe concentration in trimester 1, mean±SD (µmol/L)	241.6±121.6
Phe concentration in trimester 2, mean±SD (µmol/L)	132.7±36.4
Phe concentration in trimester 3, mean±SD (µmol/L)	185.3±57.4
% of phe assessments >360µmol/L during pregnancy, mean±SD	8.4±8.8
% of phe assessments <120µmol/L during pregnancy, mean±SD	36.0±11.2
Time of delivery, mean±SD (weeks of gestation)	39.5±1.0
Caesarean section[2] (%)	30
Low-phe diet 12 months after delivery (%)	60
Sex of offspring, ratio M:F	6:4
PKU-affection in offspring (%)	0
Phe concentration at newborn screening, mean±SD (µmol/L)	86.2±16.1
Offspring with congenital anomalies (%)	20
Infant birth weight, mean±SD (g)	3341±377
Infant head circumference, mean±SD (cm)	34.0±1.1
Breastfeeding >1 month (%)	50

phe – phenylalanine;[1] pre-pregnancy weight (kg) of patients with two pregnancies and their phe tolerance (mg) in the pre-conceptional period and at the end of trimester three were: 48.5(310/1800)/46.6(240/1800), 53.0(395/1784)/58.7(532/1600) and 48.2(275/1037)/45.4(268/410) respectively. The first and third patients abandoned their low-phe diet after pregnancies. Pre-conceptional low-phe diet before the first pregnancy was initiated from unrestricted diet only in the third patient;[2] indications for caesarean delivery were prolonged labour (n=1), hydramnion (n=1) and combined amputation and conisation of the uterine cervix (n=1).

supplementation was given before and during pregnancy. A diet restricting natural protein and supplemented with special protein-reduced foods, (bread, biscuits, flour, pancake mix, rice, noodles, milk replacers, chocolate bars, energy jelly, savoury foods etc.) and phe-free amino acid substitutes (Milupa PKU3 tempora, Milupa PKU3 advanta, XP Maxamum, P-AM Maternal, Phenyl-Free 2HP, PKU express, PKU cooler) was implemented. The function of special protein-reduced foods in the PKU diet is to provide energy from carbohydrate-fat sources and variety in the diet. Tyrosine-augmented phe-free amino acid substitutes (synthetic protein) were consumed at least four times daily, because they are absorbed and oxidised more rapidly than intact protein sources. Fruit and vegetable consumption was restricted. The mean daily protein intake from amino acid supplement(s) at 14, 28 and 37 weeks of pregnancy was: 69.3±5.6g, 87.8±9.8g and 93.7±8.7g, respectively. The mean total daily energy intake was calculated at 14, 28 and 37 weeks of pregnancy of 1921±307kcal, 2451±429kcal and 2467±437kcal, respectively. Nutritional requirements were extrapolated from non-PKU maternal requirements. The available evidence suggests that energy requirements are not increased in PKU, but protein targets based on free amino acid mixtures should be approximately 120% of the RDI (1, 2).

Table II shows mean phe tolerance at the end of each trimester in pregnancies of PKU women, who went on a phe restricted diet pre-conceptionally. The mean phe tolerance ranged from 545 mg in the first trimester to 1348 mg before delivery. The mean ratio of phe tolerance to the patient's body weight increased three times from 6.6mg/kg b.w. before conception to 18.5mg/kg b.w. in the third trimester (Table II). Despite the same *PAH* mutation in reported PKU patients, in the third trimester the highest phe tolerance was 4.4 fold higher compared to the observed lowest value. In the first and second pregnancy of one PKU woman (IQ 86), who returned to low-phe diet 24 and 12 months before each conception respectively, there were similar values of phe tolerance pre-conceptionally and in trimesters one and two: 275mg/375mg/530mg and 268mg/294mg/515mg, respectively. Contrary to the increase of phe tolerance in trimester three of the first pregnancy up to 1037 mg, in the second pregnancy a reduction of phe tolerance of 20% was noted (to 410 mg). With a similar supply of energy, the mean trimester three phe concentrations in the first and second pregnancies were 156 µmol/L (range 38–353) and 304µmol/L (range 140–530) respectively. Total pregnancy weight gain was 13.8 kg and 14.6 kg respectively.

Breastfeeding and metabolic status of offspring

After labour, more than half of the patients continued strict or relaxed low-phe diet for at least one year. Patients opted to discontinue their diet based upon social convenience. For eight out of ten newborns breastfeeding was started, but only half of the babies were breastfed for longer than one month (Table I). With the exception of two cases with congenital heart defects (membranous and muscular ventricular septal defects), birth defects were not diagnosed in offspring. None of the infants had PKU or any degree of persistent hyperphenylalaninaemia (Table I).

DISCUSSION

Women with PKU who are pregnant need appropriate management to avoid the teratogenic properties of raised phe levels (1, 2, 6). A low-phe diet is challenging for pregnant phenylketonurics and they need much support and education about the treatment of PKU in pregnancy (1,2). The practical education of patients and the supply of information and skills to manage their dietary treatment is a key component of care. Prediction of phe tolerance changes might help patients and medical teams to estimate the scale of needs of natural protein restriction for a longer period of time during pregnancy. To our knowledge, this is the first report on phe tolerance in pregnancies of treated PKU patients with a selected genotype. In patients homozygous for the mutation p.R408W, mean phe tolerance increased four times during pregnancy. Interestingly, we observed in the second trimester a similar range of phe tolerance, as in the American College of Medical Genetics (ACMG) guidelines

on PKU (1). In the first trimester, however, in one out of ten analysed pregnancies, phe tolerance was strongly above the upper limit of recommended phe intake in the ACMG guidelines on PKU (1300 mg *vs* 770 mg; in this case, IQ 96, pre-conceptional phe tolerance was 310 mg) (1). This value is also higher than the reported phe tolerance in other references (2). In the third trimester, in a pregnancy from our sample, phe tolerance was strongly below the lower limit of recommended phe intake in the ACMG guidelines on PKU (410 mg *vs* 700 mg) (1). Kohlschütter et al. (4) reported a pregnancy of a PKU patient with the genotype p.R408W/p.R261Q with a foetus homozygous for PKU (genotype: p.R408W/p.R408W), in which phe intake could not exceed 400–500 mg/day without risking highly increased phe blood levels. In our case of very low phe tolerance during the course of the whole second pregnancy and even phe tolerance reduction in trimester three, the foetus was not affected by PKU. The pregnancy resulted in a full-term female infant without congenital anomalies, who had normal birth weight (2630 g, 10p.), length (52 cm, >90p.) and head circumference (33 cm, >10p.). This case of pregnancy in a PKU patient with genotype p.R408W/p.R408W does not confirm the observation that lack of impacting phe tolerance increase in pregnancy is a marker of foetal PKU-affection (2,4). To the best of our knowledge, in a classical PKU patient (unknown genotype) with dietary treatment started ten weeks before conception, Thompson et al. (7) showed the highest increase of phe tolerance from 6 mg/kg b.w. to 30 mg/kg b.w. In our study, the highest phe tolerance expressed per kg of pregnant woman's body weight was 26.9 mg.

Dietary management of pregnant PKU patients that is too strict, may be associated with a risk of intrauterine growth restriction (IUGR) (1,2). In our sample of pregnancies, 36% of phe concentration assessments were <120µmol/L, but IUGR was not diagnosed in the offspring. Dietary intake of phe should be increased by 50–100mg/day without delay if phe concentrations are <120µmol/L (2). In our study, mean birth weight was 3.34 kg. Birth weights between 3.1 and 3.6 kg (mean 3.3 kg) are associated with the optimal ratio of maternal and foetal health outcomes (2). It is noteworthy that the highest mean trimester phe concentration was in trimester one. Meal requirements vary considerably for women in the first trimester due to changes in eating behaviour and physical activity. Low energy intake is associated with higher blood phe concentrations (2). The range of total pregnancy weight gain between 13.8 kg and 27 kg showed that energy demand was sufficiently covered in the reported PKU mothers.

Ventricular septal defect is among the most common birth defects, with an average prevalence of 3.1/10,000 live births in Poland. The mean first trimester phe concentrations in two pregnancies resulting in offspring with congenital heart defects were 266µmol/L and 254µmol/l respectively. Five and three months before the conceptions, low-phe pre-pregnancy feeding plans were clarified. Interestingly, there was a difference between the two mothers

Table II. *Phenylalanine tolerance during pregnancy in maternal PKU.*

Phe tolerance in ten pregnancies of PKU patients with genotype p.R408W/p.R408W															
Preconceptional period				**Trimester 1**				**Trimester 2**				**Trimester 3**			
Total tolerance (mg/day)		**Tolerance per kg of body weight** (mg/kg b.w./day)		**Total tolerance** (mg/day)		**Tolerance per kg of body weight** (mg/kg b.w./day)		**Total tolerance** (mg/day)		**Tolerance per kg of body weight** (mg/kg b.w./day)		**Total tolerance** (mg/day)		**Tolerance per kg of body weight** (mg/kg b.w./day)	
Mean± SD	Range	Mean± SD	Range	Mean± SD	Range	Mean± SD	Range	Mean± SD	Range	Mean± SD	Range	Mean± SD	Range	Mean± SD	Range
344± 85	240-532	6.6± 1.6	5.2-10.8	545± 288	294-1300	10.0± 5.5	6.6-24.5	923± 389	515-1600	14.8± 6.3	9.4-26.7	1348± 466	410-1800	18.5± 6.4	6.8-26.9

(IQ: 128 and 99) with respect to the proportion of time during pregnancy when the phe concentrations were <120µmol/L and >360µmol/L (22% and 5% compared to 40% and 1%, respectively). Phe tolerance (mg) increased from 595 and 393 in trimester one to 1600 and 1150 in trimester three respectively. It is important to note that the offspring was not affected by microcephalia and low birth weight, which are very typical features of maternal PKU syndrome (1, 2, 6). Questions remain as to what the optimal 120–360µmol/L range is. Moreover, some offspring may have satisfactory outcome despite very poor metabolic control of maternal PKU, which suggests that important, but as yet undetermined factors like maternal, placental or foetal may be at play (8). Other aspects of nutrition should be considered beyond blood phe control. Decreased triiodothyronine production has been observed in patients on specific diets, such as for PKU (9). Thyroid hormones strongly influence histiotrophic nutrition during the first trimester of pregnancy prior to hemotrophic nutrition after the onset of maternal blood flow toward the placenta (10).

Many women discontinue their low-phe diet after pregnancy (2, 11, 12). In our study, a similar rate of patients started a pre-pregnancy low-phe diet from an unrestricted diet level and discontinued dietetic therapy during the first twelve months after labour, 50% *vs* 40%. Interestingly, two out of three multiparous women abandoned the low-phe diet, even in relaxed form, after both the first and second pregnancies. There are no reports available about phe toxicity to the mother post-delivery and the risk of depressive symptoms (2). Unaffected infants of PKU women, however, are able readily to metabolise the phe contained in their mothers' breast milk (2). Only every second baby was breastfed longer than one month in our sample, which is a typical rate for the Polish general population. Conversely both, especially motivated mothers of babies with congenital heart defects breastfed for three and 11 months respectively.

The current study has notable strengths. The PKU patients under investigation were ethnically homogenous and under the regular supervision of the same metabolic dietitian. The study has also certain limitations that need to be taken into account. The number of pregnancies is limited and there was lack of information regarding history of nausea and vomiting. Unfortunately, blood vitamins and micronutrient levels were also unavailable. Despite these limitations, this study provides an opportunity to understand better the issue of phe tolerance in maternal PKU and provides insight into the potential need to modify the recommended phe supply.

In conclusion, phe tolerance varies greatly even between pregnancies of patients with the same PKU genotype. Clearly, much remains to be learnt from the outcome of pregnant PKU patients on various modalities of low-phe dietary treatment. Further research is needed to identify biological regulators of phe tolerance during pregnancy, which is a neglected area in the PKU research (6), and provide evidence-based guidelines to optimise the care of PKU in females of childbearing age.

ACKNOWLEDGEMENTS

We are indebted to Dr. Maria Nowacka for setting up maternal PKU service in Mazovia (Central Poland) and for her constant encouragement.

REFERENCES

1. Vockley J, Andersson HC, Antshel KM, et al. Phenylalanine hydroxylase deficiency: diagnosis and management guideline. Gen Med 2014; 16:188-200.
2. van Wegberg AM, MacDonald A, Ahring K, et al. The complete European guidelines on phenylketonuria: diagnosis and treatment. Orphanet J Rare Dis 2017; 12:162.
3. Byck S, Morgan K, Tyfield L, Dworniczak B, Scriver CR. Evidence of origin, by recurrent mutation, of the phenylalanine hydroxylase R408W mutation on two haplotypes in European and Quebec populations. Hum Mol Genet 1994; 3:1675-77.
4. Kohlschütter B, Ellerbrok M, Merkel M, Tchirikov M, Zschocke J, Santer R, Ullrich K. Phenylalanine tolerance in three phenylketonuric women pregnant with fetuses of different genetic PKU status. J Inherit Metab Dis 2009; 32 (Suppl 1):S1-S4.
5. Polska Grupa Robocza Fenyloketonurii. Zalecenia. Warszawa 2006.

6. Resta R. Generation n+1: Projected numbers of babies born to women with PKU compared to babies with PKU in the United States in 2009. Am J Med Genet 2012; 158A:1118-23.
7. Thompson GN, Francis DE, Kirby DM, Compton R. Pregnancy in phenylketonuria: dietary treatment aimed at normalising maternal plasma phenylalanine concentration. Arch Dis Child 1991; 66:1346-49.
8. Maillot F, Lilburn M, Baudin J, Morley DW, Lee PJ. Factors influencing outcomes in the offspring of mothers with phenylketonuria during pregnancy: the importance of variation in maternal blood phenylalanine. Am J Clin Nutr 2008; 88:700-705.
9. Köhrle J. Thyroid hormone deiodinases: a selenoenzyme family activity as gate keepers to thyroid hormone action. Acta Med Austriaca 1996; 26:17-30.
10. Knabl J, Vattai A, Ziegelmüller B, Ditsch N, Jeschke U. Role of nuclear receptors in spontaneous and recurrent miscarriage. EMJ Repro Health 2015; 1:95-100.
11. Marszałek A, Walaszek R. The review of results of research on breastfeeding considering medicinal and prophylactic aspects. Health Probl Civil 2016; 10:39-45.
12. Fox-Bacon C, McCamman S, Therou L, Moore W, Kipp DE. Maternal PKU an breastfeeding: case report of identical twin mothers. Clin Pediatr 1997; 36:539-42.

LETTER TO THE EDITOR

SERUM OXIDATIVE STRESS, INFLAMMATORY RESPONSE AND PLATELET ACTIVATION IN PATIENTS WITH VASCULAR VERTIGO

SX. QIAN, JX. GU, QB. GUAN, XL. ZHANG and YP. WANG

Department of Neurology, The Second Affiliated Hospital of Jiaxing University, Jiaxing, Zhejiang Province, China

Received November 1, 2018 – Accepted December 19, 2018

The aim of this study was to investigate the correlation and clinical significance of oxidative stress and inflammatory response in vascular vertigo (VV). The subjects were divided into three groups: vascular vertigo (group A), non-vascular vertigo (group B) and controls (group C). The serum levels of IL-6 (interleukins-6), SOD (superoxide dismutase), MDA (malondialdehyde) and TNF-α (tumor necrosis factor-α) and CD62P (also called P-Selectin) activation rates were determined and compared among the three groups. The levels of IL-6, TNF-α, MDA and CD62P in group A were significantly higher than those of group B and group C ($P < 0.05$). The SOD level of group A was lower than that of group B and group C ($P < 0.05$). There was no significant difference between groups B and C in IL-6, TNF-αMDA, SOD and CD62P (P>0.05). In patients with vascular vertigo, TNF-α levels had a weak linear correlation with those of low-density lipoprotein ($P = 0.025$, r = 0.312). There was no linear correlation between TNF-α and SOD in patients with VV and non-VV. The occurrence of inflammatory reaction and oxidative stress may cause abnormal lipid metabolism in the body and promote the occurrence of VV, and platelet activation may be involved in its formation.

To the Editor,

Posterior circulation ischemia (PCI) is a common cerebrovascular disease, including post-circulatory transient ischemic attack (TIA) and posterior circulation infarction (1). Dizziness is the most common clinical symptom of PCI (2), and the risk factors are similar to those of the internal carotid artery system (3). Aortic atherosclerosis is the most important cause of PCI (4). Several studies showed that 35% of PCI was caused by macrovascular atherosclerosis, and 13% was caused by small vessel disease. Numerous studies showed that the formation of arteriosclerosis and the resulting reperfusion injury were associated with oxidative stress and inflammatory response (5). It is believed that arteriosclerosis is a chronic inflammatory process that damages the arterial wall by inflammatory factors (6). In many chronic diseases, oxidative stress plays a key role. It is a common notion that oxidative stress is a common pathogenic pathway leading to atherosclerosis and cerebral ischemic attacks due to various risk factors. Despite the advancement in neuroimaging and examination methods, there are still many difficulties in the diagnosis of PCI, and the diagnosis of vascular vertigo (VV) is still a major problem in clinical work. This study aimed to determine the biomarkers of oxidative stress and inflammatory cytokine expressions in serum

Key words: vascular vertigo; oxidative stress; inflammatory response; platelet activation

Corresponding Author:
Dr Yanping Wang,
Department of Neurology,
The Second Affiliated Hospital
Jiaxing University, No.1518 North Ring Road,
Jiaxing, 314000, Zhejiang Province, China
e-mail: ypwang_93@163.com

0393-974X (2019)

DISCLOSURE: ALL AUTHORS REPORT NO CONFLICTS OF INTEREST RELEVANT TO THIS ARTICLE.

of patients with VV caused by PCI, and analyze its changes in VV.

MATERIALS AND METHODS

Patients

Patients seeking medical treatment and requiring radiotherapy in The Second Affiliated Hospital of Jiaxing University were enrolled from February 2017 to September 2018. Forty-two cases of VV (VV group, group A), 44 cases of non-VV (non-VV group, group B), and 40 healthy subjects who had no previous vertigo (control group, group C) were included in this study. The clinical data of the enrolled patients were recorded in detail, and the physical examination and auxiliary examination of the nervous system were performed. Auxiliary examinations included routine blood test, routine urine test, biochemical test, cervical artery color Doppler ultrasonography, TCD, head MRI (MRA), and head computed tomographic angiography (CTA). Informed consent was signed by all patients, and the protocol was approved by the Ethics Committee of The Second Affiliated Hospital of Jiaxing University.

Inclusion criteria for group A: a) the onset was within one week; b) the patient was mainly characterized by dizziness, with or without head and limb numbness, paresthesia, swallowing or dysarthria, hemianopia, etc.; c) evidence of insufficient blood supply to the vestibular system, hemodynamic abnormalities or stenosis, occlusion or infarction of the posterior cerebral artery, basilar artery, vertebral artery; d) more than one risk factor for vascular disease; e) patients aged over 45 years.

The patients with vertigo but showing no evidence of cerebrovascular disease were excluded.

Inclusion criteria for group B: onset was within one week; aged over 45 years; no abnormality in blood vessel assessment; no neurological deficit syndrome; diagnosed as BPPV (benign paroxysmal positional vertigo), Meniere's disease, and vestibular neuritis.

Exclusion criteria: severe infection and high fever two weeks before onset; recent drug intake affecting immune function and anticoagulation and anti-platelet aggregation drugs; angina pectoris, myocardial infarction, cardiomyopathy, rheumatic heart disease, heart failure; malignant tumors; serious endocrine disease; severe lung infection; immune diseases; chronic renal insufficiency; obviously abnormal liver function.

Blood samples

Six mL of fasting venous blood was drawn from the elbow of each patient at 8:00 a.m. on the first day after admission. Two mL of blood was placed in an anticoagulant tube for CD62P activity detection, and 4 mL of blood was added to a biochemical tube for IL-6, TNF-α, SOD and MDA determination.

CD62P-PE detection

Two mL of venous blood was collected in the EDTA-k2E anticoagulation tube (Wuhan Zhiyuan Medical Technology Co., Ltd., China). Fresh samples were allowed to stand for 30 min (or centrifuged at 700 rpm for 5 min) to harvest platelet-rich plasma. The Falcon tube numbers were marked with control tubes and test tubes. 10 μL each of anti-human IgG1-PE, PAC-1-FITC, CD61 PerCP and RGDS (Glycoprotein ii b/iiia Antagonist) (BD Company, USA) was added to the control tube. 10 μL each of CD62P-PE, PAC-1-FITC, and CD61PerCP (BD Company, USA) was added to the test tube, then 10 μL of the treated blood sample was added to the test tube and the control tube by a micropipette (Shanghai Qiujing Biochemical Reagent Instrument Co., Ltd., China), respectively, and the reaction lasted 20 min under strict exclusion of light. The above anti-platelet monoclonal antibody immunofluorescent staining specimens were tested on a flow cytometer (BD Company, USA). CellQuest software was used to analyze the percentage of CD62-Percp positive platelets.

Detection of SOD and MDA

Two mL of fresh venous blood was centrifuged at 3000 rpm for 20 min. The supernatant was collected and the concentration of SOD and MDA was measured using an ELISA-kit (R&D, USA). The serial dilution was performed in a small test tube according to the following protocol: (a) 80 U/mL standard No. 5, 150 μL of the original standard 150 μL + standard dilution 150 μL; (b) 40 U/mL standard No. 4, No. 5 standard 150μL + standard dilution 150 μL; (c) 20 U/mL standard No. 3, No. 4 standard 150 μL + standard dilution 150 μL; (d) 10U/mL standard No. 2, No. 3 standard 150 μL + standard dilution 150 μL; (e) 5 U/mL standard No. 1, No. 2 standard 150 μL + standard dilution 150 μL. Three wells were set as blank, standard, and sample, respectively. 50 μL of the standard was applied to the plate on the enzyme label. 40 μL of the sample dilution was added to the sample well followed

by adding 10 μL of the tested sample, and the mixture was shaken slightly. After sealing, the plate was incubated at 37°C in a constant temperature water bath (Shanghai Yuejin Medical Instrument Factory, China) for 30 min. The 30-fold concentrated washing solution was diluted 30 times with distilled water (Qinhuangdao Weimansi Environmental Engineering Group Co., Ltd., China) to working solution. The sealing film was removed, the liquid was discarded, and the well was dried. Each well was filled with diluted washing solution standing for 30 s. The waste liquid was removed and the rinsing was repeated 5 times. As for the blank wells, 50 μL of the enzyme labeling reagent was added to each well. After sealing, the plate was incubated at 37°C in a constant temperature water bath for 30 min. The sealing film was gently peeled off, and the liquid was removed and dried. Each well was filled with washing solution. After standing for 30 s, the waste liquid was removed, and after repeated 5 times, the wells were patted dry. 50 μL of developer A was added to each well, and then 50 μL of the developer B was added, which was carefully shaken, mixed, and developed at 37°C for 10 min in the dark; 50 μL of the stop solution was added to each well to terminate the reaction. The blank wells were zeroed, and the absorbance

Table I. *Demographic and clinical data.*

Category	Group A	Group B	Group C	*P* value
Age	62.36±15.82	63.14±16.92	61.52±20.18	0.448
Gender (male/ female)	23/19	24/20	21/19	0.792
Diabetes (case)	11	15	10	0.553
LDL (case)	7	12	12	0.561
Hypertension (case)	13	19	19	0.126
Hypotension (case)	11	17	17	0.083

Table II. *Serum SOD expression levels in each group.*

	Group A	Group B	Group C
SOD(U/mL)	54.628±3.291$^{*\#}$	61.419±6.193*	69.021±6.012
MDA(nmoL/mL)	5.928±2.103$^{*\#}$	3.577±0.391*	3.829±0.382
TNF-α(pg/mL)	17.281±3.338$^{*\#}$	15.829±3.830*	14.183±3.119
IL-6(pg/mL)	20.228±10.573$^{*\#}$	15.182±4.119*	14.492±3.834

Note: $^{\#}P<0.05$, compared with the non-vascular vertigo group; $^{*}P<0.05$, compared with the control group.

(OD value) of each well was measured at a wavelength of 450 nm. A standard curve was drawn and the OD value of the sample was calculated from the linear regression equation of the standard curve.

Detection of TNF-α and IL-6

Two mL of fresh venous blood was centrifuged at 3000 rpm for 20 min. The supernatant was collected for detection of TNF-α and IL-6 concentrations by ELISA-kit (R&D, USA). The detection range of the kit was 7.8pg/mL to 500pg/mL and 10.2pg/mL to 2000pg/mL, respectively. The blank, standard, and sample wells were set as described in the previous section. The rest of the steps referred to the SOD and MDA protocol.

Statistical analysis

Statistical analysis was performed using SPSS 22.0 statistical software. The continuous data were presented

Table III. *Correlation between serum TNF-α levels and LDL levels.*

	Group	r	P
TNF-α	Group A	0.312	0.025
	Group B	0.016	0.883
SOD	Group A	0.109	0.418
	Group B	0.213	0.301

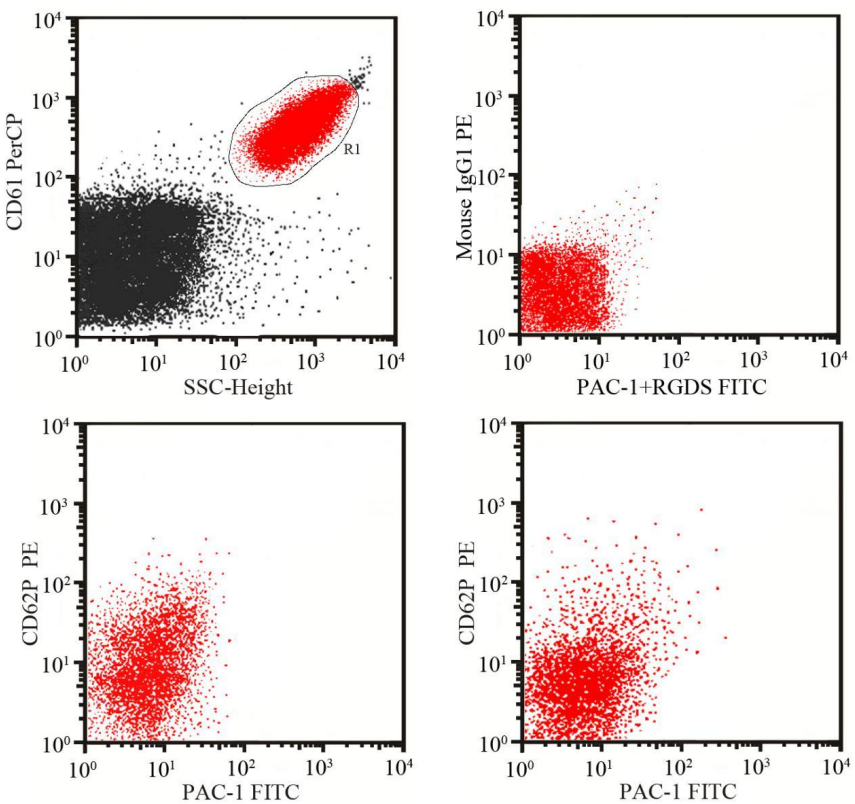

Fig. 1. *CD62P scatter plot.*

as $\bar{x} \pm s$. Inter-group analysis was performed using one-way ANOVA. Correlation analysis was performed using Spearman rank correlation analysis. $P < 0.05$ indicated statistical significance.

RESULTS

Demographic and clinical data of the patients

As shown in Table I, there was no significant difference in the composition ratio of age, gender, diabetes, blood lipid (LDL) and blood pressure between group A, group B and group C ($P<0.05$).

Oxidative stress and inflammatory response levels in each group

Serum SOD levels in group A were lower than those in group B and group C ($P<0.05$). The levels of MDA, TNF-α and IL-6 were higher than those of group B and group C ($P<0.05$). Compared with the levels of SOD, MDA, TNF-α, and IL-6 in group C, there was no significant difference in the non-VV group ($P>0.05$) (Table II).

The serum CD62P level in group A was higher than that in groups B and C ($P<0.05$) (Table II, Fig. 1). The results of non-VV were not significantly different from those of group C ($P>0.05$).

Correlation between serum TNF-α and SOD expressions and LDL

As shown in Table III, serum TNF-α levels in group A were correlated with LDL levels, but the correlation was weak. There was no correlation between serum SOD levels and LDL.

DISCUSSION

TNF-α induces an increase in IL-6 levels (7), which increases leukocyte adhesion to the endothelium (8). Lipid metabolism is also affected by TNF-α (9). Huang et al. (10) found that inhibition of TNF-α activity can reduce the degree of cerebral edema *in vivo*, which was consistent with our results.

Thromboembolism caused by arteriosclerosis is the main pathological mechanism of VV (11). After the vascular endothelium is stimulated by adverse factors, the blood vessels are damaged and collagen fibrous tissues are exposed. Inducers that trigger changes in platelet morphology and thrombin react with calcium ions in blood cells. Vascular endothelial cells adhere to platelets, which connect with fibrinogen. Then platelets are aggregated to release a large amount of active substances and thrombi are formed. Therefore, platelet activation plays an important role in the process of thrombosis (12).

In summary, oxidative stress and inflammatory response are involved in the pathophysiological process of VV and are associated with the formation of atherosclerosis. It is a sensitive biomarker in the early stage of vascular vertigo.

ACKNOWLEDGEMENTS

This work was supported by Research Project of Clinical Research Fund of Zhejiang Provincial Medical Association for Cardiovascular and Cerebrovascular Diseases (2017ZYC-B11).

REFERENCES

1. Zhang C, Wang Y, Zhao X, et al. Prediction of recurrent stroke or transient ischemic attack after noncardiogenic posterior circulation ischemic stroke. Stroke 2017; 48(7):1835-41.
2. Chen R, Su R, Deng M, Liu J, Hu Q, Song Z. A posterior circulation ischemia risk score system to assist the diagnosis of dizziness. J Stroke Cerebrovasc Dis 2018; 27(2):506-12.
3. Blasberg TF, Wolf L, Henke C, Lorenz MW. Isolated transient vertigo: posterior circulation ischemia or benign origin? BMC Neurol 2017; 17(1):111.
4. Guo Y, Zhou H, Ni C. Assessment of auditory function in patient with posterior circulation transient ischemic attack. Lin Chung Er Bi Yan Hou Tou Jing Wai Ke Za Zhi 2014; 28(16):1222-24.
5. Deng YM, Chen DD, Wang LY, et al. Visual field impairment predicts recurrent stroke after acute posterior circulation stroke and transient ischemic attack. CNS Neurosci Ther 2018; 24(2):154-61.
6. Song X, Xue S, Fan C, Li X, Wu J. Prevalence of ischemic stroke in young adults and Fabry disease. Zhonghua Yi Xue Za Zhi 2014; 94(47):3717-20.
7. Athilingam P, Moynihan J, Chen L, D'Aoust R, Groer

M, Kip K. Elevated levels of interleukin 6 and C-reactive protein associated with cognitive impairment in heart failure. Congest Heart Fail 2013; 19(2):92-98.

8. Atzeni F, Talotta R, Salaffi F, et al. Immunogenicity and autoimmunity during anti-TNF therapy. Autoimmun Rev 2013; 12(7):703-8.
9. Chen X, Xun K, Chen L, Wang Y. TNF-alpha, a potent lipid metabolism regulator. Cell Biochem Funct 2009; 27(7):407-16.
10. Huang LQ, Zhu GF, Deng YY, et al. Hypertonic saline alleviates cerebral edema by inhibiting microglia-derived TNF-α and IL-1β-induced Na-K-Cl Cotransporter up-regulation. J Neuroinflammation 2014; 11:102.
11. Huang Y, Teng Z, Sadat U, He J, Graves MJ, Gillard JH. In vivo MRI-based simulation of fatigue process: a possible trigger for human carotid atherosclerotic plaque rupture. Biomed Eng Online 2013; 12:36.
12. Xianghong G, Guanping C, Fenghua Y, Jiayin W. Changes in platelet functional parameters and CD62 P expression in liver cirrhosis. Afr Health Sci 2013; 13(4):1079-83.

LETTER TO THE EDITOR

AF1q GENE POLYMORPHISM PROTEOMIC MARKERS IN HERPES ZOSTER-INFECTED LEUKEMIA PATIENTS

X. CHENG[1], SL. ZHAO[2] and HM. ZHANG[3]

[1]The First Clinical Medical College, Southern Medical University, Guangzhou City, Guangdong Province, China; [2]The First Hospital of Jilin University, Changchun City, China; [3]The Chinese medicine hospital of Zhoukou City, Henan Province, Zhoukou City, China

Received November 1, 2018 – Accepted December 12, 2018

The present study investigated two potential AF1q gene polymorphism proteomic markers in patients with both leukemia and herpes zoster. A total of 40 individuals were randomly divided into two groups: Group A consisted of herpes zoster acute phase leukemia patients and Group B of healthy volunteers. Two polymorphisms, one in the promoter area and one in exon 1 of the AF1q gene were detected by polymerase chain reaction (PCR) - restriction fragment length polymorphism (RFLP). *Bbv*I and *Mse*I digestion of each AF1q gene polymorphism PCR amplicon revealed three distinct genotypes for each polymorphism. Proteomic results were extracted by iTraq. These results suggest that AF1q is involved in the pathogenesis of leukemia combined with herpes zoster.

To the Editor,

Advanced stage cancer patients are usually exposed to many chemical substances and radiation for therapeutic purposes. Thus, immunocompromised patients are more likely to develop diseases, such as herpes zoster (HZ) or human papillomavirus (HPV) (1, 2). Although it may occur at any age, most commonly HZ affects elderly individuals (3). HZ is an acute herpes skin infection caused by varicella zoster virus (VZV). After primary infection with VZV (chickenpox), the virus often persists asymptomatically in the ganglia of sensory cranial nerves and spinal dorsal root ganglia (3) and is released to the skin when the immune function is reduced (4). Several cancers have been associated with increased HZ risk, especially within the first 2 years after cancer diagnosis and with prevalence to younger individuals (5). HZ most commonly occurs in patients with hematologic malignancies (6). Studies report that HLA-alleles may be combined with impact molecules, peptides and T cells, which control the exogenous and antigen specificity immune response by forming different genotypes of disease susceptibility (7). Even if its function is not yet fully known, elevated AF1q expression may be associated with poor clinical outcomes in various malignancies (8). This study aimed to evaluate the AF1q gene polymorphisms and the *AF1q* blood protein concentration levels during acute HZ periods.

MATERIALS AND METHODS

Subjects

For the present study a total of 40 individuals were

Key words: AF1q gene; leukemia combined with herpes zoster; iTraq: gene polymorphism; proteomic markers

Corresponding Author:
Dr Hongmei Zhang,
The Chinese Medicine Hospital of Zhoukou City,
No.33 Qiyi West Road,
Zhoukou City, Henan Province, China
e-mail: zhang_hongmei2008@126.com

0393-974X (2019)

recruited. Participants were divided into 2 groups (Group A and Group B). Group A consisted of 20 patients, including 10 males and 10 females, aged 27-65 years (45±3.21 years), diagnosed with leukemia combined with HZ by a hematologist at the Jilin University First Hospital, who were recruited between August 2016 and August 2017. Group B (control group) consisted of 20 volunteers, 10 males and 10 females, aged 27-65 years (43±7.25 years) with normal medical laboratory test results and confirmed negative clinical evidence of any disease. All the participants signed an informed consent agreeing to be included in the study. The study was approved by the Ethics Committee of the First Jilin University Hospital.

Inclusion criteria: patients from group A were in acute HZ state, onset 1~7 days, VZV viral load gradually increasing (peripheral blood was extracted for blood sample testing then diagnosed according to serology index); disease duration ≤3 days; no antiviral or glucocorticoid treatement before study inclusion.

Exclusion criteria: patients with non-herpes zoster-caused neurological injury, patients with other severe organ functional disorders, with malignant tumor and/or immunological disease, patients with mental illness history or who had been long-term treated with glucocorticoids, immunosuppressive agents, and/or immune enhancers, and pregnant or lactating women.

Genetic screening AF1q *gene (rs10749659, rs2140709 and rs3738481)*

AF1q gene polymorphism in the promoter area was detected by polymerase chain reaction (PCR) - restriction fragment length polymorphism (RFLP). PCR was performed using 0.2 mg genomic DNA, 1 U Taq polymerase, 10 pmol of appropriate primers, and 200 mm dTNPs under the following conditions: initial denaturation for 4 min at 92°C, annealing for 45s at 52°C, extension for 30s at 70°C, denaturation for 45s at 92°C. In total, 30 cycles were carried out, and final extension for 10 min at 70°C. The amplified products were then digested with appropriate restriction edonuclease (*Mse*I) and analyzed on 3.5% agarose gels. The oligonucleotide primers used were forward 5'-AATGGAATTGGACTGGATGGT-3' and reverse 5'-TTTACGAGAAGGAAGCGGTG-3'. PCR products were cut with *Mse*I.

PCR conditions for exon 1, position 39, A/G polymorphism were the same as the previous using forward 5'-GCTCTAGTTCCTGAAGACCT-3' and reverse 5'-AGTGTCACTCACCTTTGCAG-3' as oligonucleotide primers. PCR products were then digested with *Bbv*I.

To verify successful digestion, one digested sample of each promoter and exon-1 allele, respectively, were further confirmed by sequencing.

PBMC isolation, protein extraction and quantitation

According to the Bradford method, 5 ml of venous blood from each patient were collected in heparinized tubes. Total proteins were extracted and measured using the BCA protein assay kit (Thermo Scientific), as reported previously (9). Proteins were then stored at -80°C for further analysis.

iTRAQ labeling and strong cationic exchange (SCX) fractionation

Following the iTRAQ protocol (Applied Biosystems, Foster City, CA, USA), each 100 µg protein was digested with 0.2 mL of a 50 µg/mL trypsin (Promega, Madison, WI, USA) at 37°C for 16 h. Peptides were labeled with isobaric tags 118 (normal control group), 119 (untreated rd12 group), and 121 (treated rd12 group) and incubated at room temperature for 2 h. Then the labeled mixtures were dried by vacuum centrifugation, desalted with Sep-Pak Vac C18 cartridge 1 cm3/50 mg (Waters, USA), and fractionated using a ShimazuLC-20AB HPLC Pump system (Shimazu, Japan) connected to a strong cation exchange (SCX) column (polysulfoethyl column, 2.1 mm × 100 mm, 5 µm, 200 Å, The Nest Group, Inc. USA). SCX separation was performed using a linear binary gradient of 0–45% buffer B (350 mM KCl, 10 mM KH2PO4 in 25% ACN, pH 2.6) in buffer A (10 mM KH2PO4 in 25% ACN, pH2.6) at a flow rate of 200 µL/min for 90 min, and 30 fractions were collected every 3 min. Each fraction was dried down and redissolved in buffer C [5% (v/v) acetonitrile and 0.1% formic acid solution], and the fractions with high KCl concentration were desalted with PepClean C-18 spin Column (Pierce, USA).

LC-ESI-MS/MS Analysis

Each fraction was resuspended in buffer A (2% ACN, 0.1% FA) and centrifuged at 20,000 ×g for 10 min. In each fraction, the final concentration of peptides was approximately 0.25 µg/µL. Using an autosampler, 20 µL

of supernatant was loaded onto a 2 cm C18 trap column (inner diameter 200 µm) on a Shimadzu LC-20AD nanoHPLC. Peptides were eluted onto a resolving 10 cm analytical C18 column (inner diameter 75 µm) that was assembled in-house. The samples were loaded at 15 µL/min for 4 min and eluted with a 44 min gradient at 400 nL/min from 2 to 35% B (98% ACN, 0.1% FA), followed by a 2 min linear gradient to 80% B, maintenance at 80% B for 4 min, and finally a return to 2% B over 1 min.

The peptides were subjected to nanoelectrospray ionization followed by tandem mass spectrometry (MS/MS) in an LTQ OrbitrapVelos (Thermo) coupled in-line to the HPLC. Intact peptides were detected in the Orbitrap. Peptides were selected for MS/MS using the high-energy collision dissociation (HCD) operating mode with a normalized collision energy setting of 45%. Ion fragments were detected in the LTQ. A data-dependent procedure that alternated between one MS scan followed by eight MS/MS scans was applied for the eight most abundant precursor ions above a threshold ion count of 5,000 in the MS survey scan with the following Dynamic Exclusion settings: repeat counts: 2; repeat duration: 30 s; and exclusion duration: 120 s. The applied electrospray voltage was 1.5 kV. Automatic gain control (AGC) was used to prevent overfilling of the ion trap; 1 × 104 ions were accumulated in the ion trap to generate HCD spectra. For MS scans, the m/z scan range was 350 to 2,000 Da.

Statistical analysis

Distributions of alleles in patients and controls were compared using Fisher's exact test. Values of $P < 0.05$ were regarded as significant. MASCOT version 2.3.02 (Matrix Science, Ltd., London, UK) was used to analyze the identification and quantification of the proteins. The peptide sequences were searched in the nonredundant NCBI database. The search criteria were set to permit a maximum of 1 missed cleavage. Certain peptide modifications were permitted: for example, Gln.>pyro.Glu, iTRAQ 8plex, Phospho. The values supplied with the Applied Biosystems reagents were used to carry out automatic isotope correction through both software packages. Subsequently, Gene Ontology (GO) (http://www.geneontology.org) was used to elucidate the molecular function, biological process and cellular component associated with each individual protein.

Table I. *AF1q exon 1 polymorphism in leukemia combined with herpes zoster acute stage patients (Group A) and controls (Group B).*

Genotype/allele/phenotype	Group A n=20(%)	Group B n=20(%)
Genotype frequencies		
GG (Ala/Ala)	5 (25)	7 (11)
AG (Thr/Ala)	11 (51)	14 (59)
AA (Thr/Thr)	4 (24)	9(30)
Allele frequencies		
G (Ala)	89 (72)	96 (56)
A (Thr)	62(28)	71 (44)
Phenotype frequencies		
G positive	83 (85)	84 (86)
A positive	62 (74)	67 (76)

RESULTS

AF1q was located at position 45. The amplified PCR product was 160bp. After *Bbv*I digestion, three genotypes could be identified, i.e. A/A allele (one band at 160 bp); A/G allele (three bands: 160, 87 and 73bp); and G/G allele (two bands at 89 and 71 bp). The heterozygous A/G allele was a predominant AF1q polymorphism genotype. An increase in the frequency of G/G allele (25 *vs* 11%) and a slight decrease in A/A allele (24 *vs* 30%) were observed in herpes zoster leukemia patients as compared to the control group. However, these differences were not statistically significant (P=0.316).

Since G to A transition at position 45 leads to an alanine to threonine amino acid substitution, phenotype and allele frequencies were further analyzed. It appeared that G positive phenotype

Table II. *Different protein expression in the two groups.*

Participants	Regulation type	proteins	Enrichment ratio	P
P02741	Upregulation	CRP	21.31	0.001
P69891	Upregulation	HBG1	12.12	0.001
P69892	Upregulation	HBG2	10.23	0.001
P0DJ18	Upregulation	SAA1	8.65	0.001
P0DJ19	Upregulation	SAA2	7.54	0.001
075636	Upregulation	FCN3	4.12	0.001
Q6UXB8	Upregulation	P116	5.12	0.001
P08519	Downregulation	APOA	7.12	0.001
P02776	Downregulation	PLF4	8.12	0.001
P05546	Downregulation	HEP2	6.21	0.001

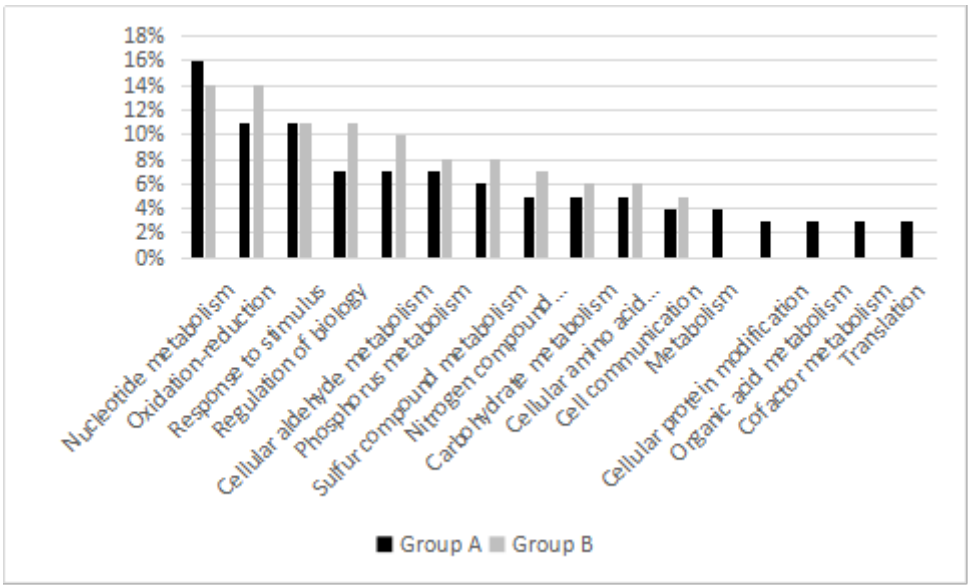

Fig. 1. *Percentage of molecular function in each group (Group A: Leukemia combined with herpes zoster acute stage. Group B: healthy volunteers.)*

and G allele frequencies were increased in leukemia accompanied by herpes zoster compared with normal controls. There were no statistically significant differences between leukemia accompanied by herpes zoster and controls (P< 0.454 and 0.182, respectively). These results are shown in Table I.

Compared with the control group, in Group A 285 proteins were upregulated and 121 proteins were downregulated (Table II). Of these, a difference of a multiple of ≥0.5 points identified 604 differential candidates, a difference of upregulated >18 points included 5 proteins and a difference of downregulated <0.13 points included 3 proteins. There was a difference between the functional and protein processes between the two groups (Fig. 1 and Fig. 2). The most expressed molecular function in each group was the nucleotide metabolism and oxidation-reduction. In the healthy control group, the cell communication presented decreased activity. In the leukaemia combined with herpes zoster acute stage, the cellular protein modification, organic acid metabolism, cofactor metabolism and translation presented the least activity.

DISCUSSION

Although the pathogenesis of the combination of leukemia and HZ is unknown, abnormalities in the immune system function certainly play a significant role. Consequently, it is reasonable to claim that the expression and function of AF1q gene might be defective in patients with leukemia and HZ. In other words, we can also indicate the significant role of AF1q in the occurrence and development of HZ. Until today, it was believed that AF1q correlates to the occurrence of leukemia, however the results

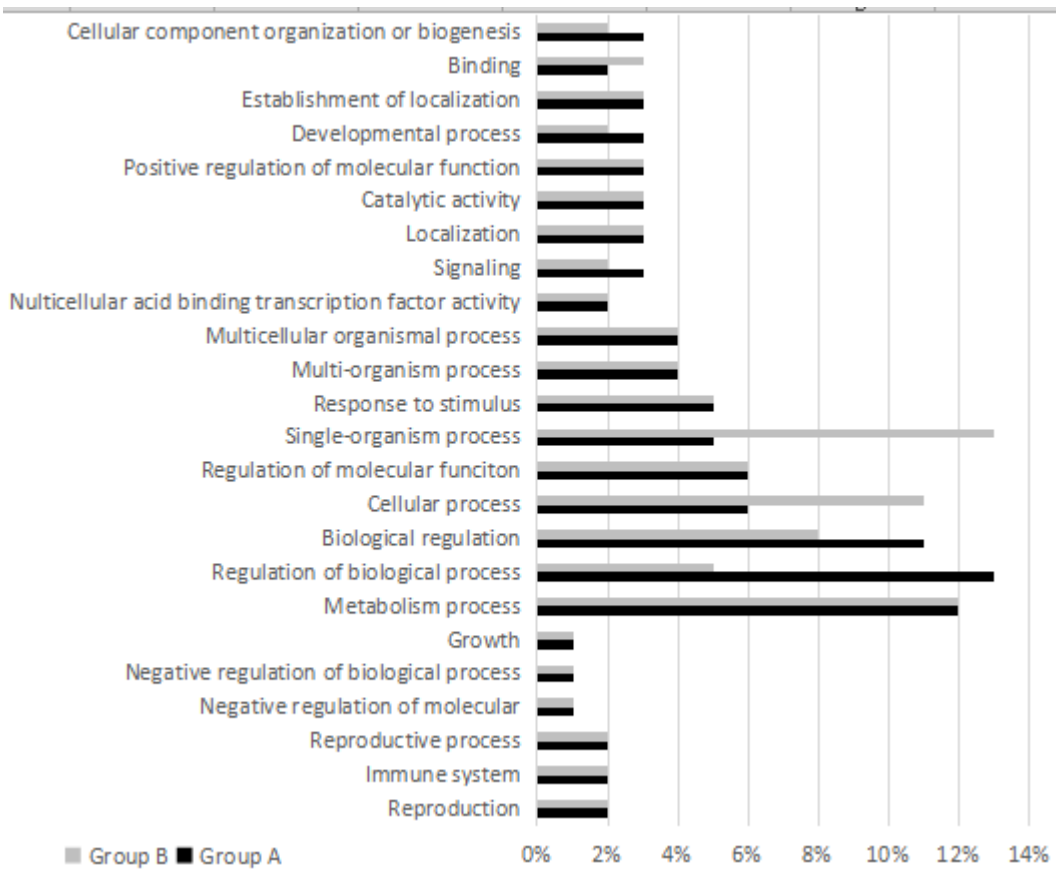

Fig. 2. *Biological process (Group A: Leukemia combined with herpes zoster acute stage. Group B: healthy volunteers).*

of this experiment led us to discover a different aspect of the AF1q, HZ and leukemia correlation. However, modified genes can affect the development of leukemia, leading to HZ (10).The results showed that the enriched protein has many differences in cell processes: single-organism processes, cellular processes and acid binding transcription factor activity.

Leukemia presents a poor prognosis especially in the types with molecular abnormalities. The recurrence rate after chemotherapy-induced remission is higher (11). We used the gene polymorphism and the quantitative analysis of proteome to observe the changes of HZ in acute periods. Although it was not clear how AF1q regulated blood protein changes, the mutation site was found. AF1q gene polymorphism was located at position 45. The same candidate proteins were SAA1 and SAA2. Further studies should be carried out to explore the correlation between specific protein and AF1q gene in order to elucidate the molecular mechanisms that regulate these processes.

REFERENCES

1. Lin HC, Chao YH, Wu KH, et al. Increased risk of herpes zoster in children with cancer: A nationwide population-based cohort study. Medicine (Baltimore) 2016; 95(30):e4037.
2. Boda D, Docea AO, Calina D, et al. Human papilloma virus: Apprehending the link with carcinogenesis and unveiling new research avenues (Review). Int J Oncol 2018; 52(3):637-55.
3. Sampathkumar P, Drage LA, Martin DP. Herpes zoster (shingles) and postherpetic neuralgia. Mayo Clin Proc 2009; 84(3):274-80.
4. Andrei G, Snoeck R. Advances in the treatment of varicella-zoster virus infections. Adv Pharmacol 2013; 67:107-68.
5. Hansson E, Forbes HJ, Langan SM, Smeeth L, Bhaskaran K. Herpes zoster risk after 21 specific cancers: population-based case-control study. Br J Cancer 2017; 116(12):1643-51.
6. Sutton E, Lopez JJ, Dao LN, Wetter DA. Disseminated herpes zoster in chronic lymphocytic leukemia. J Emerg Med 2016; 50(3):e159-60.
7. Kumar P, Krishna VD, Sulochana P, Nirmala G, Haridattatreya M, Satchidanandam V. Cell-mediated immune responses in healthy children with a history of subclinical infection with Japanese encephalitis virus: analysis of CD4+ and CD8+ T cell target specificities by intracellular delivery of viral proteins using the human immunodeficiency virus Tat protein transduction domain. J Gen Virol 2004; 85(Pt 2):471-82.
8. Park J, Schlederer M, Schreiber M, et al. AF1q is a novel TCF7 co-factor which activates CD44 and promotes breast cancer metastasis. Oncotarget 2015; 6(24):20697-710.
9. Bradford MM. A rapid and sensitive method for the quantitation of microgram quantities of protein utilizing the principle of protein-dye binding. Anal Biochem 1976; 72:248-54.
10. Ziemer M, Bornkessel A, Hahnfeld S, Weyers W. 'Specific' cutaneous infiltrate of B-cell chronic lymphocytic leukemia at the site of a florid herpes simplex infection. J Cutan Pathol 2005; 32(8):581-84.
11. Lichtenegger FS, Krupka C, Köhnke T, Subklewe M. immunotherapy for acute myeloid leukemia. Semin Hematol 2015; 52(3):207-14.

LETTER TO THE EDITOR

CYTOLOGICAL MECHANISM OF ASTRAGALOSIDE IV IN PROMOTING REPAIR OF BONE DEFECTS

X. LIAN*, CC. SHEN*, HJ. SUN and YJ. ZENG

Department of Orthopedics, Hangzhou Normal University Affiliated Hospital, Hangzhou, Zhejiang, China

Received November 6, 2018 – Accepted January 23, 2019

*These authors contributed equally to this work

To explore the possible cytological mechanism underlying the role of Astragaloside IV in promoting the repair of bone defects, osteoblasts were cultured *in vitro* and identified using inverted phase contrast microscopy, alkaline phosphatase (ALP) staining and alizarin red staining. Subsequently, cells were sub-cultured into 24-well plates with different concentrations (0.1 μg/mL, 1 μg/mL, 10 μg/mL, 100 μg/mL, and 1000 μg/mL) of Astragaloside IV before the content of ALP in the culture medium was determined. Using a similar method, a proliferative assay of the cells was carried out to determine the proliferation ability of cultured osteoblasts. The results showed that 1μg/mL, 10μg/mL and 100μg/mL Astragaloside IV solutions promoted proliferation of osteoblasts, while 10μg/mL and 100μg/mL promoted the secretion of ALP by osteoblasts. In conclusion, Astragaloside IV of concentrations in a certain range can promote the proliferation and differentiation of osteoblasts, suggesting the presence of a cytological mechanism underlying its role in promoting the repair of bone defects.

To the Editor,

Bone defect is a common disease caused by trauma, infection, tumor, osteomyelitis, debridement, and various congenital diseases (1). Traditional Chinese medicine can promote the proliferation of osteoblasts and regulate their activity (2). To date, a large number of experimental studies have confirmed that Astragaloside IV, an active component of *Astragalus membranaceus*, exerts a good osteogenic effect (3, 4). At present, bone marrow stromal cells are often used as seed cells in conjunction with other agents to promote the repair of fractures and bone defects (5, 6). Osteoblasts play an important role in the growth and metabolism of bone tissue as well as in the repair of bone defects (7). However, the mechanism underlying the role of Astragaloside IV in promoting the proliferation and differentiation of osteoblasts is still unclear. Therefore, in this study, osteoblasts derived from rat bone marrow stromal cells were cultured *in vitro* to observe the effect of Astragaloside IV on the proliferation of osteoblasts.

MATERIALS AND METHODS

Animals

Sixteen new-born rats aged < 24 h (weight 70-90g) without limitation of gender were purchased from Ji'nan Jinfeng Experimental Animal Co., Ltd, China. The housing conditions of rats were as follows: room temperature 19-24°C, noise less than

Key words: Astragaloside IV; osteoblast; bone defects; ALP

Corresponding Author:
Dr Yunji Zeng,
Department of Orthopedics,
Hangzhou Normal University affiliated Hospital,
No.126 Wenzhou Road,
Hangzhou 310015, Zhejiang, China
e-mail: zeng_yunjiyi006@163.com

0393-974X (2019)

60dB, humidity 50-60%, and illumination 12h/d; feed and bedding were sterilized by high pressure and high temperature, and drinking water was sterilized by high temperature. The experiment was approved by the Ethics Committee of Hangzhou Normal University Affiliated Hospital and conformed to the International Regulations on Animal Protection and Management.

Preparation of culture medium

Standard culture medium was used as basic culture medium and blank control culture medium. DMEM (Dulbecco's modified eagle medium) complete culture medium contains 10% fetal bovine serum, 100U/mL penicillin, and 100U/mL streptomycin). Culture medium containing Astragaloside IV (Beijing Solarbio Technology Co., Ltd. China) was used as the culture medium for the experimental group. Different concentrations of Astragaloside IV were added into the standard culture medium to generate Astragaloside IV-containing culture media. Then, L-glutamine was added to the culture medium in about two weeks after start of the culture.

Primary culture of osteoblasts

Sixteen neonatal rats aged less than 24 h were intraperitoneally injected with 10% chloral hydrate solution (Abcam, USA) (0.35mL/100g body weight) for anesthesia and sacrificed by neck dislocation. The skull was collected from the rats and disinfected with 75% ethanol for 5 min. The skull was then put into phosphate buffer solution (PBS) (pH 7.2-7.4) to remove the periosteum and its surrounding connective tissues and blood vessels. Subsequently, the skull was washed with PBS 2-3 times until no blood stains were seen. The bone tissues were then cut into blocks and digested with 0.2% I-type collagenase (Shanghai Yubo Biotechnology Co., Ltd., China) and 0.1% hyaluronidase under aseptic conditions for 5 cycles, with 20 min per cycle. After 3, 4, and 5 cycles of digestion, respectively, cells were collected and centrifuged for 10 min at 1000 r/min. After the supernatant was discarded, the cells were suspended in a DMEM medium containing 10% fetal bovine serum (Thermo Fisher Scientific, USA), mixed evenly, inoculated into culture flasks, and incubated in a 37°C and 5% CO_2 incubator (Shanghai Jinghong Experimental Equipment Co., Ltd., China), with the culture medium changed after 24 h. After the cells reached 60%~70% confluency, they were digested by 0.25% trypsin (Abcam, USA) and used as primary osteoblasts.

Subculture of osteoblasts

The primary osteoblasts were cultured for 10 days. After the cells almost fused into a monolayer, the cells were digested by 0.25% trypsin into a single cell suspension and then inoculated into a new culture flask for subculture. The cells were cultured in a 37°C and 5% CO_2 incubator of saturated humidity and observed daily under an inverted phase contrast microscope, and the culture medium was changed every 3 days. After successful subculture and when the cells almost fused into a monolayer, they were digested and sub-cultured similarly to obtain subsequent generations of cells.

Cell observation and identification

The growth, proliferation and morphological characteristics of cultured cells were observed daily under an inverted phase contrast microscope.

The Gomori calcium cobalt method was used for ALP staining. Cell cap slides were washed and incubated with PBS for 5 min. They were then fixed with cold acetone (Abcam, USA) for 10 min, washed with distilled water for several times, and incubated with ALP in an incubator (5 mL 3% ß-sodium glycerophosphate, 5 mL 2% barbiturate (Abcam, USA), 10 mL 2% $CaCl_2$, 1 mL 2% $MgSO_4$, and 10 mL distilled water) at 37°C for 4 ~ 6 hours. Subsequently, the slides were rinsed with distilled water several times, soaked in 2% cobalt nitrate solution for about 3-5 min, rinsed with distilled water again, and then placed in 1% ammonium sulfide solution for 2 min. After being rinsed with tap water, the slides were dried, mounted and observed under a light microscope.

The purified cells derived from the 4th generation were inoculated into a 24-well plate at a concentration of 1 x 10^7 cells/L and cultured in an incubator (Shanghai Jinghong Experimental Equipment Co., Ltd., China) at 5% CO_2 and 37°C

for 25 days. Subsequently, the cells were stained with 0.1% alizarin red to observe the formation of mineralized nodules.

Quantitative determination of ALP

After the osteoblasts cultured in 10% fetal bovine serum were made into a cell suspension at a density of 5 x 10^4/mL, they were seeded into a 24-well culture plate in 1mL/well of culture medium and cultured in a 37°C and 5% CO_2 incubator. After the cells were cultured for 1 day, the medium was replaced with a fresh culture medium containing 10% fetal bovine serum, and then the medium was changed once every 3 days. When the osteoblasts attached to the bottom of the plate, the culture medium was aspirated and the cultured osteoblasts were divided into 4 groups, with 6 compound holes for each group. The control group was cultured in a DMEM medium containing no fetal bovine serum; the other three groups were cultured in the presence of 1μg/mL, 10μg/mL, and 100μg/mL Astragaloside IV. After 4 h, the supernatant in each well was collected and the ALP content in the supernatant was quantified by an Olympus 2500 automatic biochemical analyzer. No repetitive tests were required.

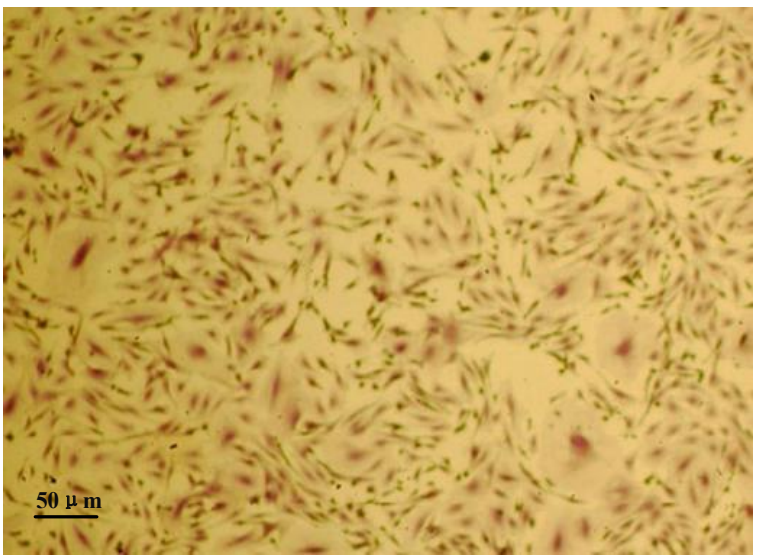

Fig. 1. *Osteoblast morphology observed under microscope (10-14 days) (40X).*

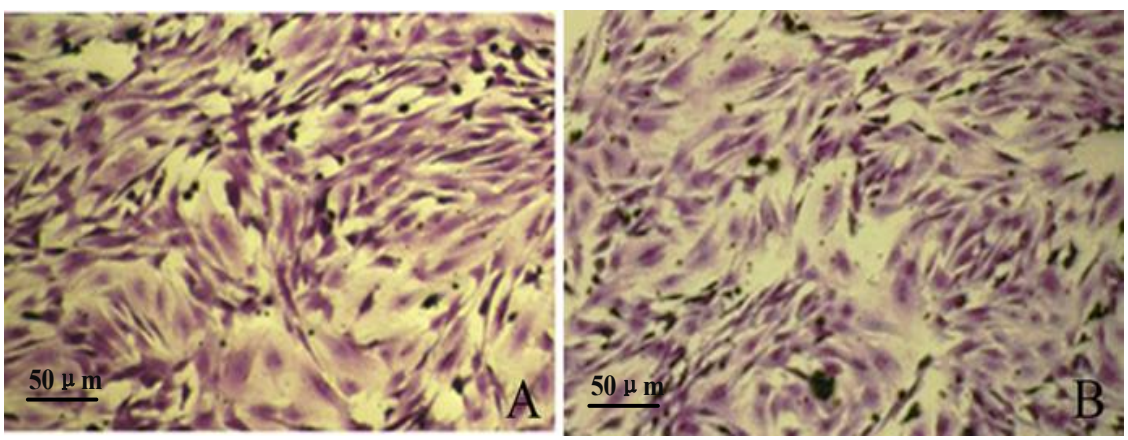

Fig. 2. *The changes of cytoplasmic substances in cells were observed by staining (40X) (A: ALP staining; B: alizarin red staining).*

Cell proliferation assay

Osteoblasts of the second generation were digested and suspended in 0.25% trypsin. The cells were then inoculated into five 96-well plates at 1 x 10^3 cells/well in 200μL/well of culture medium. The cells were then incubated in a 5% CO_2 and 37°C incubator until the cells formed a single layer at the bottom of the wells (in 96-well plates with a flat bottom). Subsequently, different concentrations of Astragaloside IV (with final concentrations of 0.1μg/mL, 1μg/mL, 10μg/mL, 100μg/mL, and 1000μg/mL, respectively) were added into culture media according to the experimental design. Each concentration of Astragaloside IV was tested in five wells in parallel. On days 1, 3, 5, 7, and 9 after the addition of Astragaloside IV, one plate was observed under an inverted microscope (Olympus Corporation, Japan). Twenty μL of MTT solution (5mg/mL, i.e., 0.5% MTT) was then added to each well and incubated for 4 h. After the incubation was terminated, the culture medium in each well was aspirated and 100 μL of dimethyl sulfoxide (DMSO) (Suzhou xiong Chemical Technology Co., Ltd., China) was added in each well, and the plate was incubated at 37°C for half an hour to fully dissolve the crystals. The OD value of each well was measured at a wavelength of OD 490nm by an enzyme labeling apparatus. The blank wells (with 200 μL Astragaloside IV-free culture medium and no cells) and normal control wells (containing cells and 200 μL culture medium but without Astragaloside IV) were also set up. The experiment was repeated 3 times.

Statistical analysis

SPSS 19 software was used for statistical analysis, and the experimental results were expressed as $\bar{x} \pm s$. One-way ANOVA was used to compare multiple groups. $P < 0.05$ indicated that the difference was statistically significant, and $P < 0.01$ indicated that the difference was extremely significant.

RESULTS

Observation by the inverted phase contrast microscope

The primary cells were mostly round, with a large cell size and single nuclei. The adherent cells began to adhere to the wall of the culture flask within 24-36 h, and the number of adherent cells increased significantly after 36-48 h. After 72 h, the adherent cells showed spindle-shaped appearance with many long cytoplasmic processes and large nuclei. After 5~8 days, the cells proliferated and the number of cells further increased to form colonies. After 10~14 days, monolayer of cells fused and the cells were transformed into a fusiform (Fig. 1). After trypsin digestion, the cells became round and could be detached from the bottom of the culture flask. Most of the cells adhered to the wall within 24 h after subculture and proliferated rapidly in 72 h after subculture. The cells fused into a monolayer in 5-7 days after subculture, and the cells were mostly spindle-shaped with about 2-3 large protrusions.

Staining results

ALP staining results showed that there were gray-black granular or massive precipitates in the cells, and the staining was obviously seen in the cytoplasm, as shown in Fig. 2A. The results of alizarin red staining showed that the presence of red-positive nodules with different size and shapes confirmed the mineralization of these nodules, as shown in Fig. 2B.

Results of qualitative measurement of ALP

ALP content in the culture medium was measured. The statistical analysis showed obvious difference in ALP values of 10μg/mL and 100μg/mL groups compared with the control group, but no obvious difference was found between the l μg/mL group and the control group (Table I).

Results of cell proliferation measurement

On days 1, 3, 5, 7, and 9 after mouse-derived osteoblasts were treated with different concentrations of Astragaloside IV, significant difference was observed among 1μg/mL, 10μg/mL, 100μg/mL groups and the control group ($P<0.05$), especially among 10μg/mL, 100μg/mL and 1000μg/mL groups ($P<0.01$). As a result, 1μg/mL, 10μg/mL, and 100μg/mL Astragaloside IV could promote the proliferation of osteoblasts, but 1000μg/mL Astragaloside IV

showed an inhibitory effect on the proliferation of osteoblasts. Over time, different concentrations of Astragaloside IV increased the number of osteoblasts, and the cells in the 100μg/mL group showed most significant proliferation on the seventh day (Table II).

DISCUSSION

Traditional Chinese medicine can promote the proliferation and differentiation of osteoblasts derived from bone marrow stromal cells (8). As an enzyme secreted by osteoblasts with high specificity (9), ALP is an important marker of osteoblast differentiation and maturation (10). ALP is also the most common marker used to evaluate bone formation/turnover and the activity of osteoblasts (11, 12).

In this study, Astragaloside IV of different concentrations (0μg/mL, 0.1μg/mL, 1μg/mL, 10μg/mL, 100μg/mL, and 1000μg/mL) was used to treat osteoblasts before the proliferation of osteoblasts was detected after 1, 3, 5, 7 and 9 days of treatment. The results showed that Astragaloside IV of 0.1μg/mL and 1000μg/mL could not promote the proliferation of osteoblasts. In addition, Astragaloside IV of 10μg/mL and 100μg/mL could promote the secretion of ALP from osteoblasts.

To sum up, Astragaloside IV of a proper concentration can promote the proliferation and differentiation of osteoblasts. Therefore, it is theoretically possible to use Astragaloside A as a growth factor in controlled-release bone repair materials, thus providing a new way for the screening of traditional Chinese medicine.

ACKNOWLEDGEMENTS

This project was supported by Medical and Health Research Project of Zhejiang province (grant No. 2018PY041); Traditional Chinese Medicine Science and Technology Project of Zhejiang province (grant No. 2018ZB102); Health Science and Technology Project of Hangzhou City (grant No. 2016A17) and Social Development Research Project of Hangzhou City (grant No. 20180533B47).

Table I. *Results of ALP determination .*

Groups	Control group	1μg/mL experimental group	10μg/mL experimental group	100μg/mL experimental group
ALP content	5.27±1.02	6.48±1.06$^{\&}$	9.53±1.36$^{*\#}$	12.66±1.39$^{*\#}$

Note: (unit: μ/mL); $^{\&}P>0.05$; $^{*}P<0.05$; $^{\#}P<0.01$.

Table II. *The effect of different concentrations of Astragaloside IV on the proliferation of osteoblasts.*

	Control group	0.1μg/mL	1μg/mL	10μg/mL	100μg/mL	1000μg/mL
1 day	0.215±0.004	0.215±0.008	0.254±0.008$^{*\#}$	0.281±0.008$^{*\#}$	0.296±0.017$^{*\#}$	0.305±0.008$^{*\#}$
3 days	0.421±0.006	0.434±0.010	0.441±0.007$^{*\#}$	0.482±0.005$^{*\#}$	0.486±0.009$^{*\#}$	0.502±0.005$^{*\#}$
5 days	0.769±0.011	0.648±0.013	0.826±0.011$^{*\#}$	0.829±0.006$^{*\#}$	0.846±0.014$^{*\#}$	0.613±0.012$^{*\#}$
7 days	0.968±0.009	0.968±0.038	1.059±0.041*	1.122±0.048$^{*\#}$	1.211±0.041$^{*\#}$	0.733±0.041$^{*\#}$
9 days	0.831±0.006	0.883±0.015	1.012±0.008*	1.076±0.014$^{*\#}$	1.202±0.011$^{*\#}$	0.636±0.037$^{*\#}$

$^{*}P<0.05$; $^{\#}P<0.01$. Comparison between the experimental group and the control group.

REFERENCES

1. Xie J, Wang H, Song T, et al. Tanshinone IIA and Astragaloside IV promote the migration of mesenchymal stem cells by up-regulation of CXCR4. Protoplasma 2013; 250(2):521-30.
2. Wong KC, Lee KS, Luk HK, Wan HY, Ho CK, Zhang Y, Wong MS. Er-xian Decoction exerts estrogen-like osteoprotective effects in vivo and in vitro. Am J Chin Med 2014; 42(2):409-26.
3. Li M, Yu L, She T, et al. Astragaloside IV attenuates Toll-like receptor 4 expression via NF-κB pathway under high glucose condition in mesenchymal stem cells. Eur J Pharmacol 2012; 696(1-3):203-9.
4. Fan D, Liu S, Jiang S, et al. The use of SHP-2 gene transduced bone marrow mesenchymal stem cells to promote osteogenic differentiation and bone defect repair in rat. J Biomed Mater Res A 2016; 104(8):1871-81.
5. Yoon JK, Kim HN, Bhang SH, et al. Enhanced bone repair by guided osteoblast recruitment using topographically defined implant. Tissue Eng Part A 2016; 22(7-8):654-64.
6. Li C, Ding J, Jiang L, et al. Potential of mesenchymal stem cells by adenovirus-mediated erythropoietin gene therapy approaches for bone defect. Cell Biochem Biophys 2014; 70(2):1199-204.
7. He Y, Lu A, Zha Y, et al. Correlations between symptoms as assessed in traditional Chinese medicine (TCM) and ACR20 efficacy response: a comparison study in 396 patients with rheumatoid arthritis treated with TCM or Western medicine. J Clin Rheumatol 2007; 13(6):317-21.
8. Honma T, Itagaki T, Nakamura M, Kamakura S, Takahashi I, Echigo S, Sasano Y. Bone formation in rat calvaria ceases within a limited period regardless of completion of defect repair. Oral Dis 2008; 14(5):457-64.
9. Murray E, Provvedini D, Curran D, Catherwood B, Sussman H, Manolagas S. Characterization of a human osteoblastic osteosarcoma cell line (SAOS-2) with high bone alkaline phosphatase activity. J Bone Miner Res 1987; 2(3):231-38.
10. Rawadi G, Vayssière B, Dunn F, Baron R, Roman-Roman S. BMP-2 controls alkaline phosphatase expression and osteoblast mineralization by a Wnt autocrine loop. J Bone Miner Res 2003; 18(10):1842-53.
11. Farley JR, Hall SL, Tanner MA, Wergedal JE. Specific activity of skeletal alkaline phosphatase in human osteoblast-line cells regulated by phosphate, phosphate esters, and phosphate analogs and release of alkaline phosphatase activity inversely regulated by calcium. J Bone Miner Res 1994; 9(4):497-508.
12. Rey A, Manen D, Rizzoli R, Ferrari SL, Caverzasio J. Evidences for a role of p38 MAP kinase in the stimulation of alkaline phosphatase and matrix mineralization induced by parathyroid hormone in osteoblastic cells. Bone 2007; 41(1):59-67.

LETTER TO THE EDITOR

EFFECTS OF EXERCISE ON SEX HORMONES AND EXPRESSION OF RELEVANT GENES IN THE HYPOTHALAMUS IN OBESE MICE

JM. WANG[1], TY. GONG[1] and ZJ. ZHAO[2]

[1]School of Sports Science, Nantong University, Nantong, Jiangsu, China; [2]School of Sports Science, Zhengzhou University, Zhengzhou, Henan, China

Received November 11, 2018 – Accepted January 11, 2019

This study aimed to investigate the effect of different exercise loads on sex hormones and expressions of relevant genes in hypothalamus in obese mice. Sixty weaning male C57BL/6 mice were used as subjects. Among them, 15 mice were randomly classified into the normal diet group (CON group), and the remaining 45 mice into high-fat diet group (MOB group). The obesity was successfully achieved by high-fat diet 10 weeks later. Then the rats were randomly divided into three groups based on weight, namely, obesity control group (OBC group), obesity with moderate-intensity exercise group (MOBC group), and obesity with high-intensity exercise group (HOBC group), with 15 mice in each group. Mice in the MOBC group and HOBC group were offered 8 weeks of swimming training, and the exercise time increased incrementally until 2 h and 4 h per day. After the training was over, ELISA method was used to determine the serum levels of Adiponectin (Adipo), luteotropic hormone (LH), follicle-stimulating hormone (FSH) and testosterone (T). Real-time PCR was implemented to detect the transcriptional levels of genes of Adipo and other relevant proteins in the hypothalamus. The result showed that compared with the CON group, there was a significant reduction in the serum levels of Adipo, LH, FSH and T in the OBC group (P<0.05). As compared with the OBC group, the serum levels of Adipo, LH, FSH and T increased significantly in the OBC group (P<0.05). There was a significant increase in the transcriptional levels of Adipo, Adipo receptor 1 (Adipo R1), and AMP-activated protein kinase (AMPK) in the OBC group (P<0.05) compared to in the CON group; meanwhile, the transcriptional levels of kisspeptin (Kiss) and gonadotropin-releasing hormone (GnRH) decreased significantly (P<0.05). In conclusion, long-term moderate-intensity exercise could improve the negative effect of obesity on sex development. Long-term high-intensity exercises could not improve the inhibitory effect of obesity on sex development.

To the Editor,

With social and economic development, China has witnessed a growing incidence of childhood obesity, which is usually associated with endocrine disorders and disorders of sex development (1). Before adolescence, the hypothalamic- pituitary gland-gonad (HPG) (2) axis remains at a low activity level. After the initiation of adolescence, the hypothalamus secretes gonadotropin-releasing hormone (GnRH), which acts on the anterior pituitary gland to promote the secretion of luteotropic hormone (LH), and follicle-stimulating hormone (FSH). These two sex hormones enter the blood circulation to act on the sex gland, promoting the secretion of sex hormones and synthesis of sperms and ova by the sex gland (3). The central nervous system regulates the endocrine

Key words: exercise intervention; obesity; Adiponectin; HPG axis; endocrine

Corresponding Author:
Dr Zijian Zhao,
School of Sports Science,
Zhengzhou University (main campus),
No.100 Science Avenue,
Zhengzhou, 450001, Henan, China.
email: zhao_zijian1976@126.com

0393-974X (2019)

system through several pathways, which involves many hormones and transmitters. Some hormones promote the release of GnRH, while others have an opposite effect (4). It has been shown that kisspeptin (Kiss) plays a key role in promoting the release of GnRH. Kiss promotes the release of GnRH, thus activating the HPG axis (5). In addition, fat-secreted Adipo is crucial to reproductive regulation (6). It has been reported that an overexpression of Adipo in the hypothalamus damages the fertility of male mice (7). Among the males with testicular hypoplasia, most are associated with the mutation in the Adipo gene (8). The interaction between Adipo in the hypothalamus and regulatory mechanism of the HPG axis under different exercise loads was discussed in our study. The regulatory mechanisms of different exercise loads improving the regulation of the reproductive system were proposed.

MATERIALS AND METHODS

Animals

Sixty male C57BL/6 mice (Nanjing Junke Bioengineering Co., Ltd., China) were maintained at a temperature of 22±5°C, relative humidity of 50±10%, and 12h/12h dark/light cycle. The mice were allowed free access to food and water, and the cage was replaced with padding and water every day. The main ingredients and energy composition of the two diets are shown as follows:

Ordinary feed (100g): 20g barley flour, 10g cabbage, 20g soybean flour, 1g yeast, 5g bone meal, 16g corn flour, 16g bran, 10g fish meal, and 2g salt; 11.7kJ/g energy (53.21% carbohydrate, 26.99% protein, and 19.8% fat).

High-fat feed (100g): 34.1g sucrose, 19.5g casein, 21g butter, 5g cellulose, 15.5g wheat starch, 4.9g mineral; 12.57kJ/g energy (32.99% carbohydrate, 25.53% protein, and 41.48% fat).

The animal experiment procedures were in accordance with the International Regulations on Animal Protection and Management. The study was approved by the Ethics Committee of Nantong University.

Mouse models of obesity induced by high-fat diet

Fifteen mice were randomly classified into a normal diet group (CON group), and 45 mice were classified into a high-fat diet group (MOB group). Mice in the CON group were fed with ordinary diet for 10 weeks with free access to water. Mice in the MOB group were fed with high-fat diet for 10 weeks with free access to water. After the 10-week dietary intervention was over, the average body weight of the mice in the MOB group was higher than that of the mice in the CON group by >20%. The obesity model of mice was considered successful. The mice in the MOB group were further randomly divided into three groups based on body weight: obesity control group (OBC group, n=15), obesity with moderate-intensity exercise group (MOBC group, n=15), and obesity with high-intensity exercise group (HOBC group, n=15). Mice in the CON group were fed with ordinary diet for further 8 weeks, while the other three groups were fed with high-fat diet for further 8 weeks. Mice in the MOBC and HOBC groups received exercise intervention, and were housed in separate cages with free access to food and water. The body weight of the mice was measured each week.

Exercise intervention for different groups

The obesity model of mice was considered successfully built if the average body weight of mice in the MOB group was higher than that of the CON group by over 20%. All mice in the MOB group were further given high-fat diet. MOBC group and HOBC group began swimming training from week 11 (6 days a week, with one day off per week, for 8 weeks in total). The water temperature was kept at 32-36°C during training, and the water depth was 25 cm, so that the mouse tails would not touch the bottom of the pool. The surface area of swimming was about 50cm^2 for each mouse. For the MOBC group, the exercise load was increased incrementally from week 1 to 2. After reaching the maximum of 2 h at the end of week 2, the exercise load was kept at 2 h per day for the next 6 weeks. For the HOBC group, the exercise load was increased incrementally from week 1 to 2. The maximum load was 4 h at the end of week 2, with 2 h in the morning and 2 h in the afternoon. This exercise load was maintained for the next 6 weeks.

Sample collection

All mice were fasted for 12 h before sample collection and anesthetized by intraperitoneal injection of 10% chloral hydrate (Guangzhou Peiyu Biological Products Co., Ltd., China). Blood samples were collected from orbital venous plexus and immediately centrifuged for 25 min (4°C, 3000

rpm). Serum was isolated and preserved at -80°C prior to the detection of serum Adipo, LH, FSH and T. Adipose tissues around the testicles, kidneys and mesentery were rapidly isolated and weighed. The mice were sacrificed by decapitation and the skull was opened to isolate the hypothalamus, which was preserved at -80°C prior to real-time PCR of the hypothalamus (transcriptional levels of Adipo, Adipo R1, AMPK, Kiss and GnRH).

Indicator measurement

Body weight: The mice were weighed on the analytical balance before anesthesia and the anesthetic dose was calculated on this basis.

Weighing of abdominal adipose tissues: The abdomen was opened after anesthesia, and the abdominal adipose tissues were harvested and weighed on the electronic balance (AE200 analytical balance, Hangzhou Jiaxuan Technology Co., Ltd., China). Weight of abdominal adipose tissues=Weight of adipose tissues around the testicles+adipose tissues around the kidneys+adipose tissues around the mesentery.

Ratio of adipose tissue weight to body weight (%) = (Weight of abdominal adipose tissues/body weight) ×100%.

Determination of serum levels of Adipo, LH, FSH and T levels: Mouse serum Adipo ELISA kit, mouse serum LH ELISA kit, mouse serum FSH ELISA kit and mouse serum T ELISA kit (all the kits were purchased from Shanghai Lianlian Biotechnology Co., Ltd., China) were employed. Ten wells were set up for the standard sample on the ELISA plate (loading sample was 50 ul per well), along with blank wells (control wells without samples or ELISA reagents) and test wells. Into the test wells, 40 μl of sample diluent was first added, followed by 10 ul of the test samples (the final dilution fold was 5). The samples were loaded to the bottom of the wells and the plate was sealed with sealing film. The plate was incubated at 37°C for 30 min. The 30-fold concentrate washing solution was diluted by 30-fold with distilled water. Then, the sealing film was removed, the liquid was discarded and the plate was dried by shaking. The washing buffer was added to each well and stood for 30 s before being discarded. This process was repeated for 5 times. Into each well 50 μl of ELISA reagents were added, except for the blank wells. The plate was sealed with sealing film and incubated at 37°C for 30 min. Then, the sealing film was removed, the liquid was discarded and the plate was dried by shaking. The washing buffer was added to each well and stood for 30 s before being discarded. This process was repeated for 5 times, and the plate was slapped dry. Into each well 50 ul of chromogenic reagent A and 50 ul of chromogenic reagent B were added successively, which were mixed by oscillation. Color development reaction proceeded in the dark at 37°C for 15 min, and the reaction was stopped by adding 50 ul of stopping solution into each well (with blue color turning yellow). The absorbance was measured for each well at a wavelength of 450 nm (OD value) and the standard curve was plotted. Sample concentrations were calculated by introducing OD value of the sample into the equation. The sample concentration multiplied by dilution fold was the actual concentration of the sample.

RNA extraction from the hypothalamus and real-time PCR: the frozen hypothalamus was taken out for RNA extraction. Reverse transcription (Semerfly Technology (China) Co., Ltd., China) was performed using the extracted RNA in accordance with the manufacturer's instructions. Real-time PCR reaction solution was performed for the reaction. Based on the Ct values of each reaction well and by taking GAPDH as the internal reference, the relative expressions of each target gene were calculated for the samples. The primer sequences used in the experiment are shown below.

Adipo: forward: 5'-ACCCATAGCCCATACACCAG-'3, Reverse:5'-AGTCGTGGAGACCAGGGAGT-'3;
Adipo R1: forward:5'-CTTGACGATGCTGAGACCAA-'3, reverse:5'-CCAGGAGAAACTGAGGCAGA-'3;
AMPX: forward:5'-CCACCAAATTCAACCTATGACTACTTC-'3, everse:5'AGCTGTCTCATAATGTCCATTCGA-'3;
Kiss: forward:5'-GACCTGTCCACCTACAACTGG-'3, reverse: 5'-CTGCCTTGGCCTCTACAATC-'3;
GnRH: forward:5'-CTCAACCTACCAACGGAAGC-'3, reverse :5'-TCCAAACACACAGTCAGCAGT-'3;
GAPDH: forward :5'-GCTCTCTGCTCCTCCCTGTTC-'3, reverse: 5'-GAGGCTGGCACTGCACAA-'3 .

Statistical analysis

All statistical analyses were performed using SPSS 22.0 software. The results were reported as mean±standard deviation. Intergroup comparison was performed between the CON group and the OBC group using *t*-test. Comparison among the OBC group, MOBC

group and HOBC group was performed using one-way ANOVA. P<0.05 indicated significant difference.

RESULTS

Construction of obesity models of mice

Before inducing obesity, the MOB group and CON group showed no significant difference in body weight (P>0.05) (Fig. 1). After 10 weeks of high-fat diet, the average body weight of the MOB group was significantly increased as compared with the CON group (P<0.01). Thus the obesity model of mice was successfully built.

In the MOB group, 45 mice survived, and 2 were excluded due to failed modeling, with a successful modeling rate of 95.56%. As shown in Table I, one mouse died in both the MOBC group and HOBC group, respectively, during 8 weeks of swimming training with different loads. The death rate of mice was 6.67% for the two groups compared to 0% for the CON group and OBC group. For the two exercise groups, the mice died from drowning.

Changes in body weight, weight of abdominal adipose tissues, and ratio of abdominal adipose tissue weight to body weight in each group

As shown in Table II, the body weight, abdominal adipose tissue weight and ratio of abdominal adipose tissue weight to body weight increased in the OBC group as compared with the CON group (P<0.05). The obesity was severe in the OBC group. The above three indicators decreased apparently in the MOBC group as compared with the OBC group (P<0.05), and so did the HOBC group (P<0.05). These indicators were all much lower in the HOBC group than in the MOBC group (P<0.05).

Changes in the serum levels of Adipo, LH, FSH and T in each group

The serum level of Adipo decreased significantly in the OBC group as compared with the CON group (P<0.01), and so did LH, FSH and T, though to a lesser extent (P<0.05). The serum level of Adipo increased significantly in the MOBC group as compared with the OBC group (P<0.05), and so did

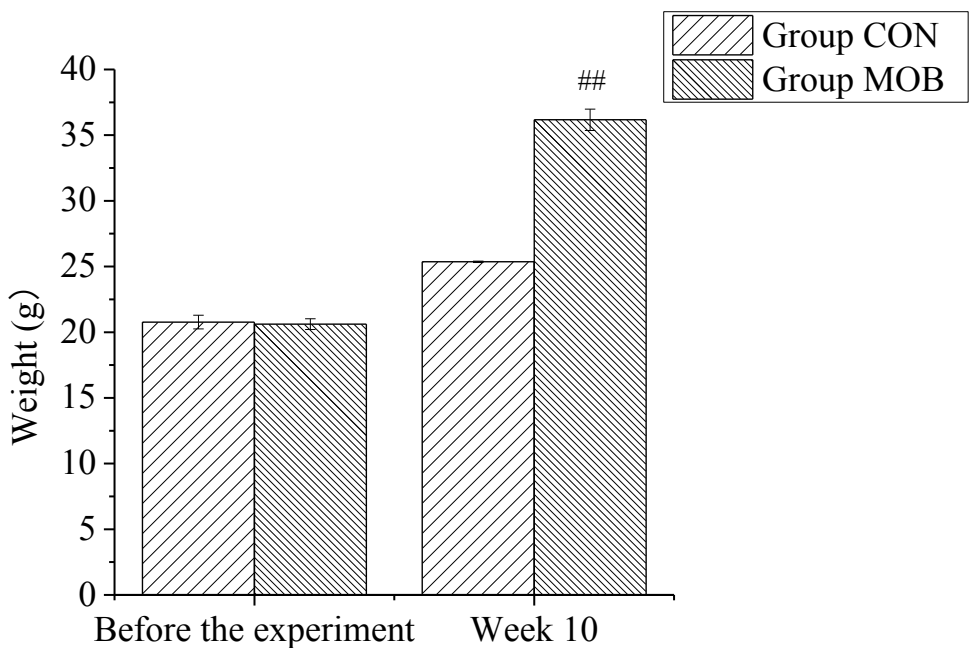

Fig. 1. *Weight comparison of mice during modeling. ##P<0.01, vs CON group.*

Table I. *Death rates of mice under different exercise loads.*

Group	CON group	OBC group	MOBC group	HOBC group
Week 11 (n)	0	0	0	0
Week 18 (n)	0	0	1	1
Death rate (%)	0	0	6.67	6.67

Table II. *Changes in body weight, weight of abdominal Adipose tissues, and ratio of abdominal Adipose tissue weight to body weight across the groups.*

Group	CON group	OBC group	MOBC group	HOBC group
Body weight (g)	29.87±2.31	45.11±3.45$^{\#\#}$	33.58±2.54**	30.52±2.23$^{**\&}$
Abdominal Adipose tissue weight (g)	1.56±0.37	3.64±0.36$^{\#\#}$	2.71±0.42*	1.73±0.17$^{*\&}$
Ratio of abdominal Adipose tissue weight to body weight (%)	5.06±0.81	8.31±0.83$^{\#}$	6.78±0.66*	5.69±0.51$^{*\&}$

$^{\#}P<0.05$, $^{\#\#}P<0.01$, compared with CON group; $^{*}P<0.05$, $^{**}P<0.01$, compared with OBC group; $^{\&}P<0.05$, $^{\&\&}P<0.01$, compared with MOBC group.

Table III. *Serum levels of Adipo, LH, FSH and T across the groups.*

Group	CON group	OBC group	MOBC group	HOBC group
Adipo(ug/L)	182.21±32.83	73.43±28.19$^{\#\#}$	102.11±43.12*	79.39±35.22$^{\&}$
LH(ng/L)	1995.92±361.03	1668.03±302.84$^{\#}$	2041.92±277.83**	1537.38±208.03$^{\&\&}$
FSH(IU/L)	12.34±1.35	8.79±1.21$^{\#}$	11.12±0.73**	8.13±1.05$^{\&\&}$
.T(ng/L)	267.45±43.19	207.39±41.51$^{\#}$	251.54±34.03*	197.39±18.22$^{\&\&}$

$^{\#}P<0.05$, $^{\#\#}P<0.01$, compared with CON group; $^{*}P<0.05$, $^{**}P<0.01$, compared with OBC group; $^{\&}P<0.05$, $^{\&\&}P<0.01$, compared with MOBC group

Table IV. *Adipo, Adipo R1, AMPK, Kiss and GnRH mRNA expressions in the hypothalamus in each group.*

Group	CON group	OBC group	MOBC group	HOBC group
Adipo	0.31±0.02	1.00±0.04$^{\#}$	0.66±0.11**	0.93±0.07$^{\&}$
Adipo R1	0.64±0.04	1.00±0.07$^{\#}$	0.65±0.08**	0.94±0.09$^{\&}$
AMPK	0.55±0.13	1.00±0.06$^{\#}$	0.65±0.15*	0.98±0.26$^{\&}$
Kiss	2.27±0.45	1.00±0.12$^{\#\#}$	2.01±0.41*	1.43±0.38$^{\&\&}$
GnRH	2.16±0.17	1.00±0.15$^{\#\#}$	1.68±0.34*	1.12±0.31$^{\&\&}$

$^{\#}P<0.05$, $^{\#\#}P<0.01$, compared with CON group; $^{*}P<0.05$, $^{**}P<0.01$, compared with OBC group; $^{\&}P<0.05$, $^{\&\&}P<0.01$, compared with MOBC group.

LH, FSH and T to a lesser extent (P<0.05). There was no significant difference in the serum levels of Adipo, LH, FSH and T between the OBC group and HOBC group (P>0.05). There were lower serum levels of Adipo (P<0.05), and much lower levels of LH, FSH and T in the HOBC group as compared with the MOBC group (P<0.01) (Table III).

Gene expressions of Adipo, Adipo R1, AMPK, Kiss and GnRH in the hypothalamus in each group

The gene expressions of Adipo, Adipo R1 and AMPK were upregulated significantly in the OBC group than in the CON group (P<0.05), while those of Kiss and GnRH were downregulated (P<0.01) (Table IV). There was a dramatic downregulation of Adipo, Adipo R1 and AMPK genes in the MOBC group as compared with the OBC group (P<0.05), with a significant upregulation of Kiss and GnRH genes (P<0.05). There were no significant changes in the gene expressions of Adipo, Adipo R1 and AMPK between the OBC group and HOBC group (P>0.05). The gene expressions of Kiss and GnRH only increased insignificantly in the HOBC group (P>0.05). As compared with the MOBC group, there were much higher gene expressions of Adipo, Adipo R1 and AMPK in the HOBC group (P<0.05). The gene expressions of Kiss and GnRH were downregulated significantly in the HOBC group as compared with the MOBC group (P<0.01).

DISCUSSION

A large number of studies have confirmed that obese children often suffer endocrine and metabolic disorders and adolescent developmental abnormalities, and reproductive dysfunction occurs during adulthood (9). After maturation of the male reproductive axis, the hypothalamus begins to secrete GnRH, which acts on the anterior pituitary lobe to secrete LH and FSH (10). George et al. (11) showed that the secretion of GnRH in hypothalamus of male mice exhibited a downward trend in obesity. In this study, it was revealed that long-term moderate exercise effectively reduced body fat, improved metabolic disorders in mice, down-regulated Adipo in hypothalamus, alleviated the inhibition of Kiss-GnRH gene expressions and HPG axis, and improved the negative effects of obesity on sexual development. Long-term high-intensity exercise had a more significant effect on reducing body fat and improving metabolic disorders in mice, but Adipo in hypothalamus was not regulated, which did not improve the gene expression of Kiss-GnRH, the inhibition of HPG axis, and the negative effect of obesity on sexual development. Therefore, it is hypothesized that the effect of exercise on hypothalamic Adipo may be related to exercise time, exercise intensity and physical fitness.

REFERENCES

1. Holst JJ. Enteroendocrine secretion of gut hormones in diabetes, obesity and after bariatric surgery. Curr Opin Pharmacol 2013; 13(6):983-88.
2. Dudek M, Kołodziejski PA, Pruszyńska-Oszmałek E, Sassek M, Ziarniak K, Nowak KW, Sliwowska JH. Effects of high-fat diet-induced obesity and diabetes on Kiss1 and GPR54 expression in the hypothalamic-pituitary-gonadal (HPG) axis and peripheral organs (fat, pancreas and liver) in male rats. Neuropeptides 2016; 56:41-49.
3. Davolli GM, Ball BA, Estellervico A, et al. Reversible downregulation of the hypothalamic-pituitary-gonadal axis in stallions with a novel GnRH antagonist. Theriogenology 2016; 86(9):2272-80.
4. Matsui H, Asami T. Effects and therapeutic potentials of kisspeptin analogs: regulation of the hypothalamic-pituitary-gonadal axis. Neuroendocrinology 12014; 99(1):49-60.
5. Yeo SH, Colledge WH. The Role of Kiss1 neurons as integrators of endocrine, metabolic, and environmental factors in the hypothalamic-pituitary-gonadal axis. Front Endocrinol (Lausanne) 2018; 9:188.
6. Klenke U, Taylorburds C, Wray S. Metabolic influences on reproduction: Adiponectin attenuates GnRH neuronal activity in female mice. Endocrinology 2014; 155(5):1851-63.
7. Gui Y, Silha JV, Murphy LJ. Sexual dimorphism and regulation of resistin, Adiponectin, and leptin expression in the mouse. Obes Res 2004; 12(9):1481-91.
8. Heinonen S, Korhonen S, Helisalmi S, Koivunen R, Tapanainen J, Hippeläinen M, Laakso M. Associations

between two single nucleotide polymorphisms in the Adiponectin gene and polycystic ovary syndrome. Gynecol Endocrinol 2005; 21(3):165-69.
9. Tena-Sempere M. The Endocrine Society Centennial: genes and hormones in obesity… or how obesity met endocrinology. Endocrinology 2016; 157(3):979-82.
10. Kimura M, Shinozaki T, Tateishi N, et al. Adiponectin is regulated differently by chronic exercise than by weight-matched food restriction in hyperphagic and obese OLETF rats. Life Sci 2006; 79(22):2105-11.
11. George JT, Millar RP, Anderson RA. Hypothesis: kisspeptin mediates male hypogonadism in obesity and type 2 diabetes. Neuroendocrinology 2010; 91(4):302-7.

LETTER TO THE EDITOR

EFFICACY OF CONTINUOUS RENAL REPLACEMENT ON ACUTE RENAL INJURY DEVELOPED IN SEVERE SEPSIS

Y. ZHANG[1], DR. SHAO[2], ZP. HE[3], XX. MA[2] and CJ. SHI[2]

[1]ICU, Affiliated Hongqi Hospital of Mudanjiang Medical University, MuDanJiang, Heilongjiang, China; [2]Department of Nephrology, The Second Affiliated Hospital of Mudanjiang Medical University, MudanJiang, Heilongjiang, China; [3]Department of Pathophysiology, College of Basic Medical Science of Mudanjiang Medical University Heilongjiang, China

Received September 27, 2018 – Accepted January 23, 2019

Sepsis is a systemic inflammatory response that can further develop into severe sepsis (septic shock), which eventually leads to multiple organ dysfunction syndrome (MODS). This study aimed to assess the effects of continuous renal replacement therapy (CRRT) on acute renal injury caused by severe sepsis by monitoring biochemical parameters. A total of 60 patients with septic shock and acute kidney injury were included. The control group (30 cases) was treated with routine treatment and intermittent renal replacement therapy (IRRT). The experimental group (30 cases) was treated with routine treatment and continuous renal replacement therapy CRRT. The changes in inflammation and biochemical indexes and APACHE- II score were evaluated before the treatment and 1, 3, and 7days after the treatment. The inflammatory markers (neutrophil percentage, C-reactive protein (CRP) and procalcitonin (PCT) levels) in the experimental group decreased significantly after treatment. In the control group, the index of inflammation still increased one day after treatment and decreased on day 3 of treatment. After treatment, blood lactate, serum creatinine and urea nitrogen levels decreased, but the urine volume increased. After treatment, the vasoactive dose in the experimental group was significantly lower than that of the control group (P<0.05). CRRT is a good treatment for septic shock-related acute kidney injury, which improves biochemical indicators and protects kidney function.

To the Editor,

Sepsis is a systemic inflammatory response that can further develop into severe sepsis (septic shock), which eventually leads to multiple organ dysfunction syndrome (MODS) (1). The most common germ involved in septic shock is *Staphylococcus aureus* which is difficult to treat, especially in patients with clinical comorbidities such as kidney disease or diabetes (2). Sepsis-induced acute kidney injury is diagnosed in up to 47% of human ICU patients and is a major health concern (3). The treatment mainly includes symptomatic supportive treatment and etiological treatment that often fails when germ resistance is increased (4). In recent years, blood purification has become an important part of the treatment of sepsis-related acute kidney injury (5). Methods of blood purification include peritoneal dialysis, intermittent renal replacement therapy (IRRT) and continuous renal replacement therapy (CRRT) (6). Although the cost of peritoneal

Key words: continuous renal replacement therapy; severe sepsis; acute kidney injury; inflammatory response

Corresponding Author:
Dr Chunjing Shi,
Department of Nephrology,
The Second Affiliated Hospital, Mudanjiang Medical University,
No.15 Dongxiaoyun Street, Aimin District, MudanJiang,
Heilongjiang 157009, China
e-mail: shi_chunjingmm@yeah.net

0393-974X (2019)

DISCLOSURE: ALL AUTHORS REPORT NO CONFLICTS OF INTEREST RELEVANT TO THIS ARTICLE.

dialysis is cheaper and easier to carry out, it has the potential of aggravating abdominal infection and has poor controllability (7). IRRT can quickly clear inflammatory mediators and metabolites (8), but it can cause severe hemodynamic fluctuations. CRRT can remove metabolic toxins in the body and improve the balance of electrolytes and liquids (9). Hemodynamics is more stable than in IRRT. Even in patients with hemodynamically stable sepsis, CRRT demonstrated some advantages over intermittent hemodialysis, such as the control of temperature, pH, and fluid homeostasis (10). A large amount of fluid loss and visceral edema were avoided in a short period of time. The aim of this study was to evaluate the improvement of the vital signs, and inflammatory and biochemical indexes in patients with acute renal injury associated with septic shock after CRRT.

MATERIALS AND METHODS

Patients

Sixty patients who were diagnosed with septic shock associated with acute renal injury from July 1, 2015 to December 31, 2017 in the Affiliated Hongqi Hospital of Mudanjiang Medical University were selected. According to renal replacement therapy, the selected patients were divided into a control group (conventional therapy + IRRT) and an experimental group (conventional therapy + CRRT), 30 patients per group. All patients signed the informed consent for participating in the study which was approved by the Ethics Committee of Affiliated Hongqi Hospital of Mudanjiang Medical University.

Inclusion criteria: patients with acute renal injury induced by septic shock in the first 48 h from onset.

Exclusion criteria: patients with shock determined by other causes that led to acute renal injury, patients with chronic renal failure or renal replacement therapy, patients who died in the first 48 h after admittance to the hospital.

Conventional therapy

All patients were treated according to the Chinese Guidelines for Management of Severe Sepsis and Septic Shock (2014). According to the patient's condition, they received fluid replacement, oxygen inhalation, nutritional support and empirical antibiotics. Dopamine and norepinephrine were given to maintain mean arterial pressure >65 mmHg. 200,000 U ulinastatin (Guangdong Tianpu Biochemical Pharmaceutical Co., Ltd., China) was administered intravenously by micro-pump for 1 hour every 8 h for 5 days. Patients with fungal infections were treated with fluconazole. In the case of respiratory failure, mechanical ventilation was performed.

Kidney replacement therapy

A cardiopulmonary bypass was established using a single needle and central double-lumen veno-venous catheters were inserted through the femoral vein or the subclavian vein or the internal jugular vein by the Seldinger wire technique. After extracorporeal circulation establishment IRRT or CRRT was performed.

The control group was treated using IRRT for 6 months started in the first 24-48h after admission. The frequency of IRRT was three times per week, 4 hours each time. For the procedure, a GermanFresenius 4008B, Campbell AK96 and Nipro dialyzer FB-150U were used. Blood flow rate was 300mL/min. The patients received heparin as anticoagulant in doses of 0.3-0.5mg/kg body weight and respectively 2-10mg/h twice. The patients with bleeding tendency received low molecular weight heparin and those with severe bleeding or immediately after surgery did not received anticoagulant medication.

The experimental group was treated with CRRT for 6 months started in the first 24-48 h after admission. For the procedure, a Baxter ACCURA bedside blood filtration machine with a high flux filter and an alum membrane (HF1200, Baxter, USA) was used according to standard procedure. The treatment dose was set as 50-60mL·kg^{-1}·h^{-1} and the rate of blood flow was 120 ~ 250mL/h. The ultrafiltration was performed continuously for 24 h with a flow <400mL/h. The electrolyte levels were monitored during the treatment, and the replacement solution was adjusted according to the results. The composition of replacement solution was 3000 mL normal saline solution, 1000 mL 5% glucose solution, 250 mL 5% sodium bicarbonate solution, 30 mL 10% calcium gluconate solution, 3.2 mL 25% magnesium sulfate solution and 0-18 mL 10% potassium chloride solution. According to the electrolytes and blood gas levels the dosage of each ion and of sodium bicarbonate was adjusted in the formula of the replacement liquid. In order to prevent blood coagulation in the pipeline, 100mg/L heparin saline was used before the treatment to pre-wash the blood

Table I. *General clinical data.*

Category	Experimental group (n = 30)	Control group (n = 30)
Age	64.83±13.49	66.03±14.71
Gender (male / female)	19/11	17/13
Urinary tract infection (case)	3	4
Abdominal infection (case)	10	9
Pulmonary infection (case)	10	12
Number of damaged organs	2.50±1.21	2.39±1.33
APACHE-II score	23.82±6.3	22.16±4.51

Table II. *Blood inflammation and biochemical indexes before and after treatment.*

Category	Group	Before treatment	1d after treatment	3d after treatment	7d after treatment
APACHE-II score	Experimental group	23.12±6.24	19.23±4.34	16.71±3.56	14.28±3.37
	Control group	20.81±3.34	20.79±3.72	19.71±2.856	16.81±265
Body temperature (°C)	Experimental group	38.34±0.86	37.68±0.64*	37.42±0.43*	37.06±0.41*
	Control group	38.11±0.89	38.16±0.61	37.87±0.51	37.43±0.37
Neutrophil percentage	Experimental group	90.07±2.43	88.12±2.57*	84.65±2.45*	79.56±2.35*
	Control group	89.56±2.46	90.78±2.26	87.54±2.49	83.12±3.35
CRP(mg/L)	Experimental group	94.82±13.43	86.41±4.15*	81.35±4.61*	66.14±8.82*
	Control group	92.25±10.65	91.23±4.25	85.51±3.27	76.31±6.89
PCT(ng/mL)	Experimental group	45.82±12.69	32.37±10.65*	21.14±7.86*	10.41±4.69*
	Control group	46.52±12.76	38.79±11.71	28.12±8.15	18.12±8.02
Blood lactate (mmoL / L)	Experimental group	6.41±1.12	5.72±1.03	4.52±1.13*	2.59±0.75*
	Control group	6.34±1.10	6.12±1.07	5.46±1.09	4.12±1.12
Creatinine (umoL / L)	Experimental group	252.15±24.14	221.84±27.14*	188.35±21.73*	155.32±18.47*
	Control group	253.37±25.73	242.56±24.14	215.82±23.76	184.12±21.45
Urea nitrogen (mmoL / L)	Experimental group	18.56±3.43	15.24±3.12*	12.36±2.78*	9.86±2.12*
	Control group	18.71±2.78	17.91±2.87	15.79±2.47	14.12±3.15
Urine volume (mL / h)	Experimental group	19.54±6.14	31.34±8.35*	41.71±8.37*	51.67±11.41*
	Control group	20.83±7.43	23.45±9.31	30.62±8.46	42.58±12.43

*Note: The experimental and control groups were compared, * P <0.05.*

pipe, filter, replacement fluid pipeline and ultrafiltration pipeline. The amount of the first dose of heparin was 15-20 mg, and the maintenance amount was 2-10mg/h. The dose of heparin was adjusted according to the activated partial thromboplastin time (APTT). APTT was maintained at about 1-1.5 times normal value. In cases where there was a bleeding tendency, the dosage was adjusted according to the global patient condition and the blood coagulation function. The postoperative patients and those with severe bleeding tendency discontinued the heparin according to the particular condition for 6 months.

The criteria for final cessation of renal replacement therapy were: improvement of the disease, recovery of renal function, infection control, stability of the vital signs, or the death of the patient.

Blood tests and severity of disease

The clinical data of the two groups of patients, the changes of APACHE- II score, blood lactic acid, neutrophil percentage, C-reactive protein (CRP), Procalcitonin (PCT), Serum creatinine (Scr), urea nitrogen and urine volume per hour of patients before treatment and 1, 3, and 7 days after treatment at 6:00 in the morning, the types of vasoactive drugs that maintain average arterial pressure greater than 65 mmHg in a day, maximum dose and peak temperature of body temperature were monitored.

The biochemistry tests were performed by automatic biochemical analyzer (Beckman Coulter, Inc., USA). The hematological tests were performed by ABL90 FLEX blood gas analyzer (Radiometer medical equipment (Shanghai) Co., Ltd., Shanghai, China). All testing steps were strictly in accordance with the operating procedures. The normal reference value of the related serological index: white blood cell (WBC): 3.5-9.5×10^9/L; neutrophil percentage (N%): 40-75%; C-reactive protein (CRP): 0.00-8.00mg/L; procalcitonin (PCT): 0-0.09ng/ml; serum creatinine (Scr): 59-104umol/L; blood urea nitrogen (BUN): 2.86-7.14mmol/L; lactic acid (Lac): 0.5-1.7mmol/L; blood potassium (K): 3.5-5.3mmol/L; blood sodium (Na): 137-147mmol/L.

Severity of disease

The severity of the disease was assessed by the acute physiological and chronic health status score II (APACHE- II score) (9).

Statistical analysis

The data obtained in this study were analyzed by SPSS19.0 statistics software. The measurement data conforms to the normal distribution and is represented by the average number of standard deviations. An independent sample Student's *t*-test was used for the

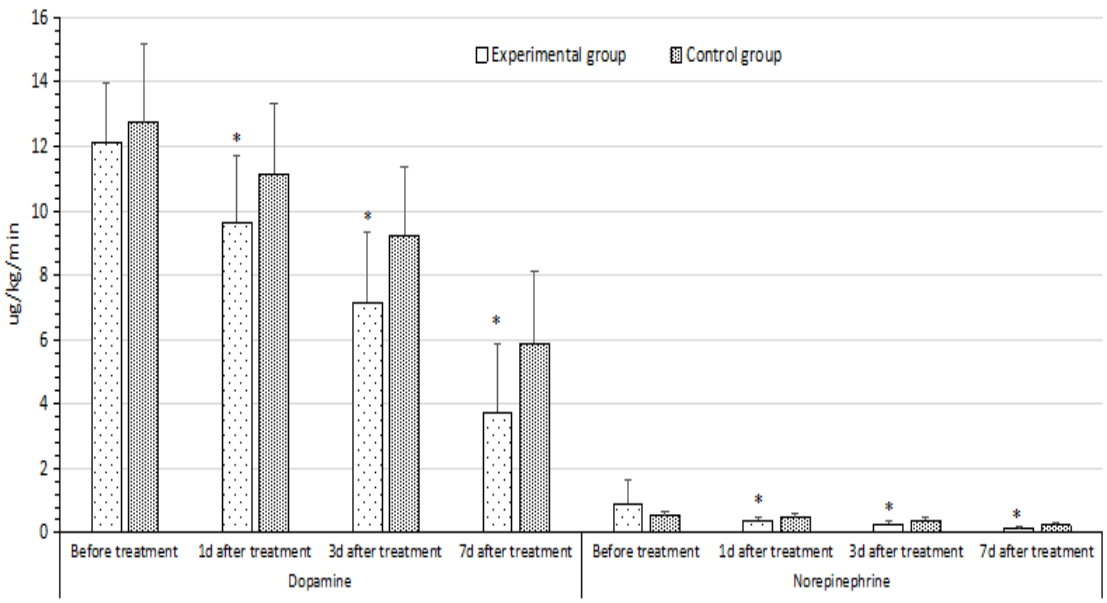

Fig. 1. *Medication before and after treatment (the experimental and control groups were compared, * P <0.05.)*

comparison between the groups. The standard α value of the test is 0.05. P<0.05 indicated that the difference was statistically significant.

RESULTS

General clinical data of the patients

There was no significant difference in the general clinical data between the two groups (P>0.5) (Table I).

Blood inflammation and biochemical indexes before and after treatment

There was no statistical difference between the two groups before treatment (P>0.05) (Table II). After the treatment, the scores of APACHE- II in the experimental group and the control group decreased compared with those before the treatment. At 3 days and 7 days after treatment, APACHE- II score in the experimental group was significantly lower compared with the control group (P<0.05). The inflammatory indices (neutrophil percentage, CRP, PCT) at days 1, 3 and 7d after treatment in the two groups were decreased compared with the levels before the treatment. In the control group, the index of partial inflammation still increased 1 day after treatment. In the treatment group the inflammatory indices were lower compared to the control group at 1, 3 and 7 days (P<0.05). The blood lactic acid values of the two groups were all lower than those before the treatment. On day 1 after treatment the decrease of blood lactic acid in the experimental group was greater than that of the control group, but with no statistical significance (P>0.05). At days 3 and 7 after treatment, the decrease of blood lactic acid in the experimental group was significantly greater than that of the control group (P<0.05).

Medication before and after treatment

There was no significant difference in the maximum dose of dopamine and norepinephrine before treatment in the two groups (P>0.05) (Fig. 1). After the treatment of early CRRT, the hemodynamics of the experimental group tended to be stable with the clearance of inflammatory mediators and metabolites, improvement of the internal environment and increase of urine output. The amount of vasoactive drug decreased. The effect was significantly better than the intermittent renal replacement therapy group (P <0.05).

DISCUSSION

After treatment, the APACHE-II score showed that both IRRT and CRRT could reduce the blood lactate level and reduce the mortality rate. The therapeutic effect of CRRT was better than that of IRRT. In addition, the index of inflammation was significantly reduced after 1 day of CRRT. When the control group was treated for 1 day with IRRT, some of the inflammatory indexes were still rising. Three days after the treatment, inflammatory cytokines were decreased in the control group. It has been shown that in the plasma of patients with acute renal injury associated with septic shock, cytokines are increased and are associated with poor prognosis (11). Microbes and their metabolites can induce inflammatory reactions which can lead to local microvascular damage. The infection has a potential to spread and produce serious consequences in different organs, resulting in multiple organ failure (12). Although a large number of inflammatory mediators can be produced in the infected area, the stress response of the body can also produce anti-inflammatory mediators.

This study showed that the dose of vasoactive drug for maintaining the mean arterial pressure over 65 mmHg was not different before treatment between the groups, but after treatment in the experimental group the effect was improved compared to the control group (P <0.05). IRRT can quickly remove the solute and water. In patients with septic shock, hemodynamic stability should be maintained first. However, even in patients with stable hemodynamic sepsis, CRRT can still show some advantages compared to other renal replacement treatments. Studies have shown that the avoidance of severe fluctuations in intracranial blood flow can only be passed through CRRT (13). After treatment, the serum creatinine and urea nitrogen decreased significantly in the experimental group (P<0.05), but the decrease in the control group was not obvious (P>0.05). The urine volume increased in the two

groups after treatment, and the increase of urine volume in the treatment group was greater than that in the control group ($P<0.05$). Low urine volume is an important risk factor associated with mortality in patients with acute kidney injury due to septic shock (14). The urine output of the experimental group was better than that of the control group and the prognosis was improved.

In summary, CRRT is a worthy treatment for patients with acute kidney injury associated with septic shock as it can effectively protect renal function, reduce inflammation and improve hemodynamics.

REFERENCES

1. Shum HP, Chan KC, Kwan MC, Yeung AW, Cheung EW, Yan WW. Timing for initiation of continuous renal replacement therapy in patients with septic shock and acute kidney injury. Ther Apher Dial 2013; 17(3):305-10.
2. Ungureanu A, Zlatian O, Mitroi G, et al. Staphylococcus aureus colonisation in patients from a primary regional hospital. Mol Med Rep 2017; 16(6):8771-80.
3. Keir I, Kellum JA. Acute kidney injury in severe sepsis: pathophysiology, diagnosis, and treatment recommendations. J Vet Emerg Crit Care (San Antonio) 2015; 25(2):200-209.
4. Călina D, Docea AO, Roşu L et al. Antimicrobial resistance development following surgical site infections. Mol Med Rep 2017; 15(2):681-88.
5. Jeong EG, Nam HS, Lee SM, et al. Role of B-type natriuretic peptide as a marker of mortality in acute kidney injury patients treated with continuous renal replacement therapy. Renal Failure 2013; 35(9):1216.
6. Baek SD, Yu H, Shin S, et al. Early continuous renal replacement therapy in septic acute kidney injury could be defined by its initiation within 24 hours of vasopressor infusion. J Crit Care 2017; 39:108-14.
7. Barbar SD, Binquet C, Monchi M, Bruyère R, Quenot JP. Impact on mortality of the timing of renal replacement therapy in patients with severe acute kidney injury in septic shock: the IDEAL-ICU study (initiation of dialysis early versus delayed in the intensive care unit): study protocol for a randomized controlled trial. Trials 2014; 15:270.
8. Martin A, Acierno MJ. Continuous renal replacement therapy in the treatment of acute kidney injury and electrolyte disturbances associated with acute tumor lysis syndrome. J Vet Intern Med 2010; 24(4):986-89.
9. Mayumi K, Yamashita T, Hamasaki Y, et al. Impact of continuous renal replacement therapy intensity on septic acute kidney injury. Shock 2016; 45(2):133.
10. Mayeur N, Rostaing L, Nogier M B, et al. Kinetics of plasmatic cytokines and cystatin C during and after hemodialysis in septic shock-related acute renal failure. Crit Care 2010; 14(3):R115.
11. Chou CY, Yeh HC, Chen W, et al. Norepinephrine and hospital mortality in critically ill patients undergoing continuous renal replacement therapy. Artif Organs 2011; 35(2):E11-17.
12. Hanafusa N. Application of continuous renal replacement therapy: what should we consider based on existing evidence? Blood Purif 2015; 40(4):312-19.
13. Zarbock A, John S, Jörres A, Kindgen-Milles D. Kidney disease: improving global outcome. [New KDIGO guidelines on acute kidney injury. Practical recommendations]. Anaesthesist 2014; 63(7):578-88.
14. Lahmer T, Rasch S, Schnappauf C, Schmid RM, Huber W. Influence of volume administration on Doppler-based renal resistive index, renal hemodynamics and renal function in medical intensive care unit patients with septic-induced acute kidney injury: a pilot study. Int Urol Nephrol 2016; 48(8):1327-34.

LETTER TO THE EDITOR

CHANGES OF BLOOD PRESSURE, SERUM INFLAMMATORY FACTORS AND ENDOTHELIN LEVELS IN PATIENTS WITH HYPERTENSION UNDER REHABILITATIVE AEROBIC EXERCISE

W. XIE, JH. SU and J. WANG

Department of Rehabilitation, West China Hospital of Sichuan University, Chengdu, Sichuan Province, China

Received November 11, 2018 – Accepted December 17, 2018

The aim of this study was to evaluate the effects of rehabilitative aerobic exercise on blood pressure, serum inflammatory factors, endothelin and quality of life in patients with hypertension. NInety patients with mild hypertension visiting West China Hospital of Sichuan University from June 2017 to December 2017 were enrolled and randomly divided into an experimental group and a control group. Patients in both groups were given a low-salt diet, and the experimental group was given an extra three-month treadmill training. Systolic blood pressure (SBP), diastolic blood pressure (DBP), serum tumor necrosis factor α (TNF-α), serum interleukin-6 and endothelin-1, body mass index (BMI), triglyceride (TG) and other indicators were examined in both groups before and after exercise, SF-36 scale was used to evaluate the quality of life. The results showed that after 3 months of exercise, SBP and DBP in the experimental group were significantly lower than those in the control group ($P < 0.05$). Compared with the control group, the concentrations of TNF-α, interleukin-6 and endothelin-1 in the experimental group were significantly decreased ($P < 0.05$). Correlation analysis showed that IL-6 was positively correlated with SBP ($P < 0.05$), and TNF-α and ET-1 were positively correlated with diastolic blood pressure ($P < 0.05$). The general health status, energy, mental health, social function, emotional function and health changes of the experimental group were significantly improved compared with before exercise ($P < 0.05$). In conclusion, rehabilitative aerobic exercise can lower blood pressure and improve the overall quality of life in mild hypertension patients by inhibiting vascular inflammation and lowering plasma endothelin-1.

To the Editor,

At present, cardiovascular disease is one of the major health threats across the world and hypertension is the most important risk factor (1, 2). Prevention and control of hypertension are the key points in reducing the incidence and mortality of cardiovascular diseases. Several studies showed that high-risk hypertensive patients tended to develop myocardial infarction and stroke even if interventional measures of lowering blood pressure and lipid levels were taken (3, 4). It is therefore necessary to apply more strenuous therapies to patients with low and moderate-risk hypertension to delay the progress of hypertension.

The pathogenesis of hypertension is very complicated (5), and its occurrence is related to many risk factors, such as lack of exercise or insufficient physical activity. Rehabilitative exercise

Key words: aerobic exercise; rehabilitative exercise; hypertension; inflammatory factors; endothelin-1

Corresponding Author:
Dr Wei Xie,
Department of Rehabilitation, West China Hospital
Sichuan University, No.37 Guoxuexiang,
Chengdu, 610041,
Sichuan Province, China
e-mail: xieweihuaxi1974@163.com

0393-974X (2019)

therapy is an important measure for the treatment (6). Cornelissen et al. (7) carried out 6-52 weeks of aerobic exercise training on more than 600 volunteers and it was found that their systolic and diastolic blood pressure was decreased by 3.2 mmHg and 2.7 mmHg, respectively. In this study, serum TNF-α, IL-6 and ET-1 concentrations in mild hypertension patients were determined, and their correlation with blood pressure was analyzed by observing the effect of three-month bicycle exercise on blood pressure; the relationship between exercise hypotension and serum inflammatory factors was evaluated, in order to provide new insight into the exercise pressure reduction mechanism.

MATERIALS AND METHODS

Patients

Ninety outpatients with mild essential hypertension visiting West China Hospital of Sichuan University from June 2017 to December 2017 were enrolled. Among them, 32 patients had simple elevated systolic blood pressure (SBP), 25 patients had simple elevated diastolic blood pressure, and 33 patients had both elevated systolic and diastolic blood pressure. The patients were randomly divided into an experimental group and a control group, 45 in each group. There were 24 males and 21 females aged 53-70 in the experimental group, and 22 males and 23 females aged 51-69 in the control group. This study was approved by the ethics committees of West China Hospital of Sichuan University and each participant completed the written consent form.

Exclusion criteria: regular exercise within the previous year; secondary hypertension, cerebrovascular disease, diabetes, coronary atherosclerotic heart disease, myocardial infarction, myocardial hypertrophy and heart failure; proteinuria, hematological diseases, immune diseases, severe hepatorenal insufficiency, inflammatory diseases and connective tissue diseases; dysfunction of lower extremity muscles and joints.

Procedure for intervention and testing

The patients in the control group received assessment of cardiopulmonary function in our hospital at baseline, and then they all had 2 weeks of low-salt and low-fat diet and received another cardiopulmonary function examination 3 months after the baseline evaluation. On the basis of the control group, the experimental group imderwent aerobic training for 3 months after the baseline evaluation.

Cardiopulmonary function was evaluated by using a bicycle exercise program (no more than 6 g of salt and 40 g of fat each day). Meanwhile, SF-36 Simple Health Questionnaire on Quality of Life (8) was used to record the lifestyle of the two groups and evaluate their quality of life, and the exercise intensity of each patient in the experimental group within three months was determined by treadmill exercise test.

According to the FITT principle, the patients' exercise plan was designed as follows: bicycle exercise training was applied and the frequency of exercise was twice per day for 3 months; the intensity of exercise was 50-70% HRmax; the total duration of each exercise was 40 min, including 30 min of exercise, 5 min of warm-up, and 5 minutes of relaxation after exercise. The whole training process was well prepared for emergency to prevent accidents.

The exercise effect of the experimental group was evaluated. The blood pressure and heart rate of all patients were measured by electronic blood pressure and heart rate meters before and after treatment. All subjects were fasting for more than 12 hours, and 10 mL venous blood was collected in the morning. 5 mL venous blood was used to examine blood lipids of the two groups, including triglyceride (TG), total cholesterol (TC), low density lipoprotein cholesterol (LDL), high density lipoprotein cholesterol (HDL). 5 mL venous blood was centrifuged for 10 min at 3 000 r/min and stored at -70°C. All the above tests were completed within 4 hours. Enzyme-linked immunosorbent assay (ELISA) was used to determine serum TNF-α, IL-6, and ET-1 according to the manufacturer's instructions (Shanghai Jianglai Biological Technology Co., Ltd., China).

SF-36 simple scale was used to assess the quality of life from eight dimensions: physiological function (PF), role of physiology (RP), general health status (GH), vitality (VT), social function (SF), role of emotion (RE), mental health (MH), and reported health transition (HT).

Statistical analysis

SPSS22.0 statistical software was used for statistical analysis. The data were presented by mean ± standard deviation or median and interquartile. Statistical differences

between continuous variables with normal distribution were tested by Student's *t*-test, while those not obeying normal distribution were tested by Wilcoxon signed rank test. Correlation analysis of normal distributed data was performed by Pearson analysis, and multivariate analysis by multivariate linear regression analysis. A *P*-value (two-tailed) of <0.05 was considered statistically significant.

RESULTS

Effects of rehabilitative exercise on body mass index and blood lipid

The comparison of the baseline data between the two groups showed no significant difference in age, gender, height, BMI, TG, TC, LDL, and HDL. After 3-month training, body mass index (BMI) of the experimental group was significantly lower than that of the control group ($P < 0.05$), but there was no significant difference between the experimental group and the control group in TG, TC, LDL, and HDL, as shown in Table I.

Effects of rehabilitative exercise on blood pressure, inflammatory factors and plasma endothelin-1 in patients and correlation analysis

There was no significant difference in SBP, DBP, serum TNF-α, IL-6 and ET-1 between the two groups before exercise. After 3-month exercise, SBP and DBP in the experimental group dropped to normal levels, while the serum TNF-α, IL-6 and ET-1 levels in the experimental group were lower than those in the control group and before exercise ($P < 0.05$), as shown in Table I. The correlation analysis showed that SBP and DBP were both positively correlated with IL-6 ($P < 0.05$), and DBP was positively correlated with TNF-α and ET-1 ($P < 0.05$). The details are shown Fig. 1. Multiple linear regression analysis showed that the concentrations of TNF-α and ET-1 in the experimental

Table I. *Effects of exercise training on body mass index, blood lipids, blood pressure, inflammatory factors and plasma endothelin-1 in patients with hypertension (x±SD).*

Detection index	Control group (n=45)		Experimental group (n=45)	
	Before experiment	After experiment	Before exercise	After exercise
BMI(Kg/M^2)	24.83±3.25	24.97±2.49	25.50±2.43	23.57±2.43#*
TG(mmol/L)	1.45±0.36	1.47±0.33	1.42±0.25	1.41±0.29
TC(mmol/L)	4.80±0.67	4.95±0.74	4.85±0.64	4.64±0.67
LDL(mmol/L)	2.69±0.44	2.81±0.49	2.79±0.55	2.63±0.61
HDL(mmol/L)	1.47±0.30	1.51±0.31	1.57±0.26	1.61±0.33
SBP(mmHg)	143.71±8.82	145.52±6.87	144.85±7.18	135.49±7.22#*
DBP(mmHg)	90.52±6.84	92.78±5.76	92.96±5.45	86.84±5.82#*
TNF-α(pg/mL)	28.64±5.37	28.87±5.06	28.75±4.78	22.81±4.80#*
IL-6(pg/mL)	36.51±3.68	36.84±3.98	37.61±4.26	32.73±4.79#*
ET-1(pg/mL)	90.77±16.78	91.73±16.70	92.45±13.61	79.56±13.07#*

P<0.05, compared with the control group; P<0.05, compared with before exercise.

group were closely related to the changes of diastolic blood pressure ($P < 0.05$) (Table II).

Effects of rehabilitative exercise on quality of life in patients with hypertension

The results showed that there were no significant differences in PF, GH, VT, and MH between the two groups before exercise. After 3 months of exercise training, GH, VT and MH in the experimental group were significantly improved compared with those in the control group ($P < 0.05$). PF in the experimental group was not significantly different from that in the control group and before exercise. Before exercise, there was no significant difference in the scores of RP, SF, RE and HT between the two groups; after 3 months of exercise, SF, RE and HT in the experimental group were significantly improved compared with those in the control group ($P < 0.05$), but there was no significant difference in RP between the two groups, as shown in Table III.

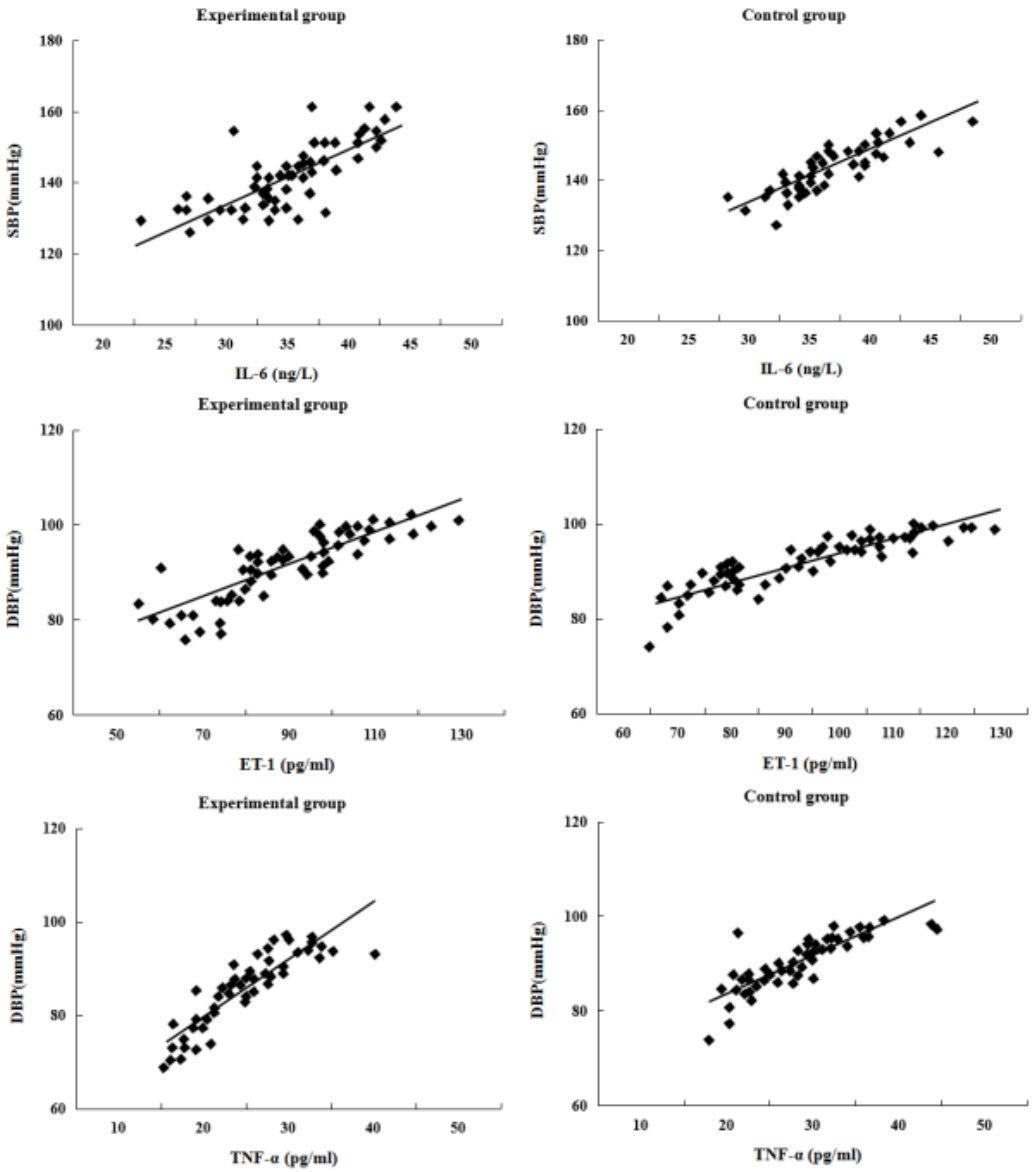

Fig. 1. *Correlation analysis of TNF-α, IL-6 and ET-1 with SBP and DBP.*

Table II. *Multiple linear regression analysis of changes of DBP and different indexes in the experimental group.*

Variable	Parameter estimation	Standard deviation	T	P
Intercept	58.403	2.989	19.545	<0.05
TNF-α	0.637	0.108	5.845	<0.05
IL-6	-0.079	0.074	-1.081	0.287
ET-1	0.207	0.040	5.326	<0.05

Table III. *Comparison of PF, GH, VT, and MH between the two groups (x± SD).*

Detection index	Control group (n=45)		Experimental group (n=45)	
	Before experiment	After experiment	Before exercise	After exercise
PF	82.15±10.52	78.82±10.26	80.36±10.61	84.12±10.21
GH	63.54±20.15	58.63±20.55	63.75±20.78	69.64±16.27#*
VT	71.45±15.35	68.27±13.85	71.56±14.22	76.15±13.22#*
MH	59.48±16.89	56.04±17.49	59.64±17.61	65.24±18.01#*
RP	83.51±10.32	81.20±11.78	81.98±13.55	82.54±11.24
SF	62.78±14.59	59.86±15.21	64.12±10.33	71.65±14.28#*
RE	68.39±17.85	69.51±18.20	67.42±15.18	75.95±12.53#*
HT	57.45±10.23	54.69±12.17	55.83±13.57	68.26±14.84#*

*Note:#P<0.05, compared with the control group; *P<0.05, compared with before exercise.*

DISCUSSION

Our study showed that after three-month exercise SBP and DBP in the experimental group were significantly lower than those in the control group and compared to before exercise. Furthermore, there was no serious cardiovascular reaction during exercise. Our results were consistent with the study of Krieger et al. (9), who reported that low-to-moderate intensity exercise had better anti-hypertensive effects than high intensity exercise.

It was found that the ET-1 level in the experimental group was lower than that in the control group ($P < 0.05$). Zheng et al. (10) reported that Baduanjin exercise decreased plasma ET-1 concentration in elderly patients with hypertension, which was consistent with our results. Correlation analysis showed that the decrease of blood pressure was positively correlated with the changes of TNF-α and IL-6, suggesting that exercise-induced decrease of TNF-α and IL-6 might be related to exercise-induced hypotension. In addition, multiple linear stepwise

regression analysis showed that the change of DBP before and after treatment was closely related to the change of TNF-α concentrations, suggesting that TNF-α may affect the change of DBP alone. Our results showed that after three months of aerobic exercise training, the scores of GH, VT, SF, RE, MH and HT in patients with hypertension were improved.

In conclusion, the changes of blood pressure in hypertensive patients were positively correlated with serum TNF-α, IL-6 and ET-1. Aerobic exercise can reduce blood pressure and improve the life quality of patients with mild hypertension by inhibiting inflammation and lowering the level of ET-1.

REFERENCES

1. Townsend N, Wilson L, Bhatnagar P, Wickramasinghe K, Rayner M, Nichols M. Cardiovascular disease in Europe: epidemiological update 2016. Eur Heart J 2016; 37(42):3232-45.
2. Leong DP, Joseph PG, McKee M, Anand SS, Teo KK, Schwalm JD, Yusuf S. reducing the global burden of cardiovascular disease, part 2: prevention and treatment of cardiovascular disease. Circ Res 2017; 121(6):695-710.
3. Mosca L, Appel LJ, Benjamin EJ, et al. Evidence-based guidelines for cardiovascular disease prevention in women. J Am Coll Cardiol 2007; 49(11):1230-50.
4. Sever PS, Dahlöf B, Poulter NR, et al. Prevention of coronary and stroke events with atorvastatin in hypertensive patients who have average or lower-than-average cholesterol concentrations, in the Anglo-Scandinavian CardiacOutcomes Trial--Lipid Lowering Arm (ASCOT-LLA): a multicentre randomised controlled trial. Lancet 2003; 361(9364):1149-58.
5. Bonadei I, Vizzardi E, D'Aloia A, Sciatti E, Raddino R, Metra M. Role of Aliskiren on arterial stiffness and endothelial function in patients with primary hypertension. J Clin Hypertens (Greenwich) 2014; 16(3):202-6.
6. Thompson PD. Exercise and physical activity in the prevention and treatment of atherosclerotic cardiovascular disease. Arterioscler Thromb Vasc Biol 2003; 23(8):1319-21.
7. Cornelissen VA, Buys R, Smart NA. Endurance exercise beneficially affects ambulatory blood pressure: a systematic review and meta-analysis. J Hypertens 2013; 31(4):639-48.
8. López-Pérez P, Miranda-Novales G, Segura-Méndez NH, Del Rivero-Hernández L, Cambray-Gutiérrez C, Chávez-García A. [Study of quality of life in adults with common variable immunodeficiency by using the Questionnaire SF-36]. Rev Alerg Mex 2014; 61(2):52-8. Spanish.
9. Krieger EM, Brum PC, Negrão CE. State-of-the-Art lecture: influence of exercise training on neurogenic control of blood pressure in spontaneously hypertensive rats. Hypertension 1999; 34(4 Pt 2):720-3.
10. Zheng L, Chen Q Y, Chen F. The influence of ba duan jin exercise on vascular endothelium function in old patients with hypertension grade 1. Chin J Rehabil Med 2014; 29(3):223-27.

LETTER TO THE EDITOR

EFFECTS OF DIFFERENT LEVELS OF SOLUBLE PD-L1 PROTEIN ON THE GROWTH OF LEWIS LUNG CANCER TRANSPLANTED TUMOR

KN. YANG, W. HAN, YJ. QIN and LN. CHEN

Respiratory and Critical Care Medicine, Weifang Respiratory Disease Hospital (Weifang No.2 people's Hospital), Weifang, Shandong, China

Received November 1, 2018 – Accepted January 10, 2019

To investigate the effects of different doses of soluble PD-L1 (soluble form of Programmed death ligand 1, sPD-L1) protein on Lewis lung cancer cells, flow cytometry was used to detect the expression of PD-L1 (Programmed death ligand 1) on the surface of Lewis lung cancer cell lines and the expression of PD-1 on the surface of T lymphocytes in peripheral blood and spleen cells of C57BL/6 mice. A Lewis lung cancer animal model of C57BL/6 mice was established by transplanting Lewis lung cancer cells subcutaneously. The sPD-L1 protein was injected into the abdominal cavity of the mouse (sPD-L1 Ig) (working dose: 2.5, 5, 10 μg per mouse), while the sPD-L1 control protein was injected as a control. The growth of Lewis lung cancer xenografts was observed. On the 18th day after tumor cell inoculation, T lymphocyte subsets in mouse spleen were determined by flow cytometry. The PD-1 molecules on the surface of Lewis lung cancer cell line, C57BL/6 mouse spleen T lymphocytes and peripheral blood T lymphocytes were positively expressed. Compared with the control group, the volume of the transplanted tumor of Lewis lung cancer in C57BL/6 mice was larger with 10 μg sPD-L1 I g injection ($P < 0.05$), and no significant difference was observed in tumor volume with 2.5 μg and 5 μg injection ($P > 0.05$). A certain level of soluble PD-L1 (10 μg/mouse) could promote the growth of transplanted tumors of Lewis lung cancer in C57BL/6 mice.

To the Editor,

Lymphocytes play an important role in the immune response, in which T lymphocytes have a variety of biological functions, such as directly killing target cells, assisting or inhibiting the production of antibodies by B lymphocytes, and resisting pathogenic infection (1, 2), thereby forming the first line of defense against tumor. Programmed death ligand-1 (PD-L1) is one of the important negative costimulatory molecules in the regulation of T lymphocyte immune response (3, 4). PD-L1 is one of PD-1 (Programmed death-1). It is also a member of the CD28/B7 superfamily. There are two forms of cell membrane types which are soluble. sPD-L1 combines with its receptor in the same manner as the membrane-type PD-L1 molecule and plays biological functions. Studies have confirmed that PD-1/PD-L1 can significantly inhibit the function of T lymphocytes, attenuate activation of T lymphocytes and reduce cytokine (e.g. IL-2, IL-4 and IL-6) production. PD-L1 exists in cell membrane type and soluble form (5, 6). The soluble form of PD-L1 (sPD-L1) has a certain biological role in the occurrence and progression of various diseases, and was reported to be associated with the stage, metastasis and efficacy of lung cancer (7).

However, the effect of sPD-L1 on lung cancer growth *in vivo* remains to be clarified. In this study, we established a Lewis lung cancer animal model by

Key words: soluble PD-L1; T lymphocyte subsets; lung cancer; immune response

Corresponding Author:
Dr Lina Chen,
Respiratory and Critical Care Medicine,
Weifang Respiratory Disease Hospital
Weifang No.2 people's Hospital),
No. 7 Yuanxiao Street,
Kuiwei District, Weifang 261041, Shandong, China
e-mail: chenlina7888@163.com

0393-974X (2019)

DISCLOSURE: ALL AUTHORS REPORT NO CONFLICTS OF INTEREST RELEVANT TO THIS ARTICLE.

transplanting cancer cells into C57BL/6 mice, which were then injected with different doses of sPD-L1 into the abdominal cavity. The growth of tumors was observed.

MATERIALS AND METHODS

Animals

Four/five week-old male C57BL/6 mice weighing 18~22g were selected. All mice were raised at room temperature (24±1)°C and relative humidity (50±5) % and were kept in 12h/12h light/dark cycle. The mice were given free access to food and water. The mice were tested after one week of adaptation. The operations and medications involved in this experiment are in line with international animal protection regulations and the study was approved by the Ethics Committee of Weifang Respiratory Disease Hospital (Weifang No.2 People's Hospital).

Cell culture and passage

Lewis lung cancer cells (Nanjing Senbeijia Biotechnology Co., Ltd., China) were cultured in a high glucose DMEM (Dulbecco's Modified Eagle Medium)(including 10% fetal bovine serum, penicillin 100 U/ml, streptomycin 100 μg/ml) (Guangzhou Fulbo Biotechnology Co., Ltd., China) in a 5% CO_2 and 37°C incubator. 0.25% trypsin was used for digestion and passage (1:5). Depending on the cell growth condition, 2 to 3 passages were performed weekly. Logarithmic growth phase cells were selected for the experiments.

Expressions of PD-L1 in Lewis lung cancer cells

Lewis lung cancer cells in log phase were collected and centrifuged at 1000 rpm for 5 min. The supernatant was discarded. After resuspending the cells in DMEM, 1 μl of PE-labeled mouse PD-L1 antibody (Shanghai Meilian Bioengineering Co., Ltd., China) was added. The PE-labeled control antibody (Shanghai Meilian Bioengineering Co., Ltd., China) served as an isotype control antibody. After shaking, the reaction was protected from light at 4°C for 30 min, and 3 mL PBS (phosphate buffered saline solution, PH=7.3) (Shanghai Jingke Chemical Technology Co., Ltd., China) was added thereto, followed by centrifugation at 1000 rpm for 5 min. The supernatant was discarded. The cells were resuspended in 0.5 mL of PBS (PH=7.3). Lewis lung cancer cells without any antibody were used as blank controls. Lewis lung cancer cells with 1 μl of PE-labeled control antibody were used as isotype controls. Cell labeling was detected by flow cytometry at PE wavelength.

Expressions of PD-1 in peripheral blood T lymphocytes of C57BL/6 mice

The mice were intraperitoneally injected with propofol 100mg/kg. Then, eyeball was removed to collect whole blood. The blood diluted 1:1 with PBS was added to the lymphocyte separation solution and then centrifuged. The single nuclear cell layer was separated. After washing, it was incubated with FITC-labeled mouse CD3 monoclonal antibody (Shanghai Meilian Bioengineering Co., Ltd., China), and PE-labeled mouse PD-1 antibody for 30 min. The peripheral blood T lymphocytes of mice without any antibody were used as a blank control. The cell labeling was detected by flow cytometry.

Expressions of PD-1 in spleen T lymphocytes of C57BL/6 mice

K57BL/6 mice were anesthetized with ketamine by intraperitoneal injection of 100 mg/kg bw, and sacrificed by cervical dislocation. The body was then soaked in 75% alcohol for 5 minu. The skin and peritoneum of the abdominal junction of the mouse were cut open, and the spleen was taken out and placed on a 200-mesh steel net. Approximately 3 mL of PBS was added and. The splenocyte suspension was collected. The splenocyte suspension was added to the lymphocyte separation solution and centrifuged at 1800 rpm for 5 min. The single nuclear cell layer was separated. After washing, it was incubated with 1 μl of FITC-labeled mouse CD3 monoclonal antibody, and PE-labeled mouse PD-1 antibody for 30 min. 1 μl of PE-labeled control antibody and mouse spleen T lymphocytes without any antibody were used as an isotype control and blank control, respectively. Cell labeling was detected by flow cytometry.

Establishment of ectopic model of Lewis lung cancer in C57BL/6 mice

After culture and passage with DMEM medium containing 100mL/L FCS (fetal bovine serum), Lewis lung cancer cells in log phase were washed twice with PBS and trypsinized for 2~3 min. Digestion was stopped after addition of the medium. The cell fluid was pipetted and

centrifuged at 1000 rpm for 5 ~ 10 min. The supernatant was discarded. The remaining cell solution was washed twice with PBS and repeatedly mixed 5~6 times. The cell suspension was obtained. The cells were counted at 10^7/mL and placed in a 1.5 mL EP (Eppendorf) tube; 0.2 mL of the cell suspension was taken and the inoculated site was wiped with 75% ethanol. C57BL/6 mice were inoculated subcutaneously with a 1 mL disposable syringe. The growth of the tumor was observed. On day 8 post inoculation, the tumor lumps were observed. All the mice were divided into four groups, with six in each group, and were treated with different doses of sPD-L1 Ig (Shanghai Meilian Bioengineering Co., Ltd., China) at day 0, 3, 4, 9. The mice were injected with 2.5 μg, 5 μg and 10 μg sPD-L1 Ig into the abdominal cavity respectively, and mice in the control group were injected with sPD-L1 Ig control protein.

The tumor growth after the injection was observed. At day 5, 7, 9, 11, 14 and 16 post-injection, the long diameter (a) and the short diameter (b) of the tumor were measured with a vernier caliper. The volume was calculated using the following formula: $V=0.4a\times b^2$.

Splenic T lymphocyte subsets in each group of mice

At day 18 after inoculation of the tumor cells, the mice in the 10-μg group and the model control group and mock group were sacrificed. After treatment, the splenocyte suspension was collected and added to 2 mL of lymphocyte separation solution and centrifuged at 1800 rpm for 20 min. The single nuclear cell layer was separated. After washing twice with PBS, the suspension was incubated with 500 μL PBS to adjust the spleen lymphocyte suspension to 5×10^6 cells/mL. 100 uL of the cell suspension in dedicated tubes was used for flow cytometry analysis. Two tubes were prepared for each sample and labeled with FITC and PE two-color fluorescent antibody. The first tube was supplemented with 1 uL of PE-labeled anti-CD3 antibody and 1 μL of FITC-labeled anti-CD4 antibody (Shanghai Meilian Bioengineering Co., Ltd., China). The second tube was supplemented with 1 μL of PE-labeled anti-CD3 antibody and 1 μL of FITC-labeled anti-CD8 antibody (Shanghai Meilian Bioengineering Co., Ltd., China). After incubation for 30 min at room temperature, 500 μL PBS was added to each tube and shaken. The upflow analyzer recorded the proportion of CD3+CD4+ cells and CD3+CD8+ cells of the samples.

Statistical analysis

Continuous data were presented as the mean±standard deviation, or median (1st quartile, 3rd quartile). Differences between variables were examined by Student's *t*-test or Mann-Whitney U test. Statistical analysis was carried out using SPSS 22.0 software. A P value of < 0.05 (two-tailed) was considered statistically significant. $P<0.05$ indicated significant difference.

Table I. *Volume of Lewis lung cancer transplanted tumors in C57BL/6 mice after different levels of sPD-L1 intervention (mm^3).*

Days	sPD-L1 control protein	sPD-L1:2.5ug	sPD-L1:5ug	sPD-L1:10ug
5d	0.68	1.13	1.52	3.43
7d	1.16	12.19	18.82	49.18
9d	2.86	18.33	25.38	62.33
11d	6.28	19.12	28.19	80.82
14d	14.73	22.72	30.22	147.91
16d	29.11	36.28	40.73	185.68

RESULTS

Expressions of PD-L1 in Lewis lung cancer cell lines

As shown in Fig. 1, the PD-L1 on the Lewis lung cancer cell line was positive, and the positive rate was 17.09%.

Expressions of PD-1 on the surface of peripheral blood T lymphocytes in C57BL/6 mice

The positive rate of PD-1 expression on the surface of peripheral blood T lymphocytes of C57BL/6 mice was only 3.23% (Fig. 2).

Expressions of PD-1 on the surface of spleen T lymphocytes in C57BL/6 mice

The PD-1 on the surface of spleen T lymphocytes of C57BL/6 mice was positive, and the positive rate was 18.13% (Fig. 3).

Effects of different levels of sPD-L1 on the growth of Lewis lung cancer transplanted tumors

When the sPD-L1 Ig working dose was 10 μg per mouse, the tumor volume was significantly larger than that in the sPD-L1 control protein group (P <

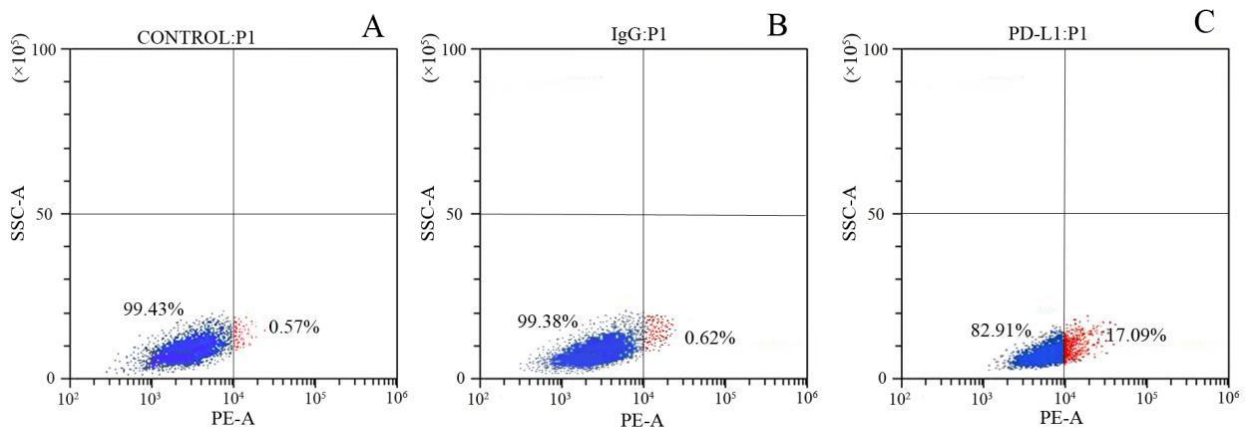

Fig. 1. *Expressions of PD-L1 on the surface of Lewis lung cancer cell lines (IgG and PD-L1 are PE-labeled antibodies). **A**) blank group; **B**) IgG group; **C**) PD-L1 group.*

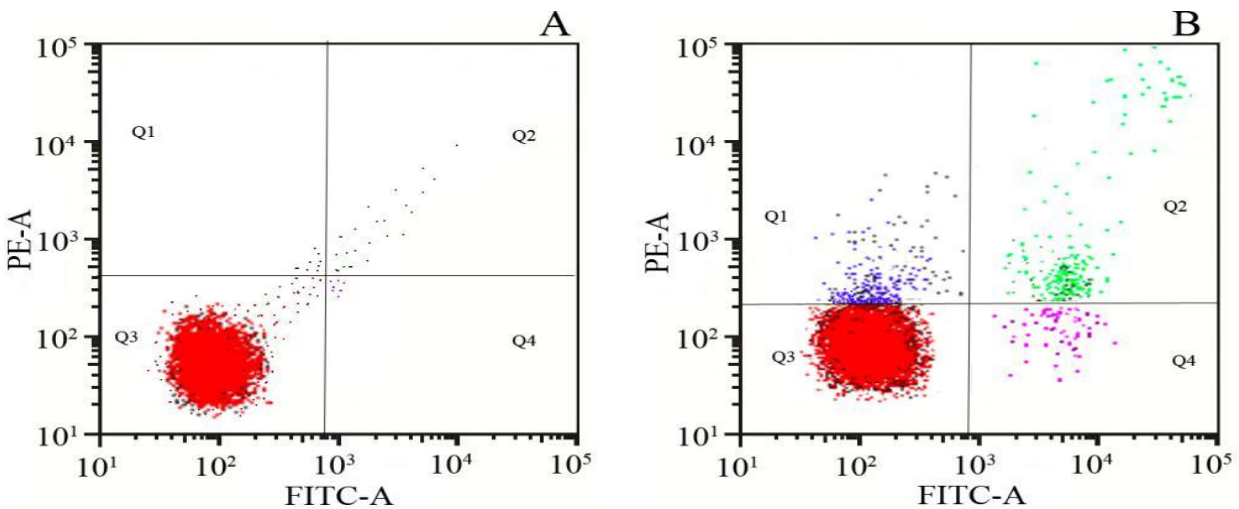

Fig. 2. *Expressions of PD-1 on the surface of peripheral blood T lymphocytes in C57BL/6 mice (PD-1 is a PE-labeled antibody; CD3 is a FITC-labeled antibody). **A**) peripheral blood blank group; **B**) peripheral blood CD3+PD-1 group).*

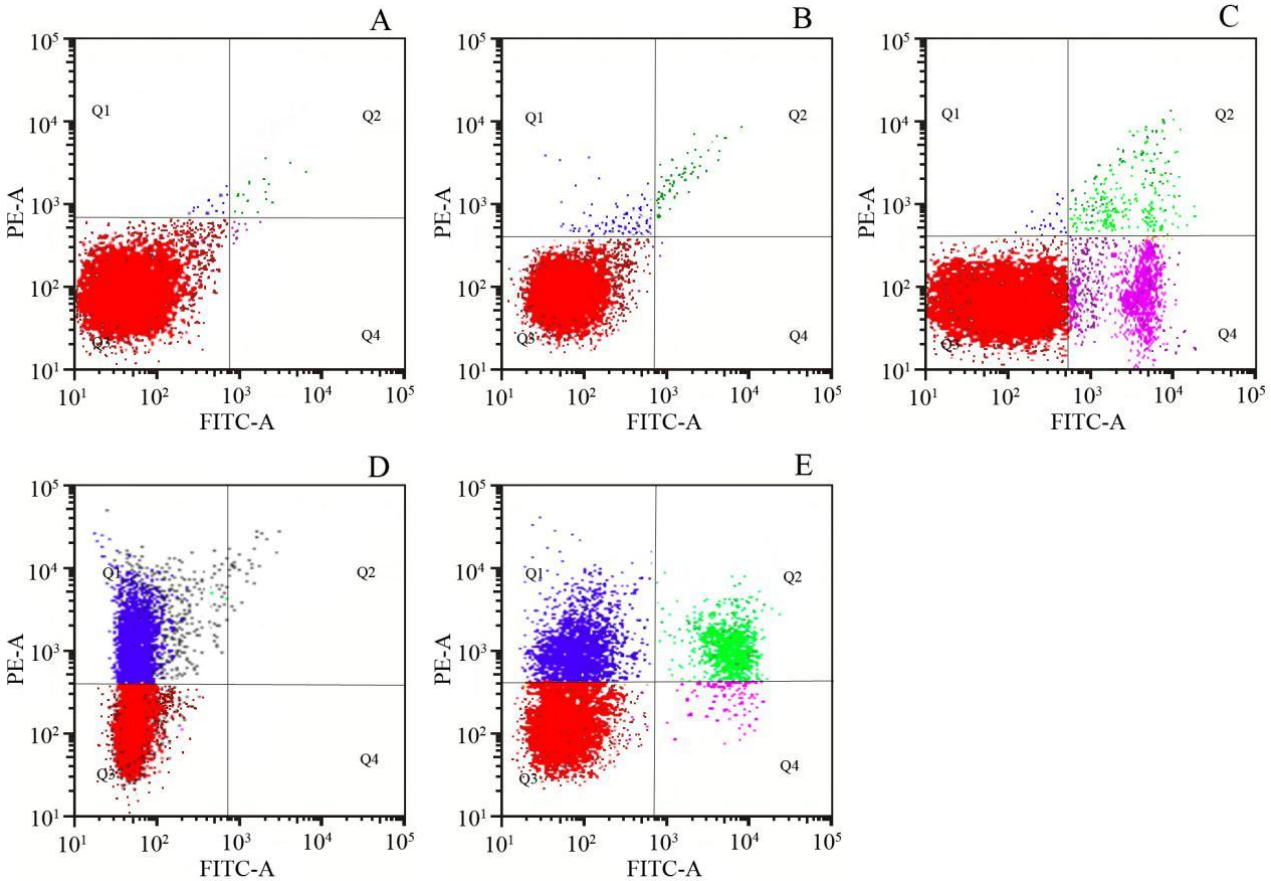

Fig. 3. *Expressions of PD-1 on the surface of spleen T lymphocytes in C57BL/6 mice (IgG and PD-1 are PE-labeled antibodies; CD3 is a FITC-labeled antibody).* ***A)*** *spleen blank group;* ***B)*** *spleen IgG group;* ***C)*** *spleen CD3 group;* ***D)*** *spleen PD-1 group;* ***E)*** *spleen CD3+PD-1 group.*

0.05). When the working dose was 2.5 μg per mouse and 5 μg per mouse, the volume of the tumor was not significantly different from that of the sPD-L1 control protein group (P>0.05) (Table I).

Effects of sPD-L1 on spleen T lymphocyte subsets of mice

On day 18 after inoculation of tumor cells, the CD4/CD8 ratios of normal mice and sPD-L1 control protein mice were 1.94 and 1.89, respectively. The CD4/CD8 ratio of sPD-L1 10 μg/mouse was 1.59.

DISCUSSION

T cell-mediated cellular immunity plays a very important role in human immune response (8). Previous studies found that sPD-L1 can exert negative immunomodulatory effects by binding with PD-1 receptors on the surface of T lymphocytes and B lymphocytes (9, 10). It has been (11) shown that sPD-L1 can inhibit T lymphocyte function and promote tumor growth.

Our results showed that the PD-L1 on the Lewis lung cancer cell line was positive. The PD-L1, receptor of PD-1, was confirmed to be positively expressed on the surface of spleen T lymphocytes of C57BL/6 mice. The PD-1 expression was also detected on the surface of peripheral blood T lymphocytes. Our results showed that compared with the sPD-L1 control protein group, the volume of Lewis lung cancer transplanted tumors with a sPD-L1 Ig working dose of 10 μg/mouse was significantly increased (P<0.05). When the working dose was 2.5 μg/mouse and 5 μg/mouse, the volume of Lewis lung transplanted tumors was not significantly

different from that of sPD-L1 control protein group ($P>0.05$). The underlying mechanism could be that a certain threshold level of sPD-L1 molecules inhibited PD-1+ T cells through the PD-1/sPD-L1 pathway. The inhibition of killing function of T lymphocytes could lead to the apoptosis of tumor-specific T cells.

In summary, different doses of soluble PD-L1 have different effects on the growth of Lewis lung transplanted tumors. A certain threshold level of soluble PD-L1 could promote the growth of transplanted tumors of Lewis lung cancer in C57BL/6 mice.

REFERENCES

1. Yang X, Brunham R. T lymphocyte immunity in host defence against Chlamydia trachomatis and its implication for vaccine development. Can J Infect Dis 1998; 9(2):99-108.
2. Podshivalova K, Salomon DR. MicroRNA regulation of T-lymphocyte immunity: modulation of molecular networks responsible for T-cell activation, differentiation, and development. Crit Rev Immunol 2013; 33(5):435-76.
3. Goto T, Nishida T, Takagi E, et al. Programmed Death-Ligand 1 on Antigen-presenting Cells Facilitates the Induction of Antigen-specific Cytotoxic T Lymphocytes: Application to Adoptive T-Cell Immunotherapy. J Immunother 2016; 39(8):306-15.
4. Kassardjian A, Shintaku PI, Moatamed NA. Expression of immune checkpoint regulators, cytotoxic T lymphocyte antigen 4 (CTLA-4) and programmed death-ligand 1 (PD-L1), in female breast carcinomas. PLoS One 2018; 13(4):e0195958.
5. Teng F, Meng X, Kong L, et al. Tumor-infiltrating lymphocytes, forkhead box P3, programmed death ligand-1, and cytotoxic T lymphocyte-associated antigen-4 expressions before and after neoadjuvant chemoradiation in rectal cancer. Transl Res 2015; 166(6):721-32.
6. Kawazoe A, Kuwata T, Kuboki Y, et al. Clinicopathological features of programmed death ligand 1 expression with tumor-infiltrating lymphocyte, mismatch repair, and Epstein–Barr virus status in a large cohort of gastric cancer patients. Gastric Cancer 2017; 20(3):407-15.
7. Sangkhamanon S, Jongpairat P, Sookprasert A, et al. Programmed Death-Ligand 1 (PD-L1) expression associated with a high neutrophil/lymphocyte ratio in cholangiocarcinoma. Asian Pac J Cancer Prev 2017; 18(6):1671-74.
8. Mansfield AS, Aubry MC, Moser JC, Harrington SM, Dronca RS, Park SS, Dong H. Temporal and spatial discordance of programmed cell death-ligand 1 expression and lymphocyte tumor infiltration between paired primary lesions and brain metastases in lung cancer. Ann Oncol 2016; 27(10):1953-58.
9. Kozako T, Yoshimitsu M, Akimoto M, et al. Programmed death-1 (PD-1)/PD-1 ligand pathway–mediated immune responses against human T-lymphotropic virus type 1 (HTLV-1) in HTLV-1-associated myelopathy/tropical spastic paraparesis and carriers with autoimmune disorders. Hum Immunol 2011; 72(11):1001-6.
10. Birtas A E, Tarkun P, Demirsoy ET, et al. Soluble programmed death 1 (PD-1) Is decreased in patients with immune thrombocytopenia (ITP): potential involvement of PD-1 pathway in ITP immunopathogenesis. Clin Appl Thromb Hemost 2016; 22(3):248-51.
11. Hasita H, Ma C, Yano H, et al. An IL-27/Stat3 axis induces expression of programmed cell death 1 ligands (PD-L1/2) on infiltrating macrophages in lymphoma. Cancer Sci 2016; 107(11):1696-704.

LETTER TO THE EDITOR

EXPRESSION OF RNF8 ON COCHLEAR APOPTOSIS AND AGING IN MICE OF DIFFERENT AGES

TT. LI, P. XU, ZG. BAI, ZT. CUI, XG. CAI and B. ZHOU

Department of Otorhinolaryngology, The Fourth Affiliated Hospital of Harbin Medical University, Harbin, Heilongjiang, China

Received November 18, 2018 – Accepted January 21, 2018

This study aimed to investigate the role of RNF8 (RING finger protein 8) in DNA damage repair in mice of different ages, and to provide new insight into the pathology and treatment of senile deafness. Sixteen C57BL/6J mice aged 8 weeks, 16 weeks and 32 weeks were obtained by paired reproduction. The mice of three age groups were equally divided into two groups, named experimental group (RNF8 gene knockout) and control group (no knockout). The cochlear hair cells, stria vascularis and spiral ganglion cells were observed by HE (hematoxylin-eosin) staining. The degree of DNA damage and the related expressions were observed by immunofluorescence γ-H2AX staining and 8-OH immunohistochemical staining, and the aging of damaged cells was detected by lipofuscin and β-galactosidase staining. HE staining showed that the changes of cochlear hair cells, stria vascularis and spiral ganglion cells were obvious in the same group of mice at different ages. Compared with the control group, the aging changes of cochlear hair cells, stria vascularis and spiral ganglion cells were more significant in the experimental group. Immunofluorescence γ-H2AX staining showed H2AX phosphorylation in injured cells. The aging of cochlea in mice changed, and staining of β-galactosidase in the experimental group suggested that the striae of blood vessels were changed with age at 32 weeks old and staining of lipofuscin showed dark brown staining around the nucleus ($P < 0.05$). In conclusion, the deletion of RNF8 is an important cause of morphological changes in the cochlea of mice. The deletion of RNF8 accelerates the aging of the cochlea of mice, suggesting that the apoptosis of the cochlea could contribute to aging in RNF8 gene-deficient mice.

To the Editor,

Senile deafness is the aging manifestation of binaural, progressive and aging hearing impairment in aging organisms, and it is also a typical manifestation of the aging process in auditory organs (1). The symptoms and signs of aging are highly individualized, and increasing evidence indicates that the onset time of senile deafness does not have a clear boundary (2). Therefore, early prevention and early treatment of senile deafness are very important. The mechanism of cochlear aging has not yet been fully elucidated (3, 4). Molecular studies have found that nuclear gene ahl2 may be associated with early-onset senile deafness and ahl3 is associated with late-onset senile deafness (5).

Many studies have reported that targeted silencing of RNF8 can increase the sensitivity of cell therapy (6-8), therefore RNF8 could be the next key solution for the cochlear aging problem in the DNA damage response (DDR) network (9). In this study, the

Key words: RNF8 gene; DNA damage repair; cochlea; aging

Corresponding Author:
Dr Bin Zhou,
Department of Otorhinolaryngology,
The Fourth Affiliated Hospital
Harbin Medical University,
No. 37 Yiyuan Street, Nangang District,
150001, Harbin, Heilongjiang, China
e-mail: zhoubin3358@126.com

0393-974X (2019)

natural aging mouse model by knocking out RNF8 gene was established, and the cochlear hair cells, stria vascularis and spiral ganglion of experimental animals were harvested and detected by biological techniques. By analyzing their morphological and qualitative indexes of aging, we evaluated the effect of RNF8-knockout on the mice cochlea aging and its potential mechanism. Our study could provide a novel and precise therapeutic target for hearing in aging.

MATERIALS AND METHODS

Animals

Sixteen C57BL/6J mice aged 8 weeks, 16 weeks and 32 weeks were obtained by paired reproduction (Beijing Weitong Lihua Laboratory Animal Technology Co., Ltd., China). The mice of the three age groups were equally divided into two groups (8 mice in each age group), named experimental group (RNF8 gene knockout) and control group (no knockout). The feeding conditions of mice were as follows: room temperature 19-24°C, noise less than 60 dB, humidity 50-60%, illumination 12h/d, autoclave sterilization of feed, and strictly-pasteurized drinking water. The animal experiment procedures were in accordance with the International Regulations on Animal Protection and Management and was approved by the ethics committee of The Fourth Affiliated Hospital of Harbin Medical University.

Primer design

Promega kit (Shanghai Sixin Biotechnology Co., Ltd., China) was used to extract DNA from target mice and amplify target genes. The primers were designed as follows: RNF8-control group: 5'-TGACCTTGCAGCCATTAGGGAGATT-3'; RNF8-experimental group: 5'-AGACCTTGGGACCACCTCATCAGAA-3'.

Material preparation

After routine disinfection, mice were anesthetized by intraperitoneal injection of 2% pentobarbital sodium (Beijing Chemical Plant Co., Ltd., China) 40-50mg/kg. After anesthesia, the left ventricle was perfused with 0.9% normal saline and 4% paraformaldehyde (Beijing Chemical Plant Co., Ltd., China). After successful perfusion, the brain tissue of mice was removed. The cochlea was separated and fixed in a tubule containing 4% poly-formaldehyde. After 8 h, the attached muscles and bones were removed, the ossicles were removed, and the cochlea was exposed. The cochlear top was broken by fine needling, so that the cochlea could be fixed adequately with the fixed solution. The fixed cochlea was replaced by decalcification, dehydration, paraffin and xylene (Pengcheng Biological Co., Ltd., China), then soaked with soft wax and placed on the base of the embedding box. After pouring hard wax into the wax block, the cochlea was maintained for 24 h (Thermo Fisher Scientific, USA) at –25°C. Before section, 0.5-0.6 cm wax was removed horizontally from the top of the wax block with a knife and the base of the embedding box and unwanted bone tissues were also removed. The sections were paraffin fixed or frozen for regular slicing and baking.

HE staining

Different sections of paraffin-fixed mouse cochlea were used. They were dehydrated with 55%, 75%, 85%, 95% and 100% ethanol; the sections were treated with xylene twice; re-hydrated with absolute ethanol (Beijing Chemical Plant Co., Ltd., China) twice; dehydrated with 95%, 85% and 75% ethanol; washed briefly in distilled water; stained in hematoxylin (Shanghai Maikun Chemical Co., Ltd., China) for 8 min; differentiated in 1% hydrochloric (Beijing Chemical Plant Co., Ltd., China) alcohol for 30 s; washed in running tap water; stained in eosin for 2 min; re-hydrated with absolute ethanol twice; and treated with xylene twice. After staining, the slices were placed under neutral gum and then observed under a microscope.

γ-H2AX immunofluorescence staining

The slices were dewaxed with xylene twice; dehydrated with 100%, 95%, 85%, 75% ethanol twice; washed briefly in distilled water; and fixed by 4% PA (Paraformaldehyde). After washing with PBS (Phosphate buffered solution) (TaKaRa Biological Co., Ltd., Japan), the slices were sealed in goat serum working fluid at 37°C, and the blocking solution was discarded. Primary antibody γ-H2AX (Kehao Biological Co., Ltd., China) was added and they were incubated overnight at 4°C. After PBS washing, they were incubated at 37°C for 1 h after adding second antibody CY3. After PBS washing, DAPI (4',6-diamidino-2-phenylindole) was added and washed by PBS. The sections were sealed with fluorescence attenuation professional seal liquid and observed under a fluorescence microscope (Olympus, Japan).

8-OH immunohistochemical staining

The slices were dewaxed with xylene twice; dehydrated with 100%, 95%, 85%, 75% ethanol twice; washed briefly in distilled water; fixed in 9.4% PA; washed by PBS and incubated at room temperature with 0.3% hydrogen peroxide. Antigen was repaired after PBS washing, and CB (0.01M Ph6.0 Citrate buffer) was

boiled under high pressure and cooled to room temperature. After PBS washing, they were sealed with goat serum working fluid at 37°C; primary antibody was added and the slices were incubated for overnight at 4°C. After PBS washing, second antibody was added and the slices were incubated at 37°C. Following PBS washing, SABC (Strept avidin-biotin complex) was added and they were incubated at 37°C. DAB (3,3'-diaminobenzidin) was washed in 0.1 M TrisCl, and stained, dehydrated and transparent after rinsing with clean water. Neutral gum was observed under a microscope (Nikon, Japan) after sealing.

Detection of aging by β-galactosidase staining

The slices were dewaxed with xylene twice; dehydrated with 100%, 95%, 85%, 75% ethanol twice; washed briefly in distilled water; fixed solution of β-galactosidase staining was added, and incubated overnight at 37°C. They slices were observed under a microscope after neutral gum sealing.

Cochlear lipofuscin staining

The slices were routinely dewaxed; rinsed with distilled water for three times, and covered with fuchsin staining solution overnight at room temperature. After rinsing with distilled water, they were differentiated into transparent background with long acid differentiation solution; after rinsing with distilled water, they were re-stained with methylene blue nuclei; after rinsing with acetic acid, they were dehydrated and made transparent; after sealing with neutral gum, they were observed under a microscope.

Statistical analysis

SPSS 19.0 software was used for statistical analysis. The data were presented by mean ± standard deviation. The difference between continuous variables obeying normal distribution was tested by Student's *t*-test. A P-value (two-tailed) of <0.05 was considered statistically significant.

RESULTS

Morphological changes of cochlea in the two groups

HE staining results showed that hair cells of 8-week-old mice in the two groups were well arranged, uniformly stained, orderly arranged, and had no nuclear deletion. The number of hair cells in the basal gyrus of the 16-week-old mice in the control group decreased compared with the 8-week-

Table I. *Comparisons of three-cycle hair cell count, stria vascularis thickness and spiral ganglion results in cochlear sections of mice between the two groups (`x±s).*

		8 weeks old			16 weeks old			32 weeks old		
		Top	Middle	Bottom	Top	Middle	Bottom	Top	Middle	Bottom
Control group	The number of three hair cells	24±2		24±2	23±2		242	17±1	15±1	13±1
Experimental group		22±2		22±2	21±2		202	13±1	11±1	7±1
P			>0.05			<0.05			<0.05	
Control group	Stria striae thickness		12±1			10±0.5			7±1	
Experimental group			11±1			7±0.5			6±0.5	
P			>0.05			<0.05			<0.05	
Control group	Spiral ganglion of cochlea		24±2			19±2			13±1	
Experimental group			22±2			13±1			7±2	
P			>0.05			<0.05			<0.05	

old mice; the number of hair cells in the 32-week-old mice decreased compared with the 16-week-old mice, and some hair cells were arranged disorderly, stained unevenly, and had nuclear deletion; the number of hair cells in the cochlea of 16-week-old mice decreased compared with the 8-week-old mice; the number of hair cells in 32-week-old mice was sparse compared with the 16-week-old mice, and most hair cells were disorderly arranged, unevenly stained, and the loss of nuclei was obvious, as shown in Fig. 1A and Table I.

HE staining results showed that the stria vascularis of 16-week-old mice in the control group was thinner than that of 8-week-old mice in the marginal cell layer and sparse in the middle cell layer. Compared with 16-week-old cells, 32-week-old cells showed a decrease in the number of three layers. The size of nuclei was not uniform, and the staining was uneven and the nuclei were missing. The stria vascularis of the cochlea of 16-week-old mice showed a decrease in the number of three layers of cells, thinning and

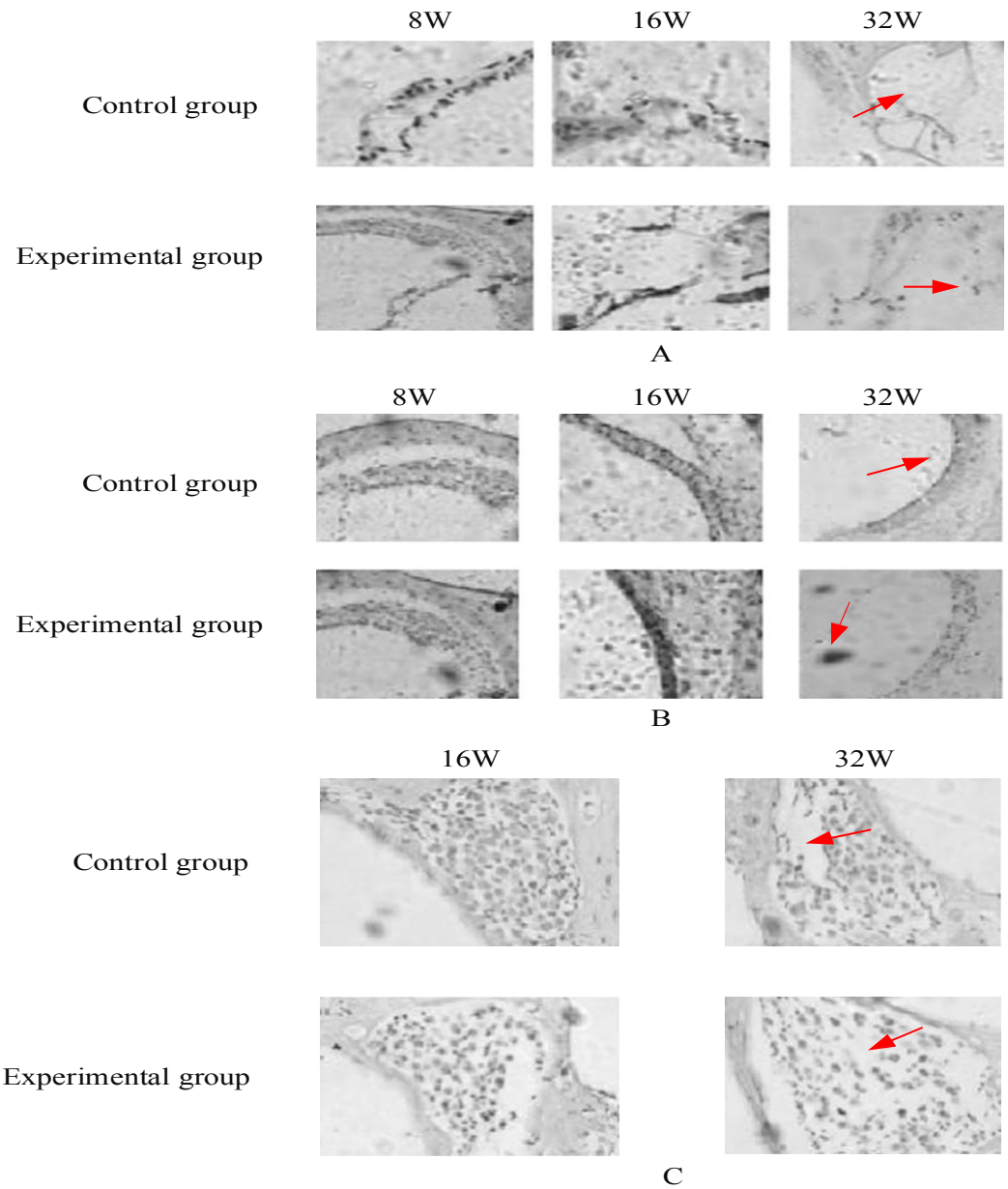

Fig. 1. *Comparison of HE staining of mice in two groups. **A**) hair cells; **B**) striated cells; **C**) spiral ganglion cells) (20X)*

abnormal rupture of the marginal layer compared with the 8-week-old mice. Compared with the 16-week-old three-layer structure, 32-week-old cells showed a decrease in the number, irregular cell arrangement, uneven nuclear staining, three-layer separation of stria vascularis and serious breakage of marginal layer, as shown in Fig. 1B and Table I.

HE staining results showed that the number of cochlear spiral ganglion cells in the 16-week-old mice decreased compared with the 8-week-old mice. Compared with 16-week-old cells, 32-week-old cells showed a decrease in number, disordered arrangement, not uniform nuclei size and nuclear deletion. The number of cochlear spiral ganglion cells decreased and slight fissures appeared in 16-week-old mice compared with the 8-week-old mice. Compared with 16-week-old cells, 32-week-old cells were sparse, mostly disorderly arranged, with not uniform size of nuclei, uneven staining, obvious nuclear deletion, and serious fissures, as shown in Fig. 1C and Table I.

Overall, compared with the 8-week-old mice, the 16-week-old mice showed different aging changes in cochlear hair cells, stria vascularis and spiral ganglion. Hair cell loss was more obvious, while changes of stria vascularis and spiral ganglion were not apparent. The age-related changes of hair cells, stria and spiral ganglia were more significant at 32-week-old mice compared with the 16-week-old mice. Compared with the cochlea of mice in the RNF8 control group, the aging changes of hair cells, stria vascularis and spiral ganglion in the cochlea of the RNF8 experimental group were greater at the age of 16 weeks and 32 weeks.

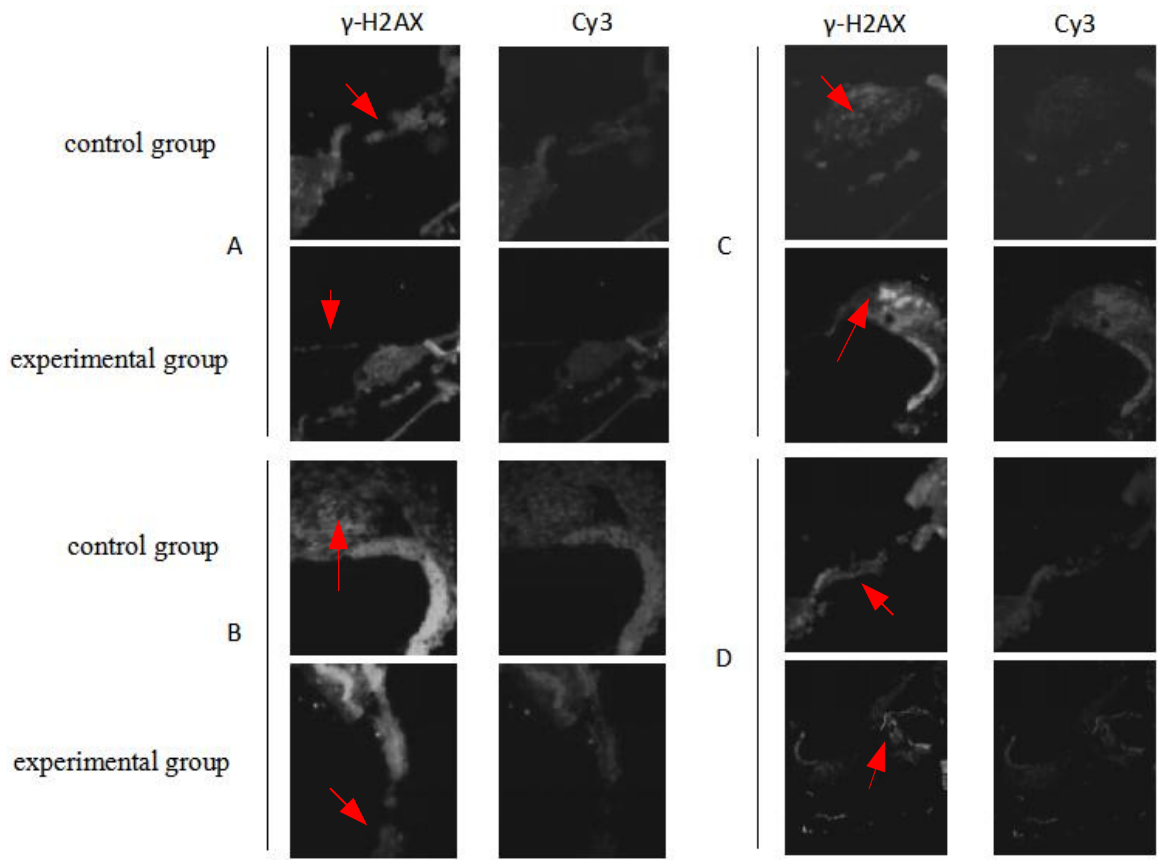

Fig. 2. *The comparison results of γ-H2AX staining in 32-week-old mice of the two groups.* ***A)*** *Cochlear hair cells γ-H2AX staining;* ***B)*** *stria γ-H2AX staining;* ***C)*** *spiral ganglion γ-H2AX staining;* ***D)*** *Cochlear γ-H2AX staining) (40X).*

Damage and aging of cochlea tissues in two groups of mice

The results of γ-H2AX immunofluorescence staining showed that the cochlea of 8-week-old mice in the control group showed no difference and little color; the 16-week-old mice only had little color shown at the bottom; there were varying degrees of color in the 32-week-old mice. There was no significant change in the cochlea of 8-week-old mice. Multiple bright spots appeared in the 16-week-old mice, and bright spots were densely distributed in the 32-week-old mice. The changes of hair cells and stria vascularis were more significant, while the spiral ganglion was more concentrated, as shown in Fig.2.

The results of 8-OH immunohistochemical staining showed that there was no obvious change in parietal gyrus, middle gyrus and basal gyrus of cochlear hair cells in the control group, but positive cells were detected in stria vascularis and spiral ganglion of the 32-week-old mice. There was no obvious change in parietal gyrus, middle gyrus and basal gyrus of cochlear hair cells in the experimental group, and positive cells were distributed in different degrees in the 32-week-old mice. There were a large number of positive cells in the stria vascularis and spiral ganglion with aging changes, as shown in Fig. 3A.

The results of aging test with β-galactosidase staining showed that there was no obvious change in the three cycles of cochlear hair cells in the 8-week-old and 16-week-old control group mice, and there were a few black spots and uneven distribution in the three cycles of 32-week-old mice. There was an increase in the number of black spots in the stria vascularis along with age changes, which were obvious in the

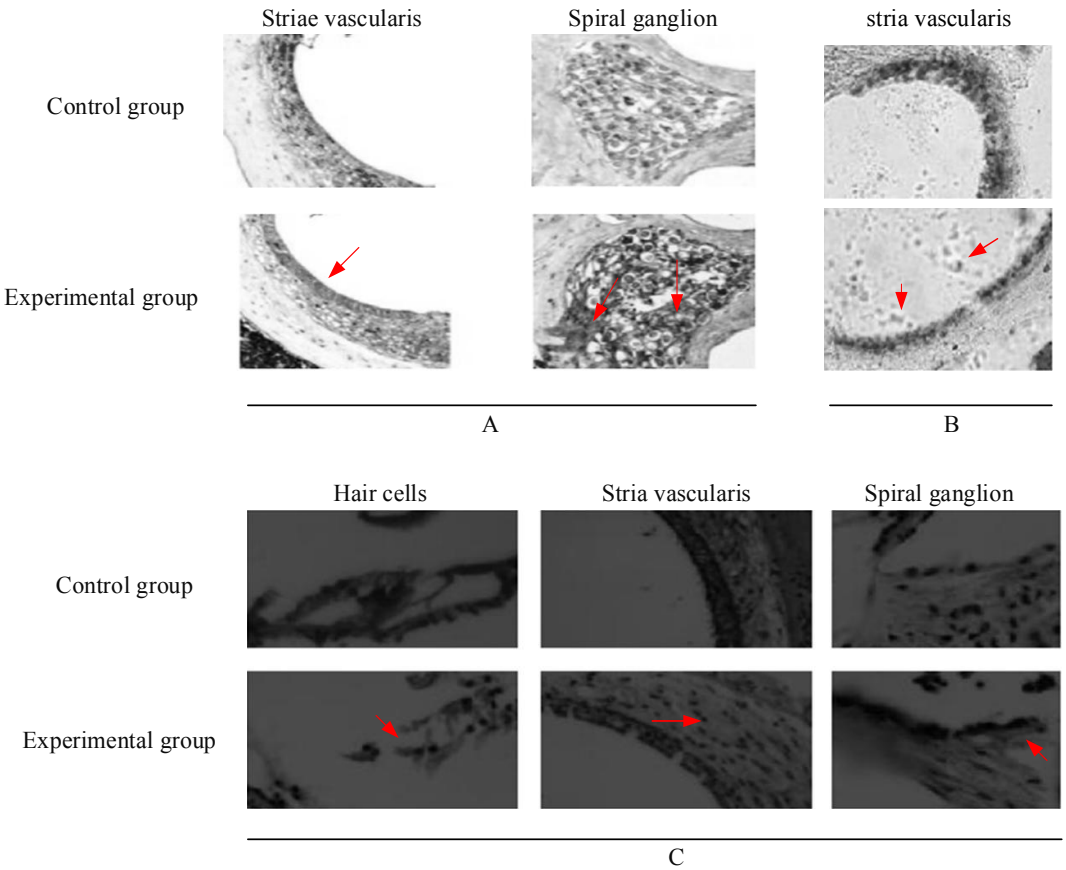

Fig. 3. *Comparison of staining in 32-week-old mice between the two groups. **A**) stria vascularis, spiral ganglion 8-OH immunohistochemical staining; **B**) stria β-galactosidase staining; **C**) hair cells, stria vascularis, and spiral ganglion lipofuscin aging change staining) (20X).*

mice aged 32 weeks. There was no obvious change in spiral ganglion. There were many black spots in the cochlea hair cells of the experimental group. The black spots of stria vascularis increased with aging, especially at 32 weeks old, and were densely distributed in the marginal layer and extended to the middle layer. The spiral ganglion only had scattered black spots, as shown in Fig. 3B.

The results of cochlear lipofuscin staining showed that there was no obvious change in cochlear hair cells, stria vascularis and spiral ganglion of mice aged 8 weeks and 16 weeks in the control and experimental groups. In the 32-week-old control group mice, the intercellular staining of hair cells was darker, and the changes of marginal and intermediate layers of stria vascularis were more evident. In the 32-week-old experimental group mice, the hair cells were sparse, most of which were disorderly arranged, and the nuclei were not uniform in size and uneven in staining. The marginal layer of stria vascularis was more obvious, stratified and dyed aggravated, as shown in Fig. 3C.

DISCUSSION

The structural features of cells and tissues are the basis of morphology. Many studies have shown that RNF8 deficiency caused neurodegenerative changes (10, 11). DNA damage accumulation triggers the apoptosis of cells. This accumulation to a certain extent can lead to pathological changes, such as morphological changes, reduction of number, etc., and hence affect physiological function. C57BL/6J mice are a kind of aging mice with congenital genetic defects. Their audiological changes with age are very similar to the clinical manifestations of senile deafness, so they have already been used as a mature animal model in the study of senile deafness. The loss of RNF8 indirectly affects the physiological function of the cochlea (12). The deletion of RNF8 in C57BL/6J mice is different from that in wild-type mice at different ages, suggesting that the effect of RNF8 on the structure of cochlea may be different at different time periods. In addition, there are obvious differences in the main structure of cochlear aging in mice with RNF8 deletion. The function of RNF8 gene has been clearly linked to DNA damage and neurodegeneration, and the molecular mechanism underlying the primary interaction between DNA damage and repair upstream and downstream has also been explored.

In conclusion, RNF8 deletion is one of the important causes of morphological changes in the cochlea of mice, and it also indirectly affects the physiological function of the cochlea. The different effects of RNF8 on the aging of cochlear structures in mice are closely related to the clinical manifestations of senile deafness. The apoptosis of cochlea in RNF8-deficient mice is closely related to aging.

ACKNOWLEDGEMENTS

This work was supported by Heilongjiang Youth Funding Project (No. QC2011C029)

REFERENCES

1. Chien WW, Isgrig K, Roy S, et al. Gene therapy restores hair cell stereocilia morphology in inner ears of deaf whirler mice. Mol Ther 2016; 24(1):17-25.
2. Buret L, Delprat B, Delettre C. Loss of function of Ywhahin mice induces deafness and cochlear outer hair cells' degeneration. Cell Death Dis 2016; 2(4):e2187.
3. Ng L, Liu H, St Germain DL, Hernandez A, Forrest D. Deletion of the thyroid hormone-activating type 2 deiodinase rescues cone photoreceptor degeneration but not deafness in mice lacking type 3 deiodinase. Endocrinology 2017; 158(6):1999-2010.
4. Jaarsma D, van der Pluijm I, de Waard MC, et al. Age-related neuronal degeneration:complementary roles of nucleotide excision repair and transcription-coupled repair in preventing neuropathology. PLoS Genet 2011; 7(12):e1002405.
5. Patuzzi R. Ion flow in stria vascularis and the production and regulation of cochlear endolymph and the endolymphatic potential. Hear Res 2011; 277(1-2):4-19.
6. West T, Ashmore J. A model of ionic transport and osmotic volume control in cochlear outer hair cells. Interface Focus 2014; 4(6):20140018.
7. Requena T, Gallego-Martinez A, Lopez-Escamez JA. Bioinformatic integration of molecular networks

and major pathways involved in mice cochlear and vestibular supporting cells. Front Mol Neurosci 2018; 11:108.
8. Huang X, Dixit VM. Drugging the undruggables: exploring the ubiquitin system for drug development. Cell Res 2016; 26(4):484-98.
9. Kinoshita M, Sakamoto T, Kashio A, Shimizu T, Yamasoba T. Age-Related hearing loss in Mn-SODHeterozygous Knockout Mice. Oxid Med Cell Longev 2013; 2013:325702.
10. Kurima K, Ebrahim S, Pan B, et al. TMC1 and TMC2 Localize at the site of mechanotransduction in mammalian inner ear hair cell stereocilia. Cell Rep 2015; 12(10):1606-17.
11. Taylor R, Bullen A, Johnson SL, et al. Absence of plastin 1 causes abnormal maintenance of hair cell stereocilia and a moderate form of hearing loss in mice. Hum Mol Genet 2015; 24(1):37-49.
12. Nolan LS, Cadge BA, Gomez-Dorado M, Dawson SJ. A functional and genetic analysis of SOD2 promoter variants and their contribution to age-related hearing loss. Mech Ageing Dev 2013; 134(7-8):298-306.

LETTER TO THE EDITOR

EFFECTS OF TRASTUZUMAB AND LAPATINIB ON HER2 POSITIVE BREAST CANCER TREATMENT

W. JIA[1] and TZ. WANG[2]

[1]Department of Clinical Pharmacy, Tonglu First People's Hospital, Zhejiang, Tonglu, Hangzhou, Zhejiang, China; [2]Department of Orthopedics, Tonglu First People's Hospital, Tonglu, Hangzhou, Zhejiang, China

Received November 289, 2018 – Accepted January 16, 2019

This study aimed to evaluate the clinical efficacy of trastuzumab combined with lapatinib in the treatment of human epidermal growth factor receptor 2 (HER2) positive breast cancer. One hundred and fifty-four patients with breast cancer were randomly divided into a trastuzumab group (group A, 52 cases), a lapatinib group (group B, 48 cases) and a combination group (group C, 54 cases). The patients from group A received trastuzumab 4 mg/kg intravenously once a week in the first 9 weeks, and 2 mg/kg iv in the second 9 weeks. The patients from group B took lapatinib 1.5 g orally once per day. The patients from group C received the combination of 4 mg/kg intravenously once a week in the first 9 weeks, and 2 mg/kg iv trastuzumab (the same doses as in group A) in the second 9 weeks and 1.5 g lipatinib orally per day for 18 weeks. After treatment, the clinical efficacy of the treatments in the three groups was observed, and the progression free survival (PFS), overall survival (OS), central nervous system (CNS), overall response rate (ORR), clinical Benefit Response (CBP) and adverse reactions were compared before and after treatment. After treatment, PFS of group A, group B and group C were 44, 42 and 58 months, respectively. PFS of group C was significantly higher compared with that of group A and group B (P<0.05). After treatment, during follow-up, OS in group A, group B and group C were 28, 20 and 22 months, respectively. After treatment, the CNS metastasis rate in group C was significantly lower than that in group A and group B (P<0.05). ORR and CBR in group C were higher than those in group A and group B (P<0.05). The incidence of adverse reactions in group C was significantly lower than that in group A and group B (P<0.05). In conclusion, the potency of lapatinib combined with trastuzumab in the treatment of HER2 positive breast cancer patients is superior to treatment with lapatinib or trastuzumab only.

To the Editor,

Breast cancer with a complex etiology is one of the most common malignant tumors in women (1). The incidence of breast cancer accounts for 7-10% of all types of malignant tumors and is the second cause of cancer in women after uterine cancer (2). It usually affects breast epithelial tissue and has a negative influence on women's physical and mental health (3). Research has shown that human epidermal growth factor receptor 2 (HER2) gene overexpression is associated with relatively poor prognosis of breast cancer, and molecular targeted therapy can be an efficient treatment option (4, 5). Trastuzumab is a specific humanized monoclonal

Key words: trastuzumab; lapatinib; HER2 positive breast cancer; progression-free survival; overall survival

Corresponding Author:
Dr Wei Jia,
Tonglu First People's Hospital,
No. 338 Xuesheng Road,
Tonglu, Hangzhou,
Zhejiang, 311500, China
e-mail: jiaweipharmacy@163.com

0393-974X (2019)

DISCLOSURE: ALL AUTHORS REPORT NO CONFLICTS OF INTEREST RELEVANT TO THIS ARTICLE.

antibody targeting the extracellular domain of HER2 that could significantly improve the 5-year disease-free survival rate and overall survival rate of HER2-positive breast cancer patients (6). Lapatinib is a new antitumor drug for breast cancer that acts through a different mechanism of action than trastuzumab. It has a dual-target mechanism by inhibiting the tyrosine kinase receptor which acts on 2 growth factor receptors - EGFR (epidermal growth factor receptor) and HER2 (7). Lapatinib can inhibit the activation of MAPK and AKT, which are the downstream effectors of EGFR and HER2, reduce the excessive signal in transduction pathway, accelerate the apoptosis of tumor cells, and inhibit cell growth (8). This study aimed to evaluate the efficacy of monotherapy with lapatinib or trastuzumab alone and their combination in the treatment of HER2 positive breast cancer.

MATERIALS AND METHODS

Patients

The study included 261 patients from Tonglu First People's Hospital diagnosed with breast cancer between February 2015 and July 2018. The course of the disease ranged from 5 months to 45 months. The study was approved by the Ethics Committee of Tonglu First People's Hospital and all the patients signed an inform consent to participate in the study.

Inclusion criteria: The patient had been diagnosed with HER2 positive breast cancer; tumor size ≥2cm, and heart, liver, kidney, bone marrow and other organs function normal; LVEF (Left Ventricular Ejection Fractions) ≥50%; patients with a Eastern Cooperative Oncology Group Performance Status of 0 to 2 grades; patients agreed to receive lapatinib or/and trastuzumab treatment and signed the informed consent; no recurrent or progressive diseases had been treated with cytotoxic or biological agents before treatment; survival ≥12 months.

Exclusion criteria: patients receiving other anti-tumor drugs during treatment; patients with serious adverse reactions during treatment; patients with other major diseases; survival less than 12 months.

Therapeutic regimen

Two hundred and sixty-one patients with breast cancer were randomly divided into a trastuzumab group (group A, 52 cases), a lapatinib group (group B, 48 cases) and a combination group (group C, 54 cases).

In group A, trastuzumab (Herceptin, Roche Pharma (Schweiz) Ltd., USA, 440mg (20mL)/bottle) was injected intravenously once a week, 4 mg/kg in the first 9 weeks and 2 mg/kg in the second 9 weeks.

In group B, the patients received 1.5g lapatinib (Tykerb, Glaxo Group Limited, UK, 0.25g/tablet) (6 tablets of 0.25g) once per day for 18 weeks.

In group C, the patients received 1.5g lapatinib (Tykerb, Glaxo Group Limited, UK, 0.25g/tablet) (6 tablets of 0.25g) once per day in combination with trastuzumab (Herceptin, Roche Pharma (Schweiz) Ltd., USA, 440mg (20mL)/bottle) intravenously injected once per week in doses of 4 mg/kg in the first 9 weeks, and 2 mg/kg in the second 9 weeks.

The response of the treatment was evaluated by complete response (CR), partial response (PR), progressive disease (PR), stable disease (SD), recovery rate and control rate. The recovery rate and control rate were calculated using the following formulas:

Recovery rate=(CR+PR)/ Total number of cases

Control rate=(CR+PR+PD)/ Total number of cases

For each patient included in the study was calculated the PFS (Progression-free survival), OS (overall survival), ORR (objective response rate) and CBR (clinical benefit rate) (9) were calculated. CNS (central nervous system) metastasis was evaluated by MRI (magnetic resonance imaging) or CT (computed tomography).

Statistical analysis

Statistical software SPSS19.0 was used to analyze the data, single weighting method was used to analyze the clinical efficacy, and Kaplan-Meier method was used to evaluate PFS, OS and other conditions. The difference was statistically significant when $P<0.05$.

RESULTS

Clinical efficacy

The recovery rate and the control rate after the treatment was significantly increased in group C treated with the transtuzumab plus lapatinib compared to group A and group B ($P<0.05$ and $P<0.01$, respectively) (Table I).

Comparison of PFS and OS between the groups

After treatment, PFS of group A, group B and group C were 44, 42 and 58 months, respectively. There was no significant difference between group A and group B. In group C, PFS was significantly longer than that of group A and group B (P<0.05) (Fig.1A). During the follow-up period, OS of group A, group B and group C were 28, 20 and 22 months, respectively (Fig.1B).

CNS metastasis status, ORR and CBR in each group

There was no statistical significant difference in the metastasis rate of CNS between groups A and B after treatment (P>0.05), but in group C the metastasis rate was significantly lower than that in groups A and B (P<0.05) (Table II).

There was no significant difference in the level of ORR and CBR between group A and group B. ORR and CBR in group C increased significantly compared with the levels of groups A and B (P<0.05) (Table II).

Evaluation of the incidence of adverse reactions in the groups

The patients from group C developed less adverse reactions compared with the patients from groups A and B. The difference between group C and group A and B were highly statistically significant for heart, liver, gallbladder and pancreas levels (P<0.01) and statistically significant for nerve, lung and upper respiratory tract level (P<0.05).

DISCUSSION

The current study showed that the treatment with lapatinib combined with trastuzumab determined an increased recovery rate and control rate in breast cancer patients compared to lapatinib or trastuzumab alone. These results are in accordance with a previous study that showed increased pathological complete response in combined HER2-targeted therapy compared with single agent therapy (10).

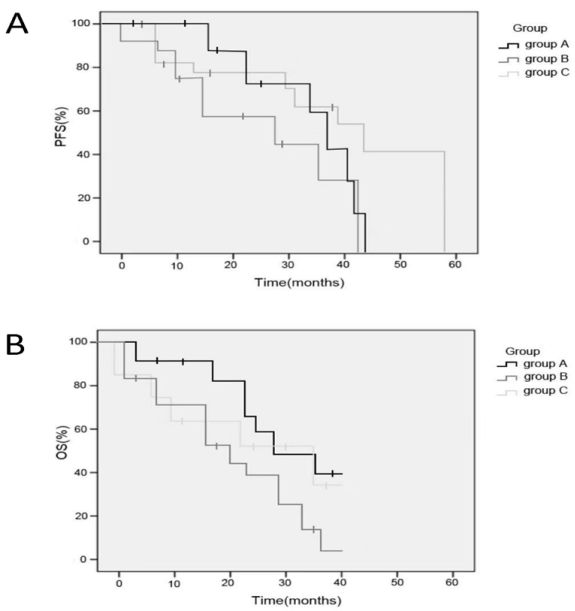

Fig. 1. *Kaplan –Meier plot of (**A**) PFS (Progession Free Survival) and (**B**) OS (overall survival) of patients in each group.*

Table I. *Comparison of clinical efficacy among the 3 groups.*

Category	Group A n	Group B n	Group C n
CR	3	2	3
PR	10	9	22
PD	16	16	17
SD	17	14	6
Others	6	7	6
Recovery rate (%)	25.00	22.93	$46.30^{\#*}$
Control rate (%)	55.77	56.25	$77.78^{\#\#**}$

Note: compared with group A: $^{\#}P<0.05$, $^{\#\#}P<0.01$; compared with group B: $^{*}P<0.05$, $^{**}P<0.01$.

Table II. *Comparison of CNS metastasis, ORR and CBR between the 3 groups.*

Groups	CNS metastasis status, n			CNS metastasis rate (%)	ORR	CBR
	Yes	No	Unknown			
Group A	15	30	7	28.85	59.65	47.27
Group B	16	22	10	33.33	56.88	43.25
Group C	10	39	5	18.52$^{\#*}$	76.73#*	68.93#*

Note: compared with group A: $^{\#}P<0.05$; compared with group B: $^{*}P<0.05$.

Table III. *Comparison the incidence of adverse reaction (%) between the groups*

Category	Group A (%)	Group B (%)	Group C (%)
Heart	5.77	6.25	0.00$^{\#\#**}$
Skin	19.23	18.75	14.81
Hepatobiliary / pancreas	5.77	4.17	1.85$^{\#\#**}$
Infection	3.85	4.17	1.85*
Lymph	19.23	16.67	12.96
Nerve	11.54	10.42	3.70$^{\#*}$
Pain	13.46	12.50	11.11
Lung / upper respiratory tract	7.69	8.33	3.70$^{\#*}$
Others	61.54	60.42	53.70

Note: compared with group A: $^{\#}P<0.05$, $^{\#\#}P<0.01$; compared with group B: $^{*}P<0.05$, $^{**}P<0.01$.

The side effects of Lapatinib are lower than those of other medicines from the same class. The main side effects are neutropenic fever, diarrhea, rash and anorexia (11). There were no differences between PFS and OS in group A and group B ($P>0.05$), while those in group C were significantly higher than those in groups A and B ($P<0.05$). This indicates that combined medication with lapatinib and trastuzumab can prolong the survival time of patients.

Trastuzumab combined with lapatinib did not increase the incidence of severe visceral damage but was significantly reduced, and the incidence of adverse reactions in group C was significantly lower than that in groups A and B ($P<0.05$). In other studies, also the incidence of cardiac damage events were lower in the combined treatment, with no significant difference compared with trastuzumab alone, and even significantly lower than that of lapatinib alone (11).

In conclusion, lapatinib combined with trastuzumab presented good tolerance and safety in patients with HER2 positive breast cancer, and showed improved efficacy in delaying tumor progression and prolonging the survival of patients.

REFERENCES

1. Fenga C, Costa C, Caruso E, et al. Current evidence on the protective effect of dietary polyphenols on breast cancer. Farmacia 2016; 64(1):1-12.
2. Alqaisi A, Chen L, Romond E, et al. Impact of estrogen receptor (ER) and human epidermal growth factor receptor-2 (HER2) co-expression on breast cancer disease characteristics: implications for tumor biology and research. Breast Cancer Res Treat 2014; 148(2):437-44.
3. Cordina-Duverger E, Koudou Y, Truong T, Arveux P, Kerbrat P, Menegaux F, Guénel P. Night work and breast cancer risk defined by human epidermal growth factor receptor-2 (HER2) and hormone receptor status: A population-based case–control study in France. Chronobiol Int 2016; 33(6):783-87.
4. Wolff AC, Hammond ME, Hicks DG, et al. Recommendations for human epidermal growth factor receptor 2 testing in breast cancer: American Society of Clinical Oncology/College of American Pathologists clinical practice guideline update. J Clin Oncol 2013; 31(31):3997-4013.
5. Gonzalez-Angulo AM, Litton JK, Broglio KR, et al. High risk of recurrence for patients with breast cancer who have human epidermal growth factor receptor 2-positive, node-negative tumors 1 cm or smaller. J Clin Oncol 2009; 27(34):5700-6.
6. Wilks S, Puhalla S, O'Shaughnessy J, et al. Phase 2, multicenter, single-arm study of eribulin mesylate with trastuzumab as first-line therapy for locally recurrent or metastatic HER2-positive breast cancer. Clin Breast Cancer 2014; 14(6):405-12.
7. Krishnamurti U, Silverman JF. HER2 in breast cancer: a review and update. Adv Anat Pathol 2014; 21(2):100-7.
8. Lin NU, Freedman RA, Ramakrishna N, et al. A phase I study of lapatinib with whole brain radiotherapy in patients with human epidermal growth factor receptor 2 (HER2)-positive breast cancer brain metastases. Breast Cancer Res Treat 2013; 142(2):405-14.
9. U.S. Department of Health and Human Services Food and Drug Administration Center for Drug Evaluation and Research (CDER), Center for Biologics Evaluation and Research (CBER). Guidance for industry: clinical trial endpoints for the approval of cancer drugs and biologics. http://www.fda.gov/downloads/Drugs/…/Guidances/ucm071590.pdf. Published May 2007. Accessed June 4, 2018.
10. Robidoux A, Tang G, Rastogi P, et al. Lapatinib as a component of neoadjuvant therapy for HER2-positive operable breast cancer (NSABP protocol B-41): an open-label, randomised phase 3 trial. Lancet Oncol 2013; 14(12):1183-92.
11. Valachis A, Nearchou A, Lind P, Mauri D. Lapatinib, trastuzumab or the combination added to preoperative chemotherapy for breast cancer: a meta-analysis of randomized evidence. Breast Cancer Res Treat 2012; 135(3):655-62.

LETTER TO THE EDITOR

DIAGNOSTIC VALUE OF TRACP5b EXPRESSION IN PATIENTS WITH BONE TUMORS

Q. ZHANG, L. CAO, XD. MIAO and YP. WU

Foot and Ankle Group of Department of Orthopaedics, The Second Hospital Affiliated to Zhejiang University School of Medicine, Hangzhou, Zhejiang University, China

Received December 16, 2018 – Accepted January 22, 2019

In order to investigate the diagnostic value of serum levels of tartrate-resistant acid phosphatase 5b (TRACP5b) in patients with bone tumors, enzyme linked immunosorbent assay (ELISA) was used to compare serum levels of TRACP5b and alkaline phosphatase (ALP) in bone tumor patients (experimental group, 80 cases) and healthy controls (control group, 36 cases). It was found that the serum level of TRACP5b in the experimental group was significantly higher than that in the control group. In addition, the sensitivity and specificity of serum TRACP5b were higher than those of serum ALP in the diagnosis of bone tumors. Furthermore, the serum level of TRACP5b was positively correlated with that of ALP. Therefore, it was concluded that the serum level of TRACP5b may be used as a sensitive indicator of bone tumors, and the sensitivity and specificity of TRACP5b are even higher than those of ALP in the diagnosis of bone tumors.

To the Editor,

Bone tumors (1) are tumors affecting bone tissues. Abnormal growth of the bone can be classified as benign (non-cancerous) or malignant (cancerous). It is easy to cure benign bone tumors, which are associated with a good prognosis. In contrast, it is usually difficult to treat malignant bone tumors. Malignant bone tumors can be divided into primary bone tumors and secondary bone tumors (2). The balance between osteogenesis and bone resorption is maintained in the process of normal bone metabolism. This balance is mainly achieved through the coordinated action of osteoclasts and osteoblasts. However, the balance between osteogenesis and bone resorption is broken during the pathogenesis of bone tumors, leading to the abnormal manifestations of osteogenesis (3).

Alkaline phosphatase (ALP) (4) has long been considered as a marker of osteoblast activity. In addition, mainly derived from osteoclasts, serum tartrate-resistant acid phosphatase 5b (TRACP5b) (5) is a marker of bone resorption. Possessing the enzyme activity of degrading mineralized calcium and phosphorus substrates in the bone matrix, TRACP5b can be used as a marker to reflect the activity of osteoclasts and the degree of bone resorption. In recent years, it has been confirmed that the expression of TRACP5b is elevated in patients with metastatic bone tumors (6), Paget disease, and osteoporosis (7). However, few studies have reported TRACP5b levels in patients with primary bone tumors (8-10). Therefore, this study explored the clinical value of using TRACP5b as a marker in the treatment of primary bone tumors.

MATERIALS AND METHODS

Subjects

Eighty bone tumor patients diagnosed by pathological examinations (bone tumor group) and 36 healthy subjects

Key words: bone tumors; tartrate-resistant acid phosphatase 5b; tumor markers; diagnosis; clinical value

Corresponding Author:
Dr Yongping Wu,
Foot and Ankle Group of Department of Orthopaedics,
The Second Hospital Affiliated
Zhejiang University School of Medicine,
No.88 Jiefang Road, Hangzhou,
31000, Zhejiang University, China
e-mail: 2504124@zju.edu.cn

0393-974X (2019)

DISCLOSURE: ALL AUTHORS REPORT NO CONFLICTS OF INTEREST RELEVANT TO THIS ARTICLE.

(normal control group) from The Second Hospital Affiliated to Zhejiang University School of Medicine between April 2017 and August 2018 were enrolled in the study. The 80 bone tumor patients included 39 females and 41 males, aged 11-70 years (average 38.3 years). There were 16 females and 20 males in the normal control group, aged 9-76 years (average 43.1 years). Informed consent was obtained from all patients, and this study was approved by the ethics committee of The Second Hospital Affiliated to Zhejiang University School of Medicine.

Inclusion criteria of the bone tumor group: patients diagnosed with bone tumors by pathological examinations; patients who had not taken any drugs affecting bone metabolism or received any surgical treatment in the previous six months; patients who signed the informed consent.

Exclusion criteria of the bone tumor group: patients who had history of locomotor system trauma in the past six months; patients with diseases affecting bone metabolism; patients who had taken drugs affecting bone metabolism in the previous six months; patients with impaired liver or kidney functions.

Sample collection, processing and preservation

2-3mL of fasting venous blood samples were collected from each subject using vacuum blood collection tubes (Shanghai Yuanye Biotechnology Co., Ltd., China) containing no anticoagulant. After being placed at room temperature for l-2 h, each blood sample was centrifuged at 4000 rpm (Zhengzhou Honglang Instrument Equipment Co., Ltd., China) for l0 min. The serum was collected and aliquoted into 100 uL Eppendorf tubes and stored in a -80°C cryocontainer (China Haier Company, China) for subsequent testing. During testing, the samples were thawed at room temperature for at least 30 min. Subsequently, the samples were detected at room temperature (20-23°C).

Detection of serum TRACP5b

The kit (Shanghai Source Leaf Biotechnology Co., Ltd., China) and sample serum were taken from the freezer and placed at room temperature for at least 30 min. The blank well was not porous, but the standard and sample wells were both porous. 120 uL, 240 uL, 360 uL, 480 uL and 600 uL of standard diluents were added to 120 uL of standard solution, respectively. The first well was used as the blank control well, which contained only Tetramethylbenzidine (TMB) color reagents A/B and H_2SO_4 termination solution. 50 uL diluted standard products and 50 uL streptavidin-HRP were added to each of other wells, respectively, followed by the addition of 40 uL samples. Subsequently, 10 uL of anti-TRACPSb antibody and 50 uL of streptavidin-HRP were added into each well before the plate was sealed with a sealing film. After being gently shaken and mixed, the plate was incubated at 37 for 60 min. In the next step, the sealing film was removed and the liquid in the plate was discarded. After blotting the plate dry, each well was washed five times (30 s each time) with a phosphate buffered saline detergent. After blotting dry the plate, 50 uL of TMB developer A liquid were added into each well, followed by the addition of 50 uL TMB developer B liquid into each well. After being gently shaken and mixed, the plate was incubated at 37°C for 10 min away from light to develop color. Finally, 50 uL of stop buffer was added to each well to terminate the reaction (at this time, the blue color would turn yellow). The absorbance (OD) of each well was then measured at a wavelength of 450 nm after zero-setting the blank well. The measurement should be completed within 10 min after adding the stop buffer. The linear regression equation of the standard curve was then calculated according to the concentration of the standard and the OD value. Subsequently, the level of TRACP5b in each sample was calculated using the regression equation according to the OD value of each sample.

Detection of serum ALP

ALP was detected by the rate method. Under certain conditions of enzymatic reaction, colorless p-nitrophenyl phosphate disodium (Beijing Soleboard Corporation, China) reacts with ALP to produce pale yellow p-nitrophenol (Beijing Soleboard Corporation, China) with specific absorption at 405 nm. By measuring the change rate of absorbance at 405 nm, the activity of ALP was calculated according to Formula 1, through the molar extinction coefficient of NADH and the microprocessor of biochemical automatic analyzer.

In the formula, 260 μL is the general volume of the reaction, 10 μL is the sample volume, $6.22x10^3$ is the micro-molar optical coefficient (ε) of NADH at 405 nm, ΔA/min is the change rate of absorbance per minute, 10^6 is the conversion factor of the unit per microliter (μL) to each liter (L).

Statistical analysis

SPSS19.0 statistical software was used for statistical analysis. The experimental results followed normal distri-

bution and were expressed as mean ± standard deviation. The data of the two groups were compared by *t*-test (*t*-test for data with homogeneous variance and adjusted *t*-test for data with uneven variance), and one-way analysis of variance (ANOVA) was used to compare the mean values of the two groups. A test level of α=0.05 was used in this study, while P <0.05 indicated significant difference. Finally, Pearson correlation analysis was used to analyze the correlation between two variables.

RESULTS

Comparison of serum levels of TRACP5b and ALP between the bone tumor and normal control groups

The serum levels of TRACPSb in the bone tumor group and normal control group were (5.925±2.913) U/L and (3.597±1.131) U/L, respectively. Therefore, the serum level of TRACPSb in the bone tumor group was significantly higher than that in the normal control group (P=0.000). The serum levels of ALP in the bone tumor group and normal control group were (140.162±117.261) U/L and (92.692±46.692) U/L, respectively. Therefore, the serum level of ALP in the bone tumor group was significantly higher than that in the normal control group (P=0.0020), as shown in Table I.

ROC curves, sensitivity and specificity of TRACP5b and ALP in the diagnosis of bone tumors

Based on the analysis of Receiver Operating Characteristic (ROC) curves, the area under the curve (AUC) of TRACP5b was 0.782 in the diagnosis of bone tumors, and its 95% confidence interval was 0.697-0.866 (P < 0.01). The AUC of ALP was 0.634 and its 95% confidence interval was 0.532-0.736 (P < 0.05) (Fig. 1A). When 3.749U/L was used as the cut-off value of TRACP5b, its sensitivity and specificity in the diagnosis of bone tumors were 76.8% and 62.2%, respectively. When 77.500U/L was used as the cutoff value of ALP, its sensitivity and specificity in the diag-

Table I. *Basic characteristic of patients in the two groups.*

Category	Bone tumor group	Normal control group
Number of cases	80	36
Male/female	41/39	20/16
Age (year)	11-70(38.3)	9-78(43.1)
TRACP5b (U/L)	5.925±2.913*	3.597±1.131
ALP (U/L)	140.162±117.261*	92.692±46.692

*Note: *P<0.05, compared with the control group.*

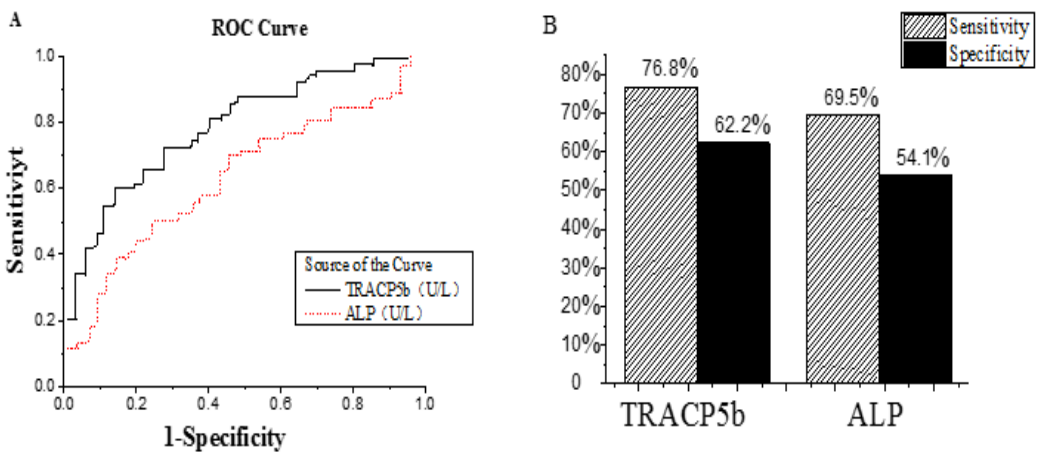

Fig. 1. *ROC curves, sensitivity and specificity of TRACP5b and ALP in the diagnosis of bone tumors. **A)** ROC curves of TRACP5b and ALP in the diagnosis of bone tumors; **B)** sensitivity and specificity of TRACP5b and ALP in the diagnosis of bone tumors.*

nosis of bone tumors were 69.5% and 54.1%, respectively (Fig. 1B).

Discrete trend of TRACP5b and ALP

For TRACPSb, its median serum level was 4.351 U/L, its average was 5.812 U/L, its quartile spacing was (3.542-6.058) U/L (Fig. 2A), and its coefficient of variation was 51.85%; For ALP, its median serum level was 85.000 U/L, its average was 124.992 U/L, its quartile spacing was (71.000-127.000) U/L, and its coefficient of variation was 81.99% (Fig. 2B).

Correlation between TRACP5b and ALP

This study showed a positive and linear correlation between TRACP5b and ALP, with a correlation coefficient of $r = 0.427$, $P < 0.01$ (Fig. 3A).

Changes in post-operative expressions of TRACP5b in patients with bone tumors (measured on the third day after operation) and in patients receiving a neo-adjuvant chemotherapy

The changes in serum TRACP5b levels were measured before and after surgery of the following pa-

Table II. *TRACP5b levels in bone tumor patients measured before and after surgery/chemotherapy.*

	Cases	Diagnosis	TRACP5b (U/L) before operation	TRACP5b (U/L) after operation
Patients with bone tumors treated with surgery	1	Osteosarcoma	4.231	5.253
	2	Osteosarcoma	3.781	4.946
	3	Osteosarcoma	12.182	13.362
	4	Osteosarcoma	5.436	8.227
	5	Giant cell tumor	4.662	8.731
	6	Bone cyst	5.082	5.602
Patients with bone tumors treated with chemotherapy	1	Osteosarcoma	3.962	3.128
	2	Osteosarcoma	10.641	5.972
	3	Chondrosarcoma	5.726	4.225

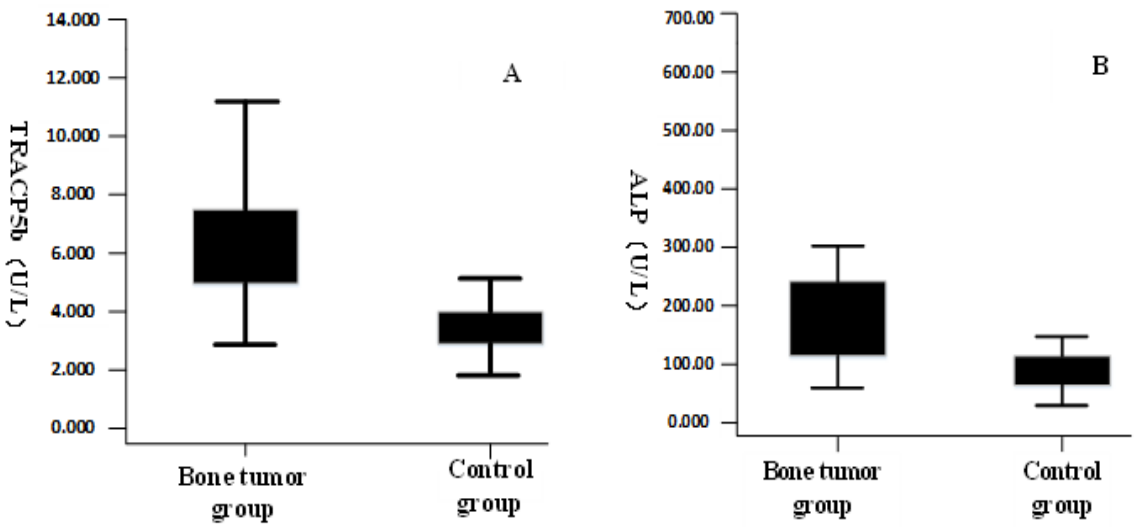

Fig. 2. *Discrete trend of TRACP5b and ALP. **A**) Discrete trend of TRACP5b; **B**) Discrete trend of ALP.*

tients: extensive tumor resection in 4 patients with osteosarcoma, marginal resection in 1 patient with giant cell tumor, and clearance of intracystic lesions in 1 patient with bone cyst. The results showed that the post-operative expression of TRACP5b in the 5 patients was higher than its pre-operative values. The changes in the serum TRACP5b levels of 2 cases of osteosarcoma and 1 case of chondrosarcoma were also measured before and after the patients being treated with a neo-adjuvant therapy. It was found that the serum level of TRACP5b after chemotherapy was lower than that before chemotherapy, as shown in Table II.

Changes in the TRACP5b expression over age

Using age as abscissa (unit: years old) and TRACP5b expressions as ordinate (unit: U/L), the curve of TRACP5b versus age (Fig. 3B) was plotted. It can be seen that TRACP5b was highly expressed in children and adolescents, especially in the peak period of puberty growth and development. In addition, TRACP5b expressions gradually increased over age after a person was aged 40 or above.

DISCUSSION

TRACP-5b is related to the activity of osteoclasts in the human body and has the activity of degrading calcium and phosphorus mineralized substrates in bone matrix (11). Therefore, TRACP-5b can be used as a marker of bone resorption and osteoclast activity in the human body (12). The present study showed that the serum level of TRACP5b in the cancer group was significantly higher than that in the normal control group. These results suggested that TRACP5b can be used as a valuable marker in the diagnosis of bone tumors.

By comparing the ROC curves of TRACP5b and APL in the diagnosis of bone tumors, it was found that TRACP5b had a higher value in the early diagnosis. It was also confirmed that TRACP5b, like ALP, could be used as a good indicator of bone metabolism and bone tumors, therefore, whenever possible, the detection of TRACP5b should be carried out in patients with bone tumors.

To sum up, the serum level of TRACP5b can be used as a sensitive indicator of bone tumors, and the sensitivity and specificity of TRACP5b are even higher than those of ALP in the diagnosis of bone tumors. However, TRACP5b as an evaluation index of therapeutic efficacy of bone tumors still needs further study in large sample prospective trials.

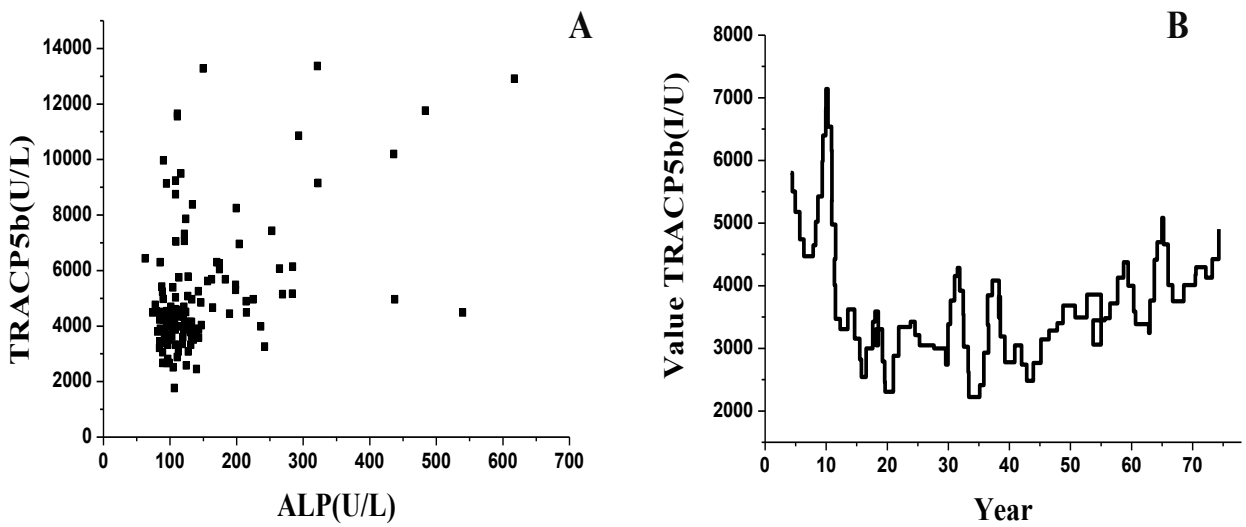

Fig. 3. *Correlation between TRACP5b and ALP and changes in TRACP5b expressions over age. **A**) Correlation between TRACP5b and ALP; **B**) Changes in TRACP5b expressions over age.*

REFERENCES

1. Chen J, Younusi A, Cao L, Xu L, Zhou Y, Zhen T, Song X. Serum levels of NTx and TRACP5b in giant cell tumor of bone and its clinical implications. Clin Lab 2015; 61(8):1077-81.
2. Sun D, Zheng X, Chen Y, et al. Enhancement of osteogenesis post-splenectomy does not attenuate bone loss in ovariectomized rats. J Orthop Res 2015; 33(9):1356-63.
3. Nwosu LN, Allen M, Wyatt L, Huebner JL, Chapman V, Walsh DA, Kraus VB. Pain prediction by serum biomarkers of bone turnover in people with knee osteoarthritis: an observational study of TRAcP5b and cathepsin K in OA. Osteoarthritis Cartilage 2017; 25(6):858-65.
4. Nakamura Y, Suzuki T, Kato H. Serum bone alkaline phosphatase is a useful marker to evaluate lumbar bone mineral density in Japanese postmenopausal osteoporotic women during denosumab treatment. Ther Clin Risk Manag 2017; 13:1343-48.
5. Sarvari BK, Sankara Mahadev D Rupa S, Mastan SA. Detection of bone metastases in breast Cancer (BC) patients by serum tartrate-resistant acid phosphatase 5b (TRACP 5b), a bone resorption marker and serum alkaline phosphatase (ALP), a bone formation marker, in lieu of well body skeletal scintigraphy with technetium 99m MDP. Indian J Clin Biochem 2015; 30(1):66-71.
6. Lumachi F, Basso SM, Camozzi V, Tozzoli R, Spaziante R, Ermani M. Bone turnover markers in women with early stage breast cancer who developed bone metastases. A prospective study with multivariate logistic regression analysis of accuracy. Clin Chim Acta 2016; 460:227-30.
7. Jing D, Yan Z, Cai J, Tong S, Li X, Guo Z, Luo E. Low-level mechanical vibration improves bone microstructure, mechanical properties and porous titanium implant osseointegration by promoting a major skeletal anabolic response in type 1 diabetic rabbits. Bone 2018; 106:11-21.
8. He B, Wang J. Chitooligosaccharides prevent osteopenia by promoting bone formation and suppressing bone resorption in ovariectomised rats: possible involvement of COX-2. Nat Prod Res 2015; 29(4):359-62.
9. Lin CM, Fan HC, Chao TY, Chu DM, Lai CC, Wang CC, Chen SJ. Potential effects of valproate and oxcarbazepine on growth velocity and bone metabolism in epileptic children- a medical center experience. BMC Pediatr 2016; 16:61.
10. Yu L, Li H, Hou S, et al. Abnormal bone mineral density and bone turnover marker expression profiles in patients with primary spontaneous pneumothorax. J Thorac Dis 2016; 8(6):1188-96.
11. Nowak B, Matuszewska A, Filipiak J, et al. The negative impact of selective activation of retinoic acid receptors on bone metabolism and bone mechanical properties in rats. Adv Clin Exp Med 2016; 25(2):213-18.
12. Sousa DM, Conceição F, Silva DI, et al. Ablation of Y1 receptor impairs osteoclast bone-resorbing activity. Sci Rep 2016; 6:33470.

LETTER TO THE EDITOR

EXPRESSION OF MUCIN 1 IN SALIVARY GLAND TUMORS AND ITS CORRELATION WITH CLINICOPATHOLOGICAL FACTORS

S. MA[1], F. AN[1], LH. LI[1], YY. LIN[2] and J. WANG[1]

[1]Department of Stomatology, The First Affiliated Hospital of Hebei North University, Zhangjiakou City, Hebei Province, China; [2]Department of Pathology, The First Affiliated Hospital of Hebei North University, Zhangjiakou City, Hebei Province, China

Received December 19, 2018 – Accepted January 18, 2019

This study aimed to detect the expression of Mucin 1 (MUC1) in acinic cell carcinoma (AciCC) of salivary gland and to explore the relationship between MUC1 and clinicopathological factors of AciCC of salivary gland. Patients with salivary gland tumors who were treated at our hospital were enrolled in this study. The pathological sections collected from all subjects were classified by histological examinations. In addition, 40 cases of primary salivary gland AciCC tissues were selected and classified into experimental group, whereas 40 cases of normal salivary gland (NSG) tissues were selected and classified into control group. MUC1 positive cells in both experimental and control groups were detected by immunohistochemistry assays, while all clinical data were analyzed statistically. The results showed that MUC1 was only expressed in the ductal epithelium of NSG and distributed at the apical side of the cell membrane. In primary salivary gland AciCC tissues, scattered expressions of MUC1 were found both on the cell membrane and in the cytoplasm of tumor cells, and sometimes even in the cell nuclei, thus completely eliminating the polarized distribution of MUC1 expressions. The percentage of MUC1 positive cells in experimental group was significantly higher than that in control group ($P < 0.05$). In addition, the expression of MUC1 in salivary gland AciCC was correlated with gender, age, histological type, lesion location, cervical lymph node metastasis, local recurrence, and distant metastasis. In conclusion, MUC1 is related to the occurrence and development of salivary gland AciCC. Therefore, MUC1 may be used as a novel tumor marker in the clinical diagnosis and treatment of salivary gland AciCC.

To the Editor,

The clinical manifestations of acinic cell carcinoma (AciCC) in salivary gland are not characteristic (1, 2). Most researchers believe that the degree of malignance of AciCC is low, and most of AciCC cases are treated with local excision (3-5). If necessary, AciCC of salivary gland can be cured by neck dissection in conjunction with post-operative radiotherapy and chemotherapy, although this method may lead to local recurrence and distant metastasis. Mucin 1 (MUC1) is a high molecular weight type I transmembrane protein encoded by the MUC1 gene. Usually, MUC1 is widely expressed on the apical surface of human mucosal epithelial cells. Abnormal expressions of MUC1 are often found in tumor tissues (6). MUC1 can enhance the invasiveness of tumor cells by reducing the adhesion between tumor cells and by promoting

Key words: mucin 1; acinar cell carcinoma; salivary gland tumor; tumor markers

Corresponding Author:
Dr Feng An,
Department of Stomatology, The First Affiliated Hospital
Hebei North University, No. 12 Changqing Road,
Zhangjiakou City, 075000,
Hebei Province, China
e-mail: anfengkouqiang0313@163.com

0393-974X (2019)

their metastasis. MUC1 may be used as a marker for the diagnosis of tumor invasion in surrounding tissues and the distant metastasis of squamous cell carcinoma. Additionally, MUC1 may be used as a new molecular marker to improve the prognosis of MEC patients in the future. The relationship between the expression of MUC1 and the clinicopathological factors of salivary gland AciCC was discussed in this study, and the results may provide a theoretical basis for the early diagnosis, treatment and prognosis of salivary gland AciCC.

MATERIALS AND METHODS

Subjects

Patients with salivary gland tumors who were treated in The First Affiliated Hospital of Hebei North University from March 2015 to September 2018 were enrolled in this study. The clinical and follow-up data of the patients were analyzed. In addition, the histological sections collected from all subjects were classified. According to the location of AciCC, 40 samples of primary salivary gland AciCC were classified into experimental group, while 40 normal salivary gland (NSG) tissues were incorporated into control group. Informed consent was signed by all patients. In addition, this study was unanimously approved by the Ethics Committee of The First Affiliated Hospital of Hebei North University.

Inclusion criteria: primary salivary gland, salivary gland tumors with no signs of metastasis or recurrence; clear histopathological diagnosis; all cases were treated for the first time or treated for less than 3 months after surgery.

Exclusion criteria: No operation or biopsy was performed and hence the histopathological features were not clear.

Detection of MUC1 expressions

Eighty paraffin specimens were selected and sectioned with a thickness of 4μm (7). The Max Vision method was used for immunohistochemical staining (8). The PBS solution was used as the negative control. Positive quality control tablets (BIO-RAD, America) of breast carcinoma MUC1 were used as the positive control. The specific steps of the experiment were as follows:

First, paraffin sections were dewaxed and hydrated, followed by the addition of 1000 mL of citrate buffer into a pressure cooker for antigen repair. The sections were then washed by tap water for 1 min, and the tissue area to be measured was marked and washed for 3 min x3 times using distilled water (Axyen, China). 100 μL of endogenous peroxidase blocker (Axyen, China) was then added onto the marked area of each slide and incubated for 10 min at 18-28°C. Following another PBS (Axyen, China) washing for 3 min x3 times, 100 μL of anti-MUC1 antibody ab15481 (Beckman, Germany) was dripped onto each section and incubated for 120 min at 18-28°C. Following another PBS washing for 3 min x3 times, 100 μL of enzyme-labeled sheep/rabbit IgG polymer (Axyen, China) was added onto the marked area and incubated for 15 min at 18-28°C. Following another PBS washing for 3 min x3 times, 100 μL of freshly prepared DAB color solution (Sigma, America) was dripped onto each slide and incubated for 3-5 min at 18-28°C. After rinsing with tap water, 100 μL of hematoxylin (InvitroGen, America) staining solution was added onto each slide to stain the nucleus to light blue, which subsequently turned blue upon PBS rinsing. The slides were then dehydrated, made transparent and mounted for observation.

Result judgment

The expression of MUC1 in cell membrane or cytoplasm/nuclei in 80 immunohistochemically stained specimens was observed under a light microscope. The expression intensity of MUC1 in a single cell was divided into four grades: negative (colorless), weak positive (weak yellowish), moderately positive (yellow) and strongly positive (strongly yellowish brown). Cells with a grade higher than moderately positive were identified as positive cells. Microscopically, the distribution of tumor parenchymal cells was observed to select the area with a high expression. Subsequently, 5 cells positive for MUC1 expressions were counted in a high power field of vision to calculate the rate of positive cells. The rate of MUC1 positive cells = (number of positive cells/total number of cells of the same type) x100%.

Statistical analysis

SPSS19.0 statistical software was used for statistical processing. Data were expressed as mean ± standard deviation. Independent sample *t*-test was used for the comparison between two groups, while one-way

analysis of variance was used for the comparison among multiple groups. In addition, SNK-q test was used for the comparison between two groups. The test level was α=0.05, and P <0.05 was considered significant.

RESULTS

General features

Among the 40 patients with primary salivary gland AciCC, there were 19 males and 21 females, with a male-to-female ratio of 1:1.11; the average age was 49 years old, and 47.50% (19/40) of the patients were aged 51~60 years old; the most common site of tumor was parotid gland, 67.50% (27/40), followed by palate, 12.50% (5/40), submandibular gland, 7.50% (3/40), and small salivary gland, 12.50% (5/52). Pathological section of the patient is shown in Fig.1. No normal tubular mucinous acinar structure is found in solid section (Fig. 1A). A large number of vesicles appear in microcystic section (Fig. 1B). A large number of papillary vesicles appear in papillary cystic section (Fig. 1C). A large number of vacuolar structures appear in follicular section (Fig. 1D). According to the statistics of different types of patients, it is found that among all tumor specimens, 12 cases were of solid type, 12 cases of microcapsule type, 6 cases of papillary cystic type and 1 case of follicular type (Fig. 1). The 40 cases were followed up for 6-105 months, with a median follow-up of 45 months. The rate of local recurrence was 12.50% (5/40) while the rate of distant metastasis was 5.00% (2/40).

Expressions of MUC1 in normal salivary gland tissue

Fig. 2A shows that normal salivary gland tissue is filled with tubular mucinous acinar structure and interstitial cells. Fig. 2B shows that dark staining is in the medial part of ductal epithelium of NSG tissue, but not in other parts. This indicates that

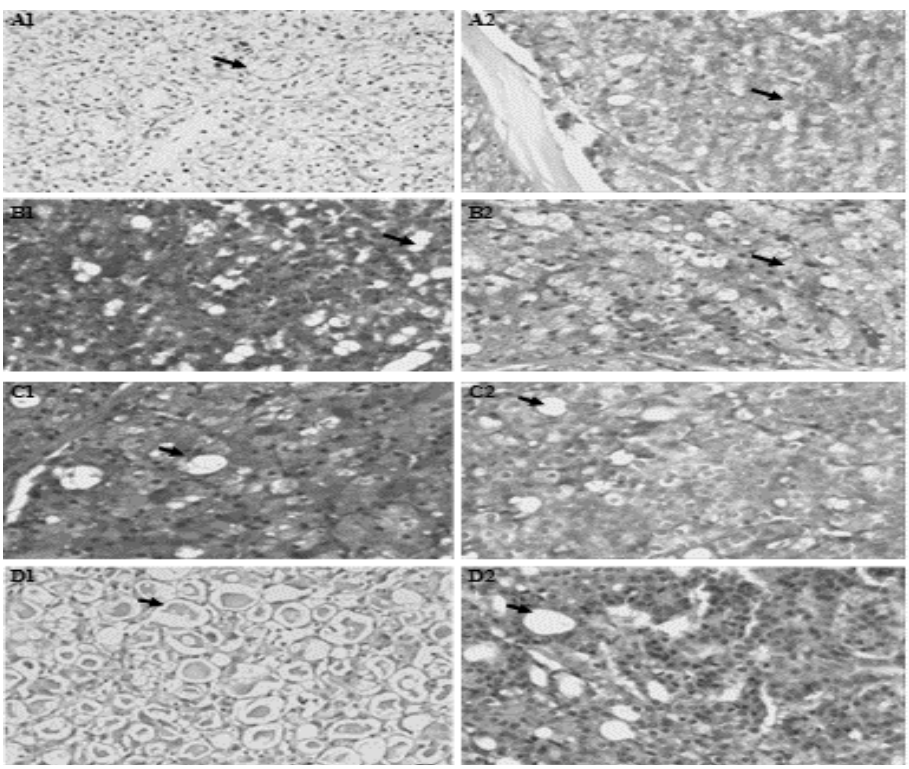

Fig. 1. *Salivary gland neoplasm cell type.* ***A****) 1, 2: solid type, the arrows point to solid type structure;* ***B****) 1, 2: microcapsule type, the arrows point to microcapsule type structure;* ***C****) 1, 2: papillary cystic type, the arrows point to papillary cystic structure;* ***D****) 1, 2: follicular type, the arrows point to follicular structure) (HE x 200).*

Table I. *The relationship between the expression of MUC1 in salivary gland AciCC and its clinicopathological factors.*

Groups		Case (n)	Rates of MUC1 positive cells (%)	t/F	P
Gender	Male	19	82.16±2.32	-15.646	<0.001
	Female	21	89.92±1.54		
Age (years old)	0~20	2	84.79±1.87	11.841	<0.001
	21~40	6	87.36±2.19		
	41~60	25	91.36±3.28		
	61~80	7	88.48±1.73		
Location of disease	Parotid gland	27	86.77±2.68	14.671	<0.001
	Palate	5	81.16±3.50		
	Salivary gland	3	93.36±2.37		
	Other minor salivary glands	5	83.14±1.28		
Tissue type	Microcapsule type	12	80.33±2.55	115.33	<0.001
	Papillary cystic type	6	78.26±1.69		
	Solid type	21	92.82±3.13		
Cervical lymph node metastasis	Yes	5	88.71±1.51	4.016	<0.001
	No	35	86.81±1.83		
Local recurrence or distant metastasis	Yes	7	93.41±2.06	8.148	<0.001
	No	33	85.60±2.61		

MUC1 is only expressed in the ductal epithelium of NSG tissue, and is distributed at the top of cell membrane facing the lumen side cells and shows polarity distribution.

MUC1 expression in primary salivary gland AciCC

As can be seen from Fig. 3, dark staining was found in solid (Fig. 3A), microcapsule (Fig. 3B), papillary cystic (Fig. 3C) and follicular (Fig. 3D) histopathological sections which suggested that MUC1 was expressed in AciCC tissues of primary salivary glands. Compared with normal tissues (Fig. 2B), the staining site was not only confined to the medial ductal epithelium of NSG tissues, but also scattered in cell membrane and cytoplasm of tumor cells. The expression of MUC1 was also found in some nuclei, indicating that the polar distribution of MUC1 expression disappeared.

The rate of MUC1 positive cells

The rate of positive MUC1 cells in experimental and control groups was (86.36±2.48)% and (9.06±2.15)%, respectively. There was significant difference between the two groups ($P < 0.05$).

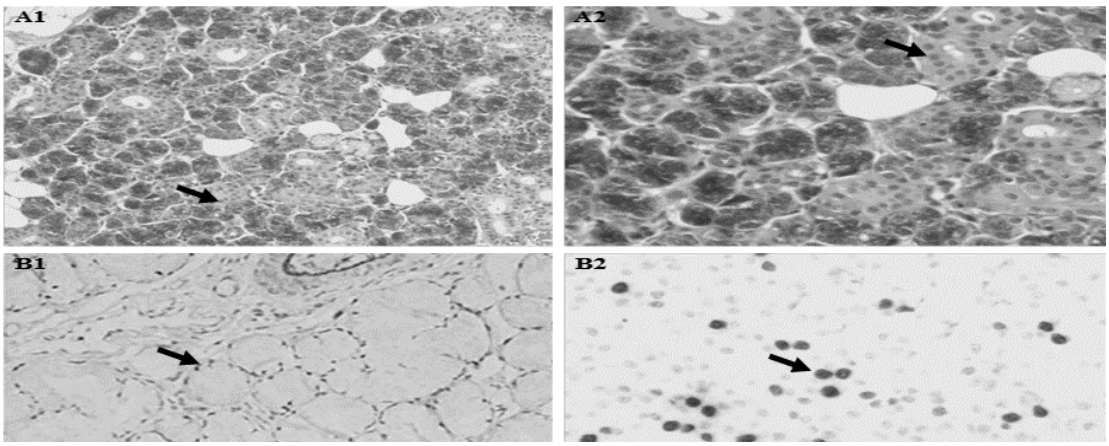

Fig. 2. ***A)*** *1,2: Normal salivary gland, the arrows point to the normal tubular mucinous acinar structure (HEx200);* ***B)*** *1, 2: MUC1 expression in normal salivary gland tissue, the arrows point to the MUC1 positive expression location (Max Vision x 200).*

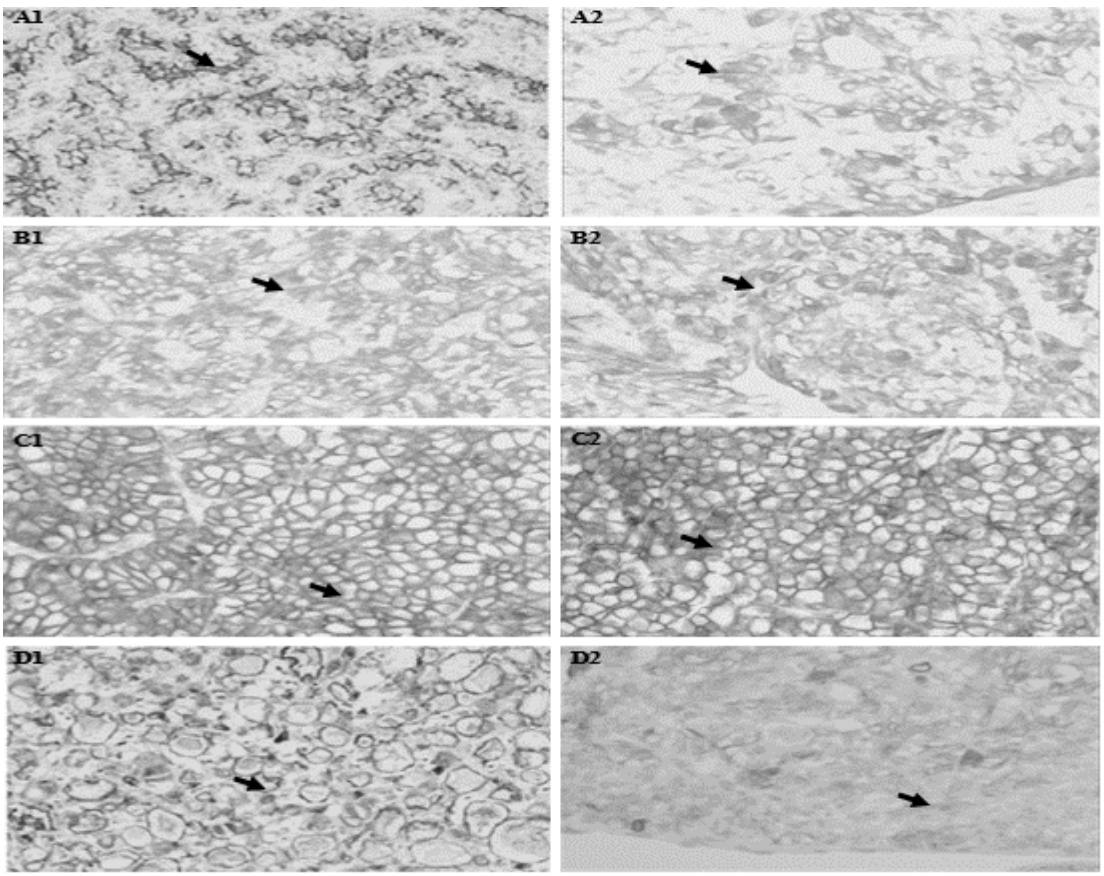

Fig. 3. *The expression of MUC1 in AciCC of salivary gland, the arrow points to the positive expression of MUC1.* ***A)*** *1, 2: MUC1 expression in solid type;* ***B)*** *1, 2: MUC1 expression in microcapsule type;* ***C)*** *1, 2: MUC1 expression in papillary cystic type;* ***D)*** *1, 2: MUC1 expression in follicular type) (Max Vision x 200)*

The relationship between the expression of MUC1 in salivary gland AciCC and clinicopathological factors

Only one case of follicular type was found among 40 samples of AciCC of salivary glands and hence was excluded from the analysis (Table I). The positive rates of MUC1 in solid type, microcapsule type and papillary cystic type AciCC were (92.82±3.13)%, (80.33±2.55)% and (78.26±1.69)%, respectively ($P<0.05$, compared to AciCC tissues of salivary gland of the same tissue type). Among these tissue types, there was significant difference between solid type and both microcapsule type and papillary cystic type.

In addition, the positive rate of MUC1 in females was higher than that in males. The positive rate of MUC1 in the 41-60 years group was higher than that in other age groups. The positive rate of MUC1 in submandibular gland was higher than that in other parts of the body. The positive rate of MUC1 was higher in cases with cervical lymph node metastasis. The positive rate of MUC1 in cases with local recurrence or distant metastasis was also higher. All differences were statistically significant ($P<0.05$).

DISCUSSION

MUC1 was only expressed in salivary gland AciCC tissues and NSG tissues at the apical surface of ductal gland epithelium (9). The expression of MUC1 in salivary gland AciCC was significantly higher than that in control group ($P<0.05$). The expression of MUC1 in NSG tissues indicated that MUC1 was an essential factor for the development of NSG (10-12). In this study, the expression of MUC1 in experimental group was significantly higher than that in control group.

This study showed that the positive rate of MUC1 cells in patients with cervical lymph node metastasis was significantly higher than that in those without cervical lymph node metastasis ($P<0.05$). In addition, the positive rate of MUC1 cells in patients with local recurrence or distant metastasis was significantly higher than that in those without local recurrence or distant metastasis ($P<0.05$). The abnormal high expression of MUC1 suggested that the risk of cervical lymph node metastasis, local recurrence and distant metastasis was high in patients with salivary gland AciCC. Therefore, the expression level of MUC1 acts as an important factor affecting the prognosis of salivary gland AciCC.

In conclusion, it was speculated that MUC1 may play an essential role in the malignant transformation, invasion and metastasis of salivary gland AciCC, and hence the MUC1 expression may be used as a tumor marker in the diagnosis of salivary gland AciCC. Therefore, in clinical research and treatment, it is recommended to pay attention to patients with an abnormally high expression of MUC1.

ACKNOWLEDGEMENTS

This work was supported by Self-financing Project of Key Research in Hebei Province (Project No.: 172777144).

REFERENCES

1. Hoffman HT, Karnell LH, Robinson RA, Pinkston JA, Menck HR. National cancer data base report on cancer of the head and neck: Acinic cell carcinoma. Head Neck 1999; 21(4):297-309.
2. Savla R, Taratula O, Garbuzenko O, Minko T. Tumor targeted quantum dot-mucin 1 aptamer-doxorubicin conjugate for imaging and treatment of cancer. J Control Release 2011; 153(1):16-22.
3. Besmer DM, Curry JM, Roy LD, et al. Pancreatic ductal adenocarcinoma mice lacking mucin 1 have a profound defect in tumor growth and metastasis. Cancer Res 2011; 71(13):4432-42.
4. Chen D1, Xia J, Tanaka Y,et al. Immunotherapy of spontaneous mammary carcinoma with fusions of dendritic cells and mucin 1-positive carcinoma cells. Immunology 2003; 109(2):300-7.
5. Xing-Mao Z, Hong-Juan Z, Qing L, Qiang H. Pancreatic acinar cell carcinoma-case report and literature review. BMC Cancer 2018; 18(1):1083.
6. Liu S, Ruan M, Li S, Wang L, Yang W. Increased expression of MUC1 predicts poor survival in salivary gland mucoepidermoid carcinoma. J Craniomaxillofac Surg 2014; 42(8):1891-6.
7. Zhu L, Jiang L, Wang W, et al. Angiopoietin-like protein

3 is an indicator of prognosis in esophageal cancer patients. Int J Clin Exp Med 2015; 8(9):16101-6.
8. Pan BJ, Xu C, Ping GQ, et al. Correlation analysis of PD-L1 expression and prognosis in triple-negative breast cancers. Zhonghua Bing Li Xue Za Zhi 2017; 46(12):822-826.
9. Moniaux N, Escande F, Porchet N, Aubert JP, Batra SK.. Structural organization and classification of the human mucin genes. Front Biosci 2001; 6:D1192-206.
10. Kato K, Lillehoj EP, Park YS, Umehara T, Hoffman NE, Madesh M, Kim KC. Membrane-tethered MUC1 mucin is phosphorylated by EGFR in airway epithelial cells and associates with TLR5 to inhibit recruitment of MyD88. J Immunol 2012; 188(4):2014-22.
11. Munteanu MC, Mărgăritescu C, Cionca L, Niţulescu NC, Dăguci L, Ciucă EM. Acinic cell carcinoma of the salivary glands: a retrospective clinicopathologic study of 12 cases. Rom J Morphol Embryol 2012; 53(2):313-20.
12. Biron VL, Lentsch EJ, Gerry DR, Bewley AF. Factors influencing survival in acinic cell carcinoma: a retrospective survival analysis of 2061 patients. Head Neck 2015; 37(6):870-7.

LETTER TO THE EDITOR

EFFECTS OF DIFFERENT DRAINAGE METHODS ON SERUM BILE ACID AND HEPATOCYTE APOPTOSIS AND REGENERATION AFTER PARTIAL HEPATECTOMY IN RATS WITH OBSTRUCTIVE JAUNDICE

Q. SUN, F. FANG, GC. LU, HH. MAO, JH. XU, SK. ZHOU, XM. TONG, Y. GUO, JF. WU and B. JIANG

Department of Surgery 2, TongLu First People's Hospital, Tonglu, Hangzhou, Zhejiang Province, China

Received November 26, 2018 – Accepted January 24, 2019

The aim of this study was to investigate the mechanism of hepatocyte apoptosis and regeneration after partial hepatectomy in obstructive jaundice (OJ) rats under different drainage methods of bile acid intervention. Forty male Sprague Dawley rats were randomly divided into five groups. An OJ rat model was established by the following protocols. Seven days after obstruction, an SD rats model with 70% partial hepatectomy was established by different drainage methods of OJ. Blood and liver tissue samples were collected from rats 72 h after surgery; 72 h after partial hepatectomy (PH), the liver regeneration rate, the expression of proliferating cell nuclear antigen (PCNA) and the level of mitotic index (MI) in the internal biliary drainage (IBD) group were higher than those in external biliary drainage (EBD) group ($P < 0.05$). Those in the EBD group were higher compared to the OJ group ($P < 0.05$). There was no significant difference among the IBD group, EBD+CA group and (SO) sham operation group ($P > 0.05$). Bax expressions had the same trend as AI in the five groups. The expression of Bcl-2 was increased in the IBD group and EBD+CA group, which was statistically higher compared to the SO group ($P < 0.05$). In conclusion, both internal and external drainage can relieve biliary obstruction. The difference in liver regeneration caused by external drainage and internal drainage may be attributed to the destruction of bile acid enterohepatic circulation, which increases hepatocyte apoptosis and affects liver regeneration.

To the Editor,

Hilar cholangiocarcinoma (HC) refers to bile duct epithelial cancer located in the common hepatic duct and left and right hepatic ducts (1). The vast majority of HCs have various degrees of OJ (obstructive jaundice), and complete obstruction is observed in most cases (2).

To ensure patient safety during operating, it is necessary to enhance the patient's tolerance to surgery before an operation. It is reported that preoperative biliary drainage (PBD) can significantly improve liver function and liver regeneration after surgery (3). According to different drainage methods, PBD can be divided into internal biliary drainage (IBD) and external biliary drainage (EBD) (4). IBD is more of a physiological process, which restores bile intestinal and hepatic circulation. The patient recovers well, but the operation is difficult and the diagnostic value is not as good as external drainage (5). Although EBD has a desirable drainage effect, patients may have destruction in bile enterohepatic circulation, and worse long-term recovery. Complications such

Key words: internal and external drainage; bile acid; liver regeneration; obstructive jaundice; apoptosis

Corresponding Author:
Dr Fu Fang,
Department of Surgery 2,
Tonglu First People's Hospital,
Xuesheng Road 338, Tonglu, 311500, Hangzhou,
Zhejiang Province, China
email: fangfutonglu11@163.com

0393-974X (2019)

DISCLOSURE: ALL AUTHORS REPORT NO CONFLICTS OF INTEREST RELEVANT TO THIS ARTICLE.

as disturbance of acid-base balance of electrolytes, poor digestion and absorption, and translocation of intestinal flora often occur (6). In the present study, an animal model of 70% hepatectomy in OJ rats was established under different drainage methods, in order to simulate the clinical course of extensive hepatectomy after hepatic portal cholangiocarcinoma with preoperative drainage and yellowing and to understand the related mechanisms of different drainage methods in liver regeneration after partial hepatectomy.

MATERIALS AND METHODS

Animals

Forty male Sprague-Dawley rats (SPF grade) weighing 260-300g were purchased from Nanjing Junke Bioengineering Co., Ltd., China. The experimental animals were fed regularly, and allowed free access to food and water. The circadian rhythm was maintained properly. The ambient temperature was 15-20°C and humidity was 45-65%. The protocol was approved by the ethics committee of TongLu First People's Hospital, and the experiment followed the regulations of the State Science and Technology Commission on the management of laboratory animals.

Preparation and grouping of animal model

Forty Sprague Dawley rats were randomly divided into five groups: Obstructive jaundice group (OJ), internal bile drainage group (IBD), external bile drainage group (EBD), external bile acid drainage + 0.2%CA group (EBD+CA) and sham operation group (SO), with eight rats in each group. Before the operation, food was forbidden for 12 h and water was not provided for 4 h. The rats were anesthetized by intraperitoneal injection of 10% chloral hydrate solution (Abcam, USA) (0.35ml/100g body weight). Seven days after the common bile duct ligation, the left outer lobe, the left inner lobe, and the middle lobe were removed, which together consisted of about 70% of the liver volume, and then drainage was performed in the tube. After 7 days of internal drainage, the left hepatic lobe and middle lobe were removed, and the liver volume was about 70%. After 7 days of external drainage, the left and middle lobe of the liver were resected, and about 70% of the liver volume was taken.

Postoperative management and observation

After the operation, the rats were kept in separate cages, and a lamp was used for warmth until the anesthesia was over. General conditions such as hair color, activity, diet, mental state, and response to stimuli were recorded. Rats were allowed free access to food and water. The cages were kept clean constantly to prevent infection of the incision.

Specimen collection

At 72 h after 70% PH, the rats in each group were laparotomized. 3-5 ml of blood was taken from lower inferior vena cava, and maintained at room temperature for 15 min, followed by centrifugation (Shanghai Precision Instruments Co., Ltd., China) at 3000 rpm for 15 min. 1.5-2ml of the supernatant was collected in an EP tube (Leica, Germany) and stored at -80°C. The liver tissue with a volume of 1.0×1.0×0.5 cm^3 was immersed in 10% formalin (Shanghai Weiao Biotechnology Co., Ltd., China) and stored. The liver tissue with a volume of 0.5×0.5×0.5 cm^3 was put into 2 ml cryotubes (Thermo Scientific, USA) and quickly transferred into liquid nitrogen and stored at -80°C.

General indexes

The automatic biochemical detector (Nanjing Beiden Medical Co., Ltd., China) was used to detect the changes of serum aspartate transaminase (AST), Alanine transaminase (ALT), total bilirubin (TBIL) and albumin (ALB) levels. Conventional pathological sections and H&E staining were performed. The proportion of mitotic or binucleated cells in 1000 hepatocytes which were counted under a light microscope was defined as the mitotic index (MI). Liver regeneration rate (%) = [C-(A-B)] / (A-B) × 100, where A refers to the liver mass before surgery, B refers to the liver mass removed in the surgery and C indicates the liver mass after regeneration. The expression of proliferating cell nuclear antigen (PCNA) in liver tissues was evaluated by immunohistochemical surfactant protein A. Five visual fields were selected under the microscope at high magnification. The percentage of PCNA-positive cells (brownish yellow nuclei) in 1000 hepatocytes was counted.

Serum total bile acid test

Before the test, the concentration of samples were

estimated and hence the samples were diluted to fit in the detection threshold of the kit. All liquid reagents were mixed prior to use. 100 µL of sample dilution was added to the blank well, and 100 µL standard samples or test samples were added to other wells. The plate was covered and incubated at room temperature at 37°C for 2 h. The solution was thoroughly aspirated from wells and the liquid was discarded. 100 µL of working solution of the test solution A was added to each well. The plate was covered and incubated at 37°C for 1 h. 100 µL of working solution of the test solution B was added to each well. The plate was covered and incubated at 37°C for 1 h. Ninety µL of substrate solution was added to each well. The plate was developed at 37°C in the dark for 30 min. The stop solution was added to each well. At this time, the blue color turns yellow, and the stop liquid is no longer added. The solution in each well was made up to the same level with secondary water. The optical density (OD value) of each well was read at 450 nm. The plate was evaluated right after the stopping the reaction.

Liver pathology test

The liver specimens were fixed and dehydrated. They were then immersed in wax and embedded, followed by paraffin sectioning. Baked slices were produced, and the slices were subjected to HE staining.

Detection of Bcl-2 and Bax expressions in liver tissues by immunohistochemistry

The tissues were dewaxed with xylene twice, for 10 min each time. The tissues were washed with 100%, 95%, 90%, 80%, 70% ethanol and distilled water for 5 min each time, and then washed with PBS (pH 7.4) for 3 times, 5 min each time. The endogenous peroxidase activity was blocked at room temperature by 30-min incubation in 0.3% H_2O_2 and 80% methanol. The sections were rinsed with PBS three times, 5 min each time. 0.01M citrate microwave antigen was repaired at 92~98°C for 15 min. The primary antibody (rabbit anti-mouse Bax, Bcl-2) was applied dropwise at 4°C overnight. The sections were rinsed three times, 2 min each time. The goat anti-rabbit IgG antibody-HRP multimer was added dropwise and incubated at 37°C for 20-30 min. The sections were washed three times, 2 min each time. 50 µl of DAB substrate buffer was added to 950 µl of distilled water to get a working solution. 50 µl of DAB chromogen and 50 µl of 0.6% hydrogen peroxide were added. The DAB coloring solution was added dropwise to the background color, and the reaction was controlled under a microscope. They were rinsed by tap water. The slides were counterstained in hematoxylin, followed by a series of dehydration and transparency. The slides were sealed with neutral gums and observed under a light microscope.

Negative controls were applied in the staining process by replacing the primary antibody with PBS. A known Bcl-2 positive tonsil was used as a positive control. The cytoplasm was brownish yellow as a positive reaction cell.

Detection of hepatocyte apoptosis by TUNEL method

The slides were washed with xylene (Shanghai Yuanye Biotechnology Co., Ltd., China) twice, 5 min each time, followed by washing by 100% ethanol for 5 min. They were washed in the order of 100%, 95%, 85%, 70%, and 50% ethanol for 3 min each time, followed by washing by 0.85% NaCl for 5 min. They were rinsed with PBS for 5 min each time, and incubated with the fixing solution (4% paraformaldehyde) for 15 min at room temperature. They were rinsed with PBS twice, 5 min each time, and the moisture was removed. 100 µl of 20 µg/ml proteinase (Beijing Zhongshang Jinqiao Biotechnology Co., Ltd., China) K solution (after 1:500 dilution) was added to cover the tissue and incubated at room temperature for 10~30 min. They were rinsed with PBS for 5 min, and incubated with the fixing solution (4% paraformaldehyde in PBS) for 5 min at room temperature. They were rinsed with PBS twice, 5 min each time, and the moisture was removed. 100 µl of Equilibration buffer was added and incubated for 5~10 min at room temperature. They sections were incubated in 100 ul/slide of rTd T reaction mixture, followed by incubation with 2×SSC solution for 15 min to terminate the reaction. They were rinsed with PBS three times, 5 min each time. They were incubate with 0.3% H_2O_2 for 3~5 min, and rinsed with PBS three times, 5 min each time. 100 ul/slide of the streptavidin HRP solution (after 1:500 dilution) was added and incubated at room temperature for 30 min. 50 ul of DAB 20 × chromogen and 50 µl of 20 × hydrogen peroxide were added. 100 µl DAB was added onto the slides and developed in a room until pale brown appeared. They were dehydrated through gradient ethanol and treated in xylene twice, 10 min each time. The slides were sealed with neutral gum and observed under an optical microscope. The apoptotic

cells stained with brownish yellow in the nucleus were observed under a light microscope. Five hundred-fold visual fields were counted in each case. The average number of apoptotic cells per 100 nuclei was used as the apoptotic index (AI).

Statistical analysis

Statistical analysis and plotting of data were performed by SPSS statistics 19.0 and Excel. Data were presented as mean ± standard deviation. One-way analysis of variance was used for comparison between groups. $P<0.05$ was considered statistically significant.

RESULTS

Establishment of animal models

As shown in Table IA, the body weight of the rats in the IBD group was higher than that in OJ group and EBD group 7 days after drainage and 3 days after partial hepatectomy, respectively. There was no significant difference between the IBD group and EBD+CA group.

Detection of liver function in each group after PH

The liver function of OJ group was better after

Table I. *Comparison of test results of five groups of rats.*

	Groups	OJ group	IBD group	EBD group	EBD+CA group	SO group
A	Preoperative	271.33±8.11	269.15±8.26	270.28±8.53	270.52±8.22	271.17±8.13
	7d after bile duct ligation	278.17±16.21	277.57±17.43	277.15±14.54	279.16±15.67	278.51±13.72
	7d after different methods of drainage	278.09±14.34	302.13±12.11	269.54±26.13	296.88±11.54	312.41±12.11
	3d after partial hepatectomy	282.12±16.15	308.87±14.65	273.75±18.55	301.08±11.03	318.22±11.32
B	AST(U/L)	583.13±42.33*#	215.14±31.22&	360.14±47.37*#&	231.65±23.11&	36.14±6.36&
	ALT(U/L)	246.45±21.27*#	84.55±5.53&	138.22±21.35*#&	104.54±6.42&	123.725±11.43&
	TBiL(umoL/L)	68.65±6.34*#	13.13±0.59&	7.93±0.52*#&	11.06±1.57&	19.65±1.96&
	ALB(g/L)	28.82±5.54*#	35.87±3.07&	30.34±5.45*#&	34.14±4.18&	37.26±2.25&
C	Liver regeneration rate (%)	40.92±5.51*#	92.03±12.16&	65.16±9.16*#&	89.15±10.69&	99.14±10.16&
	PCNA	55.06±8.15*#	64.13±6.34&	56.87±7.14*#&	62.26±7.15&	78.47±9.87&
	MI(%)	12.33±2.37*#	16.32±2.41&	14.16±3.24*#&	17.06±2.54&	19.11±3.47&
D	TBA	141.34±21.17*#	71.87±14.75*&	54.24±9.26*#&	88.36±13.54*&	91.22±10.38#&

***A)** Changes in body weight of rats (g); **B)** Results of liver function tests in each group; **C)** Changes in liver regeneration rate, PCAN, and mitotic index in each group; **D)** Changes in serum TBA after liver incision (μmol/L)*
**P<0.05, compared with the same period in SO group; #P<0.05, compared with the same period in IBD group; &P<0.05, compared with the same period in OJ group.*

PH, which was significantly different compared to other groups ($P < 0.05$) (Table IB). There was significant difference among the OJ group, IBD group, EBD group and SO group ($P < 0.05$).

Changes of liver regeneration ration, PCNA, and MI in all groups after PH

PCNA was weakly expressed in hepatocytes of the OJ group (Fig. 1A), which was positively expressed in the IBD group (Fig.1B). The expression level of PCNA in the EBD group and EBD+CA group was higher than that in the OJ group but lower than that in the IBD group (Fig. 1C, D). PCNA was strongly expressed in hepatocytes of SO group (Fig.1E).

The liver regeneration rate, PCNA and MI of the OJ group were significantly lower than those of the other groups ($P<0.05$) (Table IC). There was significant difference among the OJ group, IBD group, EBD group and SO group ($P<0.05$).

Changes of TBA levels

As can be seen in Table ID, the overall TBA of the OJ group was significantly increased, which was significantly higher compared to the other groups ($P < 0.05$). There was significant difference among the OJ group, IBD group, EBD group and SO group ($P<0.05$).

Detection of liver pathology

The OJ group showed an alleviation in liver congestion. The swelling at 72 h after the operation was significantly relieved 7 days after obstruction. The obvious dilatation of bile ducts above the obstructive segment was significantly reduced. The liver of the IBD group was significantly relieved of the swelling before drainage. The color was ruddy and bright. The texture of liver was soft, and the dilatation of bile ducts at all levels was significantly reduced. The liver color of rats in the EBD group was brighter than that in the OJ group, however, compared to the liver of EBD+CA group and SO group, the color was darker and the texture was tough. The liver of the EBD+CA group was roughly the same as that of the IBD group. The surface of the liver of the SO group was ruddy, bright and soft.

Observation of H&E staining under a light microscope

Obvious inflammatory cell infiltration was

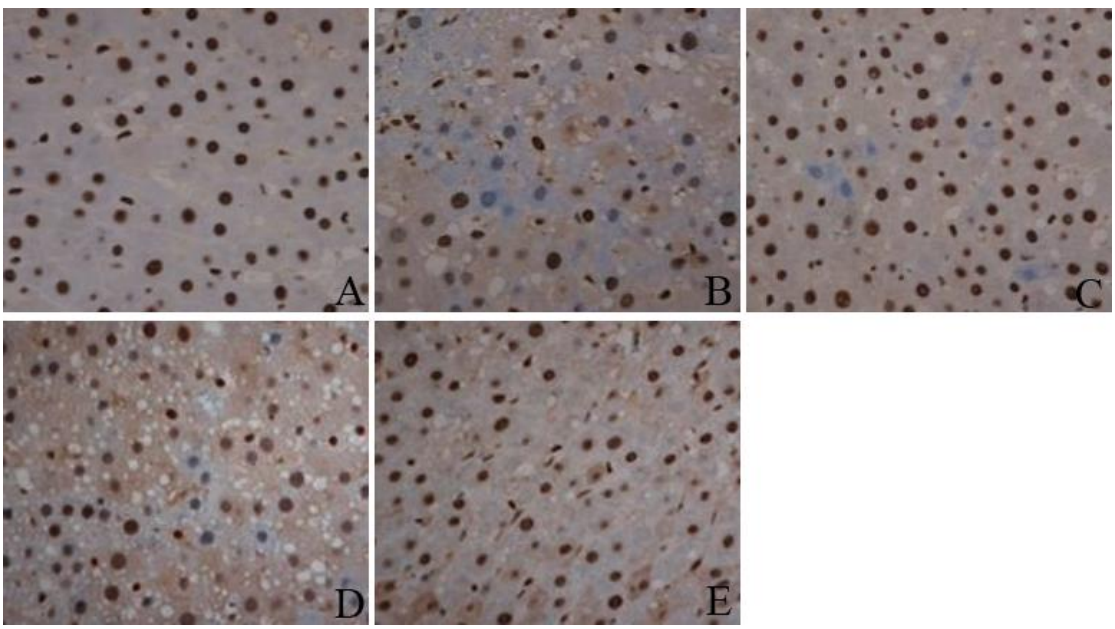

Fig. 1. *The expression of PCNA in liver of each group by immunohistochemistry. **A**) OJ group; **B**) IBD group; **C**) EBD group; **D**) EBD+CA group; **E**) SO group) (100×).*

observed in the liver of the OJ group, with focal necrosis, bile duct dilatation and moderate hyperplasia (Fig. 2A). Hepatocyte or intercellular cholestatic changes in the IBD group were significantly less than those in the OJ group. The bile duct was slightly dilated and proliferated, with focal necrosis and a small amount of inflammatory cell infiltration (Fig. 2B). The changes under the light microscope in the EBD group and EBD+CA group were less than those of the OJ group but more than those of the IBD group (Fig. 2C, D). There were no obvious abnormalities in the liver cell morphology of the SO group. The structure of the hepatic lobule, central vein, and portal area was clear, and only a small number of inflammatory cells were scattered (Fig. 2E).

Detection of Bax and Bcl-2 expressions and apoptosis in hepatocytes

The immunohistochemical positive reaction showed brownish yellow particles. Both Bax and Bcl-2 positive reactions were localized in the cytosol.

As shown in Fig. 3A, Bax was strongly positive in the OJ group. Bax was weakly expressed in the IBD group. The expression of Bax in the EBD group and EBD+CA group was lower than that of the OJ group but higher than that of the IBD group. Bax was rarely expressed in the SO group.

As shown in Fig. 3B, little Bcl-2 was expressed in hepatocytes of the OJ group, and was positively expressed in I the BD group. The expression of Bcl-2 in the EBD group and EBD+CA group was higher than that of the OJ group but lower than that of the IBD group. Almost no Bcl-2 expression was found in the SO group.

Determination of hepatocyte apoptosis by TUNEL method

As shown in Fig. 3C, substantial apoptosis was found in the OJ group, but little in the IBD group. Apoptosis in the EBD group and EBD+CA group was less than that in the OJ group but greater than that in IBD group. Very little apoptosis was found in the SO group.

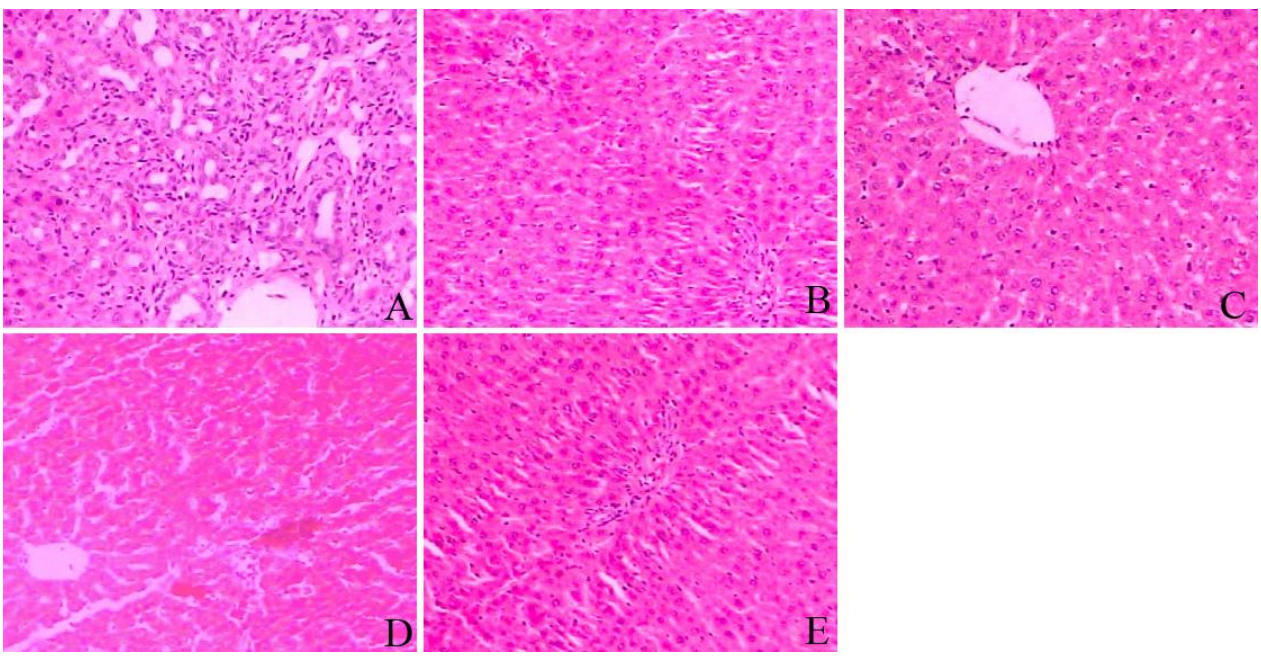

Fig. 2. *HE staining results of liver in each group. A) OJ group; B) IBD group; C) EBD group; D) EBD + CA group; E) SO group) (100 ×).*

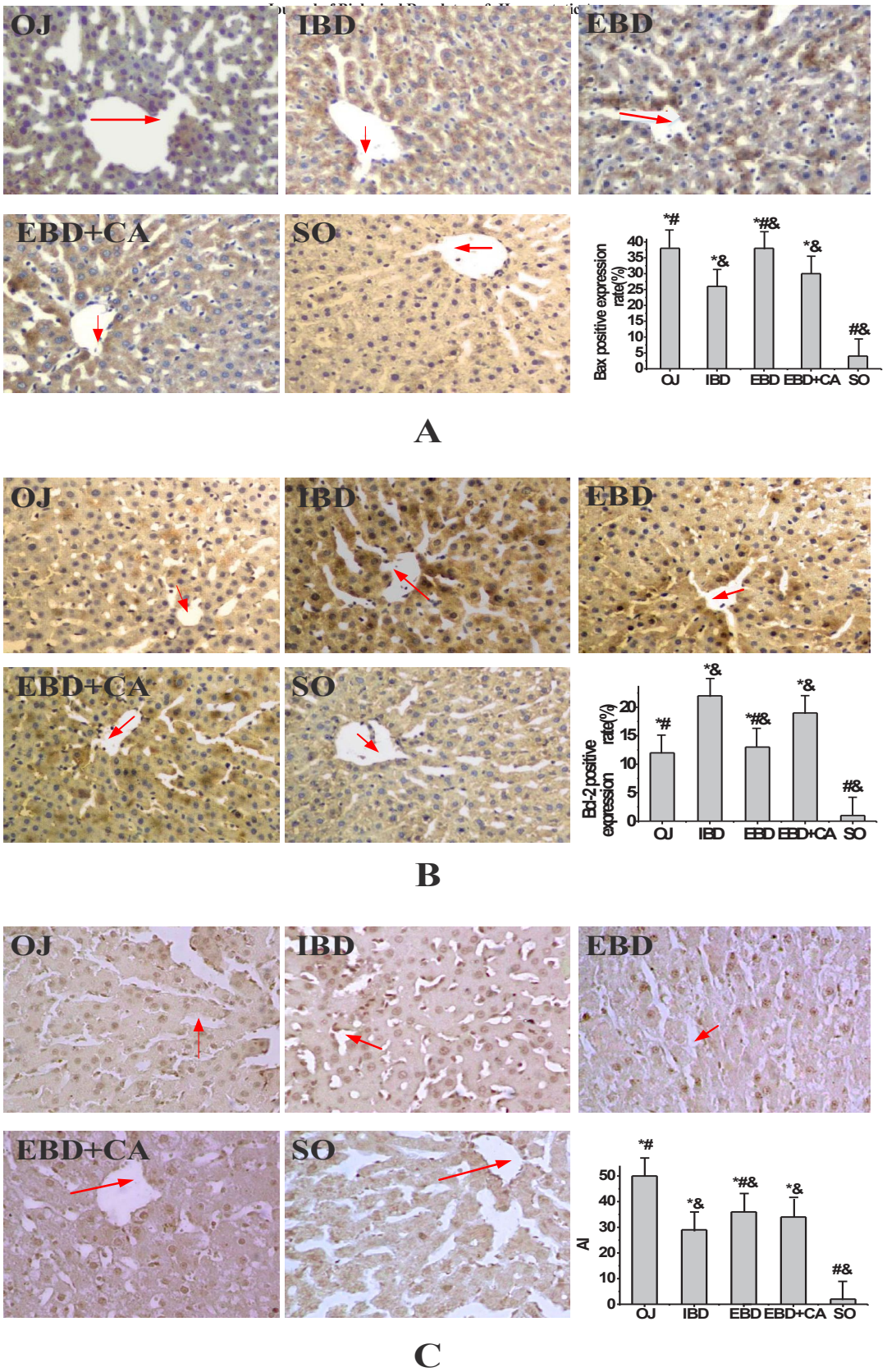

Fig. 3. *Liver indexes of rats in each group. **A)** Expression of Bax in rat liver of each group; **B)** Expression of bcl-2 in rat liver of each group; **C)** Liver TUNEL results of rats in each group) (Note: *P<0.05, compared with SO group; #P<0.05, compared with IBD group; &P<0.05, compared with OJ group) (100×)*

DISCUSSION

Bcl-2 is an apoptosis inhibitory gene (7), and Bax has an opposite function of Bcl-2 (8). The presence of Bcl-2 in the mitochondrial outer membrane protects cells from apoptosis. Bile acid is a general term for a class of choline acids in bile (9). After liver synthesis, the bile salt output pump enters the small intestine with bile and participates in metabolic processes (10). Recent studies found that bile acids can act as a signaling molecule to play an important regulatory role in liver regeneration by activating related signaling pathways (11, 12). There was no significant difference in the exogenous bile acid intervention between the EBD group and the IBD group. It is speculated that bile acid may inhibit hepatocellular apoptosis by directly or indirectly down-regulating the proapoptotic gene Bax and up-regulating the expression of anti-apoptotic gene Bcl-2.

The results of this study indicated that Bax played a very important role in the regulation of hepatocyte apoptosis. Bile acid had an inhibitory effect on hepatocyte apoptosis after hepatectomy in different drainage modes of OJ rats, and had a promoting effect on liver regeneration of residual liver. There was no significant difference in the exogenous bile acid intervention between the EBD group and IBD group. Bile acid may inhibit the apoptosis of hepatocytes by directly or indirectly down-regulating the proapoptotic gene Bax and up-regulating the expression of anti-apoptotic gene Bcl-2. In conclusion, Bax and Bcl-2 promoted liver regeneration by inhibiting apoptosis in liver tissues during early liver regeneration. The regulatory mechanisms and their signaling pathways remain to be further studied.

REFERENCES

1. Heimbach JK, Sanchez W, Rosen CB, Gores GJ. Trans-peritoneal fine needle aspiration biopsy of hilar cholangiocarcinoma is associated with disease dissemination. HPB (Oxford) 2011; 13(5):356-60.
2. Li M, Li K, Qi X, et al. Percutaneous transhepatic biliary stent implantation for obstructive jaundice of perihilar cholangiocarcinoma: a prospective study on predictors of stent patency and survival in 92 patients. J Vasc Interv Radiol 2016; 27(7):1047-55.e2
3. Xu C, Huang XE, Wang SX, Lv PH, Sun L, Wang FA. Comparison of infection between internal-external and external percutaneous transhepatic biliary drainage in treating patients with malignant obstructive jaundice. Asian Pac J Cancer Prev 2015; 16(6):2543-46.
4. Tang X, Ma W, Zhan W, et al. Internal biliary drainage superior to external biliary drainage in improving gut mucosa barrier because of goblet cells and mucin-2 upregulation. Biosci Rep 2018; 38(3):BSR20171241.
5. Mori A, Ito S, Yumura T, Hachiya H, Sawada M, Hayashi S, Ohashi N. Development of an external-to-internal convertible endoscopic biliary drainage device – a preliminary prospective feasibility study. Endosc Int Open 2018; 6(1):E123-E126.
6. Shestopalov SS, Mikhaylova SA, Abramov EI, Ozhigina EV. [Malignant obstructive jaundice management via external biliary drainage followed by bile examination]. Khirurgiia (Mosk) 2018; (10):44-50.
7. Tessoulin B, Papin A, Gomez-Bougie P, Bellanger C, Amiot M, Pellat-Deceunynck C, Chiron D. BCL2-Family dysregulation in B-cell malignancies: from gene expression regulation to a targeted therapy biomarker. Front Oncol 2019; 8:645.
8. Niu H, Gao W, Cheng J, Liu B, Li Y, Huang K, Yang H. Improvement of percutaneous transhepatic biliary internal-external drainage and its initial experience in patients with malignant obstruction of the upper biliary tree. Hepatogastroenterology 2012; 59(117):1368.
9. Wu L, Li W, Wang Z, Yuan Z, Hyder Q. Bile acid-induced expression of farnesoid X receptor as the basis for superiority of internal biliary drainage in experimental biliary obstruction. Scand J Gastroenterol 2013; 48(4):496-503.
10. Cao J, Chen J, Wang J, Jia R, Xue W, Luo Y, Gan X. Effects of fluoride on liver apoptosis and Bcl-2, Bax protein expression in freshwater teleost, Cyprinus carpio. Chemosphere 2013; 91(8):1203-12.
11. Chen Q, Chen L, Wu X, et al. Dihydroartemisinin prevents liver fibrosis in bile duct ligated rats by inducing hepatic stellate cell apoptosis through modulating the PI3K/Akt pathway. IUBMB

Life 2016; 68(3):220-31.
12. Webster CR, Anwer MS. Hydrophobic bile acid apoptosis is regulated by sphingosine-1-phosphate receptor 2 in rat hepatocytes and human hepatocellular carcinoma cells. Am J Physiol Gastrointest Liver Physiol 2016; 310(10):G865-73.

LETTER TO THE EDITOR

MAGNETIC RESONANCE ARTHROGRAPHY ACCURACY IN THE DETECTION OF LABRAL TEARS IN YOUNG PATIENTS WITH CHRONIC UNSTABLE SHOULDER: CORRELATION WITH ARTHROSCOPY

D. BEOMONTE ZOBEL[1], C. DELL'ATTI[1], N. MAGARELLI[1], D. COVIELLO[1], G. BELMONTE[1], M.F. SACCOMANNO[2], A. PALADINI[3], G. MILANO[2], A. LEONE[1] and C. COLOSIMO[1]

[1]Institute of Radiology, Fondazione Policlinico Universitario A. Gemelli IRCCS, Catholic University of the Sacred Heart, Rome, Italy; [2]Institute of Orthopedics and Traumatology, Fondazione Policlinico Universitario A. Gemelli IRCCS, Catholic University of the Sacred Heart, Rome, Italy; [3]SCDU Diagnostic and Interventional Radiology, University Hospital Maggiore della Carità, Novara, Italy

Received June 21, 2018 – Accepted December 18, 2018

The aim of this study is to determine the diagnostic performance of Magnetic Resonance Arthrography (MRA) in evaluating lesions of the glenoid labrum, in young active patients with chronic unstable shoulder, compared to shoulder arthroscopy. We retrospectively considered 65 MRA examinations, performed between December 2011 and January 2018. Among them, thirty-five patients (31 men, 4 women; mean age, 27.3 years; range, 16-53 years; 4 patients with a previous arthroscopy of the same shoulder) underwent shoulder arthroscopy after MRA. Arthroscopic reports were collected and analyzed for the correlation with MRA results. The inclusion criteria were: a) clinical symptoms of chronic shoulder instability with at least 2 episodes and less than 5 episodes of shoulder dislocation; b) arthroscopy performed by surgeons in our institution; c) non-professional sportsmen, that is occasional or amateur sport practice. MRA examinations, carried out with a 1.5 T superconductive magnet, were evaluated by two radiologists. The authors observed complete agreement between MRA evaluation and arthroscopic findings in 31 patients, and disagreement in 4 patients. Sensitivity was 93%, specificity 71%, positive predictive value 93%, negative predictive value 71% and the diagnostic accuracy for all glenoid lesions 88%. In patients with chronic shoulder instability, MRA confirmed its high sensitivity and positive predictive value for the diagnosis of labral lesions, providing useful information on the size and extent of the tears. The lower value of specificity and negative predictive value were probably due to the small number of patients who underwent arthroscopy after an MRA negative for glenoid injuries.

To the Editor,

The shoulder is the most inherently unstable joint in the body, prone to frequent subluxation or dislocation (incidence of 24/100.000 cases per year); in 96-98% of cases, the shoulder displaces in an anterior direction (1). Glenoid labral damage is frequently identified as the source of recurrent subluxation or luxation following a major trauma or

Key words: MR-arthrography; shoulder instability; chronic unstable shoulder; glenoid labrum lesion and MR-arthrography

Corresponding Author:
Dr Nicola Magarelli,
Institute of Radiology, Fondazione Policlinico Universitario A. Gemelli, IRCCS,
Catholic University of the Sacred Heart.
Largo Francesco Vito 1, 00168, Rome, Italy
Tel.: +39 3382438340 - Fax: +39 0630155428
e-mail: nicola.magarelli@unicatt.it

0393-974X (2019)

repeated micro traumatisms, especially in patients affected by ligamentous laxity (2). To plan the correct surgical treatment, for improved outcome in young patients (under the age of 30), it is essential to identify the precise location of labral injuries, according to a clockwise approach (3) or by dividing the labrum into six segments (4), and the associated lesions. Usually, in patients with acute symptoms, magnetic resonance imaging is the modality of choice, without using any contrast material, considering that the soft-tissue changes and the presence of joint effusion are able to produce enough intrinsic contrast to obtain a characterization of the lesions (5). On the contrary, in patients with recurrent shoulder luxation, and when the clinical evaluation suggests the presence of some insufficiency of the glenoid labrum, magnetic resonance arthrography (MRA), with intra-articular contrast injection, is the preferred technique as it distends the capsule, giving a better demonstration of intra-articular structures, and allows the passage of the contrast agent into the labrum, in case of tears, or between the labrum and the glenoid, in case of labral detachment. While there are several reports on the accuracy and sensitivity of MRA *versus* arthroscopy in the detection of Superior Labral tear from Anterior to Posterior (SLAP) lesions (6) or in elite level athletes (7), and there is a well-known high prevalence of labral pathology on MRA, with a lack of association with symptomatic injuries in athletes (8), less articles have been devoted to evaluate the role of MRA in identifying labral lesions in young active patients with unstable shoulder. Considering the arthroscopic findings as the reference standard, we therefore retrospectively evaluated the accuracy of MRA in detecting the type and location of labral tears in young patients with chronic shoulder instability.

MATERIALS AND METHODS

An institutional review board approved the retrospective study and each patient, at the time of MRA examination, gave a full written informed consent.

Sixty-five MRA examinations of patients with chronic shoulder instability performed between December 2011 and January 2018 were retrospectively analyzed. Of these, only patients who underwent arthroscopy after MRA were considered. The inclusion criteria were: a) clinical symptoms of shoulder chronic instability with at least 2 episodes and less than 5 episodes of shoulder dislocation; b) arthroscopy performed by orthopedic surgeons in our institution; c) non-professional sport performers, that is occasional or amateur sport practice.

We excluded patients who: a) did not proceed to

Table I. *Correlation between MR arthrography and arthroscopy findings.*

		Arthroscopy							
		NO lesion	SLAP I	SLAP II	SLAP III	SLAP IV	BANKART	REVERSE BANKART	ALPSA
MR Arthrography	NO lesion	5	0	1	0	0	0	0	1
	SLAP I	0	2	0	0	0	0	0	0
	SLAP II	1	0	8	0	0	0	0	0
	SLAP III	1	0	0	0	0	0	0	0
	SLAP IV	0	0	0	0	2	0	0	0
	BANKART	0	0	0	0	0	8	0	0
	REVERSE BANKART	0	0	0	0	0	0	4	0
	ALPSA	0	0	0	0	0	0	0	2

arthroscopy and those who performed arthroscopy in another hospital with unavailable surgical reports; b) performed arthroscopy after a time interval > 1 year from MRA; c) had complete tears involving at least one tendon of the rotator cuff (that lesion could be related to multidirectional instability). A previous surgical shoulder arthroscopy was not considered a criterion to exclude a patient from the study. Only 35 patients met the inclusion criteria (31 men, 4 women; mean age, 27.3 years; range 16-53 years; 19 right shoulders; 16 left shoulders; 4 patients with a previous operative arthroscopy for labral repair of the same shoulder), and all carried out occasional sport practice. MR arthrograms were retrospectively reviewed by two radiologists by consensus. The mean interval between MRA and arthroscopy was 3 months (range 2-7 months).

All MRA studies were carried out with a dedicated 8-channel shoulder coil using a 1.5 T superconductive magnet (Optima MR 450 W GEM, General Electric Health Care, Milwaukee, USA). Before MRA examination, local anesthesia was performed (Mepicain 2%, 5 ml). Then, approximately 2 ml of iodinated contrast agent (Iopamiro 300; Bracco, Italy) were injected using a 22-gauge spinal needle, in the glenohumeral joint, under fluoroscopic guidance, with an anterior approach. Subsequently, 15-20 ml of gadolinium based-contrast medium (Magnevist; Bayer-Schering, Berlin, Germany) solution, diluted to a concentration of 2 mmol/l (1:20), were injected using the same 22-gauge spinal needle. All procedures were carried out respecting sterile conditions and no complications, such as extravasation, anesthetic drug reaction, bleeding or infection were recorded.

MRA was performed immediately after or no more than 15 min after contrast injection. All patients underwent MRA imaging with the upper arm in a neutral position. Standard protocol included coronal, sagittal, and axial fat-saturated T1-weighted, and axial T1-weighted fast Spin Echo images.

Considering their location, according to a clockwise approach (3) or dividing the labrum in six segments (4), the labral tears were classified into: SLAP lesions, considering ten different types (4), involving the superior labrum; Bankart lesion, GLAD (Gleno-Labral Articular Disruption), and Bankart variants, such as Perthes, ALPSA (Anterior Labroligamentous Periosteal Sleeve Avulsion), involving the antero-inferior labrum; reverse-Bankart lesion, posterior GLAD (Gleno-Labral Articular Disruption), and reverse-Bankart variants, such as reverse Perthes, POLPSA (Posterior Labroligamentous Periosteal Sleeve Avulsion), involving the postero-inferior labrum (5).

Additional findings such as anatomic variants (sublabral recess and sublabral foramen) were also reported.

Reports from all arthroscopies were collected from orthopedic and considered as reference standard for confirming or excluding the MRA findings.

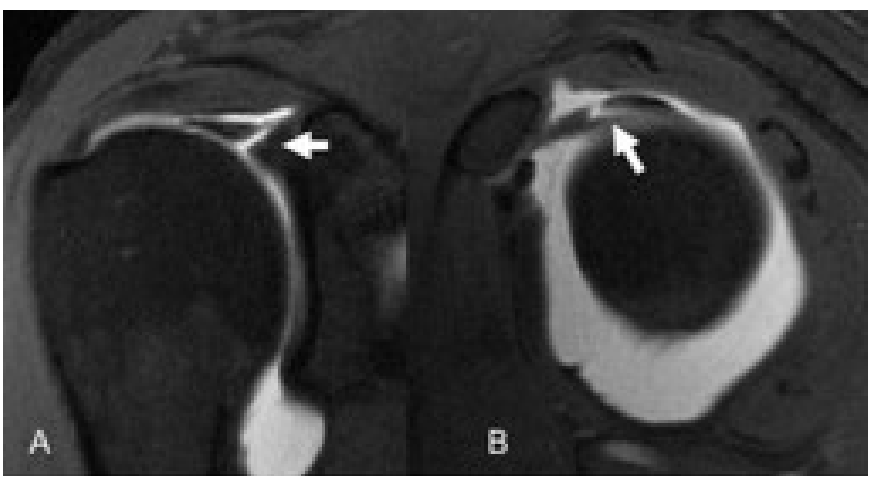

Fig. 1. *A 32-year-old man with SLAP lesion type II.* ***A)*** *Coronal T1-weighted fat-suppressed MR image shows a tear of the anterosuperior glenoid labrum (arrow);* ***B)*** *sagittal T1-weighted fat-suppressed MRA image demonstrates involvement of the biceps labral complex (arrow).*

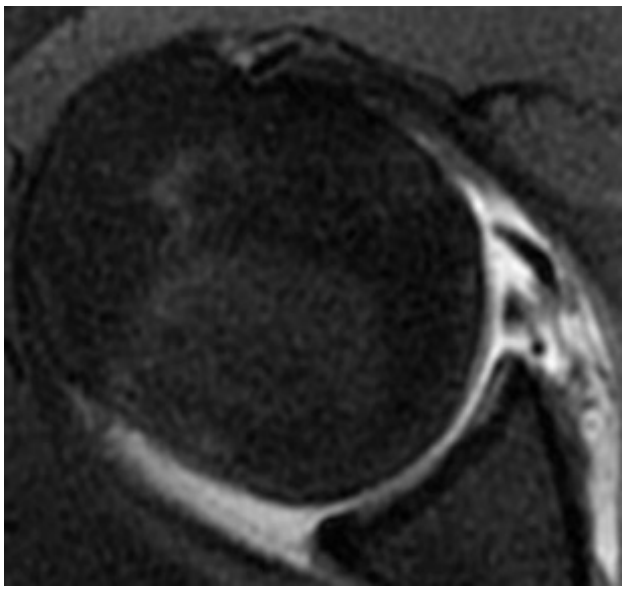

Fig. 2. *A 22-year-old man with Bankart lesion. Axial T1-weighted fat-suppressed MRA image shows a large interruption of the continued hypointense linear profile of the anteroinferior glenoid labrum.*

RESULTS

MRA and arthroscopic results are reported in Table I. MRA showed 12 SLAP lesions (34.3%) (Fig. 1), 8 Bankart (22.8%) (Fig. 2), 2 ALPSA (5.7%) (Fig. 3) and 4 reverse-Bankart (11.4%). Among the SLAP lesions, 2 cases were classified as SLAP I (16.7%), 8 as SLAP II (66.6%), 2 as SLAP IV (16.7%). Among Bankart lesions, 4 patients presented an associated bone fracture of the glenoid. All these injuries were confirmed at arthroscopy.

MRA demonstrated 2 injuries that were not confirmed during arthroscopy: 1 SLAP II and 1 SLAP III. Furthermore, MRA failed to demonstrate 2 injuries: 1 ALPSA e 1 SLAP II; in both these cases, the patients had undergone previous surgery. Therefore, we obtained 26 true positives, 5 true negatives, 2 false positives, and 2 false negatives. MRA achieved a sensitivity of 93%, a specificity of 71%, a positive predictive value of 93%, a negative predictive value of 71% and a diagnostic accuracy, for all glenoid lesions, of 88 %.

In one true positive diagnosis, arthroscopy confirmed Bankart lesion but depicted a sublabral foramen which was not detected on MRA. In another case, MRA overestimated the grade of SLAP lesion, judging as SLAP lesion type II a SLAP type I observed on arthroscopy.

DISCUSSION

Our retrospective evaluation showed a significant correlation ($P < 0.05$) between the results of MRA and the arthroscopic findings. The sensitivity and positive

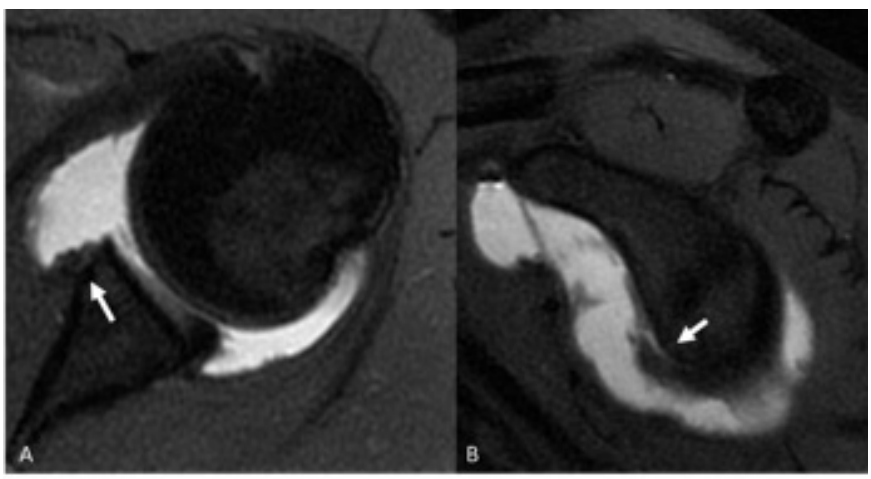

Fig. 3. *A 24-year-old man with ALPSA lesion.* ***A)*** *Axial T1-weighted fat-suppressed MRA image shows a detachment of the anteroinferior labrum which remains attached to the periostium and is shifted medially (arrow);* ***B)*** *Sagittal T1-weighted fat-suppressed MRA image demonstrates the presence of contrast material between the anteroinferior glenoid and the labrum (arrow).*

predictive value are in agreement with those reported in other studies (9, 10). The lower values of specificity and negative predictive value, compared with other published results, are probably due to the inclusion of patient who had undergone previous surgery and to the small number of patients who had undergone arthroscopy after an MRA negative for glenoid lesions. In one false positive case, we indicated as SLAP II a case of sublabral foramen, whereas in the other case the hypointense rounded image, referred as SLAP III on MRA, was related to an air bubble. The process of distinguishing labral tears from normal anatomic variants may be a challenging task for the radiologist. Concerning the false negative cases (1 ALPSA e 1 SLAP II), the two patients had undergone previous surgery, therefore the normal anatomy was subverted with a more difficult detection of labral tears.

One of the strengths of the present study is the homogeneity of the study group, as only two radiologists performed and reviewed all MRA examinations and only two orthopedic surgeons carried out the arthroscopic repairs. Another very important aspect is to consider the efficacy of MRA exclusively in the evaluation of labral injuries in unstable shoulder, which is the recognized indication to carry out an MRA.

The study had limitations as it was a retrospective evaluation with a relatively small sample size from a single institution, thus the incidence of Bankart lesions resulted lower than SLAP lesions in unstable shoulders, considering the previously published articles (11, 12). Furthermore, four patients who had undergone previous shoulder arthroscopy were also included, although there are few reports considering the accuracy of MRA in such cases. Another limitation was the lack of ABER position, that could be useful in detection of labral tear. Lastly, the control group was small, composed of only five patients with positive clinical signs (apprehension test) whose instability was not related to the presence of labral pathologies.

In conclusion, MRA is a valid diagnostic tool to identify and classify labral tears in young active patients with chronic unstable shoulder. In our experience, the sensitivity and the positive predictive value are sufficient to guide the orthopedic surgeon in choosing the right surgical approach, arthroscopy *versus* open treatment, or in planning the arthroscopic repair.

REFERENCES

1. Knapik DM, Voos JE. Magnetic resonance imaging and arthroscopic correlation in shoulder instability. Sports Med Arthrosc Rev 2017; 25(4):172-78.
2. Kim DS, Yoon YS, Yi CH. Prevalence comparison of accompanying lesions between primary and recurrent anterior dislocation in the shoulder. Am J Sports Med 2010; 38:2071-76.
3. Mohana-Borges AV, Chung CB, Resnick D. Superior labral anteroposterior tear: classification and diagnosis on MRI and MR arthrography. Am J Roentgenol 2003; 181(6):1449-62.
4. Clavert P. Glenoid labrum pathology. Orthop Traumatol Surg Res 2015; 101(1 Suppl):S19-24.
5. De Coninck T, Ngai SS, Tafur M, Chung CB. Imaging the glenoid labrum and labral tears. Radiographics 2016; 36(6):1628-47.
6. Symanski JS, Subhas N, Babb J, Nicholson J, Gyftopoulos S. diagnosis of superior labrum anterior-to-posterior tears by using MR Imaging and MR arthrography: A systematic review and meta-analysis. Radiology 2017; 285(1):101-13.
7. Jarraya M, Roemer FW, Gale HI, Landreau P, D'Hooghe P, Guermazi A. MR-arthrography and CT-arthrography in sports-related glenolabral injuries: a matched descriptive illustration. Insights Imaging 2016; 7(2):167-77.
8. Knapik DM, Gebhart JJ, Sheehan J, Tanenbaum JE, Salata MJ, Voos JE. recurrent labral tearing on magnetic resonance imaging is not predictive of diminished participation among national football league athletes. Arthroscopy 2018; 34(1):66-72.
9. Saqib R, Harris J, Funk L. Comparison of magnetic resonance arthrography with arthroscopy for imaging of shoulder injuries: retrospective study. Ann R Coll Surg Engl 2017; 99(4):271-74.
10. Holzapfel K, Waldt S, Bruegel M, et al. Inter- and intraobserver variability of MR arthrography in the detection and classification of superior labral anterior posterior (SLAP) lesions: evaluation in 78 cases with arthroscopic correlation. Eur Radiol 2010;

20(3):666-73.
11. Gutierrez V, Monckeberg JE, Pinedo M, Radice F. Arthroscopically determined degree of injury after shoulder dislocation relates to recurrence rate. Clin Orthop Relat Res 2012; 470(4):961-964.
12. Durban CM, Kim JK, Kim SH, Oh JH. Anterior shoulder instability with concomitant superior labrum from anterior to posterior (SLAP) lesion compared to anterior instability without SLAP lesion. Clin Orthop Surg 2016; 8(2):168-74.

JOURNAL OF BIOLOGICAL REGULATORS & HOMEOSTATIC AGENTS Vol. 33, no. 2, 587-592 (2019)

LETTER TO THE EDITOR

AEROBIC EXERCISE AND OREXIN A: ROLE OF SYMPATHETIC ACTIVITY AND REDOX SYSTEM

V. MONDA[1], I. VILLANO[1], A. MESSINA[1], A. VALENZANO[2], M. SALERNO[2], S. SANTO SIGNORELLI[3], M. MONDA[1], V. RUSSO[4], F. SESSA[2] and G. MESSINA[2]

[1]Department of Experimental Medicine, University of Campania "Luigi Vanvitelli", Naples, Italy; [2]Department of Clinical and Experimental Medicine, University of Foggia, Foggia, Italy; [3]Department of Clinical and Experimental Medicine, University of Catania, Catania, Italy; [4]Department of Ophthalmology. University of Foggia, Foggia, Italy

Received August 24, 2018 – Accepted January 8, 2019

Aerobic exercise is associated with the sympathetic activation evoking adaptive responses to sustain muscle engagement. Physical exercise can cause alterations in the cardiovascular activity and cellular stress may occur which could be marked by either heart rate (HR), or galvanic skin response (GSR). Moderate plasma levels of reactive oxygen species (ROS) are considered as health markers, absolving to important roles such as adaptive cellular responses to exercise. Orexin A, a hypothalamic peptide, causes a widespread stimulation of the sympathetic nervous system, playing a role in many physiological functions. The aim of this study was to analyze the effects of aerobic exercise on Orexin A plasma levels, evaluating the possible association with physical exercise and oxidative stress, both involved in the sympathetic and thermogenic reactivities. Three blood samples were collected at various periods of time from all participants (25 males with mean age of 23.4±2.1 years): resting time (0 min), exercise time (at the start and at end of exercise) and recovery time (30-45 min after training). At the same interval times, heart rate (HR), galvanic skin response (GSR), rectal temperature, and d-ROMs test were monitored. Exercise induced a significant increase in the following parameters: HR ($p < 0.01$); GSR ($p < 0.05$); rectal temperature ($p < 0.01$); and plasma Orexin A ($p < 0.01$). No significant increase of the d-ROMs values were found. The results of this study confirmed that physical activity is associated with the sympathetic activation, as demonstrated by HR and GSR increases after training. Changes in the Orexin A plasma levels reveal the presence of hormonal adaptations in response to exercise, indicating that this peptide might be involved in cardiovascular regulation. Further studies could confirm the multitasking role of this neuropeptide.

To the Editor,

Physical activity (PA) is an effective, practical and inexpensive way to improve health, to balance the internal homeostatic process, to control body weight and to reduce age-related cognitive decline (1, 2).

PA increases the metabolic rate, leading to higher reactive oxygen species (ROS). ROS are molecules or ions formed by the incomplete one-electron reduction of oxygen; the production was performed especially via NADPH oxidase and the mitochondrial respiratory chain (3). At moderate

Key words: exercise; orexin A; sympathetic activity; reactive oxygen species; UCPs

Corresponding Author:
Dr Giovanni Messina,
Department of Clinical and Experimental Medicine,
University of Foggia,
Foggia, Italy
Tel.: +39 0881588095
e-mail: giovanni.messina@unifg.it

0393-974X (2019)

concentrations, ROS participate in redox regulation acting as regulatory mediators in signaling processes, re-establishing "redox homeostasis" thanks to the ROS-mediated responses (4). By contrast, exhaustive exercise increases ROS generation, leading to oxidative stress (OS) and damage to physiological functions (5).

The Orexin A (hypocretin-1), a neuropeptide synthesized by neurons located in the perifornical region of the lateral hypothalamus area (LHA), plays several roles in the regulation of various body systems. It was described that a dose of Orexin A, given by intracerebroventricular (IVC) injection, causes effects on food intake; it is also responsible for an increase in blood pressure (BP), heart rate (HR) and metabolic rate (6, 7). In addition to the regulation of food intake, BP, HR, and metabolism, the Orexin A system plays an important role in sleep regulation and in temperature control. The aim of this study is the analysis of the aerobic exercise effects on Orexin A plasma levels; moreover, this paper aims to describe a possible link between PA and oxidative stress.

MATERIALS AND METHODS

Twenty-five male athletes (mean age 24.9 years; SD ± 1.3), at the lower agonistic level (regional level), were enrolled by the Unit of Dietetics and Sports Medicine of the University of Campania "L. Vanvitelli". Low agonistic level training corresponds to the moderate level of physical exercise. According to the American Heart Association's Recommendations for Physical Activity in Adults, exercise with values between 11 and 14 of the Borg Rating of Perceived Exertion scale (or RPE) is defined as "moderate activity". The principal physiological parameters are summarized in Table I.

All participants gave their written informed consent to take part in the study and signed permission for the use plasma samples. The study protocol was approved by the Ethics Committee of the "University of Campania" and all procedures were performed in accordance with the Declaration of Helsinki.

Study protocol

The protocol consisted of a single testing day in which each subject performed their usual daily routine. The blood samples were collected during the experiment at 5 different time-points: resting time (0 min), exercise time (at the start and at end of exercise) and recovery time (30-45 min after training). The physical activity consisted of a cycle ergometer exercise at 75 W for 15 min, performed at 1-15 min periods (moderate intensity).

Measurement of heart rate (HR), galvanic skin response (GSR), and rectal temperature (RT)

The measurements of HR, GSR, and RT were recorded at 5 different time-points: resting time (0 min), exercise time (at the start and at end of exercise) and recovery time (30-45 min after training). Each subject wore a chest belt hard-wired to a digital R-R recorder (BTL08 SD ECG), where the QRS-signal wave-form R-R signal was sampled at the resolution of 1 ms. The HR (beats min-1) was calculated using the formula: HR = 60 R-R interval-1; the R-R interval was converted into seconds. The GSR parameters were measured simultaneously using the SenseWear Pro Armband™ (version 3.0, BodyMedia, Inc. PA, USA), which was worn on the right arm over the tricep muscles at the midpoint between acromion and olecranon processes, as recommended by the manufacturer. Rectal temperatures were measured

Table I. *Principal biological parameters for the study group.*

PARAMETERS	MEAN VALUES
Body Mass Index	23.4±7
Systolic blood pressure	122±8
Diastolic blood pressure	72±6

with electronic thermometer thermistor/thermocouple (Ellab A/S, Hilleroed, Denmark).

Plasma Orexin A detection

Blood samples from the forearm vein were drawn at 8:00 a.m., using Vacutainer tubes (BD, Franklin Lakes, NJ, USA) containing EDTA and 0.45 TIU/ml of aprotinin.. After centrifugation, the plasma was stored at −80°C until analysis. Enzyme-linked immunoassay kits (ELISA) were used to measure plasma Orexin A levels (Phoenix Pharmaceuticals). The minimal detectable concentration was 0.37 ng/ml, the intra-assay error < 5% and the inter-assay error < 14%.

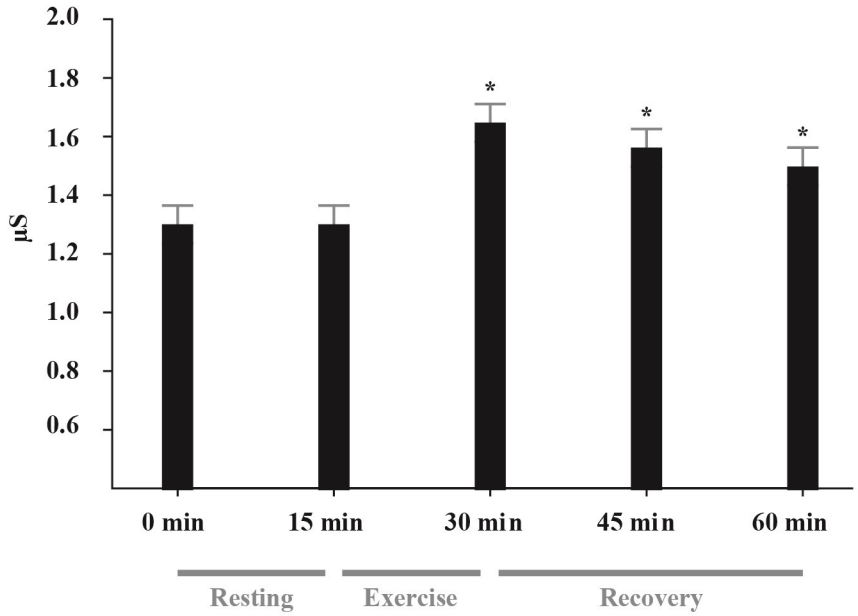

Fig. 1. *GSR variations among pre-exercise status, during exercise status and in the recovery periods.*

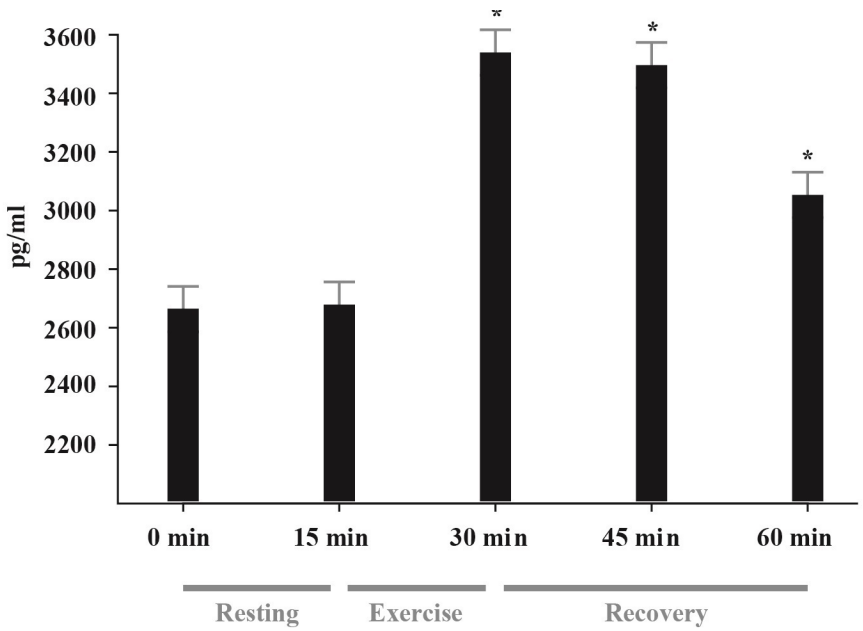

Fig. 2. *Variations of Orexin A plasma values between pre-exercise status, during exercise status and in the recovery periods.*

d-ROMs test

The d-ROMs test was tested with the Free Radical Analytical System 4 (FRAS4), analyzing a single drop of peripheral (finger) blood. The d-ROMs values were expressed in the arbitrary unit U. CARR (Carratelli Units), as established by the manufacturer (1 U. CARR corresponds to 0.08 mg of H2O2/dL). Normal values range between 250 and 300 U. CARR and values higher than 300 U. CARR suggest increased oxidative stress.

Statistical analysis

The values are presented as means ± SD. Statistical analysis was performed using analysis of variance (ANOVA). Multiple comparisons were performed by the Newman-Keuls post hoc test. All data were analyzed with GraphPad Prism-version 5.01 statistical software package (GraphPad, CA, USA).

RESULTS

PA caused an increase in RT: the maximum level was recorded at 30 min. RT (°C) changed from a basal value of 37.36±0.88 to 37.81±0.12, and diminished to 37.48±0.09 at 60 min. The ANOVA showed significant effects [$F(3, 48) = 5.29$, $p < 0.01$]. The post-hoc test showed a difference between pre-exercise and post-exercise values at 30, 45, and 60 min.

The physical activity caused an increase in HR with the maximum level at 30 min. Heart rate (beats/min) changed from a basal value of 70±5.3 to 137.9±4.7 at 30 min, and returned almost to basal value at 60 min. The ANOVA Test showed significant effects [$F(3,48) = 91.54$, $p < 0.01$]. The post-hoc test showed a difference between pre-exercise and post-exercise values at 30 min.

The physical activity caused an increase in GSR with the maximum level at 30 min. GSR (μS) increased from a basal value of 1.33±0.11 to 1.66±0.12 at 30 min, and it decreased to 1.49±0.12 at 60 min (Fig. 1).

The ANOVA showed significant effects [$F(3, 48) = 3.87$, $p < 0.05$]. The post-hoc test showed a difference between pre-exercise and post-exercise values at 30, 45, and 60 min.

The physical activity caused an increase in Orexin A from a basal value of 2612±189 pg/mL to a maximum level (3592±189 pg/mL) at 30 min. Orexin A decreased to a value of 2961±193 at 60 min (Fig. 2). The ANOVA showed significant effects [$F(3, 48)$

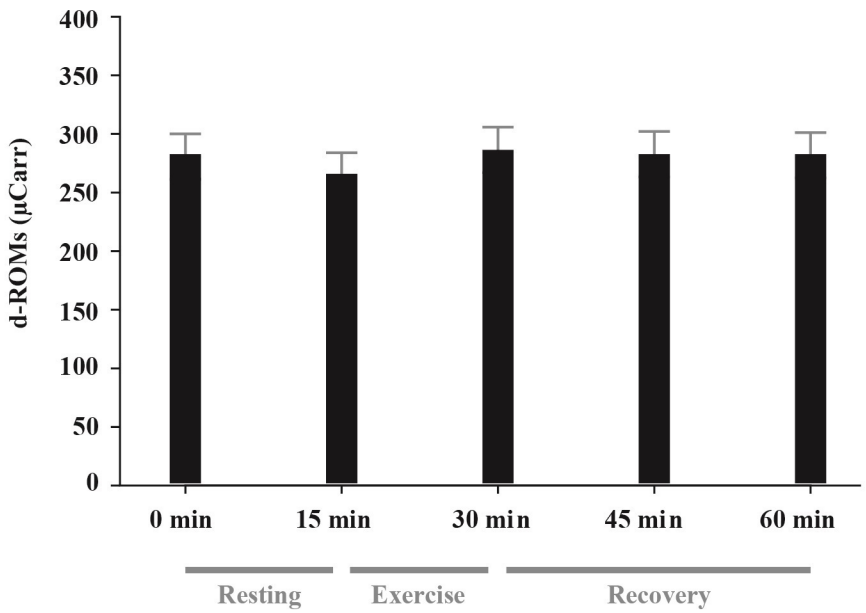

Fig. 3. *d-ROM variations between pre-exercise status, during exercise status and in the recovery periods.*

=5.03, p <0.01]. The post-hoc test showed a difference between pre-exercise and post-exercise values at 30, 45, and 60 min. The same values at basal times (0 and 15 min) suggest that the monitored variables do not change over a short period. This justifies the lack of a control group.

The physical activity did not cause an increase in d-ROMs from a basal value of 268±20 μCarr to a maximum level (281±17 μCarr) at 30 min. d-ROMs decreased to a value of 267±17 at 60 min (Fig. 3). The ANOVA did not show significant effects.

There was a normal distribution of all data. Multivariate regression analysis showed that there were no significant correlations between the variables examined.

DISCUSSION

It is well known that aerobic exercise is associated with the sympathetic activation eliciting adaptive responses, sustaining muscle engagement. The results of the present study demonstrated that the HR increased in all participants during PA, reaching the maximum value at the end of the training session. Moreover, the plasmatic orexin A levels shown similar values to a previous study (8). The increase of the Orexin A plasma levels could be considered as a hormonal adaptation, responding to PA. During exercise, there is also an enhancement of the cortisol secretion, and an association between Orexin A and cortisol has been described (9).

While previous studies have described that cerebral Orexin A is related to the sympathetic discharge, our research is the first that demonstrates a correlation between plasmatic Orexin A and HR as an expression of the sympathetic activity. In a broader vision of the physiological role of Orexin A, the benefits of PA in the control of body weight could be linked to peripheral secretion of this peptide. Since Orexin A is involved in the regulation of body weight (6), and in the pathophysiology of obesity, secretion of plasmatic Orexin A during physical activity, as described in this experimental model, could influence body weight, probably through an activation of energy expenditure (10).

Considering our findings, we also need to take into account that PA increases the metabolic demands of skeletal muscles leading to a greater oxygen uptake and blood flow to the muscles and other organs, also with a higher ROS generation (11). In particular, we have also evaluated the possible association of plasma Orexin A levels with exercise and oxidative stress. PA increases oxygen consumption and in our study it would be expected to observe higher plasmatic d-ROMs levels due to the increase in ROS production. As described in this study, regular and moderate exercise decreases the aging-associated development of oxidative stress reducing the oxidative stress markers in the mitochondrial membranes; contrariwise, the mitochondrial antioxidant enzyme activities were increased (5, 12). On the other hand, several studies have demonstrated that exercise leads to oxidative stress only when exhaustive due to an increase in lipid peroxidation products and, consequently, to oxidative stress and muscle mitochondrial membrane damage (12). In this case, the ROS generation is not counterbalanced by the antioxidant defense system determining an imbalance definite as "active OS" (12). Considering this evidence, our results confirm the previous data.

In conclusion, our study demonstrates that exercise induces an increase in plasmatic Orexin A and this peptide could play an important role in the peripheral adaptations to physical activity. Furthermore, it is certainly premature to speak of the beneficial effect of increased exercise-induced Orexin A in reducing oxidative stress and/or ROS generation. To date, it is only possible to hypothesize a positive role for Orexin A. Further experiments will have to be carried out to verify this hypothesis, confirming a multitasking role for this neuropeptide.

ACKNOWLEDGEMENTS

This study was supported by grants from the Section of Human Physiology and Unit of Dietetic and Sport Medicine and Department of Experimental Medicine, Università degli Studi della Campania "L. Vanvitelli."

REFERENCES

1. Chieffi S, Messina G, Villano I, et al. Neuroprotective

effects of physical activity: Evidence from human and animal studies. Front Neurol 2017; 8:188.
2. Sessa F, Anna V, Messina G, et al. Heart rate variability as predictive factor for sudden cardiac death. Aging (Albany NY) 2018; 10(2):166-77.
3. Yoshida T, Tabony AM, Galvez S, Mitch WE, Higashi Y, Sukhanov S, Delafontaine P. Molecular mechanisms and signaling pathways of angiotensin II-induced muscle wasting: Potential therapeutic targets for cardiac cachexia. Int J Biochem Cell Biol 2013; 45(10):2322-32.
4. Li G, He H. Hormesis, allostatic buffering capacity and physiological mechanism of physical activity: A new theoretic framework. Med Hypotheses 2009; 72(5):527-32.
5. Radák Z, Naito H, Kaneko T, et al. Exercise training decreases DNA damage and increases DNA repair and resistance against oxidative stress of proteins in aged rat skeletal muscle. Pflugers Arch Eur J Physiol 2002; 445(2):273-78.
6. Monda M, Viggiano A, Viggiano A, Fuccio F, De Luca V. Injection of orexin a into the diagonal band of Broca induces symphatetic and hyperthermic reactions. Brain Res 2004; 1018(2):265-71.
7. Jochem J, Zwirska-Korczala K, Zabielski R, Kato I, Kuwahara A. Cardiovascular effects of centrally acting orexin A in haemorrhage-shocked rats. J Physiol Pharmacol 2006; 57(S11):115-24.
8. Messina G, Di Bernardo G, Viggiano A, et al. Exercise increases the level of plasma orexin A in humans. J Basic Clin Physiol Pharmacol 2016; 27(6):611-16.
9. Bertozzi G, Sessa F, Albano GD, et al. The role of anabolic androgenic steroids in disruption of the physiological function in discrete areas of the central nervous system. Mol Neurobiol 2018; 55(7):5548-56.
10. Monda M, Viggiano A, Viggiano A, Viggiano E, Messina G, Tafuri D, De Luca V. Sympathetic and hyperthermic reactions by orexin A: Role of cerebral catecholaminergic neurons. Regul Pept 2007; 139(1–3):39-44.
11. Messina A, Monda V, Avola R, et al. Role of the orexin system on arousal, attention, feeding behaviour and sleep disorders. Acta Medica Mediterr 2017; 33(4):645-49.
12. Monda M, Messina G, Scognamiglio I, et al. Short-term diet and moderate exercise in young overweight men modulate cardiocyte and hepatocarcinoma survival by oxidative stress. Oxid Med Cell Longev 2014; 2014:131024.

LETTER TO THE EDITOR

MAGNESIUM ALGINATE IN CHILDREN WITH UNCONTROLLED ASTHMA

M. MIRAGLIA DEL GIUDICE[1], C. INDOLFI[1], G. CIPRANDI[2], F. DECIMO[1], G. CAMPANA[1], G.R. UMANO[1], E. GIANNETTI[3] and M. MAGLIONE[3]

[1]Department of Woman, Child and of General and Specialized Surgery, University of Campania "Luigi Vanvitelli," Naples, Italy; [2]Ospedale Policlinico San Martino, Genova; [3]Department of Translational Medical Sciences, Section of Pediatrics, Federico II University, Naples, Italy

Received October 11, 2018 – Accepted December 6, 2018

Gastroesophageal reflux disease (GERD) may be frequently associated with asthma in children and may affect asthma control. Proton pump inhibitors (PPI) are commonly prescribed in asthmatic children, despite uncertain efficacy on respiratory symptoms and risk of relevant adverse effects. We investigated whether Magnesium Alginate (MA), an alternative option to PPI in GERD management, improves symptom control in children with uncontrolled asthma. Children with uncontrolled asthma were prospectively enrolled at two tertiary care pediatric respiratory centers over 4 years. The recruited subjects were randomly assigned to three groups, receiving, in addition to current asthma therapy, PPI, MA or no specific GERD treatment, respectively, for 8 weeks. Lung function, asthma control test (ACT), and asthma control questionnaire (ACQ) were assessed at baseline, at the end of the treatment, and at the follow-up. Both PPI and MA significantly improved ACT and ACQ in comparison with the control group. ACQ improvement at follow-up resulted more relevant in the MA than in the PPI group (p=0.004). No difference between MA and PPI was detected with regard to ACT improvement. In conclusion, added to standard asthma medications, MA may improve symptom control in children with uncontrolled asthma.

To the Editor,

Gastro-esophageal reflux (GER) is the physiological retrograde passage of gastric content (gaseous or liquid) into the esophagus which may occur up to 50 times during the day. On the other hand, gastro-esophageal reflux disease (GERD) is defined when GER determines the onset of symptoms, affecting quality of life of the child and/or his/her family or causing complications (1). GERD-related clinical manifestations are commonly classified as gastro-esophageal (or typical) symptoms, such as heartburn or regurgitation, and extra-esophageal (atypical) events, including respiratory manifestations such as asthma, chronic cough, and laryngo-pharyngeal reflux (2). Even though a clear causal relationship between asthma and GERD is still debated, a frequent association between the two conditions has been widely reported. The first description of GERD-associated respiratory symptoms was reported by Kennedy in 1962. Up to 61% of children with recurrent respiratory symptoms were later reported to have GERD, and a study of uncontrolled asthmatic children found GERD in 75% of them (3). Nevertheless, a study conducted on 24 asthmatic children, showed mild correlation among multichannel intraluminal impedance pH

Key words: asthma; gastroesophageal reflux disease; magnesium alginate; proton pump inhibitor; asthma control; children

Corresponding Author:
Giorgio Ciprandi, M.D.
Via Boselli 5,
16146 Genoa, Italy
e-mail: gio.cip@libero.it

0393-974X (2019)

monitoring, respiratory symptoms, and reflux episodes. A recent meta-analysis, including 20 observational studies, reported a 22.8% mean prevalence of GERD in asthmatic children and underlined a possible association between the two disorders, even in the absence of evident cause/effect relationship (4). Moreover, it has been hypothesized that also increased intra-thoracic and intra-gastric pressure, occurring in asthma, may allow GERD occurrence. Despite the absence of conclusive evidence of causal association between asthma and GERD, the prescription of anti-reflux medication in infants and children with respiratory symptoms suggestive for GERD has become very common in clinical practice (5). This pragmatic approach is based on some clinical experiences showing improved wheezing after anti-reflux treatment (6).

On the other hand, very few studies have investigated the effectiveness of proton pump inhibitors (PPI) in uncontrolled asthma. A prospective study on 27 children with moderate persistent asthma and GERD showed a reduced use of anti-asthmatic medications after a 1-year course with combined esomeprazole and metoclopramide (7). In the following 6 months, the children continuing the combined treatment showed less asthma exacerbations in comparison with those treated with ranitidine alone (8). More recently, a large randomized-controlled study enrolled 306 children (mean age 11 years) with uncontrolled asthma, who were treated with lansoprazole in addition to their current asthma medications (9). This treatment did not affect patient-reported respiratory symptoms, nor lung function in comparison with placebo. In addition, children treated with PPI experienced more frequent side effects, including respiratory infections. This circumstance may depend on the reduced defense mechanisms against microbial colonization because of acid-suppression by PPI and on the possible presence of weakly acid or alkaline reflux (9). Similarly, it was demonstrated that PPI were effective in reducing typical symptoms due to acid reflux, but were poorly effective in reducing symptoms due to weakly acid or alkaline reflux.

Alginate is a fruitful medication in the management of GERD. It precipitates as a gel after the exposure to the gastric acid, thus forming a raft that represents a barrier to the reflux of the gastric content into the esophagus (9). However, there are different formulations containing alginate, and data on their efficacy are conflicting, probably depending on the different compositions (10, 11). Therefore, the North American and European Society for Pediatric Gastroenterology, Hepatology and Nutrition

Table I. *Demographic and clinical characteristics at baseline in the three groups.*

	Group A N= 46	**Group B N=40**	**Group C N=36**	**p-value**
Age (years)	8.4±3.2	10.9 ±3.3	11.5 ±2.9	<0.0001
Gender (M/F, %)	50/50	70.7/29.3	27.8/72.2	0.05
FEV_1 (% of predicted)	107.4±15.9	100.2±15.1	97.6±12.9	0.02
ACT score	16.9±2.9	17.4±1.8	16.3±2.9	0.62
ACQ score	1.60±0.3	1.3±0.1	1.9±0.5	0.06
ACT class (% of subjects) (<20/20-24/>25)	77.1/20.8/2.1	70.7/26.8/2.5	83.3/6.7/0.0	0.71

(NASPGHAN/ESPGHAN) guidelines define the positioning of alginate formulations, considering the indications, the durations, and the potential combinations (2). On the other hand, no study has investigated the effectiveness of alginate and PPI in the control of respiratory symptoms in children with uncontrolled asthma.

As GERD comorbidity commonly affects asthma control in children, the hypothesis to be tested was to verify the effectiveness of alginate in improving respiratory symptoms in uncontrolled asthma. Therefore, this two-center, prospective, randomized, controlled study aimed at comparing alginate, PPI, and non-specific GERD medication in children with uncontrolled asthma.

MATERIALS AND METHODS

Patients

The inclusion criteria were: i) asthma diagnosis according to the Global Initiative for Asthma (GINA) criteria (21); ii) uncontrolled asthma according to the GINA document; iii) age between 6 and 17 years; iv) documented diagnosis of GERD; and v) written informed consent signed by the parents of the children involved in the study.

The exclusion criteria were: i) controlled asthma; ii) change of anti-asthmatic treatment 8 weeks prior to enrollment in the trial; iii) past or current anti-acid treatment; iv) delayed psychomotor development; v) chronic disorders; vi) hepatic, cardiac, or renal disease; vii) systemic infections; and viii) allergy to cow milk.

Asthma diagnosis was based on history positive for typical asthma symptoms, including cough, recurrent wheezing and dyspnea, chest tightness, night awakening, seasonal symptoms, atopy, symptom worsening after climatic change, exposure to smoke, pollution, pollens, pets, respiratory infections (mainly viral), drugs, physical exercise, and emotional stress. In addition, in compliant patients, reversible bronchial obstruction was documented by positive response to bronchodilation test, methacholine challenge, or exercise test.

Uncontrolled asthma was defined according to validated criteria, including: i) use of short acting bronchodilators >2 time/week in the previous month; ii) night awakening >1/week in the previous month; iii) two or more emergency room visits, unscheduled medical visits, oral corticosteroid course, and hospital admissions for asthma; iv) ≥1.25 score for ACQ and <20 for ACT.

The ACT questionnaire includes 5 questions concerning asthma symptoms and perceived quality of life. The ACQ test considers symptoms and lung function.

Children were enrolled at the Pediatric Department of Naples University Federico II and the Pediatric

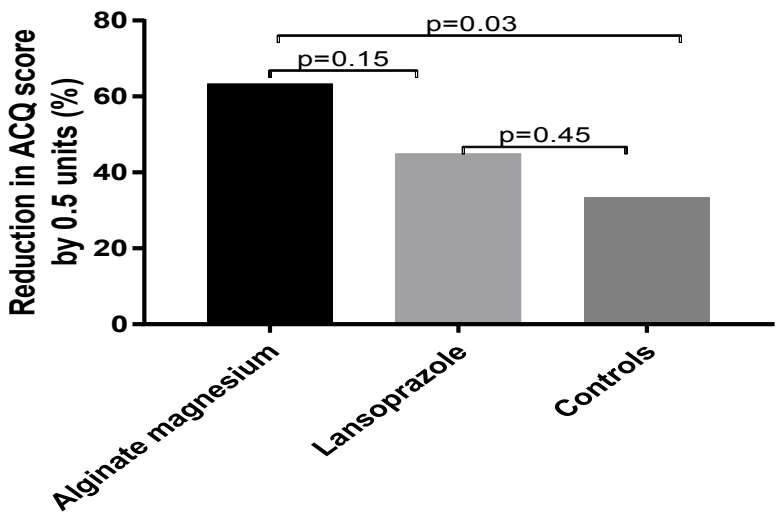

Fig. 1. *Reduction in ACQ score by 0.5 units (%) in the 3 Groups at T1.*

Department of University of Campania Luigi Vanvitelli. The Ethic Committees approved the protocol.

Study design

The present study was conducted as two-center, prospective, randomized, and single-blind controlled. During the first visit (T0), children were visited, screened for the requested requisites, and completed two questionnaires (asthma control test - ACT and asthma control questionnaire - ACQ). The selected children were randomly divided into 3 groups: Group A treated with oral Magnesium Alginate (Gastrotuss baby) 10 mL 3 times/day after meals; Group B treated with Lansoprazole 15 mg/day (if <30 Kg bw) or 30 mg/day (if ≥30 Kg bw); Group C without GERD treatment. The treatment duration was 8 weeks for all children.

Dietetic and behavioral recommendations to prevent reflux episodes were suggested to all patients. A daily diary for GERD symptoms, treatment adherence, and side effects was given to the parents. Every patient was re-visited four (T1) and eight (T2) weeks after the start of the treatment.

Clinical examination, diary assessment, ACT, ACQ, and lung function were carried out at each visit.

Statistical analysis

The power analysis revealed the need of a sample size of 32 subjects in each arm in order to achieve a power of 90% with an alpha error of 0.05 to detect a difference of 0.5 units in ACQ score with a mean DS of 1.5. Differences in categorical variables were investigated by *Chi*-squared test. Kruskal-Wallis test was performed to evaluate differences for continuous variables. All analyses were performed using SAS version 9.4 (SAS Institute, Cary, NC, USA), and statistical significance was assessed at the two-tailed 0.05 threshold.

RESULTS

A total of 122 children with uncontrolled asthma were enrolled in the study and demographic and clinical data are reported in Table I. All children concluded the 8-week treatment and none reported any clinically relevant adverse event.

ACQ test

Fig. 1 and Table II show the reduction of ACQ score, evaluated by 0.5 units, in the 3 Groups at T1. In Group A, 63.2% of subjects had a reduction of 0.5 units; 46.8% of Group B children, and 33.3% of Group C children. There was a significant difference between Group A and C (p=0.03). The mean Δ scores were -0.7, -0.5, and -0.3, respectively: the comparison among Groups showed a significant difference (p=0.006 Kruskal-Wallis test).

Fig. 2 shows the reduction of ACQ score,

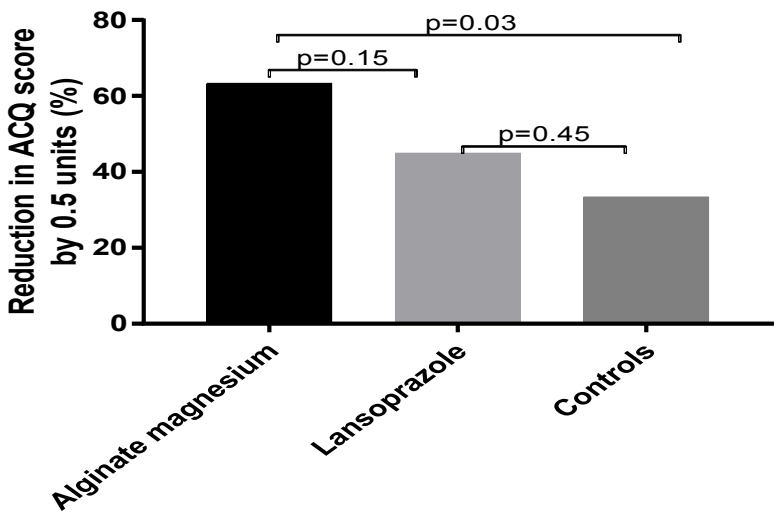

Fig. 2. *Reduction in ACQ score by 0.5 units (%) in the 3 Groups at T2.*

evaluated by 0.5 units, in the 3 Groups at T2. In Group A, 89.1% of subjects had a reduction of 0.5 units; 55.6% of Group B children, and 33.3% of Group C children. There was a significant difference between Groups A and C, and between Groups A and B ($p<0.0001$ and $=0.004$, respectively). The mean Δ scores were -0.9, -0.6, and -0.3, respectively: the comparison among Groups showed a significant difference ($p<0.0001$ Kruskal-Wallis test).

ACT questionnaire

Patients were divided into 3 classes according to the ACT scores: <20; 20-24; and 25. At baseline, 77.1% of Group A, 70.7% of Group B, and 83.3% of Group C subjects had ACT values <20, as reported in Table I.

The percentages of subjects with ACT score >20 in the 3 Groups at T1 are shown in Fig. 3A. In Group A, 70.8% of subjects had ACT score >20, 72.3% of Group B, and 28.6% of Group C. There was a significant difference between Groups A and C, and between Groups B and C.

The percentages of subjects with ACT score >20 in the 3 Groups at T2 are shown in Fig. 3B. In Group A, 81.1% of subjects had ACT score >20, 65% of Group B, and 33.3% of Group C. There was a significant difference between Groups A and C, and between Groups B and C.

Lung function

There was no significant difference for Δ FEV_1 among Groups either at T1 ($p=0.62$) or T2 ($p=0.22$).

DISCUSSION

Even though the relationship between asthma and GERD is still debated, there is no doubt that refluxate inhalation into the bronchi may significantly affect asthma. In fact, GERD is a well-recognized comorbid disorder that should be ruled out in the work-up of patients with uncontrolled asthma. This statement is supported by the evidence that treating GERD could improve asthma control (1).

However, GERD treatment is controversial, the guidelines suggest to give advice about GERD and reassure patients and caregivers (8-11). Patients with suspected GERD could be treated with empirical full-dose PPI therapy for 4 or 8 weeks. If symptoms recur after initial treatment, a PPI could be offered at the lowest dose possible to control symptoms. In addition, it is recommended to encourage people who need long-term management of dyspepsia

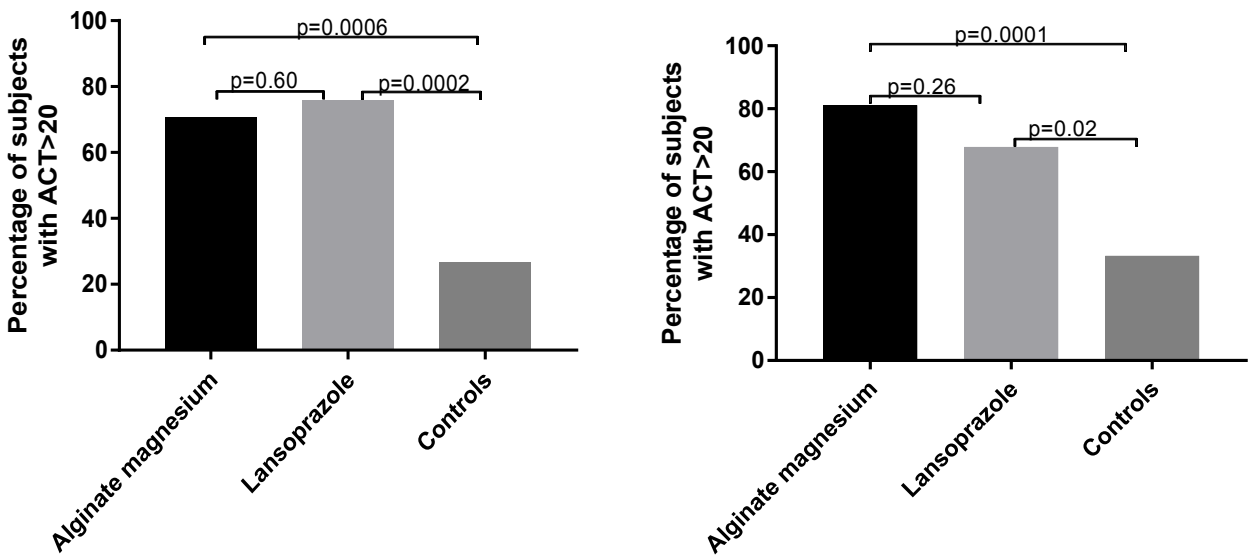

Fig. 3. ***A)*** *Percentage of subjects with ACT score >20 in the 3 Groups at T1.* ***B)*** *Percentage of subjects with ACT score >20 in the 3 Groups at T2.*

symptoms to reduce their use of prescribed medication stepwise: by using the effective lowest dose, by trying 'as-needed' use when appropriate, and by returning to self-treatment with antacid and/or alginate therapy (unless there is an underlying condition or co-medication that needs continuing treatment). It is also necessary to advise people that it may be appropriate for them to return to self-treatment with antacid and/or alginate therapy (either prescribed or purchased over-the-counter and taken as needed). Finally, it is important to avoid long-term, frequent doses and continuous antacid therapy (it only relieves symptoms in the short term rather than preventing them). On the other hand, the exact role of PPI in the treatment of respiratory symptoms in children is hotly debated, mainly concerning potential side effects during long-term treatment, as recently highlighted (12).

On the basis of these considerations, alginates may be considered as a valid and reasonable therapeutic option for children with uncontrolled asthma. The current study demonstrated that an 8-week course of magnesium alginate is able to significantly decrease the number of children with uncontrolled asthma. In particular, considering two validated parameters commonly used in the assessment of asthma control, such as ACT and ACQ tests, up to 80% of children with uncontrolled asthma treated with magnesium alginate had a clinically relevant reduction of both scores. Interestingly, this outcome was better in children treated with alginate than in PPI-treated subjects.

The current study has some strengths, such as the study design and duration, but also some limitations, including the lack of follow-up. Therefore, other studies are needed to confirm the current findings.

The main implication of our results is that alginate may be a valid therapeutic option in children with uncontrolled asthma. In particular, this could suggest that an empirical magnesium alginate trial could be prescribed in children with uncontrolled asthma to try to improve asthma control. Magnesium alginate is safe and generally well tolerated.

In conclusion, the present study demonstrated that magnesium alginate may be able to improve asthma control in children with uncontrolled asthma in clinical practice.

REFERENCES

1. Vandenplas Y, Rudolph CD, Di Lorenzo C, et al. Pediatric Gastroesophageal Reflux Clinical Practice Guidelines: Joint Recommendations of the North American Society for Pediatric Gastroenterology, Hepatology, and Nutrition (NASPGHAN) and the European Society for Pediatric Gastroenterology, Hepatology, and Nutrition (ESPGHAN). J Pediatr Gastroenterol Nutr 2009; 49:498-547.
2. Thakkar K, Boatright RO, Gilger MA, El-Serag HB. Gastroesophageal reflux and asthma in children: a systematic review. Pediatrics 2010; 125:e925-30.
3. Khoshoo V, Haydel R Jr. Effect of antireflux treatment on asthma exacerbations in nonatopic children.J Pediatr Gastroenterol Nutr 2007; 44:331-35.
4. Committee for the American Lung Association Asthma Clinical Research Centers Lansoprazole for Children With Poorly Controlled Asthma A Randomized Controlled Trial. JAMA 2012; 307:373-81.
5. Iwakiri K, Kawami N, Sano H, et al. Acid and non-acid reflux in Japanese patients with non-erosive reflux disease with persistent reflux symptoms, despite taking a double-dose of proton pump inhibitor: a study using combined pH-impedance monitoring. J Gastroenterol 2009; 44:708-12.
6. Turk H, Hauser B, Breceli J, Vandenplas Y, Orel R. Effect of proton pump inhibition on acid, weakly acid and weakly alkaline gastro-esophageal reflux in children. World J Pediatr 2013; 9:36-41.
7. Corvaglia L, Monari C, Martini S, Aceti A, Faldella G. Pharmacological therapy of gastroesophageal reflux in preterm infants. Gastroenterol Res Pract 2013; 2013:714564.
8. Internal Clinical Guidelines Team (UK). Dyspepsia and Gastro-Oesophageal Reflux Disease: Investigation and Management of Dyspepsia, Symptoms Suggestive of Gastro-Oesophageal Reflux Disease, or Both. London: National Institute for Health and Care Excellence (UK); Sept 2014.
9. Davies I, Burman-Roy S, Murphy MS: Guideline Development Group. Gastroesophageal reflux disease in children: NICE guidance. BMJ 2015; 350:g7703.
10. Kahrilas P, Yadlapati R, Roman S. Emerging dilemmas in the diagnosis and management of gastroesophageal

reflux disease. F1000Res 2017; 6:1748.
11. Iwakiri K, Kinoshita Y, Habu Y, et al. Evidence-based clinical practice guidelines for gastroesophageal reflux disease 2015. J Gastroenterol 2016; 51:751-67.
12. Rosen R, Rahbar R. Proton pump inhibitor use and outcomes in children with respiratory symptoms. JAMA Otolaryngol Head Nech Surg 2018 published online May 3, 2018.

LETTER TO THE EDITOR

SINERGA MAY PREVENT RECURRENT RESPIRATORY INFECTIONS IN ALLERGIC CHILDREN

F. AMELI[1] and G. CIPRANDI[2]

[1]Otorhinolaryngology Unit, Villa Montallegro, Genoa, Italy; [2]Allergy Clinic, Villa Montallegro, Genoa, Italy

Received October 17, 2018 – Accepted December 6, 2018

Recurrent respiratory infections (RRI) are an intriguing challenge for both otolaryngologists and paediatricians. Therefore, to prevent RRI is an ambitious target in clinical practice. In this regard, modulation of the immune system may have a critical role. Sinerga, a dietary supplement (containing: palmitoylethanolamide (PEA), *Kluyveromyces marxianus* B0399, bovine colostrum, and phenylalanine), was supplemented in 20 allergic children with RRI (20/30 days per 3 months) and treated with standard therapy (antihistamine plus intranasal corticosteroid). Other 20 allergic children with RRI were treated only with standard therapy. Sinerga significantly reduced the number of RI and the size of both inferior and middle turbinate consistently with the postulated mechanisms of action. In conclusion, the current study demonstrated that Sinerga supplementation in allergic children with RRI may significantly prevent RI and reduce events depending on allergic inflammation.

To the Editor,

Children with recurrent respiratory infections (RRI), mainly allergic, are an emerging problem for paediatricians and otolaryngologists in clinical practice. The diagnosis of RRI is performed according to the following criteria: i) > 6 RI per year; ii) > 1 RI per month involving upper airways from September to April; iii) > 3 RI involving lower airways (1). RRI have a relevant impact on pharmaco-economy and are a burden for both the family and society.

Many factors may be involved in promoting and/or causing RRI, including age (for a relative immaturity of the immune system), early attending at nursery school, air and home pollution, passive tobacco smoking, low socio-economic level, and atopy. In particular, allergy plays a crucial role in promoting RI recurrence as the immune response is impaired in allergic subjects and allergic inflammation favours infections. Allergic subjects have a defect of the type 1 immune response that is appointed to hinder infections producing anti-infective cytokines, namely IFN-γ. In fact, allergic children have more numerous and severe infections than normal subjects (2). Moreover, allergic subjects typically present the so-called minimal persistent inflammation, i.e. mucosal inflammatory cell infiltrate closely associated to allergen exposure (3). This event may account for sustained susceptibility to infections because of impaired type 1 response, increased ICAM-1 expression (the main rhinovirus receptor) on epithelial cells, and local inflammation that represents a *pabulum* for pathogens. In addition, viral infections may increase the probability of contracting frequent RI because of the high number of circulating viruses and the numerous sub-types. Viral infections are predominant, but bacterial super-

Key words: recurrent respiratory infection; allergy; Sinerga; immune system; mast cell; children

Corresponding Author:
Giorgio Ciprandi, MD
Via P. Boselli 5,
16146 Genoa, Italy
Tel.: +39 10 35338120
e-mail: gio.cip@libero.it

0393-974X (2019)

DISCLOSURE: ALL AUTHORS REPORT NO CONFLICTS OF INTEREST RELEVANT TO THIS ARTICLE.

infections may frequently appear. Consequently, there is an overuse/misuse of antibiotics which, in turn, induces antibiotic resistance (4). Moreover, biofilm causes frequent antibiotic unsuccess, and 25-45% of children with severe RRI need surgical intervention.

Moreover, allergic patients with IRR show a Type 2 polarization, reduction of macrophage phagocytosis, reduction of neutrophil chemotaxis, and a partial IgA and/or IgG subclass deficiency. In this scenario, mast cells play a pivotal role, as they produce several mediators and cytokines that in turn maintain and amplify Type 2 polarization and consequently allergic inflammation, also minimal (2, 3).

RI treatment is generally based on administration of symptomatic drugs (e.g. acetaminophen) and antibiotics, but frequently without precise indication and empirically prescribed. Consequently, prevention of RRI is at present a goal in common practice. Bacterial derivates, including probiotics, are also used with mild results in reducing respiratory morbidity in clinical practice (5). Thus, there is interest in preventive and alternative treatment by doctors. In this regard, immunomodulants are widely used in daily practice.

Sinerga is a dietary supplement containing palmitoylethanolamide (PEA), *Kluyveromyces marxianus* B0399, bovine colostrum, and phenylalanine. PEA is an autacoid, namely an endocannabinoid, and has a clear analgesic and anti-inflammatory activity, and virtually no side effects. PEA is a self-body fatty compound and is produced by our own living cells to restore balance in chronic pain and chronic inflammation. Its anti-inflammatory and painkilling properties have been known in science since the first description of this compound in 1957. In 1993, the Nobel Prize winner Levi-Montalcini pointed out the relevance of PEA in medicine as a potent inhibitor of activated mast cells, as recently reviewed. In particular, PEA has a peripheral anti-inflammatory activity mediated by a CB_2-like receptor, present also on mast cells (6).

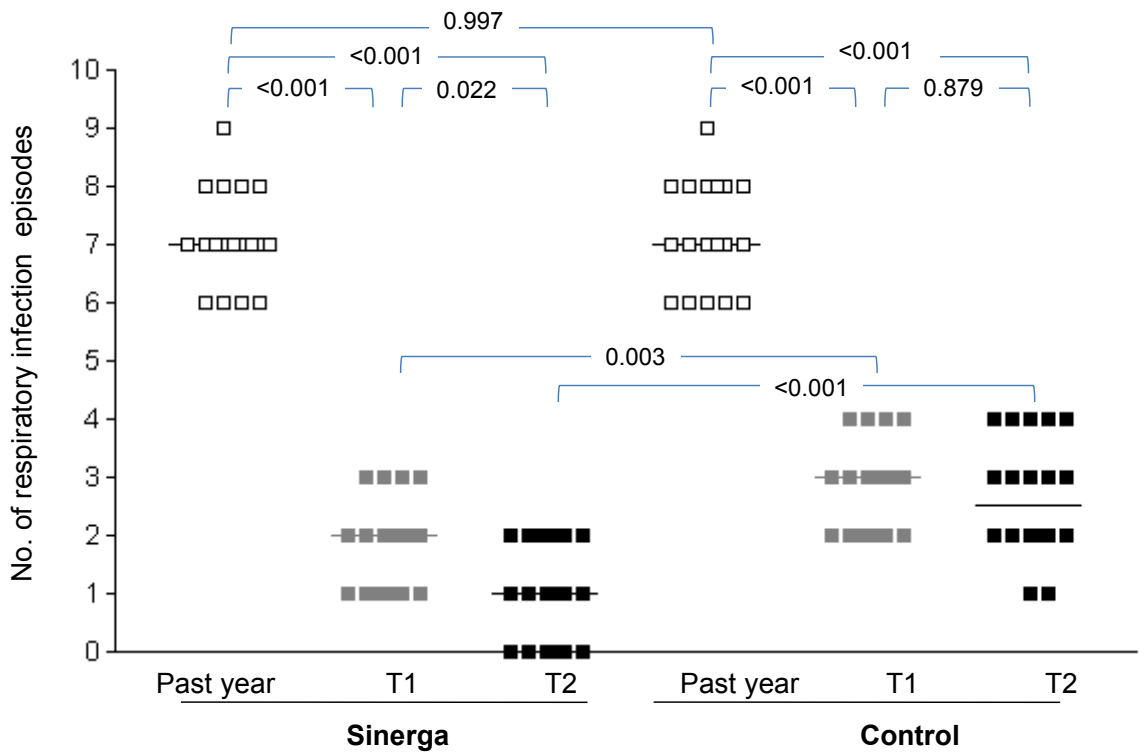

Fig. 1. *Number of respiratory infections in the Sinerga group and the control group in the previous year, after the 3-month treatment (T1), and after the 3-month follow-up (T2).*

Kluyveromyces marxianus B0399 is a lactic yeast isolated from different dairy products, mainly kefir; a recent study showed that it decreased production of pro-inflammatory cytokines, increased the bifidobacterial concentration, the production of secretory immunoglobulin A, the short-chain fatty acid acetate and propionate (potent anti-inflammatory agents), and decreased the potential cytotoxic activity in a colonization model (7). The bovine colostrum extract, used in Sinerga product, contains immunoglobulin G (G1 + G2 subclasses) class antibodies, α2-glycoprotein, and AP glycoprotein: these proteins may significantly reinforce the immunological mechanisms of defence (8). Phenylalanine is an essential amino acid that is converted in L-DOPA, in turn converted to dopamine; normal concentrations of dopamine inhibit mast cell activation (9).

On the basis of this background, Sinerga could exert a relevant activity in preventing RRI acting on different steps of the inflammatory cascade, potentially including mast cell stabilization, consequent to infections and allergy. A recent retrospective study demonstrated that Sinerga supplementation significantly reduced the number of RI in children with an RRI history (10). However, these authors did not consider the role of allergy as adjunctive risk factor for RRI. Therefore, we aimed to confirm this outcome in a group of children with RRI and allergy.

MATERIALS AND METHODS

Forty children (18 males, 22 females, mean age 6.5 years, ranging between 4 and 9 years) with RRI and allergy were enrolled in the current study. All patients were evaluated by an otolaryngologist, who performed a fibre-optic nasal endoscopy. The inclusion criteria were: i) age between 4 and 9 years; ii) both genders; iii) history of RRI in the past year; and iv) documented allergy to house dust mites. The exclusion criteria were: i) severe allergic symptoms (such as to interfere with the assessment of

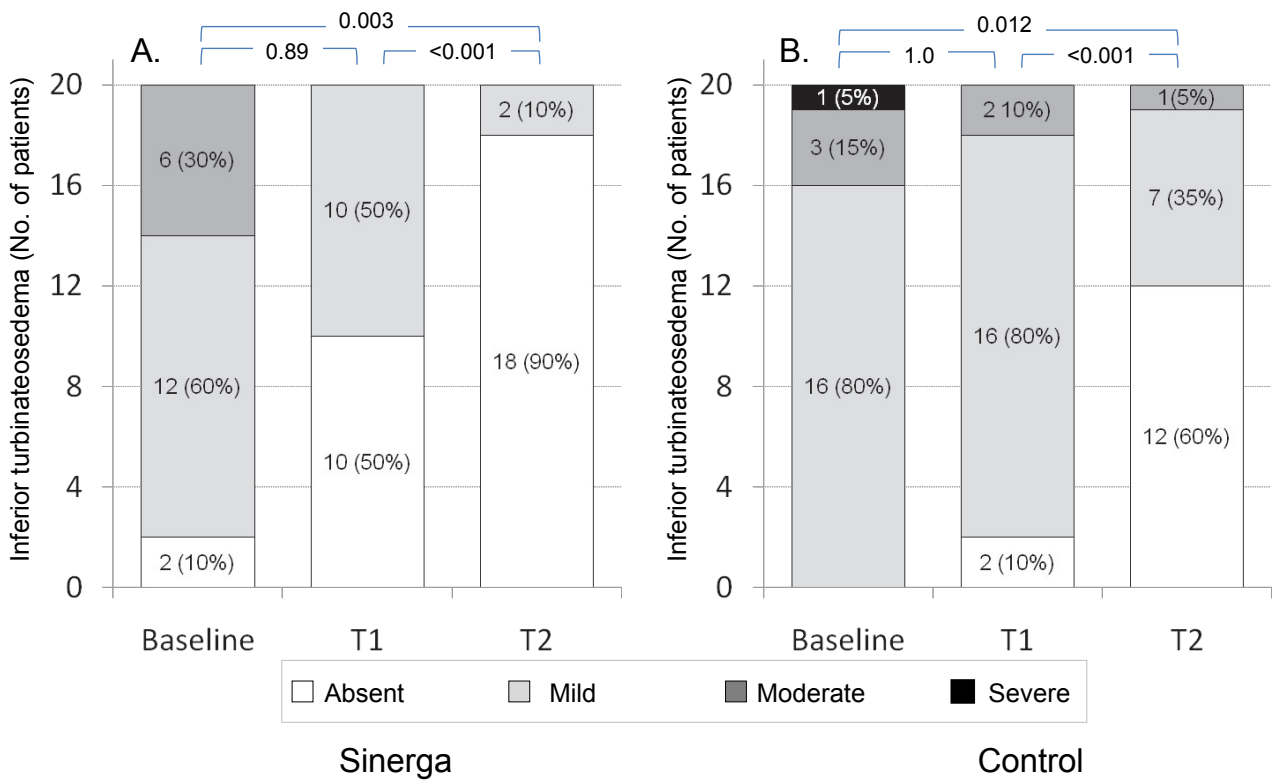

Fig. 2. *Grading of the oedema of inferior turbinate in the Sinerga group and the Control group, at baseline, after the 3-month treatment (T1), and after the 3-month follow-up (T2).*

treatments); ii) congenital or acquired immunodeficiency; iii) craniofacial abnormalities; iv) sleep apnoea syndrome; v) Down syndrome; vi) chronic disease (including metabolic disorders, cystic fibrosis, cancer, etc.); vii) clinically relevant passive smoking; and viii) previous (last 3 months) or current administration of drugs able to interfere with the study (e.g. immunomodulants, homeopathic therapy, or systemic corticosteroids for at least 2 consecutive weeks).

The study was conducted according the Helsinki Conference Document and the parents or legal tutor, after receiving information on the study, gave their written informed consent to participate.

All children were treated with a standard treatment, including cetirizine drops (5 mg/die) and intranasal budesonide (50 mcg/nostril/die) for 3 months. The children were randomly (1:1) and consecutively subdivided in two groups at baseline. The first group was supplemented with Sinerga: one sachet/die for 20 consecutive days/month for 3 months. The second group was treated with the standard therapy alone and considered as Control.

The primary outcome was the number of RI during the study period and also compared with the previous year. RI was diagnosed on the basis of the symptoms reported by the parents, as previously defined (3). The RI diagnosis was made when at least 2 symptoms or fever (axillary temperature ≥38°C), in addition to one other symptom (see below), were present for at least 48 hours. The considered symptoms were mucopurulent rhinorrhoea, stuffy or dripping nose or both, sore-throat, cough (dry or productive), otalgia (earache), fever, dyspnoea, and mucopurulent secretion.

Secondary outcomes were: i) the number of acute otitis media (AOM) episodes; ii) oedema of turbinate inferior and middle (0=absent; 1=mild; 2=moderate; 3=severe); iii) visual analogue scale for the parents' perception of treatment effectiveness, sleep quality, and treatment tolerability, measured according to methods described in a previous study (11).

All children were visited at baseline, after the 3-month treatment (T1), and after a 3-month follow-up (T2). The study was conducted between October 2017 and May 2018.

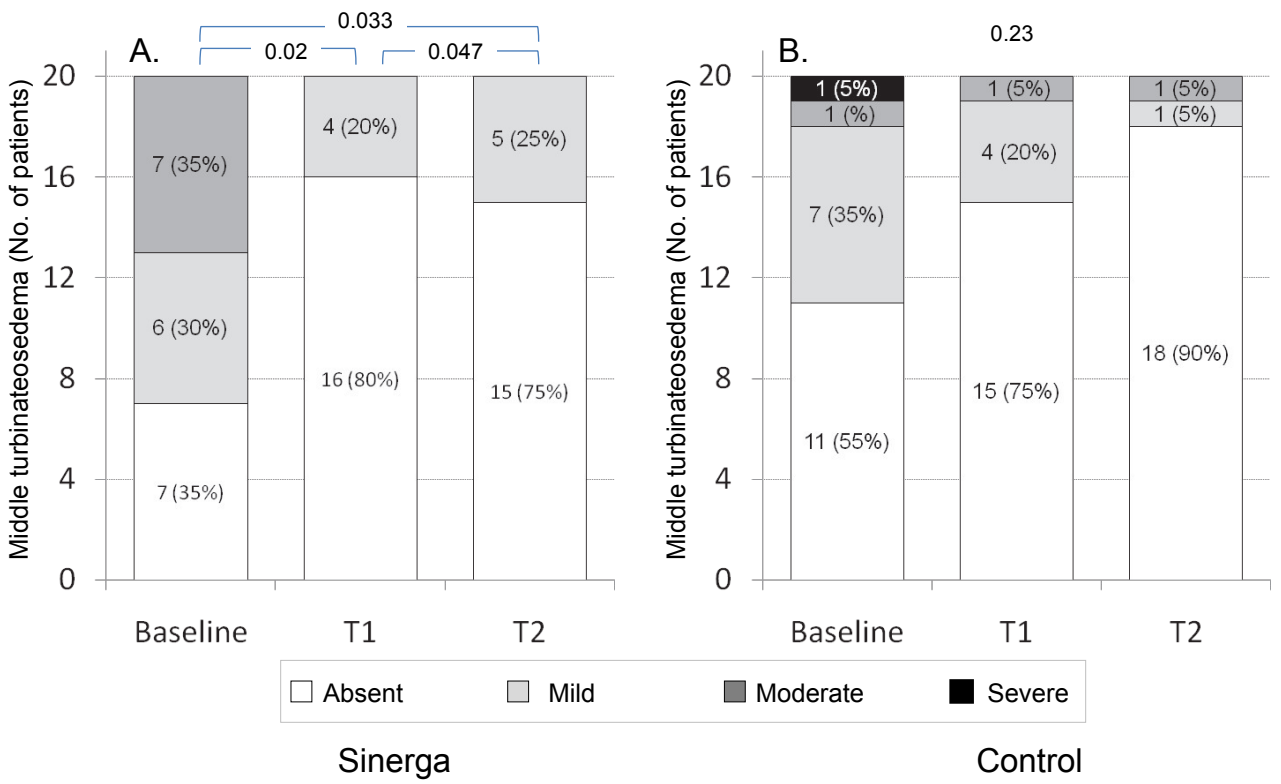

Fig. 3. *Grading of the oedema of middle turbinate in the Sinerga group and the Control group, at baseline, after the 3-month treatment (T1), and after the 3-month follow-up (T2).*

Demographic and clinical characteristics are described using means with SDs for normally-distributed continuous data (i.e. age) or medians with lower and upper quartiles (LQ-UQ) for not normally-distributed. Any statistically significant difference in the mean values or in the median values of each continuous variable was evaluated with the Wilcoxon signed rank test or with Mann U Whitney test, respectively. Statistical significance was set at $p < 0.05$, and the analyses were performed using GraphPad Prism software, GraphPad Software Inc, CA, USA.

RESULTS

Table I reports the demographic data and the outcomes in the two groups of allergic children with RRI. The groups were homogeneous for the considered parameters at baseline. Forty subjects completed the study; 4 children dropped out because of Sinerga unpleasantness.

Fig. 1 shows the number of RI in the two groups: both treatments significantly reduced the RI episodes both at T1 and at T2, but Sinerga supplementation was more effective than standard therapy both at T1 and T2 ($p=0.003$ and <0.001 respectively).

The number of AOM was significantly reduced in both groups without significant difference (Table I). The perception of effectiveness significantly ($p=0.024$) improved at T2 only in the Sinerga group; the sleep quality significantly improved in both groups at T2 without intergroup difference; the tolerability was optimal in both groups without significant difference (Table I).

The oedema of inferior turbinate significantly diminished in both groups ($p<0.001$ for both between T1 and T2), but there was difference at T1 and T2 between groups ($p=0.018$ and 0.04 respectively) as shown in Fig. 2. In addition, the oedema of middle turbinate significantly diminished only in the Sinerga group ($p=0.02$ between baseline and T1 and 0.047 between T1 and T2), and there was difference at T1 and T2 between groups ($p=0.018$ and 0.08, respectively) as shown in Fig. 3.

DISCUSSION

Respiratory infections, mainly if recurrent, constitute a burdensome task for many doctors in clinical practice. RI account for the first reason of antibiotic prescription. Moreover, RI in childhood cause frequent school absences and consequently parents' work days loss. Therefore, contrasting RI represents a crucial and compelling challenge in medical practice.

The immune system fights RI, involving the innate and the adaptive response by both humoral and cellular signalling. The immune system responds to pathogens through very complex and complicated mechanisms (12). An effective response results from a balance between aggressive and reparative processes finely modulated by regulatory pathways.

On the basis of this background, we tested the hypothesis that Sinerga, a mixture compound, could modulate immune response toward a more efficient contrast to pathogens in children with allergy. The current outcomes demonstrate that Sinerga supplementation was able to significantly reduce the number of RI episodes. In addition, Sinerga supplementation was able to reduce the turbinate size. Remarkably, the parents' perception of the treatment effectiveness, the sleep quality, and the treatment tolerability was optimal in the Sinerga group.

These findings could be explained by the complex mechanism of action of Sinerga. In fact, the single components exert several positive effects that could be summarized in two principal mechanisms: modulation of the immune system (exerted by the colostrum extract and the probiotic) and mast cell protection (exerted by the PEA and the phenylalanine). The first mechanism may improve the physiological immune response to pathogens, the latter may reduce the phenomena related to the allergic inflammation. In particular, PEA exerts its activity likely as a gatekeeper of local homeostasis. In fact, PEA exerts anti-inflammatory activity in several experimental models of immune-mediate and neurogenic inflammation, characterized by mast cell involvement. Especially, PEA inhibits the plasmatic exudation induced by substance P and passive cutaneous anaphylaxis (23) and the paw oedema induced by carragenin, dextran, and formalin (13). Therefore, the mast cell stabilization induced

by PEA might contribute to reduce the respiratory inflammation in RRI. These effects on mast cell might also contribute to restore a physiological switch from the Th2 polarization to the physiological Th1 prevalence.

Of course, the positive effects observed also in the control group depend on the activity exerted by antihistamine and intranasal corticosteroids that reduce allergic inflammation and relieve respiratory symptoms. However, Sinerga supplementation could prevent infections better than the standard pharmacological option as it notably reinforces immune response and stabilizes mast cells, a relevant source of allergic mediators. The current findings support this interpretation as the reduction of turbinate oedema is consistent with a reduction of allergic inflammation. In fact, it is well known that turbinate oedema is a surrogate marker for allergic inflammation, as previously demonstrated (14). Therefore, the putative Sinerga effect on mast cell could explain the observed reduction of turbinate oedema (15). On the other hand, the reduced number of RI can be dependent on the stimulation of the immune system by Sinerga.

However, the present study has some limitations, including the open design, the limited number of enrolled subjects, the lack of documented infection diagnosis, and the absence of mediator measurements. In fact, the current study cannot define the real mechanisms of action involved in the obtained outcomes. As Sinerga is a multi-compound product, there is not the possibility to identify the single activity of each component, therefore, the findings could not allow to draw definitive conclusions. Thus, further studies should be designed to answer these unmet needs.

In conclusion, the current study demonstrated that Sinerga supplementation in allergic children with RRI might significantly prevent RI and reduce allergic inflammation.

REFERENCES

1. Gruppo di Studio di Immunologia della Società Italiana di Pediatria. Le infezioni ricorrenti nel bambino: definizione ed approccio diagnostico. Riv Immunol Allergol Ped 1988; 2:127-34.
2. Ciprandi G, Tosca MA, Fasce L. Allergic children have more numerous and severe respiratory infections than non-allergic children. Ped Allergy Immunol 2006; 17:389-91.
3. Ciprandi G, Buscaglia S, Pesce GP, et al. Minimal persistent inflammation is present at mucosal level in asymptomatic rhinitic patients with allergy due to mites. J Allergy Clin Immunol 1995; 96:971-79.
4. Li J, Song X, Yang T, Chen Y, Gong Y, Yin X, Lu Z. A systematic review of antibiotic prescription associated with upper respiratory tract infections in China. Medicine (Baltimore) 2016; 95(19):e3587.
5. Lanzilli G, Falchetti R, Cottarelli A, Macchi A, Ungheri D, Fuggetta MP. In vivo effect of an immunostimulating bacterial lysate on human B lymphocytes. Int J Immunopathol Pharmacol 2006; 19(3):551-59.
6. Conti S, Costa B, Colleoni M, Parolaro D, Giagnoni G. Antiinflammatory action of endocannabinoid palmitoylethanolamide and the synthetic cannabinoid nabilone in a model of actute inflammation in the rat. Br J Pharmacol 2002; 135:181-87.
7. Maccaferri S, Klinder A, Brigidi P, Cavina P, Costabile A. Potential probiotic Klyveromyces marxianus B0399 modulates the immune response in Caco-2 cells and peripheral blood mononuclear cells and impacts in the human gut microbiota in an in vitro colonic model system. Appl Environ Microbiol 2012; 78:956-64.
8. Jones AW, Thatcher R, March DS, Davison G. Influence of 4 weeks of bovine colostrum supplementation on neutrophil and mucosal immuneresponses to prolonged cycling. Scand J Med Sci Sports 2015; 25:788-96
9. Xue L, Li X, Ren HX, et al. The dopamine D3 receptor regulates the effects of methamphetamine on LPS-induced cytokine production in murine mast cells. Immunobiology 2015; 220:744-52.
10. Nigro A, Nicastro A, Trodella R. Retrospective observational clinical study to evaluate the safety and efficacy of Sinerga, a nutritional product, in the prevention of recurrent respiratory infections in children. Int J Immunopathol Pharmacol 2014; 27:455-60.
11. Barberi S, D'Auria E, Bernardo L, et al. Hypertonic

saline monotherapy in children with perennial allergic rhinitis: a pilot study. J Biol Res 2016; 30:271-75.

12. Simon AK, Hollander GA, McMichael A. Evolution of the immune system in humans from infancy to old age. Proc Biol Sci 2015; 282:2014308.
13. Mazzari S, Cannella R, Petrelli L, Marcolongo G, Leon A. N-(2-hydroxyethyl) hexadecanamide is orally active in reducing edema formation and inflammatory hyperalgesia by down-modulating mast cell activation. Eur J Pharmacol 1996; 300:227-36.
14. Ciprandi G, Marseglia GL, Klersy C, Tosca MA. Relationships between allergic inflammation and nasal airflow in children with persistent allergic rhinitis due to mite sensitization. Allergy 2005; 60:957-60.
15. Ciprandi G, Klersy C, Cirillo I, Marseglia GL. Quality of life in allergic rhinitis: relationship with clinical, immunological, and functional aspects. Clin Exp Allergy 2007; 37:1528-35.

LETTER TO THE EDITOR

BROSER® (BROMELAIN, ESCIN AND SELENIUM), ORAL NUTRACEUTICAL, MONOTHERAPY IN PATIENTS WITH INFLAMMATORY OTORHINOLARYNGOLOGICAL DISORDERS

G.F. CUPIDO[1], M. GELARDI[2], I. LA MANTIA[3], S.E. ARAGONA[4], G. CIPRANDI[5] and ITALIAN STUDY GROUP ON INFLAMMATORY OTORHINOLARYNGOLOGICAL DISORDERS[*]

[1]ENT Department, University of Palermo, Palermo, Italy; [2]Otolaryngology Unit, Department of Basic Medical Science, Neuroscience and Sensory Organs, University of Bari Aldo Moro, Bari, Italy; [3]ENT Department, University of Catania, Catania, Italy; [4]Center of Regenerative Medicine, Humanitas Mater Domini, Castellanza (VA), Italy; [5]Allergy Clinic, Casa di Cura Villa Montallegro, Genoa, Italy

[*]Italian Study Group of inflammatory otorhinolaryngological disorders: Aielli Federica, Albanese Gianluca, Allosso Giuseppe, Amadori Maurizio, Antoniacomi Giovanni, Asprea Francesco, Auletta Pasquale, Azzaro Raffaele, Balduzzi Attilio, Bellini Vito, Benedetto Domenico, Berardi Carlo, Bernardi Rosanna, Bianchi Alessandro, Bordonaro Carla, Brindisi Annamaria, Buccolieri Marcello, Bulzomì Antonio Giovanni, Caligo Giacomo, Cantaffa Antonio, Carboni Sebastiano, Cascio Felice, Cassano Michele, Castagna Giovanni, Castellani Francesca, Chillura Mario, Colombo Giovanni, Corbetta Marco, Cordier Aldo, Costanzo Marcello, Cupido Francesco, Cupido Gianfranco, Danza Carlo, De Luca Carlo, Di Maria Domenico, Falcetti Saverio, Falciglia Roberto, Ferraro Guglielmo, Forte Sebastiano, Franco Teresa, Franzetti Andrea, Frisina Antonio, Gambardella Giuseppe, Gambardella Tullio, Iannello Franco, Ierace Michelangelo, Ingria Federico, La Mantia Ignazio, La Paglia Alessandro, Leone Mirko, Lingua Cristiano, Lovotti Paolo, Machetta Giacomo, Maddalena Gianluca, Maffezzoni Enrico, Mangiatordi Francesco Gerardo, Maniscalco Francesco, Melis Andrea, Mercurio Antonio, Milone Vincenzo, Mirra Nicola, Montanaro Salvatore Carmine, Moro Davide, Muià Fernando, Mussella Tommaso, Nacci Andrea, Padovani Davide, Panetti Maria Luisa, Paoletti Matteo, Piccolo Marcello, Pizzolante Maurizio Cosimo, Principi Pietro, Sari Marianna, Scarpa Alfonso, Serraino Eugenio Maurizio, Stabile Carlo, Tomacelli Giovanni, Tombolini Alberto, Trichini Antonio Fabio, Vergari Alessandro, Zaraca Giorgio

Received December 5, 2018 – Accepted January 16, 2019

Inflammation is a common pathogenic mechanism involved in many otorhinolaryngological (ORL) disorders. Broser® is an oral nutraceutical currently containing bromelain 100 mg, escin 30 mg, and selenium 42.5 mcg. It could exert a safe and effective anti-inflammatory activity by virtue of these components. Therefore, the aim of the current survey, conducted in clinical practice of 84 Italian ORL centers, was to evaluate its safety and efficacy in the treatment of patients with: i) high-tract acute illness; ii) low-tract acute illness; iii) high-tract chronic illness; iv) low-tract chronic illness; or v) post-surgery condition. The 3,203 (1,604 females and 1,599 males, mean age 44.9±8.9 years) patients were evaluated at baseline (T0) and after a 2-week treatment (T1) with Broser® monotherapy (2 tablets/daily). Signs and symptom severity were measured by visual analogue scale. Broser® significantly and safely diminished the clinical features in ORL disorders all sub-groups (p<0.001 for all). In conclusion, Broser® is an oral nutraceutical able to exert a safe and effective anti-inflammatory activity in patients with inflammation.

To the Editor,

Inflammatory disorders may be classified according to the duration, namely acute and chronic diseases. In clinical otorhinolaryngological practice, inflammatory disorders represent the most frequent cause of visit. From a clinical point of

Key words: inflammation; otorhinolaryngology; bromelain; escin; selenium

Corresponding Author:
Dr Giorgio Ciprandi,
Via P. Boselli 5,
16146 Genoa, Italy
e-mail gio.cip@libero.it

0393-974X (2019)

DISCLOSURE: ALL AUTHORS REPORT NO CONFLICTS OF INTEREST RELEVANT TO THIS ARTICLE.

view, the inflammatory otorhinolaryngology (ORL) diseases may be subdivided into 4 categories: i) high-tract acute illness, including common cold, acute rhinosinusitis, acute rhinopharyngitis, acute pharyngitis, acute otitis, and bacterial tonsillitis; ii) low-tract acute illness, including acute laryngitis and acute laryngotracheitis; iii) high-tract chronic illness, including chronic rhinosinusitis, chronic rhinopharyngitis, chronic pharyngitis, and chronic tonsillitis; and iv) low-tract chronic illness, i.e. chronic laryngitis. Another common ORL inflammatory illness is the post-surgery condition.

The common cold is the most frequent respiratory disease and involves the entire upper respiratory tract, and it is usually self-limiting. Two main guidelines for rhinosinusitis management have been published recently, both consider the best pragmatic approach in clinical practice (1, 2). Similarly, pharyngitis, laryngitis, and tracheitis are very common and are usually managed as reported in detail elsewhere (3, 4). On the other hand, surgery represents a usual therapeutic approach in the treatment of many ORL diseases (5), but pain and inflammation constitute an unavoidable consequence of operation. Therefore, inflammatory ORL disorders are usually treated using antibiotics if infection occurs, but anti-inflammatory medications are the mainstay in clinical practice. However, anti-inflammatory drugs may also have serious adverse events, therefore many doctors and patients prefer complementary medicine as they retain it more trustworthy (6). In this regard, Broser®, an oral nutraceutical, has been recently marketed. One Broser® tablet currently contains: bromelain 100 mg, escin 30 mg, and selenium 42.5 mcg.

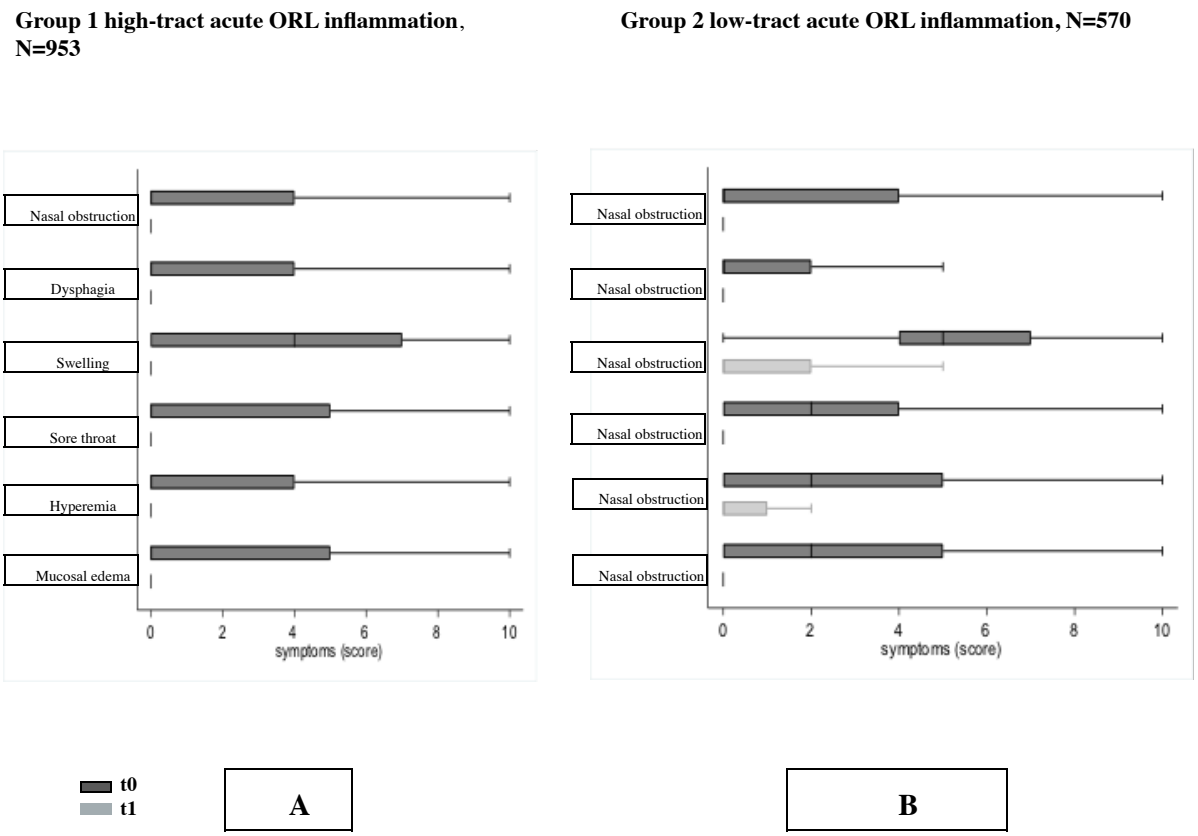

Fig. 1. ***A)*** *Visual Analogue Scale scores in Group 1 (high-tract acute ORL inflammation), at baseline (T0) and after treatment (T1).* ***B)*** *Visual Analogue Scale scores in Group 2 (low-tract acute ORL inflammation), at baseline (T0) and after treatment (T1).*

Bromelain is a complex mixture of protease extracted from the fruit or stem of the pineapple plant (7). Bromelain gained universal acceptability as a phytotherapeutic agent due to its history of safe use and lack of side effects. The beneficial effects are due to multiple factors. Bromelain increases bioavailability and reduces the side effects that are associated with various antibiotics. Furthermore, bromelain acts as an immunomodulator, and has anti-oedematous, anti-thrombotic, and anti-inflammatory activity. Bromelain has the *in vitro* ability to modulate surface adhesion molecules on T cells, macrophages, and natural killer cells and also may induce the secretion of IL-1β, IL-6, and tumour necrosis factor α (TNFα) by peripheral blood mononuclear cells (8). Bromelain influences blood coagulation by increasing the serum fibrinolytic ability and by inhibiting the synthesis of fibrin, a protein involved in blood clotting (8). In addition, bromelain can reduce the average number of days for complete disappearance of pain and post-surgery inflammation.

Escin is the major active principle from *Aesculus hippocastanum* (Hippocastanaceae), such as the horse chestnut tree (9). Escin is a natural mixture of triterpene saponins and has been shown to be effective in preventing the formation of oedema in models of inflammation that reproduce the initial exudative phase. The mechanism of the anti-oedematous effect, in addition to the earlier described sensitization to Ca ions, resulting in a 'sealing effect' on small vessels permeable to water, has also been related to a reduced hypoxia-induced activation of human endothelial cells. Escin can well antagonize the reduction in ATP content and increased phospholipase A2 responsible for the release of precursors of inflammatory mediators. There is, furthermore, a reduced neutrophil adherence/activation, all resulting in the protection of veins and reduced oedema. Escin exerts also antiviral and

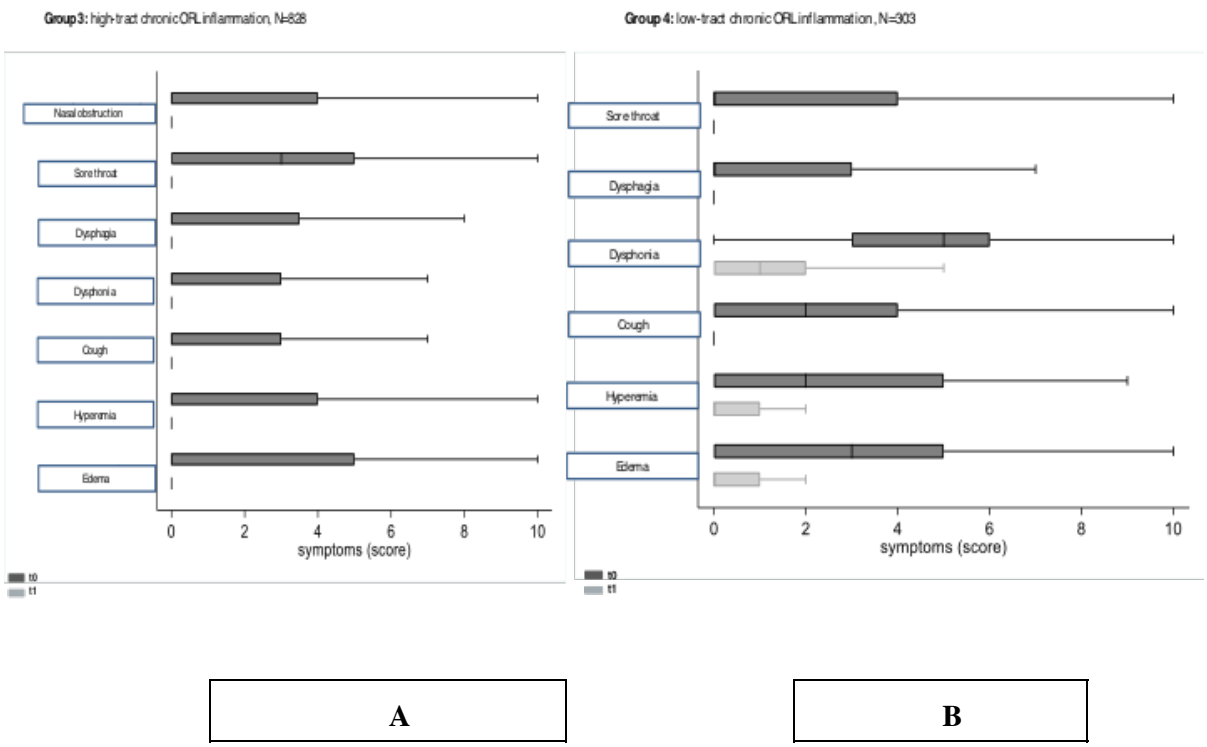

Fig. 2. ***A)*** *Visual Analogue Scale scores in Group 3 (high-tract chronic ORL inflammation), at baseline (T0) and after treatment (T1).* ***B)*** *Visual Analogue Scale scores in Group 4 (low-tract chronic ORL inflammation), at baseline (T0) and after treatment (T1).*

antiallergic activity (10).

Selenium is an essential trace element that exerts many functions, including anti-inflammatory activity (11). Epidemiological data suggest a positive association between selenium deficiency and chronic inflammation. Selenium supplementation of patients with chronic disorders has improved their health status and quality of life. In septic shock patients characterized by acute inflammation accompanied by severe pathology, selenium supplementation at high concentrations lessened mortality and improved health status (11). Adequate concentrations of selenium are essential for initiating immunity in addition to regulating excessive immune responses and chronic inflammation. Selenium-dependent effects are mediated via the downregulation of the redox-sensitive transcription factor NF-kB in addition to the epigenetic control of gene expression regulation (12). The selenium-metabolites modulate cell signalling, DNA methylation (directly or through one-carbon metabolism), histone acetylation, and finally, gene expression (12).

On the basis of this background, an Italian survey explored the pragmatic approach of a group of otorhinolaryngologists in the management of inflammatory upper-airway disorders in clinical practice. Therefore, the aim of the current survey was to evaluate the efficacy and safety of Broser® as monotherapy in outpatients with acute, chronic or post-surgery ORL diseases.

MATERIALS AND METHODS

The current survey was conducted in 84 Italian ORL centers, distributed in the whole of Italy, so assuring a wide and complete national coverage, during fall-winter 2017-2018. Otorhinolaryngologists endorsed to the Italian Study Group of inflammatory otorhinolaryngological disorders were asked to recruit all consecutive patients visited because of inflammatory illness, including post-surgery.

Patients were consecutively recruited during the specialist visit. The inclusion criteria were: a diagnosis of inflammatory ORL disorder, both genders, and adulthood. Exclusion criteria were comorbidities able to interfere the evaluation of the outcomes. As this survey was based on a real-world practice, the doctors had the complete liberty of choosing the preferred medications on the basis of the best practice. The patients treated with Broser®, prescribed as monotherapy, were included in the present analysis.

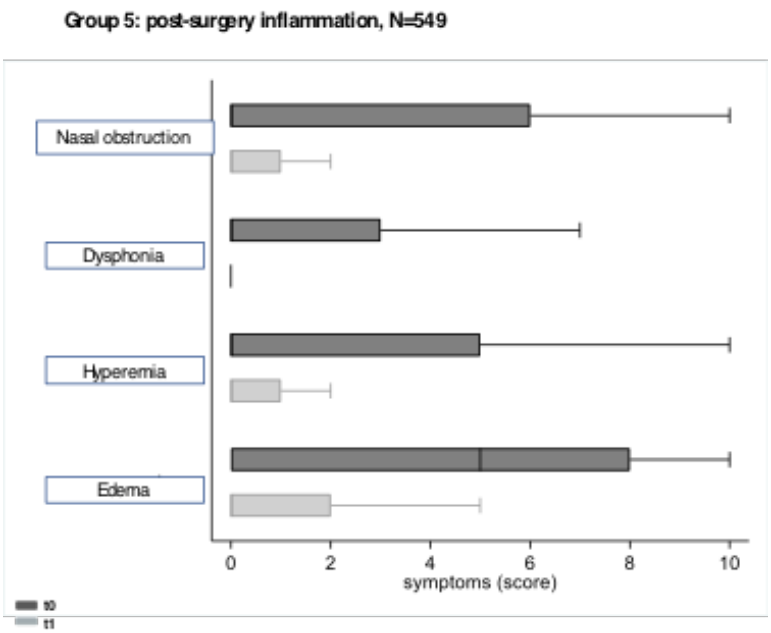

Fig. 3. *Visual Analogue Scale scores in Group 5 (post-surgery ORL inflammation), at baseline (T0) and after treatment (T1).*

The patients were subdivided into 5 sub-groups, suffering from: i) high-tract acute illness, including common cold, acute rhinosinusitis, acute rhinopharyngitis, acute pharyngitis, acute otitis, and bacterial tonsillitis; ii) low-tract acute illness, including acute laryngitis and acute laryngotracheitis; iii) high-tract chronic illness, including chronic rhinosinusitis, chronic rhinopharyngitis, chronic pharyngitis, and chronic tonsillitis; iv) low-tract chronic illness, i.e. chronic laryngitis; and v) post-surgery.

All patients signed an informed consent to participate in the study. The treatment course lasted 2 weeks. The oral nutraceutical was taken following specific indications, such as two tablets/daily. Patients were visited at baseline (T0) and after the treatment (T1).

Clinical examination and fiber-endoscopy were evaluated in all patients at T0 and T1. The following parameters were investigated: nasal obstruction, mucosal edema, hyperemia, earache, swelling, sore throat, dysphagia, dysphonia, and cough. Signs and symptoms were assessed by a visual analogue scale (VAS). VAS is a psychometric test widely used to measure the patient's perception of symptom severity, emotions, pain, etc. Currently, VAS is a reliable and valid tool to assess the perception of symptoms and signs (13). The VAS consisted of one rule asking for signs and symptoms severity perception. In this study, the VAS was a 10-cm horizontal line on which 0 implied the absence of sing or symptom, while 10 corresponded to maximal severity. With a movable marker, the patient or the doctor could mark any point on the 10-cm segment which best described his/her perception. No interval marker was visible on the line. VAS is considered a routine and validated parameter to assess disease severity in clinical practice (13). Safety was measured by reporting the occurrence of adverse events.

The paired *t*-test was used. Statistical significance was set at $p < 0.05$. Data are expressed as medians and 1th and 3rd quartiles. The analysis was performed using STATA, College Station, Texas, USA.

RESULTS

A total of 3,203 (1,604 females and 1,599 males, mean age 44.9±8.9 years) patients were visited and completed the treatment course.

Group 1, high-tract acute ORL inflammation, consisted of 953 patients. Fig. 1A shows the scores before (T0) and after (T1) the Broser® monotherapy treatment course: all of them significantly diminished ($p<0.001$ for all).

Group 2, low-tract acute ORL inflammation, consisted of 570 patients. Fig. 1B shows the scores before (T0) and after (T1) the Broser® monotherapy treatment course: all of them significantly diminished ($p<0.001$ for all).

Group 3, high-tract chronic ORL inflammation, consisted of 828 patients. Fig. 2A shows the scores before (T0) and after (T1) the Broser® monotherapy treatment course: all of them significantly diminished ($p<0.001$ for all).

Group 4, low-tract chronic ORL inflammation, consisted of 303 patients. Fig. 2B shows the scores before (T0) and after (T1) the Broser® monotherapy treatment course: all of them significantly diminished ($p<0.001$ for all).

Group 5, post ORL surgery, consisted of 549 patients. Fig. 3 shows the scores before (T0) and after (T1) the Broser® monotherapy treatment course: all of them significantly diminished ($p<0.001$ for all).

The treatment was well tolerated by all patients and no relevant adverse event was reported. The most common not-relevant adverse events were headache (11%), sore throat (9%), itching (6%), and stomach upset (5%).

DISCUSSION

Inflammation, which is a pattern of response to injury, involves the accumulation of cells and exudates in involved tissues, that allows protection from further damage. Inflammation has been studied for thousands of years with the aim of contrasting its effects on the body. In 30 AD, Celsius described the 4 classic signs of inflammation (*rubor, calor, dolor,* and *tumor*) and used extracts of willow leaves to relieve them. For many years, salicylate-containing plants were applied therapeutically and led to the production of a major anti-inflammatory drug (acetylsalicylate). Acetylsalicylate, an agent with anti-inflammatory activity, is derived from natural sources, and is used extensively in current clinical practice. It represents the paradigmatic example of the use of plant-derived

compounds in medicine. Many other salicylate-like drugs are now available including non-steroid anti-inflammatory drugs (NSAIDs).

Natural products with anti-inflammatory activity have long been used as a folk remedy for inflammatory conditions such as fevers, pain, migraine and arthritis. As the inflammatory basis of disease becomes clear, anti-inflammatory food products become of greater interest. In this regard, the oral nutraceutical Broser® belongs to the plant-derived food supplements, as it contains extracts of pineapple, namely the bromelain, and of horse chestnut, i.e. escin. In addition, Broser® includes selenium, an oligo-element.

Currently, the mechanisms of action of these molecules have been identified and examined in depth, thus, their clinical use is no longer empirical but based on solid scientific grounds. In particular, Broser® may exert a clinically relevant anti-inflammatory activity and could be considerably better tolerated than NSAIDs.

The current survey demonstrated that Broser® significantly improved the clinical feature in acute, chronic, and post-surgery inflammatory disorders in ORL clinical practice. As previously reported, bromelain, escin, and selenium may significantly affect the inflammatory events cascade. In this scenario, this food supplement even alone may safely reduce inflammatory phenomena. The present findings are consistent with previous studies that explored the therapeutic effects of similar multi-component nutraceuticals in the treatment of ORL diseases.

Bromelain has commonly been used in rhinosinusitis as an anti-inflammatory and mucolytic. A 2005 German clinical study found that children suffering from acute rhinosinusitis exhibited statistically significant faster symptom recovery than standard treatment (14). Bromelain appeared also to thin nasal secretions and has been shown to be an effective mucolytic agent in other respiratory tract diseases (15). This is in addition to bromelain's proteolytic activity at inflammatory sites, which is thought to promote the inhibition of pro-inflammatory prostaglandin biosynthesis and the initiation of prostaglandin-E1 accumulation, inhibiting the release of leukocyte lysosomal enzymes (16). A very recent study compared placebo with ibuprofen or a phytotherapeutic drug, containing baicalin, bromelain, and escin (17). This food supplement significantly decreased the severity of postoperative pain more than ibuprofen and placebo. Consistently, a recent meta-analysis reported that bromelain proved to be effective in controlling postoperative pain at 48–72 hours after surgery (8). A previous systematic review evidenced that herbal medicines could be beneficial in the treatment of rhinosinusitis (18). Another systematic review of randomized trials using herbal medicine in chronic rhinosinusitis reported that this remedy is popular and commonly used (19). The outcomes showed that special medicinal plants may be effective and safe. Moreover, it has been demonstrated that selenium-enriched hot spring water reduced inflammatory activity and mucus hypersecretion in LPS-induced experimental rhinosinusitis (20).

The present survey therefore confirms that an oral nutraceutical, such as Broser®, was able to significantly reduce clinical features in many ORL disorders characterized by an inflammatory reaction. However, the current study has some limitations, mainly concerning the open design and the lack of objective functional data. On the other hand, the strength of this survey is the high number of enrolled patients and the real-world setting, therefore the findings may mirror what occurs in daily practice.

In conclusion, the present survey evidenced that Broser® may induce a safe control of respiratory complaints in inflammatory ORL disorders.

REFERENCES

1. Fokkens WJ, Lund VJ, Mullol J, et al. European position paper on rhinosinusitis and nasal polyps 2012. Rhinology 2012; S23:1-298.
2. Orlandi R, Kingdom TT, Hwang PH, et al. International consensus statement on allergy and rhinology: rhinosinusitis. Int Forum Allergy Rhinology 2016; 6:S22-S209.
3. Wood JM, Athanasiadis T, Allen J. Laryngitis. BMJ 2014; 349:g5827.
4. Blot M, Bonniaud-Blot P, Favrolt N, Bonniaud P,

Chavanet P, Piroth L. Update on childhood and adult infectious tracheitis. Med Mal Infect 2017; 47:443-52.
5. Rudmik L, Soler ZM, Orlandi RR. Early postoperative care following endoscopic surgery: an evidence-based review with recommendations. Int Forum Allergy Rhinol 2011; 1:417-30.
6. Yuan G, Wahlqvist ML, He G, Yang M, Li D. Natural products and anti-inflammatory activity. Asia Pac J Clin Nutr 2006; 15:143-52.
7. Rathnavelu V, Alitheen NB, Sohila S, Kanagesan S, Ramesh R. Potential role of bromelain in clinical and therapeutic applications (Review). Biomed Rep 2016; 5:283-88.
8. Zehra AM, Tashfeen A. Therapeutic uses of pineapple-extracted bromelain insurgical care – a Review. J Pak Med Assoc 2017; 67:121-25.
9. Sirtori CR. Aescin: pharmacological, pharmacokinetics and therapeutic profile. Pharmacological Research 2001; 44:183-93.
10. Michelini F, Alché LE, Bueno CA. Virucidal, antiviral and immunomodulatory activities of β-escin and *Aesulus hippocastanum* extract. J Pharmacy Pharmacol 2018; 70:1561-71.
11. Prabhu KS, Lei XG. Selenium. Adv Nutr 2016; 7:415-17.
12. Costantinescu-Aruxandei D, Frincu RM, Capra L. Selenium analysis and speciation in dietary supplements based on next-generation selenium ingredients. Nutrients 2018; 10:1466
13. Ciprandi G, Mora F, Cassano M, Gallina AM, Mora R. V.A.S. and nasal obstruction in persistent allergic rhinitis. Otolaryngol Head Neck Surg 2009;141:527-29.
14. Braun JM, Schneider B, Beuth HJ. Therapeutic use, efficiency and safety of the proteolytic pineapple enzyme Bromelain-POS in children with acute sinusitis in Germany. In Vivo 2005; 19:417-21.
15. Taub SJ. The use of bromelains in sinusitis: a double-blind clinical evaluation. Eye Ear Nose Throat Mon 1967; 46:361-62.
16. Rimoldi R, Ginesu F, Giura R. The use of bromelain in pneumological therapy. Drugs Exp Clin Res 1978; 4:55-66.
17. Isola G, Matarese M, Ramaglia L, Iorio-Siciliano V, Cordasco G, Matarese G. Efficacy of a drug composed of herbal extracts on postoperative discomfort after surgical removal of impacted mandibular third molar: a randomized, triple blind, controlled clinical trial. Clin Oral Invest 2018 (in press) doi: 10.1007/s00784-018-2690-9.
18. Guo R, Canter PH, Ernst E. Herbal medicines for the treatment of rhinosinusitis: a systematic review. Otolaryngol-HNS 2006; 135:496-506.
19. Anushiravani M, Bakhshaee M, Taghipour A, Naghedi-Baghdar H, Farshchi MK, Hoseini SS, Mehri MR. A systematic review of randomized controlled trials with herbal medicine on chronic rhinosinusitis. Phytother Res 2018; 32:395-401.
20. Kim DH, Yeo SW. Effects of normal saline and selenium-enriched hot spring water on experimentally induced rhinosinusitis in rats. Int J Ped Otorhinolaryngol 2013; 77:117-22.

LETTER TO THE EDITOR

A POLYCENTRIC, RANDOMIZED, DOUBLE BLIND, PARALLEL-GROUP, PLACEBO-CONTROLLED STUDY ON LERTAL®, A MULTICOMPONENT NUTRACEUTICAL, AS ADD-ON TREATMENT IN CHILDREN WITH ALLERGIC RHINOCONJUNCTIVITIS: PHASE I DURING ACTIVE TREATMENT

GL. MARSEGLIA[1], A. LICARI[1], G. CIPRANDI[2] and ITALIAN STUDY GROUP ON PEDIATRIC ALLERGIC RHINOCONJUNCTIVITIS*

[1]Pediatrics Clinic, Pediatrics Department, Policlinico San Matteo, University of Pavia, Pavia, Italy; [2]Allergy Clinic, Casa di Cura Villa Montallegro, Genoa, Italy

*Italian Study Group on Pediatric Allergic Rhinoconjunctivitis: Brambilla I, Cardinale F, Cherubini S, Giordano P, Leonardi S, Marchisio P, Martelli A, Minasi D, Miraglia del Giudice M, Paravati F, Pellegrini G, Podestà A, Pogliani L, Salpietro C, Tosca MA, Verrotti A, Zicari A

Received January 17, 2019 – Accepted January 25, 2019

Allergic rhinoconjunctivitis (AR) treatment is usually pharmacological in children, but medications are merely symptomatic, may not be completely effective, and may have relevant side effects. Thus, doctors and parents look at complementary medicine, including nutraceuticals. Lertal®, an oral nutraceutical, contains extract of Perilla, quercetin, and Vitamin D_3 It has been reported that adults with AR diminished allergic symptoms and medication use during Lertal® therapy. Therefore, the current polycentric, randomized, double blind, parallel-group, placebo-controlled study aimed to evaluate the efficacy and safety of Lertal® as an add-on treatment in children with AR. In this study, 146 children (94 males and 52 females, mean age 9.1±1.88) were randomly assigned to Lertal® + standard treatment or Placebo + standard treatment and were visited at baseline (W0), and after 2 (W2) and 4 weeks (W4). Standard treatment consisted of continuous antihistaminic schedule. The primary endpoint was the Total Symptom Score (TSS - last 12 hours) change from the baseline to the end of the 4-week treatment. Both groups significantly ($p<0.0001$ for both) reduced TSS (last 12 hours) after 4 weeks (% change: - 63.6% in Lertal®-group and – 60.7% in Placebo-group; p= n.s. intergroup analysis). Notably, 24 children had symptom worsening between W2 and W4: 8 in the Lertal®-group and 16 in the Placebo-group, with significant intergroup difference ($p<0.05$). All of them were poly-allergic subjects exposed to multiple allergens. There was no relevant adverse event. The present study documented that Lertal®, as add-on treatment, was able to significantly prevent the occurrence of clinical worsening and was safe in AR poly-allergic children.

To the Editor,

Allergic rhinoconjunctivitis (AR) is characterized by ocular and nasal symptoms, such as itching, congestion, sneezing (1).

Treatment is usually pharmacological, including antihistamines and corticosteroids, even though drugs exert only a symptomatic effect as they do not cure allergy (2). Aggressive therapy and use of

Key words: allergic rhinoconjunctivitis; nutraceutical; Perilla frutescens; quercetin; vitamin D_3; add-on treatment

Corresponding Author:
Dr Giorgio Ciprandi,
Via P. Boselli 5,
16146, Genoa, Italy
e-mail: gio.cip@libero.it

0393-974X (2019)

drugs with significant side effects should however be limited or avoided altogether in children. For this reason, it is growing interest in using complementary medicine. Nutraceuticals with proven efficacy may be associated with conventional therapy to speed up recovery, make it long lasting, and avoid aggressive therapeutic regimens, including systemic corticosteroids, or at least limit their duration (3).

Lertal® is a novel oral food supplement. Each tablet contains the following active ingredients in a double-layer "fast-slow" release: Quercetin 150 mg, *Perilla frutescens* 80 mg (as dry extract of the seeds containing rosmarinic acid, luteolin, apigenin and chrysoeriol), and Vitamin D3 5 mcg (200 IU).

The dry seed extract of *Perilla frutescens* contains rosmarinic acid and other flavonoids and has shown anti-allergic activity *in vivo* and *in vitro*, mainly concerning 5-lipoxygenase and 12-lipoxygenase (4-6). Quercetin is a bioflavonoid found in red wine, grapefruit, onions, apples, and black tea (7). Quercetin has a strong affinity for mast cells and basophils and tends to stabilize their cell membranes and block degranulation, inhibiting the release of pro-inflammatory mediators and cytokines implicated in allergic inflammation (8, 9). Vitamin D3 is important for its contribution to the normal function of the immune system by preventing and potentially treating AR, as it restores physiological T regulatory activity and exerts also anti-inflammatory activity (10-15). Lertal® is formulated in bilayer tablets composed of a fast-release layer that allows the rapid antihistamine activity of *Perilla*, and a sustained-release layer that enhances Quercetin and Vitamin D3 bioavailability and anti-allergy activity spread over time, as recently reported (16).

Moreover, it is well known that a possible symptom worsening may occur both during the active antihistaminic treatment or after its suspension, as expression of insensitivity or excessive allergen exposure. Consequently, we tested two hypotheses: i) to investigate the Lertal® capability to amplify the response to standard antihistaminic AR medications and/or reduce the insensitivity during the active treatment, and ii) to demonstrate the Lertal® potentiality to prevent possible relapse after treatment. Therefore, the current polycentric, randomized, study was designed in two phases: the first as double blind, placebo-controlled trial during standard active AR treatment and the second as open follow-up after it. The first phase aimed to evaluate the efficacy and safety of Lertal® as an add-on treatment in children with AR.

MATERIALS AND METHODS

The first phase of the present study was a 4-week, randomized, polycentric, double-blinded, parallel-group, placebo-controlled trial. One hundred and sixty patients suffering from AR were planned for enrolment in 17 Italian Paediatric Allergy clinics. AR diagnosis was performed, according to validated criteria (1), such as nasal symptom history being consistent with documented sensitization.

Inclusion criteria were: age range 6-12 years, AR diagnosis, sensitization to house dust mites or pollens, Total Symptoms Score (TSS) $\geq$ 15 and at least 1 for nasal congestion, written informed consent of patients and of parents or legal guardians. Exclusion criteria were: uncontrolled asthma, secondary rhinitis to other causes, concomitant acute or chronic rhinosinusitis, nasal polyps, current use of topical or systemic corticosteroids, antihistamines, antileukotrienes, inadequate washout of them, nasal anatomic defect, respiratory infections in the previous 2 weeks, participation in other clinical studies in the previous month, documented hypersensitivity to the study product or its excipients, and trips planned outside of the study area.

After a 2-week run-in period, eligible patients were randomly (1:1 ratio) treated with Lertal® double-layer tablets (1 tab/day for 4 weeks) plus standard therapy, or Lertal® placebo tablets (1 tab/day for 4 weeks) plus standard therapy. As Lertal® was considered as add-on treatment, the standard therapy was continuous antihistaminic treatment. Systemic or intranasal corticosteroids, leukotriene antagonists, and sodium cromoglicate were prohibited during the study. Four visits were performed: Visit 1 at run-in, Visit 2 at baseline (W0), Visit 3 after 2 weeks (W2), and Visit 4 after 4 weeks, i.e. end of treatment (W4).

Patient-reported outcomes and diary-recorded data, including the use of rescue medication/concomitant medication and the occurrence of adverse events, were

collected at Visits 2, 3 and 4. Clinical data were reported in an electronic Case Report Form (eCRF).

The primary endpoint of this study was the TSS change from the baseline to the end of the treatment (4 weeks). The secondary objectives were: overall symptom control assessed by means of a VAS after 2 and 4 weeks of treatment, change from baseline of the Total Symptom Score (TSS) after 2 weeks of treatment, number of responders (at least 30% reduction of TSS) after 2 and 4 weeks of treatment, time to maximum effect on TSS *vs* placebo, change of TSS from 2 and 4 weeks (worsening was defined as at least 30% increase of TSS), use of rescue treatment, change from baseline of Total Nasal Symptom Score (TNSS), Total Ocular Symptom Score (TOSS), and Total Throat Symptom Score (TTSS) after 2 and 4 weeks of treatment, issues interfering with quality of life at baseline and after 4 weeks, duration of symptom-free or mild symptoms.

Nasal symptoms (TNSS) included itching, sneezing, rhinorrhea, nasal congestion; ocular symptoms (TOSS): itching, hyperemia of conjunctiva, tearing; throat symptoms (TTSS): itching, coughing. With the help of their parents, patients scored symptoms severity on a 4-point scale: 0 = absent or irrelevant, 1 = mild, 2 = moderate, 3 = severe.

At Visit 3 and Visit 4 the patient was asked to indicate overall system distress on a 100 mm Visual Analogue Scale (VAS) where 0 is equal to no discomfort and 100 the worst possible discomfort.

The Pediatric Rhinoconjunctivitis Quality of Life Questionnaire (PRQLQ) consists of 23 questions in 5 domains (nasal symptoms, ocular symptoms, practical issues, limitation of activities, other symptoms), that are answered on a 7-point scale (0-6), where 0 represents the absence of problems and 6 the greatest symptom distress. Children completed the questionnaire together with a parent at baseline and at Visit 4.

Safety was assessed on the incidence of adverse events for each treatment and on physical examinations.

The sample size was *a priori* calculated, using nQuery 4.0 and adjusted for an expected dropout rate of 12% using Freedman's formula. The study protocol was approved

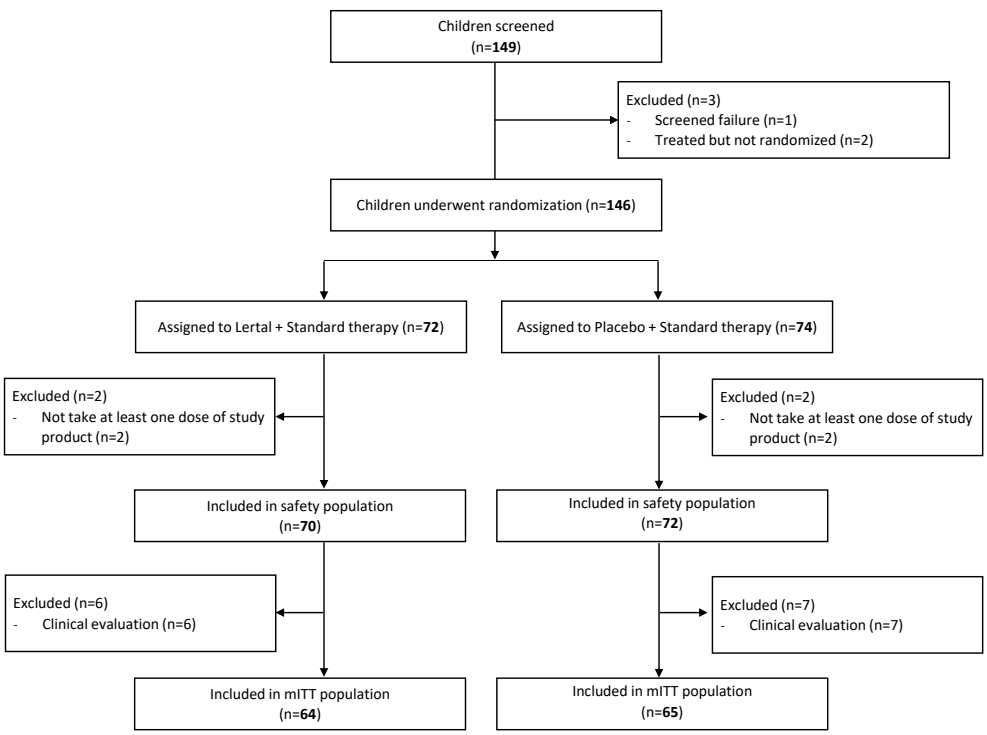

Fig. 1. *Patients' disposition during the study.*

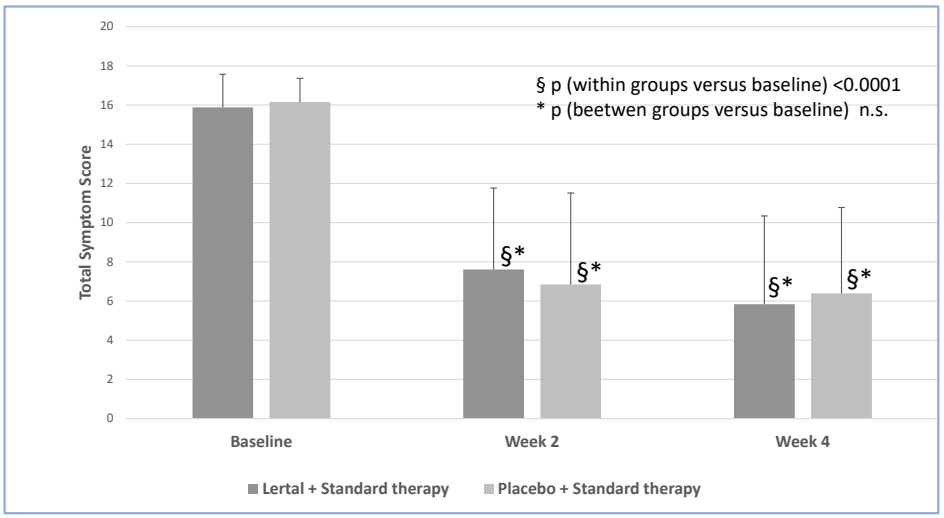

Fig. 2. *Total Symptom Score: trend over time by treatments.*

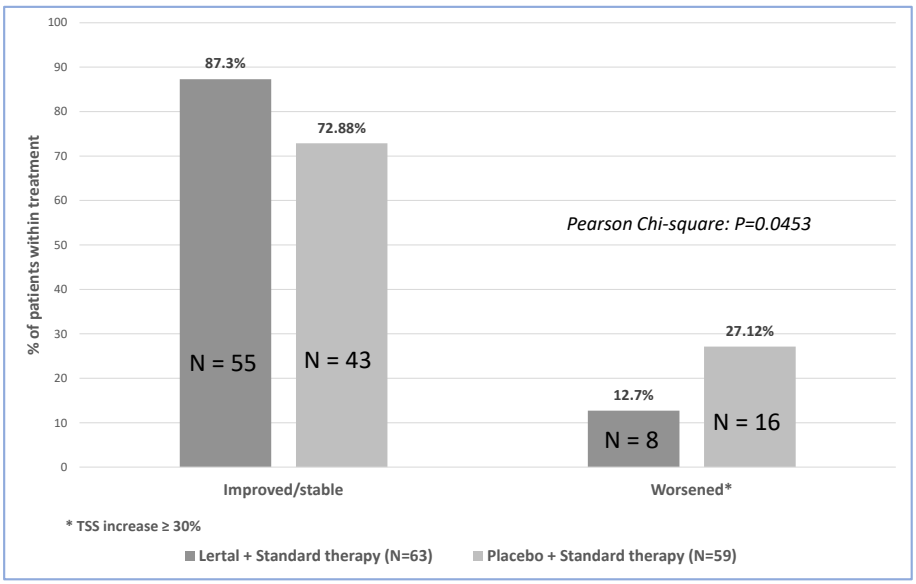

Fig. 3. *Total Symptom Score: class change between W2 and W4 by treatments.*

by the Ethics Committees of each center. The study was registered at ClinicalTrials.gov ID NCT03365648.

The between-group analysis was performed by means of a *t*-test for independent samples or analogous non-parametric test or a *Chi*-squared test in contingency tables.

RESULTS

Globally, 146 children (94 males and 52 females, aged 6-12 years, mean age 9.1±1.88) were randomized. The patients' disposition is reported in Fig. 1. Four patients were excluded from safety analysis (4 did not take at least one dose of the study product) and other 13 patients were excluded from efficacy analysis after clinical evaluation. The efficacy analysis therefore included a total of 129 patients, of whom 64 were assigned to Lertal® + standard therapy, and 65 to placebo + standard therapy. The two groups were homogeneous as far as age, gender, BMI, type of allergy, time from

diagnosis and symptom severity are concerned at baseline (p=n.s.).

The TSS at baseline was 15.9 (±1.7) in the Lertal®-group and 16.1 (±1.2) in the Placebo-group (p= n.s.). Both groups significantly ($p<0.0001$ for both) reduced TSS (last 12 hours) after 2 and 4 weeks, without between-group difference (Fig. 2). In particular, TSS at W4 was: 5.83 (±4.5) in the Lertal®-group and 6.39 (±4.38) in the Placebo-group (p=n.s.). There was a trend between groups about the percentage Δ change: - 63.6% in the Lertal®-group and - 60.7% in the Placebo-group.

Notably, 24 children had total symptom score worsened (i.e. ≥ 30% increased TSS) between W2 and W4: 8 in the Lertal®-group and 16 in the Placebo-group, the difference between treatments being significant ($P<0.05$). Fig. 3 shows the percentages of improved/stable patients and worsened ones in the two groups between W2 and W4.

All other secondary endpoints (TNSS, TOSS, TTSS, PRQL) after 2 and 4 weeks improved in both groups, without significant between-group difference (data not shown).

Both treatments were well tolerated and no serious adverse events were reported. There were only two adverse events related to the treatment in the Lertal® group (mild allergic conjunctivitis and moderate tooth disorder).

DISCUSSION

The clinical relevance of AR depends on several issues, including bothersome complaints, frequent co-morbidities, negative impact on personal and social quality of life, familiar involvement, and overall the awareness that AR is a chronic disease not curable with medications alone (17).

The current study showed that standard antihistaminic treatment is able to improve the clinical feature in children with AR. Furthermore, it has been evidenced that Lertal®, used as add-on therapy, was able to tendentially improve the effect of the standard AR treatment. The Lertal®-group achieved a mean reduction of about 64% of symptom severity, whereas the Placebo-group of 60%. However, a relevant difference was not expected because of both the obviously antihistaminic activity and the characteristics of the nutraceutical. Notably, Lertal® significantly reduced the possible occurrence of intercurrent relapse during the standard treatment in children with AR. Indeed, the most important finding of the present study was the capability of Lertal® to prevent symptom worsening during conventional antihistaminic treatment, mainly concerning the second period of the treatment. In the current trial, 28 patients (8 in the Lertal® group and 16 in the Placebo group) had a clinical relapse between the third and the fourth week, despite an initial improvement. Therefore, the possible explanation of this behaviour was deeply investigated. The common characteristic of these children was poly-allergy. Very recently, Togias reported that children suffering from perennial allergic rhinitis with seasonal exacerbations, such as poly-allergy, present the most severe AR phenotype (18). Consequently, the children enrolled in the present study, worsened, despite ongoing treatment, as they were exposed to multiple allergens, thus developing more severe allergic reaction. Nevertheless, add-on Lertal® preserved clinical relapse in a larger number of poly-allergic children than standard therapy. This finding is particularly interesting if contextualized as part of a continuous effective antihistaminic treatment and this preventive activity may allow to avoid the recourse to corticosteroids. The plausible reason of this phenomenon could be explained by the multifaceted mechanisms of action exerted by Lertal®. In particular, Lertal® effects seem to be grounded in the complex anti-inflammatory and anti-allergic activity exerted on the immune response by the three compounds.

In conclusion, the present study documented that add-on Lertal® treatment was able to partially improve standard AR treatment in children, significantly prevent the occurrence of clinical worsening in a subgroup of poly-allergic children, and was safe.

REFERENCES

1. Brożek JL, Bousquet J, Agache I, et al. Allergic Rhinitis and its Impact on Asthma (ARIA) guidelines-2016

revision. J Allergy Clin Immunol 2017; 140(4):950-58.
2. Wise SK, Lin SY, Toskala E, et al. International Consensus Statement on Allergy and Rhinology: Allergic Rhinitis. Int Forum Allergy Rhinol 2018; 8(2):108-352.
3. El-Qutob López D. New methods of prevention and treatment of allergic diseases. Recent Pat Inflamm Allergy Drug Discov 2012; 6(1):46-64.
4. Yu H, Qiu JF, Ma LJ, Hu YJ, Li P, Wan JB. Phytochemical and phytopharmacological review of Perilla frutescens L. (Labiatae), a traditional edible-medicinal herb in China. Food Chem Toxicol 2017; 108(Pt B):375-91.
5. Makino T, Furuta Y, Wakushima H, et al. Anti-allergic effect of Perilla frutescens and its active constituents. Phytother Res 2003; 17(3):240-43.
6. Igarashi M, Miyazaki Y. A review on bioactivities of Perilla: progress in research on the functions of Perilla as medicine and food. Evid Based Complement Alternat Med 2013; 2013:925342.
7. Shaik YB, Castellani ML, Perrella A, et al. Role of Quercetin (a natural herbal compound) in allergy and inflammation.J Biol Regul Homeost Agents 2006; 20(3-4):47-52.
8. Chirumbolo S. The role of Quercetin, Flavonols and Flavones in modulating inflammatory cell function. Inflamm Allergy-Drug Targets 2010; 9(4):263-85.
9. Mlcek J, Jurikova T, Skrovankova S, Sochor J. Quercetin and its anti-allergic immune response. Molecules 2016; 2:,623.
10. Muehleisen B, Gallo RL J. Vitamin D in allergic disease: shedding light on a complex problem Allergy Clin Immunol 2013; 131(2):324-29.
11. Bozzetto S, Carraro S, Giordano G et al. Asthma, allergy and respiratory infections: the vitamin D hypothesis. Allergy 2012; 67(1):10-17.
12. Yepes-Nunes JJ, Brozek JL, Fiocchi A, et al. Vitamin D supplementation in primary allergy prevention: systematic review of randomized and non-randomized studies. Allergy 2018; 73:37-49.
13. Kim YH, Kim KW, Kim MJ, et al. Vitamin D levels in allergic rhinitis: a systematic review and meta-analysis. Ped Allergy Immunol 2016; 27:580-90.
14. Aryan Z, Rezaei N, Camargo CA. Vitamin status, aeroallergen sensitization, and allergic rhinitis: a systematic review and meta-analysis. Int Rev Immunol 2017; 36:41-53.
15. Loo EXL, Tham EH, Phang KW, et al. Associations between maternal vitamin D levels during pregnancy and allergic outcomes in the offspring in the first 5 years of life. Pediatr Allergy Immunol 2018 Oct 19. doi: 10.1111/pai.12995.
16. Ariano R. Efficacy of a novel food supplement in the relief of the signs and symptoms of seasonal allergic rhinitis and in the reduction of the consumption of anti-allergic drugs. Acta Biomed 2015; 86(1):53-58.
17. Ciprandi, G, Klersy C, Cirillo I, Marseglia GL. Quality of life in allergic rhinitis: relationship with clinical, immunological, and functional aspects. Clin Exp Allergy 2007; 37(10):1528-35.
18. Togias A, Gergen PJ, Hu JW, et al. Rhinitis in children and adolescents with asthma. Ubiquitous, difficult to control, and associated with asthma outcomes. J Allergy Clin Immunol 2018; Jul 27. pii: S0091-6749(18)31064-9. doi: 10.1016/j.jaci.2018.06.043

LETTER TO THE EDITOR

DELAYED TOOTH REPLANTATION AND INFLAMMATORY ROOT RESORPTION IN CHILDHOOD AND ADOLESCENCE

E. SPINAS[1], L. GENERALI[2], A. MAMELI[1], C. DEMONTIS[1], D. MARTINELLI[3] and L. GIANNETTI[2]

[1]Department of Surgical Sciences, Sports Dental Research Center, University of Cagliari, Cagliari, Italy; [2]Department of Surgical Sciences, Pedodontics Division, University of Modena-Reggio, Modena, Italy; [3]Department of Medical, Oral and Biotechnological Sciences, University "G. d'Annunzio" of Chieti and Pescara, Chieti, Italy

Received October 17, 2018 – Accepted January 23, 2019

Avulsion of one or more permanent teeth represents an emergency in dentistry. The main treatment is the replantation of the tooth/teeth as soon as possible to decrease possible complications. However, this is not always possible, and, in many cases, the patient undergoes a delayed replantation and subsequently prosthetic and implant treatments. This becomes problematic when the traumatized patient is a child; in this case, the goal is to maintain the space for the subsequent implant positioning and to give an adequate aesthetic result until the bone growth has ceased. A review on the incidence of the inflammatory root resorption onset after delayed replantation was carried out to check the frequency and severity of these complications.

To the Editor,

Traumas of the stomatognatic system have considerable social importance: traumatic events in the oral region occur frequently and represent 5% of all injuries for which people require treatment (1). According to Andreasen, dental traumas are very common during childhood and adolescence, and current statistics show that one-third of all preschool children and one-quarter of school children have suffered a trauma, respectively, to the primary and permanent dentition (1). The most frequent causes are accidental falls and sports activities. In these traumas, maxillary central incisors are the most involved teeth, followed by lateral maxillary incisors. The most serious injury is universally identified in avulsion. Avulsion consists in the complete displacement of the involved tooth out of the socket, with or without alveolar tissue loss, and represents 0.5-3% of all dental injuries and involves especially anterior teeth in subjects aged 9-11 years. The treatment consists in replanting the avulsed tooth in as little time as possible with an immediate replantation, which is the Gold Standard for this type of injury (2). Sometimes this treatment cannot be performed before 60 minutes, which is the case of delayed replantation (1-2), a treatment that needs a rigid follow-up and a multidisciplinary team who have to work in synergy. The inflammatory root resorption (IRR) is one of the most frequent complications that occurs after delayed replantation and can lead to tooth loss.

The aim of this work is a literature review focusing on incidence, diagnosis and treatment of IRR after delayed dental replantation.

Key words: dental trauma; avulsion; ankylosis; guided bone regeneration; delayed replantation; inflammatory root resorption

Corresponding Author:
Prof. Luca Giannetti,
University of Modena and Reggio Emilia,
Department of Paediatric Dentistry,
Via del Pozzo, 71, 41125 Modena, Italy
Tel.: +39 059 422432
e-mail: luca.giannetti@unimore.it

0393-974X (2019)

DISCLOSURE: ALL AUTHORS REPORT NO CONFLICTS OF INTEREST RELEVANT TO THIS ARTICLE.

MATERIALS AND METHODS

A mini-review of the literature was carried out on IRR after delayed replantation. Studies concerning only delayed replantation which developed an IRR were included. Ten works were selected from 1995 to 2016. Data are shown in Tables I and II. The incidence of IRR varies between 6.8-62.5%. The interval time from the avulsion to the replantation goes from 1 hour (minimum time to decide on delayed replantation, https://dentaltraumaguide.org) to 24 hours. Time elapsed from the replantation to the diagnosis of IRR goes from 1 month to 6 years; patients were followed up for 1-12 years with an average of 6 years. Regarding the treatment performed after the diagnosis of IRR, Table II lists the most utilized type of treatment and materials

DISCUSSION

Delayed replantation means the replantation of a tooth when it has been found for more than 60 minutes outside the alveolus and stored dry, or when the tooth is stored in a non-physiological storage media (1). The long-term prognosis is scarce. After the replantation, pulp necrosis and root resorption can occur. Root resorption can be divided into internal and external (3); external root resorption can be also divided in surface resorption, a type of periodontal healing; replacement resorption (or ankylosis), which is a fusion of bone and dental tissues and IRR which is caused by infections and pulp necrosis and can lead to a complete erosion of the root (3).

In the literature, quantifying the incidence of IRR in delayed replantation appears to be difficult because in many studies there is no clear differentiation of complications between delayed and immediate replantation. However, it can be said that this complication has an incidence ranging between 6.8% and 62.5% in all avulsed and replanted teeth (4-8)

At the beginning this lesion is asymptomatic, but later it can manifest with signs of inflammations, pain when chewing, increase of tooth mobility (grades I, II and III) and subsequently dental migration, and change in colour of the crown of the involved tooth (3). The IRR can be seen as a radio transparent lesion which erodes the root of the tooth (3) (Fig. 1).

A late diagnosis can lead to an early extraction of the replanted tooth. The follow-up periods listed in Table II goes from a minimum of 2 years (9) to a maximum of 12 years (5). The IRR can be solved with endodontic treatment, using different materials, such as Ca(OH)2 (6, 7, 9), MTA (10); if the root is compromised, extraction is the only option (4, 7, 11, 12). One study reported that in 14 years of follow-up, only 10% of teeth replanted within 30 minutes after avulsion did not present root resorption, as compared to 95% of teeth that were beyond the 2 hours outside alveolus which had no survival chance.

The only way to prevent the onset of the inflammatory root resorption is the preservation of an intact and vital periodontal ligament. If the root surface of an avulsed tooth remains dry, 50% of the periodontal ligament cells die in 30 minutes, and almost no cell is vital up to 60 minutes. Endodontic treatment could be performed with gutta-percha, to prevent the inflammatory resorption as much as possible. Splinting of avulsed teeth should be semi-rigid to allow movement of the replanted tooth

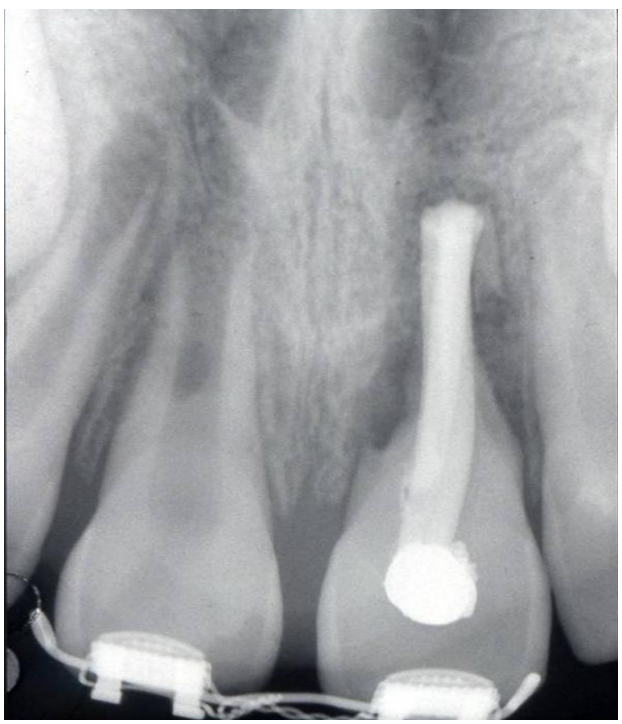

Fig. 1. *Six months after the trauma: the X-ray examination of the tooth 2.1 revealed the presence of a root surface resorption with a moderate bone defect area.*

Table I. *Data on incidence of inflammatory root resorption.*

Author and Year	Sample (teeth)	Incidence (%)
Hecova et al. 2010	58	26.5
Lin et al. 2016	74	6.8
Majorana et al. 2003	73	16.4
Petrovic et al. 2010	32	62.5
Schatz et al. 1995	33	54.5

Table II. *Data on time between avulsion and replantation, diagnosis of IRR, follow-up and treatment.*

Author and Y ear	Time from trauma to replantation	Time to Diagnosis of the inflammatory root resorption	Follow-up	Treatment for the inflammatory root resorption
Calliskan et al. 2000	3h	1 m	2y	Endodontic treatment with $Ca(OH)_2$
Aggarwal et al. 2010	2h	3m	4y	Endodontic treatment with MTA
Dhillon et al. 2011	1.30h	6y	No follow-up (the patient returned to the dentist 6 years after replantation)	Extraction
Ines et al. 2016	3-24h	1y	NS	Extraction
Hecova et al. 2010	60-120m	NS	5y	Extraction
Lin et al. 2016	/	6m	1-12y	NS
Majorana et al. 2003	> 2h	NS	5y	IRR stopped in 6 teeth (endodontic treatment with $Ca(OH)_2$; no data about the others 6 teeth
Petrovic et al. 2010	2h	1m-2y	1-6y	Endodontic treatment with $Ca(OH)_2$; 55% of the teeth were extracted after endodontic treatment
Schatz et al. 1995	1-3h	NS	5y (2-9y)	Endodontic Treatment

h: hours; m: months; y: years, NS: Not Specified

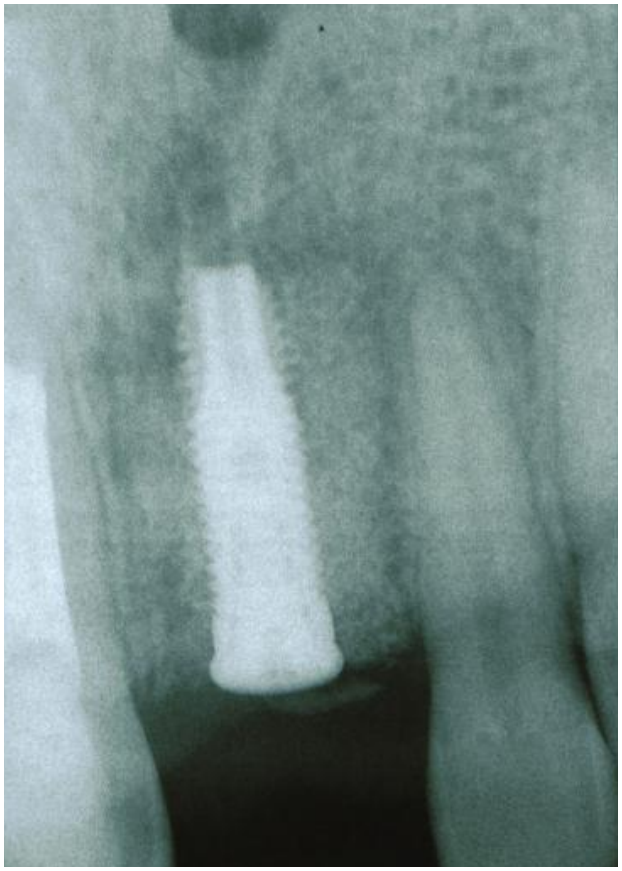

Fig. 2. *Nine months after the GBR: X-ray examination after removal of the membrane and the simultaneous placement of a dental implant.*

comparable to the physiological movement of the healthy teeth, and should not be extended beyond 14/21 days (1).

The immature dental element must not be endodontically treated like a tooth with complete root development. Instead of utilizing gutta-percha as canal filling material, it would be advisable to utilize calcium hydroxide, which would slow the root resorption process and ankylosis onset. In fact, calcium hydroxide has antibacterial activity, dentinogenic action, and is resorbable, preventing any foreign body reaction, in contrast to gutta-percha, which is not absorbable, and may facilitate the onset of root resorption (13).

Sometimes patients could take advantage of the technique of decrowning (13, 14), which, during the peak of bone growth, should be performed as soon as the dental ankyloses and the next infraocclusion is diagnosed; this technique would avoid or limit future bone regeneration intervention with membranes (13).

Original tooth replantation can enable natural dental arch space preservation and, by maintaining the natural tooth, it is not necessary to make any temporary prosthetic replacement, with decrease of biological and economic costs, and obtaining a good patient compliance.

When the trauma affects a young patient, at the time of the loss of the dental crown, it is always recommended to perform a two-stage intervention: guided bone regeneration with placement of a titanium-reinforced Gore-Tex membrane, retained *in-situ* for 6 months, and only subsequently dental implant placement (Fig. 2).

After approximately three months, to complete the prosthetic rehabilitation, a direct impression should be taken (15) and a full fixed crown made.

The literature shows that, in case of dental avulsion, the delayed replantation technique is frequently used, and therefore IRR often occurs. If not diagnosed early with a strict follow-up, IRR can cause the loss of the injured tooth/teeth with relevant consequences for the patient's health.

The damage caused by IRR can be prevented/mitigated with adequate follow-up as well as endodontic treatment. Rehabilitation of teeth which have suffered an avulsion and subsequently a delayed replantation requires bone regeneration and the use of osseointegrated implants consistent with the age of the injury and its degree of osteo-skeletal maturation.

REFERENCES

1. Andersson L, Andreasen JO, Day P, et al. Guidelines for the Management of Traumatic Dental Injuries: 2. Avulsion of Permanent Teeth. Pediatr Dent 2017; 39: 412-19.
2. Giannetti L, Murri A. Clinical evidence and literature to compare two different therapeutic protocols in tooth avulsion. Eur J Paediatr Dent 2006; 7(3):122-30.
3. Finucane D, Kinirons MJ. External inflammatory and replacement resorption of luxated, and avulsed replanted permanent incisors: a review and case presentation. Dental Traumatol 2003; 19:170-74.

4. Hecova H, Tzigkounakis V, Merglova V, Netolicky J. A retrospective study of 889 injured permanent teeth. Dent Traumatol 2010; 26:466-75.
5. Lin S, Pilosof N, Karawani M, Wigler R, Kaufman AY, Teich ST. Occurrence and timing of complications following traumatic dental injuries: A retrospective study in a dental trauma department. J Clin Exp Dent 2016; 8:e429-e36.
6. Majorana A, Bardellini E, Conti G, et al. Root resorption in dental trauma: 45 cases followed for 5 years. Dent Traumatol 2003; 19:262-65.
7. Petrovic B, Markovic D, Peric T, Blagojevic D. Factors related to treatment and outcomes of avulsed teeth. Dent Traumatol 2010; 26:52-59.
8. Schatz JP, Hausherr C, Joho JP. A retrospective clinical and radiologic study of teeth reimplanted following traumatic avulsion. Endod Dent Traumatol 1995; 11:235-39.
9. Caliskan MK, Turkun M, Gokay N. Delayed replantation of avulsed mature teeth with calcium hydroxide treatment. J Endod 2000; 26:4727-6.
10. Aggarwal V, Singla M. Management of inflammatory root resorption using MTA obturation - a four year follow up. Br Dent J 2010; 208:287-89.
11. Dhillon JS, Narula NB, Kumar M. Complete root resorption after reimplantation of maxillary central incisor - A case report. Endodontology 2011; 98-103.
12. Ines K, Nabiha D. Delayed tooth replantation after traumatic avulsion resulting in complete root resorption. J Paediatr Dent 2016; 4:5.
13. Schwartz-Arad D, Levin L, Ashkenazi M. Treatment options of untreatable traumatized anterior maxillary teeth for future use of dental implantation. Implant Dent 2004; 13:120-28.
14. Spinas E, Aresu M, Canargiu F, Gianetti L. Preventive treatment of post-traumatic dental infraocclusion: study on the knowledge of dental decoronation in a sample of Italian dental students and dentists. Eur J Paediatr Dent 2015; 16:279-83.
15. Bambini F, Giannetti L, Memè L, Pellecchia M, Selvaggio R. Comparative analysis of direct and indirect implant impression techiques: An in vitro study Minerva Stomatol 2005; 54(6):395-402.

LETTER TO THE EDITOR

TOOTH AVULSION WITH EXTRA ORAL TIME IN LESS THAN 60 MINUTES: TWO DIFFERENT THERAPEUTIC PROTOCOLS WITH 13-YEAR FOLLOW-UP

L. GIANNETTI[1], E. SPINAS[2] and A. MURRI DELLO DIAGO[1]

[1]Department of Paediatric Dentistry, University of Modena and Reggio Emilia, Modena, Italy;
[2] Department of Surgical Science, University of Cagliari, Cagliari, Italy

Received October 17, 2018 – Accepted January 9, 2019

The aim of this study is to assess what needs to be the priority in tooth avulsion: replantation as quickly as possible and deferred endodontic treatment, or replantation and elimination of every irritating stimulus for the periodontal ligament. Twenty patients were selected and divided into 2 groups: in group A attention was focused on the rapidity of replantation and postponed endodontic therapy, in group B we focused on the elimination of the necrotic pulp with extraoral endodontic therapy. Clinically, there was no difference in stability, but there were 3 elements in infraocclusion in group A, and 4 in group B. Radiographically, a similar incidence of radicular resorption caould be observed in group B compared to group A. In conclusion, as a result of dental avulsion, the speed of replanting always seems to be a priority.

To the Editor,

Teeth avulsion accounts for up to 16% of all traumatic injuries in the permanent dentition and is considered to be the most serious (1). It causes severe damage to supporting tissues and neurovascular structures, which negatively affects the outcome of replantation (2-4). In fact, if it is not possible to perform the re-implantation or the replanting fails, implant replacement may be a good alternative. An accurate pre-surgical evaluation, including the growth expectation assessment, make it possible to place the mini implants without interfering with subsequent sagittal and transversal growth of the maxillary bones (5). Even the immediate aesthetic and functional success is achievable by easy indirect impression techniques (6) and provisional restoration crown in acrylic resin.

In case of avulsion of permanent teeth, however, replanting is the elective therapy. Therapy aims to avoid or minimize the inflammatory reactions occurring as direct consequence of the avulsion (7).

The objective of the present study is to determine which has to be the priority - replantation or elimination of every irritating stimulus for the periodontal ligament. Twelve years ago we thought it was better to perform extraoral endodontic therapy. Do we have the same response nowadays?

MATERIALS AND METHODS

The patients included in the study are among those visited and treated, from January 2004 to January 2006, at the Dentoalveolar Traumatology Division of the University of Modena. The selection was based on the following criteria: patients of both sexes, with permanent avulsed dental elements, with complete root formation

Key words: tooth avulsion; endodontic treatment; extra oral dry time

Corresponding Author:
Prof. Luca Giannetti,
Department of Paediatric Dentistry,
University of Modena and Reggio Emilia,
Via del Pozzo, 71, 41125 Modena, Italy
Tel.: +39 059 4224325
e-mail: luca.giannetti@unimore.it

0393-974X (2019)

and with an extraoral dry time greater than 60 minutes. Eleven males and 9 females were selected and randomly divided into 2 groups (Group A - Group B).

Group A

In Group A the attention was focused on the rapidity of replantation. At the first appointment the avulsed element was grasped by the crown and, under constant irrigation with salt solution, the residual fragments of LPD and any other possible irritating stimulus were removed from the radicular surface then it was replanted with delicate manual pressure and splinted. The correct replantation of the avulsed element was radiographically checked.

At the second appointment (after one week), endodontic therapy of the avulsed element was performed: access to the pulpal room with a three-step standardized technique, pulpectomy with manual steel tools, type K-files, and partial outlining of the radicular channels system, under constant irrigation with EDTA at 17% and NaOCl at 5.25% (8), then application of calcium hydroxide, diluted with physiological, inside the canal system, positioning of a cotton pellet and temporary filling with zinc oxide-eugenol.

At the third appointment (after two weeks) the splint was removed and clinical/radiographic evaluation of the replanted element was performed. The endodontic therapy was finalized with a mixed technique using standardized steel and Ni-TI tools, then a three-dimensional filling of the canal system by thermafil technique.

Group B

The main objective was the complete removal of the necrotic pulp and any possible irritating stimuli that could lead to radicular resorption of inflammatory type. In this case the priority was not the replantation as quickly as possible, as it was in GROUP A.

At the first appointment an extra-oral endodontic therapy was performed: access to the pulpal room with a three-step standardized technique, outlining of the canal system with a mixed technique using steel and standardized Ni-Ti and instruments, alternate irrigation with EDTA liquid at 17% and sodium hypochlorite at 5.25%, three-dimensional filling of the canal system by thermafil technique. The avulsed element was then replanted with delicate manual pressure and splinted.

At the second appointment (after two weeks), the splint was removed and clinical/radiographic evaluation of the replanted element was performed.

After 12 years all the patients were recalled for clinical and radiographic evaluation. From the clinical perspective, the presence or not of the replanted tooth was the first goal, then the degree of mobility was appraised for all of the replanted elements according to Miller's classification.

Radiographic evaluation

To establish the degree, intensity and extension of the resorption, it was decided to use a classification we described in 2006:

i. light degree: radicular point resorption < 1 mm^2

ii. moderate degree: radicular point resorption > 1 mm^2

iii. severe degree: radicular resorption in different locations

In order to optimize the evaluation, the root of every dental element was divided into three parts (coronal, middle and apical third) and subsequently a value was assigned to every third.

RESULTS

All 20 patients came for the 12-year follow-up and all the teeth were still *in situ*. Clinically, we had similar results in both groups; in fact, there was no mobility at all.

We observed an infraocclusion of some teeth: in group A 3 elements and in group B 4 elements.

Radiographically, in Group A there were 2 cases with RR of a light degree, 3 cases with RR of a moderate degree and 3 cases with RR of severe degree. In Group B there were 3 cases with RR of a light degree, 2 cases with RR of a moderate degree and 4 cases with RR of severe degree.

DISCUSSION

There are guidelines (3) available to assist the clinician in the management of avulsed teeth. The consensus from these guidelines is that the pulp should be removed 7–14 days after replantation (9-11). This guidance appears to be based on the known high risk of inflammatory root resorption in replanted

teeth in cases where the pulp has not been extirpated. Extraoral endodontic treatment is contraindicated as this extends extraoral time, further damaging periodontal ligament cells, although this has been recommended for teeth with extended extraoral dry times.

From the revision of the literature, it is clear that a standardized approach does not exist, therefore this is the reason for this study. Although at 12 months (12) the results indicated clearly that the extra oral therapy was to be preferred as it could reduce root resorption, after 13 years the results became similar to the point of overlapping values. In some cases even, the elements treated with extra-oral therapy had a greater root resorption.

In conclusion, as a result of dental avulsion, the speed of replanting always seems to be a priority.

REFERENCES

1. Andreasen JO, Borum M, Jacobsen HL, Andreasen FM. Replantation of 400 traumatically avulsed permanent incisors. 2. Factors related to pulp healing. Endod Dent Traumatol 1995; 11(2):59-68.
2. Giannetti L, Murri A, Vecci F, Gatto R. Dental avulsion: therapeutic protocols and oral health related quality of life. Eur J Paediatr Dent 2007; 8(2):69-75.
3. Andersson L, Andreasen JO, Day P, et al. Guidelines for management of traumatic dental injuries: 2 Avulsion of permanent teeth. Pediatr Dent 2017; 15(6):412-19.
4. Sardana D, Goyal A, Gauba K. Delayed replantation of avulsed tooth with 15-hours extra-oral time: 3-year follow-up. Singapore Dent J 2014; 35:71-76
5. Giannetti L, Murri Dello Diago A, Vecci F, Consolo U. Mini-implants in growing patients: a case report. Pediatr Dent 2010; 32(3):239-44.
6. Bambini F, Giannetti L, Memè L, Pellecchia M, Selvaggio R. Comparative analysis of direct and indirect implant impression techniques an in vitro study. An in vitro study. Minerva Stomatol 2005; 54(6):395-402.
7. Souza BDM, DDS, Dutra KL, Kuntze MM et all. Incidence of root resorption after the replantation of avulsed teeth: a meta-analysis. J Endod 2018; 44(8):1216-27.
8. Giardino L, Cavani F, Generali L. Sodium hypochlorite solution penetration into human dentine: a histochemical evaluation. Int Endod J 2017; 50(5):492-98.
9. Kenny DJ, Barrett EJ, Casas MJ. Avulsions and intrusions: the controversial displacement injuries. J Can Dent Assoc 2003; 69(5):308-13.
10. Pohl Y, Filippi A, Kirschner H. Extraoral endodontic treatment by retrograde insertion of posts: a long term study on replanted and transplanted teeth. Oral Surg Oral Med Oral Pathol Oral Radiol Endod 2003; 95:355-63
11. Trope M Clinical management of the avulsed tooth: present strategies and future directions. Dent Traumatol 2002; 18(1):1.
12. Giannetti L, Murri A. Clinical evidence and literature to compare:two different therapeutic protocols in tooth avulsion. Eur J Paediatr Dent 2006; 7(3):122-30.

LETTER TO THE EDITOR

THE USE OF ONLY ENAMEL MATRIX DERIVATIVE ALLOWS OUTSTANDING REGENERATION RESULTS IN PERIODONTAL INTRABONY DEFECT TREATMENT: A RETROSPECTIVE STUDY

C. BERTOLDI[1], M. FERRARI[2] and L. GIANNETTI[1]

[1]Section of Periodontology and Fixed Dental Prosthesis, Department of Surgery, Medicine, Dentistry and Morphological Sciences with Transplant Surgery, Oncology and Regenerative Medicine Relevance, University of Modena and Reggio Emilia, Modena, Italy; [2]Private Practice, Modena- MO, Italy

Received January 4, 2019 – Accepted January 24, 2019

Periodontal tissue regeneration depends on several biological, homeostatic and regulative variables that directly induce the clinical features. The aim of this study is to compare the clinical results obtained using the enamel matrix derivative peptide (EMP) compared to the less manageable association of EMP and bovine bone xenographic (BPBM) in the treatment of deep intraosseous defects. Ten healthy patients, suffering from moderate or severe chronic periodontitis, having at least two deep and narrow intrabony defects in the same dental arch and needing surgical treatment, were selected. The same patient was treated with the two different materials: EMP –TG1 in one defect and the association-TG2 in the other. Immediately before surgery (T0) and 12-month after (T2) the probing depth (PD) and gingival recession (GR) were registered at the experimental sites. No statistically significant differences were shown between TG1 and TG2 at T0 nor at T1 in term of PD and GR, while a statistically significant PD decrease was found both in TG1 and TG2 between T0 and T1 ($p<0.05$). GR increase resulted statistically significant in TG1 ($p<0.05$) but not in TG2 between T0 and T1 ($p\geq0.05$). In this split-mouth retrospective study, both the treatments achieve favourable clinical results but the TG1 shows a significant increase in GR probably because EMP is not able to support the gingiva covering the intrabony defect. Therefore, the choice of the type of periodontal defect to be treated with EMP will be a therapeutic key-point.

To the Editor,

The regenerative treatment of intraosseous defects is achieved by following different methodologies. In particular, bovine bone xenographic (BPBM) derivatives have proved to be safe and beneficial both on animals and humans in terms of bone regeneration, clinical attack gain (CAL-gain), probing depth reduction (PD- reduction), defect filling and defect resolution when used in intraosseous defects (1-3). However, the periodontal regeneration would make much of the use of the enamel matrix derivative peptide (EMP). All the minimally invasive surgical techniques, permitting a less invasive approach to the patients, are particularly suited to the use of only EMP (4, 5).

The aim of this study is to compare the clinical results obtained using the sole EMP compared to the association of EMP and BPBM in the treatment of deep intraosseous defects.

Key words: enamel matrix derivative; minimally invasive surgery; periodontal regeneration

Corresponding Author:
Prof. Carlo Bertoldi,
Dipartimento Chirurgico, Medico, Odontoiatrico
e di Scienze Morfologiche
con Interesse Trapiantologico, Oncologico e di Medicina Rigenerativa,
Università di Modena e Reggio Emilia,
Via del Pozzo 71, 41124, Modena, Italy
Tel.: +39 0594224101 - Fax: +39 0594224795
e-mail: carlo.bertoldi@unimore.it

0393-974X (2019)

MATERIALS AND METHODS

This retrospective study was performed at the Periodontology Unit of Dentistry and Oral-Maxillofacial Surgery of Modena University Hospital. Subjects referred for dental and periodontal therapy were among those visited and treated from January 2007 and January 2009. The patients considered in this retrospective study, signed informed consent detailing all procedures of the treatment, as requested by the Helsinki protocols. They were suffering from moderate or severe chronic periodontitis (6). Moreover, they had to satisfy the following systemic and local inclusion criteria: absence of relevant medical conditions (7), to be of age, non-pregnant or lactating. The full-mouth plaque score (FMPS) and the full-mouth bleeding score (FMBS), had to be maintained ≤25% (measured at 4 aspects per tooth).

Patients selected had at least two intrabony defects not adjacent in the same dental arch needing surgical treatment with the following properties: pocket depth (PD) ≥ 5mm with a radiologic intrabony component of at least 3 mm. The defect angle had to be < 36° (3, 4). The defects considered could not include furcations and had to be either two- or three-wall intraosseous defects.

Dental-periodontal procedures and clinical measurements

The minimally invasive surgery principles and papillary preservation was always implemented on angular intraosseous defects (4). The treatment was performed in the same dental arch using EMP (Emdogain, Biora AB, Malmö, Sweden) (treatment group 1- TG1) or EMP + BPBM (Bio-Oss, Geistlich Pharma, Wolhusen, Switzerland) in the periodontal defects (Treatment group 2- TG2). So, the same patient was treated with the two different materials (EMP in one defect and the association in the other) but with the same surgical principle on equal defects.

The following clinical measurements were taken at the experimental site at baseline (T0), before the surgical treatment, and 12-month after (T2): probing depth (PD) end gingival recession (GR). The greater values of these indices in relation to the periodontal defects were considered in this study during TO and T1 measurements. Also, FMPS and FMBS were measured at the same time points. Bleeding on probing was never marked in relation to sites considered.

Statistical analysis

The 12-months primary outcomes of this study were: PD and GR comparison between TG1 and TG2. Secondary outcome was the evaluation of PD and GR changes along the study follow-up.

Statistical analysis was performed using the parametric paired t-test for the clinical data taken before and after the surgical treatment or the variance analysis parametric test for two groups of different defects.

For all measured variables, the null hypothesis (H_0) of no difference among groups was rejected for a critical significance level of $p < 0.05$.

RESULTS

Ten patients, 4 women and 6 men, aged 33-68 years (mean ± SD, 55.6±10.2 years) fulfilled the entry criteria to the perspective study.

At baseline (T0), the full-mouth plaque and bleeding scores were 16.8±2.8% and 15.6±3.5%, respectively. An average PD resulted 6.1±0.9mm and 5.8±0.6mm in TG1 and TG2, respectively. An average GR resulted both in TG1 and TG2 0.5±0.5mm. The difference between TG1 and TG2 at T0 was not statistically significant for both PD and GR indices ($p>0.05$, variance analysis test).

Twelve months afterward (T1), FMPS and FMBS were 15.6±3.5% and 4.7±1.7%, respectively; the difference between the baseline and 12-month measurements was statistically significant for both the indices ($p<0.05$, paired *t*-test). An average probing depth (PD) of 1.8±0.64mm and 1.5±0.7mm was recorded in TG1 and TG2, respectively. The gingival recession (GR) average was 0.9±0.6mm and 0.7±0.7mm in TG1 and TG2, respectively. The difference in PD and GR between TG1 and TG2 groups was statistically not significant ($p>0.05$, variance analysis test).

The difference in PD between T0 (baseline) and T1 (12-month afterwards) was statistically

significant ($p<0.05$, paired *t*-test) for both TG1 (treated with EMP) and TG2 (treated with EMP + BPBM) whereas the difference in GR between T0 and T1 resulted statistically significant for TG1 ($p=0.037$, paired t-test) and not significant for TG2 ($p=0.343$-paired *t*-test) for TG2.

DISCUSSION

Tissue regeneration depends on several variables, on materials used (1, 3), on the devices used to apply these materials (8, 9), but the defect properties and the surgical technique chosen to obtain the stability of the coagulum also play a fundamental role (4, 5, 8). All of these variables have to produce a biological environment suitable for tissue regeneration (4, 5, 8). Moreover, several other factors could be involved in periodontological regeneration such as the biochemical structure of the periodontal pocket and its homeostasis. The modern pathogenetic model suggests dynamic biologic processes based on a multilevel framework that includes disease-initiating and -resolving mechanisms that are regulated by innate and environmental factors, by the type of inflammation and the regulation of the same that characterizes the disease (18, 19). Probably, the periodontal pocket pathologic tissue loses its physiologic homeostasis and acquires the autonomic property to proceed in a pathological sense (10). Besides, even the patients' lifestyles and psychological profile, matter (11). Several variables that can influence the result of a therapy are probably still not very clear and therefore the choice of the therapy has to be carried out very carefully. So, the study design requested stringent criteria of enrollment to the retrospective study, is to characterize as much as possible the periodontal defects considered. In this study, carried out on patients characterized by a good hygienic control, affected by deep and narrow periodontal defects with 2-3 bone walls and treated with an advanced model of minimally invasive surgical therapy, we found no significant differences in PD and GR between TG1 and TG2 both at baseline and 12-month after surgery. The patients-pool considered (TG1 and TG2), improved significantly their periodontal conditions in terms of FMPS, FMBS and PD. However, GR showed an increasing trend that resulted statistically significant only in TG1. Most probably, the gingival shrinkage following the periodontal pocket removal, caused in several ways the GR increase. However, this effect must be reduced as far as possible because it hinders the regenerative purpose of the periodontal therapy. The greater is the increase of GR after surgery, the lower is the decrease of PD due to periodontal ligament regeneration (CAL-gain) because PD+GR = CAL. This effect could become so relevant as to induce a soft tissue crater. In conclusion, in our retrospective study none significant difference resulted between TG1 and TG2 in terms of PD and GR measured at the periodontal defect. The difference in selection and treatment between TG1 and TG2 was only in relation to the material used to favor the periodontal regeneration. The EMP has no relevant mechanical properties, it is not a space-maintaining regenerative material (12), able to keep the gingiva in position once the periodontal pocket tissue has been removed. So, the periodontal defect selection, that has to be strictly a self-maintaining space defect if only EMP is used, is most probably a key-point of the therapeutic strategy.

REFERENCES

1. Camargo P, Lekovic V, Weinlaender M, Vasilic N, Kenney EB, Madzarevic M. The effectiveness of EMPs used in combination with BPBM in the treatment of intrabony defects in humans. J Clin Periodontol 2001; 28:1016-22.
2. Bertoldi C, Zaffe D. In vivo comparison of two bone substitutes in the distal femur of the rabbit. Int J Oral Maxillofac Implants 2012; 27:119-27.
3. Bertoldi C, Pellacani C, Lalla M, Consolo U, Pinti M, Cortellini P, Cossarizza A. Herpes Simplex I virus impairs regenerative outcomes of periodontal regenerative therapy in intrabony defects: a pilot study. J Clin Periodontol 2012; 39:385-92.
4. Cortellini P, Tonetti MS. Improved wound stability with a modified minimally invasive surgical technique in the regenerative treatment of isolated interdental intrabony defects. J Clin Periodontol 2009; 36:157-63.

5. Farina R, Simonelli A, Rizzi A, Pramstraller M, Cucchi A, Trombelli L. Early postoperative healing following buccal single flap approach to access intraosseous periodontal defects. Clin Oral Investig 2013; 17:1573-83.
6. Caton JG, Armitage G, Berglundh T, et al. A new classification scheme for periodontal and peri-implant diseases and conditions - Introduction and key changes from the 1999 classification. J Periodontol 2018; 89 Suppl 1: S1-S8.
7. Bertoldi C, Balli F, Tanza D, Bertolani P, Chiarini L. Experimentation and clinical analysis of the interrelationships between dental damage and celiac disease. Minerva Stomatol 1995; 44: 395-405.
8. De Stavola L, Tunkel J. A new approach to maintenance of regenerated autogenous bone volume: delayed relining with xenograft and resorbable membrane. Int J Oral Maxillofac Implants 2013; 28:1062-7.
9. Bertoldi C, Pradelli JM, Consolo U, Zaffe D. Release of elements from retrieved maxillofacial plates and screws. J Mater Sci Mater Med 2005; 16:857-61.
10. Bertoldi C, Bellei E, Pellacani C, et al. Non-bacterial protein expression in periodontal pockets by proteome analysis. J Clin Periodontol 2013; 40:573-82.
11. Bertoldi C, Venuta M, Guaraldi G, et al. Are periodontal outcomes affected by personality patterns? A 18-month follow-up study. Acta Odontol Scand 2018; 76: 48-57.
12. Barboza EP, de Souza RO, Caúla AL, Neto LG, Caúla Fde O, Duarte ME. Bone regeneration of localized chronic alveolar defects utilizing cell binding peptide associated with anorganic bovine-derived bone mineral: a clinical and histological study. J Periodontol 2002; 73:1153-9.

LETTER TO THE EDITOR

DESQUAMATIVE GINGIVITIS: A SYSTEMATIC REVIEW OF POSSIBLE TREATMENTS

M. CABRAS, A. GAMBINO, R. BROCCOLETTI and P.G. ARDUINO

Department of Surgical Sciences, Oral Medicine Section, CIR-Dental School, University of Turin, Turin, Italy

Received June 20, 2018 – Accepted November 5, 2018

The occurrence of epithelial desquamation, erythema, and erosions on the gingival tissue could be described in literature as "desquamative gingivitis" (DG), mostly due to a wide range of autoimmune/dermatological disorders. The objective of this systematic review was to assess the efficiency of the different treatments for DG. The research was conducted using the following databases: PubMed, Google Scholar, NIH (National Institute of Health), Up to Date, Scopus, Cochrane Library, Web of Science. The P.I.C.O. (Patient, Intervention, Control, Outcome) question was as follows: human patients with clinical-pathological diagnosis of DG (Patients); any topic, systemic medication, photobiomodulation or periodontal treatments (Intervention); no treatment, placebo or other drug (Comparison); and effectiveness in terms of improvement of symptoms (primary Outcome) and signs (secondary Outcome). The PROSPERO record is number CRD42018084531. A total of 2,174 potential results were acquired from the various databases, of which 998 were duplicates; the remaining 1,176 studies were submitted to a first reading of title and abstract: 1,137 articles had to be excluded, with 994 not being inherent to the purposes of this review, and 143 being published in languages other than English. The remaining 39 articles were subjected to full reading; 4 randomized controlled trials were considered eligible but only 2 finally analysed. To date, 0.05% clobetasol propionate ointment compared with placebo, in the management of signs and symptoms of DG, showed no statistically significant differences. Differently, a structured plaque control appeared to be successful in reducing plaque and improving signs and related pain, with statistically significant differences regarding related symptoms, plaque index and mucosal disease score. Regarding the clinical relevance based on our results, it is actually not possible to draw certain and positive conclusions as to the best management modalities for DG. Future research should be conducted in order to establish a proper therapy for this condition, primarily considering that it is mainly a characteristic clinical representation of dissimilar autoimmune bullous diseases. A promising field could be that of periodontal therapy, however, more data are needed.

To the Editor,

Desquamative gingivitis (DG) is a characteristic clinical representation of many autoimmune diseases, such as oral lichen planus (OLP), mucous membrane pemphigoid (MMP), pemphigus vulgaris (PV), bullous pemphigoid, erythema multiforme, linear IgA disease, systemic lupus erythematosus, epidermolysis bullosa, and dermatitis herpetiformis. It can also arise as consequence of hypersensitivity reaction to some antigens contained in toothpastes, mouth rinses, chewing gum or foods, and less frequently in patients with plasma cell gingivitis,

Key words: systematic review; desquamative gingivitis; gingival pain; therapy; outcome

Corresponding Author:
Dr. Marco Cabras,
Department of Surgical Sciences, CIR - Dental School,
School of Medicine, University of Turin,
Oral Medicine Unit, Via Nizza 230, I-10126 Turin, Italy
Tel.: +39 011 6331522 - Fax: +39 011 618639
e-mail: cabrasmarco300@gmail.com

0393-974X (2019)

chronic ulcerative stomatitis and orofacial granulomatosis (1, 2).

DG usually presents with erythema, shedding and ulceration of both free and attached gingiva (mainly vestibular), and, differently from plaque-induced inflammation, it could extend beyond the marginal border, involving the full width of the gums and often the alveolar mucosa (3, 4).

To date, there are no generally established guidelines for the treatment of DG (1-4). Treatment should be undertaken with the goal of achieving control of symptoms with minimum side effects (1). In the last decade some evidence suggested that DG could play a role in increasing the long-term risk for periodontal tissue breakdown (5), detailing that an inappropriate home oral hygiene could worsen the gingival status in DG patients, if compared to controls (6). For these reasons, some Authors have decided to start periodontal therapies for patients with DG (7).

Consequently, with such dissimilar conclusions at hand, we sought to systematically review therapies for DG to incorporate research in order to provide a base for the elaboration of more consistent and effective management approaches.

MATERIALS AND METHODS

This study on the treatment of DG was carried out from December 2016 to December 2017. The P.I.C.O. (Patient, Intervention, Control, Outcome) question [based on the Preferred Reporting Items for Systematic Review and Meta-analysis (PRISMA)] for this investigation was: "In populations with DG, which intervention is effective in improving pain and/or relieving related symptoms compared to other intervention or placebo?" The P.I.C.O. question was then developed as follows: human patients with clinical diagnosis of DG (Patients) related to any possible cause; any topic, systemic medication, photobiomodulation or periodontal treatments (Intervention); no treatment, placebo or other drug (Comparison); and effectiveness in terms of improvement of symptoms (primary Outcome) and clinical signs (secondary Outcome).

Inclusion criteria were: randomized and controlled clinical trials conducted on human beings affected by DG, treated by dentist/odontostomatologist, in the presence of a comparison group, under placebo or proper medications.

Exclusion criteria were: case reports, case series, reviews, open clinical trials, prospective or retrospective studies, letters to editors concerning DG therapy, as well as studies published in non-English language, and "non-inherent" studies, defined as such when:

- Not performed on humans;
- DG was not mentioned in any way;
- DG was simply cited as one of the many clinical manifestations observed in patients, without further specification;
- DG was documented and treated together with other atrophic-erosive oral lesions, without offering any distinctive data on the efficacy and/or tolerability of a given therapeutic protocol in the management of DG alone.

The PROSPERO record is number CRD42018084531.

Search strategy

The research was conducted on the following databases: PubMed, Google Scholar, NIH (National Institute of Health), Up to Date, Scopus, Cochrane Library, Web of Science. Initially, there were no restrictions regarding the language, with not-in-English studies excluded in the first phase of study selection. Conversely, no restriction regarding the publishing year was applied whatsoever.

Study selection and data extraction

References were exported into the EndNote® program (Thomson Reuters). Two reviewers independently from one another, proceeded to classify the various results. Any disagreements were resolved by consulting other reviewers until a consensus was reached.

After excluding not-inherent and not-in-English studies, based on the reading of titles and abstracts, full texts of the remaining articles were acquired and read; later, their classification was carried out, based on the eligibility criteria mentioned above.

Quality assessment

The reviewers proceeded to assess the quality of the studies included using the PEDro scale, applied in previous systematic reviews, up to the current year. This scale considers the following parameters: random allocation, concealed allocation, similarity between the groups at

baseline, subject, therapist and assessor blinding, less than 15% dropouts, intention-to-treat analysis, statistical comparisons between the groups, point measures and variability data. According to this scale, a controlled clinical trial can be considered of good quality if the PEDro score is ≥6 with a maximum score of 10.

Table I. *Characteristics of RCT examining treatment on patients with desquamative gingivitis.*

Authors, year	Country	Oral disease	Sample	Groups under comparison	Duration	Drug/dose
Motta *et al.* 2009	Brazil	PV, MMP, OLP	22 (17 F)	5 *vs* 17	8 wks	0.05% propionate clobetasol ointment *vs* hydroxylhetyl cellulose
Stone *et al.* 2015	UK	OLP	82 data from 79 patients	39 *vs* 43	20 wks	Powered toothbrush/interdental cleaning aids *vs* normal plaque control

Patients age	Inclusion criteria	Exclusion criteria	Collected data	Main results
25-78 yrs	Presence of erythema, atrophy, vesicobullous areas, erosions, ulcerations and desquamative lesions, in multiple associations or not	Patients with disseminated mucocutaneous diseases or exacerbation of their diseases during the study period, or undergoing treatment potentially OLL-evoking	Patients examined before the trial and then at 2-week intervals throughout the trial; clinical evaluation through diagram of the gingival mucosa involved in DG with 6 sites for tooth; response defined as complete (100%), excellent (75% to 99%), good (50% to 74%), poor (1% to 49%), no response, and worsened	No statistically significant difference was found between clobetasol and placebo ($p>0.05$). Within the period designed to treat the gingival lesions of the patients, clobetasol propionate did not significantly outperform the placebo.
61.2 yrs	Patients ≥ 18 yrs, willing and able to complete questionnaires; able to provide consent, newly referred or under review at Newcastle Dental Hospital with a provisional diagnosis of OLP with clinical signs of gingival involvement	Unable to attend for the additional appointments prior to biopsy; unable to complete questionnaires, involved in a research study within the previous 28 days.	OHIP ordinal, OHIP dichotomous, VAS, PI, Escudier score	OHIP ordinal and OHIP dichotomous scores showed statistically significant improvements when compared with control. Intervention was successful in reducing plaque compared to control ($p < 0.001$) improvements were observed using the mucosal disease indices at the 4 and 20 weeks follow-up ($p< 0.001$)

DG: desquamative gingivitis; OLP: oral lichen planus; MMP: mucous membrane pemphigoid; OLL: oral lichenoid lesion; OHIP: oral health impact profile; PI: plaque index; VAS: visual analogue scale; WTP: willingness to pay

Data synthesis

Through the compilation of an Excel sheet, information was extracted from each of the selected studies regarding study design, main characteristics of the selected sample (country of origin, size, distribution by gender and age), type of therapeutic protocol, duration of the intervention and results.

In light of the limited number of RCTs and the high degree of diversification regarding both methods and therapies, a meta-analysis could not be performed, therefore, a narrative description of the results is presented in this current review.

RESULTS

A total of 2,174 potential results were acquired from the various databases, of which 998 were duplicates. The remaining 1,176 studies were submitted to a first reading of title and abstract: 1,137 articles had to be excluded, with 994 not being

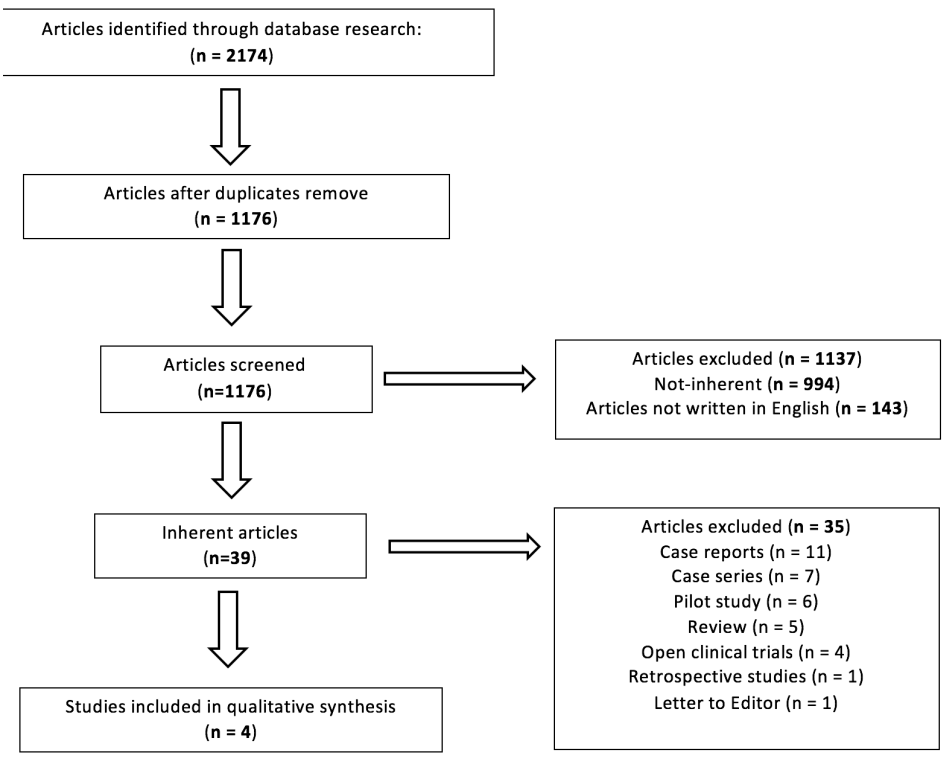

Fig. 1. *Flow-chart of systematic review synthesis.*

Table II. *Quality assessment PEDro scale.*

Authors, year	1	2	3	4	5	6	7	8	9	10	11	Total
Motta *et al.* 2009	Yes	No	Yes	Yes	Yes	Yes	Yes	Yes	Yes	Yes	Yes	9 of 10
Stone *et al.* 2015	Yes	Yes	No	Yes	No	No	No	Yes	Yes	Yes	Yes	6 of 10

inherent to the purposes of this review, and 143 being published in languages other than English. The remaining 39 articles were subjected to full reading: 2 Randomized Controlled Trials were considered eligible for this review (10, 11). Furthermore, 11 case reports, 7 case-series, 6 pilot studies, 5 reviews, 4 open clinical trials, 2 not-inherent RCT, 1 retrospective study and 1 letter to the Editor were also excluded (Fig. 1).

Table I summarizes the main characteristics of the two included trials.

Quality assessment

The quality assessment using the PEDro scale revealed values ranging from 6 to 10 with the scale ranging from 0 to 10. Grade 6 of the study by Stone and co-workers was due to the absence of a blinded approach (Table II).

General characteristics of the sample

The size of the trial samples varies from 22 to 82, with an age-range between 25 and 78 years, and an approximate female to male ratio of 6:1.

In 2009, Motta and co-workers (10) carried out an 8-week double-blind, crossover, placebo-controlled clinical trial on 22 Brazilian patients, divided into two groups in order to compare the efficacy of 0.05% clobetasol propionate ointment with placebo (hydroxyethyl cellulose) in the management of signs and symptoms of DG, showing no statistically significant differences ($p>0.05$). Group 1 was a sample of 5 PV female patients, treated systemically with prednisone and/or azathioprine in the previous six months, whereas group 2 consisted of 9 patients with OLP, 5 with MMP and 3 with PV, thus consisting of a total of 17 patients.

Later, in 2015, Stone and co-workers (11) conducted a 20-week randomized controlled trial on 82 British patients affected by OLP-related DG, in order to determine the clinical efficacy of structured plaque control provided to 43 patients through the addition of a powered toothbrush and inter-dental cleaning aids TePe® extra soft inter-dental brushes (TePe Munhygienprodukter, Malmo, Sweden) ranging from ISO size 1–6 or Oral-B dental floss (Procter & Gamble, Weybridge, UK). Such addition, when compared to the normal plaque control regimen maintained by the 39 control cases, appeared to be successful in reducing plaque and improving signs and symptoms of DG, with statistically significant differences regarding related symptoms, plaque index and mucosal disease score.

DISCUSSION

The aim of this systematic review was to investigate the current state of the art regarding the therapy of DG. Based on these current results, it is actually not possible to draw certain and encouraging conclusions as to the best management modalities.

Corrocher and co-workers' RCT (8) was excluded due to the questionable eligibility criteria provided, as was Stone and co-workers' RCT (9), due to the incompatibility of its outcome with the P.I.C.O. question of the present review.

On the other hand, the double-blind, crossover, placebo-controlled trial published by Motta and co-workers (10), assessing the efficacy of topical clobetasol propionate on DG patients, met our criteria of inclusion, showing a slight, not-significant improvement of clinical signs and symptoms between topical steroid and placebo.

Stone and co-workers (11) reported a statistically significant improvement through a structured plaque control both in plaque control and oro-mucosal disease ($p<0.001$ for Plaque Index and Escudier index), with no statistically significant changes regarding perception of pain ($p>0.05$ for OHIP and VAS).

The present systematic review reveals a substantial lack in current understanding of the pathogenesis and risk factors of DG. Hence, further clinical trials on large samples of patients are required to establish whether clobetasol propionate is as unreliable as shown by Motta and co-workers, not only on patients with OLP-related DG, but also PV/PMM-related DG, where DG tends to persist, despite the healing of the cutaneous and oral signs.

Similarly, to assess the role of periodontal therapy in the management of DG, although our group provided evidence of microbiologic alterations in subgingival plaque between autoimmune and

plaque-induced gingivitis (12), further and larger randomized prospective studies are needed to investigate this fascinating association.

ACKNOWLEDGEMENTS

The work was supported by the Department of Surgical Sciences, School of Medicine, University of Turin, Turin, Italy.

REFERENCES

1. Arduino PG. Oral complications of dermatologic disorders. Atlas Oral Maxillofac Surg Clin North Am 2017; 25:221-28.
2. Mustafa MB, Porter SR, Smoller BR, Sitaru C. Oral mucosa manifestations of autoimmune skin diseases. Autoimmunity Rev 2015; 14: 930-51.
3. Lo Russo L, Fedele S, Guiglia R, et al. Diagnostic pathways and clinical significance of desquamative gingivitis. J Periodontol 2008; 79:4-24.
4. Arduino PG, Broccoletti R, Sciannameo V, Scully C. A practical clinical recording system for cases of desquamative gingivitis. Br J Dermatol 2017; 177:299-301.
5. Lo Russo L, Guiglia R, Pizzo G, et al. Effect of desquamative gingivitis on periodontal status: a pilot study. Oral Dis 2010; 16:102
6. Lo Russo L, Gallo C, Pellegrino G, et al. Periodontal clinical and microbiological data in desquamative gingivitis patients. Clin Oral Investig 2014; 18:917-25.
7. Guiglia R, Di Liberto C, Pizzo G, et al. A combined treatment regimen for desquamative gingivitis in patients with oral lichen planus. J Oral Pathol Med 2007; 36:110-16.
8. Corrocher G, Di Lorenzo G, Mansueto P, et al. Comparison of topical tacrolimus 0.1 % in pectin ointment with clobetasol 0.5% ointment in adults with moderate to severe desquamative gingivitis: A 4-week, randomized, double-blind clinical trial. Clin Ther 2006; 28:1296-302.
9. Stone SJ, McCracken GI, Heasman PA, Staines KS, Pennington M. Cost-effectiveness of personalized plaque control for managing the gingival manifestations of oral lichen planus: a randomized controlled study. J Clin Periodontol 2013; 40:859-67.
10. Motta AC, Domaneschi C, Komesu MC, Souza Cda S, Aoki V, Migliari DA. Double-blind, crossover, placebo-controlled clinical trial with clobetasol propionate in desquamative gingivitis. Braz Dent J 2009; 20:2313-6.
11. Stone SJ, Heasman PA, Staines KS, McCracken GI. The impact of structured plaque control for patients with gingival manifestations of oral lichen planus: a randomized controlled study. J Clin Periodontol 2015; 42:356-62.
12. Arduino PG, Romano F, Sasia D, et al. Subgingival microbiota in white patients with desquamative gingivitis: a cross-sectional study. J Periodontol 2017; 88:643-50.

LETTER TO THE EDITOR

EFFECTIVENESS OF A VENTILATOR-ASSOCIATED PNEUMONIA PREVENTION BUNDLE IN CRITICALLY ILL CHILDREN

I. VITALI[1], O. GENOVESE[2], G. CONTI[2], L. RAFFAELLI[1], A. D'ADDONA[1], A. DELL'ANNA[3] and L. DASSATTI[1]

[1]A. Gemelli University Hospital Foundation, School of Dental Medicine, Catholic University of the Sacred Heart, Rome; [2]Paediatric Intensive Care Unit and Paediatric Trauma Center, A.Gemelli University Hospital Foundation,[2]Catholic University of the Sacred Heart, Rome; [3]Anaesthesiology, Resuscitation, Intensive Care Unit and Clinical Tossicology, A.Gemelli University Hospital Foundation, Catholic University of the Sacred Heart, Rome

Ventilator Associated Pneumonia (VAP) is a serious complication in critically ill patients, and oral hygiene care may effectively reduce its incidence. The prevention of VAP is much more effective through the implementation of several interventions that together give rise to a potentially synergistic effect. From January 2018, according to the latest guidelines and the internal department protocol at the Paediatric Intensive Care Unit of A. Gemelli University Hospital, the measures for the management of the VAP have been implemented. Chlorhexidine 0.12% has been used, within the oral hygiene procedures established by the protocol, to evaluate its microbiological and clinical effectiveness on the development of ventilator-associated pneumonia in paediatric patients admitted to intensive care undergoing invasive mechanical ventilation. The main purpose of the present study was to verify the effectiveness of the prevention protocol, during its implementation, in reducing the incidence of pneumonia associated with invasive mechanical ventilation. The survey also aimed to evaluate the predictive power of the culture of the pharyngeal swabs, routinely performed according to the scientific evidence, in identifying the colonization of the trachea, in the patients admitted to our intensive care unit and subjected to mechanical ventilation for at least 48 hours. Finally, the research has evaluated the conditions of the stomatognathic apparatus and of all the tissues and organs associated with it in the patients who use ventilators.

To the Editor,

Ventilator-associated pneumonia (VAP) is one the most common (2) hospital-acquired infections (HAIs), occurring in about 12% of paediatric patients admitted to intensive care (1) and accounting for almost a quarter of nosocomial infections with more than 5% of ventilated patients affected. Oral health and the VAP development are correlated by numerous factors (3).

VAP is defined as a pulmonary bacterial infection involving patients under mechanical ventilation for 48 hours or longer. Given the strict correlation between VAP and mechanical ventilation, no signs and symptoms that suggest a development of the lower respiratory tract infection before intubation must be present (4). Bacterial colonization of the respiratory tract in patients undergoing mechanical ventilation is the responsible of VAP initiation (5). Tracheobronchitis associated with ventilation (VATB) are caused by bacterial colonization of the oropharyngeal tract and prompt ventilator-associated pneumonia development (6).

Key words: VAP; prevention; pediatric intensive care unit; chlorexidine

Corresponding Author:
Dr Ilaria Vitali,
School of Dental Medicine,
A. Gemelli University Hospital Foundation,
Catholic University of Rome,
8, Largo Agostino Gemelli, 00168 Rome, Italy
Tel.: +39 3477688137 - Fax: +39 0883 664596
e-mail: ilaria.vitali01@icatt.it

0393-974X (2019)

DISCLOSURE: ALL AUTHORS REPORT NO CONFLICTS OF INTEREST RELEVANT TO THIS ARTICLE.

Such bacterial colonization of the inferior respiratory tract, physiologically sterile, is related mainly to the aspiration of secretions, to the colonization of the aerodigestive tract or to the use of contaminated instruments (5). Immobility and the reduced reflex of cough make intubated patients more suitable to VAP development. Furthermore, the VAP risk is higher for intubated children than for adults in the same condition (7) because of different anatomy, physiology and underlying illnesses from adults. Pseudomonas aeruginosa, Staphylococcus aureus and Haemophilus influenzae are the pathogens most frequently associated with VAP in paediatric intensive care (2).

In patients admitted to intensive care and subjected to mechanical ventilation, oral health may be compromised by the state of the disease and by mechanical ventilation itself (8). The effects of oral hygiene on the development of VAP are of great interest to clinicians (9).

In our paediatric intensive care unit (PICU), a new bundle of treatment for VAP prevention was introduced in clinical practice in January 2018. Our aim was to compare the incidence of VAP in this population before and after VAP prevention bundle implementation.

MATERIALS AND METHODS

Trial design and oversight

This is a prospective longitudinal monocentric cohort study with a retrospective control group (before-after observational analysis).

This protocol evaluates primarily the incidence of VAPs between two groups (before and after VAP prevention bundle implementation) and secondarily bacterial colonization of the oropharynx. Since January 2018 the implementation of the care measures has been adopted in accordance with the latest guidelines, 2016-2017 (12).

Patients were enrolled at the Paediatric Intensive Care Unit (PICU) of the Fondazione Policlinico Agostino Gemelli-IRCSS in Rome. In the study, among those admitted to paediatric intensive care, patients requiring invasive mechanical ventilation were enrolled. In line with the internal protocol of our department, these patients received the measures scheduled in the protocol for the management of VAP.

Patients

Implementation of the management of patients at VAP risk has started on January 2018, once the present protocol has been approved by the Ethics Committee. All paediatric patients admitted to our PICU receiving mechanical ventilation with a duration greater than or equal to 48 hours have been considered eligible for our study. All consecutive patients admitted from January 2018 have been included, and demographic and clinical data have been collected anonymously, as long as data regarding infections and therapies prescription, including antibiotics ("after" group). The retrospective control cohort ("before" group) is represented by a group of patients admitted in our PICU in the period from January 2016 up to December 2017. Patients have been matched with prospective group.

Patients undergoing invasive mechanical ventilation for at least 48 hours. and aged <18 years were included in the study. Reasons for exclusion were: the parents did not give informed consent; pregnancy; previous endotracheal antibiotic therapy; penicillin (amoxicillin; ampicillin); cephalosporins 1° and 2°; macrolide; presence of tracheostomy.

For each patient, the study was considered completed after weaning from mechanical ventilation or in the case of need for tracheostomy.

Intervention and procedures

Parents or those who have the child's legal responsibility were informed about the objectives of the study and how to carry out the treatment, and once they signed the informed consent, their children were enrolled in the investigation.

Each enrolled patient was identified with a code, recorded on a special register kept by the investigators. For the patients, data (date of enrolment, age at time of enrolment, sex, clinical history, results of the physical examination, possible notes) were collected and managed through appropriate electronic apparatus, in respect of their privacy.

According to the routine protocol, the treatments for the prevention of bacterial colonization were the following:

- aspiration of tracheobronchial secretions through the closed-circuit system;

- changing ventilator circuits and suction catheters when visibly dirty or malfunctioning;
- drainage of endotracheal tube where indicated by the clinical examination;
- drying the condensation from the ventilation circuit when needed;
- hand hygiene before and after contact with the patient and/or with the ventilation circuit;
- practicing oral hygiene according to the age group to which the patient belongs, as shown below.

Infants and edentulous children: cleaning the oral cavity with swabs soaked in physiological saline solution every 12 hours; soothing the lips with paraffin-based products every 12 hours and as needed.

Children under the age of 6 years in deciduous dentition: cleaning the oral cavity with a pad soaked in physiological saline solution every 12 hours; soothing the lips with paraffin-based products every 12 hours and as needed.

Children over 6 years of age in mixed and permanent dentition: cleaning the oral cavity with a swab dipped in chlorhexidine digluconate in a concentration of 0.12%. every 12 hours; not rinsing the oral cavity; soothing the lips with paraffin-based products every 12 hours and as needed.

Alongside the measures implemented to prevent bacterial colonization, the following procedures were implemented to prevent aspiration of secretions from the oropharynx:

- raising, where possible, the headboard by 30-40°;
- always drying the ventilator circuit before repositioning the patient;
- using endotracheal tubes with the dorsal lumen that opens above the tracheal tube cuff to facilitate the suction of the secretions from the cuff for children over the age of 12 years.

After 24 hours of mechanical ventilation, tracheal secretions were collected from all patients, as well as samples using oropharyngeal swabs to be analysed; these collections were repeated twice a week (once every 3-4 days). The samples were taken before the oral hygiene procedures stated in the protocol, that included the use of physiological saline or chlorhexidine in the effective and safe concentration of 0.12%.

In cases where there was evidence of colonization by hospital germs, the existing PICU protocols were adopted (12). In patients who had developed clinical signs of pneumonia whilst receiving mechanical ventilation, a bronchoalveolar lavage (BAL) was performed blindly, as required by the internal protocol of the department in case of clinical suspicion of pneumonia. Pneumonia is suspected in infants when increased body temperature or leukopenia are accompanied by at least three of the following signs: unstable body temperature, appearance of purulent sputum or sputum modification or increased respiratory secretions or increased drainage requirement, apnoea, tachypnoea, nasal burning with retraction of the rib cage or with grunts, breath whistling rantolii or ronchii, cough, bradycardia or tachycardia. In children over 1 year of age or under 12 years, the suspicion of VAP relied on fever or leukopenia accompanied by at least three of the following signs: fever or hypothermia, leukopenia or leucocytosis, onset of purulent sputum or sputum modification or increased respiratory secretions or increased drainage needs, onset or worsening of cough or dyspnoea, apnoea or tachypnoea, rales or bronchial respiratory noises, worsening gaseous exchanges, increased oxygen requirements or increased fan demand. In children above the age of 12, pneumonia is suspected when the chest radiograph reveals a new or progressive pulmonary infiltrate and at least two of the following criteria are present: temperature >38°C or <36°C, purulent respiratory secretions, white blood cells >12,000/mm3 or <4,000/mm3.

The monitoring of the clinical condition of the oral cavity was carried out by assigning a score provided in an evaluation form, which analysed the status of lips, mucous membranes and tongue, gums, teeth (where present) and saliva. The score was assigned according to a reference table, which assigned value 1 in the case of a physiological picture, value 2 if there are signs of pathological changes, value 3 where the pathological picture was established. This form had to be completed daily and was repeated upon discharge from the operative unit.

The aim of the study was to measure the number of tracheobronchial tree and lower respiratory tract infections both during the period of admission under invasive mechanical ventilation in the intensive care unit and within 48 hours of extubation.

Statistical analysis

The incidence of VAP in our PICU is around 30%.

Accepting an Alpha error of 0.05 and a Beta error of 0.2 and estimating an absolute 15% reduction in the incidence of VAP, the total population enrolled was calculated as N = 242 and N per group = 121.

The data distribution was evaluated by the Kolmogorov-Smirnov test. The continuous variables with normal distribution were expressed as mean ± standard deviation and evaluated by the Student *t*-test. Continuous variables with non-normal distribution were expressed as median and interquartile ranges and evaluated by the Mann-Whitney test. The categorical variables were reported as percentages and analysed using the *Chi*-squared test or Fisher's test when appropriate.

The predictive ability of the study test (culture of samples from the oropharynx) was evaluated by calculating the sensitivity, the specificity, and the positive and negative predictive value of the test with the respective 95% confidence intervals, constructing ROC curves with selection of the incidence of tracheobronchial colonization and VAP, respectively. The AUC of the curves were compared to each other to understand whether one of the samples taken had a better predictive power than the others.

A $p < 0.05$ was considered statistically significant. The analysis was elaborated with the statistical software MedCalc Statistical Software version 14.12.0 (MedCalc Software bvba, Ostend, Belgium; http://www.medcalc.org; 2014).

RESULTS

Colonization of the tracheal tract was defined as the presence of one or more germs in the culture of tracheal secretions regardless of the microbial load and the type of germ (qualitative measure).

The culture of the oropharyngeal samples (study test), independently of the microbial charge and the type of germ (qualitative measure), was defined as true positive if there had been a growth of the germ in the cultures both in these sites and in the tracheal secretions. The test was defined as false positive if the growth of the germ had occurred in the oropharynx cultures but not the tracheal secretions. The test was defined as true negative if there had been no growth of the germ in the oropharynx cultures or tracheal secretions. Finally, the test was defined as false negative if the growth of the germ had occurred in the cultures of the tracheal secretions but not the oropharynx.

The status of oral health was based on a score assigned by evaluating lips, mucous membranes and tongue, gums, teeth (where present), saliva. The score ranged from 1 to 3, and was recorded during the whole length of stay in the intensive care unit, indicating the progression of the status of oral health during the ventilation period.

DISCUSSION

The main purpose of this study was to evaluate the effectiveness of the VAP prevention bundle in reducing the number of ventilation-associated-pneumonia events in the paediatric population of the intensive care. The survey also aimed to evaluate the predictive power of the culture of the pharyngeal swabs in identifying the colonization of the trachea. These measures were routinely performed according to the latest scientific evidence in all the patients admitted to the intensive care unit and subjected to mechanical ventilation for at least 48 hours (12). Finally, the research evaluated the conditions of the stomatognathic apparatus and the oral health in the patients who use ventilators.

The primary outcome is monitoring the effectiveness of the protocol in the prevention of ventilator-associated pneumonia in a cohort of paediatric patients admitted to intensive care undergoing invasive mechanical ventilation. Additional secondary outcomes are evaluating the orotracheal colonization of patients undergoing mechanical ventilation, observing the status of oral health in these patients, and comparing the incidence of VAP before and after the implementation of the VAP prevention bundle.

Exploratory outcomes are evaluating the orotracheal colonization of the subpopulation of patients who develop pneumonia and any related relapses on the empiric antibiotic therapy approach; finally, the study also aims to observe the status of oral health in the subpopulation of patients who develop pneumonia.

The processing of data was carried out in compliance with the measures of the "Code regarding

the protection of personal data"; the database was developed using Microsoft Office Excel. The trial was conducted in accordance to the principles of good clinical practice and current regulations.

REFERENCES

1. Casado RJ, De Mello MJ, De Aragão RC, Correia JB. Incidence and risk factors for health care-associated pneumonia in a paediatric intensive care unit. Crit Care Med 2011; 39(8):1968-73.
2. Venkatachalam V, Hendley JO, Willson DF. The diagnostic dilemma of ventilator-associated pneumonia in critically ill children. Pediatr Crit Care Med 2011; 39(12):286-96.
3. Munro CL, Grap MJ, Jones DJ, McClish DK, Sessler CN. Chlorhexidine, toothbrushing, and preventing ventilator-associated pneumonia in critically ill adults. Am J Crit Care 200; 18(5):428-38.
4. Centers for Disease Control and Prevention. Ventilator-associated pneumonia (VAP) event. Device Assoc Events 2012: 6:1-6:13.
5. Coffin SE, Klompas M, Classen D, et al. Strategies to prevent ventilator associated pneumonia in acute care hospitals. Infect Control Hosp Epidemiol 2008; 29:S31-S40.
6. Teramoto S, Yoshida K, Hizawa N. Update on the pathogenesis and management of pneumonia in the elderly-roles of aspiration pneumonia. Respir Investig 2015; 53 (5):178-84.
7. Liu B, Li S-Q, Zhang S-M, et al. Risk factors of ventilator-associated pneumonia in pediatric intensive care unit: a systematic review and meta-analysis. J Thorac Dis 2013; 5(4):525-31.
8. Gupta A, Gupta A, Singh TK, Saxsena A. Role of oral care to prevent VAP in mechanically ventilated Intensive Care Unit patients. Saudi J Anaesth 2016; 10(1):95-7.
9. Klompas M, Speck K, Howell MD, Greene LR, Berenholtz SM. Reappraisal of routine oral care with chlorhexidine gluconate for patients receiving mechanical ventilation: systematic review and meta-analysis. JAMA Intern Med 2014; 174(5):751-61.
10. Kalil AC, Metersky ML, Klompas M, et al. Management of Adults with Hospital-acquired and Ventilator-associated Pneumonia: 2016 Clinical Practice Guidelines by the Infectious Diseases Society of America and the American Thoracic Society. Clinical Infectious Diseases, IDSA GUIDELINE. Clin Infect Dis 2016; 63(5):e61-e111
11. Torres A, Niederman MS, Chastre J, et al. International ERS/ESICM/ESCMID/ALAT guidelines for the management of hospital-acquired pneumonia and ventilator-associated pneumonia. ERS/ESICM/ESCMID/ALAT evidence-based recommendations for HAP/VAP diagnosis, treatment and prevention. Eur Respir J 2017: 10;50(3)
12. Brusselaers N, Labeau S, Vogelaers D, Blot S. Value of lower respiratory tract surveillance cultures to predict bacterial pathogens in ventilator-associated pneumonia: systematic review and diagnostic test accuracy meta-analysis. Intensive Care Med 2013; 39:365-75.

LETTER TO THE EDITOR

ROLE OF ADAMTS4 AND ADAMTS5 DURING EARLY ORTHODONTIC TOOTH MOVEMENT

S. MURAGLIE[1], G. MUSUMECI[2], C. LORETO[2] and R.M. LEONARDI[1]

[1]Department of Orthodontics, University of Catania, Catania, Italy; [2]Department of Biomedical and Biotechnological Sciences, Human Anatomy and Histology Section, School of Medicine, University of Catania, Catania, Italy

Received May 29, 2018 – Accepted November 7, 2018

The aim of this study was to evaluate the expression of ADAMTS4 and ADAMTS5 in human gingival crevicular fluid (GCF) at different time-points following the application of an orthodontic force. Thirty-two healthy patients (20 females, 12 males, mean age 13.8) who had undergone orthodontic treatment and needed upper first premolar extractions were enrolled in this study. For each patient, one maxillary canine was used as the test side and was subjected to a standardized orthodontic force while the contra-lateral canine was used as a control and not subjected to any force. A GCF sample was taken on the compression and test sides of the test tooth and on the control tooth at baseline, after 1, 4, 24 hours and 7 and 21 days. Western blot analysis was performed to detect protein levels on controls and test teeth. Following the application of a force, the expression of ADAMTS4 increased significantly ($p \leq 0.001$) peaking at 4 hours in the tension side, while on the compression side it reached a peak, in a time-dependent way, at 21 days ($p \leq 0.001$). ADAMTS5 levels peaked, on both tension and compression sides, at 1 hour following the application of force ($p \leq 0.05$), and on the compression side also at 24 hours and 7 days. These results suggest that both ADAMTS4 and 5 are involved during the early stages of orthodontic tooth movement.

To the Editor,

Orthodontic tooth movement (OTM) is the result of a specifically balanced remodeling process between the alveolar bone and periodontal ligament (PDL). When an orthodontic force is applied to a tooth, a response from the periodontal tissue allows tooth movement (1). It has been shown that the mechanical stress during OTM induces PDL cells to release different mediators, such as cytokines, growth factors, matrix metalloproteinases (MMPs) and enzymes, which are fundamental for connective tissue remodeling and maintenance (1-5). The ADAMTS (a disintegrin and metalloproteinase with thrombospondin motif protein), is a subfamily of metalloproteinases and enzymes that possess the ability to degrade proteoglycans (PGs), acting at a different cleavage site to MMPs (6). Moreover, it has been shown that PGs, like collagens, are involved during OTM. It was shown that, in rat tooth eruption, ADAMTS plays a key role in the remodeling of periodontal extracellular matrix (ECM) (7). In that study, it was demonstrated that during tooth eruption osteoblasts, osteocytes and fibroblasts of PDL expressed versican, ADAMTS1, ADAMTS4

Key words: ADAMTS4; ADAMTS5; orthodontic movement

Mailing address:
Dr. Simone Muraglie,
Department of Orthodontics,
Policlinico Universitario "Vittorio Emanuele", University of Catania,
Via Santa Sofia, 78, 95123 Catania (CT), Italy
Tel./Fax: +39 095 3782759
e-mail: simonemuraglie@live.it

0393-974X (2019)

DISCLOSURE: ALL AUTHORS REPORT NO CONFLICTS OF INTEREST RELEVANT TO THIS ARTICLE.

and ADAMTS5 (7). Therefore, it was supposed that ADAMTS 1, 2 and 5 are important in the signaling and regulation of the extracellular accumulation of large proportions of proteoglycan in the ECM of the periodontal ligament cells. Gingival crevicular fluid (GCF) analysis constitutes a non-invasive method to dynamically investigate the inflammatory mediators and signaling molecules in periodontal tissues and it has been used to analyze the biochemical and molecular processes of the soft and hard tissues that are involved during OTM. Identifying and mapping the molecular changes following the application of orthodontic force may help the clinician to identify the optimal force that can be used to obtain an appropriate tooth movement. For these reasons, given the important role of ADAMTSs in ECM and periodontal remodeling and metabolism, this study aimed to determine the composition and early time-dependent changes of ADAMTS4 and ADAMTS5 in GCF during orthodontic tooth movement before and after the application of a standardized orthodontic force to further understand the dynamic periodontal changes that facilitate the early phases of OTM.

MATERIALS AND METHODS

Study population

A power analysis was carried out using the results obtained from 10 random patients to evaluate the correct sample size for this research. The analysis indicated that 30 participants would yield a confidence level of 95% and a Beta error level of 20%.

Thirty-two patients (20 females, 12 males; 13-15 years of age; mean 13.8) who needed orthodontic treatment were selected for this study. Informed consent was obtained from all patients' guardians before the experimentation. Then the protocol was reviewed and approved by the local ethics committee.

The inclusion criteria were: i) general good health; ii) orthodontic treatment requiring a fixed appliance and upper first premolar extraction; iii) possessing a fully erupted maxillary canine; iv) healthy periodontium without gingival inflammation or radiographic evidence of bone loss; v) a full-mouth probing depth (PD) of ≤3 mm; vi) full-mouth plaque and full-mouth bleeding scores less or equal to 20%. The full-mouth plaque and full-mouth bleeding scores were evaluated by a 20g controlled force probe (Vivacare TPS Probe, Vivadent; Schaan, Lichtenstein) for supra-gingival plaque on the tooth surfaces or bleeding up to 30 seconds after probing.

The exclusion criteria were: i) previous orthodontic treatment; ii) pregnancy; iii) any systemic condition which might affect the study; iv) use of anti-inflammatory or antimicrobial drugs during the previous 3 months; v) use of mouthwash containing antimicrobials during the previous 3 months; vi) use of hormonal contraceptives; and vii) smoking.

Before bonding the orthodontic appliances, all subjects underwent a detailed periodontal examination and received an oral hygiene instruction protocol from a clinician not involved in the subsequent study phase and follow-up.

Study design

During the first phase of the orthodontic treatment, the maxillary first premolar teeth were extracted 21 days before starting the therapy with a fixed straightwire appliance. A fixed edgewise orthodontic appliance (MBT, 3M Unitek, Monrovia, CA, USA) was bonded along with an archwire sequence of 0.014-in, 0.016-in nickel titanium and 0.016-in stainless steel (MBT, 3M-Unitek).

For each patient, one maxillary upper canine was randomly chosen as a test tooth (for applying orthodontic force) and the other one as a control tooth (unbonded, without applying orthodontic force). The orthodontic force was applied, between the test tooth and the first molar, with a 150 gr Sentalloy coil spring (GAC International, Bohemia, NY, USA), controlled by a calibrated tension gauge which was activated once, at the baseline. One side of the test tooth was the compression side, the other the tension side. After the experiment, orthodontic treatment also included the control tooth. During the observation period the patients were told to avoid any anti-inflammatory or antimicrobial drugs.

GCF sampling

GCF samples were taken from the mesiobuccal and distobuccal sides of both the test and control teeth (1), according to the following schedule: T0, before application of the orthodontic force (baseline); T1, 1 h; T2, 4 h; T3, 24 h; T4, 7 days and T5, 21 days after applying a standardized orthodontic force. The sample

collection started at 9a.m.

At each appointment for all subjects, all the clinical periodontal data was assessed. Before GCF collection from the selected sites, any plaque deposit was removed with a sterilized cotton roll, and gently dried by air stream. GCF was collected with sterile strips on the control tooth and on the tension and compression sides of the test tooth (Inline, Torino, Italy). The strip was gently subgingivally placed on 1 mm for 30 seconds. Strips contaminated by saliva or blood were disposed of. The valid strips were then immediately placed in individual sealed plastic tubes (Cryotube, 2.0 mL, NUNC, Roskilde, Denmark) and snap frozen in liquid nitrogen at –70°C.

During the experimental period, the total amount of control and test tooth movement was calculated with a calibrated digital caliper. After completing the clinical assessments, intra-examiner repeatability and method error were evaluated. Intra-examiner calibration and reproducibility were guaranteed during the baseline calibration sessions by obtaining duplicate measurements of the GCF parameters from randomly selected patients. Intra-examiner agreement was calculated by Cohen's k

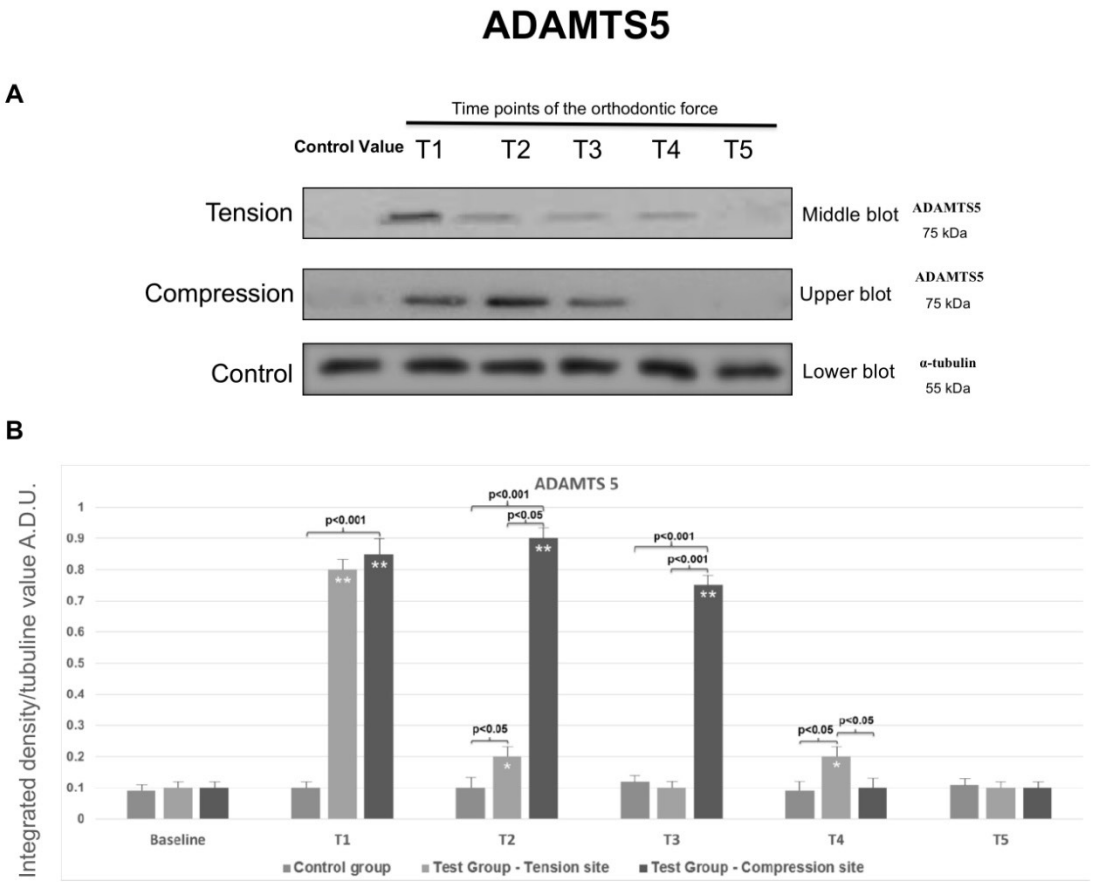

Fig. 1. ***A)*** *Western blot analyses for ADAMTS5. ADAMTS5 protein levels in gingival crevicular fluid (GCF) at: T0, before application of the orthodontic force (baseline); T1, 1 hour; T2, 4 hours; T3, 24 hours; T4, 7 days and T5, 21 days after exertion of the standardized orthodontic force (upper blot, compression; middle blot, tension).* ***B)*** *Graph for ADAMTS5, T1, 1 hour; T2, 4 hours; T3, 24 hours; T4, 7 days and T5, 21 days after exertion of the standardized orthodontic force. Data showed the relative expression (mean ± SEM) of ADAMTS5 protein calculated as arbitrary densitometric units (A.D.U.), collected from three independent experiments. Representative immunoblots were obtained using 30 μg of cell homogenates for each group. β-Tubulin was used as the loading control in each experiment. * $p < 0.05$ and ** $p < 0.01$, when compared to the control group.*

** $p \leq 0.05$; ** $p \leq 0.001$, values between baseline and analyzed group at different time points.*

coefficient which predicted a good degree of test-retest reliability.

Protein extraction

The proteins were extracted in a buffer containing lysis (150 mmol/L NaCl, 50 mmol/L Tris- HCl [pH 7.5], 5 mmol/L ethylenediaminetetraacetic acid (EDTA), 1 mmol/L Na3VO4, 30 mmol/L Na pyrophosphate, 50 mmol/L NaF, 1 acid mmol/L phenyl-methyl- sulfonyl-fluoride, 5 Ag/mL aprotinin, 2 Ag/mL leupeptin, 1 Ag/mL pepstatin, 10% glycerol, and 0.2% Triton X-100) and subsequently centrifuged in supernatants at 14,000 rpm at 4°C for 10 min. The protein concentration was determined by the Bradford method using BSA as a standard.

Western blot analysis

Western blot analysis was carried out to analyze the production of ADAMTS5 and ADAMTS4. Briefly, all samples were homogenized in a buffer containing T-Per buffer (Thermoscientific, Rockford, IL, USA) and a protease inhibitor cocktail (Roche Diagnostics) in a Teflon-glass homogenizer followed by sonication. The protein concentrations were determined using the Bradford method with bovine serum albumin as a standard. Sample proteins (30 µg) were diluted in sodium dodecyl sulphate protein gel loading solution (Invitrogen, Monza, Italy), boiled for 5 min, separated on 4–12% Bis-tris gel (Invitrogen) and electroblotted onto nitrocellulose membranes (Invitrogen).

The following antibodies were used: rabbit antihuman ADAMTS5 (ab41037 abcam, Cambridge, UK) and rabbit antihuman ADMTS4 (ab84792, abcam, Cambridge, UK); diluted 1:1000 in TBS-T buffer overnight at 4°C and α-tubulin (Santa Cruz Biotechnology Inc, Bergheimer, Germany; 1:20,000), which was used as a loading control. The HRP-conjugated secondary antibody (Santa Cruz Biotechnology Inc, Bergheimer, Germany) was diluted 1:10,000. Nonspecific binding was blocked for 2 h at 37°C with 5% non-fat dried milk in Tween-Tris-buffered saline. All antibodies were prepared in 5% non-fat dried milk solution in Tween-Tris-buffered saline. Blots were developed using the enhanced chemiluminescence ECL technique (GE Healthcare, Milan, Italy) and relative band densities were quantified using ImageQuantTL 7.0 software (GE Healthcare, Milan, Italy). No signal was detected when the primary antibody was omitted (data not shown). All experiments were repeated at least 3 times.

Statistical analysis

ADAMTS5 and ADAMTS4 protein expressions were calculated by mean levels ± standard deviations (SD) for the control teeth and for the tension and compression sides of the test teeth, at each interval throughout the experiment.

The Kolmogorov–Smirnov test was used to test the normality of the data. Since the data were not normally distributed with inhomogeneous variance, non-parametric tests were used. The data were analyzed by Friedman test to statistically evaluate any significant differences in the expression levels of ADAMTS5 and ADAMTS4 protein on the compression and tension sides during each interval session *vs* control values.

The Kruskall Wallis test was applied to determine whether there were any significant differences among the groups at each time point. Additionally, to identify the significance in each pair of groups, multiple comparison analyses were also performed; for these multiple comparisons, Bonferroni's correction was applied, for which the alpha significance level 0.050 was divided by the number of possible comparisons (three). Thus, the new 'adjusted' significance level was 0.017.

The data were crunched by SPSS (version 11.5 for Windows SPSS, Chicago, IL) and $p<0.05$ was considered to be statistically significant.

RESULTS

All 32 participants completed the study. During the observation period, all the enrolled subjects maintained good oral hygiene. There were no dropouts throughout the clinical trial. The mean movement of the canines toward the second premolars was 2.23±0.35 mm.

α-tubulin was used as an internal control for protein load (Fig. 1A, lower blot). The ADAMTS5 and ADAMTS4 GCF levels, recorded for the control (group) and compression and tension sides (test group) at each interval are shown in Figs. 1 and 2.

The ADAMTS5 GCF levels in the control samples were lower compared to the values of both sides of the test group (Fig. 1). Compared to the baseline, the test group tension sites showed a rapid

and significant increase in ADAMTS5 protein at T1 (1 h) ($p<0.001$) while showing a drastic reduction at T2 (4 h) and T3 (24 h) with an applied force (Fig. 1, A upper blot and B). Even in the test group, on the compression side, the GCF expression of the ADAMTS5 protein showed significantly increased time-dependent levels at T1, T2 and T3 ($p<0.001$), while showing a drastic reduction at T4 and T5. Moreover, at T5, the ADAMTS5 levels were similar on both test sides and with the control group (Fig. 1, *A* middle blot and *B*).

Comparing the two sides of the test group, there was a higher significant expression of ADAMTS5 on the compression side at T2, T3 ($p<0.001$) and T4 ($p<0.05$) compared to the tension side (Fig. 1).

ADAMTS4 was constitutively highly expressed in GCF compared to ADAMTS5 (Fig. 2 B). ADAMTS4 levels were more highly expressed in the test group, compared to controls, both on the compression and tension sides, even though differently. On the tension

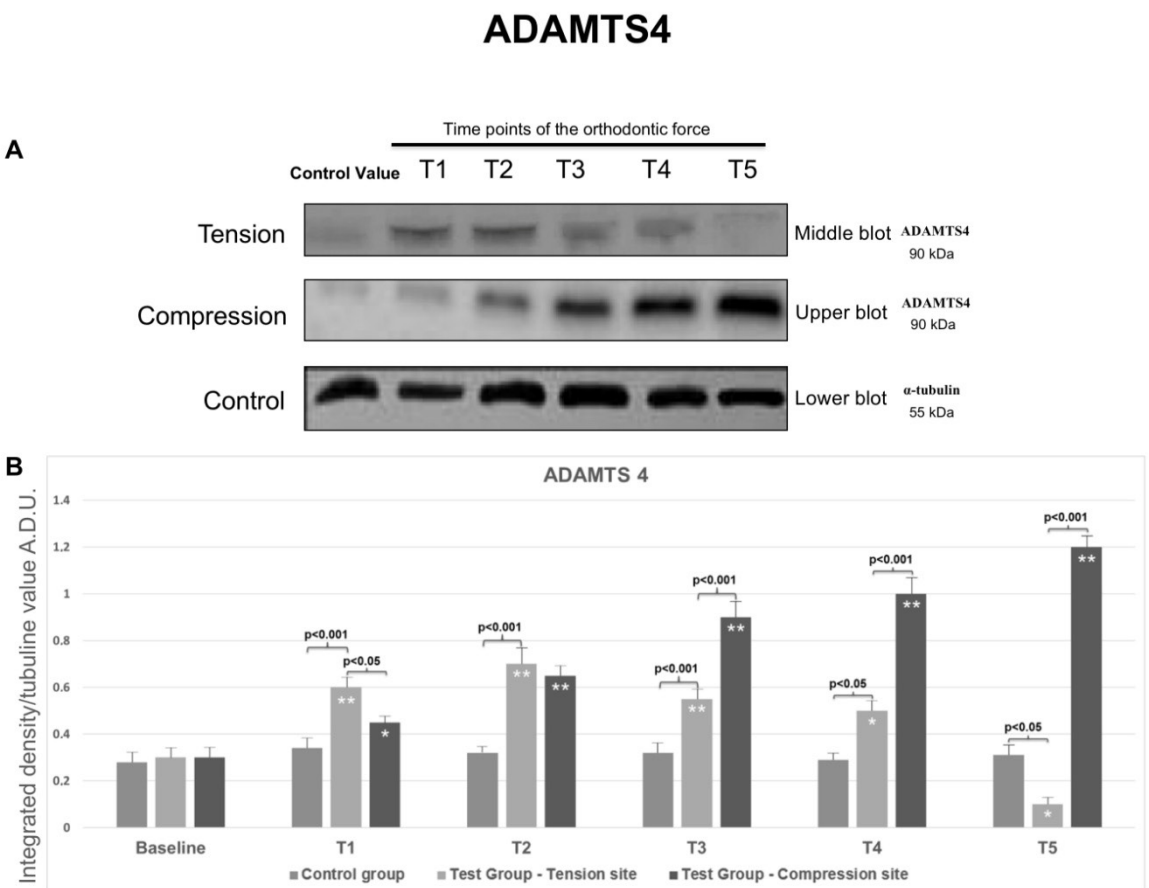

Fig. 2. ***A****) Western blot analyses for ADAMTS4. ADAMTS4 protein level in gingival crevicular fluid (GCF) at: T0, before application of the orthodontic force (baseline); T1, 1 hour; T2, 4 hours; T3, 24 hours; T4, 7 days and T5, 21 days after exertion of the standardized orthodontic force (upper blot, compression; middle blot, tension). (B) Graph for ADAMTS4. T1, 1 hour; T2, 4 hours; T3, 24 hours; T4, 7 days and T5, 21 days after exertion of the standardized orthodontic force. Data showed the relative expression (mean ± SEM) of ADAMTS4 protein calculated as arbitrary densitometric units (A.D.U.), collected from three independent experiments. Representative immunoblots were obtained using 30 μg of cell homogenates for each group. β-Tubulin was used as the loading control in each experiment.*

** $p < 0.05$ and ** $p < 0.01$, when compared to the control group.*

** $p \leq 0.05$; ** $p \leq 0.001$, values between baseline and analyzed group at different time points.*

side, the expression increased significantly at T1 and T2 ($p<0.001$), while it decreased at T3, T4 and T5 throughout the experiment (Fig. 2, A upper blot, and B). On the compression side, the ADAMTS4 protein expression levels increased time-dependently and reached a peak at T5 ($p<0.001$) with a force applied (Fig. 2, middle blot).

DISCUSSION

This study demonstrated that both ADAMTS4 and 5 play an important role in ECM maintenance and remodeling, and that they are constitutively expressed and their levels change due to OTM. MMPs and aggrecanases are two main molecules capable of hydrolyzing and degrading the PG proteins in PDL. ADAMTS-4 and ADAMTS-5, also called aggrecanase 1 and aggrecanase 2, play an important role in aggrecan degradation (8). Moreover, the aggreganases are expressed by PDL cells and cementoblasts which also balance, alongside ADAMTS 1 and 4, the accumulation of PGs in the ECM (7). In many human tissues, it has been described that ADAMTSs can be mechano-regulated: it has been reported that dynamic compressive loading on meniscal explants leads to increased expression of ADAMTS4 and ADAMTS5 and MMPs (9). These results were also confirmed by a similar report, which showed that levels for aggrecanases were up-regulated during the first 8 hours after a compression force (10). Thus, according to the results of this study, as well as being mechano-regulated, ADAMTSs are also time-dependently regulated during OTM. Data from this study is in line with previous reports. Furthermore, this study demonstrates differences in ADAMTS expression levels between the compression and tension sides, although ADAMTS 4 and 5 were more up-regulated on the tension side than on the compression side (6, 10, 11). Interestingly, a previous study on a PDL sample demonstrated that during experimental tooth movement, versican was more expressed on the compression side than the tension side (12), and this could be somehow linked to ADAMTS up-regulation on the same side according to the results of the present study. Therefore, the time-dependent expressions of versican and ADAMTS4 and 5 are similar, speculating on their participation in alveolar bone and PDL remodeling during OTM (7). An up-regulation of ADAMTS4 and ADAMTS5 in response to applying an orthodontic force suggests a potential role for these enzymes being mechanically induced early in the ECM remodeling of PDL. Based on the results of the present study, we conclude that ADAMTS4 and ADAMTS5 are constitutively expressed during the early phases of OTM and their up-regulation is observed, interestingly, more on the tension side than the compression side. Moreover, it is essential to identify the changes in these biomarkers to better understand how tissue response, following the application of an orthodontic force, could influence the physiology of tooth movement.

REFERENCES

1. Cantarella G, Cantarella R, Caltabiano M, Risuglia N, Bernardini R, Leonardi R. Levels of matrix metalloproteinases 1 and 2 in human gingival crevicular fluid during initial tooth movement. Am J Orthod Dentofacial Orthop 2006; 130:11-16.
2. Leonardi R, Talic NF, Loreto C. MMP-13 (collagenase 3) immunolocalisation during initial orthodontic tooth movement in rats. Acta Histochem 2007; 109:215-20.
3. Ingman T, Apajalahti S, Mantyla P, Savolainen P, Sorsa T. Matrix metalloproteinase-1 and -8 in gingival crevicular fluid during orthodontic tooth movement: a pilot study during 1 month of follow-up after fixed appliance activation. Eur J Orthod 2005; 27:202-7.
4. Apajalahti S, Sorsa T, Railavo S, Ingman T. The in vivo levels of matrix metalloproteinase-1 and -8 in gingival crevicular fluid during initial orthodontic tooth movement. J Dent Res 2003; 82:1018-22.
5. Leonardi R, Loreto C, Talic N, Caltabiano R, Musumeci G. Immunolocalization of lubricin in the rat periodontal ligament during experimental tooth movement. Acta Histochem 2012; 114:700-4.
6. Wang SL, Yu YL, Tang CL, Lv FZ. Effects of TGF-beta1 and IL-1beta on expression of ADAMTS enzymes and TIMP-3 in human intervertebral disc degeneration. Exp Ther Med 2013; 6:1522-26.

7. Sone S, Nakamura M, Maruya Y, Takahashi I, Mizoguchi I, Mayanagi H, Sasano Y. Expression of versican and ADAMTS during rat tooth eruption. J Mol Histol 2005; 36:281-88.
8. Tortorella MD, Malfait F, Barve RA, Shieh HS, Malfait AM. A review of the ADAMTS family, pharmaceutical targets of the future. Curr Pharm Des 2009; 15:2359-74.
9. Zielinska B, Killian M, Kadmiel M, Nelsen M, Haut Donahue TL. Meniscal tissue explants response depends on level of dynamic compressive strain. Osteoarthritis Cartilage 2009; 17:754-60.
10. Fitzgerald JB, Jin M, Dean D, Wood DJ, Zheng MH, Grodzinsky AJ. Mechanical compression of cartilage explants induces multiple time-dependent gene expression patterns and involves intracellular calcium and cyclic AMP. J Biol Chem 2004; 279:19502-11.
11. Valhmu WB, Stazzone EJ, Bachrach NM, Saed-Nejad F, Fischer SG, Mow VC, Ratcliffe A. Load-controlled compression of articular cartilage induces a transient stimulation of aggrecan gene expression. Arch Biochem Biophys 1998; 353:29-36.
12. Sato R, Yamamoto H, Kasai K, Yamauchi M. Distribution pattern of versican, link protein and hyaluronic acid in the rat periodontal ligament during experimental tooth movement. J Periodontal Res 2002; 37:15-22.